P-1

THE INTERNATIONAL HYDROGRAPHIC REVIEW

VOL. 30 · Nº 1
MAY 2024

IHO International Hydrographic Organization

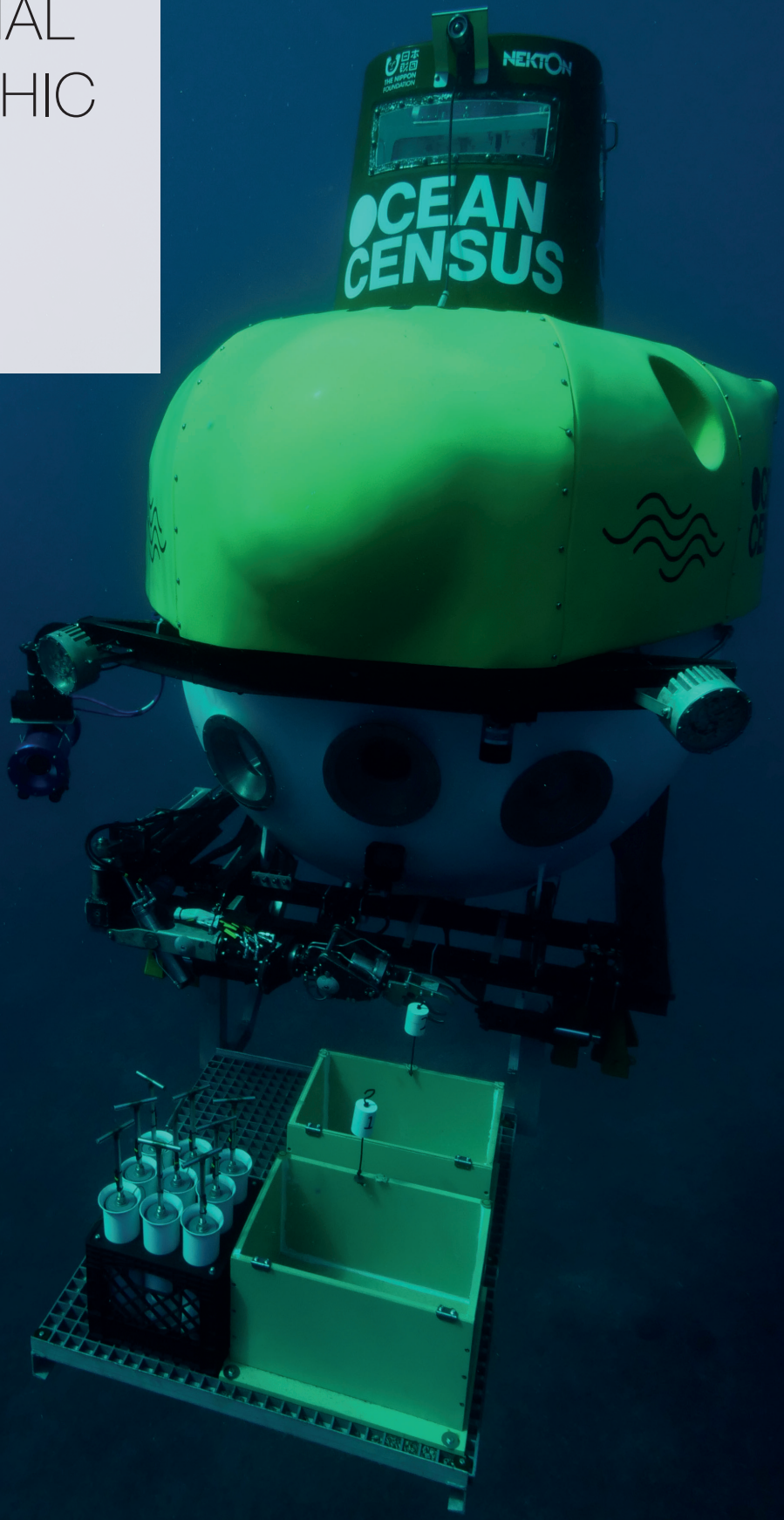

P-1

THE INTERNATIONAL HYDROGRAPHIC REVIEW

VOL. 30 · Nº 1
MAY 2024

IHO
International Hydrographic Organization

International Hydrographic Organization
Vol. 30 · Nº 1 — May 2024

Cover image

The cover image shows the Pisces VI deep-sea research submersible, which provides access to the deep ocean to study marine ecosystems. The related article by Alex David Rogers & Eva Ramirez-Llodra (pp. 10–37) shows how quantitative sampling methods and deep submergence technologies, as well as advances in fields such as acoustics and marine navigation, are enabling deep-sea exploration of marine ecosystems. The Nippon Foundation Nekton Ocean Census programme is an important initiative to accelerate the discovery of marine life. Photo: Nekton Foundation.

Open Access Policy

This journal provides immediate open access to its content on the principle that making research freely available to the public supports a greater global exchange of knowledge.

About the Journal

The International Hydrographic Review (IHR) is an international scientific journal publishing peer-reviewed papers on all aspects of hydrography and associated subjects, ranging from the latest technical developments and significant events to book reviews and historical recollections. The IHR was first published in 1923 and since then has been published regularly.

Editorial

Patrick Westfeld

Welcome to the first issue of the 30th volume of The International Hydrographic Review (IHR).

What a success! Over 1 billion crowdsourcing depth data points, collected by hundreds of vessels using standard navigation equipment during routine maritime operations, are stored in the IHO Data Center for Digital Bathymetry (DCDB). The DCDB is hosted by the U.S. National Oceanographic and Atmospheric Administration (NOAA) on behalf of the IHO Member States. In addition to data from the IHO Crowdsourced Bathymetry (CSB) initiative, the DCDB archives and shares ocean depth soundings collected since 1990 by hydrographic, oceanographic and industrial vessels using multibeam and single beam sonars during surveys or transits.

Each of these 1,008,164,463 CSB depth soundings (as of April 2024) has the potential to fill data gaps and to contribute to a safer navigation at sea. But it is not only for this purpose. The hydrographic data required is no longer limited to water depths along shipping routes. Rather, the derived spatio-temporally resolved seabed topography plays a crucial role in the acquisition, processing and analysis of other expert data, e.g. ocean profile data in oceanography and habitat mapping in marine geology. Hydrographic data are therefore essential for e.g. assessing the impact of climate change on ocean circulation, mapping mussel habitats, predicting coastal erosion and identifying suitable areas for offshore renewable energy infrastructure.

Knowledge of our waters in general, and CSB data in particular, can help take informed decisions and is therefore key to protecting and sustainably using our oceans. The fact that our hydrographic community, as well as the neighbouring disciplines of oceanography and geodesy, are rising to the challenge of providing data that were previously non-existent or very sparse is also reflected in the number of related papers in this issue – five on crowdsourcing and four on ocean exploration. Let us begin with the first...

In honour of IHR's centenary in 2023, Prof Dr Alex David Rogers has been invited to contribute to the special Jubilee Issue with a keynote article on the exploration of deep-sea biodiversity. As this was not possible in the Jubilee year, we are publishing the manuscript now. This is not such a big worry, as Alex David Rogers & Eva Ramirez-Llodra's article also fits perfectly into the thematic focus of this issue. Their contribution provides an excellent summary of the activities to discover the diversity of species in the deep sea over the last hundred years, and shows that as human impact increases, knowledge of the distribution of life must be constantly improved through further *deep-sea exploration of marine ecosystems* (pp. 10–37).

The second article in this issue is also an invited contribution. Manuela Ammann from the University of Applied Sciences Northwestern Switzerland is the current winner of the IFHS Student Award for her Master's thesis on *robotic photogrammetric underwater inspections* (pp. 38–44).

The following three of the five peer-reviewed scientific articles also address the task of filling data gaps. What is exciting is that they do so from three different disciplines, in very different ways, for different tasks. First, Bruce Enki Oscar Thomas et al. present a novel *cargo ship-based Global Navigation Satellite System (GNSS) network* in the Pacific Ocean that analyses sea surface heights in real time *for tsunami detection*, thereby adding accurate tsunami observations to an existing geodetic data gap (pp. 46–63). In the following article, Mathieu Rondeau et al. use the Canadian Hydrographic Service's (CHS) *Community Hydrography Program* as an

ISSN print: 0020-6946
DOI prefix: 10.58440
URL: https://ihr.iho.int/

Publisher:
International Hydrographic Organisation
4b Quai Albert 1er
98011 Monaco

Editorial Board:
https://ihr.iho.int/editorial-team/

example of how *to go from a volunteer ping to a bathymetric community map* in the span of a few weeks (pp. 64–77). In a third article, Matthias Hinz et al. present a workflow for fully automated *AI-based boulder detection* in sonar data, which has the potential to efficiently provide accurate, reliable and unbiased knowledge about the presence of boulders on the seabed for a variety of applications such as marine geological and biological habitat mapping (pp. 78–98).

Another two peer-reviewed scientific articles focus on *improving the energy efficiency of a ship using tidal current information* (Jinyoung Yang & Do-Seong Byun, pp. 100–110) and *exploring the possibility of adding Discrete Global Grid Systems (DGGS) support to the S-100 Universal Hydrographic Data Model* (Kimberly Mason & Jens Schröder-Fürstenberg, pp. 112–123).

I am pleased to announce that for the first time in this issue we are publishing selected papers from HYDRO, the annual hydrographic conference of the International Federation of Hydrographic Societies (IFHS). First of all, Aldo Monaca, President of the Organizing Committee of HYDRO 2023, will give you his greetings (pp. 125–126). This is followed by two conference papers on exploring our oceans, with the aim of providing the knowledge to use them sustainably and to protect them: Tanja Dufek et al. use *deep-towed multibeam echosounder data to locate active hydrothermal vents* that are thought to be metal-rich sulphide deposits on the seafloor (pp. 128–134). Hannah Brocke et al. are also helping to *fill data gaps by creating automated maps of seabed health to provide nature-based solutions* for policy decisions, support investment in the blue economy, and encourage the development of markets for blue carbon and biodiversity credits (pp. 136–142). Matthew Woodlief will conclude with his conference paper on *unlock insights from hydrographic data with GeoAI* (pp. 144–149).

Due to the rapid technological development in the field of hydroacoustic data acquisition and processing, CSB can make a valuable contribution to filling the gaps, provided that the associated uncertainty constraints are understood and adequately addressed. In this new issue of the IHR you will find two notes / technical reports on the subject of CSB: Jennifer Jencks & Belen Jimenez Baron present *CSB as part of the modern hydrographic toolbox* (pp. 150–160) and Hains et al. examine CSB data quality and legal concerns (pp. 162–170).

Two further notes / technical reports deal with *Science Monitoring and Reliable Technology (SMART)* to monitor the ocean using submarine cables (Matías Sifón, pp. 172–177) and the *Baltic Sea e-Nav project, a partnership for the future of marine navigation* to unlock the full potential of the S-100 paradigm shift towards e-navigation (Benjamin Hell et al., pp. 178–181).

The current issue concludes with valuable information from the IFHS on *empowering hydrographic professionals* (Lekkerkerk et al., pp. 182–187), from the International Federation of Surveyors (FIG) presenting its forthcoming *four-year work plan for Commission 4 – Hydrography* (M. D. Eranda K. Gunathilaka et al., pp. 188–192) and a *review of the book „The deepest map – The high-stakes race to chart the world's oceans"* by Laura Tretheway (Douglas Paul Brunt, pp. 194–195).

On behalf of the Editorial Board, I hope you enjoy reading this new edition of IHR!

Dr Patrick Westfeld
Chief Editor, IHR

https://doi.org/10.58440/ihr-30-1-e01

Content

Notes / Technical reports

General information

Book review

INVITED ARTICLE

Deep-sea exploration of marine ecosystems – Knowledge and solutions for marine biodiversity

Authors

Alex David Rogers[1,2] and Eva Ramirez-Llodra[2]

Preamble

In honour of the centenary of The International Hydrographic Review (IHR) in 2023, Prof Dr Alex David Rogers was invited to contribute to the special Jubilee Issue* with a keynote article on the exploration of deep-sea biodiversity over the past 100 years and a look into the future of deep-sea exploration of marine ecosystems. As this was not possible in the Jubilee year, we are now publishing the manuscript.

* *The International Hydrographic Review, 29*(1). International Hydrographic Organization, Monaco.https://ihr.iho.int/issues volume-29-1/ (accessed 20 April 2024).

Abstract

We review discoveries in deep-sea biodiversity since the establishment of the International Hydrographic Organisation in 1921. Over the last century it has been demonstrated that the deep sea harbours a great variety of habitats which host a large diversity of species rivalling that of other marine and terrestrial ecosystems. This was possible through the invention of quantitative sampling methods and deep-submergence technologies as well as advances in fields such as acoustics and marine navigation. Increasing human activities impacting the deep ocean now demand knowledge of the distribution of life in the deep sea is greatly improved through further exploration.

Keywords

deep-sea · biodiversity · ecology · sampling technology

Résumé

Nous passons en revue les découvertes en matière de biodiversité des grands fonds marins depuis la création de l'Organisation hydrographique internationale en 1921. Au cours du siècle dernier, il a été démontré que les eaux profondes abritent une grande variété d'habitats qui hébergent une large diversité d'espèces rivalisant avec celles des autres écosystèmes marins et terrestres. Ces résultats ont pu être obtenus grâce à l'invention de méthodes d'échantillonnage quantitatif et de technologies d'immersion en profondeur, ainsi que grâce aux progrès réalisés dans des domaines tels que l'acoustique et la navigation maritime. L'augmentation des activités humaines qui ont un impact sur les grands fonds océaniques exige désormais que la connaissance de la diffusion de la vie dans les grands fonds soit grandement améliorée par de nouvelles explorations.

✉ Alex David Rogers · alex.rogers@oceancensus.org

[1] Ocean Census, Oxfordshire, OX5 1PF, United Kingdom

[2] REV Ocean, 1327 Lysaker, Norway

https://doi.org/10.58440/ihr-30-1-a09

Resumen

Revisamos los descubrimientos en biodiversidad de los fondos marinos desde la creación de la Organización Hidrográfica Internacional en 1921. A lo largo del último siglo se ha demostrado que las profundidades marinas albergan una gran variedad de hábitats que acogen una gran diversidad de especies que rivaliza con la de otros ecosistemas marinos y terrestres. Esto ha sido posible gracias a la invención de métodos cuantitativos de toma de muestras y tecnologías de inmersión profunda, así como avances en campos como la acústica y navegación marinas. El aumento de las actividades humanas que afectan a las profundidades oceánicas exige ahora que se mejore considerablemente el conocimiento de la distribución de la vida en las profundidades marinas mediante más exploraciones.

1 The emergence of modern deep-sea biodiversity research

By the time of the establishment of the International Hydrographic Organisation (IHO; then the International Hydrographic Bureau) in 1921, the results to many oceanic and transoceanic expeditions had been published. The circumglobal voyage of *HMS Challenger* (1872–1876) alone resulted in 50 volumes of scientific research, the last of which was published in 1895 (Corfield, 2004). In 1935, the Swedish zoologist Sven Ekman synthesised findings on species distributions from the results of these expeditions to summarise current knowledge of the biogeography of the global ocean including the deep sea. Ekman (1935) concluded that the deep-sea fauna was distinctive and diverse (the *Challenger* expedition described more than 1,500 species living below 500 fathoms [914 m]), although the abundance and diversity of species declined with increasing depth and distance from the continental shelf. He also concluded that the fauna of hard substrata was different to that found on sediments (Ekman, 1935). His descriptions of the zones of transition from the shelf biota to the deep sea and then within the deep sea itself remain largely consistent with our understanding today.

It is fascinating to note that just before Ekman published his seminal work in on ocean biogeography two Americans, William Beebe and Otis Barton had taken the first dives into the deep sea using the *Bathysphere*, essentially a hollow iron ball lowered on a cable with a single viewing window. Deep-submergence technology had emerged for the first time for the purposes of marine scientific research. This paper reviews the exploration of deep-sea biodiversity over the last 100 years describing important technological advances and the landmark discoveries in the field. We finish by looking into the future of deep-ocean biodiversity science and how it is critical to halting the decline of marine species through providing evidence for decision making and management related to human activities in the ocean.

2 Plumbing the depths: over-the side sampling

Much of the work discovering deep-sea biodiversity has been undertaken through over-the-side sampling using dredges, trawls, sleds, corers and pelagic nets. This has involved painstaking work in the field and back in the laboratory to carefully identify marine species, still poorly known from the deep sea (e.g. Bouchet et al., 2023), to obtain quantitative data on the distribution of life. This equipment began as mechanical devices deployed by wire or rope from a ship but have developed overtime to incorporate sensors, telemetry and precise control of sampling.

2.1 Benthic sampling

2.1.1 Dredges and sleds

The naturalist's dredge became the workhorse of 19th Century deep-sea biology and work undertaken during expeditions such as that of *HMS Challenger* (1872–1876) provided some of the first insights into the diversity and distribution of deep-sea organisms (Ekman, 1935; Kaiser & Brenke, 2016; Table 1). Post World War 2 scientists tried to design more quantitative dredges. Howard Sanders from Woods Hole Oceanographic Institution (WHOI) developed the anchor dredge for semi-quantitative sampling, revealing an astonishing diversity of small animals living on or in deep-sea sediments (Sanders et al. 1965). This was followed by the development of the WHOI epibenthic sled (Hessler & Sanders, 1967) and more complex sleds which incorporated acoustic telemetry and cameras to better estimate the area / volume of sediment sampled and to photograph seafloor communities prior to disturbance from the gear (Table 1).

In subsequent decades iterations of the WHOI epibenthic sledge were designed (e.g. Snell sledge; Snell, 1998) whilst much heavier and more robust instruments have been used to sample rough seafloors associated with seamounts and other rugged topography (e.g. New Zealand Institute of Water and Atmospheric Research's [NIWA] seamount sled; Kaiser & Brenke, 2016; Fig. 1). These instruments have provided data on the abundance and diversity of seamount benthic fauna (e.g. Clark & Rowden, 2009). Sleds were also developed to sample small organisms

https://doi.org/10.58440/ihr-30-1-a09

Fig. 1 Examples of (a) the NIWA seamount sled, (b) beam trawl (c) Brenke sled, (d) otter trawl. All photos by A. D. Rogers taken during The Nippon Foundation Nekton Ocean Census NIWA Bounty Trough Expedition, South West Pacific, 2024 (a, b, c) and on the *RV Helmer Hanssen* in Svalbard, Arctic June, 2019.

living on and in sediments as well as the hyperbenthos including the Rothlisberg and Pearcy epibenthic sampler or sled and the Brenke sledge (Brenke, 2005; Kaiser & Brenke, 2016; Table 1; Fig. 1). The latter can recover intact samples of small organisms and has also been equipped with stills and video cameras as well as oxygen sensors (Brandt et al., 2013).

2.1.2 Trawls

Beam and otter trawls (Fig. 1) have been adapted for science from fishing gear. Using a beam trawl *HMS Challenger* recovered megafauna living on the surface of the seafloor down to abyssal depths (Table 2). These trawls were simplified by Alexander Agassiz, a scientist and Captain Charles D. Sigsbee of the U.S. Coast Survey Steamer *Blake* (Murray & Hjort, 1912; Rozwadowski, 2005; Table 2). They also pioneered the use of wire rope a material which is now standard for many research vessels. Sizes of Agassiz trawl vary from small light trawls of 1 m width and 0.3 m height to much larger trawls of 3.5 m width and 1 m in height (Clark et al., 2016). Otter trawls (Table 2) can be large and need to be towed at speed to keep the doors open. This type of trawl enabled the capturing of large numbers of leptocephali of the European and America eels (*Anguilla anguilla* and *Anguilla rostrata*) on a series of fisheries investigations eventually enabling the Danish scientist Johannes Schmidt to uncover the approximate location of the eel spawning grounds in the Sargasso Sea (Hjort, 1910; Schmidt, 1923; see account in Svensson, 2019).

Modern otter trawls are often twin warped and the angle and spreading effect of the doors can be altered to reduce or increase bottom contact influencing the species collected (Clark et al., 2016; Fig. 1). Wires connect back from the doors to the net, the upper headline of which is held up in the water by buoyant floats to hold the mouth open (Clark et al., 2016). The ground rope is often equipped with rollers or bobbins to help it jump over obstacles (Clark et al., 2016). These nets can be modified for very rough seafloors such as found on seamounts or in canyons through including heavier ground gear with wide discs or rollers (Clark et al., 2016). Smaller otter trawls can be towed on single warps where the vessel is small and available power limited (e.g. *Michael Sars*; Murray & Hjort, 1912; Clark et al., 2016).

2.1.3 Corers

Trawls and dredges can only generate qualitative or semi-quantitative data for deep-sea megafauna and macrofauna (Gage & Tyler, 1991; Narayanaswamy et al., 2016). Grabs and later corers were developed to take a known quantity of the seafloor so that organisms living both on and in the sediments could be identified, enumerated and their biomass estimated. These include the macrofauna (animals retained in a sieve of mesh size 250–300 μm) and meiofauna (animals retained in a sieve of mesh size 20–32 μm) that make up most of the biological communities of

https://doi.org/10.58440/ihr-30-1-a09

deep-sea sediments (Narayanaswamy et al., 2016).

The first grabs were developed for use in shallow water for investigations of the role of benthic communities in supporting fish stocks in Danish fjords (Petersen & Boysen Jensen, 1911; Table 3). This work gave rise to the concept of animal communities on the seafloor (Petersen, 1913). Penetration of grabs into the seafloor was an issue as was the bow-wave effect where the water pushed in front of the equipment "blows away" organisms living on the surface (Narayanaswamy et al., 2016). Given these and other issues such as sample wash out on retrieval, these devices have been largely replaced by corers for quantitative sampling of deep-sea sediments (Narayanaswamy et al., 2016; Table 3). Video guided grab systems have more typically been used to take geological samples or to take samples from places where corers or other equipment cannot sample or where habitat is very patchy such as on seamount, cold-water coral reef ecosystems (e.g. Pratt et al., 2019) or sulphide-rich deposits (Narayanaswamy et al., 2016). Some of these are hydraulic and may even be equipped with ROV thrusters to enable more precise positioning of the system for sampling (e.g. HYBIS, Table 3).

Gravity corers were first developed in the mid-late 19th Century and included the Brooke Sounder and the Baillie Sounding Machine, used during the *Challenger* Expedition for soundings (Murray & Renard, 1891; Schönfeld, 2012; Table 3). The desire for longer cores led to the development of a corer driven into the seafloor by an explosive charge which obtained cores up to 10 meters long from depths as great as 4,846 m depth (Piggot, 1936; Table 3). However, this was superseded by the piston core (Kullenberg, 1947) deployed on the Swedish *Albatross* expedition and was used to collect 250 core samples as long as 13 m from the deep sea (Pettersson, 1949). This has remained largely unchanged to the present day and can obtain cores up to 60 m long.

Gravity corers still suffered from the issue of bow waves and also the use of core catchers, devices which prevent a core falling from the coring tube or liner

Table 1 The evolution of benthic sleds and dredges. Through time trends included more accurate quantification of samples, inclusion of closing mechanisms for nets and greater levels of telemetry and instrumentation.

Equipment	Inventor/adaptor	Innovation	Reference
Oyster dredge	Count Luigi Ferdinando Marsigli (Italy)	Dredging of shallow water animals published in Histoire Physique de la Mer 1725	Rehbock, 1979
Müller dredge	Otto Frederic Müller (Denmark)	Modified oyster dredge with square mouth. Deep water sampling of Oslofjord and other fjords in southern Norway.	Brattegard et al., 2011
Ball's dredge or naturalists dredge	Robert Ball (Ireland)	Rectangular mouth and scrapers on upper and lower sides of dredge so it would operate regardless of which side landed on the seafloor. Towing arms of dredge also folded down so device could be packed into portable bag. Used in the *Challenger* Expedition.	Rozwadowski, 2005
Anchor dredge	Forster, modified by Howard Sanders (U.S.A.)	Dredge with horizontal plate attached to a metal frame dividing the mouth into two equal halves so it would dig in up to the level of the plate (about 11 cm). Semi-quantitative and samples sieved through 0.42 mm mesh to collect small animals.	Forster, 1953; Sanders et al., 1965; Kaiser & Brenke, 2016
WHOI Epibenthic sled	Hessler and Sanders (U.S.A.)	Fine-mesh plankton net (000 monofilament nylon) surrounded by a flat metal frame fixed to metal runners on the top and bottom. Rectangular mouth with adjustable cutting edges to alter the penetration depth of the sled. Semi quantitative.	Hessler & Sanders, 1967
IOS Epibenthic sled	Aldred (U.K.)	Steel frame with broad weighted skids; an opening and closing mouth to prevent contamination by planktonic organisms; main net of 4.5 mm terylene mesh and a 1.5 m cod end of 1 mm mesh; acoustic telemetry; oblique camera pointing forwards with electronic flash. Modified by replacement of single central net with a central net of 1.0 mm mesh either side of which were additional nets of 4.5 mm mesh size (Rice et al., 1982). Above the central net was an additional net of 0.33 mm mesh to capture organisms living above the seabed (hyperbenthos); also odometer and height adjustable camera.	Aldred, 1976; Rice et al., 1982
Rothlisberg and Pearcy (R-P) epibenthic sampler or sledge		Sampling box, with closing door to prevent contamination during hauling, enclosing a fine-meshed nylon net (571 μm), fitted into a steel frame on runners. Modified with an additional supranet on top of the existing net to sample fauna from 25–60 cm and 77–105 m above the seafloor.	Rothlisberg & Pearcy, 1977; Brandt & Barthel, 1995; Kaiser & Brenke, 2016.
Brenke sled	Brenke (Germany)	Large and strong metal frame surrounding epi- and supra-net; opening and closing system; small mesh sized nets (300–500 μm) for capturing both meiofauna and macrofauna; can be broken into three parts for transport.	Brenke, 2005.

Table 2 The evolution of scientific trawls.

Equipment	Inventor/adaptor	Innovation	Reference
Beam trawl	Sir Charles Wyville Thomson (U.K.)	Use of a fisheries beam trawl for deep-sea sampling (2,650 fathoms or 4,846 m).	Murray and Hjort, 1912; Rozwadowski, 2005.
Agassiz, Sigsbee or Blake trawl	Alexander Agassiz, Captain Charles D. Sigsbee (U.S.A.)	Simple steel frame forming a rectangular mouth attached to the trawl net and with a towing bridle; the front edges of the frame are oval to enable the trawl to skip over small obstacles and it can operate either side up; use of wire rope to save on space and weight compared to hemp rope.	Murray & Hjort, 1912; Gage &Tyler, 1991; Rozwadowski, 2005; Clark et al., 2016
Otter trawl	Johan Hjort (Norway)	Adapted from fisheries trawl. Heavy doors used to hold the entrance of the net open.	Hjort, 1910; Murray & Hjort, 1912; Clark et al., 2016.
Pelagic young fish trawl	C. G. Joh. Petersen	Mesh comprising thickly woven hemp (19 threads to 3 cm).	Hjort & Petersen, 1905; Murray & Hjort, 1912.

Fig. 2 Examples of (a) Multicorer, (b) Box corer. Photos by A. D. Rogers taken during The Nippon Foundation Nekton Ocean Census NIWA Bounty Trough Expedition, Southwest Pacific, 2024.

which tend to disturb the surface of the core (Craib, 1965; Schonfeld, 2012). The solution to this was the development of a corer with a hydraulic dampener a device that slows the penetration of the core tube into the sediment (Craib, 1965; Table 3). This was further developed into modern day multicorers and megacorers (Table 3; Fig. 2) routinely deployed for sampling of deep-sea meiofauna and macrofauna.

Box corers are designed to take a cuboid section of sediment from the seafloor (Table 3; Fig. 2). These samplers can take precise areas of the seafloor (0.25 m^2 for USNEL box corer) and can provide a large amount of material for sampling or subsampling of animals and for recording the physical and chemical characteristics of the sediment including porewater. Bow wave effects can be an issue with box corers although careful operation can reduce this problem considerably.

2.2 Pelagic Sampling

2.2.1 Ring nets

The German scientist Victor Hensen first used the term "plankton" and developed the first quantitative approaches to sampling pelagic communities. Hensen believed that plankton production might fuel marine food webs and was interested in characterising the horizontal and vertical distribution of plankton (Wiebe & Benfield, 2003; Dolan, 2021). The Hensen Net comprised a metal ring from which a conical net was suspended, and which could be lowered to a set depth and the volume of water it had filtered calculated (Dolan, 2021; Table 4). Hensen also invented a method to enumerate planktonic organisms on an etched glass plate (Dolan, 2021). He undertook the Plankton Expedition on the steamer *National* which sampled the North Atlantic (Dolan, 2021) and versions of this net are still used. Chun, Petersen and Nansen modified this net to be sent to the required depth closed, mechanically opened through the use of a messenger sent down the cable (a weight) and then closed after the required length of time of fishing using another messenger (Murray & Hjort, 1912; Bigelow, 1913).

2.2.2 Deep pelagic trawls

Following World War 2 scientific and military interest in characterising the deep scattering layer led to the need for nets that could open at mesopelagic or bathypelagic depths, maintain an open mouth while being towed horizontally and at a greater speed than previous designs (Hersey & Backus, 1962; Devereux & Winsett, 1953). Two main designs appeared in the 1950s, the Tucker Trawl and the Isaacs-Kidd Midwater Trawl (IKMT; Tucker, 1951; Devereux & Winsett, 1953; Table 4). These nets were effective at capturing micronekton which typically comprised of crustaceans such as euphausiids, small fish such as myctophids and squid (e.g. Tucker, 1951; Devereux & Winsett, 1953). The rectangular mouth of the Tucker Trawl enabled subsequent development as an opening and closing net and then the further development of multinets (Wiebe & Benfield, 2003; Table 4). Systems

https://doi.org/10.58440/ihr-30-1-a09

Table 3 The evolution of quantitative seafloor corers.

Equipment	Inventor/adaptor	Innovation	Reference
Grabs	Petersen and Boysen-Jensen	Adapted from industrial coal grab; semi quantitative.	Petersen & Boysen Jensen, 1911; Holme, 1964; Narayanaswamy et al., 2016.
Heavy grabs e.g. Okean grab; Campbell grab	Various	Increase of the size and weight of grab to increase seafloor penetration; semi-quantitative.	Spärck, 1956; Lisitsin & Udintsev, 1955; Hartman, 1955; Hartman and Barnard, 1958.
Van Veen grab, Aberdeen Grab, Baird Sampler	Various	Use of levers and pulleys to increase the closing force of the grab; semi-quantitative.	Thamdrup, 1938; Smith & McIntyre, 1954; Baird, 1958; Narayanaswamy et al., 2016.
Video-guided grab samplers (Russian GTVD-2/Preussag grab; Hydraulic Benthic Interactive Sampler [HYBIS])	Bramley Murton (HYBIS)	Live video feed to enable sampling of specific geological features or habitats. Addition of thrusters for steering (HYBIS); semi-quantitative.	Sheremet & Efimova, 1996; Murton, 2012; Narayanaswamy et al., 2016.
Brooke Sounder	John M Brooke (U.S.A.)	Shot weight with a hole bored through it into which a metal rod was inserted with a hollow at one end to obtain a sample of the seabed. Semi-quantitative.	Rozwadowski, 2005
Baillie Sounding Machine	Murray and Renard (U.K.)	Series of iron weights or sinkers with holes in the centre through which a hollow iron rod was inserted. The weights were detached on striking the seafloor and the tube retrieved containing a sample of the seafloor. Semi-quantitative.	Murray & Renard 1891.
Explosive corer	Snowden Piggot (U.S.A.)	Steel tube inside of which was a brass tube which on contact with the seafloor was propelled into the sediment by an explosive charge at the upper end. Obtained 10 m cores. Quantitative.	Piggot, 1936
Piston corer	Hans Pettersson and B. Kullenberg	Piston added to coring tube which moves up tube as core is collected and forms an airtight seal. Collect core with minimal disturbance to surface, up to 60 m long. Quantitative.	Kullenberg, 1947; Pettersson, 1949
Hydraulically dampened corer	Craib	Core tube with weights on top is mounted in a frame and connected to a hydraulic dampener, that slows the penetration of the core tube into the sediment minimising disturbance of core. Ball drawn over the bottom end of the coring tube by two elastic cords holding the column of sediment in the tube. Quantitative.	Craib, 1965.
Multicorer e.g. Scottish Marine Biological Association (SMBA) multicorer Barnett	Barnett	Development of hydraulically dampened corer with 12 core tubes with a diameter of 5 cm. Megacorer is a development of multicorer with wider-bore coring tubes. Quantitative.	Barnett et al., 1984; Narayanswamy et al., 2016.
Box corer e.g. United States Naval Laboratory [USNEL] box corer or Royal Netherlands Institute for Sea Research [NIOZ] box corer	Hessler and Jumars	Removable square or round sample box attached below a weighted central column carrying a pivoting spade which closes the box after it samples the seafloor. A gimballed support frame may also attach to the central column. Can take precise areas of the seafloor (0.25 m^2 for USNEL box corer). Quantitative.	Hessler & Jumars, 1974; Narayanaswamy et al., 2016.
Grey-O'Hara [GOMEX] box corer		Box corer with double-jawed closure	Boland & Rowe, 1991

such as the RMT1+8 and MOCNESS were generally targeted at micronekton and large zooplankton. However, smaller modern multinets targeted at macrozooplankton are based on an original design by Bé et al. (1959; also Bé 1962; Table 4; Fig. 3).

3 The evolution of deep-submergence technology

In this section we focus on the deep-submergence technologies which have driven scientific advances in our understanding of deep-ocean biodiversity. These technologies are used for the remote exploration of the deep ocean using manned or unmanned platforms.

3.1 Drop cameras

It was not until the pioneering work of a group of scientists and engineers at Lamont/Woods Hole that it was demonstrated that remotely operated cameras could be used for scientific observations in the deep sea (Ewing et al., 1946, 1967; Southward & Nicholson, 1985; Table 5). These camera systems were based on 35 mm film and evolved to be contained in tubular housings which had strong pressure-resistance and could be designed so the cameras as well as electronics and batteries could be spread along an internal chassis (Southward & Nicholson, 1985). Photographs were taken by closure of than electrical contact either by timer or through a switch linked to a triggering mechanism (Southward & Nicholson, 1985). Early flash units used either tungsten lights or flash bulbs but rapidly gave way to the use of electronic flash units in cylindrical housings (Southward & Nicholson, 1985).

Early deep-sea cameras were mounted on poles, in cages on sleds or on a variety of other towed gear such as trawls or grabs (Southward & Nicholson, 1985). Pole-mounted deep-sea cameras had their flash units mounted beneath to reduce backscatter and were typically activated when a weight suspended from a line hit the seafloor triggering a spring-loaded switch (e.g. Ewing, 1946). The bottom of the pole sometimes included a gravity corer and direct contact with the seafloor acted as a trigger (see example in Heezen & Hollister, 1971). Pole mounted cameras were improved with the introduction of a pinger which indicated when the camera was triggered and when it

had recycled, ready for another photograph. This allowed the equipment to be repeatedly lifted 10–20 m off the seafloor before being lowered again for another photograph (Southward & Nicholson, 1985). The development of cages for deep-sea cameras gave them protection from knocks during launch and recovery and when operating within 2 m to <1 m of the seafloor, an advantage when trying to photograph deep-sea life (Southward & Nicholson, 1985).

Fig. 3 Multinet being recovered after sampling microzooplankton on the Southwest Indian Ridge, southern Indian Ocean, 2009 during the IUCN – NERC Seamount Project. Photo by A. D. Rogers.

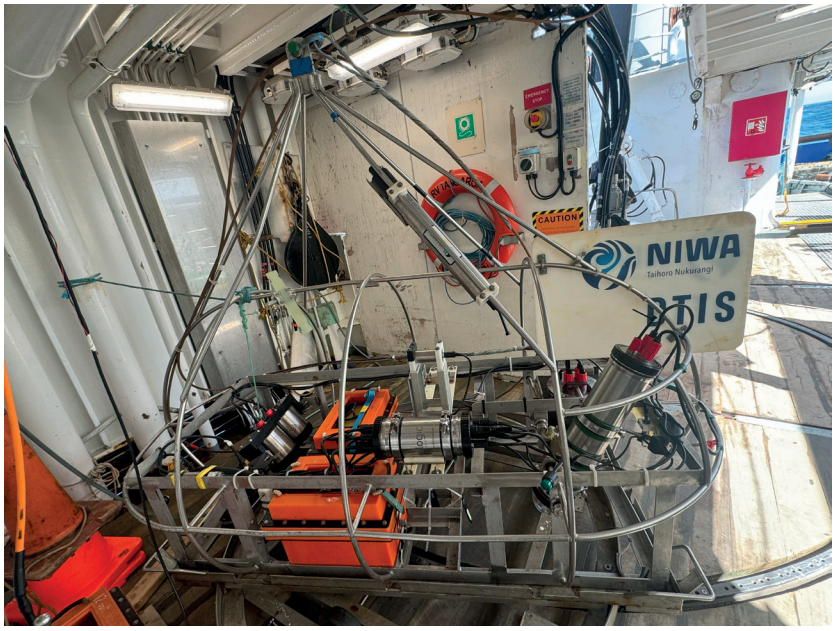

Fig. 4 The Deep-Towed Imaging System (DTIS) deployed by the National Institute for Water and Atmospheric Research (NIWA) in New Zealand. Photo by A.D. Rogers taken during The Nippon Foundation Nekton Ocean Census NIWA Bounty Trough Expedition, South West Pacific, 2024.

Suspended and drop camera systems provided our first views of a variety of deep-sea ecosystems revealing how variable the composition of the seafloor is, a large diversity of megafauna (animals large enough to be seen in cameras), the influence of biological activity on the seafloor through generation of lebenspurren such as tracks, burrows, worm casts etc. and evidence of strong currents in the deep sea (e.g. ripple marks). They also provided evidence of how seafloor is generated along the mid-ocean ridges through structures such as pillow lavas. Importantly, images of the deep-sea floor and its inhabitants could be shown to the public for the first time, a good example being Heezen & Hollister's (1971) book The *Face of the Deep* which contained hundreds of such images.

3.2 Camera sleds

Camera sleds are platforms towed on or just off the seafloor. The first deep-water camera sled was Cousteau's *Troika*, so named because it resembled the traditional Russian snow sled (Southward and Nicholson, 1985; Crylen, 2018). This sled was built by Cousteau and his team alongside Harold Edgerton from MIT, a pioneer of underwater camera and lighting equipment as well as side-scan sonar (Crylen, 2018). Modern camera sleds comprise a robust metal framework made of marine grade steel or aluminium to allow attachment and protection of cameras, lighting and other equipment (e.g. the Deep Towed Imaging System [DTIS]; Bowden & Jones, 2016; Fig. 4). Stills cameras and/or video cameras are set up for oblique or vertical imagery (ideally both). These orientations have advantages and disadvantages such as organisms being more easily identified in oblique camera images but vertical cameras being better able to count and estimate area coverage of organisms (see Bowden & Jones, 2016 for review). Even lighting is important for image analysis and is more easily achieved for vertical cameras. Lighting has to be set at an angle to cameras to avoid backscatter from suspended particulate matter in seawater (less of an issue in the deep-sea). Lighting has developed considerably over the last 60–70 years and modern high-intensity discharge (HDI or HMI) and LED (light emitting diodes) lights can allow operation of cameras 2–5 m above the seafloor and even up to 10 m in some cases (Bowden & Jones, 2016). High-capacitance strobe lighting is required for stills images (Bowden & Jones, 2016).

Scaling of camera images is an important aspect of extracting data from video or stills images. This can be achieved by placing an object of known scale within the image frame (Bowden & Jones, 2016) or by testing cameras in a water-filled tank with a grid which can then be superimposed on images from the deep sea to measure and quantify organisms (e.g. Rice & Collins, 1985). Now this is usually achieved through the use of two or more red or green scaling lasers set in parallel, so the beams are a fixed distance apart

https://doi.org/10.58440/ihr-30-1-a09

(Bowden & Jons, 2016). Stereo cameras can also be used with commercial software that can quantify and measure organisms although such cameras usually require calibration in water (e.g. Stefanoudis et al., 2019a). The use of USBL or long baseline (LBL) acoustic positioning systems can help to superimpose the tracks of towed camera systems onto multibeam bathymetry or from pre-existing data or charts (Bowden and Jones, 2016). This can be very helpful in associating the diversity and abundance of benthic organisms and fish to seafloor topography (e.g. Clark & Rowden, 2009; Williams et al., 2010).

3.3 Submersibles

The first deep-sea exploration in a human occupied vehicle (HOV) was that of William Beebe and Otis Barton in the *Bathysphere* (Busby, 1976; Table 6). This comprised a single cast steel sphere weighing about 2.27 tonnes with a space just 1.35 m across inside. Between 1930 and 1934 Beebe and Barton conducted a series of dives observing deep-sea animals in their own habitat for the first time in human history, reaching 923m depth, a record at the time (Beebe, 1934; Busby, 1976).

Following WWII, the Swiss physicist and inventor,

Table 4 The evolution of plankton / micronekton nets.

Equipment	Inventor/adaptor	Innovation	Reference
Plankton net	J. Vaughan Thompson	First plankton net	Wheeler, 1975; Wiebe & Benfield, 2003
Conical plankton net	Johannes Müller	Conical net with small mesh.	Murray & Hjort, 1912; Fraser, 1968
Hensen net	Victor Hensen	Metal ring from which a conical net was suspended. Volume of water sampled could be calculated. Also invented etched plate for enumerating plankton.	Dolan, 2021
Closing conical net	Chun, Petersen and Nansen	Version of Hensen net that could be sent to depth closed and then opened using a messenger (weight) sent down cable and closed using a second messenger.	Murray & Hjort, 1912; Bigelow, 1913.
Tucker trawl	Tucker	Rectangular opening comprising of two horizontal iron bars forming the top and the bottom of the net mouth with the sides formed of manila line forming a square 183 cm (6 feet) to a side. The net was about 9 m long with a mesh size of about 19 mm for the first 4.5 m, then 12.5 mm to the cod end forming the last 1.5 m, made of course plankton or muslin netting. Weights were suspended from the lower horizontal bar and a depth recorder from the top.	Tucker, 1951
Isaacs-Kidd Midwater Trawl (IKMT)		Net with a pentagonal opening with a depressor vane on the lower part of the net mouth made of metal and forming a shallow V-shape aimed to keep the net mouth open whilst it was being towed. IKMTs came in a range of sizes and were towed obliquely at speeds of up to 8.5 knots	Devereux & Winsett, 1953; Wiebe & Benfield, 2003
Opening and closing mid-water trawl (modified Tucker trawl)		Tucker trawl with opening and closing mechanism based on timer.	Davis & Barham, 1969
Rectangular mid-water trawl (RMT)	Clarke	Net with 8 m^2 mouth, 10 m in length with a 4.5 mm mesh apart from the last 1.5 m which were 0.33 mm nylon ending in the cod end formed by a bucket. Opened and closed using an acoustic signal. Pinger to monitor depth.	
RMT 1+8	Baker	Addition of a 1 m^2 mouth opening net which was suspended above the 8 m^2 net and had a mesh size of 0.32 mm.	Baker et al., 1973
IOS Multinet	Roe and Shale	Three 8 m^2 nets and three 1 m^2 nets.	Roe & Shale, 1979
Multiple Opening/Closing Net and Environmental Sensing System (MOCNESS)	Wiebe and co-workers	Based on Tucker trawl with rigid mouth (side bars were of steel rods) ensuring a fixed area for calculation of filtered volume. Up to nine opening and closing fine-meshed nets (0.333 mm) of 6 m in length. Number of variations including different mouth sizes (up to 20 m^2), up to 20 nets and with different mesh sizes (64 μm – 3.0 mm). Can also carry sensors for pressure, temperature, conductivity, fluorometer, transmissometer, oxygen, light and net operation data (flow, net-frame angle, net-bar release).	Wiebe et al., 1976, 1985; Wiebe & Benfield, 2003
Macrozooplankton trawl (multinet)	Bé	Mouth of the net is formed by sheet aluminium or steel and encloses rods which are vertical when the nets enter the water, but which pivot to form the lower edge of the nets when triggered. The original net was activated by messenger, replaced by a pressure release system (Bé et al., 1962). Can have from 5–9 nets attached and net openings of 0.125 m^2, 0.25 m^2, 0.5 m^2 and 1.0 m^2 (MultiNet Type Mammoth). Can be triggered via cable or by a self-contained released unit and sensors include flow meters, temperature and conductivity probes.	Bé et al., 1959, 1962; Christiansen, 2016; Hydrobios, 2020

Table 5 The evolution of remote camera systems.

Equipment	Inventor/adaptor	Innovation	Reference
Underwater camera	Louis Boutan (France)	Waterproof camera housing and underwater lighting flash	Boutan, 1900
Remotely operated pole-mounted deep submergence cameras	Maurice Ewing (U.S.A.)	Bottom contact exposure triggering; free fall pop-up cameras; flash lighting; time lapse automatic exposure; tubular pressure housings; use of lens or spherical domes to correct distortion	Southward & Nicholson, 1985
Deep-water camera sled	Jacques Cousteau (France)	*Troika* system – self-righting camera sled	Southward & Nicholson, 1985; Crylen, 2018
Modern deep-tow camera systems	Various	e.g. National Institute of Water and Atmospheric Research (NIWA, New Zealand) Deep-Tow Imaging System (DTIS). Platforms carrying cameras, lighting and a range of other sensors such as CTDs (conductivity, temperature, depth recorders), fluorimeters, positioning transponders (e.g. Ultra Short Baseline systems) and water sampling (Niskin) bottles.	Bowden & Jones, 2016

August Piccard, constructed the *FNRS2*, a submersible comprising a cast-steel sphere, larger than the *Bathysphere*, and formed by two halves bolted together, suspended under a thin-skinned metal structure containing gasoline as buoyancy (Busby, 1976). Unfortunately, during the first mission to the Cape Verde islands to test the submersible rough seas destroyed the gasoline buoyancy tanks of *FNRS2* whilst the vehicle was on tow (Busby, 1976). Piccard built a new bathyscaph, the *Trieste* which following a number of successful missions was purchased by the US Navy Electronics Lab and upgraded with a new pressure sphere and more buoyancy (Busby, 1976). It was with this modified submersible that Jacques Piccard and Don Walsh in 1960 undertook the first dive to the bottom of the Challenger Deep in the Marianas Trench during the Nekton Mission, a depth of 35,814 feet (10,916 m) and the deepest part of the ocean (Busby, 1976).

The *Bathyscaph* design was large and cumbersome and as early as 1953 the underwater pioneer Jacques Cousteau was considering designs for a smaller, lighter and more easily transported vehicle. This resulted in the first modern submersible, the famous *Diving Saucer (SP-350) Denise*. The *Diving Saucer* could be launched and retrieved by a 10-ton crane but could be transported rapidly anywhere on its mothership and was highly agile underwater (Bline, 1977). It was also the first positively buoyant submersible with a 55 lb weight being manually jettisoned to the allow the vehicle to ascend to the surface (Busby, 1976; Bline, 1977). The *Diving Saucer* was successfully operated from Cousteau's vessel *Calypso* and appeared in films such as *World Without Sun* (*Le Monde sans soleil*) completing over 1,000 dives (Bline, 1977).

The early 1960s saw a burst in submersible development spurred on by the potential of perceived markets in tourism, leisure, scientific, commercial and military research and object recovery and rescue (Busby, 1976). It was during this time that the DSV *Alvin*, the most famous deep-sea submersible used for research on biodiversity was designed and built. *Alvin* was used to discover deep-sea high temperature hydrothermal vents on the Galapagos Ridge in 1976 and undertook the first dives to the wreck of the *Titanic* ten years later (Ballard, 2000). The destruction of a B52 bomber in 1966 following a mid-air collision over southern Spain resulted in the loss of four hydrogen bombs, one of which was located by *Alvin* in over 2000 ft of water, further spurred military interest in submersibles. The late 1960s saw the building of submersibles including the *Deepstar 4000* and the International Hydrodynamics (HYCO) *Pisces* series submersibles. By 1976 more than 120 submersibles had been built with the offshore oil and gas industry adding further to the market for the use of these vehicles (Bline, 1977). Deep-diving research submersibles soon followed including the *Pisces VI*, *Alvin*, *Mir*, *Shinkai 6500*, *Nautile* and *Jialong* (Table 6; Fig. 5).

The advent of superyachts and adventure cruising has spurred the development of a new generation of small submersibles mostly with acrylic spheres or hemispheres if the vehicle has a tubular hull. These submersibles have been adapted for science and are increasingly being built with science capabilities as yacht owners want their assets to be used for science as a philanthropic activity. The deepest diving acrylic submersible to date is the *Triton 7K3* operated by REV Ocean, which is equipped with scientific sampling equipment (Fig. 5). They have particularly been used for biological surveys in the mesophotic, rariphotic and upper bathyal zones for both surveys of fish and benthic communities (e.g. Stefanoudis et al., 2019a, 2019b; Fig. 5).

The first submersible capable of repeated diving to the deepest parts of the ocean, the *Limiting Factor*, was completed in 2018 by Triton funded by the philanthropist Victor Vescovo (Jamieson et al., 2019; Young, 2020). This submersible has a sphere constructed from titanium but the exostructure and faring are designed for rapid descent and ascent, so the submersible has a different shape to other currently constructed submersibles with a narrow cross section and greater height (see photos in Jamieson et al., 2019). It has enabled human exploration of the deepest parts of the ocean.

3.4 Remotely Operated Vehicles

Remotely Operated Vehicles (ROVs) are self-propelled platforms which are tethered by cable to a surface craft from which they are powered and controlled and through which they feed data (Busby, 1976). ROVs were developed in the 1960s because of the need to selectively sample and study the seafloor, to recover lost military assets and to visually inspect, build, maintain and monitor underwater facilities (Busby, 1976). The US Naval Underwater Warfare Centre, Pasadena, California, developed the CURV I (Cable-controlled Underwater Research Vehicle) to retrieve torpedoes from depths of more than 305 m and it showed many of the basic features found in ROVs today (Table 7; Busby, 1976). It was later used to recover a lost hydrogen bomb from off the coast of Spain (found by *Alvin*) and CURV III, a later version of the vehicle was used to rescue the *Pisces III* and its crew from off the coast of Cork in 1973 (Talkington, 1977; Capocci et al., 2017). Oil and gas discoveries in the North Sea in the 1970s led to rapid development of ROVs for commercial operations which expanded in the 1980s (Busby, 1976; Capocci et al., 2017). By the 2000s the oil and gas industry were operating over 200 work-class ROVs capable of diving to 1,000 m depth or more whilst about 20 such vehicles were available for scientists (Jones, 2009).

ROVs comprise a metal frame, usually aluminium or stainless steel, to mount equipment and provide support and protection to the vehicle (Capocci et al., 2017; Fig. 6). Smaller ROVs may employ plastic frames (e.g. high density polyethylene or polypropylene; Capocci et al., 2017). Buoyancy is attached

https://doi.org/10.58440/ihr-30-1-a09

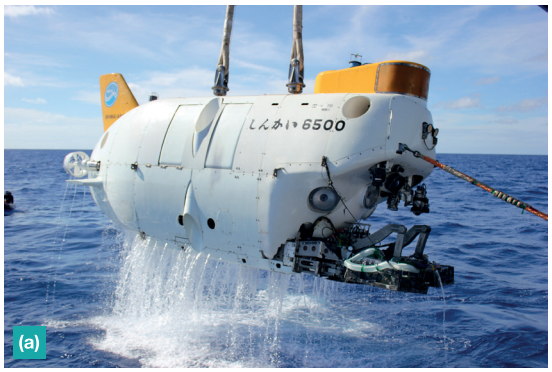

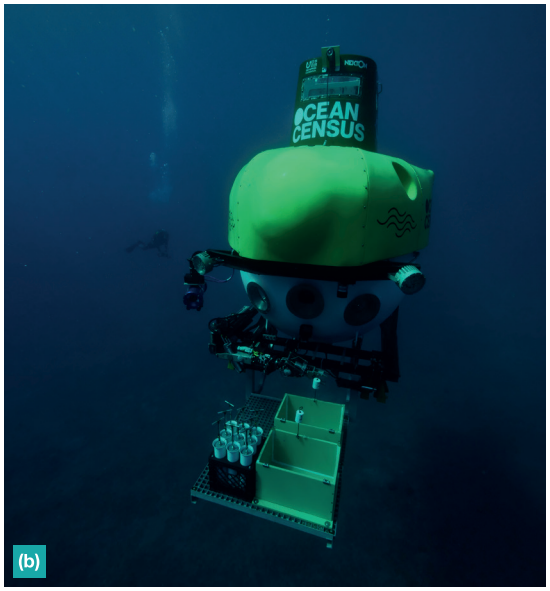

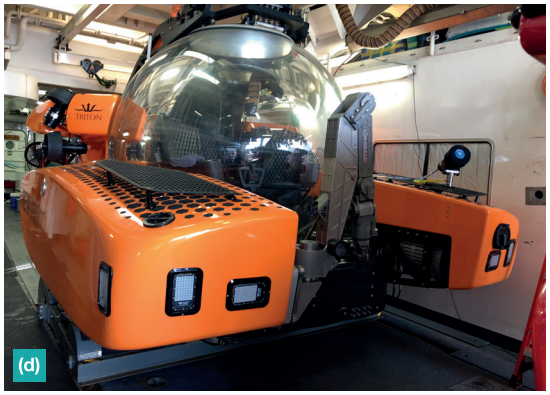

Fig. 5 Deep-sea submersibles currently in use including (a) the Japan Agency for Marine Science and Technology (JAMSTEC) *Shinkai 6500* (b) the *Pisces VI* (c) *Triton 1K3* (d) REV Ocean's *Triton 7K3*. Photos by A. D. Rogers (a, c, d) and the Nekton Foundation (b).

to the frame which may be a dynamic system (e.g. buoyancy tanks) or buoyancy blocks with a lower density than seawater. For shallower water ROVs these blocks can be formed of polymer foam (e.g. polyurethane, polyisocyanurate or polyvinyl chloride) or for deep-water ROVs syntactic foam is used, a composite material formed with hollow glass microspheres in epoxy resin (Capocci et al., 2017; Fig. 6). The *Nereus* ROV developed by Woods Hole Oceanographic Institute used ceramic spheres to provide buoyancy (Capocci et al., 2017). Power distribution and control equipment are held in metal pressure bottles and ROVs may be equipped with electric or hydraulic manipulators. Propulsion is provided by an array of electric thrusters designed to allow multidirectional movement (Capocci et al., 2017). Navigation is achieved using a combination of depth sensors, altimeter (echosounder), fluxgate compass, Inertial Navigation System integrated with a Doppler Velocity Log and USBL systems (Capocci et al., 2017; Petillot et al., 2019). Ideally areas where ROVs (and submersibles) are used should be mapped prior to dives to assist in mission planning as well as real time tracking. Scientific equipment including cameras, lighting, sample containers, corers and suction guns tend to be mounted on the front of the vehicle, although CTDs, water sampling bottles and multibeam sonar can be positioned underneath or on the rear (Fig. 6). Larger ROVs may be operated with a Launch and Recovery System (LARS) and a Tether Management System (TMS; Fig. 6).

Two ROVs that are worth special mention are *Kaiko*, developed by JAMSTEC and the *Nereus* developed by WHOI (Table 7). *Kaiko* achieved dives to the bottom of the Challenger Deep in the Mariana Trench to a depth of 10,911 m (Kyo et al., 1995). *Nereus* was designed as a Hybrid ROV system whereby it could dive as a self-powered ROV tethered by fibreoptic cable for data telemetry or as an autonomous platform (Fletcher et al., 2009). The vehicle was designed to overcome the limitations of use of cables beyond 7,000 m depth (Fletcher et al., 2009). *Nereus* was lost to a catastrophic implosion in 2014 whilst undertaking a 9,900 m dive in the Kermadec Trench.

ROVs have been used to investigate both deep benthic and pelagic ecosystems globally. Benthic ecosystems have included seamounts (e.g. Pratt et al., 2019; Auscavitch et al., 2020), cold-water coral reefs (e.g. Lim et al., 2018), chemosynthetic environments, including deep-sea hydrothermal vents (e.g. Rogers et al., 2012) and seeps (e.g. Ondréas et al., 2005), abyssal plains (e.g. Vanreusel et al., 2016) and trenches (e.g. Nunally et al., 2016). Pioneering work on pelagic ecosystems using ROVs has been undertaken particularly by Monterey Bay Aquarium Research Institute (MBARI; Robison et al., 2017).

3.5 Autonomous Underwater Vehicles

Autonomous Underwater Vehicles (AUVs) are unmanned and untethered underwater vehicles driven

Table 6 The evolution of submersibles for research and industrial purposes.

Equipment	Inventor/adaptor	Innovation	Reference
Argonaut First	Simon Lake (U.S.A.)	First submarine; sealed hull; gasoline engine; propeller; wet diving chamber; wheeled so operated on seafloor; attached to surface via pipe.	Busby, 1976
Bathysphere	William Beebe and Otis Barton (U.S.A.)	Steel sphere; CO_2 scrubber; calcium chloride to control humidity; quartz window; suspended from cable with electrical cable providing power for lights and communication to surface.	Beebe, 1934; Busby, 1976
FNRS2 / Bathyscaph	Auguste Piccard (Swiss)	Thin-skinned metal buoyancy tank containing 6,600 gallons of gasoline in 6 compartments; conical-shaped acrylic plastic for windows; pressure-compensated lead-acid batteries; electrical penetrators into hull of pressure sphere suspended beneath the buoyancy tank.	Busby, 1976
Trieste	Auguste Piccard (Swiss)	Stronger, cylindrically shaped buoyancy tank with a keel for better towing characteristics, containing 22,600 gallons of gasoline; forged steel for the construction of the sphere; use of silver-zinc batteries.	Busby, 1976
Diving Saucer (SP-350) *Denise*	Jacques Cousteau (France)	Disc-shaped pressure hull; acrylic viewports; pressure-compensated batteries; first positively buoyant submersible; highly portable design (launched with 10-tonne crane)	Busby, 1976; Bline, 1977
Research submersibles e.g. *Alvin, Shinkai 6500, Pisces VI, Mir, Nautile, Jialong, Limiting factor*	Various	Titanium or steel pressure sphere; life support system; submersible control systems; communication system; exostructure, usually a metal framework, ballast and trim including buoyancy provided by syntactic foam, propulsion and batteries and external faring (shell). A range of navigation and scientific equipment is usually attached to the outside of the submersible including Ultra Short Baseline (USBL) beacons, sonar, CTD, multibeam, cameras, lighting, manipulators, containers for samples and sometimes a suction gun with rotating sample chambers.	Busby, 1976; Ballard, 2000; Bline, 1977; Jamieson et al., 2019; Young, 2020
New generation submersibles e.g. Triton; UBoat Worx; Seamagine	Various	Acrylic sphere, air or oil-based ballast systems, manipulator, cameras, science skid (sample drawer, slurp gun and rotary containers), Niskin bottles etc.	e.g. Stefanoudis et al., 2019a, 2019b

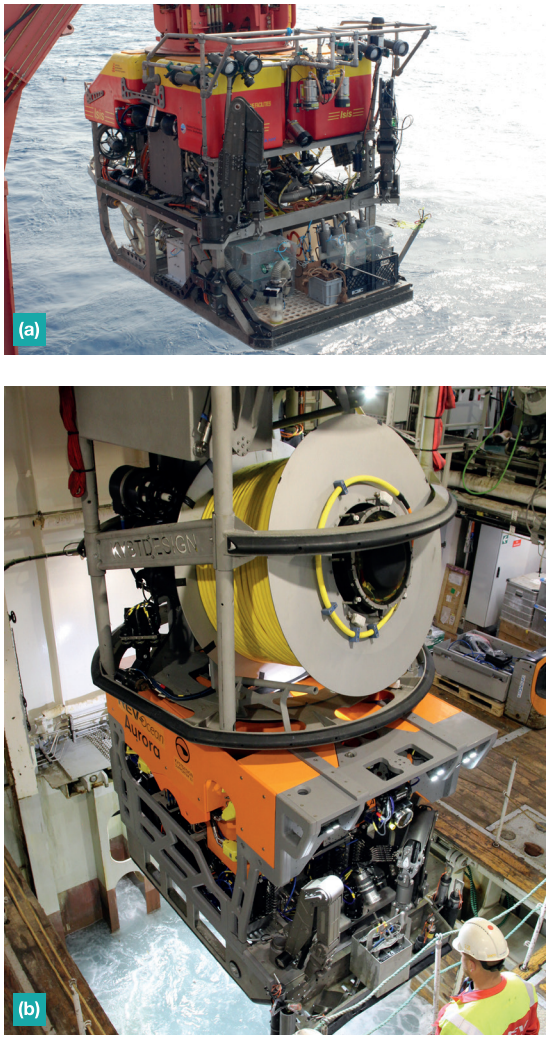

Fig. 6 Remotely Operated Vehicles (ROVs) (a) the Natural Environment Research Council's (NERC) *Isis* ROV and (b) REV Ocean *Aurora* ROV with Tether Management System. Note the ROV manipulators, sample containers, cameras and lighting. The square red, orange or yellow blocks are syntactic foam for buoyancy. Photos by A. D. Rogers.

through the water by a propulsion system, controlled and piloted by onboard computers and are manoeuvrable in three dimensions (von Alt, 2003). The first AUV, *Sea Spook*, was developed by the pioneering underwater photographer and film maker, Dmitri Rebikoff in 1960 (Michel, 1998). This was followed by the University of Washington's (Seattle) Self-Propelled Underwater Research Vehicle (SPURV 1) in 1963 and the Unmanned Arctic Research Vehicle (UARS) in 1972, and SPURV 2 in 1973 (Francois, 1973, 1977; Widditsch, 1973; Busby, 1976, Michel, 1998).

Development of AUVs continued through the 1970s and early 1980s spurred on by military funding because of the perceived importance of AUVs as stealth reconnaissance platforms (Michel, 1998). By 1984 there were 17 AUVs under development in different countries but only the SPURV systems and the French *Epaulard*, operated by IFREMER could be considered as operational (Michel & Wernli, 1998; Table 8). *Epaulard* was built in 1981 and had a maximum depth rating of 6,000 m and within five years had undertaken more than 800 km of underwater survey (Michel, 1988). Many of the AUVs developed during the 1980s and early 1990s were either military or designed as test-bed platforms and were perceived as high-tech and high risk (Michel & Wernli, 1998). Many of these AUVs were also expensive which spurred the development of low cost, smaller AUVs at academic institutions such as MIT (*Odyssey I, Odyssey II* and *Odyssey IIb*) and Florida Atlantic University (e.g. *Ocean Voyager II* and *Ocean Explorer*; Michel, 1998). These small, more cost-effective AUVs paved the way for evolution of this technology for a wide range of industrial, military and scientific applications. This was further promoted by the adoption of this technology by the oil and gas industry (Michel, 1998).

Most AUVs are torpedo-shaped (e.g. Kongsberg

https://doi.org/10.58440/ihr-30-1-a09

Table 7 The evolution of Remotely Operated Vehicles (ROVs) for research, military and industrial purposes.

Equipment	Inventor/adaptor	Innovation	Reference
CURV I (Cable-controlled Underwater Research Vehicle)	US Navy (U.S.A.)	First remotely operated vehicle. Frame, buoyancy, camera, propulsion, hydraulically-operated manipulator.	Busby, 1976
Consub 1	British Aircraft Coorporation (U.K.)	Early example of offshore industry ROV	Busby, 1976
Kaiko	JAMSTEC (Japan)	Two-component system comprising the launcher and the ROV; launcher includes the cable handling equipment, navigation equipment including Long Baseline receiver, a Super Short Baseline receiver, obstacle avoidance sonar, an altimeter, depth sensor, a gyrocompass and roll/pitch sensor; scientific equipment including a CTD, side scan sonar and a sub-bottom profiler.	Kyo et al., 1995; Barry & Hashimoto, 2009
NEREUS	Woods Hole Oceanographic Institution (U.S.A.)	Hybrid ROV system can dive as a self-powered ROV tethered by fibreoptic cable for data telemetry or as an autonomous vehicle. Autonomous mode equipped with a CTD, optical backscatter sensor, a redox potential sensor, a side-scan sonar and camera and could be used for mapping and photographic survey. ROV-mode *Nereus* was fitted with an electro-hydraulic arm, sampling equipment and additional cameras. Ceramic spheres used for buoyancy.	Fletcher et al., 2009.

REMUS and General Dynamics *Blue Fin*; Sahoo et al., 2019) in order to reduce drag. However, other shapes have been adopted including platforms with a more rectangular cross-section to egg-shaped or even spherical AUVs for more manoeuvrability and some with hydrofoils (Sahoo et al., 2019). Biomimetic AUVs have also been designed which are inspired by nature with a fish-like or snake-like shape (Sahoo et al., 2019). Some AUVs have adopted more complex shapes, especially those capable of hovering including WHOI's *Autonomous Benthic Explorer* (*ABE*; German et al., 2008; Table 8) and *Sentry*, designed to operate close to the seafloor at up to 6,000 m depth (Kaiser et al., 2016).

Propulsion for AUVs is provided by propellers or thrusters with rudders and fins for directional control (Sahoo et al., 2019). Power in early AUVs was provided by lead-acid batteries but silver zinc batteries have also been deployed although these are expensive (Blidberg, 2001). The *ABE* system uses lithium-ion batteries whilst NiMH batteries are used in some newer AUVs (Blidberg, 2001). Aluminium – oxygen semi cells have also been employed extending the range of the DARPA UUV (Blidberg, 2001). Navigation is usually achieved through use of arrays of acoustic beacons on the seafloor (Long Base Line beacons) or by a combination of Ultra Short Base Line acoustic communication, GPS positioning, and inertial navigation (Wynn et al., 2014). AUVs are programmed to undertake specific missions but the advent of acoustic communications and subsea docking stations are providing a new order of flexibility and complexity in AUV deployment. Sensor packages for AUVs vary greatly and they are used for a wide range of scientific missions including seafloor mapping, physical oceanographic measurements, chemical and turbidity measurements, biological acoustics and seafloor photography. Some AUVs are modular in design so specific sensor modules can be changed to suit a specific mission (e.g. Teledyne Gavia system).

AUVs have been used for a wide range of scientific missions including detection and location of deep-sea hydrothermal vents and fluid escape features, habitat mapping, mapping of seafloor morphology, under ice mapping of the seafloor and ice profiling, fisheries research and physical oceanographic measurements (e.g. Manly, 2004; German et al., 2008; McPhaill et al., 2009; Morris et al., 2014; Wynn et al., 2014; Barker et al., 2020).

3.6 Landers

Landers are autonomous, free-fall platforms used to undertake physical oceanographic or biogeochemical observations, experiments on the seafloor or to photograph and/or capture deep-sea organisms (e.g. Baited Remote Underwater Video or BRUVs; Tengberg et al., 1995; Fig. 7). The platforms generally comprise a rigid framework on which is mounted instrumentation, batteries, buoyancy, ballast weights and a ballast release mechanism (Tengberg et al., 1995). Release is usually achieved by an acoustic signal from a surface vessel or by a timed-release device (Jamieson, 2016). Landers have been deployed for hours to up to a year or more (Jamieson, 2016). They have the advantage that once deployed research vessels are free to undertake other activities (Tengberg et al 1995).

The first landers were developed in the late 1960s / early 1970s for photographing the scavenging fauna of the deep-sea floor (e.g. Isaacs, 1969; Heezen & Hollister, 1971; Isaacs & Scwartlose, 1975) and for biogeochemical measurements. Early examples of baited landers include the Monster Camera (Isaacs, 1969; Heezen & Hollister, 1971; Isaacs & Scwartlose, 1975) and the baited version of the U.K.'s Bathysnap system known as Bathysnack (Thurston et al., 1995). Early examples of biogeochemical landers include the Free Vehicle Respirometer (FVR) developed to undertake measurements of oxygen consumption in the deep sea (Smith & Clifford, 1976; Smith, 1978) and the free vehicle developed for the Manganese Nodule Programme (MANOP) during the International Decade for Ocean Exploration (IDOE; Weiss et al., 1977). The latter could take water samples for *in-situ* experiments, measuring oxygen and pH and also retrieving box core samples (Weiss et al., 1977). Further development of landers mainly for biogeochemical analysis were developed through the 1980s

Table 8 The evolution of Autonomous Underwater Vehicles for research, military and industrial purposes.

Equipment	Inventor/adaptor	Innovation	Reference
Sea Spook	Dmitri Rebikoff (France)	First autonomous underwater vehicle; used for filming	Michel, 1998
SPURV1 / Unmanned Arctic Research Vehicle (UARS) / SPURV2	University of Washington (U.S.A.)	SPURV1 capable of speeds up to 2.5 m/s at depths to 3,600 m. Developed to measure ocean temperature and sound velocity. UARS operated to 457 m depth and equipped with an under-ice acoustic profiling system.	Francois, 1973, 1977; Widditsch, 1973; Busby, 1976, Michel, 1998
Epaulard	IFREMER (France)		Michel, 1998
Odyssey I, Odyssey II and *Odyssey IIb*	MIT (U.S.A.)	New generation of small, more cost effective AUVs.	Michel, 1998
Ocean Voyager II and *Ocean Explorer*	Florida Atlantic University (U.S.A.)		Michel, 1998
Autosub	NERC (U.K.)	Long-range power via arrays of D-cells (early innovation); transmission of data to satellites (later versions).	
Remus	Kongsberg (Norway)		
Autonomous Benthic Explorer (ABE)	Woods Hole Oceanographic Institution (U.S.A.)	Two upper pods containing buoyancy (glass spheres) from which is suspended a lower pod containing the batteries and other electronics; three lateral and two vertical thrusters allowing it to move in three dimensions close to the seafloor.	Blidberg, 2001; German et al., 2008
Sentry	Woods Hole Oceanographic Institution (U.S.A)	High aspect hull and four propellers mounted on articulated hydrofoils; two housings, the upper for electronics made of titanium and the lower for batteries made of alumina, ceramics and titanium, with a titanium framework to support the elements of the vehicle; instrument packages and emergency transponders are housed in separate titanium pods; buoyancy is provided by syntactic foam.	Kaiser et al., 2016

and 1990s (see Tengberg et al., 1995).

The main use of landers for biodiversity studies has been for the study of scavenger communities attracted by bait as well as colonisers of organic materials such as wood and whale bone (Bailey et al., 2007; Jamieson, 2016; Figs. 7a and 7b). The design of baited landers is reviewed in Bailey (2007) and Jamieson (2016). These can comprise some or all of the following components: bait, imaging systems, lighting, baited traps, ingestible acoustic devices (swallowed by scavengers feeding on bait), sensors (e.g. CTDs, ADCPs) and the lander delivery system (Bailey et al., 2007; Jamieson, 2016). Baits tend to include oily fish which may be macerated or liquidised, squid, cat food, sometimes thickened with breadcrumbs or sawdust and are held in a perforated receptacle or mesh bag (Jamieson, 2016). Entire carcasses have been used to simulate food falls ranging in size from fish to dolphins, porpoises and sharks (Jamieson, 2016). The latter can form temporary habitats as consumption of the entire carcass including bones can take time. Alternatively, artificial baits have been used comprising natural chemical attractants found in squid and fish (Jamieson, 2016). Jellyfish have also been used in baited landers to improve understanding of the role of these animals in carbon transport from the water column to the seafloor (e.g. Sweetman et al., 2014).

Landers have been particularly important in understanding the biodiversity and ecology of the hadal zone (ocean trenches as well as deep fracture zones, troughs and basins; Weston et al., 2021) because there are few other deep-submergence assets capable of deployment to depths beyond 6,000 m. Deployment of hadal lander systems have enabled the sampling of large numbers of scavenging amphipods from the families Lysianassoidea and Allicelloidea which can be dominant components of communities below 8,000 m depth. This has enabled the use of these organisms as model taxa to study the ecological dynamics of hadal fauna (e.g. patterns of genetic connectivity; Weston et al., 2021; Weston & Jamieson, 2022). These studies have confirmed an abrupt change in biological communities from an abyssal fauna to hadal at depths 6,000 m and 7,000 m (Weston et al., 2021). They have also revealed the Liparidae (snail fishes) as the deepest living fish family with the deepest record currently at 8,336 m depth in the Izu- Ogasawara Trench in the northwest Pacific Ocean (Jamieson et al., 2023).

3.7 Acoustics

3.7.1 Habitat mapping

Prior to the 20th century the depth of the ocean was measured using the lead and line system in which a plumb attached to a cable is allowed to sink to the seafloor (Menandro & Bastos, 2020). Echosounders were developed as a response to the *Titanic* disaster of 1912 for the detection of icebergs (Hersey & Backus, 1962). Reorientation of the directional transducer vertically downwards enabled emitting regular pulses of sound so that between pulses they could serve as the receiver of the bottom echo (Vigoureux & Hersey, 1962). A graphic recorder for collecting echosounder data was introduced by Marti (1922) and in 1925–1927 the German *Meteor* Expedition surveyed the South Atlantic Ocean using echo sounding equipment identifying the continuous nature of the Mid-Atlantic Ridge (Menandro & Bastos, 2020).

Multibeam bathymetry systems were developed in the 1960s by the military for seafloor mapping. These systems emit a fan-shaped wave of acoustic pulses (>100 sound beams and in some cases >200; Brown & Blondel, 2009; Harris and Baker, 2012) which are reflected from across a swath of the seafloor and picked up by the transceiver. They revolutionised seafloor mapping by enabling a broad track of the seafloor to be mapped under a vessel.

https://doi.org/10.58440/ihr-30-1-a09

Fig. 7 Benthic landers including (a) mooring deployed with sunken wood and bone on a seamount on the South West Indian Ridge deployed during the IUCN – NERC Seamount Project, (b) fish trap deployed during The Nippon Foundation Nekton Ocean Census NIWA Bounty Trough Expedition, South West Pacific, 2024. Photos by IUCN – NERC Seamounts Expedition (a) and A. D. Rogers (b).

The first civilian systems were installed on the French research vessel *Jean Charcot* and employed on an expedition in 1977. Multibeam sonar when combined with Geographic Positioning System (GPS data) produces high resolution geopositioned contour maps of the seafloor (Harris & Baker, 2012). The properties of the backscatter data from echo sounders (e.g. the strength of the return echo) are dependent on seafloor hardness, texture and roughness (de Moustier, 1986). Different frequencies of echosounders are used to map different water depths with higher frequencies used for shallower water mapping (Harris & Baker, 2012). Sidescan-sonar only collects acoustic backscatter data but because it is usually deployed as a tow-fish behind a ship it is not easy to georeference the map produced and has significant disadvantages for habitat mapping (Harris and Baker, 2012). Approaches to analysis of backscatter data are discussed in Brown and Blondel (2009). This method is now improving with the advent of multifrequency acoustic backscatter data (e.g. Brown et al., 2019).

Both seafloor topography and backscatter data give important information on benthic habitat, the first for identifying important topographic features (e.g. seamounts, ridges, canyons) and the second on the texture of the seafloor (e.g. basalt, sand, coral). Both provide information on physical habitats, the ecological or environmental areas that are inhabited by species (Harris and Baker, 2012). The same types of habitats are consistently associated with biological communities or assemblages of species which occur together (Harris and Baker, 2012). Currently, it is still the case that our ability to map the physical structure of the seabed greatly exceeds our ability to observe what species live in these habitats (Harris and Baker, 2012). Biological observations using video survey or other methods on a small subset of the seafloor for which acoustic data has generated topographic maps and backscatter data can be used to model community distribution at much larger geographic scales. The mapping of biophysical variables of the seafloor which have a quantifiable correspondence to the occurrence of benthic species and communities is referred to as surrogacy (Harris, 2012). Processing methods for multibeam data from the water column have also now been used to identify habitats such as gas plumes from hydrocarbon seeps (e.g. Schneider von Deimling et al., 2007; Wilson et al., 2015).

Habitat classification and mapping is an important area of biodiversity research with many applied and scientific applications. The combination of further refinements in acoustic mapping technologies (e.g. multifrequency multibeam bathymetry; synthetic aperture sonar) and navigation together with application of new methods such as deep machine learning to habitat classification are increasing the resolution and accuracy of acoustic mapping of habitat.

3.7.2 Biological acoustics

The first use of active acoustics to study pelagic ecology occurred in the 1920s and 1930s with Kimura (1929) being the first scientist to record echoes from a fish (Benoit-Bird & Lawson, 2016). In the 1930s the pioneering British fisherman Captain Ronald Balls installed an echosounder in his herring drifter *Violet and Rose* and was able to set his nets on mid-water echoes correctly attributed to herring shoals (Balls, 1948, 1951; Hersey & Backus, 1962). Early work on the use of echosounders was also undertaken in Norway with the plotting of echoes in a time-depth plot (Sund, 1935).

The principle behind biological acoustics is that sound pulses are produced and their echoes from living organisms in the water column are received by a transducer mounted in the hull of a vessel, autonomous- or towed platform (Jennings et al., 2001; Benoit-Bird & Lawson, 2016). When a sound pulse meets an object with a density different from seawater sound waves are scattered in all directions (Jennings et al., 2001). Early sounders recorded single echoes, but development of the echo-integrator allowed the strength of many echo returns to be summed over depth and distance (Jennings et al., 2001). The advent of multifrequency echosounders, multiple echosounders emitting sound pulses at different

frequencies or a single echosounder with multiple processing units (Korneliussen, 2018) has been critical in the ability of acoustics to discriminate among species and taxa (Benoit-Bird & Waluk, 2020). This has been further developed with the use of broadband echosounders that transmit and receive a frequency-modulated signal from a single transducer to allow acoustic backscattering to be measured continuously over a range of frequencies (Benoit-Bird & Waluk, 2020).

Different types of organisms have different sound reflection properties, for example, those with gas-filled cavities such as siphonophores or fish with swim bladders have a resonant sound scattering frequency that depends on the depth and size of the cavity (Benoit-Bird & Lawson, 2016; Benoit-Bird & Waluk, 2020; Korneliussen, 2018). The aim of acoustic target classification is to categorise sound scatter into groups which then hopefully correspond to different species or groups of organisms for which abundance and biomass can then be estimated (Korneliussen, 2018). Approaches to classification of echograms is based on model-based approaches or on empirical approaches (use of previously-collected data on sound scattering properties of monospecific aggregations of a species; Korneliussen, 2018). If species aggregations are known to have specific sizes or shapes these can be used to identify species from the dimensions and shapes of echograms (echo envelope; Korneliussen, 2018). Multivariate statistical approaches have been used to classify species on the basis of echo envelopes, other information on aggregation shape and size and also physical environmental data (Korneliussen, 2018). Increasingly, Artificial Neural Networks are being applied to the identification of species (e.g. Brautaset et al., 2020; Korneliussen, 2018).

3.8 Navigation

Ocean mapping and the operation of deep submergence technologies are not possible without accurate navigation. It is important to understand exactly where depth and backscatter are measured on the seafloor or where an underwater platform is in respect to the surrounding environment. Ship's navigation has transformed over the last 50 years from the use of the sextant in the 1960s with accuracy of ~1 nautical mile, to the Global Positioning System (GPS) from the early 1990s with an accuracy of up to 100 m continuously to Real Time Kinematic GPS with an accuracy up to 5 cm (Mayer, 2006). The precise angles at which multibeam sonar signals leave a vessel and are received by its transducers are also critical to mapping. Therefore, technology has also developed to precisely monitor and correct soundings for vessel motion (Mayer, 2006). Accurate estimation of the positioning of an acoustic reflection from the seafloor requires the estimation of the sound velocity profile through the water column from measurement of temperature and salinity with depth using a Sound Velocity Profiler (SVP; Mayer, 2006).

Deployment of deep-sea sampling equipment and deep—submergence technologies that are tethered to a vessel or which need to be carefully deployed and recovered demands a stable ship's position and heading. Such vessel stability is achieved through Dynamic Positioning Systems (DP or DPS) a technology that has also undergone a transformational advance since the late 1960s under the driving force of the offshore oil and gas industry (Mehrzadi et al., 2020). DP controls a vessel heading and position by using thrusters that are continuously dynamic to counter environmental forces induced by waves, winds and currents (Mehrzadi et al., 2020). Modern research vessels are often equipped with DP systems to enable the use of tethered equipment such as towed cameras and ROVs as well as launch and recovery of submersibles, AUVs or other deep-submergence equipment.

Georeferenced location of scientific observations from a submerged platform or sensors enables multiple datasets to be co-registered across multiple dives or deployments from a single system or across multiple systems (Barker et al., 2020). Georeferenced data can then be placed into context with physical and biogeochemical environmental data, bathymetric and other geophysical maps (Barker et al., 2020). It is also important to know the position of deep-submergence equipment to target specific localities, environmental features (e.g. hydrothermal vents) or to avoid hazards. Because GPS signals cannot be received underwater, submerged platforms deploy a range of technologies for underwater navigation including (Kinsey et al., 2006; Barker et al., 2020):

- Depth sensors (strain gauges or quartz crystal)
- Magnetic heading sensors
- Roll and pitch sensors (e.g. pendulum or fluid tilt sensors, accelerometer pitch sensors)
- Angular rate sensors (e.g. Fibre Optic Gyroscopes or Ring Laser Gyroscopes)
- Long Baseline Navigation (LBL; platform determines position by triangulation in a network of acoustic transponders)
- Ultra Short Baseline Navigation (USBL; ship's location is telemetered to the platform continuously)
- Doppler sonar (measures bottom velocity using acoustics)
- Inertial Measurement Unit (IMU; employs Doppler Velocity Logs [DVL] and GPS or acoustic navigation systems to estimate position)

Multiple such systems may be used on a platform such as an ROV.

4 100 years of discovery

4.1 Continental drift and plate tectonics

In 1912, Alfred Wegener proposed the theory of continental drift where he hypothesised that the continents had drifted apart (Wegner, 1912a, 1912b). He was, however, unable to provide robust evidence for the processes that had led to this drift of continents and the theory remained controversial for years. Between 1920 and 1930, the geologist Arthur

https://doi.org/10.58440/ihr-30-1-a09

Holmes published work proposing that plate junctions under the ocean and convective cells and radioactive heat in the Earth's mantle might drive the process of continental drift (Holmes, 1928, 1929). The discovery of the continuous nature of the mid-ocean ridges by Ewing's team in the 1950s and 1960s (e.g. Heezen et al., 1959) and the development of the theory of seafloor spreading by Hess (1960, 1962) and Dietz (1961) proposed that new seafloor formed at the ridge was being carried away from the point of formation. Evidence of alternating stripes of magnetic orientation in basalt that were symmetrical around the mid-ocean ridges could only be explained by the formation of seafloor at the ridges and then it being drawn away (Vine & Matthews, 1963; Conveyer Belt Theory). These geological investigations, supported by Marie Tharpe's cartographic works, led to the acceptance of Wegener's hypothesis on continental drift (Le Pichon, 1968). It was not until 1968 that American geophysicist Jack Oliver with colleagues Bryan Isacks & Lynn R. Sykes provided the first seismologic evidence of plate tectonics that explained the process for continental drift (Isacks et al., 1968).

Recent studies suggest that plate tectonics have had a major role in the distribution of life in the ocean including the occurrence of biodiversity hotspots and endemism (e.g. Leprieur et al., 2016; Zaffos et al., 2017; Pellissier et al., 2018). It also explains phenomena such as the regional endemism of the Antarctic biota which has been isolated as a result of continental drift and the decline of environmental temperatures over millions of years (Rogers, 2007, 2012). In the deep sea, plate tectonics have also determined large-scale patterns of diversity in the hydrothermal vent fauna (e.g. Tunnicliffe et al., 1996).

4.2 Establishment of thermohaline circulation

In 1987 Wallace Smith Broecker published the paper that established the concept of the ocean conveyor belt, through which large-scale ocean circulation is explained by global density and temperature gradients – the thermohaline circulation. Surface currents driven by wind move water masses poleward in the Atlantic. As these water masses, enriched in salt through evaporation move northwards, they cool down, resulting in the sinking of dense water at high latitudes that form the North Atlantic Deep Water. This cold-water flows southward and into the Southern Ocean, circulating around it and also moving into the Indian and Pacific Oceans before it upwells to form warm surface currents. In the Southern Ocean, the strong cooling of the water caused by Antarctic winds and the formation of sea ice decrease temperature and increase salinity respectively, resulting in the formation of the Antarctic Bottom Water, joining the circumpolar circulation. Broecker (1987, 1997) also described the mechanism which leads to abrupt changes in ocean circulation and the climate over time, the freshening of seawater in the North Atlantic disrupting the thermohaline circulation and leading to its breakdown.

The thermohaline circulation is critical for the generation of cold, oxygenated water supporting the high biodiversity of deep-sea ecosystems. During climate warming events the disruption of the thermohaline circulation has caused episodes of hypoxia and anoxia in deep waters. This flip-flop from thermohaline oxygenated conditions to halothermal hypoxic or anoxic conditions in the global deep sea is thought to have played a major role in shaping the past and current distribution of many deep-sea taxa thus contributing to past and present distributions of deep-sea biodiversity (e.g. Rogers, 2000; Strugnall et al., 2008; Thuy, 2013; Košt'ák et al., 2021; Horowitz et al., 2023).

4.3 Discovery of high deep-sea biodiversity

In the 1960s, deep-sea biology shifted from descriptive to more quantitative ecological, evolutionary and experimental approaches. Sampling along a transect in the Northwest Atlantic (Gay-Head to Bermuda) revealed an astonishing density of animals living in the deep sea, 6,000–23,000 animals/m^2 on the upper continental slope dropping to 150–270 animals/m^2 on the abyssal plain (Sanders et al., 1965). Polychaetes were the most abundant and diverse group, followed by peracarid crustaceans (mainly amphipods) and bivalve molluscs (Sanders et al., 1965). This provided evidence that, contrary to previous doctrine, the deep sea supported one of the highest levels of biodiversity on Earth, mainly comprising meio- and macrofauna living in and on the sediments (Hessler & Sanders, 1967; Grassle & Maciolek, 1992; Fig. 8a). Early findings also showed that in the abyssal soft sediments (Fig. 8a), there is an even distribution of species abundance, with the most abundant species not exceeding 20 % of the total and many species being rare taxa or occurring as singletons (e.g. Grassle & Maciolek, 1992). Later studies described a parabolic distribution of diversity with depth (Rex, 1981, 1983), with the biodiversity peak often found at bathyal depths (Rex, 1981; Maciolek et al., 1987), although the depth at which this peak occurs varies with region and taxon considered (reviewed in Rex & Etter, 2010). This is now thought to result from declining food supplies preventing competitive dominance at intermediate depths, along with a combination of other environmental factors promoting biodiversity (Rex & Etter, 2010).

In shallow waters analyses of species occurrence indicates that for many groups of species (but not all), and overall, there is a latitudinal gradient in biodiversity with highest levels occurring at low latitudes and the lowest at the poles, especially in the northern hemisphere (Rogers et al., 2022). For most groups of deep-sea organisms there is insufficient knowledge to elucidate such patterns with the exception to date of the Ophiuroidea (brittlestars). For this group of echinoderms, it has been demonstrated that peak diversity in the deep sea occurs at mid-latitudes (Woolley et al., 2016). This is likely a result of the higher input of particulate organic matter, the predominant food

supply for the deep sea at mid-latitudes (Woolley et al., 2016). Time lapse photography as well as other forms of repetitive or long-term sampling of deep-sea biodiversity has also demonstrated that communities vary interannually and over longer time periods (reviewed in Rogers, 2015). The dependency of the deep-sea fauna on the rain of organic material from the ocean surface means that these ecosystems are coupled. Annual and longer-term variation in both the quantity and quality of food, mainly phytodetritus (dead phytoplankton cells) as well as dead organisms and faecal pellets drives temporal changes in the abundance and diversity of seafloor communities (Rogers, 2015; Sweetman et al., 2017). This has profound consequences in considering the impacts of climate change which is causing large-scale changes in the patterns of ocean primary production and may in turn strongly influence deep-sea biodiversity (Rogers, 2015; Sweetman et al., 2017).

Increasing interest in exploiting deep-sea resources has driven studies on deep-sea biodiversity. On the continental margins exploration and exploitation of oil and gas deposits as well as deep-sea fisheries led to the rediscovery of cold-water coral reef ecosystems. Cold-water corals had been known from northern Europe since the eighteenth century (Roberts et al., 2009) and the extensive nature of cold-water coral habitats was described in the mid-twentieth century (e.g. Le Danois, 1948). However, it was the use of submersibles such as *Alvin* and the *Pisces III* that allowed direct observations of the habitats formed by corals such as *Desmophyllum pertusum* and *Dendrophyllia profunda* (Roberts et al., 2009; Fig. 8b). These habitats were found to support high diversities of associated species (e.g. Rogers, 1999; Roberts et al., 2009). The realisation that such habitats were impacted primarily by bottom trawl fisheries gave rise to the concept of Vulnerable Marine Ecosystems (VMEs; FAO, 2009). It has been recognised that many groups of sessile marine invertebrates can form habitats in the deep sea associated with high biodiversity of other species. These include coral gardens formed by Scleractinia, Octocorallia, Stylasterida and Antipatharia, and habitats formed by Demospongiae, Hexactinellida and xenophyophores (e.g. Buhl-Mortensen et al., 2010).

Development of deep-sea mining began in the 1960s but whilst deep-sea mineral resources were mapped and technology for recovery of polymetallic nodules developed in the 1970s and 1980s economic conditions were inimical to commercial mining (Glasby, 2000). Interest in deep-sea mining has re-emerged driving studies focusing on the biodiversity of deep-sea ecosystems potentially impacted by mineral extraction. This has focused on abyssal ecosystems of the Clarion Clipperton Fracture Zone (CCFZ) in the equatorial eastern Pacific (e.g. Smith et al., 2021) but also on seamounts (e.g. Schlacher et al., 2014) and seabed massive sulphides (e.g. Boschen et al., 2016). Work on the CCFZ has confirmed the remarkable diversity of abyssal ecosystems with >5,500 species identified 92 % of which are undescribed and a predicted diversity of up to nearly 8,000 species (Rabone et al., 2023). They have also shown that communities vary across the CCFZ related to factors including topography, nodule density and particulate organic carbon concentration (Smith et al., 2021). Only a small proportion of the species found in the CCFZ seem to have wide geographic distributions whilst many have only been found at single sites and often are represented by a single specimen (singletons; Smith et al., 2021). This work and other studies, including metabarcoding analysis of the deep-sea water column and sediments point to large undocumented biodiversity in the deep sea, including at higher taxonomic levels (e.g. Cordier et al., 2022). Communities on cobalt crusts at seamounts and on seabed massive sulphides are also different to those that occur on the surrounding seafloor (e.g. Schlacher et al., 2014; Boschen et al., 2016). Deep-sea hydrothermal vent communities are characterised by having a high proportion of endemic species (e.g. Wolff, 2005). This is exemplified by the scaly foot snail, *Chrysomallon squamiferum*, which is found on just three vent sites in the Indian Ocean covering an estimated 0.02 km^2 (Sigwart et al., 2019). Collectively these findings mean that management of the environmental impact of deep-sea mining is highly challenging.

4.4 The Structure of pelagic communities

Ekman (1935) summarised the findings of the expeditions of mid-19th and early 20th Centuries with respect to pelagic biodiversity. These expeditions, alongside the work of coastal marine research stations, founded our understanding of the biogeography of pelagic organisms. Findings included the existence of neritic (coastal) versus oceanic plankton communities, the occurrence of cosmopolitan and circumglobal distributions amongst some planktonic organisms and the association of species and communities with water masses of specific temperatures, generally divided latitudinally (e.g. polar, sub-tropical, tropical, Ekman, 1935). At this time a significant change in pelagic communities at a depth of 150–200 m was recognised dividing the shallower epipelagic zone from the deeper bathypelagic zone. For many groups of organisms limited sampling meant that depth zonation in the bathypelagic was obscure but it is notable that Dahl, as early as 1894 had identified three depth zones on the basis of copepod distribution, 0–200 m (epipelagic), 200–1,000 m (mesopelagic) and below 1,000 m (bathypelagic; Ekman, 1935). Studies in the second half of the 20th Century confirmed the differences between neritic and oceanic plankton communities (Haedrich & Judkins, 1979). The former lacked elements of the micronekton (e.g. small pelagic fish, decapod shrimps and squid) present in oceanic environments and meroplankton were more abundant inshore than offshore (Haedrich & Judkins, 1979). Neritic plankton and their

https://doi.org/10.58440/ihr-30-1-a09

communities tended to have a much narrower latitudinal distribution than oceanic species which could be defined by temperature. For oceanic species work on fish and invertebrates suggested that distribution was associated with temperature and salinity (density), in other words water mass (Haedrich & Judkins, 1979). However, work on mesopelagic fish demonstrated that water mass alone was insufficient to explain horizontal and vertical distribution and other factors such as seafloor topography, temperature alone, the edges of major current systems and fronts all had influence (Backus et al., 1970; Headrich & Judkins, 1979).

The advent of satellite remote sensing provided a different perspective on pelagic biogeography. Observations of sea-surface colour enabled the classification of ecological domains in the surface ocean based on seasonal and spatial patterns of phytoplankton production driven by turbulence, stratification and irradiance at the ocean surface (Yentsch & Garside, 1986; Platt, et al. 1991). This resulted in the classification of the surface ocean into biomes (polar, westerlies, trades and coastal) within which were defined multiple provinces (e.g. Longhurst, 1995, 1998). Recently, attempts to analyse both epipelagic and mesopelagic biogeography patterns have been undertaken using analysis of species distributions through cluster analyses and expert opinion (Sutton et al., 2017; Reygondeau et al., 2018; Reygondeau & Dunn, 2019). These approaches to defining epipelagic and deep-pelagic biogeography resemble the biogeochemical provinces of Longhurst (1995, 1998) but differ significantly in detail.

4.5 The deep scattering layer

During World War 2 sound propagation experiments undertaken by workers at the University of California's Division of War Research identified a consistent layer of mid-water sound scattering (Eyring et al., 1948). This became known as the 'deep-scattering layer' (DSL) and early observations indicated that it shifted in depth diurnally from shallow depths at night to greater depths at day suggesting a biological origin (Johnson, 1948). The identity of the organisms reflecting sound energy remained elusive for many years because of difficulties in sampling deep-water pelagic ecosystems (Hersey & Backus, 1962). Early speculation was that the sound scatterers were likely to be midwater fish (e.g. myctophids) because their swim bladders were capable of reflecting sound (Marshall, 1951). Correlation of net captures from equipment such as the Tucker trawl and IKMTs with the depths of acoustic scattering in the northeastern Pacific found that euphausiids and mid-water fish, particularly myctophids, were the most conspicuous inhabitants of the DSL (e.g. Boden, 1950; Tucker, 1951; Barham, 1957; Hersey & Backus, 1962). Subsequent observations, including from the bathyscaphe *Trieste* and Cousteau's diving saucer (Barham, 1963, 1966) indicated that a wider range of organisms were likely to contribute to the DSL including physonectid siphonophores which have a gas-filled pneumatophore. Description of the species that constitute the DSL, its behaviour and geographic variation remain in progress today.

It has now been recognised that vertically migrating organisms that cross from the mesopelagic and upper bathypelagic zone into the epipelagic zone on a daily basis make a significant contribution to the export of carbon from the surface of the ocean into the deep sea where it can be stored for centuries or millenia. Estimates for the annual organic carbon sequestration by mesopelagic organisms ranges between 900–3600 Tg C_{org} yr^{-1} although these are highly uncertain because of the lack of studies of mesopelagic food webs and biogeochemical processes (e.g. Childress et al., 1980; Davison et al., 2013; Aumont et al., 2018; Boyd et al., 2019). These organisms are therefore likely to be significant in terms of the ocean carbon cycle and consideration of blue carbon ecosystems.

4.6 Discovery of hydrothermal vents, cold seeps, other chemosynthetic systems

The discovery of high-temperature hydrothermal vents and their biota has been one of the most exciting and unexpected findings in oceanography over the last 100 years. The first "black smokers" were discovered in early 1977 between the Galápagos islands and mainland Ecuador by the submersible *Alvin* whilst looking for evidence of heat flow from the seafloor (Grassle, 1987; German et al., 1995; van Dover, 2000). The high abundance and biomass of clams, mussels and tube worms in these ecosystems was immediately recognised as unusual leading to them being referred to as deep-sea oases (Corliss et al., 1979; Turner & Lutz, 1984; Grassle, 1985; van Dover, 2000). For the first time, samples of large vesicomyid clams, mussels, limpets, and tube worms were collected and brought to surface for examination and identification (Corliss et al., 1979).

It was soon recognised that at vents, reduced chemicals such as hydrogen sulphide and methane dissolved in the hydrothermal fluids provide energy for chemoautotrophic microorganisms to fix carbon. The free-living bacteria grow in direct contact with hydrothermal fluid in a variety of habitats, forming microbial mats, as well as episymbionts on the external surfaces of vent organisms, or suspended in plumes of diluted hydrothermal fluid (Grassle, 1987; Winn et al., 1986). Not only were free-living bacteria crucial for sustaining vent fauna, but also symbiotic bacteria occurred in the tissues of the dominant vent species. In some cases, these symbiotic relationships have resulted in highly specialised physiologies, such as in the tubeworm *Riftia pachyptila*, which lacks a mouth and digestive system and depends completely on the production of its endosymbiotic microorganisms (Cavanaugh et al. 1981). The discovery of chemosynthesis changed the way we understand life on Earth and primary productivity in the ocean (Baker et al., 2010) as well as how life may have originated and where it might

occur elsewhere in the universe, including within the solar system (e.g. Longo and Damer, 2020). The systematic study of mid-ocean ridges has led to the discovery of new hydrothermal active sites, with 722 confirmed high-temperature vents to date, and an additional 720 vents inferred from water-column chemistry data (Beaulieu & Szafranski, 2020; Fig. 8c). Since the discovery in the Pacific Ocean, hydrothermal vents have been found in all ocean basins, including in the ultra-slow spreading ridges of the Indian and Arctic oceans (Hashimoto et al. 2001; Ramirez-Llodra et al., 2007, 2023).

Following the discovery of chemoautrophic-based ecosystems at hydrothermal vents, similar communities based on the primary productivity of autotrophic microorganism were found in cold seeps and large organic falls. Cold seep ecosystems were discovered in the Gulf of Mexico in 1984 (Paull et al., 1984). These habitats are characterised by the seepage through the sediment of cold fluid with high concentrations of methane that sustains chemoautotrophic bacteria at the base of the food web, which support high abundances of specialised megafauna (Sibuet & Olu, 1998; Tunnicliffe et al., 2003).

5 The future

The deep ocean has now been recognised as harbouring high biodiversity, rivalling that of other marine and terrestrial ecosystems. However, it remains the least explored ecosystem in the ocean, particularly the deep pelagic (Webb et al., 2010). Increasing human activities in the deep ocean or those indirectly affecting it through pollution or climate change (e.g. Ramirez-Llodra et al., 2011; Sweetman et al., 2017) mean that reaching a better understanding of the distribution of life in the ocean is now a key scientific challenge of the 21st Century. The Agreement

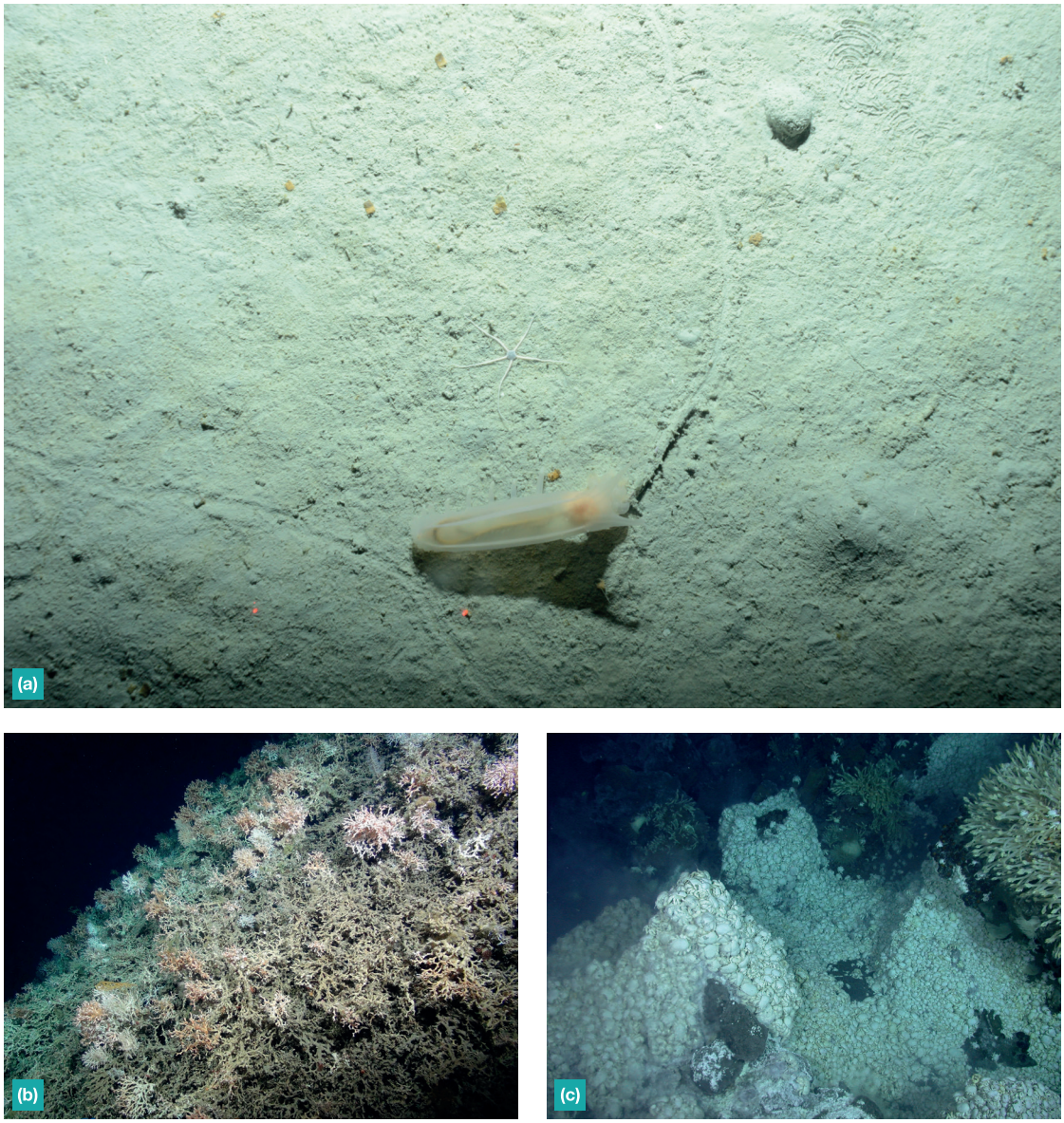

Fig. 8 Examples of deep-sea ecosystems (a) abyssal mud, Bounty Trough, Southwest Pacific (b) cold-water coral reef, Anton Dohrn Seamount, 400m depth, Northeast Atlantic (c) aggregations of yeti crabs (Kiwa tyleri) on deep-sea hydrothermal vents, southern East Scotia Ridge, Antarctica. Photos taken during The Nippon Foundation Nekton Ocean Census NIWA Bounty Trough Expedition, South West Pacific, 2024 (a); NERC Deep Links Expedition (b); NERC CHESSO Project.

https://doi.org/10.58440/ihr-30-1-a09

under the United Nations Convention on the Law of the Sea on the Conservation and Sustainable Use of Marine Biological Diversity of Areas beyond National Jurisdiction treaty now provides a legal framework for protection of pelagic and benthic species in the high seas and the Area (seafloor in areas beyond national jurisdiction; UN, 2023). However, without improved knowledge of the biodiversity of the deep sea, connectivity between its communities and better understanding of the functional ecology of species, implementation will be difficult.

One challenge in studying the deep sea is its vast size. At present, studying deep-sea biodiversity involves sampling the water column or seafloor, recovering animals and identifying and quantifying them. This science requires large, ocean-going research vessels of which there are a finite number operating globally, mainly belonging to high-income countries or wealthy philanthropic non-governmental organisations (Rogers et al., 2021). The process of identifying species through taxonomy is challenging, slow and significantly impaired by a lack of human capacity (Rogers et al., 2023). Enhancing ship-based science with autonomous platforms for biological studies is extremely challenging but may be important in expanding the geographic scope and resolution of biodiversity studies and lowering the carbon footprint of ocean science. This may be tractable first in the much smaller size fractions of organisms such as microbial taxa and the pelagic fauna that may be documented through a combination of advanced imaging and DNA sequencing. Meiofauna and macrofauna that live in sediments might also be sampled and preserved using autonomous platforms. These may be tractable to automated sorting and identification using technologies such as flow cytometry (e.g. Kitahashi et al., 2018).

DNA sequencing is providing further resolution to our knowledge of deep-sea biodiversity demonstrating that even in apparently homogenous pelagic environments what were considered as cosmopolitan or widespread species can be complexes of geographically separated cryptic species (e.g. mesopelagic fish; Miya & Nishida, 1997). Integrated taxonomic approaches whereby both morphological and genetic data are collected to enable the discovery and description of species are now key to species discovery and ultimately description (Rogers et al., 2022, 2023). Metabarcoding approaches are beginning to yield new information on the distribution and diversity of life in the deep sea. Application of these approaches to deep-sea sediments have revealed previously undocumented diversity, including at higher taxonomic levels and new information on species range and turnover for different size classes of organisms (e.g. Cordier et al., 2022). However, wider application of environmental DNA (eDNA) for biodiversity monitoring requires barcoding libraries that are much better populated with sequences from species identified or described by taxonomists along with accompanying voucher specimens and archived tissue / DNA samples in biological collections (Rogers et al., 2022).

Such a major challenge requires a coordinated global approach to species discovery and description whether from existing collections or from new expeditions to poorly sampled parts of the ocean such as the deep sea. The Nippon Foundation Nekton Ocean Census programme is one such effort aimed to accelerate the discovery of ocean life. Here a combination of the use of new technologies, human capacity development and the nurturing of global networks of taxonomists, institutions, technology and infrastructure providers are aimed at meeting the challenge of better understanding the distribution of life in the ocean (Rogers et al., 2023). It is critical that such global initiatives are inclusive of low- and middle-income countries which are not only located in some of the most biodiversity rich parts of the ocean but also have a wealth of human talent to help solve this challenge. For this programme and others to be successful in transforming our knowledge of life in the deep ocean biodiversity must be valued by society for the critical services it provides to humankind. Only through such recognition will the investment be made and maintained in capacity and infrastructure to study and understand life in the ocean and to use the knowledge gained to better manage human activities to restore it to health.

Acknowledgements

The authors would like to thank Dr Patrick Westfeld, the Editor of The International Hydrographic Review for the invitation to write this paper. They would also like to thank REV Ocean, The Nippon Foundation and the Nekton Foundation for support during the production of this synthesis.

References

Aldred, R. G., Thurston, M. H., Rice, A. L. and Morley D. R. (1976). An acoustically monitored opening and closing epibenthic sledge. *Deep-Sea Research, 23*, pp. 167–174.

Aumont, O., Maury, O., Lefort, S. and Bopp, L. (2018). Evaluating the potential impacts of the diurnal vertical migration by marine organisms on marine biogeochemistry. *Global Biogeochemical Cycles, 32*, pp. 1622–1643.

Auscavitch, S. R., Deere, M. C., Keller, A. G., Rotjan, R. D., Shank, T. M. and Cordes, E. E. (2020). Oceanographic drivers of deep-sea coral species distribution and community assembly on seamounts, islands, atolls, and reefs within the Phoenix Islands Protected Area. *Frontiers in Marine Science, 7*, 42.

Backus, R. H., Craddock, J. E., Haedrich, R. L. and Shores, D. L. (1970). The distribution of mesopelagic fishes in the equatorial and western North Atlantic Ocean. In G. B. Farquhar (Ed.), *Proceedings of the International Symposium on Biological Sound Scattering in the Ocean, March 31–April 2, 1970 Airlie House Conference Center Warrenton, Virginia* (pp. 20–40). U.S. Government Printing Office, Washington DC, U.S.A.

Bailey, D. M., King, N. J. and Priede, I. G. (2007). Cameras and carcasses: historical and current methods for using artificial food falls to study deep-water animals. *Marine Ecology Progress Series, 350*, pp. 179–191.

Baird, R. H. (1958). A preliminary account of a new half square metre bottom sampler. *I. C. E. S. Shellfish Committee, 70*, 4 pp.

Baker, A., de C., Clarke, M. R. and Harris, M. J. (1973). THE N. I. O. combination net (RMT 1 + 8) and further developments of rectangular midwater trawls. *Journal of the Marine Biological Association of the U. K., 53*, pp. 167–184.

Baker, M. C., Ramirez-Llodra, E. Z., Tyler, P. A., German, C. R., Boetius, A., Cordes, E. E., Dubilier, N., Fisher, C. R., Levin, L. A., Metaxas, A., Rowden, A. A., Santos, R. S., Shank, T. M., van Dover, C. L., Young, C. M. and Warén, A. (2010). Biogeography, ecology, and vulnerability of chemosynthetic ecosystems in the deep sea. In A. D. McIntyre (Ed.), *Life in the World's Oceans* (pp. 161–182). Blackwell Publishing Ltd., Oxford, U. K.

Ballard, R. D. (2000). *The Eternal Darkness*. Princeton University Press, Princeton, New Jersey, U.S.A, 388 pp.

Balls, R. (1948). Herring fishing with the echometer. *Journal du Conseil, 15*, pp. 193–206.

Balls, R. (1951). Environmental changes in herring behaviour: a theory of light avoidance as suggested by echo-sounding observations in the North Sea. *Journal du Conseil, 17*, pp. 274–298.

Barham, E. G. (1957). The ecology of sonic scattering layers in the Monterey Bay area. *Hopkins Marine Station, Stanford University Technical Report, 1*, 182 pp.

Barham, E. G. (1963). The deep scattering layer as observed from the bathyscaph Trieste. In J. A. Moore (Ed.), *Proceedings of the 16th International Congress of Zoology, Washington, 20th–27th August 1963 Volume 4* (pp. 298–300).

Barham, E. G. (1966). Deep scattering layer migration and composition: observations from a diving saucer. *Science, 151*, pp. 1399–1403.

Barker, L. D. L., Jakuba, M. V., Bowen, A. D., German, C. R., Maksym, T., Mayer, L., Boetius, A., Dutrieux, P. and Whitcomb, L. L. (2020). Scientific challenges and present capabilities in underwater robotic vehicle design and navigation for oceanographic exploration under-ice. *Remote Sensing, 12*, 2588.

Barnett, P. R. O., Watson, J. and Connelly, D. (1984). A multiple corer for taking virtually undisturbed samples from shelf, bathyal and abyssal sediments. *Oceanologica Acta, 7*, pp. 399–408.

Barry, J. P. and Hashimoto, J. (2009). Revisiting the Challenger Deep using the ROV Kaiko. *Marine Technology Society Journal, 43*, pp. 77–78.

Bé, A. W. H. (1962). Quantitative multiple opening-and-closing plankton samplers. *Deep-Sea Research, 9*, pp. 144–151.

Bé, A. W. H., Ewing, M. and Linton, L. W. (1959). A quantitative multiple opening-and-closing plankton sampler for vertical towing. *Journal du Conseil / Conseil Permanent International pour l'Exploration de la Mer, 25*, pp. 36–46.

Beaulieu, S. E., and Szafranski, K. (2020). *InterRidge Global Database of Active Submarine Hydrothermal Vent Fields, Version 3.4.* https://vents-data.interridge.org/ (accessed 28 March 2024).

Beebe, W. (1934). *Half Mile Down*. Harcourt Brace and Company, New York, U.S.A., 344 pp.

Benoit-Bird, K. J. and Lawson, G. L. (2016). Ecological insights from pelagic habitats acquired using active acoustic techniques. *Annual Review of Marine Science, 8*, pp. 463–490.

Benoit-Bird, K. J., Waluk, C. M. (2020). Exploring the promise of broadband fisheries echosounders for species discrimination with quantitative assessment of data processing effects. *Journal of the Acoustical Society of America, 147*, pp. 411–427.

Bigelow, H. B. (1913). A new closing net for horizontal use, with a suggested method of testing the catenary in fast towing. *Internationale Revue der gesamten Hydrobiologie und Hydrographie, 5*, pp. 576–580.

Blidberg, R. D. (2001). The development of Autonomous Underwater Vehicles (AUV); A brief summary. Autonomous Undersea Systems Institute, Lee New Hampshire, USA, 12 pp.

Bline, D. (1977). The unique roles and history of manned and unmanned submersibles in oceanography. In R. A. Geyer (Ed.), *Submersibles and Their Use in Oceanography and Ocean Engineering, Elsevier Oceanography Series, 17* (pp. 61–76).

Boden, B. P. (1950). Plankton organisms in the deep scattering layer. *United States Navy Electronics Laboratory Reports, 186*, pp. 1–29.

Boland, G. S. and Rowe, G. T. (1991). Deep-sea benthos sampling with the GOMEX box corer. *Limnology and Oceanography, 36*, pp. 1015–1020.

Boschen, R. E., Rowden, A. A., Clark, M. R., Pallentin, A. and Gardner, J. P. A. (2016). Seafloor massive sulfide deposits support unique megafaunal assemblages: Implications for seabed mining and conservation. *Marine Environmental Research, 115*, pp. 78–88.

Bouchet, P., Decock, W., Lonneville, B., Vanhoorne, B. and Vandepitte, L. (2023). Marine biodiversity discovery: The metrics of new species descriptions. *Frontiers in Marine Sciences, 10*, 929989.

Boutan, L. (1900). *La Photographie Sous Marine et Les Progres de la Photographie*. Schleicher Frères, Éditeurs, Paris, France, 332 pp.

Bowden, D. A., Jones, D. O. B. (2016). Towed cameras. In M. R. Clark, M. Consalvey and A. Rowden (Eds.), *Biological Sampling in the Deep Sea* (pp. 260–284). John Wiley & Sons Ltd., Chichester, Sussex, U. K.

Boyd, P. W., Claustre, H., Levy, M., Siegel, D. A. and Weber, T. (2019). Multi-faceted particle pumps drive carbon sequestration

https://doi.org/10.58440/ihr-30-1-a09

in the ocean. *Nature, 568*, pp. 327–335.

Brandt, A. and Barthel, D. (1995). An improved supra- and epibenthic sledge for catching peracarida (Crustacea, Malacostraca). *Ophelia, 43*, pp. 15–23.

Brandt, A., Elsner, N., Brenke, N., Golovan, O., Malyutina, M. V., Riehl, T., Schwabe, E. and Würzberg, L. (2013). Epifauna of the Sea of Japan collected via a new epibenthic sledge equipped with camera and environmental sensor systems. *Deep-Sea Research II 86–87*, pp. 43–55.

Brautaset, O., Waldeland, A. U., Johnsen, E., et al. (2020). Acoustic classification in multifrequency echosounder data using deep convolutional neural networks. *ICES Journal of Marine Science, 77*, pp. 1391–1400.

Brattegard, T., Høisæter, T., Sjøtun, K., Fenchel, T. and Uiblein, F. (2011). Norwegian fjords: From natural history to ecosystem ecology and beyond. *Marine Biology Research, 7*, pp. 421–424.

Brenke, N. (2005). An epibenthic sledge for operations on marine soft bottom and bedrock. *Marine Technology Society Journal, 39*, pp. 10–21.

Broecker, W. S. (1987). Unpleasant surprises in the greenhouse? *Nature, 328*, pp. 123–126.

Broecker, W. S. (1997) Thermohaline circulation, the Achilles heel of our climate system: will man-made CO_2 upset the current balance? *Science, 278*, pp. 1582–1588.

Brown, C. J., Beaudoin, J., Brissette, M. and Gazzola, V. (2019). Multispectral multibeam echo sounder backscatter as a tool for improved seafloor characterization. *Geosciences, 9*, p. 126.

Brown, C. J. and Blondel, P., 2009. Developments in the application of multibeam sonar backscatter for seafloor habitat mapping. *Applied Acoustics, 70*, pp. 1242–1247.

Buhl-Mortensen, L., Vanreusel, A., Gooday, A. J., Levin, L. A., Priede, I. G., Buhl-Mortensen, P., Gheerardyn, H., King, N. J. and Raes, M. (2010). Biological structures as a source of habitat heterogeneity and biodiversity on the deep ocean margins. *Marine Ecology, 31*, pp. 21–50.

Busby, R. F. (1976). *Manned Submersibles*. Office of the Oceanographer of the Navy, U.S.A., 764 pp.

Capocci, R., Dooly, G., Omerdič, E., Coleman, J., Newe, T. and Toal, D. (2017). Inspection-class remotely operated vehicles—a review. *Journal of Marine Science and Engineering, 5*, 13.

Cavanaugh, C. M., Gardiner, S. L., Jones, M. L., Jannasch, H. W. and Waterbury, J. B. (1981). Prokaryotic cells in the hydrothermal vent tube worm *Riftia pachyptila* Jones: Possible chemoautotrophic symbiont. *Science, 213*, pp. 340–342.

Childress, J. J., Taylor, S. M., Calliet, G. M. and Price, M. H. (1980). Patterns of growth, energy utilization and reproduction in some meso- and bathypelagic fishes off southern California. *Marine Biology, 61*, pp. 27–40.

Christiansen, B. (2016). Deep-sea zooplankton sampling. In M. R. Clark, M. Consalvey and A. Rowden (Eds.), *Biological Sampling in the Deep Sea* (pp. 103–125). John Wiley & Sons Ltd., Chichester, Sussex, U. K.

Clark, M. R., Bagley, N. W. and Harley, B. (2016). Trawls. In M. R. Clark, M. Consalvey and A. Rowden (Eds.), *Biological Sampling in the Deep Sea* (pp. 126–158). John Wiley & Sons Ltd., Chichester, Sussex, U. K.

Clark, M. R. and Rowden, A. A. (2009). Effect of deepwater trawling on the macro-invertebrate assemblages of seamounts on the Chatham Rise, New Zealand. *Deep Sea Research I, 56*, pp. 1540–1554.

Clarke, M. (1969). A new midwater trawl for sampling discrete depth horizons. *Journal of the Marine Biological Association of the United Kingdom, 49*, pp. 945–960.

Cordier, T., Angeles, I. B., Henry, N., Lejzerowicz, F., Berney, C., Morard, R., Brandt, A., Cambon-Bonavita, M.-A., Guidi, L., Lombard, F., Arbizu, P. M., Massana, R., Orejas, C., Poulain, J., Smith, C. R., Wincker, P., Arnaud-Haond, S., Gooday, A. J., de Vargas, C. and Pawlowski, J. (2022). Patterns of eukaryotic diversity from the surface to the deep-ocean sediment. *Science Advances, 8*, eabj9309.

Corfield, R. (2004). *The Silent Landscape: In the Wake of HMS Challenger 1872–1876*. John Murray, London, U. K., 285 pp.

Corliss, J. B., Dymond, J., Gordon, L. I., Edmond, J. M., von Herzen, R. P., Ballard, R. D., Green, K., Williams, D., Bainbridge, A., Crane, K. and van Andel, T. H. (1979). Submarine thermal springs on the Galápagos Rift. *Science, 203*, pp. 1073–1083.

Craib, J. S. (1965). A sampler for taking short undisturbed marine cores. J*ournal du Conseil / Conseil Permanent International pour l'Exploration de la Mer, 30*, pp. 34–39.

Crylen, J. (2018). Living in a world without sun. *Journal of Cinema and Media Studies, 58*, pp. 1–23.

Davis, I. E. and Barham, E. G. (1969). An in-situ surge-temperature recorder. *Limnology and Oceanography, 14*, pp. 638–641.

Davison, P. C., Checkley Jr., D. M., Koslow, J. A. and Barlow, J. (2013). Carbon export mediated by mesopelagic fishes in the northeast Pacific Ocean. *Progress in Oceanography, 116*, pp. 14–30.

De Moustier, C. (1986). Beyond bathymetry: Mapping acoustic backscattering from the deep seafloor with Sea Beam. J*ournal of the Acoustical Society of America, 79*, pp. 316–331.

Devereux, R. F. and Winsett, R. C. (1953). *Isaacs-Kidd Midwater Trawl*. Final Report. Designers J. D. Isaacs and L. W. Kidd. University of California, Scripps Institute of Oceanography, California, U.S.A., 18 pp. + 3 Diagrams.

Dietz, R. S. (1961). Continent and ocean basin evolution by spreading of the seafloor. *Nature, 190*, pp. 854–857.

Dolan, J. R. (2021). Pioneers of plankton research: Victor Hensen (1835–1924). *Journal of Plankton Research, 43*, pp. 507–510.

Ehlers, P. (2002). Hydrographic services at the crossroads. *The International Hydrographic Review, 3*, pp. 6–13.

Ekman, S. (1935). *The Zoogeography of the Sea*. Sidgewick and Jackson Limited, London, U. K., 417 pp. (note this is an English translation of Ekman's work Tiergeographie des Meeres published in 1953).

Ewing, M., Vine, A. and Worzel, J. L. (1946). Photography of the ocean bottom. *Journal of the Optical Society of America, 36*, pp. 307–321.

Ewing, M., Worzel, J. L. and Veine, A. (1967). Early development of ocean bottom photography at Woods Hole Oceanographical Institution and Lamont Geological Observatory. In J. B. Hersey (Ed.), *Deep-Sea Photography* (pp. 13–39). Johns Hopkins Press, Baltimore, U.S.A.

Eyring, C. F., Christensen, R. J. and Raitt, R. W. (1948). Reverberation in the sea. *Journal of the Acoustical Society of America, 20*, pp. 462–475.

FAO (2009a). *International Guidelines for the Management of Deep-Sea Fisheries in the High Seas*. Food and Agricultural Organisation of the United Nations, Rome, Italy, 73 pp.

Fletcher, B., Bowen, A., Yoerger, D. R. and Whitcomb, L. L. (2009). Journey to the Challenger Deep: 50 years later with the *Nereus*

hybrid remotely operated vehicle. *Marine Technology Society Journal, 43*, pp. 65–76.

Forster, G. R. (1953). A New Dredge for Collecting Burrowing Animals. *Journal of the Marine Biological Association of the United Kingdom, 32*, pp. 193–198.

Francois, R. E. (1973). The Unmanned Arctic Research Submersible System. *Marine Technology Science Journal, 7*, (republished in 2006 in Vol. 40, pp. 75–77 as an archive paper).

Francois, R. E. (1977). *High Resolution Observations of Under-Ice Morphology*. Applied Physics Laboratory, University of Washington, Seattle, Washington State, U.S.A.

Fraser, J. H. (1968). The history of plankton sampling. In *Zooplankton Sampling. Monographs on Oceanographic Methodology 2* (pp. 11–18). United Nations Educational, Scientific and Cultural Organization, Paris France.

Gage, J. D. and Tyler, P. A. (1991). *Deep-Sea Biology: A Natural History of Organisms at the Deep-Sea Floor*. Cambridge University Press, 504 pp.

German, C. R., Baker, E. T. and Klinkhammer, G. (1995). Regional setting of hydrothermal activity. *Geological Society of London Special Publications, 87*, pp. 3–15.

German, C. R., Yoerger, D. R., Jakuba, M., Shank, T., Lin, J. and Nakamura, K. (2008). Hydrothermal exploration by AUV: Progress to-date with ABE in the Pacific, Atlantic & Indian Oceans. *2008 IEEE/OES Autonomous Underwater Vehicles*, Woods Hole, MA, USA, pp. 1–5.

Glasby, G. P. (2000). Lessons learned from deep-sea mining. *Science, 289*, pp. 551–553.

Grassle, J. F. (1985). Hydrothermal vent animals: distribution and biology. *Science, 229*, pp. 713–717.

Grassle, J. F. (1987). The ecology od deep-sea hydrothermal vent communities. *Advances in Marine Biology, 23*, pp. 301–362.

Grassle, J. F. and Maciolek, N. J. (1992). Deep-sea species richness: regional and local diversity estimates from quantitative bottom samples. *The American Naturalist, 139*, pp. 313–341.

Haedrich, R. L. and Judkins, D. C. (1979). Macrozooplankton and its environment. In S. van der Spoel and A. C. Pierrot-Bults (Eds.), *Zoogeography and diversity in plankton* (pp. 4–28). Bunge Scientific, Utrecht, Netherlands.

Harris, B. (2000). 400 Years of Subs. https://www.pbs.org/wgbh/nova/lostsub/history.html (accessed 18 August, 2023).

Harris, P. T. (2012). Surrogacy. In P. T. Harris and E. K. Baker (Eds.), *Seafloor Geomorphology as Benthic Habitat: GEOHAB Atlas of Seafloor Geomorphic Features and Benthic Habitats* (pp. 93–108). Elsevier, London, U. K.

Harris, P. T and Baker, E. K. (2012). Why map benthic habitats? In P. T. Harris and E. K. Baker (Eds.), *Seafloor Geomorphology as Benthic Habitat: GEOHAB Atlas of Seafloor Geomorphic Features and Benthic Habitats*. Elsevier, London, U. K., 3–22.

Hartman, O. (1955). *Quantitative survey of the benthos of San Pedro Basin, Southern California*. Part I. Preliminary results. Allan Hancock Pacific Expeditions 19, 185 pp.

Hartman, O., and Barnard, J. L. (1958). *The benthic fauna of the deep basins off southern California*. Allan Hancock Pacific Expeditions 22, 67 pp.

Harvey, E. N. (1939). Deep-sea photography. *Science, 90*, p. 187.

Hashimoto, J., Ohta, S., Gamo, T., Chiba, H., Yamaguchi, T., Tsuchida, S., Okudaira, T., Watabe, H., Yamanaka, T. and Kitazawa, M. (2001). First hydrothermal vent communities from the Indian Ocean discovered. *Zoological Science, 18*, pp. 717–721.

Heezen, B. C. and Hollister, C. D. (1971) *The Face of the Deep*. Oxford University Press, London, U. K., 659 pp.

Hersey, J. B. and Backus, R. H. (1962). Sound scattering by marine organisms. In M. N. Hill (Ed.), *The Sea: Ideas and Observations on Progress in the Study of the Seas*. Vol. 1. Physical Oceanography. Interscience Publishers, John Wiley & Sons, New York, pp. 498–539.

Hess, H. H., (1960). *The Evolution of Ocean Basins*. Preprint/technical report to the Office of Naval Research, dated December 1960, Department of Geology, Princeton University, 38 pp.

Hess, H. H. (1962). History of ocean basins. In A. E. J. Engel, H. L. James and B. F. Leonard (Eds.), *Petrologic Studies: A Volume to Honor A. F Buddington* (pp. 599–620). Geological Society of America, New York, U.S.A.

Hessler, R. R. and Jumars, P. A. (1974). Abyssal community analysis from replicate box cores in the central North Pacific. *Deep-Sea Research, 21*, pp. 185–209.

Hessler, R. R. and Sanders, H. L. (1967). Faunal diversity in the deep-sea. *Deep-Sea Research, 14*, pp. 65–78.

Hjort, J. (1910). Eel-larvae (*Leptocephalus brevirostris*) from the Central North Atlantic. *Nature, 85*, pp. 104–106.

Hjort, J. and Petersen, C. G. J. (1905). Short Review of the Results of the international Investigations (mostly Norwegian and Danish). *Rapports et procès-verbaux des réunions, 3*, Appendix G. 43 pp. + 10 plates. https://doi.org/10.17895/ices.pub.19272014

Holme, N. A. (1964). Methods of sampling the benthos. *Advances in Marine Biology, 2*, pp. 171–260.

Holmes, A. (1928). Radioactivity and continental drift. *Geological Magazine, 65*, pp. 236–238.

Holmes, A. (1929). Radioactivity and earth movements. *Transactions of the Geological Society of Glasgow, 18*, pp. 559– 606.

Horowitz, J., Quattrini, A. M., Brugler, M. R., Miller, D. J., Pahang, K., Bridge, T. C. L. and Cowman, P. F. (2023). Bathymetric evolution of black corals through deep time. *Proceedings of the Royal Society B 290*, 20231107.

Hydrobios (2020). *Multi Plankton Sampler MultiNet® Type Mammoth Catalogue No. 438 180*. Operation Manual. Hydrobios, Altenholz, Germany, 42 pp.

Isaacs, J. D. (1969). Nature of oceanic life. *Scientific American, 221*, pp. 146–162.

Isaacs, J. D. and Schwartzlose, R. A. (1975). Active animals of deep-sea floor. *Scientific American, 233*, pp. 85–91.

Isacks, B., Oliver, J. and Sykes, L. R. (1968). Seismology and the new global tectonics. *Journal of Geophysical Research, 73*, pp. 5855–5899.

Jamieson, A. J. (2016). Landers baited cameras and traps. In M. R. Clark, M. Consalvey, and A. Rowden (Eds.), *Biological Sampling in the Deep Sea* (pp. 228–259). John Wiley & Sons Ltd., Chichester, Sussex, U. K.

Jamieson, A. J., Maroni, P. J., Bond, T., Niyazi, Y., Kolbusz, J., Arasu, P. and Kitazato, H. (2023). New maximum depth record for bony fish: Teleostei, Scorpaeniformes, Liparidae (8336 m, Izu-Ogasawara Trench). *Deep-Sea Research I, 199*, p. 104132.

Jamieson, A. J., Ramsey, J. and Lahey, P. (2019) Hadal manned submersible: Five Deeps Expedition explores deepest point in every ocean. *Sea Technology, 60*, pp. 22–24.

Jennings, S., Kaiser, M. J. and Reynolds, J. D., 2001. *Marine*

https://doi.org/10.58440/ihr-30-1-a09

Fisheries Ecology. Blackwell Publishing, Oxford, U. K., 417 pp.

Johnson, E. R. F. (1939). Undersea cinematography. *Journal of the Society of Motion Picture Engineers, 32*, pp. 3–17.

Johnson, M. W. (1948). Sound as a tool in marine ecology, from data on biological noises and the deep scattering layer. *Journal of Marine Research, 7*, pp. 443–458.

Jones, D. O. B. (2009). Using existing industrial remotely operated vehicles for deep-sea science. *Zoologica Scripta, 38*(1), pp. 41–47.

Kaiser, S., Brenke, N. (2016). Epibenthic sledges. In: Clark, M. R., Consalvey, M., Rowden, A. (Eds.), Biological Sampling in the Deep Sea. John Wiley & Sons Ltd., Chichester, Sussex, U. K., pp. 184–206.

Kaiser, C. L., Yoerger, D. R., Kinsey, J. C., Kelley, S., Billings, A., Fujii, J., Suman, S., Jakuba, M., Berkowitz, Z., German, C. R. and Bowen, A. D. (2016). The design and 200 day per year operation of the Autonomous Underwater Vehicle Sentry. *2016 IEEE/OES Autonomous Underwater Vehicles (AUV)*, Tokyo, Japan, 2016, pp. 251–260.

Kimura, K. (1929). On the detection of fish groups by an acoustic method. *Journal of the Imperial Fisheries Institute of Tokyo, 24*, pp. 451–458.

Kinsey, J. C., Eustice, R. M. and Whitcomb, L. L. (2006). A survey of underwater vehicle navigation: recent advances and new challenges. *7th Conference on Manoeuvring and Control of Marine Craft (MCMC'2006)*, Lisbon, Portugal, September 20–22, 2006. 12 pp.

Kitahashi, T., Watanabe, H. K., Tsuchiya, M., Yamamoto, H. and Yamamoto, H. (2018). A new method for acquiring images of meiobenthic images using the FlowCAM. *MethodsX, 5*, pp. 1330–1335.

Korneliussen, R. J., (2018). *Acoustic target classification*. ICES Cooperative Research Report No. 344. 104 pp. https://doi.org/10.17895/ices.pub.4567

Košťák, M., Schlögl, J., Fuchs, D., Holcová, K., Hudáčková, N., Culka, A., Fözy, I., Tomašových, A., Milovský, R., Šurka, J. and Mazuch, M. (2021). Fossil evidence for vampire squid inhabiting oxygen-depleted ocean zones since at least the Oligocene. *Communications Biology, 4*, 216.

Kullenberg, B. (1947). The piston core sampler. Svenska Hydrografisk-Biologiska Kommissionens Skrifter. *Third Series: Hydrography, 1*, pp. 1–46.

Kyo, M., Miyazaki, E., Tsukioka, S., Ochi, H., Amitani, Y., Tsuchiya, T., Aoki, T. and Takagawa, S. (1995). The sea trial of "*Kaiko*", the full ocean depth research ROV. *Challenges of Our Changing Global Environment'. Conference Proceedings. OCEANS '95 MTS/IEEE*, San Diego, CA, USA, Vol. 3 pp. 1991–1996. https://doi.org/10.1109/OCEANS.1995.528882

Le Danois, E. (1948). *Les Profondeurs de la Mer*. Payot, Paris, France, 303 pp.

Le Pichon, X. (1968). Sea-floor spreading and continental drift. *Journal of Geophysical Research, 73*, 3661–3697.

Leprieur, F., Descombes, P., Gaboriau, T., Cowman, P. F., Parravicini, V., Kulbicki, M., Melián, C. J., de Santana, C. N., Heine, C., Mouillot, D., Bellwood, D. R. and Pellissier, L. (2016). Plate tectonics drive tropical reef biodiversity dynamics. *Nature Communications, 7*, p. 11461.

Lim, A., Kane, A., Arnaubec, A. and Wheeler, A. J. (2018). Seabed image acquisition and survey design for cold water coral mound characterisation. *Marine Geology, 395*, pp. 22–32.

Lisitsin, A. I. and Udintsev, G. B. (1955). A new type of grab. (In Russian). *Trudy Vses Gidrobiol Obsch, 6*, pp. 217–222.

Longhurst, A. (1995). Seasonal cycles of pelagic production and consumption. *Progress in Oceanography, 36*, pp. 77–167.

Longhurst, A. (1998) *Ecological Geography of the Sea*. Academic Press Inc. London, U. K., 398 pp.

Longo, A. and Damer, B. (2020). Factoring origin of life hypotheses into the search for life in the solar system and beyond. *Life, 10*, p. 52.

Maciolek, N., Grassle, J. F., Hecker, B., Brown, B., Blake, J. A., Boehm, P. D., Petrecca, R., Duffy, S., Baptiste, E. and Ruff, R. E. (1987). *Study of Biological processes on the U. S. North Atlantic Slope and Rise*. Final report prepared for U. S. Department of Interior, Minerals and Management Service, Washington DC, USA, 362 pp. + Appendices A-L.

Manly, J. E. (2004). Multiple AUV Missions in the National Oceanic and Atmospheric Administration. *2004 IEEE/OES Autonomous Underwater Vehicles (IEEE Cat. No.04CH37578)*, Sebasco, ME, USA, 2004, pp. 20–25.

Marshall, N. B. (1951). Bathypelagic fishes as sound scatterers in the ocean. *Journal of Marine Research, 10*, pp. 1–17.

Marti, M. (1922). *Brevet d'Invention XII, 3 No. 568–075, Oscillographe enregistreur continu à grande sensibilité et son application au sondage continu par le son*.

Mayer L. A. (2006). Frontiers in seafloor mapping and visualization. *Marine Geophysical Research, 27*, pp. 7–17.

McPhail, S. D., Furlong, M. E., Pebody, M., Perrett, J. R., Stevenson, P., Webb, A. and White, D. (2009). Exploring beneath the PIG Ice Shelf with the Autosub3 AUV. *OCEANS 2009–EUROPE*, Bremen, Germany, 2009, pp. 1–8.

Mehrzadi, M., Terriche, Y., Su, C.-L., Othman, M. B., Vasquez, J. C. and Guerrero, J. M. (2020). Review of dynamic positioning control in maritime microgrid systems. *Energies, 13*, 3188.

Menandro, P. S. and Bastos, A. C. (2020). Seabed mapping: A brief history from meaningful words. *Geosciences, 10*, 273.

Michel, D. (1998). *Operational Effectiveness of Unmanned Underwater Systems*. Marine Technology Society ROV Committee, Washington DC, USA, 594 pp.

Miya, M. and Nishida, M. (1997). Speciation in the open ocean. *Nature, 389*, pp. 803–804.

Morris, K. J., Bett, B. J., Durden, J. M., Huvenne, V. A. I., Milligan, R., Jones, D. O. B., McPhail, S., Robert, K., Bailey, D. M. and Ruhl, H. A. (2014). A new method for ecological surveying of the abyss using autonomous underwater vehicle photography. *Limnology and Oceanography: Methods, 12*, pp. 795–809.

Murray, J. and Hjort, J. (1912). *The Depths of the Ocean: A General Account of the Modern Science of Oceanography Based Largely on the Scientific Researches of the Norwegian Steamer Michael Sars in the North Atlantic*. Macmillan and Co., London, U. K. (Reprinted 1965 by J. Cramer Weinheim, Wheldon & Wesley Ltd., Codicote, U. K.), 821 pp, + 4 maps and 9 plates.

Murray, J. and Reynard, A. F. (1891). *Report on Deep-Sea Deposits Based on the Specimens Collected During the Voyage of H. M. S. Challenger in the Years 1872–1876*. Report on the Scientific Results of the Voyage of H. M. S. Challenger During the Years 1873–1876 Under the Command of Captain Sir George S. Nares, R. N., F. R. S., and the Late Captain Frank Tourle Thomson, R. N. Prepared Under the Superintendence of the Late Sir C. Wyville Thomson and Now of John Murray. 525

pp. + 29 Plates, 43 Charts and 22 Diagrams.

Murton, B. J., Hühnerbach, V. and Garrard, J. (2012). Exploring ultradeep hydrothermal vents In the Cayman Trough by ROV. *Sea Technology*, September 2012, pp. 15–20.

Narayanaswamy, B. E., Bett, B. J., Lamont, P. A., Rowden, A. A., Bell, E. M. and Menot, L. (2016). Corers and grabs. In M. R. Clark, M. Consalvey and A. Rowden (Eds.), *Biological Sampling in the Deep Sea* (pp. 207–227). John Wiley & Sons Ltd., Chichester, Sussex, U. K.

Nunnally, C. C., Friedman, J. R. and Drazen, J. C. (2016). In situ respiration measurements of megafauna in the Kermadec Trench. *Deep–Sea Research I, 118*, pp. 30–36.

Ondréas, H., Olu, K., Fouquet, Y., Charlou, J. L., Gay, A., Dennielou, B., Donval, J. P., Fifis, A., Nadalig, T., Cochonat, P., Cauquil, E., Bourillet, J. F., Le Moigne, M. and Sibuet, M. (2005). ROV study of a giant pockmark on the Gabon continental margin. *Geo-Marine Letters, 25*, pp. 281–292.

Paull, C. K., Hecker, B., Commeau, R., Freeman-Lynde, R. P., Neumann, C., Corso, W. P., Golubic, S., Hook, J. E., Sikes, E. and Curray, J. (1984). Biological communities at the florida escarpment resemble hydrothermal vent taxa. *Science, 226*, pp. 965–967.

Pellissier, L., Heine, C., Rosauer, D. F. and Albouy, C. (2018). Are global hotspots of endemic richness shaped by plate tectonics? *Biological Journal of the Linnean Society, 123*, pp. 247–261.

Petersen, C. G. J. (1913). Valuation of the sea. 11. The animal communities of the sea-bottom and their importance for marine zoogeography. *Reports of the Danish Biological Station, 21*, pp. 44–68.

Petersen, C. G. J. and Boysen Jensen, P. (1911). Valuation of the sea. I. Animal life of the sea-bottom, its food and quantity. *Report of the Danish Biological Station, 20*, p. 81.

Petillot, Y. R., Antonelli, G., Casalino, G. and Ferreira, F. (2019). Underwater robots: From Remotely Operated Vehicles to Intervention-Autonomous Underwater Vehicles. *IEEE Robotics and Automation Magazine, 26*, pp. 94–101.

Petterssen, H. (1949). The Swedish Deep-Sea Expedition. *The Geographical Journal, 114*, pp. 151–154.

Piggot, C. S. (1936). Apparatus to secure core samples from the ocean-bottom. *Bulletin of the Geological Society of America, 47*, pp. 675–684.

Platt, T., Caverhill, C. and Sathyendranath, S. (1991). Basin-scale estimates of oceanic primary production by remote sensing – The North Atlantic. *Journal of Geophysical Research, 96*, p. 15.

Pratt, N., Chen, T., Li, T., Wilson, D. J., van de Flierdt, T., Little, S. H., Taylor, M. L., Robinson, L. F., Rogers, A. D. and Santodomingo, N. (2019). Temporal distribution and diversity of cold-water corals in the southwest Indian Ocean over the past 25,000 years. *Deep-Sea Research I, 149*, 103049.

Rabone, M., Wiethase, J. H., Simon-Lledó, E., Emery, A. M., Jones, D. O. B., Dahlgren, T. G., Bribiesca-Contreras, G., Wiklund, H., Horton, T. and Glover, A. G. (2023). How many metazoan species live in the world's largest mineral exploration region? *Current Biology, 33*, pp. 2383–2396.

Ramirez-Llodra, E., Argentino, C., Baker, M., Boetius, A., Costa, C., Dahle, H., Denny, E. M., Dessandier, P.-A., Eilertsen, M. H., Ferre, B., German, C. R., Hand, K., Hilário, A., Hislop, L., Jamieson, J. W., Kalnitchenko, D., Mall, A., Panieri, G., Purser, A., Ramalho, S. P., Reeves, E. P., Rolley, L., Pereira, S. I., Ribeiro, P. A., Sert, M. F., Steen, I. H., Stetzler, M., Stokke, R., Victorero, L., Vulcano, F., Vågenes, S., Waghorn, K. A. and Buenz, S. (2023). Hot vents beneath an icy ocean. *Oceanography, 36*, pp. 6–17.

Ramirez-Llodra, E., Shank, T. M. and Tyler, P. A. (2007). Biodiversity and biogeography of hydrothermal vent species: thirty years of discovery and investigations. *Oceanography, 20*, pp. 30–41.

Ramirez-Llodra, E., Tyler, P. A., Baker, M. C., Bergstad, O. A., Clark, M. R., Escobar, E., Levin, L. A., Menot, L., Rowden, A. A., Smith, C. R. and van Dover, C. L. (2011). Man and the last great wilderness: human impact on the deep sea. *PLoS ONE, 6*, e22588.

Rehbock, P. F. (1979). The early dredgers: Naturalizing" in British Seas, 1830–1850. *Journal of the History of Biology, 12*, pp. 293–368.

Rex, M. (1981). Community structure in the deep-sea benthos. *Annual Review of Ecology, Evolution and Systematics, 12*, pp. 331–353.

Rex, M. (1983). Geographic patterns of species diversity in the deep-sea benthos. In G. T. Rowe (Ed.), *The Sea: Ideas and Observations of Progress in the Study of the Seas* (pp. 453–472). Volume 8 Deep-Sea Biology, Harvard University Press, Cambridge, Massachusetts, U.S.A.

Rex, M. A. and Etter, R. J. (2010). *Deep-Sea Biodiversity: Pattern and Scale*. Harvard University Press, Cambridge, Massachusetts, USA, 354 pp.

Reygondeau, G. and Dunn, D. (2018). Pelagic biogeography. In J. K. Cochran, H. J. Bokuniewicz, and P. L. Yager (Eds.), *Encyclopedia of Ocean Sciences* (pp. 588–598). Elsevier, Amsterdam, Netherlands.

Reygondeau, G., Guidi, L., Beaugrand, G., Henson, S. A., Koubbi, P., MacKenzie, B. R., Sutton, T. T., Fioroni, M. and Maury, O. (2018). Global biogeochemical provinces of the mesopelagic zone. *Journal of Biogeography, 45*, pp. 500–514.

Rice, A. L., Aldred, R. G., Billett, D. S. M. and Thurston, M. H. (1982). The combined use of an epibenthic sledge and a deep-sea camera to give quantitative relevance to macro-benthos samples. *Ambio Special Report, 6*, pp. 59–63, 65–72.

Rice, A. L. and Collins, E. P. (1985). The use of photography in deep-sea benthic biology at the Institute of Oceanographic Sciences. In J. D. George, G. . Lythgoe, J. N. Lythgoe (Eds.), *Underwater Photography and Television for Scientists* (pp. 153–164). Clarendon Press, Oxford, U. K.

Roberts, J. M., Wheeler, A. J., Freiwald, A. and Cairns, S. D. (2009). *Cold-Water Corals: The Biology and Geology of Deep-Sea Coral Habitats*. Cambridge University Press, Cambridge, U. K., 334 pp.

Robison, B. H., Reisenbichler and Sherlock, R. E. (2017). The co-evolution of midwater research and ROV technology at MBARI. *Oceanography, 30*, pp. 26–37.

Roe, H. S. J. and Shale, D. M. (1979). A new Multiple Rectangular Midwater Trawl (RMT 1+8M) and some modifications to the Institute of Oceanographic Sciences' RMT 1+8. *Marine Biology, 50*, pp. 283–288.

Rogers A. D. (1999) The biology of *Lophelia pertusa* (Linnaeus 1758) and other deep-water reef-forming corals and impacts from human activities. *International Review of Hydrobiology, 84*, pp. 315–406.

Rogers, A. D. (2000). The role of the oceanic oxygen minima in generating biodiversity in the deep sea. *Deep-Sea Research II, 47*, pp. 119–148

https://doi.org/10.58440/ihr-30-1-a09

Rogers, A. D. (2007). Evolution and biodiversity of Antarctic organisms: a molecular perspective. *Philosophical Transactions of the Royal Society B, 362*, pp. 2191–2214.

Rogers, A. D. (2012). Evolution and biodiversity of Antarctic organisms: a molecular perspective. In A. D. Rogers, N. M. Johnston, E. J. Murphy and A. Clarke (Eds.), *Antarctic Ecosystems: An Extreme Environment in a Changing World* (pp. 417–467). Wiley Publishers, Oxford, U.K.

Rogers, A. D. (2015). Environmental change in the deep ocean. *Annual Review of Environment and Resources, 40*, pp. 1–38.

Rogers, A. D., Appeltans, W., Assis, J., Balance, L. T., Cury, P., Duarte, C., Favoretto, F., Hynes, L. A., Kumagai, J. A., Lovelock, C. E., Miloslavich, P., Niamir, A., Obura, D., O'Leary, B. C., Ramirez-Llodra, E., Reygondeau, G., Roberts, C., Sadovy, Y., Steeds, O., Sutton, T., Tittensor, D. P., Velarde, E., Woodall, L. and Aburto-Oropeza, O. (2022). Discovering marine biodiversity in the 21st Century. *Advances in Marine Biology, 93*, pp. 23–115.

Rogers, A. D., Appiah-Madson, H., Ardron, J. A., Bax, N. J., Bhadury, P., Brandt, A., Buttigieg, P.-L., De Clerke, O., Delgado, C., Distel, D. L., Glover, A., Gobin, J., Guilhon, M., Hampton, S., Harden-Davies, H., Hebert, P., Hynes, L., Lowe, M., MacIntyre, S., Madduppa, H., Mazzuco, A. C. D'A., McCallum, A., McOwen, C., Nattkemper, T. W., Odido, M., O'Hara, T., Osborn, K., Pouponneau, A., Provoost, P., Rabone, M., Ramirez-Llodra, E., Scott, L., Sink, K. J., Turk, D., Watanabe, H. K., Weatherdon, L. V., Wernberg, T., Williams, S., Woodall, L., Wright, D. J., Zeppilli, D. and Steeds, O. (2023). Accelerating ocean species discovery and laying the foundations for the future of marine biodiversity research and monitoring. *Frontiers in Marine Science, 10*, 1224471.

Rogers, A. D., Baco-Taylor, A., Currie, D., Escobar-Briones, E., Gjerde, K., Gobin, J., Jaspars, M., Levin, L., Linse, K., Rabone, M., Ramirez-Llodra, E., Lopez, J. S., Shank, T. M., Sink, K., Snelgrove, P. V. R., Taylor, M. L., Wagner, D. and Harden-Davies, H. (2021). Marine genetic resources in areas beyond national jurisdiction: promoting marine scientific research and enabling equitable benefit sharing. *Frontiers in Marine Science, 8*, 667274.

Rogers, A. D., Tyler, P. A., Connelly, D. P., Copley, J. T., James, R., Larter, R. D., Linse, K., Mills, R. A., Naveira-Garabato, A., Pancost, R. D., Pearce, D. A., Polunin, N. V. C., German, C. R., Shank, T., Boersch-Supan, P. H., Alker, B., Aquilina, A., Bennett, S. A., Clarke, A., Dinley, R. J. J., Graham, A. G. C., Green, D., Hawkes, J. A., Hepburn, L., Hilario, A., Huvenne, V. A. I., Marsh, L., Ramirez-Llodra, E., Reid, W. D. K., Roterman, C. N., Sweeting, C. J., Thatje, S. and Zwirglmaier, K. (2012). The discovery of new deep-sea hydrothermal vent communities in the Southern Ocean and implications for biogeography. *PLoS Biology, 10*, e1001234.

Rothlisberg, P. C. and Pearcy, W. G. (1977). An epibenthic sampler used to study the ontogeny of vertical migration of *Pandalus jordani* (Decapoda, Caridea). *Fisheries Bulletin, 74*, pp. 994–997.

Rozwadowski, H. M. (2005). *Fathoming the Ocean: The Discovery and Exploration of the Deep Sea*. The Belknap Press of Harvard University Press, Cambridge, Massachusetts, U.S.A., 276 pp.

Sahoo, A., Dwivedy, S. K. and Robi, P. S. (2019). Advancements in the field of autonomous underwater vehicle. Ocean Engineering, *181*, pp. 145–160.

Sanders, H. L., Hessler, R. R. and Hampson, G. R. (1965). An introduction to the study of deep-sea benthic faunal assemblages along the Gay Head-Bermuda transect. *Deep-Sea Research I, 12*, pp. 845–867.

Schmidt, J. (1923). The breeding places of the eel. *Philosophical Transactions of the Royal Society of London. Series B Biological Sciences, 211*, pp. 179–208.

Schneider von Deimling, J., Brockhoff, J. and Greinert, J. (2007). Flare imaging with multibeam systems: Data processing for bubble detection at seeps. *Geochemistry, Geophysics and Geosystems, 8*, Q06004.

Schönfeld, J. (2012). History and development of methods in recent benthic foraminiferal studies. *Journal of Micropalaeontology, 31*, pp. 53 –72.

Schlacher, T. A., Baco, A. R., Rowden, A. A., O'Hara, T. D., Clark, M. R., Kelley, C. and Dower, J. F. (2014). Seamount benthos in a cobalt-rich crust region of the central Pacific: conservation challenges for future seabed mining. *Diversity and Distributions, 20*, pp. 491–502.

Sheremet, V. and Efimova, T. (1996). 2D bottom sampling. In M. K. Ivanov, A. F. Limonov and B. T. Cronin (Eds.), *Mud Volcanism and Fluid Venting in the Eastern Part of the Mediterranean Ridge*. UNESCO Reports in Marine Science, 68, 126 pp.

Sibuet, M. and Olu, K. (1998). Biogeography, biodiversity and fluid dependence of deep-sea cold-seep communities at active and passive margins. *Deep-Sea Research II, 45*, pp. 517– 567.

Sigwart, J. D., Chen, C., Thomas, E. A., Allcock, L., Böhm, M. and Seddon, M. (2019). Red Listing can protect deep-sea biodiversity. *Nature Ecology & Evolution, 3*, 1134.

Smith, C. R., Clark, M. R., Goetze, E., Glover, A. G. and Howell, K. L. (2021). Editorial: Biodiversity, connectivity and ecosystem function across the Clarion-Clipperton Zone: A regional synthesis for an area targeted for nodule mining. *Frontiers in Marine Science, 8*, 797516.

Smith, K. L. (1978). Benthic Community Respiration in the N. W. Atlantic Ocean: in situ Measurements from 40 to 5200 m. *Marine Biology*, *47*, pp. 337–347.

Smith, K. L. and Clifford, C. H. (1976). A free vehicle for measuring benthic community metabolism. *Limnology and Oceanography, 21*, pp. 164–170.

Smith. W. and McIntyre, A. D. (1954). A spring-loaded bottom-sampler. *Journal of the Marine Biological Association of the U. K., 33*, pp. 257–264.

Snell, J.-A. (1998). A simple benthic sledge for shallow and deep-sea sampling. *Sarsia, 83*, pp. 69–72.

Southward, A. J. and Nicholson, D. (1985). Photography of the deep-sea bottom fauna with remotely operated cameras. In: J. D. George, G. I. Lythgoe and J. N. Lythgoe (Eds.), *Underwater Photography and Television for Scientists* (pp. 122–152). Clarendon Press, Oxford, U. K.

Spärck, R. (1956). The density of animals on the ocean floor. In A. F. Bruun, S. V. Greve, H. Mielche and R. Spärck (Eds.), *The Galathea Deep Sea Expedition 1950–1952, Described by Members of the Expedition*. George Allen and Unwin Ltd., London, U. K., 296 pp. + 1 map.

Stefanoudis, P. V., Gress, E., Pitt, J. M., Smith, S. R., Kincaid, T., Rivers, M., Andradi-Brown, D. A., Rowlands, G., Woodall, L. C. and Rogers, A. D. (2019a). Depth-dependent structuring of reef fish assemblages from the shallows to the rariphotic zone. *Frontiers in Marine Science, 6*, 307.

Stefanoudis, P. V., Rivers, M., Smith, S. R., Schneider, C. W.,

Wagner, D., Ford, H., Rogers, A. D. and Woodall, L. C. (2019b). Low connectivity between shallow, mesophotic and rariphotic zone benthos. *Royal Society Open Science, 6*, 190958.

Strugnell, J. M., Rogers, A. D., Prodöhl, P. A., Collins, M. A. and Allcock, A. L. (2008). The thermohaline expressway: The Southern Ocean as a centre of origin for deep-sea octopuses. *Cladistics, 24*, pp. 1–8.

Svensson, P. (2019). *The Gospel of the Eels*. Picador, London, U. K., 241 pp.

Sweetman, A. K., Smith, C. R., Dale, T. and Jones, D. O. B. (2014). Rapid scavenging of jellyfish carcasses reveals the importance of gelatinous material to deep-sea food webs. *Proceedings of the Royal Society B*, 281, p. 20142210.

Sweetman, A. K., Thurber, A. R., Smith, C. R., Levin, L. A., Mora, C., Wei, C.-L., Gooday, A. J., Jones, D. O. B., Rex, M., Yasuhara, M., Ingels, J., Ruhl, H. A., Frieder, C. A., Danovaro, R., Würzberg, L., Baco, A., Grupe, B. M., Pasulka, A., Meyer, K. S., Dunlop, K. M., Henry, L.-A. and Roberts, J. M. (2017). Major impacts of climate change on deep-sea benthic ecosystems. *Elementa Science of the Anthropocene, 5*, p. 4.

Sund, O. (1935). Echo sounding in fisheries research. *Nature, 135*, p. 953.

Sutton, T. A., Clark, M. R., Dunn, D. C., Halpin, P. N., Rogers, A. D., Guinotte, J., Bograd, S. J., Angel, M. V., Perez, J. A. A., Wishner, K., Haedrich, R. L., Lindsay, D. J., Drazen, J. C., Vereshchaka, A., Piatkowski. U., Morato. T., Błachowiak-Samołyk. K., Robison. B. H., Gjerde. K. M., Pierrot-Bults. A., Bernal. P., Reygondeau. G., Heino. M. (2017). A global biogeographic classification of the mesopelagic zone. *Deep-Sea Research I, 126*, pp. 85–102.

Talkington, H. (1977). Manned and Remotely Operated Submersible Systems: A Comparison. In R. A. Geyer (Ed.), *Submersibles and Their Use in Oceanography and Ocean Engineering* (pp. 77–95). Elsevier Oceanography Series, 17.

Tengberg, A., De Bovee, F., Hall, P., Berelson, W., Chadwick, D., Ciceri, G., Crassous, P., Devol, A., Emerson, S., Gage, J., Glud, R., Graziottini, F., Gundersen, J., Hammond, D., Helder, W., Hinga, K., Holby, O., Jahnke, R., Khripounoff, A., Lieberman, S., Nuppenau, V., Pfannkuche, O., Reimers, C., Rowe, G., Sahami, A., Sayles, F., Schurter, M., Smallman, D., Wehrli, B. and de Wilde, P. (1995). Benthic chamber and profiling ianders in oceanography - A review of design, technical solutions and functioning. *Progress in Oceanography, 35*, pp. 253–294.

Thamdrup, H. M. (1938). Der van Veen-Bodengreifer. Vergleichsversuche über die Leistungsfähigkeit des van Veen- und des Petersen-Bodengreifers. *Journal du Conseils / Conseil Permanent International pour l'Exploration de la Mer, 13*, pp. 206–212.

Thomson, C. W. and Murray, J. (1895). *Report on the Scientific Results of the Voyage of H. M. S. Challenger During the Years 1872–1876 Under the Command of Captain Sir George S. Nares, R. N.,* F. R. S., and the Late Captain Frank Tourle Thomson, R. N. Summary of the Scientific Results First Part (with Appendices). Eyre & Spottiswode, London, U. K. 796 pp.

Thurston, M. H., Bett, B. J. and Rice, A. L. (1995). Abyssal megafaunal necrophages: latitudinal differences in the eastern North Atlantic Ocean. *Internationale Revue der gesamten Hydrobiologie und Hydrographie, 80*, pp. 267–286.

Thuy, B. (2013). Temporary expansion to shelf depths rather than an onshore-offshore trend: the shallow-water rise and demise of the modern deep-sea brittle star family Ophiacanthidae (Echinodermata: Ophiuroidea). *European Journal of Taxonomy, 48*, pp. 1–242.

Tucker, G. H. (1951). Relation of fishes and other organisms to the scattering of underwater sound. *Journal of Marine Research, 10*, pp. 215–238.

Tunnicliffe, V., Fowler, C. M. R. and Mcarthur, A. G. (1996). Plate tectonic history and hot vent biogeography. *Geological Society, London, Special Publications, 118*, pp. 225–238.

Tunnicliffe, V., Juniper, S. K. and Sibuet, M. (2003). Reducing environments of the deep-sea floor. In P. A. Tyler (Ed.), Ecosystems of the World 28, *Ecosystems of the Deep Oceans* (pp. 81–110). Elsevier, Amsterdam, The Netherlands.

Turner, R. D. and Lutz, R. A. (1984). Growth and distribution of mollusks at deep-sea vents and seeps. *Oceanus, 27*, pp. 54–62.

UN (2023). *Agreement Under the United Nations Convention on The Law of The Sea On The Conservation and Sustainable Use of Marine Biological Diversity of Areas Beyond National Jurisdiction*. United Nations, New York, U.S.A, 62 pp.

van Dover, C. L. (2000). *The Ecology of Deep-Sea Hydrothermal Vents*. Princeton University Press, Princeton, New Jersey, 474 pp.

Vanreusel, A., Hilario, A., Ribeiro, P. A., Menot, L. and Arbizu, P. M. (2016). Threatened by mining, polymetallic nodules are required to preserve abyssal epifauna. *Scientific Reports, 6*, 26808.

Vecchione, M., Allcock, L., Priede, I. and van Haren, H. (2023). T*he Deep Ocean: Life in the Abyss*. Princeton University Press, Princeton, New Jersey, U.S.A. and Oxford, U. K., 288 pp.

Vigoureux, P. and Hersey, J. B. (1962). Sound in the sea. In M. N. Hill (Ed.), *The Sea: Ideas and Observations on Progress in the Study of the Seas. Volume 1 Physical Oceanography* (pp. 476–497). Interscience Publishers, a division of John Wiley & Sons, London.

Vine, F. J. and Matthews, D. H. (1963). Magnetic anomalies over oceanic ridges. *Nature, 199*, pp. 947–949.

von Alt, C. (2003). *Autonomous underwater vehicles. In Autonomous Underwater Lagrangian Platforms and Sensors Workshop, Vol. 3* (p. 2). Woods Hole Oceanographic Institution, Massachusetts, U.S.A.

Webb, T. J., Vanden Berghe, E. and O'Dor, R. (2010). Biodiversity's big wet secret: the global distribution of marine biological records reveals chronic under-exploration of the deep pelagic ocean. *PLoS ONE, 5*, e10223.

Wegener, A. (1912a). Die Entstehung der Kontinente. *Petermanns Geographische Mitteilungen, 58*, pp. 185–195, pp. 253–257, pp. 305–309.

Wegener, A. (1912b). Die Entstehung der Kontinente. *Geologische Rundschau, 3*, pp. 276–292.

Weiss, R., Kirsten, O. and Ackermann, R. (1977). Free vehicle instrumentation for the in situ measurement of processes controlling the formation of deep-sea ferromanganese nodules. *OCEANS '77 Conference Record*, Los Angeles, CA, USA, 1977, pp. 616–619.

Weston J. N. J. and Jamieson A. J. (2022). The multi-ocean distribution of the hadal amphipod, Hirondellea dubia Dahl, 1959 (Crustacea, Amphipoda). *Frontiers in Marine Science, 9*, 824640.

Weston, J. N. J., Peart, R. A., Stewart, H. A., Ritchie, H., Piertney, S. B., Linley, T. D. and Jamieson, A. J. (2021). Scavenging

 https://doi.org/10.58440/ihr-30-1-a09

amphipods from the Wallaby-Zenith Fracture Zone: Extending the hadal paradigm beyond subduction trenches. *Marine Biology, 168*, 1.

Wheeler, A. (1975). Thompson: marine biologist. *British Medical Journal, 3*, pp. 534–536.

Widditsch, H. R. (1973). *SPURV – The First Decade*. Applied Physics Laboratory, University of Washington, Seattle, Washington State, USA. 27 pp. + 5 p appendices.

Wiebe, P. H. and Benfield, M. C. (2003). From the Hensen net toward four-dimensional biological oceanography. *Progress in Oceanography, 56*, pp. 7–136.

Wiebe, P. H., Burt, K. H., Boyd, S. H. and Morton, A. W. (1976). A multiple opening/ closing net and environmental sensing system for sampling zooplankton. *Journal of Marine Research, 34*, pp. 313–326.

Wiebe, P. H., Morton, A. W., Bradley, A. M., Backus, R. H., Craddock, J. E., Barber, V., Cowles, T. J. and Flierl, G. R. (1985). New developments in the MOCNESS, an apparatus for sampling zooplankton and micronekton. *Marine Biology, 87*, pp. 313–323.

Williams, A., Schlacher, T. A., Rowden, A. A., Althaus, F., Clark, M. R., Bowden, D. A., Stewart, R., Bax, N. J., Consalvey, M. and Kloser, R. J. (2010). Seamount megabenthic assemblages fail to recover from trawling impacts. *Marine Ecology, 31*(1), pp. 183–199.

Wilson, D. S., Leifer, I. and Maillard, E. (2015). Megaplume bubble process visualization by 3D multibeam sonar mapping. *Marine Petroleum Geology, 68*, pp. 753–765.

Winn, C. D., Karl, D. M. and Massoth, G. J. (1986). Microorganisms in deep-sea hydrothermal plumes. *Nature, 320*, pp. 744–746.

Wolff, T. (2005). Composition and endemism of the deep-sea hydrothermal vent fauna. Cahiers *Biologie Marine, 46*, pp. 97–104.

Woolley, S. N. C., Tittensor, D. P., Dunstan, P. K., Guillera-Arroita, G., Lahoz-Monfort, J. J., Wintle, B. A., Worm, B. and O'Hara, T. D. (2016). Deep-sea diversity patterns are shaped by energy availability. *Nature, 533*, pp. 393–396.

Wynn, R. B., Huvenne, V. A. I., Le Bas, T. P., Murton, B. J., Connelly, D. P., Bett, B. J., Ruhl, H. A., Morris, K. J., Peakall, J., Parsons, D. R., Sumner, E. J., Darby, S. E., Dorrell, R. M. and Hunt, J. E. (2014). Autonomous Underwater Vehicles (AUVs): Their past, present and future contributions to the advancement of marine geoscience. *Marine Geology, 352*, pp. 451–468.

Yentsch, C. S. and Garside, J. C. (1986). Patterns of phytoplankton abundance and biogeography. In A. C. Pierrot-Bults, S. van der Spoel, B. J. Zahuranec and R. K. Johnson (Eds.), *Pelagic Biogeography, Proceedings of an International Conference, The Netherlands 29 May-5 June 1985* (pp. 278–284). Technical Paper in Marine Science, Vol. 49, UNESCO, Paris.

Young, J. (2020). *Expedition Deep Ocean: The First Descent to the Bottom of All Five of the World's Oceans*. Pegasus Books Ltd. New York, U.S.A., 320 pp.

Zaffos, A., Finnegan, S. and Peters, S. E. (2017). Plate tectonic regulation of global marine animal diversity. *Proceedings of the National Academy of Sciences of the USA, 114*, pp. 5653–5658.

Authors' biographies

Alex David Rogers is the Science Director at the Ocean Census programme, a global effort to accelerate the discovery of marine life and to raise awareness of the importance of the ocean to humankind. Alex has worked on deep-ocean biodiversity for more than 30 years, focusing on hotspot ecosystems including seamounts, cold-water coral reefs and deep-sea hydrothermal vents. He has also worked on human impacts on the deep sea, most notably on deep-sea bottom trawling but more lately on deep-sea mining and carbon dumping. During his career Alex has worked with governments, intergovernmental organisations, including the International Union for the Conservation of Nature and non-governmental organisations including the Deep-Sea Conservation Coalition and Greenpeace.

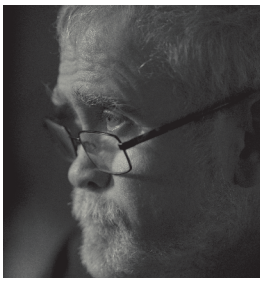

Alex David Rogers

Eva Ramirez Llodra is the Science Director at REV Ocean, a Norwegian philanthropic organisation that aims at contributing ground-breaking research and innovation towards solutions for ocean challenges, such as plastic pollution, overfishing and climate change. Eva has 25 years of research experience in marine biodiversity and ecology of deep-sea ecosystems. In the last decade, the focus has been in exploration, biodiversity and biogeography of remote ecosystems, with a particular interest in providing baseline knowledge for the development of equitable management and conservation of the ocean. Eva is a member of the Deep Ocean Stewardship Initiative (DOSI) core team and leads the Arctic regional group for the UN Ocean Decade endorsed programme Challenger 150.

Eva Ramirez Llodra

https://doi.org/10.58440/ihr-30-1-a09

INVITED ARTICLE

Robotic photogrammetric underwater inspection of hydropower plants

Author
Manuela Ammann[1]

Preamble

Manuela Ammann from the University of Applied Sciences Northwestern Switzerland is the winner of the IFHS Student Award 2023 for her Master's thesis on “Robotic Photogrammetric Underwater Inspection of Hydropower Plants”. The following article summarises her award-winning work.

Abstract

Hydropower is the most important domestic source of renewable energy in Switzerland, accounting for around 57 % of domestic electricity production. The high intensity usage of hydropower plants results in high costs for regular maintenance and inspection, which are currently carried out through manual inspections by professional divers. The aim of this work is to develop a workflow for underwater photogrammetry with Remotely Operated Vehicles (ROV) to supplement or replace these dangerous and expensive dives. A calibration frame was developed to provide a scale reference for the data collected during the inspection. With different acquisition missions, investigations on camera calibration and 3D reconstruction were performed. The reconstruction of underwater objects was successfully implemented. Well- distributed control points provide accurate results as a point cloud with a sub-centimetre accuracy at object distances of up to 6 m. 80 % of the point cloud differ less than 1 cm from the reference scan.

Keywords
underwater photogrammetry · 3D reconstruction · structure from motion · camera calibration · ROV

Resumé

L'hydroélectricité est la principale source d'énergie renouvelable en Suisse, représentant environ 57 % de la production nationale d'électricité. L'utilisation intensive des centrales hydroélectriques entraîne des coûts élevés pour la maintenance et l'inspection régulières, qui sont actuellement effectuées manuellement par des plongeurs professionnels. L'objectif de ce travail est de développer un processus de photogrammétrie sous-marine à l’aide de véhicules téléopérés (ROV) afin de compléter ou de remplacer ces plongées dangereuses et coûteuses. Un cadre d'étalonnage a été développé pour fournir une référence d'échelle pour les données collectées pendant l'inspection. Avec différentes missions d'acquisition, des études sur l'étalonnage des caméras et la reconstruction en 3D ont été réalisées. La reconstruction d'objets sous-marins a été réalisée avec succès. Des points de contrôle bien répartis fournissent des résultats précis sous la forme d'un nuage de points avec une précision inférieure au centimètre à des distances d'objets allant jusqu' à 6 m. 80 % du nuage de points diffèrent de moins de 1 cm du balayage de référence.

✉ Manuela Ammann · manuela.ammann@fhnw.ch

[1] FHNW Universities of Applied Sciences and Arts Northwestern Switzerland, Institute Geomatics, CH-4132 Muttenz, Switzerland

https://doi.org/10.58440/ihr-30-1-a04

Resumen

La energía hidráulica es la fuente nacional más importante de energía renovable en Suiza, y representa alrededor del 57 % de la producción nacional de electricidad. El uso intensivo de las centrales hidroeléctricas genera elevados costes periódicos de mantenimiento e inspección, que actualmente se realizan mediante inspecciones manuales de buceadores profesionales. El objetivo de este trabajo es desarrollar un flujo de trabajo para fotogrametría submarina con Vehículos Operados por Control Remoto (ROV) para complementar o sustituir estas inmersiones peligrosas y caras. Se desarrolló un marco de calibración para proporcionar una referencia de escala para los datos recogidos durante la inspección. Con diferentes misiones de adquisición, se realizaron investigaciones sobre calibración de la cámara y reconstrucción 3D. Se realizó con éxito la reconstrucción de elementos submarinos. Puntos de control bien distribuidos proporcionan resultados precisos como nube de puntos con una exactitud por debajo de un centímetro a distancias del elemento de hasta 6 m. El 80 % de la nube de puntos tiene menos de 1 cm de diferencia con el escaneo de referencia.

1 Introduction

Due to the topography and considerable average rainfall, Switzerland offers ideal conditions for the use of hydroelectric power. With around 57 % of domestic electricity production, hydropower is our most important domestic source of renewable energy (BFE, 2022). A major challenge associated with hydropower generation and storage is the high intensity of the plants, resulting in high costs for regular maintenance and inspection of these plants. Current underwater inspections of hydropower plants in rivers can be dangerous and expensive, as manual inspections by professional divers are necessary. The aim of this project in cooperation with Axpo Power AG and Schuck Consulting is the development and verification of a novel workflow for 3D mapping based on an ROV-based underwater structure-from-motion process.

2 Related work

3D reconstruction is used in various fields. The image-based reconstruction of in air objects is already well researched. Various applications exist, where 3D underwater reconstruction is used, for example monitoring marine ecosystems (Neyer et al., 2018), mapping archaeological heritage (Bruno et al., 2015) and underwater construction (Chemisky et al., 2021).

Underwater reconstruction applications with optical systems require images from a short distance, whereby a large number of images is needed to create complete 3D scenes (Chemisky et al., 2021). For true-to-scale 3D reconstructions, a scaling factor is applied leveraging control points with local or global coordinates, scale bars or stereo camera configurations. The accuracy of the 3D model mainly depends on the quality of the images (contrast, sharpness, exposure), the environmental conditions (visibility, particles in the field of view) and the scene (heterogeneity of texture, moving objects). Furthermore, parameters such as the scaling method or the camera calibration influence the accuracy of the reconstruction (Chemisky et al., 2021).

Comprehensive calibration is essential, when accuracy is important and especially when the measured object has a 3D surface (Shortis, 2019). There are different approaches to calibrate the camera, e.g. using a scale bar (Aragón et al., 2018), reference tape measurements (McCarthy & Benjamin, 2014), a target board or plane (Menna et al., 2017) or a geodetic network (Neyer et al., 2018).

3 Materials and methods

3.1 Materials

For this project a Sony Alpha 7 II (ILCE-7M2; Sony Europe B.V, 2022) with a lens FE 28 mm F2 (SEL28F20) with a 75° FOV is used. The camera is placed in a Sony A7 II NG V.2 Series UW underwater camera housing kit with a 8" Dome port from seafrog (seafrogs, 2023). The housing is mounted underneath a BlueROV2, which is an underwater robot with open-source electronics and software (Fig. 1; Blue Robotics Inc, 2022). Because the camera housing is larger than what the payload kit allows, the height was extended by 3D printed plates (Fig. 1, right). The ROV is manually steered on an external computer via the ROV camera stream.

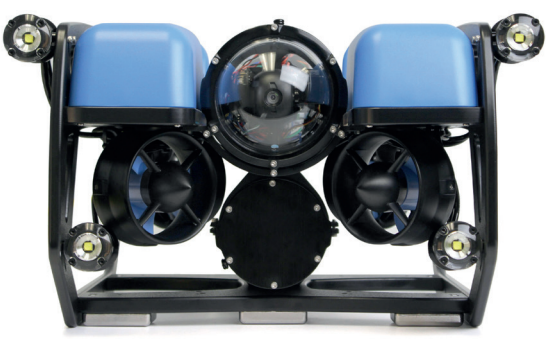

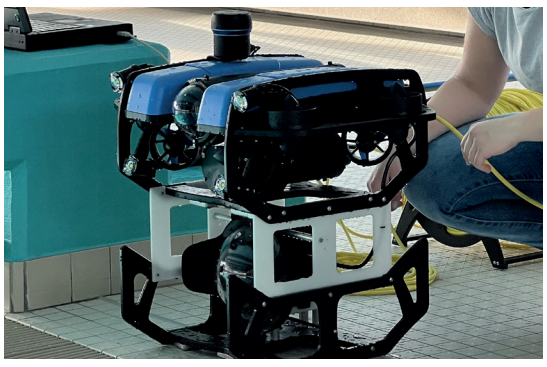

Fig. 1 ROV (left) and ROV with extended payload-kit and the camera (right).

https://doi.org/10.58440/ihr-30-1-a04

3.2 Calibration frame

A calibration frame made of aluminium was developed to perform a self-calibration during the 3D reconstruction (Fig. 2). The objects of interest are captured by moving the ROV on an arc on different heights, due to the fixed mounting of the camera, which allows horizontal image capturing only. Multiple exposures should ensure the redundancy of the images.

3.3 Study areas and data acquisition

To capture test data three different study areas were evaluated. The indoor swimming pool in Muttenz was used for test capturing in clear water. Furthermore, the water lock was used for the capturing with a reference measurement, which were performed with the laser scanner (Figs. 3 and 4). By filling the lock, different water levels can be set, simulating different depths (1–10 m) of acquisition. And finally, a water filter in the water was used to have a real object (Fig. 3).

The focus of the camera could not be set manually due to the camera trigger software available with the test system. A summary of the image acquisition at the hydropower station in Eglisau can be found in Table 1.

For reference measurements, a Leica RTC360 laser scanner was used to create a dense and very accurate scan of the empty water lock with a 3D point accuracy of approximately 2.8 mm at 20 m and a Leica TS60 total station was used to determine control points for referencing in a local coordinate system with a 3D point accuracy of approximately 2.25 mm at 20 m.

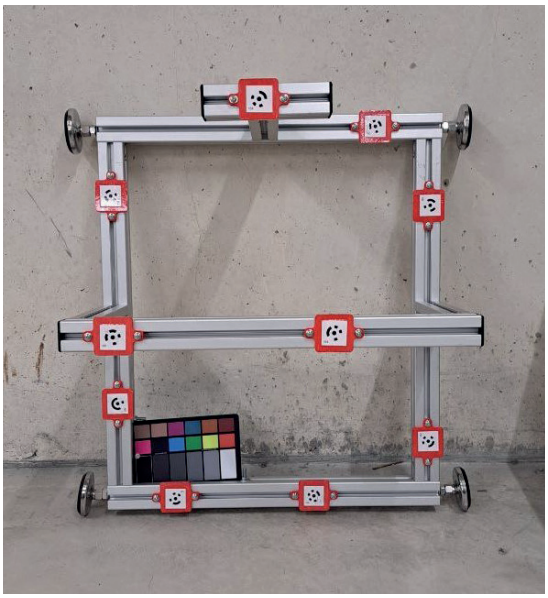

Fig. 2 Calibration frame with the colour chart int the bottom left.

Fig. 3 The Hydropower plant in Eglisau: The water lock (orange) and the water filter (blue) in the inlet basin.

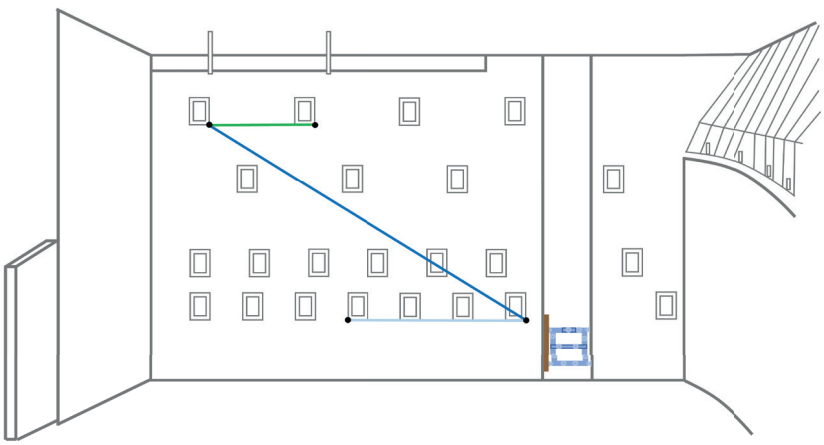

Fig. 4 Sketch of the water lock wall, the mounted calibration frame (blue object) and the measured lines for comparison: line 1 (green), line 2 (dark blue) and line 3 (light blue).

3.4 Camera calibration

The camera was calibrated in Agisoft Metashape conducting a self-calibration (Agisoft LLC, 2022). The standard frame camera model of Metashape with Brown Distortion Model was used (Brown, 1971).

The parameters focal length (f), principal point offset (x_0 and y_0), the radial distortion coefficients (K_1– K_4), the tangential distortion coefficients (P_1 and P_2) and the affinity and non-orthogonality coefficients (B_1 and B_2) were determined. Different parameter sets were examined by three methods (Table 2) with original or pre-processed white balanced images. The values are statistically tested using the Student's t-distribution as in (Harvey & Shortis, 1998).

3.5 3D Reconstruction

For 3D reconstruction, a dense point cloud was computed in Metashape with the self-calibrated cameras. The resulting point cloud of the water lock was compared to the reference scan using the plugin *M3C2* in (CloudCompare, 2023). Furthermore, the scale was controlled by three reference lines in the water lock (Fig. 4).

For the point cloud of the water filter no reference data was available. To assess the quality of this mission, a cylinder is fitted into the data using the tool *Best Cylinder* in Cyclone 3DR from Leica (Leica Geosystems AG, 2023) and the diameter is compared with the nominal value of the manufacturer (32.39 cm).

https://doi.org/10.58440/ihr-30-1-a04

Table 1 Summary of the image based acquisition.

Date	Evironement	Places	#Images	Distance [m]	Depth [m]
19.12.2022	In air	Indoor swimming pool	57	1.5-2	-
19.12.2022	In pool	Indoor swimming pool	202	2	2
30.11.2022	In river	Water lock	271	0.1-2	1, 3, 5, 7, 10
20.01.2023	In river	Water lock	1594	0.1-2	0.5-10
20.01.2023	In river	Water filter	359	0.1-2	0.5-5

Table 2 Overview calibration methods.

Method	White balanced images	f	x_0	y_0	K_1	K_2	K_3	K_4	P_1	P_2	B_1	B_2
1	-	x	x	x	x	x	x	-	x	x	-	-
2	x	x	x	x	x	x	x	-	x	x	-	-
3	-	x	x	x	x	x	x	x	x	x	x	x

4 Results

4.1 Camera calibration

All missions and methods varied significantly, hence, a mission with Method 1 was divided into three parts of 20 images each. For these parts the calibration was recalculated. Fig. 5 shows that even in one mission the camera results in significantly different parameters.

4.2 3D Reconstruction

The processed point clouds of the water lock were compared to the reference scan for each calibration method. Fig. 6 shows a close-up of the histograms of the deviation between 3D reconstruction and reference scan. 80 % of the points in the point cloud of Method 1, 78 % of Method 2 and 80 % of Method 3 differ less than 1 cm.

The reference lines show similar results (Table 3). The largest differences occur at the shortest reference distance, which is slightly extrapolating and has less image overlap. One mission (*based frame* at last column) shows greater differences with an average of 3.6 cm. The mission is orientated based on the calibration frame only and thus the lines were extrapolated.

The reconstruction of the water filter (Fig. 5) is referenced based on the calibration frame and results in a very dense point cloud (point distance up to 0.3 mm). However, the reconstructed point cloud has missing parts.

The *Best Cylinder* tool was applied to the points of the pipe and results in a cylinder with a diameter of 33.12 cm (Fig. 6). Therefore, a difference of 0.73 cm to the nominal diameter resulted.

5 Discussion

The camera calibrations of the different missions, as well as the different calibration methods, show a significant variability (Fig. 3). Possible explanations are the instable mounting in the water housing and the autofocus.

However, as discussed by Luhmann (2018), if the 3D measurements in object space later turns out

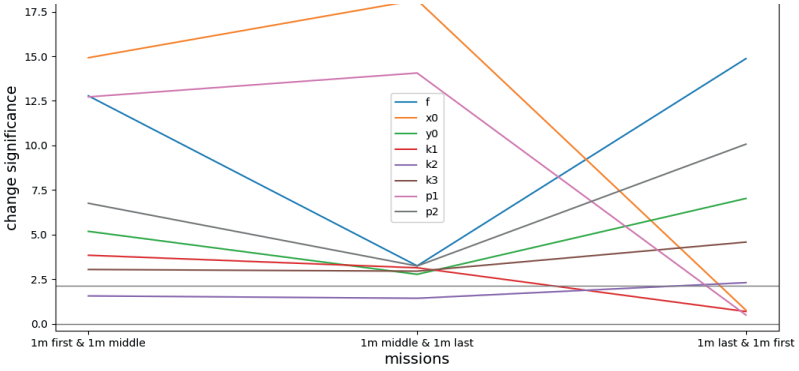

Fig. 5 Significant change of the first, middle and last part with Method 1.

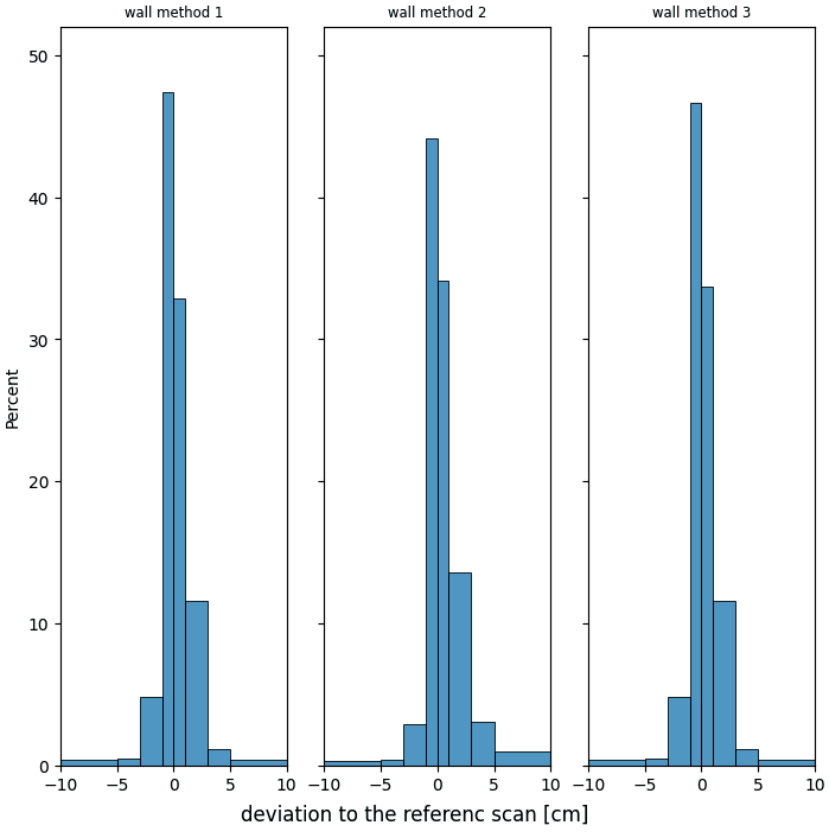

Fig. 6 Deviation per calibration method of the point cloud to the reference scan (close up).

Table 3 Comparison of line measurements in the point cloud and the reference scan.

		Reference scan	TS60 points	Photogrammetric reconstruction						Reconstruction-based frame	
				Δ Method 1 [m]	Δ Method 2 [m]	Δ Method 3 [m]	Δ Method 1 [cm]	Δ Method 2 [cm]	Δ Method 3 [cm]	Method 1 [m]	Δ Method 1 [cm]
Line	1	3.722	3.725	3.709	3.713	3,708	1.6	1.2	1.7	3.684	4.1
	2	5.835	-	5.838	5.835	5.836	0.3	0.0	0.1	5.825	1.0
	3	12.764	12.764	12.766	12.768	12.766	0.2	0.4	0.2	12.706	5.8
						Ø	0.7	0.6	0.7		3.6

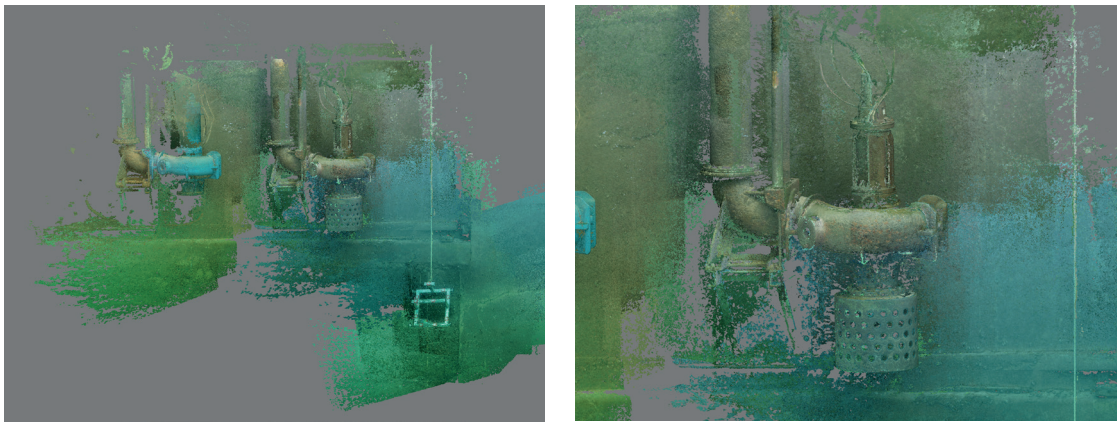

Fig. 7 Point cloud of the water filter (left) close up (right).

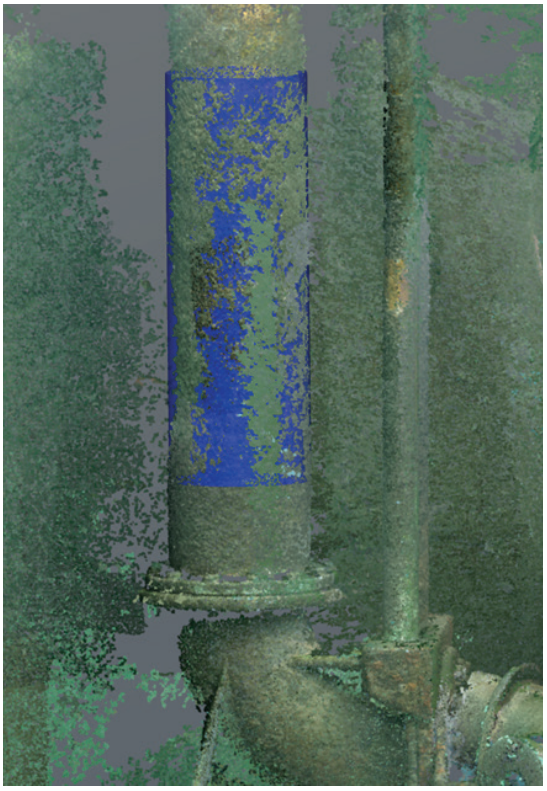

Fig. 8 Calculated cylinder for the pipe in the point cloud of the water filter.

sufficiently accurate, the corresponding camera calibration is also sufficient. Hence, the processing of the 3D reconstruction can successfully be carried out and investigated.

For each method, a point cloud was reconstructed. There are no major differences between the calibration methods (Fig. 4). Only the point clouds from Method 2 are slightly more widely distributed than those from the other methods. The white balanced images do not improve the results of these missions. Since Method 3 uses more parameters, there are more uncertainties possible. Therefore, it is recommended to use Method 1.

The largest deviations of the distances were found in the extrapolated areas of the water lock, while areas within the control points showed only a deviation of 1 cm. The results from the mission, which orientation is based on the calibration frame, revealed even larger deviations.

The water filter could be reconstructed as a 3D point cloud (Fig. 5). There are certain holes in the point cloud which are probably from a small image overlap, the fixed acquisition angle of the camera or the difficulties with the access of the object. The tool *Best Cylinder* fits a cylinder in the point cloud. Despite the large extrapolation, as is referenced based on the calibration frame, the difference is 0.73 cm to the nominal diameter.

6 Conclusion and outlook

The photogrammetric reconstruction of underwater objects was successfully implemented with the current set-up. Thanks to the calibration frame and additional control points, true-to-scale and very dense point clouds can be reconstructed, which can be used for further purposes. With well distributed control points, accuracies of sub-centimetres at distances of up to 6 m and 80 % of the points within a deviation of ± 1 cm can be achieved.

While survey areas framed by control points showed less deviation than 1 cm, the largest deviations of the distances were found in the extrapolated areas of the water lock. More calibration frames or scale positioning

https://doi.org/10.58440/ihr-30-1-a04

in the area could potentially reduce the distortion over larger distances. Future research should be in this field.

The calibration results of the different missions and methods show a significant variability. Further investigations with improved camera mounting and better camera control are needed to determine the cause of these variations. A good camera calibration could improve the accuracy of extrapolation.

The water filter was successfully reconstructed as a 3D point cloud, however there are some limitations with this set-up as the point cloud has holes. This can be attributed to low image overlap, the fixed acquisition angle of the camera or the lack of access. The tool *Best Cylinder* could successfully fit a cylinder into the point cloud, despite the large extrapolation.

References

Agisoft LLC (2022). *Agisoft Metashape*. https://www.agisoft.com/ (accessed 10 Oct. 2022).

Aragón, E., Munar, S., Rodríguez, J. and Yamafune, K. (2018). Underwater photogrammetric monitoring techniques for mid-depth shipwrecks. *Journal of Cultural Heritage, 34*, pp. 255–

260. https://doi.org/10.1016/j.culher.2017.12.007

BFE (2022). *Wasserkraft*. https://www.bfe.admin.ch/bfe/de/home/versorgung/erneuerbare-energien/wasserkraft.html (accessed 3 Oct. 2022).

Blue Robotics Inc (2022). *BlueROV2*. https://bluerobotics.com/store/rov/bluerov2/ (accessed 22 Sept. 2022).

Brown, D. C. (1971). Close-range camera calibration. *Photogramm. Eng, 37*(8), pp. 855–866.

Bruno, F., Lagudi, A., Gallo, A., Muzzupappa, M., Davidde Petriaggi, B. and Passaro, S. (2015). 3D Documentation of Archaeological Remains in the Underwater Park of Baiae. *The International Archives of the Photogrammetry, Remote Sensing and Spatial Information Sciences, XL-5/W5*, pp. 41–46. https://doi.org/10.5194/isprsarchives-XL-5-W5-41-2015

Chemisky, B., Menna, F., Nocerino, E. and Drap, P. (2021). Underwater Survey for Oil and Gas Industry: A Review of Close Range Optical Methods. *Remote Sensing, 13*(14), p. 2789. https://doi.org/10.3390/rs13142789

CloudCompare, 2023. *CloudCompare – Open Source project*. http://www.cloudcompare.org/ (accessed 1 Feb. 2023).

Harvey, E. S. and Shortis, M. R. (1998). Calibration stability of an underwater stereo-video system: implications for measurement accuracy and precision. *Marine Technology Society Journal, 32*(2), pp. 3–17.

Leica Geosystems AG, 2023. *Leica Cyclone 3DR*. https://leica- geosystems.com/de-CH/products/laser-scanners/software/leica-cyclone/leica-cyclone-3dr (accessed 1 Feb. 2023).

Luhmann, T. (2018). *Nahbereichsphotogrammetrie: Grundlagen – Methoden – Beispiele* (4th ed.). Wichmann.

McCarthy, J. and Benjamin, J. (2014). Multi-image Photogrammetry for Underwater Archaeological Site Recording: An Accessible, Diver-Based Approach. *Journal of Maritime Archaeology, 9*(1), pp. 95–114. https://doi.org/10.1007/s11457-014-9127-7

Menna, F., Nocerino, E. and Remondino, F. (2017). Flat vs Hemispherical Dome Ports in Underwater Photogrammetry. *The International Archives of the Photogrammetry, Remote Sensing and Spatial Information Sciences, XLII-2/W3*, pp. 481–487. https://doi.org/10.5194/isprs-archives-XLII-2-W3-481-2017

Neyer, F., Nocerino, E. and Gruen, A. (2018). Monitoring Coral Growth - Comparing Underwater Photogrammetry and Geodetic Control Network. *The International Archives of the Photogrammetry, Remote Sensing and Spatial Information Sciences, XLII–2*, pp. 759– 766. https://doi.org/10.5194/isprs-archives-XLII-2-759-2018

Seafrogs (2023). *Sony A7 II NG V.2 Series UW camera housing kit with 8" Dome port*. https://seafrogs.com.hk/ (accessed 17 Jan. 2023).

Shortis, M. (2019). Camera Calibration Techniques for Accurate Measurement Underwater. In J. K. McCarthy, J. Benjamin, T. Winton and W. van Duivenvoorde (Eds.), *3D Recording and Interpretation for Maritime Archaeology* (pp. 11–27). Springer International Publishing. https://doi.org/10.1007/978-3-030-03635-5_2

Sony Europe B.V (2022). *Sony Alpha 7 II*.

https://www.sony.ch/de/electronics/wechselobjektivkameras/ilce-7m2-body-kit (accessed 17 Jan. 2023).

Author's biography

Manuela Ammann

Between 2012 and 2016, Manuela Ammann learned her surveying skills in an apprenticeship, setting the course for her career. At the FHNW in Muttenz, Switzerland, she immersed herself in geomatics and obtained a Bachelor's degree from 2016 to 2019. To deepen her knowledge, Manuela completed a Master's degree in Geoinformation Technology at the FHNW from 2020 to February 2023. During this time, she worked as a research assistant for Stephan Nebiker in the field of photogrammetry. This also opened the door to underwater photogrammetry. Since March 2023, Manuela has continued her academic and professional career as a research associate at the FHNW, working with Pia Bereuter in the field of geoinformation technology.

https://doi.org/10.58440/ihr-30-1-a04

PEER–REVIEWED ARTICLE

Spatial and temporal coverage of the cargo ship network for GNSS-based tsunami detection

Authors

Bruce Enki Oscar Thomas[1], James Foster[1] and Tasnîme Louartani[1,2]

Abstract

Tracking changes in sea-surface height with ship-based GNSS can be used to detect tsunamis. One year of navigation data from ships in the Pacific is examined to investigate how well-distributed a cargo-ship network would be for tsunami detection. There is excellent coverage of the most active tsunamigenic zones, with multiple ships predicted within 30-minutes travel time of notable tsunamis. Tsunamigenic regions with low ship density, such as the Southwest Pacific, require a greater percentage of ships participating to ensure sufficient data. The global nature of GNSS and ship routes make this a promising, low-cost approach, to augment tsunami detection.

Keywords

tsunami · ship-based · GNSS · AIS · Pacific Ocean

Résumé

Le suivi des variations de la hauteur de la surface de la mer à l'aide d'un système GNSS embarqué peut être utilisé pour détecter les tsunamis. Une année de données de navigation de navires dans le Pacifique est examinée afin de déterminer l'étendue de la couverture d'un réseau de navires pour la détection des tsunamis. La couverture géographique est excellente pour les zones tsunamigènes les plus actives : plusieurs exemples notables de tsunamis soulignent qu'un grand nombre de navires est à chaque fois prédit dans un rayon de 30 minutes de temps de déplacement du tsunami. Les régions sources de tsunami à faible densité de navires, telles que le Pacifique Sud-Ouest, nécessitent un plus grand nombre de navires participants pour garantir des données suffisantes. La couverture géographique permise par l'utilisation de GNSS à bord de navires en fait une approche prometteuse et peu coûteuse pour améliorer la détection des tsunamis.

Resumen

El seguimiento de los cambios de la altura de la superficie del mar basados en datos GNSS de buques puede ser utilizado para detectar tsunamis. Se examinó un año de datos de navegación de navíos en el Pacífico con el fin de investigar qué tan bien distribuida sería una red de buques de carga para la detección de tsunamis. Existe una excelente cobertura de las zonas tsunamigénicas más activas, con múltiples embarcaciones previstas en un tiempo de viaje de 30 minutos de tsunamis considerables. En cambio, las regiones tsunamigénicas con baja densidad de buques, como el Pacífico Sudoccidental, requieren un mayor porcentaje de barcos involucrados para garantizar datos suficientes. La naturaleza global de los datos GNSS y las rutas de estas embarcaciones hacen de éste un enfoque prometedor y de bajo costo para aumentar y mejorar la detección de tsunamis.

✉ Bruce Enki Oscar Thomas · bruce.thomas@gis.uni-stuttgart.de

[1] Institute of Geodesy (GIS), University of Stuttgart, 70174 Stuttgart, Germany

[2] ENSG-Geomatics, 77420 Champs-sur-Marne, France

https://doi.org/10.58440/ihr-30-1-a05

1 Introduction

Many of the most devastating natural hazards that impact our communities are generated over, or under, the oceans. Over the last 20 years, following the Indian Ocean tsunami, the number of tsunami related research publications and governmental actions in favor of faster tsunami detection and response has increased substantially (Chiu & Ho, 2007; Cummins et al., 2009; Løvholt et al., 2014; Synolakis & Bernard, 2006). However, many recent tsunamis were surprisingly unexpected due to their amplitude, location or unusual source. For example, the 2011 Tōhoku-oki tsunami exceeded maximum predictions (Goto et al., 2011; Kagan & Jackson, 2013), and one year later, the 2012 Haida Gwaii tsunami occurred in an uncommon source region (Fine et al., 2015; Leonard et al., 2012). Later, the dual 2018 Indonesian tsunamis were generated by non-standard tsunamigenic earthquake mechanisms (Grilli et al., 2019; Schambach et al., 2021; Titov, 2021). More recently, the powerful 2022 Hunga Tonga Hunga Ha'apai (HTHH) tsunami was generated by a rare combination of atmospheric forcing, volcanic eruption, submarine landslide and local resonance (Gusman et al., 2022; Han & Yu, 2022; Lynett et al., 2022).

Most of the existing observing capacity to predict and detect these tsunamis is either located on land, like the seismic network and land-based Global Navigation Satellite System (GNSS), on the coastline, like the tide-gauges, or close to the shore, such as GNSS buoys. Deep water observations are provided by Ocean Bottom Pressure Gauges (OBPGs) and the Deep-Ocean Assessment and Reporting of Tsunami (DART) array (Bernard & Meinig, 2011; Bouchard et al., 2007). However, many tsunami events have emphasized that those sensors are sparsely located (Gusman et al., 2016) and often offline due to weather conditions, maintenance difficulties or vandalism (Xerandy et al., 2015). Moreover, the DART observing network is very costly, installed mainly by wealthy countries such as the USA or Japan, and therefore unlikely to be adopted in a dense worldwide configuration (Jin & Lin, 2011; Mulia & Satake, 2020; Qayyum et al., 2022). Current Tsunami Early Warning Systems (TEWS) implemented worldwide are typically based on detecting and characterizing tsunamigenic earthquakes occurring in subduction zones and, therefore, do not always adequately address other sources like the ones detailed above (Amato, 2020; Srinivasa Kumar & Manneela, 2021). Each of these tsunami events above showed issues with the observing capacity in the region, or during the computation of tsunami models or inundation predictions, limiting our ability to predict, detect, and respond to these hazards. They demonstrate the urgent need for well distributed, more densely spaced, observations and direct measurements from the areas between the source region and the communities that may be impacted – that is, across the oceans. A key challenge, therefore, in improving our tsunami observing capacity in the oceans and filling up this "geodetic desert" is how to achieve this at a minimal cost. Several new projects and technologies have emerged in recent years, allowing us to directly obtain data of interest for tsunami forecasting from the ocean.

First, seafloor geodetic techniques offer unique possibilities to measure crustal deformation that can result in tsunami hazards (Bürgmann & Chadwell, 2014). Several projects offshore Japan (Iinuma et al., 2021), Alaska (Brooks et al., 2023), Cascadia (Chadwell et al., 2018), Hawai'i (Brooks et al., 2021; Foster et al., 2020), and Chile (Kopp et al., 2022) have shown significant advances in the more precise understanding of the tectonic processes in areas usually inaccessible to standard geodetic instruments. While most of these techniques are expensive, recent technologies using Wave Glider ocean robots promise lower-cost seafloor geodetic systems (Brooks et al., 2021; Foster et al., 2020). Dedicated seafloor cable installations for tsunami detection and early warning have been implemented in Japan, first around the Nankai Trough with the Deep Ocean-floor Network system for Earthquakes and Tsunamis (DONET; Kawaguchi et al., 2008), then with a larger-scaled observatory along all the Japan Trench with the Seafloor Observation Network for Earthquakes and Tsunamis (S-net; Mulia & Satake, 2021). The North-East Pacific Time-Series Undersea Networked Experiments (NEPTUNE) on the west coast of Canada is another example of regional cabled ocean observatory: installed for multi-purpose research, it includes several instrumentations for tsunami monitoring (Barnes et al., 2008). Science Monitoring And Reliable Telecommunications Subsea Cables (SMART) represent another promising approach for tsunami detection and observation by using the existing submarine telecommunications cables as sensors combining a pressure sensor, seismic instrument, and an accelerometer (Howe et al., 2019). New developments aim to cover all the oceans globally through regional pilot systems, for example, the triangle Europe – Azores – Madeira (Matias et al., 2021), the Sumatra – Java region (Salaree et al., 2023), and the New Caledonia – Vanuatu – Hawai'i line in the Pacific (Howe et al., 2022).

Other projects concentrate on data coming from above the ocean. The displacement of the ocean surface during a tsunami directly transfers a fraction of this energy to the atmosphere through internal gravity waves. This causes measurable perturbations in the ionospheric total electron content (TEC) that dual-frequency GNSS systems can detect (Astafyeva, 2019; Occhipinti et al., 2008). Initial projects based on this method use continuous GNSS ground-based sites to detect these variations (e.g. 2012 Haida Gwaii tsunami: Savastano et al., 2017; 2010 Mentawai tsunami: Manta et al., 2020). A few recent projects test these systems on board of ships (e.g. 2010 Maule tsunami: Ravanelli & Foster, 2020) highlighting new possibilities for open ocean tsunami detection.

A tsunami is a perturbation of the topography of the sea surface. Measurements of sea surface height (SSH) perturbations are already made on land by tide-gauges and in the ocean by OBPGs. Some projects have explored airborne measurements of SSH using an aircraft equipped with a radar altimeter (Mulia et al., 2020). Satellite altimetry data also provides direct measurements of changes in sea level, enabling us to compare and validate tsunami models after an event (Hamlington et al., 2011; Hébert et al., 2020; Hirata et al., 2006; Okal et al., 1999). Satellites, however, are very costly and the temporal and spatial coverage remain sparse thus limits their capability. More cost-effective improvements for operational tsunami monitoring deploy sensors on existing ocean platforms. SSH measurements and tsunamis detection are already made using GNSS static buoys along the coast of Japan (Kawai et al., 2013). Several studies also demonstrated the efficiency of using a GNSS-based approach on board ships to measure SSH and even wave periods (Bonnefond et al., 2003; Foster et al., 2014; Rocken et al., 2005) and thus to be able to detect offshore tsunamis (Foster et al., 2012; Inazu et al., 2016).

Treated as moving tide gauges, ships can then provide a platform for new tsunami warning sensors. Packages have already been proposed and deployed: they are composed of a GNSS receiver and antenna for data collection, as well as a communication link with a land-based server using a satellite communication antenna (Foster et al., 2012; Foster et al., 2024). To obtain precise real-time position estimations at low-cost and avoid data loss, the onboard GNSS receiver directly processes the raw data using a commercial positioning service with a high accuracy on the vertical component (Foster et al., 2024). The final positions are then broadcasted to a server located on land through a dedicated satellite communication antenna, or even better for a cost-effective solution, by directly using the existing internet service from the ship. The vertical position given is the ellipsoidal height of the GNSS antenna. To estimate SSH perturbations from this raw data, a mean sea surface height model is applied and removed from the time series, followed by band-pass filtering to remove the ocean wave field (Foster et al., 2012, Foster et al., 2024). Tested both in coastal areas and in the deep ocean, this technique has shown the ability to detect ~10 cm tsunami amplitudes (Foster et al., 2009; Inazu et al., 2016) and ~10 $cm.s^{-1}$ accuracy of tsunami currents (Inazu et al., 2020). Using offshore observations is a powerful tool to improve field tsunami forecasting because they provide a snapshot of the open-ocean SSH and enable direct tsunami detection rather than inferring them through modeling the tsunami source (Mulia et al., 2022). The combination of offshore datasets, tsunami models and onshore datasets enables an iterative approach combining numerical modeling and comparison with observations and is already used in Japan for tsunami monitoring (Inazu et al., 2016; Mulia et al., 2017; Tsushima et al., 2014).

Dense observatories of sensors for earthquake and tsunami detection and warning would be helpful throughout the ocean. In this context, this study investigates a proposed cargo ship network for GNSS-based tsunami detection to fill this geodetic observation gap in the ocean by tracking changes in SSH and detecting even small, ~10 cm amplitude tsunamis from different sources. The first question that arises is the temporal coverage of such a cargo network, specifically: are there enough ships underway in the Pacific Ocean at all times? A correlated question concerns the spatial coverage of this network, to identify areas with less maritime traffic and therefore fewer observation points of data. A first overview of the shipping lines in the Pacific Ocean shows an excellent temporal and spatial coverage of ships (Fig. 1). Thus, this study aims (i) to analyze in detail the traffic using Automatic Identification

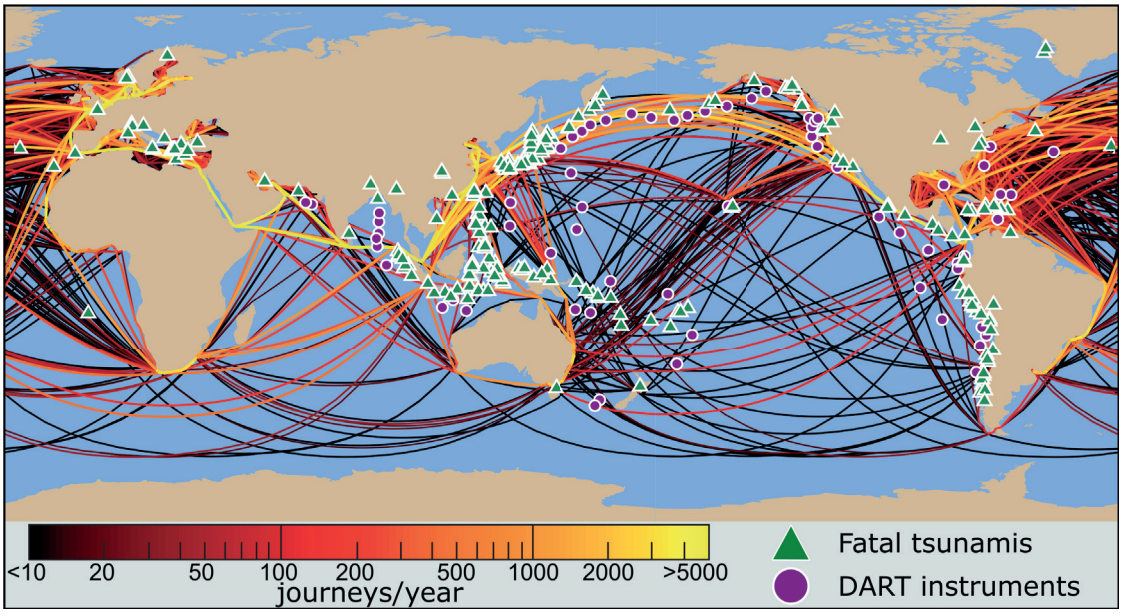

Fig. 1 Map of main commercial ship routes color-coded by frequency (data from Kaluza et al., 2010). Green triangles: sources of historical fatal tsunamis (NGDT, 2023). Purple dots: DART instruments (NOAA, 2023).

https://doi.org/10.58440/ihr-30-1-a05

Service (AIS) datasets recorded from ships and (ii) to compare an average network of ships to tsunami sources. Our goal is to assess this proposed ship network for GNSS-based tsunami detection: (i) on its contribution to trans-oceanic tsunami detection and characterization, (ii) on its early warning possibilities, and (iii) on its worldwide application as a cost-effective solution for tsunami warning. The paper finally explores the suitability of such a moving platform in the oceans to host a tsunami detection network.

2 Methodology: mapping ship traffic for a tsunami detection application

The International Maritime Organization (IMO) regulations state that all commercial ships exceeding 300 gross tonnages have to send their AIS information via very-high-frequency radio transmission: these are either received by coastal stations when the ships are less than 100 km from the coast, or through low-Earth-orbit satellites (Carson-Jackson, 2012; IMO, 2002). The AIS messages provide essential information in both static components – Maritime Mobile Service Identity (MMSI), ship type, and ship name – and dynamic components – time, coordinates except height, speed over ground, course over ground, and ship heading – (Le Tixerant et al., 2018). Real-time data is available through tracking browsers such as MarineTraffic[1].

The present study focuses on the Pacific Ocean, the region with the highest tsunamigenic potential (Gusiakov et al., 2019; Lander et al., 2003; Röbke & Vött, 2017). We use the records of hourly positions of ships (latitude and longitude) from one year of AIS navigation data from the commercial shipping fleet to generate coverage maps of large vessels in the Pacific region. Multiple records in an hour from the same ship are removed by verifying the MMSI (nominally unique) for each ship. On the contrary, breaks in the ships' AIS data stream make them not always visible in every hourly file. The data provided by commercial company SPIRE Maritime was collected from October 15, 2018 to October 14, 2019. Only records of large commercial vessels designated as cargo or tankers are used in our analysis as these are the types of ships most likely to easily and effectively participate in a tsunami detection program as they spend most of their time underway and typically have satellite internet connections. The study covers a pre-COVID-19 pandemic period with similar patterns in ship lines as now (UNCTAD, 2023). We note that the ship positions reported in AIS messages are not generally available in real-time, are low accuracy, and do not include the ship elevation, which prevents current AIS system itself to be applied to tsunami detection.

Several statistical coverage maps of ships are generated using a 500 km × 500 km grid over the Pacific Ocean. The choice of a 500 km cell size matches the average distance between DART sensors (calculated from DART data provided by NOAA, 2023). We look at the hourly mean number of ships in each cell, creating a heat map of ships in the Pacific region for different epochs. For reference, at typical propagation speeds (800 km/h), a tsunami wave would cross one of our boxes in less than 40 minutes, while a cargo ship with a typical cruise speed of 40 km/h would take more than 12 hours to cover the same distance. An overlap of these spatial and temporal coverage maps with tsunami travel time (TTT) and tsunami models enables a direct comparison with known tsunami source regions. For this study, a 10 cm tsunami threshold is used as a constraint to identify the ships' network coverage during a tsunami propagation. This choice also corresponds to ~10 cm deep-ocean tsunami threshold used in warning purposes to identify land threatening tsunamis. We note that if modern precise real-time position GNSS estimations can easily reach vertical accuracies less than 5 cm (Li et al., 2015; Nie et al., 2020; Trimble, 2024), ongoing studies show that the signal filtering process identify for now a tsunami detection threshold of 10 cm (Foster et al., 2012; Foster et al., 2024; Inazu et al., 2016).

3 Results: first insights on geographic ships' coverage of fatal tsunamis

Over one year of data, there are on average ~38,000 cargo and tanker ships at any time spread out in the Pacific Ocean (Fig. 2). Different epochs of study can be used as a base of comparison: for example, the hourly mean number of ships over each season shows a similar pattern in the overall coverage, with a density slightly higher during spring and autumn periods corresponding to an increase in trade exchange for holiday seasons, known as peak season (Yin & Shi, 2018). The highest numbers are located along coastlines, especially in East Asia: ~36,000 ships, on average, are located less than 500 km from coast at any time. More than 10,000 ships on average are in the cell centered in (29.3,122.6) corresponding to Shanghai, the busiest port in the world (WSC, 2023). Complementary monthly time series of the average number of ships for some cells locating historic tsunamis are shown in Fig. 3, highlighting an overall similar trend along the year with few seasonal variations. These patterns precisely match the common maritime routes along the coastlines in America and Asia, between the islands in Southeast Asia and Oceania, and across the North Pacific through Hawai'i (Rodrigue, 2017). However, the standard deviation and/or interquartile range of the AIS data in these cells shows some important variabilities. This can be explained partly by breaks in

[1] https://www.marinetraffic.com/ (accessed 27 March 2024).

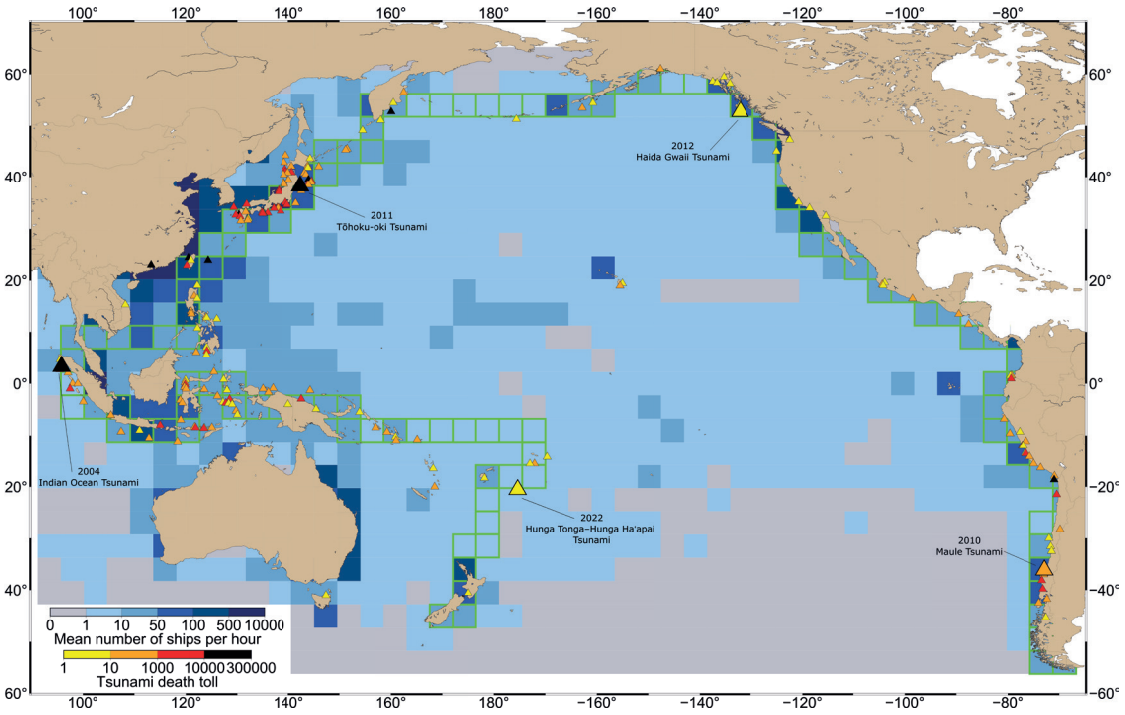

Fig. 2 Map of the hourly mean number of ships per 500 km square, based on one year of AIS data provided by SPIRE Maritime. Triangles: source location of historic fatal tsunamis color-coded by death toll (NGDT, 2023). Green highlighted cells locate the Pacific Ring of Fire, based on trench locations (Bird, 2003).

the ships' records. Secondly, when creating the grid, each cell location is defined and treated separately from the neighboring ones; thus, depending on the specific distribution of the maritime traffic and the instantaneous locations of ships with respect to the cell boundaries, the total number of vessels can significantly fluctuate. This variability is meaningful for cells with an hourly mean number of vessels above 100. For regions with low traffic, variations in the specific locations of those few ships lead to large standard deviations for the cells, but do not represent proportionately significant variations in regional traffic. In one key tsunami area with low ship counts – the South West Pacific – there is at least one ship in each cell.

Tsunamigenic areas in the Pacific Ocean are mainly located along the subduction zones where tectonic processes generate earthquakes, volcano activity, landslides and tsunamis. This so-called Pacific Ring of Fire is highlighted in Fig. 2 and unfolded as a histogram of the mean number of ships per cell location in Fig. 4: starting from the southern point of New Zealand, through the South-West Pacific islands, curving around Indonesia before reaching the Philippines then following the trench along Japan to Russia and up to Alaska, to finally run along all the west American coast (where a large section of the tectonic boundary is a strike-slip fault) from Canada to Chile. We explore the geographic relationship between the ships' locations and some of the deadliest tsunami sources. Of the 124 cells studied, half of them have been a source of a fatal tsunami: the 30-min TTT corresponds then to the cell size (for a typical deep-ocean tsunami speed of 800 km/h), meaning that we can consider that the number of ships represented in each cell (Fig. 2), or each line (Fig. 4) corresponds to the number of ships located in a 30-min TTT. Based on the deadliest tsunami taking its source from the mentioned cells, the total death count rises above 400,000 (Fig. 4). Our data suggests that a total of ~4,000 ships are located on average in the 124 cells studied. A zoom in shows that seven cells are sources of tsunamis with local and trans-oceanic death tolls above 10,000 and have a count of more than 800 ships on average per hour. As observed in Fig. 2 and confirmed in Fig. 4, the South-West Pacific zone lacks heavy ship traffic despite two thirds of its area being a source of fatal tsunamis. This is true to a lesser extent, for the Kamchatka – Alaska area and some of the Central America west coast. These maps demonstrate that commercial shipping lines offer a unique and broader range of observations that could augment the existing observing systems by providing (i) an excellent spatial coverage of the ocean globally, (ii) a spatial coverage very dense near coastlines critical for local and regional early warning, and (iii) an excellent temporal coverage of the ocean globally with few blind spots in the South Pacific.

4 Discussion: contribution of a ship-based GNSS network for tsunami detection

We envision the proposed GNSS package as being installed on ships through a voluntary participation program. As a realistic goal for our proposed network, we use the existing Voluntary Observing Ship (VOS) program which provides observations of marine meteorology (Foster et al., 2012; Kent et al., 2010) as a template. It is estimated that 11 % of the commercial fleet is part of the VOS scheme which equates to ~4,000 ships in the Pacific. For our study, we imagine a similar network of "Voluntary Tsunami Observing Ships" (VTOS) that comprise of 11 % of the cargo and tanker ships reported in the AIS database. The following discussion aims to deliver

https://doi.org/10.58440/ihr-30-1-a05

answers on the potential contribution to tsunami warning of these VTOS ships located in the near-field and in the far-field of a tsunami event.

4.1 Ships in the near-field of tsunami events

On October 28, 2012, a major Mw 7.7 thrust earthquake occurred along the Queen Charlotte Fault Zone off the southern west coast of the Haida Gwaii archipelago in Canada (USGS, 2012), and generated a non-destructive tsunami measured all along the USA west coast, in Hawai'i and throughout the Pacific (Cassidy et al., 2014; ITIC, 2012). However, apart from a few observations from post-tsunami field surveys with run-ups up to 13 m in neighboring islands (James et al., 2013; Leonard & Bednarski, 2014), no other observation in the near-field zone was reported. Few tide gauges are installed locally, and the tsunami occurred in the middle of the largest 1,360 km gap in the DART network along the North America coast (Fig. 5). Moreover, the near-field warning can be challenging with older-generation DART buoys that would likely miss a tsunami signal due to the aliasing with high-frequency acoustic noise within the source region (Tilmann et al., 2016). As summarized by Fine et al. (2015), the on-land instruments such as seismic and GPS stations do not provide enough information for a precise seafloor displacement estimation in the source area, which makes it challenging to obtain an accurate tsunami model in the near-field zone.

The 2012 Haida Gwaii tsunami provides an instructive case for examining the potential contribution to tsunami warning of ships in the near-field of a tsunami. The tsunami model and the predicted amplitudes are compared to the coverage of vessels in the Pacific (Fig. 5). On average, there are ~15 VTOS ships within the area encompassed by the 30-min TTT – where no real-time tide gauges or DART sites were located. In the dense cells with more than 50 ships (deep blue circles in Fig. 5), the standard deviation climbs to 40 % of the average of ships. The minimum count of ships in each cell shows that, temporally speaking, at least 7 VTOS ships are always present in the 30-min TTT. In the near-field of a tsunami event, the important data to obtain is estimations of heights and periods to detect the propagating tsunami wave. This zone had predicted amplitudes greater than 10 cm (color-scale in Fig. 5 in purple and red). If a ship-based network had been operational during this event, ~15 SSH observations would have been added, enabling a tsunami detection less than half an hour after the earthquake. This set-up of more than five ships would be sufficient to trigger a confident warning: Foster et al. (2012) show that with five or more vessels, the chance of a false positive detection is less than 0.1 %. Within a 1-hour TTT, the network would be composed of ~33 VTOS ships that could contribute even more to a real-time imaging of the tsunami propagation.

The 2012 Haida Gwaii tsunami can be compared to the 2011 Tōhoku-oki tsunami. As noted above, the Haida Gwaii region is not covered by permanent and overlapping instrument networks. In contrast, the Tōhoku region is surrounded by a significant number of in-land, coastal and deep-ocean instruments providing numerous records and ensuring a quick calculation of the tsunami source function (Hayashi et al., 2011; Satake et al., 2013). The Haida Gwaii area is an uncommon source region for such a tsunami; indeed, only two other very small tsunamis were reported in this region (Leonard et al., 2010; Rabinovich et al., 2008; Soloviev & Go, 1975). The low expected probability of a tsunami generated in this region (Leonard et al., 2012) demonstrates the potentially critical role of open-ocean tsunami observations in augmenting existing systems (Fine et al., 2015). Such a ship-based GPS network in this location would (i)

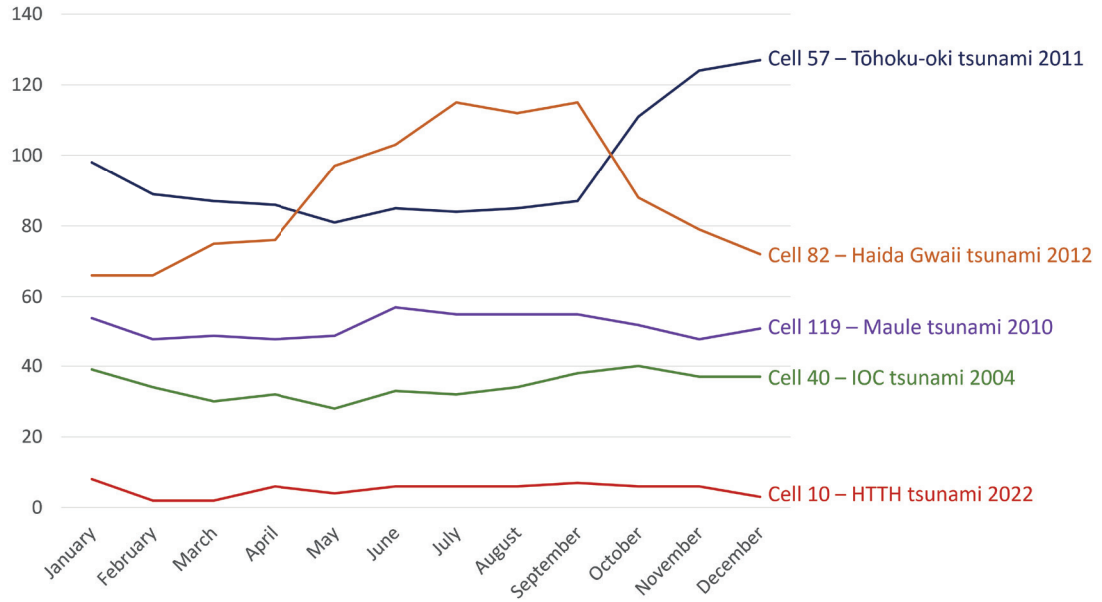

Fig. 3 Monthly time series of the hourly mean number of ships for five cells locating historic tsunamis (for the mentioned tsunamis in Fig. 2).

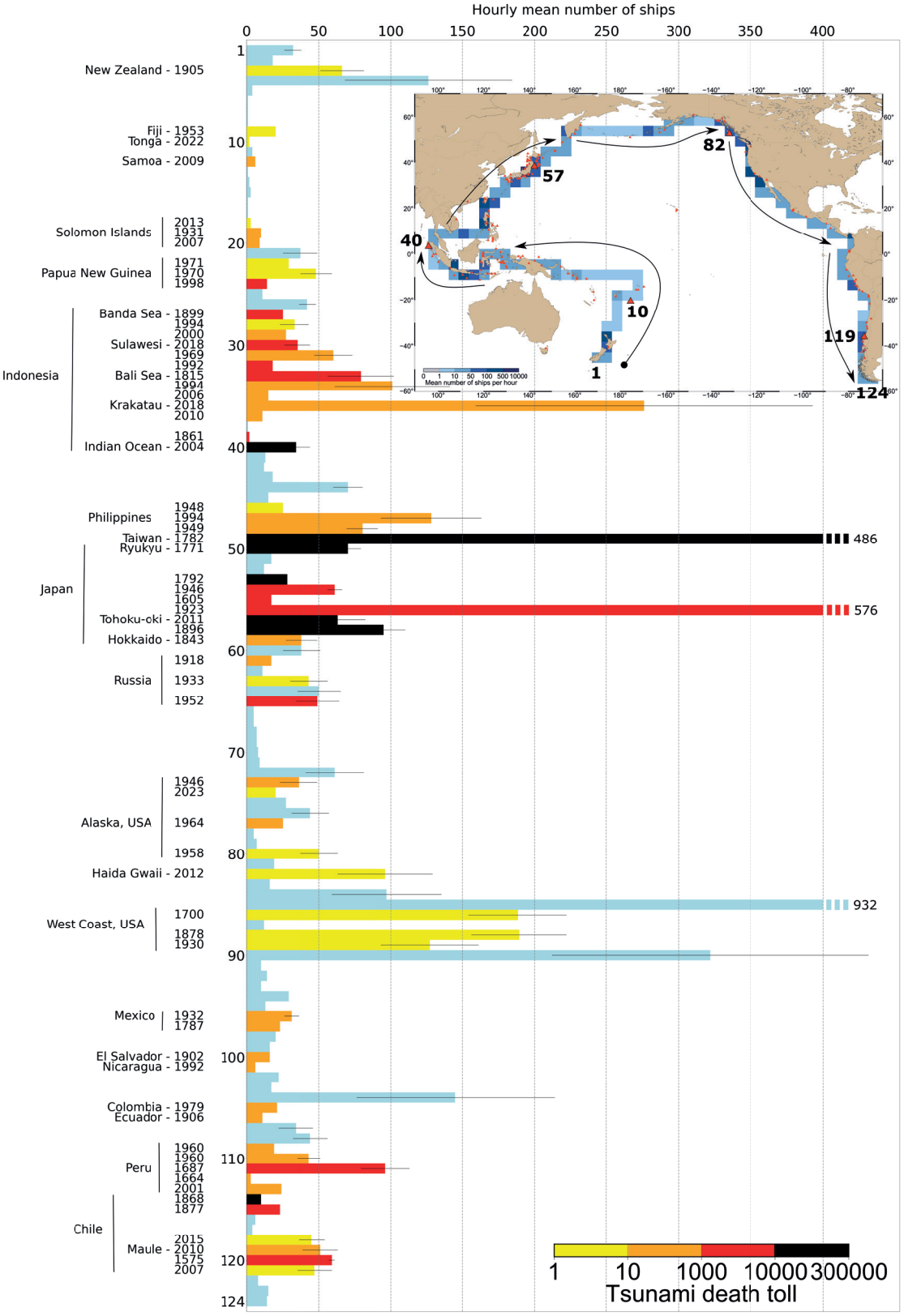

Fig. 4 Histogram of the hourly mean number of ships (axe *x*) per cell along the Pacific Ring of Fire, based on trench locations (Bird, 2003). The name of the deadliest tsunami that took source in the area defined by the cell is indicated left of each bar and the color scale shows its death toll (NGDT, 2023). The blue cells indicate possible zones source of tsunamis, but with no historic fatal tsunami recorded. The map inset precisely indicates the direction of the Pacific Ring of Fire unfolding. Numbers indicate the position of the cell / fatal tsunami along axe *y*.

validate the existence and arrival time of a tsunami and (ii) give accurate first estimates of tsunami height and period in one of the most major maritime lines in the Pacific. For the 2011 Tōhoku-oki tsunami ~100 VTOS ships on average are located in the 30-min TTT. This compares to the actual 16 near-coast ships that sent AIS information in this time frame (depth of ~100 m) (Inazu et al., 2018). Therefore, a ship-based GPS network would be a major contribution to tsunami early warning and fast response emergency by adding numerous observation points in the near-field open-ocean tsunami area (Hossen et al., 2021).

Tsunamis in the Pacific are often trans-oceanic. Although the death toll and damages are primarily focused in the near-field, they can strongly impact regions thousands of kilometers away from the initial

https://doi.org/10.58440/ihr-30-1-a05

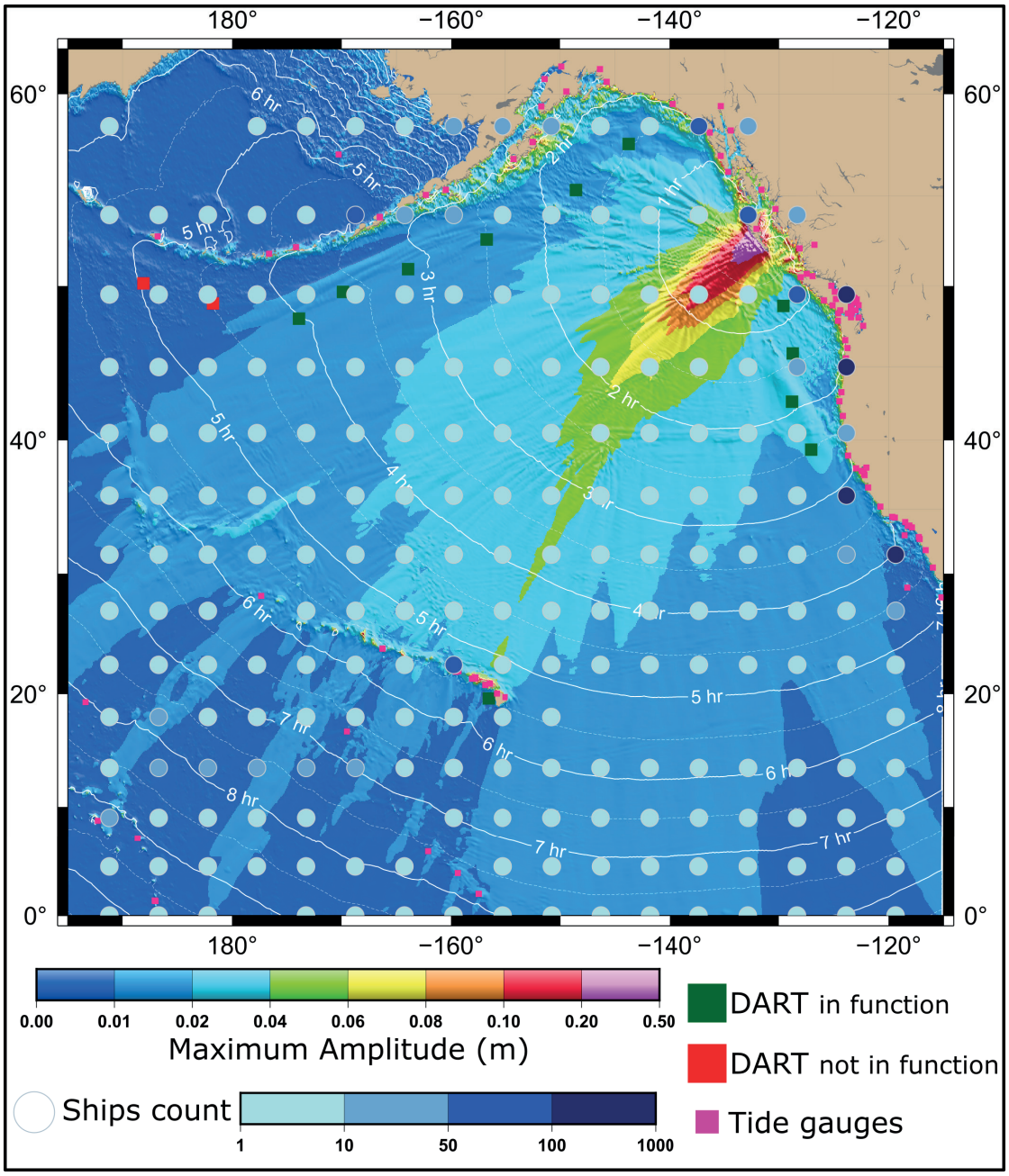

Fig. 5 Hourly mean number of ships coverage over the 2012 Haida Gwaii tsunami model. The tsunami model of maximum amplitude (colormap) is based on a RIFT model (Wang et al., 2009) from the Haida Gwaii M_W 7.7 earthquake (source parameters: Dziewonski et al., 1981; Ekström et al., 2012). White contours: TTT (http://www.geoware-online.com/). Blue-coded circles: ships coverage. Green squares: DART in function during the event. Red squares: DART not in function during the event (NOAA, 2023). Pink squares: tide gauges (Holgate et al., 2013; PSMSL, 2024).

source. The International Tsunami Information Center (ITIC) lists tsunamis that have caused deaths more than 1,000 km from the source (ITIC, 2019). Haida Gwaii is listed with one death in Hawai'i (USA) during the evacuation, as well as several tsunamis generated in Chile and impacting several South-West Pacific islands, the Philippines, Japan and North-America west coast. The Pacific Tsunami Warning Center (PTWC) also generates "enhanced products" which provide more targeted predictions of run-up for specific coastlines during tsunami events (IOC, 2014). These allow for more effective responses to events. Optimizing these products requires spatially dense imaging of the tsunami wavefield. Thus, the next step of this study is to analyze the contribution of a GNSS-based ship network tsunami detection on far-field events and impacts.

4.2 Ships in the far-field of tsunami events

On February 27, 2010, a megathrust earthquake of Mw 8.8 occurred in the subduction zone where the Nazca plate is under thrusting the South American plate and generated a destructive trans-oceanic tsunami in the Pacific known as the 2010 Maule tsunami (Fritz et al., 2011; USGS, 2010). The Maule tsunami killed hundreds of people and caused severe damage locally. It was observed and forced evacuation of coastal communities all around the Pacific. The 2010 Maule earthquake is one of a long history of similar events occurring offshore of Chile either in the same area in central-southern Chile (1928 Mw 8.0 event: Beck et al., 1998), or more north (1906 Mw 8.4 event: Lomnitz, 1970; 1985 Mw 7.8 event: Nakamura, 1992), or more south with the famous 1960 Mw 9.5 event (Cisternas et al., 2005). All these events generated tsunamis observed throughout the Pacific Ocean with significant

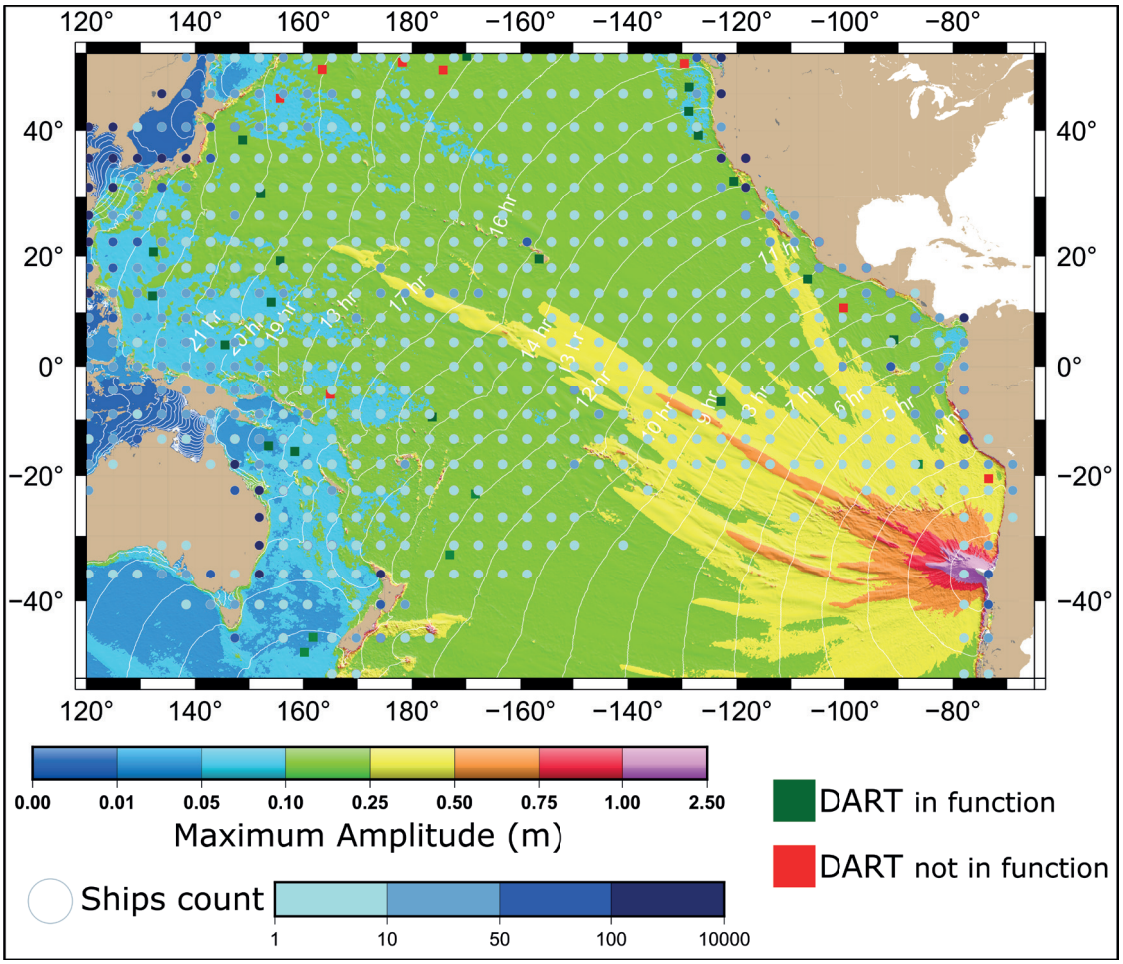

Fig. 6 Hourly mean number of ships coverage over the 2010 Maule tsunami model. The tsunami model of maximum amplitude (colormap) is based on a RIFT model (Wang et al., 2009) from the Maule M_W 8.8 earthquake (source parameters: Dziewonski et al., 1981; Ekström et al., 2012). White contours: TTT (http://www.geoware-online.com/). Blue-coded circles: ships coverage. Green squares: DART in function during the event. Red squares: DART not in function during the event (NOAA, 2023).

coastal impacts (ITIC, 2019). In comparison with the 1960 tsunami, the 2010 tsunami waves were at least three times smaller when hitting the coast of North America or Japan (Rabinovich et al., 2013).

The 2010 Maule tsunami is an interesting example of how ships both in the near-field and in the far-field of a tsunami could contribute to tsunami warning. In the 30-min TTT shown in Fig. 6, ~10 VTOS ships are located close to the coast with a standard deviation of 25 %. Thus, these ships could have provided real-time data to warning centers: a vital dataset that would contribute to more precise evacuation as the observed run-ups vary significantly on a local and regional scale (Fritz et al., 2011). In the far-field, the tsunami model shows amplitudes above 10 cm over almost two third of the Pacific (color-scale in Fig. 6 ranging from purple to green). Estimations from our AIS mapping in this area suggest ~300 VTOS ships on average. A quick comparison with the other historical events in the region and the seasonal frame of the events, shows similar numbers in ships coverage which suggest an excellent spatial and temporal coverage locally near the coast in Chile and confirms an overall excellent coverage on the Pacific. These numbers on the far-field aspect also underline that even if the tsunami event is small in amplitude, there are always ~300 new observation points capable of tsunami detection. The high number of ships in the far-field emphasizes how a warning center could benefit if this network was in place, by having large numbers of SSH observations against which to compare its numerical model predictions.

During a tsunami event, as soon as new observations of the tsunami are available, they are either incorporated into the tsunami numerical models or used to validate the numerical model predictions. The models can then be repeatedly iterated, improving the real time knowledge and calculation of the tsunami propagation and enabling a more efficient warning. Several tsunamis have shown how difficult it is to obtain a real-time precise tsunami model as uncertainties remain on the magnitude and the slip distribution. For example, the 2012 Haida Gwaii tsunami numerical models didn't predict any big inundations in Hawai'i (Santos et al., 2016). However, a tsunami warning was issued by the PTWC after misestimating wave impacts (Zimmerman, 2012). During the 2010 Maule tsunami, tsunami models also didn't closely match the reality: tsunami amplitude forecasted in the USA showed an average of 38 % error in estimation (Wilson et al., 2013), while the arrival time on the Japanese coast was delayed of about 30 min (Kato et al., 2011). If observations from ships in the far-field can seem less timely, their contribution as snapshots of the tsunami passage in the deep ocean constitute a unique dataset to improve tsunami numerical models in real time. Furthermore, despite the 2008 financial crisis, the COVID-19 pandemic and the effects of

https://doi.org/10.58440/ihr-30-1-a05

actual wars around the world, maritime trade is set to grow overall (ADB, 2020; UNCTAD, 2018; UNCTAD, 2023), with shipping costs back to pre-COVID-19 levels (UNCTAD, 2023) and minor port traffic variations (UNCTAD, 2022), assuring a stable temporal and spatial maritime coverage by ships for at least far-field events. Finally, the 2010 Maule tsunami is of great interest for the large datasets it benefited. Indeed, during the event, one ship equipped with the GNSS SSH measurement system was underway to Guam from Hawai'i and detected a ~10 cm amplitude (Foster et al., 2012), OBPGs deployed offshore Japan recorded the pressure change (Saito et al., 2010), and ground based GNSS TEC measurements were associated to the tsunami in Hawai'i and Japan (Galvan et al., 2011). The complementarity of all these datasets with the actual warning systems demonstrates how the tsunami models could be improved in real-time and in the long-term for future events.

During the 2010 Maule tsunami event, several DART buoys were out of function (NOAA, 2023). These important gaps in coverage are recurrent: in 2023, the DART system was functioning only 65 % uptime, and the new 2024-2028 mandated target performance is 70 %, lower than the one planned in 2018 (NOAA, 2024). A total of 39 DART is financed by the US in the Pacific, meaning that at least 10 DART are not in function at any time. Deployment cost for DART climbs to $0.5M/site (Bernard & Titov, 2015) and the network maintenance is estimated at $0.3M/site/year (Silva et al., 2021), which brings to a $78M total over five years. On the other hand, a complete ship-board system is estimated at $5k with $1k maintenance cost mostly dedicated to replacement (Foster et al., 2024). This does not include costs for internet and the precise positioning service as industry representatives have suggested these might be donated. Over five years, which is a reasonable lifetime for such a GNSS system, and for 4,000 VTOS ships in the Pacific, that would bring a total of $40M. The ship-based GNSS network would then clearly provide a higher spatial resolution of real-time observations complimentary to the DART system for half of the cost.

4.3 Areas with less maritime traffic

The 2022 powerful eruption of the HTHH volcano in the Kingdom of Tonga resulted in one of the most impressive and unconventional tsunamis ever observed (Gusman et al., 2022; Han & Yu, 2022). It constitutes a very instructive case in our approach as (i) the source is multi-hazard and non-seismic, (ii) the Kingdom of Tonga is located in a maritime zone with few shipping routes, (iii) however, this area is covered by hundreds of small and exposed islands with high human density on the coast, and (iv) the resulting trans-oceanic tsunami was also recorded in other oceans.

The Kingdom of Tonga is composed of 172 small islands, 45 of them inhabited distributed on a 650 km × 200 km frame along the Tonga-Kermadec subduction zone. The population is exposed to a diverse range of strong geological processes and hazards that regularly affects the archipelago (Thomas et al., 2023a). Tsunamis in Tonga may be generated from subduction megathrust earthquakes (past events: Okal et al., 2004; in 2006: Tang et al., 2008; the doublet earthquake in 2009: Lay et al., 2010), subaerial (volcano flank collapse) or submarine landslides (Frohlich et al., 2009), volcanic eruptions (Terry et al., 2022), or multi-hazard events (Lynett et al., 2022) with even a possible meteorite impact (Lavigne et al., 2021). The 2022 Tonga volcanic tsunamigenesis is often compared to the one during the 1883 Krakatau eruption and both show how crucial local and far-field observations are to improve modeling techniques and volcanic tsunami

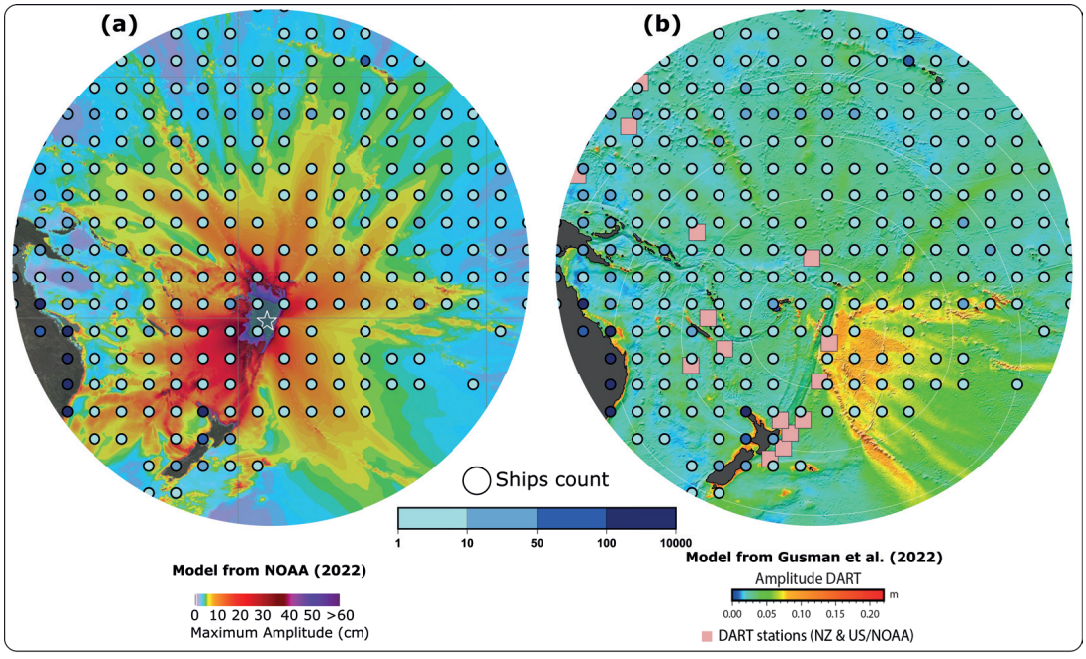

Fig. 7 Hourly mean number of ships coverage (blue-coded circles) over two 2022 Tonga tsunami models. (a) The maximum tsunami amplitudes (colormap) based on the DART-inverted model (NOAA, 2022). (b) The observed and simulated maximum tsunami amplitudes of the air-wave generated tsunami model (colormap) (Gusman et al., 2022) calculated using a COMCOT model (Wang & Power, 2011).

hazard assessment (Terry et al., 2022). Moreover, if no large earthquakes are associated with these events, the seismic networks are of limited use.

The 2022 Tonga tsunami also points out again the possibility of poor model prediction performance for non-standard source events: the tsunami surprised the scientific community by arriving two hours earlier and much larger than expected with the fast-moving atmospheric waves inducing a forerunner sea height rise (Han & Yu, 2022; Hu et al., 2023). It also lasted longer than conventionally expected due to a combination of moving and static sources (Carvajal et al., 2022; Kubota et al., 2022). Several models attempting to combine all sources have been computed. In Fig. 7a, the first quick DART-inverted model realized by the NOAA shows amplitudes in all directions above 10 cm, easily reaching New Zealand, Australia, Solomon Islands, Hawai'i and French Polynesia. In Fig. 7b, Gusman et al. (2022) analyze the air-wave generated tsunami with amplitudes above 10 cm only in the southeast direction, a propagation similar to Omira et al. (2022) model based on air-forcing. The overlap of the ships' density indicates then different estimations: between 10 to 150 ships in the +10 cm amplitude area depending on the model. A quick look at the DART observations confirms that only the nearby ones located in New Zealand had amplitudes above the 10 cm threshold (NOAA, 2023). The first classical NOAA model is thus unrealistic. However, it is used as a base for early warning and immediate action, meaning that if we consider the potential 150 ships in the +10 cm amplitude area defined by this model, we then have 150 observations of SSH perturbations in the open-ocean that would actually show smaller amplitudes or even not see the tsunami perturbation at all. This no tsunami perturbation greater than 10 cm information is also useful because the 150 ships' observations would then directly feed the real-time model and indicate that what was expected to be above 10 cm is actually way less. By providing a higher spatial resolution of real-time observations complimentary to the actual ones (c.f. Fig. 7b compared to DART locations), the ships would validate or improve real-time models. In this case, faster calculations of displaced water volume from the volcanic eruption and/or the underwater landslide could be realized (Heidarzadeh et al., 2022), models could be adapted taking into account the impact of atmospheric waves on ocean waves, by especially being able to determine the leading waves (Lamb waves) as a meteorological tsunami phenomenon (Carvajal et al., 2022; Suzuki et al., 2023). Ships equipped with ionospheric perturbations sensors as proposed in the introduction could improve the number of GNSS observations needed to analyze acoustic-gravity waves propagated by this eruption and tsunami (Ghent & Crowell, 2022).

The 2022 Tonga tsunami is of particular interest in this study due to its location away from large populated centers and thus away from observational infrastucture. Local observations from social media videos and interviews were available only a few weeks later, Tonga being under strict international lockdown during the COVID-19 pandemic. In an archipelago where more than 60 % of the population lives below 15 m elevation (Thomas et al., 2023a), communication was impossible due to deep-sea telecommunications cables being severed (Terry et al., 2022), creating a lack of real-time data. The tsunami was recorded on nearby tide gauges and DART sensors (Gusman & Roger 2022), as well as all across the Pacific Ocean, with impacts in Japan (Tsukanova & Medvedev, 2022), China (Wang et al., 2022) and Mexico (Ramírez-Herrera et al., 2022). Most records were from coastal gauges, leaving a huge gap in observations in the ocean. Most of the South-West Pacific is affected by a lower coverage of ships both temporally and spatially, while at the same time being a major geological hazard region as one quarter of the world's seismicity and tsunami sources have occurred there (calculated from NGDT, 2023). There are only on average ~7 ships within the area encompassed by the 1-hour TTT just before arriving at Fiji's east coast. With a random 11 % fleet participation, there would be no, or only one, VTOS ship in this area to capture near-field observations. This questions the potential value of a GNSS-based ship tsunami detection network in the near-field of a tsunami in areas with less maritime traffic. This lack of possible observations points in one of the highest vulnerable tsunami hazard region echoes how poorly documented this region is in tsunami-related publications compared to other regions. A literature search show that Tonga totals around 100 tsunami-related publications, half of them published after the 2022 event and almost two orders of magnitude fewer than Japan (Thomas et al., 2023b). GNSS-based ship datasets would offer a unique cost-effective tool to fill gaps in ocean observations (Metcalfe et al. 2018), contributing to more research studies and more real-time knowledge of tsunami hazard in this region. To address areas of low density of ships in our hypothetical network, we note that our VTOS concept here simply applied an 11 % selection from the full database. It is entirely possible to propose that an actual VTOS network would deliberately focus effort on soliciting collaboration from ships that operate in low-density coverage zones, resulting in a much higher percentage representation there than the 11 % average.

Another approach would be to envision the use of other type of ships in the network. Cruise ships cover all oceans and regularly transit through the South-West Pacific region making several stops around the touristic islands (e.g. cruise ships operators Compagnie du Ponant or Royal Caribbean Group destinations). Although less temporally regular, their communication links are usually excellent and would assure quick data transfer. Finally, the AIS data studied in this paper shows that 60 % of the ships in the South-West Pacific region are fishing boats, usually located all around the archipelagos and covering a wide range of the ocean never accessed by

https://doi.org/10.58440/ihr-30-1-a05

cargo ships. If the same methodology presented in this paper is applied to both cargos and fishing ships with the same rate of 11 % VOS ships, then the fishing ships contribution would definitely assure a minimum of 5 VTOS ships at all time in the near-field of any tsunami events. Additionally, it might be that the connectivity between ports of small islands in the South-West Pacific Ocean and the traditional trading partners in Oceania, Southeast Asia, East Asia and North America will increase, tending to more traffic and thus more potential VTOS data (ADB, 2020).

The worldwide impact of the 2022 Tonga tsunami (Gusman et al. 2022) even affected the atmosphere in the Black Forest in Germany, almost at the antipode of Tonga (Widmer-Schnidrig, 2022). If this can be seen as an exceptional case, several tsunamis have impacted different coastlines from different oceans: the unprecedented 2004 Indian Ocean tsunami was clearly observed in the Pacific Ocean and the 2021 South Sandwich Islands tsunami was observed in all oceans (Roger et al., 2022). Those examples reveal how crucial more observations covering all the oceans are needed to understand such extraordinary phenomenon. Our VTOS concept is not in any way limited to the Pacific, and although the Pacific Ocean is the zone of highest number of historical fatal tsunamis, they have occurred in all ocean basins. The global trade volume is at 80 % seaborne (UNCTAD, 2022) and never ceases to increase as shipping routes schedule gain in frequency and crossovers (Carlini et al., 2022; Rodrigue, 2017; Tournadre, 2014). By crossing three oceans with regular tsunami events, the Atlantic, the Indian and the Pacific, as well as the Mediterranean Sea known as another historical hotspot for tsunamis, a worldwide network of ships equipped with tsunami sensors would thus temporally and spatially cover all tsunami sources.

5 Conclusion

Tsunamis have claimed the lives of hundreds of thousands of people and are always associated with significant economic losses through infrastructure damages and costly evacuations. More temporal and spatial observations across the oceans are necessary to improve warnings and protect coastal communities. Recent studies demonstrate that a ship-based GNSS network analyzing in real-time the SSH is capable of detecting tsunamis, thus adding precise tsunami observations in an actual geodetic observational gap, and hence improving tsunami warning at a reasonable cost. We find that the commercial shipping fleet represents a vast existing infrastructure, with ~38,000 ships on average at any time in the Pacific Ocean, with the ship density highest along coastlines and most source regions of tsunamis. The one year of AIS records studied here demonstrates that 73 % of the Pacific Ocean is constantly covered by ships less than 1,000 km distant from each other, and more than 90 % of the tsunami source regions are covered by a dense ship network that could augment local and regional early warning of near-field tsunamis. For far-field events, ships would be new observations points, improving in real-time models and enabling more effective and reliable tsunami forecasting and warning. For geographic regions less visited by large ships, several options are available to densify a potential VTOS network in these low-density coverage zones. Using the global cargo ship fleet, with its persistent spatial and temporal coverage, including in tsunamigenic regions, to form a ship-based GNSS network would be a cost-effective approach for augmenting tsunami detection.

Acknowledgments

We are grateful to Dr. Aditya Gusman and Dr. Jean Roger from GNS Science, New Zealand, for sharing useful datasets and tsunami model concerning the 2022 Tonga tsunami. We would like to thank Dr. Peyman Saemian (University of Stuttgart, Germany) for his support and advice in GMT, as well as M.Sc. Vanessa Carrillo Barra (GEOAZUR, France) for the translation in Spanish of the abstract. The authors are very grateful to the editor Dr. Patrick Westfeld and three anonymous reviewers who provided constructive feedbacks to improve the quality of the article. All maps were generated using the Generic Mapping Tools (Wessel et al., 2019).

References

Amato, A. (2020). Some reflections on tsunami Early Warning Systems and their impact, with a look at the NEAMTWS. *Bollettino di Geofisica Teorica ed Applicata*, *61*(4), pp. 403–420. https://doi.org/10.4430/bgta0329

Asian Development Bank (ADB) (2020). *Trade and Maritime Transport Trends in the Pacific*. Asian Development Bank. Manila, Philippines. https://doi.org/10.22617/TCS200294-2

Astafyeva, E. (2019). Ionospheric Detection of Natural Hazards. *Reviews of Geophysics*. *57*(4), pp. 1265–1288. https://doi.org/10.1029/2019RG000668

Barnes, C. R., Best, M. M. R. and Zielinski, A. (2008). The NEPTUNE Canada Regional Cabled Ocean Observatory, *Sea Technology*, *49*(7), pp. 10–14.

Beck, S., Barrientos, S., Kausel, E. and Reyes, M. (1998). Source characteristics of historic earthquakes along the central Chile subduction Askew et alzone. *Journal of South American Earth Sciences*, *11*(2), pp. 115–129. https://doi.org/10.1016/S0895-9811(98)00005-4

Bernard, E. N. and Meinig, C. (2011). History and future of deep-ocean tsunami measurements. *Oceans'11 MTS Kona, IEEE, Waikoloa, USA*, pp. 1–7. https://doi.org/10.23919/OCEANS.2011.6106894

Bernard, E. and Titov, V. (2015). Evolution of tsunami warning systems and products, *Philosophical Transactions of the Royal Society A*, *373*, https://doi.org/10.1098/rsta.2014.0371

Bird, P. (2003). An updated digital model of plate boundaries. *Geochemistry, Geophysics, Geosystems*, *4*(3). https://doi.

org/10.1029/2001GC000252

Bonnefond, P., Exertier, P., Laurain, O., Ménard, Y., Orsoni, A., Jeansou, E., Haines, B.J., Kubitschek, D.G. and Born, G. (2003). Leveling the Sea Surface Using a GPS-Catamaran Special Issue: Jason-1 Calibration/Validation. *Marine Geodesy*, *26*(3–4), pp. 319–334. https://doi.org/10.1080/714044524

Bouchard, R., McArthur, S., Hansen, W., Kern, K.J. and Lockeet, L. (2007). Operational performance of the second generation deep-ocean assessment and reporting of Tsunamis (DART trade II). *Oceans 2007*, *IEEE, Vancouver, Canada*, pp. 1–6. https://doi.org/10.1109/OCEANS.2007.4449270

Brooks, B. A., Ericksen, T. L., DeSanto, J. B., Webb, S. C., Chadwell, C. D., Nooner, S. L., Foster, J., Thomas, B., Goldberg, D. E., Haynie, K. L., Haeussler, P. J., Witter, R. C., Zumberge, M. A., Minson, S. E. and Schmidt, D. A. (2021). *Seafloor Geodetic Constraints on an Instraslab Earthquake: The M7.6 2020 Sand Point, AK Earthquake* [Conference presentation]. AGU Fall Meeting, New Orleans, USA. https://agu.confex.com/agu/fm21/meetingapp.cgi/Paper/965198 (accessed 8 April 2024).

Brooks, B. A., Goldberg, D., DeSanto, J., Ericksen, T. L., Webb, S. C., Nooner, S. L., Chadwell, C. D., Foster, J., Minson, S., Witter, R., Haeussler, P., Freymueller, J., Barnhart, W. and Nevitt, J. (2023). Rapid shallow megathrust afterslip from the 2021 M8.2 Chignik, Alaska earthquake revealed by seafloor geodesy. *Science Advances, 9*(17), eadf9299. https://doi.org/10.1126/sciadv.adf9299

Bürgmann, R. and Chadwell, D. (2014). Seafloor Geodesy. *Annual Review of Earth and Planetary Sciences, 42*(1), pp. 509–534. https://doi.org/10.1146/annurev-earth-060313-054953

Carlini, E., Monteiro de Lira, V., Soares, A., Etemad, M., Brandoli, B. and Matwin, S. (2022). Understanding evolution of maritime networks from automatic identification system data. *GeoInformatica, 26*(3), pp. 479–503. https://doi.org/10.1007/s10707-021-00451-0

Carson-Jackson, J. (2012). Satellite AIS – Developing Technology or Existing Capability? *Journal of Navigation, 65*(2), pp. 303–321. https://doi.org/10.1017/S037346331100066X

Carvajal, M., Sepúlveda, I., Gubler, A. and Garreaud, R. (2022). Worldwide Signature of the 2022 Tonga Volcanic *Tsunami. Geophysical Research Letters, 49*(6), p. e2022GL098153. https://doi.org/10.1029/2022GL098153

Cassidy, J. F., Rogers, G. C. and Hyndman, R. D. (2014). An Overview of the 28 October 2012 Mw 7.7 Earthquake in Haida Gwaii, Canada: A Tsunamigenic Thrust Event Along a Predominantly Strike-Slip Margin. *Pure and Applied Geophysics, 171*(12), pp. 3457–3465. https://doi.org/10.1007/s00024-014-0775-1

Chadwell, C. D., Schmidt, D. A., Webb, S. C., Nooner, S. L., Ericksen, T. L., Brooks, B. A. and Foster, J. H. (2018). *Expansion of GPS-acoustic arrays offshore the cascadia and Alaska subduction zones*. AGU Fall Meeting Abstracts, San Francisco, USA.

Chiu, W.-T. and Ho, Y.-S. (2007). Bibliometric analysis of tsunami research. *Scientometrics, 73*(1), pp. 3–17. https://doi.org/10.1007/s11192-005-1523-1

Cisternas, M., Atwater, B. F., Torrejón, F., Sawai, Y., Machuca, G., Lagos, M., Eipert, A., Youlton, C., Salgado, I., Kamataki, T., Shishikura, M., Rajendran, C. P., Malik, J.K., Rizal, Y. and Husni, M. (2005). Predecessors of the giant 1960 Chile earthquake. *Nature, 437*(7057), pp. 404–407. https://doi.org/10.1038/nature03943

Cummins, P. R., Kong, L. S. L. and Satake, K. (2009). Introduction to Tsunami Science Four Years After the 2004 Indian Ocean Tsunami, Part II: Observation and Data Analysis. *Pure and Applied Geophysics*, 166(1–2), pp. 1–7. https://doi.org/10.1007/s00024-009-0442-0

Dziewonski, A. M., Chou, T.-A. and Woodhouse, J. H. (1981). Determination of earthquake source parameters from waveform data for studies of global and regional seismicity. *Journal of Geophysical Research: Solid Earth, 86*(B4), pp. 2825–2852. https://doi.org/10.1029/JB086iB04p02825

Ekström, G., Nettles, M. and Dziewoński, A. M. (2012). The global CMT project 2004–2010: Centroid-moment tensors for 13,017 earthquakes. *Physics of the Earth and Planetary Interiors, 200–201*, pp. 1–9. https://doi.org/10.1016/j.pepi.2012.04.002

Fine, I. V., Cherniawsky, J. Y., Thomson, R. E., Rabinovich, A. B. and Krassovski, M. V. (2015). Observations and Numerical Modeling of the 2012 Haida Gwaii Tsunami off the Coast of British Columbia. *Pure and Applied Geophysics, 172*(3–4), pp. 699–718. https://doi.org/10.1007/s00024-014-1012-7

Foster, J. H., Brooks, B. A., Wang, D., Carter, G. S. and Merrifield, M. A. (2012). Improving tsunami warning using commercial ships. *Geophysical Research Letters, 39*(9). https://doi.org/10.1029/2012GL051367

Foster, J. H., Carter, G. S. and Merrifield, M. A. (2009). Ship-based measurements of sea surface topography. *Geophysical Research Letters, 36*(11). https://doi.org/10.1029/2009GL038324

Foster, J., Ericksen, T., Thomas, B., Avery, J., Xie, Y. and Knogl, R. (2024). Augmenting Tsunami Detection with a Ship-based GNSS Network. *EGU General Assembly 2024, Vienna, Austria, 14–19 Apr 2024, EGU24-5841*. https://doi.org/10.5194/egusphere-egu24-5841

Foster, J. H., Ericksen, T. L. and Bingham, B. (2020). Wave Glider–Enhanced Vertical Seafloor Geodesy. *Journal of Atmospheric and Oceanic Technology, 37*(3), pp. 417–427. https://doi.org/10.1175/JTECH-D-19-0095.1

Foster, J., Li, N. and Cheung, K. F. (2014). Sea State Determination from Ship-Based Geodetic GPS. *Journal of Atmospheric and Oceanic Technology, 31*(11), pp. 2556–2564. https://doi.org/10.1175/JTECH-D-13-00211.1

Fritz, H. M., Petroff, C. M., Catalán, P. A., Cienfuegos, R., Winckler, P., Kalligeris, N., Weiss, R., Barrientos, S. E., Meneses, G., Valderas-Bermejo, C., Ebeling, C., Papadopoulos, A., Contreras, M., Almar, R., Dominguez, J. C. and Synolakis, C. E. (2011). Field Survey of the 27 February 2010 Chile Tsunami. *Pure and Applied Geophysics, 168*(11), pp. 1989–2010. https://doi.org/10.1007/s00024-011-0283-5

Frohlich, C., Hornbach, M. J., Taylor, F. W., Shen, C.-C., Moala, 'Apai, Morton, A. E. and Kruger, J. (2009). Huge erratic boulders in Tonga deposited by a prehistoric tsunami. *Geology, 37*(2), pp. 131–134. https://doi.org/10.1130/G25277A.1

Galvan, D. A., Komjathy, A., Hickey, M. P. and Mannucci, A. J. (2011). The 2009 Samoa and 2010 Chile tsunamis as observed in the ionosphere using GPS total electron content: tsunami signatures observed in TEC. *Journal of Geophysical Research: Space Physics, 116*(A6). https://doi.org/10.1029/2010JA016204

Ghent, J. N. and Crowell, B. W. (2022). Spectral Characteristics of Ionospheric Disturbances Over the Southwestern Pacific From

the 15 January 2022 Tonga Eruption and Tsunami. *Geophysical Research Letters, 49*(20), p. e2022GL100145. https://doi.org/10.1029/2022GL100145

Goto, K., Chagué-Goff, C., Fujino, S., Goff, J., Jaffe, B., Nishimura, Y., Richmond, B., Sugawara, D., Szczuciński, W., Tappin, D. R., Witter, R.C. and Yulianto, E. (2011). New insights of tsunami hazard from the 2011 Tohoku-oki event. *Marine Geology, 290*(1–4), pp. 46–50. https://doi.org/10.1016/j.margeo.2011.10.004

Grilli, S. T., Tappin, D. R., Carey, S., Watt, S. F. L., Ward, S. N., Grilli, A. R., Engwell, S. L., Zhang, C., Kirby, J. T., Schambach, L. and Muin, M. (2019). Modelling of the tsunami from the December 22, 2018 lateral collapse of Anak Krakatau volcano in the Sunda Straits, Indonesia. *Scientific Reports, 9*(1), p. 11946. https://doi.org/10.1038/s41598-019-48327-6

Gusiakov, V. K., Dunbar, P. K. and Arcos, N. (2019). Twenty-Five Years (1992–2016) of Global Tsunamis: Statistical and Analytical Overview. *Pure and Applied Geophysics, 176*(7), pp. 2795–2807. https://doi.org/10.1007/s00024-019-02113-7

Gusman, A. R. and Roger, J. (2022). *Hunga Tonga - Hunga Ha'apai volcano-induced sea level oscillations and tsunami simulations*. GNS Science webpage (accessed 20 October 2023).

Gusman, A. R., Roger, J., Noble, C., Wang, X., Power, W. and Burbidge, D. (2022). The 2022 Hunga Tonga-Hunga Ha'apai Volcano Air-Wave Generated Tsunami. *Pure and Applied Geophysics, 179*(10), pp. 3511–3525. https://doi.org/10.1007/s00024-022-03154-1

Gusman, A. R., Sheehan, A. F., Satake, K., Heidarzadeh, M., Mulia, I. E. and Maeda, T. (2016). Tsunami data assimilation of Cascadia seafloor pressure gauge records from the 2012 Haida Gwaii earthquake. *Geophysical Research Letters, 43*(9), pp. 4189–4196. https://doi.org/10.1002/2016GL068368

Hamlington, B. D., Leben, R. R., Godin, O. A., Legeais, J. F., Gica, E., and Titov, V. V. (2011). Detection of the 2010 Chilean tsunami using satellite altimetry. *Natural Hazards and Earth System Sciences, 11*(9), pp. 2391–2406. https://doi.org/10.5194/nhess-11-2391-2011

Han, P. and Yu, X. (2022). An unconventional tsunami: 2022 Tonga event. *Physics of Fluids, 34*(11), p. 116607. https://doi.org/10.1063/5.0122830

Hayashi, Y., Tsushima, H., Hirata, K., Kimura, K. and Maeda, K. (2011). Tsunami source area of the 2011 off the Pacific coast of Tohoku Earthquake determined from tsunami arrival times at offshore observation stations. *Earth, Planets and Space, 63*(7), pp. 809–813. https://doi.org/10.5047/eps.2011.06.042

Hébert, H., Occhipinti, G., Schindelé, F., Gailler, A., Pinel-Puysségur, B., Gupta, H. K., Rolland, L., Lognonné, P., Lavigne, F., Meilianda, E., Chapkanski, S., Crespon, F., Paris, A., Heinrich, P., Monnier, A., Jamelot, A. and Reymond, D. (2020). Contributions of Space Missions to Better Tsunami Science: Observations, Models and Warnings. *Surveys in Geophysics, 41*(6), pp. 1535–1581. https://doi.org/10.1007/s10712-020-09616-2

Heidarzadeh, M., Gusman, A.R., Ishibe, T., Sabeti, R. and Šepic, J. (2022). Estimating the eruption-induced water displacement source of the 15 January 2022 Tonga volcanic tsunami from tsunami spectra and numerical modelling. *Ocean Engineering, 261*, p. 112165. https://doi.org/10.1016/j.oceaneng.2022.112165

Hirata, K., Satake, K., Tanioka, Y., Kuragano, T., Hasegawa, Y., Hayashi, Y. and Hamada, N. (2006). The 2004 Indian Ocean tsunami: Tsunami source model from satellite altimetry. Earth, *Planets and Space, 58*(2), pp. 195–201. https://doi.org/10.1186/BF03353378

Holgate, S. J., Matthews, A., Woodworth, P. L., Rickards, L. J., Tamisiea, M. E., Bradshaw, E., Foden, P. R., Gordon, K. M., Jevrejeva, S. and Pugh, J. (2013). New Data Systems and Products at the Permanent Service for Mean Sea Level. *Journal of Coastal Research, 29*(3), pp. 493–504. https://doi.org/10.2112/JCOASTRES-D-12-00175.1

Hossen, M. J., Mulia, I. E., Mencin, D. and Sheehan, A. F. (2021). Data Assimilation for Tsunami Forecast With Ship–Borne GNSS Data in the Cascadia Subduction Zone. *Earth and Space Science, 8*(3). https://doi.org/10.1029/2020EA001390

Howe, B. M., Angove, M., Aucan, J., Barnes, C. R., Barros, J. S., Bayliff, N., Becker, N. C., Carrilho, F., Fouch, M. J., Fry, B., Jamelot, A., Janiszewski, H., Kong, L. S. L., Lentz, S., Luther, D. S., Marinaro, G., Matias, L. M., Rowe, C. A., Sakya, A. E., Salaree, A., Thiele, T., Tilmann, F. J., von Hillebrandt-Andrade, C., Wallace, L., Weinstein, S. and Wilcock, W. (2022). SMART Subsea Cables for Observing the Earth and Ocean, Mitigating Environmental Hazards, and Supporting the Blue Economy. *Frontiers in Earth Science, 9*, p. 775544. https://doi.org/10.3389/feart.2021.775544

Howe, B. M., Arbic, B. K., Aucan, J., Barnes, C. R., Bayliff, N., Becker, N., Butler, R., Doyle, L., Elipot, S., Johnson, G. C., Landerer, F., Lentz, S., Luther, D. S., Müller, M., Mariano, J., Panayotou, K., Rowe, C., Ota, H., Song, Y. T., Thomas, M., Thomas, P. N., Thompson, P., Tilmann, F., Weber, T. and Weinstein, S. (2019). SMART Cables for Observing the Global Ocean: Science and Implementation. *Frontiers in Marine Science, 6*, p. 424. https://doi.org/10.3389/fmars.2019.00424

Hu, G., Li, L., Ren, Z. and Zhang, K. (2023). The characteristics of the 2022 Tonga volcanic tsunami in the Pacific Ocean. *Natural Hazards and Earth System Sciences, 23*(2), pp. 675–691. https://doi.org/10.5194/nhess-23-675-2023

Iinuma, T., Kido, M., Ohta, Y., Fukuda, T., Tomita, F. and Ueki, I. (2021). GNSS-Acoustic Observations of Seafloor Crustal Deformation Using a Wave Glider. *Frontiers in Earth Science, 9*, p. 600946. https://doi.org/10.3389/feart.2021.600946

International Maritime Organization (IMO) (2002). *Guidelines for the onboard operational use of shipborne Automatic Identification Systems*.

Inazu, D., Ikeya, T., Iseki, T. and Waseda, T. (2020). Extracting clearer tsunami currents from shipborne Automatic Identification System data using ship yaw and equation of ship response. *Earth, Planets and Space, 72*(1). https://doi.org/10.1186/s40623-020-01165-7

Inazu, D., Ikeya, T., Waseda, T., Hibiya, T. and Shigihara, Y. (2018). Measuring offshore tsunami currents using ship navigation records. Progress in Earth and Planetary *Science, 5*(1). https://doi.org/10.1186/s40645-018-0194-5

Inazu, D., Waseda, T., Hibiya, T. and Ohta, Y. (2016). Assessment of GNSS-based height data of multiple ships for measuring and forecasting great tsunamis. *Geoscience Letters, 3*(1). https://doi.org/10.1186/s40562-016-0059-y

International Tsunami Information Center (ITIC) (2012). *28 October 2012 (UTC), Mw 7.7, Queen Charlotte Islands, Haida Gwaii, Canada Tsunami*. http://itic.ioc-unesco.org/index.php?option=com_content&view=article&id=1828&Itemid=2985

(accessed 20 October 2023).

International Tsunami Information Center (ITIC) (2019). *Tsunamis causing deaths greater than 1,000 km from the source location*. http://itic.ioc-unesco.org/images/stories/generalinfo/visualgallery/graphics/maps/historical/Tsunamis_causing_deaths_greater_than_1000_km_from_source_2019.jpg (accessed 20 October 2023).

Intergovernmental Oceanographic Commission (IOC) (2014). *User's Guide for the Pacific Tsunami Warning Center Enhanced Products for the Pacific Tsunami Warning System*. http://itic.ioc-unesco.org/images/stories/about_warnings/what_are_they/ts105-Rev2_eo_220368E.pdf (accessed 20 March 2024).

James, T., Rogers, G., Cassidy, J., Dragert, H., Hyndman, R., Leonard, L., Nykolaishen, L., Riedel, M., Schmidt, M. and Wang, K. (2013). Field Studies Target 2012 Haida Gwaii Earthquake. *Eos Transactions American Geophysical Union, 94*(22), pp. 197–198. https://doi.org/10.1002/2013EO220002

Jin, D. and Lin, J. (2011). Managing tsunamis through early warning systems: A multidisciplinary approach. *Ocean & Coastal Management, 54*(2), pp. 189–199. https://doi.org/10.1016/j.ocecoaman.2010.10.025

Kagan, Y. Y. and Jackson, D. D. (2013). Tohoku Earthquake: A Surprise? *Bulletin of the Seismological Society of America, 103*(2B), pp. 1181–1194. https://doi.org/10.1785/0120120110

Kaluza, P., Kölzsch, A., Gastner, M. T. and Blasius, B. (2010). The complex network of global cargo ship movements. *Journal of The Royal Society Interface, 7*(48), pp. 1093–1103. https://doi.org/10.1098/rsif.2009.0495

Kato, T., Terada, Y., Nishimura, H., Nagai, T. and Koshimura, S. (2011). Tsunami records due to the 2010 Chile Earthquake observed by GPS buoys established along the Pacific coast of Japan. *Earth, Planets and Space, 63*(6), pp. e5–e8. https://doi.org/10.5047/eps.2011.05.001

Kawaguchi, K., Kaneda, Y. and Araki, E. (2008). The DONET: A real-time seafloor research infrastructure for the precise earthquake and tsunami monitoring, *Oceans 2008, IEEE, Kobe, Japan*, pp. 1–4, https://doi.org/10.1109/OCEANSKOBE.2008.4530918

Kawai, H., Satoh, M., Kawaguchi, K. and Seki, K. (2013). Characteristics of the 2011 Tohoku Tsunami Waveform Acquired Around Japan by Nowphas Equipment. *Coastal Engineering Journal, 55*(3), pp. 1–27. https://doi.org/10.1142/S0578563413500083

Kent, E., Hall, A. D. and Leader, V. T. T. (2010). The Voluntary Observing Ship (VOS) Scheme. *Proceedings from the 2010 AGU Ocean Sciences Meeting, Washington DC, USA*, pp. 551–561.

Kopp, H. and all Cruise Participants (2022). *Conjoint Monitoring of the Ocean Bottom offshore Chile Humboldt Organic MattEr Remineralization, Cruise No. SO288, 15.01.2022 – 15.02.2022, Guayaquil (Ecuador) – Valparaiso (Chile) COMBO & HOMER*. GEOMAR Helmholtz Centre for Ocean Research Kiel. https://doi.org/10.3289/CR_SO288

Kubota, T., Saito, T. and Nishida, K. (2022). Global fast-traveling tsunamis driven by atmospheric Lamb waves on the 2022 Tonga eruption. *Science, 377*(6601), pp. 91–94. https://doi.org/10.1126/science.abo4364

Lander, J. F., Whiteside, L. S. and Lockridge, P. A. (2003). Two decades of global tsunamis. *Science of Tsunami Hazards, 21*(1), pp. 3–88.

Lavigne, F., Morin, J., Wassmer, P., Weller, O., Kula, T., Maea, A. V., Kelfoun, K., Mokadem, F., Paris, R., Malawani, M. N., Faral, A., Benbakkar, M., Saulnier-Copard, S., Vidal, C. M., Tu'I'afitu, T., Kitekei'aho, F., Trautmann, M. and Gomez, C. (2021). Bridging Legends and Science: Field Evidence of a Large Tsunami that Affected the Kingdom of Tonga in the 15th Century. *Frontiers in Earth Science, 9*, p. 748755. https://doi.org/10.3389/feart.2021.748755

Lay, T., Ammon, C. J., Kanamori, H., Rivera, L., Koper, K. D. and Hutko, A. R. (2010). The 2009 Samoa–Tonga great earthquake triggered doublet. *Nature, 466*(7309), pp. 964–968. https://doi.org/10.1038/nature09214

Le Tixerant, M., Le Guyader, D., Gourmelon, F. and Queffelec, B. (2018). How can Automatic Identification System (AIS) data be used for maritime spatial planning? *Ocean & Coastal Management, 166*, pp. 18–30. https://doi.org/10.1016/j.ocecoaman.2018.05.005

Leonard, L. J. and Bednarski, J. M. (2014). Field Survey Following the 28 October 2012 Haida Gwaii Tsunami. *Pure and Applied Geophysics, 171*(12), pp. 3467–3482. https://doi.org/10.1007/s00024-014-0792-0

Leonard, L. J., Rogers, G. C. and Hyndman, R. D. (2010). Annotated bibliography of references relevant to tsunami hazard in Canada. *Geological Survey of Canada*, 6552. https://doi.org/10.4095/285367

Leonard, L. J., Rogers, G. C. and Mazzotti, S. (2012). A preliminary tsunami hazard assessment of the Canadian Coastline. *Geological Survey of Canada*, 7201. https://doi.org/10.4095/292067

Li, X., Ge, M., Dai, X., Ren, X., Fritsche, M., Wickert, J. and Schuh, H. (2015). Accuracy and reliability of multi-GNSS real-time precise positioning: GPS, GLONASS, BeiDou, and Galileo. *Journal of Geodesy, 89*, pp. 607–635, https://doi.org/10.1007/s00190-015-0802-8

Lomnitz, C. (1970). Major earthquakes and tsunamis in Chile during the period 1535 to 1955. *Geologische Rundschau, 59*(3), pp. 938–960. https://doi.org/10.1007/BF02042278

Løvholt, F., Setiadi, N. J., Birkmann, J., Harbitz, C. B., Bach, C., Fernando, N., Kaiser, G. and Nadim, F. (2014). Tsunami risk reduction – are we better prepared today than in 2004? *International Journal of Disaster Risk Reduction, 10*, pp. 127–142. https://doi.org/10.1016/j.ijdrr.2014.07.008

Lynett, P., McCann, M., Zhou, Z., Renteria, W., Borrero, J., Greer, D., Fa'anunu, O., Bosserelle, C., Jaffe, B., La Selle, S., Ritchie, A., Snyder, A., Nasr, B., Bott, J., Graehl, N., Synolakis, C., Ebrahimi, B. and Cinar, G. E. (2022). Diverse tsunamigenesis triggered by the Hunga Tonga-Hunga Ha'apai eruption. *Nature, 609*(7928), pp. 728–733. https://doi.org/10.1038/s41586-022-05170-6

Manta, F., Occhipinti, G., Feng, L. and Hill, E. M. (2020). Rapid identification of tsunamigenic earthquakes using GNSS ionospheric sounding. *Scientific Reports, 10*(1), p. 11054. https://doi.org/10.1038/s41598-020-68097-w

Matias, L., Carrilho, F., Sá, V., Omira, R., Niehus, M., Corela, C., Barros, J. and Omar, Y. (2021). The Contribution of Submarine Optical Fiber Telecom Cables to the Monitoring of Earthquakes and Tsunamis in the NE Atlantic. *Frontiers in Earth Science, 9*, p. 686296. https://doi.org/10.3389/feart.2021.686296

Metcalfe, K., Bréheret, N., Chauvet, E., Collins, T., Curran, B. K., Parnell, R. J., Turner, R. A., Witt, M. J. and Godley, B. J. (2018).

Using satellite AIS to improve our understanding of shipping and fill gaps in ocean observation data to support marine spatial planning. *Journal of Applied Ecology, 55*(4), pp. 1834–1845. https://doi.org/10.1111/1365-2664.13139

Mulia, I. E., Hirobe, T., Inazu, D., Endoh, T., Niwa, Y., Gusman, A. R., Tatehata, H., Waseda, T. and Hibiya, T. (2020). Advanced tsunami detection and forecasting by radar on unconventional airborne observing platforms. *Scientific Reports, 10*(1), p. 2412. https://doi.org/10.1038/s41598-020-59239-1

Mulia, I. E., Inazu, D., Waseda, T. and Gusman, A. R. (2017). Preparing for the Future Nankai Trough Tsunami: A Data Assimilation and Inversion Analysis From Various Observational Systems. *Journal of Geophysical Research: Oceans, 122*(10), pp. 7924–7937. https://doi.org/10.1002/2017JC012695

Mulia, I. E. and Satake, K. (2020). Developments of Tsunami Observing Systems in Japan. *Frontiers in Earth Science, 8*, p. 145. https://doi.org/10.3389/feart.2020.00145

Mulia, I. E. and Satake, K. (2021). Synthetic analysis of the efficacy of the S-net system in tsunami forecasting. *Earth, Planets and Space, 73*(36), https://doi.org/10.1186/s40623-021-01368-6

Mulia, I. E., Ueda, N., Miyoshi, T., Gusman, A. R. and Satake, K. (2022). Machine learning-based tsunami inundation prediction derived from offshore observations. *Nature Communications, 13*(1), p. 5489. https://doi.org/10.1038/s41467-022-33253-5

Nakamura, S. (1992). An analysis of the 1985 Chilean tsunami. *Marine Geodesy, 15*(4), pp. 277–281. https://doi.org/10.1080/01490419209388064

National Geophysical Data Center (NGDT) (2023). *Global Historical Tsunami Database*. NOAA National Centers for Environmental Information. https://doi.org/10.7289/V5PN93H7

National Oceanic and Atmospheric Administration (NOAA) (2022). *Hunga Tonga-Hunga Ha'apa Volcano-generated Tsunami, January 15, 2022, Main Event Page*. NOAA Center for Tsunami Research webpage, https://nctr.pmel.noaa.gov/tonga20220115/ (accessed 20 October 2023).

National Oceanic and Atmospheric Administration (NOAA) (2023). *DART® (Deep-ocean Assessment and Reporting of Tsunamis)*. NOAA Center for Tsunami Research webpage, https://nctr.pmel.noaa.gov/Dart/ (accessed 20 October 2023).

National Oceanic and Atmospheric Administration (NOAA) (2024). *Budget Estimates, Fiscal Year 2024, Congressional Submission*. NOAA, https://www.noaa.gov/sites/default/files/2023-04/NOAA_FY24_CJ.pdf (accessed 22 March 2024).

Nie, Z., Liu, F. and Gao, Y. (2020). Real-time precise point positioning with a low-cost dual-frequency GNSS device. *GPS Solutions, 24*(9), https://doi.org/10.1007/s10291-019-0922-3

Occhipinti, G., Komjathy, A. and Lognonné, P. (2008). Tsunami detection by GPS. *GPS world, 19*(2), pp. 51–57.

Okal, E. A., Borrero, J. and Synolakis, C. E. (2004). The earthquake and tsunami of 1865 November 17: evidence for far-field tsunami hazard from Tonga. *Geophysical Journal International, 157*(1), pp. 164–174. https://doi.org/10.1111/j.1365-246X.2004.02177.x

Okal, E. A., Piatanesi, A. and Heinrich, P. (1999). Tsunami detection by satellite altimetry. Journal of Geophysical Research: *Solid Earth, 104*(B1), pp. 599–615. https://doi.org/10.1029/1998JB000018

Omira, R., Ramalho, R. S., Kim, J., González, P. J., Kadri, U., Miranda, J. M., Carrilho, F. and Baptista M. A. (2022). Global Tonga tsunami explained by a fast-moving atmospheric source. *Nature, 609*, pp. 734–740, https://doi.org/10.1038/s41586-022-04926-4

Permanent Service for Mean Sea Level (PSMSL) (2024). *Tide Gauge Data*. http://www.psmsl.org/data/obtaining/ (accessed 15 January 2024).

Qayyum, B., Ahmed, A., Ullah, I. and Shah, S. A. (2022). A Fuzzy-Logic Approach for Optimized and Cost-Effective Early Warning System for Tsunami Detection. *Sustainability, 14*(21), p. 14516. https://doi.org/10.3390/su142114516

Rabinovich, A. B., Thomson, R. E. and Fine, I. V. (2013). The 2010 Chilean Tsunami Off the West Coast of Canada and the Northwest Coast of the United States. *Pure and Applied Geophysics, 170*(9–10), pp. 1529–1565. https://doi.org/10.1007/s00024-012-0541-1

Rabinovich, A. B., Thomson, R. E., Titov, V. V., Stephenson, F. E. and Rogers, G. C. (2008). Locally generated tsunamis recorded on the coast of British Columbia. *Atmosphere-Ocean, 46*(3), pp. 343–360. https://doi.org/10.3137/ao.460304

Ramírez-Herrera, M. T., Coca, O. and Vargas-Espinosa, V. (2022). Tsunami Effects on the Coast of Mexico by the Hunga Tonga-Hunga Ha'apai Volcano Eruption, Tonga. *Pure and Applied Geophysics, 179*(4), pp. 1117–1137. https://doi.org/10.1007/s00024-022-03017-9

Ravanelli, M. and Foster, J. (2020). Detection of tsunami induced ionospheric perturbation with ship-based GNSS measurements: 2010 Maule tsunami case study. *EGU General Assembly 2020, Online, 4–8 May 2020, EGU2020-11583*. https://doi.org/10.5194/egusphere-egu2020-11583

Röbke, B. R. and Vött, A. (2017). The tsunami phenomenon. *Progress in Oceanography, 159*, pp. 296–322. https://doi.org/10.1016/j.pocean.2017.09.003

Rocken, C., Johnson, J., van Hove, T. and Iwabuchi, T. (2005). Atmospheric water vapor and geoid measurements in the open ocean with GPS. *Geophysical Research Letters, 32*(12). https://doi.org/10.1029/2005GL022573

Rodrigue, J.-P. (2017). Maritime Transport. In D. Richardson et al. (eds) *International Encyclopedia of Geography* (1st edn, pp. 1–7). Wiley. https://doi.org/10.1002/9781118786352.wbieg0155

Roger, J., Hebert, H., Jamelot, A., Gusman, A., Power, W., Hubbard, J. (2022). The South Sandwich circum-Antarctic tsunami of August 12, 2021: widespread propagation using oceanic ridges. *EGU 2022, Vienna, Austria*. https://doi.org/10.5194/egusphere-egu22-904

Saito, T., Matsuzawa, T., Obara, K. and Baba, T. (2010). Dispersive tsunami of the 2010 Chile earthquake recorded by the high–sampling–rate ocean–bottom pressure gauges. *Geophysical Research Letters, 37*(23). https://doi.org/10.1029/2010GL045290

Salaree, A., Howe, B. M., Huang, Y., Weinstein, S. A. and Sakya, A. E. (2023). A Numerical Study of SMART Cables Potential in Marine Hazard Early Warning for the Sumatra and Java Regions. *Pure and Applied Geophysics, 180*, pp. 1717–1749. https://doi.org/10.1007/s00024-022-03004-0

Santos, A., Tavares, A.O. and Queirós, M. (2016). Numerical modelling and evacuation strategies for tsunami awareness: lessons from the 2012 Haida Gwaii Tsunami. Geomatics, *Natural Hazards and Risk, 7*(4), pp. 1442–1459. https://doi.org/10.1080/19475705.2015.1065292

Satake, K., Fujuu, Y., Harada, T. and Namegaya, Y. (2013). Time and Space Distribution of Coseismic Slip of the 2011 Tohoku Earthquake as Inferred from Tsunami Waveform Data. *Bulletin*

of the Seismological Society of America, 103(2B), pp. 1473–1492. https://doi.org/10.1785/0120120122

Savastano, G., Komjathy, A., Verkhoglyadova, O., Mazzoni, A., Crespi, M., Wei, Y. and Mannucci, A. J. (2017). Real-Time Detection of Tsunami Ionospheric Disturbances with a Stand-Alone GNSS Receiver: A Preliminary Feasibility Demonstration. *Scientific Reports, 7*(1), p. 46607. https://doi.org/10.1038/srep46607

Schambach, L., Grilli, S. T. and Tappin, D.R. (2021). New High-Resolution Modeling of the 2018 Palu Tsunami, Based on Supershear Earthquake Mechanisms and Mapped Coastal Landslides, Supports a Dual Source. *Frontiers in Earth Science, 8*, p. 598839. https://doi.org/10.3389/feart.2020.598839

Silva, N., Catarino, N., Ávila, N., Baptista, M. A. and Wronna, M. (2021). Tsunami detection from Space – a nearly real-time system to detect ocean surface altimetric anomalies with satellites. deimos webpage, https://elecnor-deimos.com/tsunami-prevention-gnss-r/ (accessed 22 March 2024).

Soloviev, S. L. and Go, N. (1975). *Catalogue of tsunamis of the eastern shore of the Pacific Ocean (1513-1968)*. Nauka Publishing House. Moscow, Russia.

Srinivasa Kumar, T. and Manneela, S. (2021). A Review of the Progress, Challenges and Future Trends in Tsunami Early Warning Systems. *Journal of the Geological Society of India, 97*(12), pp. 1533–1544. https://doi.org/10.1007/s12594-021-1910-0

Suzuki, T., Nakano, M., Watanabe, S., Tatebe, H. and Takano, Y. (2023). Mechanism of a meteorological tsunami reaching the Japanese coast caused by Lamb and Pekeris waves generated by the 2022 Tonga eruption. *Ocean Modelling, 181*, p. 102153. https://doi.org/10.1016/j.ocemod.2022.102153

Synolakis, C. E. and Bernard, E. N. (2006). Tsunami science before and beyond Boxing Day 2004. *Philosophical Transactions of the Royal Society A: Mathematical, Physical and Engineering Sciences, 364*(1845), pp. 2231–2265. https://doi.org/10.1098/rsta.2006.1824

Tang, L., Titov, V. V., Wei, Y., Mofjeld, H.O., Spillane, M., Arcas, D., Bernard, E. N., Chamberlin, C., Gica, E. and Newman, J. (2008). Tsunami forecast analysis for the May 2006 Tonga tsunami. *Journal of Geophysical Research: Oceans, 113*(C12), p. 2008JC004922. https://doi.org/10.1029/2008JC004922

Terry, J. P., Goff, J., Winspear, N., Bongolan, V. P. and Fisher, S. (2022). Tonga volcanic eruption and tsunami, January 2022: globally the most significant opportunity to observe an explosive and tsunamigenic submarine eruption since AD 1883 Krakatau. *Geoscience Letters, 9*(1), p. 24. https://doi.org/10.1186/s40562-022-00232-z

Thomas, B. E. O., Roger, J., Gunnell, Y. and Ashraf, S. (2023a). A method for evaluating population and infrastructure exposed to natural hazards: tests and results for two recent Tonga tsunamis. *Geoenvironmental Disasters, 10*(1), p. 4. https://doi.org/10.1186/s40677-023-00235-8

Thomas, B. E. O., Roger, J., Gunnell, Y. and Pala, I. (2023b). *Geovisualization of Tsunami-related Studies Around the World*. AOGS 20th Annual Meeting, Singapore, Singapore, 30 July – 4 August 2023, AOGS23-6881

Tilmann, F., Howe, B., Butler, R. and Weinstein, S. (2016). *SMART Submarine Cable Applications in Earthquake and Tsunami Science and Early Warning*. Report on workshop, Potsdam, Germany, 3–4 November 2016, https://www.itu.int/en/ITU-T/climatechange/task-force-sc/Documents/Report-WS-11-2016-Potsdam.pdf (accessed 27 March 2024).

Titov, V. V. (2021). Hard Lessons of the 2018 Indonesian Tsunamis. *Pure and Applied Geophysics, 178*(4), pp. 1121–1133. https://doi.org/10.1007/s00024-021-02731-0

Tournadre, J. (2014). Anthropogenic pressure on the open ocean: The growth of ship traffic revealed by altimeter data analysis. *Geophysical Research Letters, 41*(22), pp. 7924–7932. https://doi.org/10.1002/2014GL061786

Trimble (2024). *Positioning service*. https://positioningservices.trimble.com/en/rtx (accessed 21 March 2024).

Tsukanova, E. and Medvedev, I. (2022). The Observations of the 2022 Tonga-Hunga Tsunami Waves in the Sea of Japan. *Pure and Applied Geophysics, 179*(12), pp. 4279–4299. https://doi.org/10.1007/s00024-022-03191-w

Tsushima, H., Hino, R., Ohta, Y., Iinuma, T. and Miura S. (2014). tFISH/RAPiD: Rapid improvement of near-field tsunami forecasting based on offshore tsunami data by incorporating onshore GNSS data. *Geophysical Research Letters, 41*(10), pp. 3390–3397. https://doi.org/10.1002/2014GL059863

United Nations Conference on Trade and Development (UNCTAD) (2018). *50 Years of Review of Maritime Transport, 1968-2018: Reflecting on the past, exploring the future*.

United Nations Conference on Trade and Development (UNCTAD) (2022). *Review of Maritime Transport 2022: Navigating stormy waters*. United Nations Publications. Geneva, Switzerland.

United Nations Conference on Trade and Development (UNCTAD) (2023). *Review of Maritime Transport 2023: Towards a green and just transition*. United Nations Publications. Geneva, Switzerland.

US Geological Survey (USGS) (2010). M 8.8 - 36 km WNW of Quirihue, Chile. https://earthquake.usgs.gov/earthquakes/eventpage/official20100227063411530_30/executive (accessed 20 October 2023).

US Geological Survey (USGS) (2012). M 7.8 - 206 km SW of Prince Rupert, Canada. https://earthquake.usgs.gov/earthquakes/eventpage/usp000juhz/executive (accessed 20 October 2023).

Wang, X. and Power, W. L. (2011). COMCOT : a tsunami generation, propagation and run-up model. *GNS Science report 2011/43*.

Wang, D., Walsh, D., Becker, N. C. and Fryer, G. J. (2009). A methodology for tsunami wave propagation forecast in real time. *AGU Fall Meeting, San Francisco, USA*, pp. OS43A-1367.

Wang, Y., Wang, P., Kong, H. and Wong, C.-H. (2022). Tsunamis in Lingding Bay, China, caused by the 2022 Tonga volcanic eruption. *Geophysical Journal International, 232*(3), pp. 2175–2185. https://doi.org/10.1093/gji/ggac291

Wessel, P., Luis, J.F., Uieda, L., Scharroo, R., Wobbe, F., Smith, W. H. F., and Tian, D. (2019). The Generic Mapping Tools version 6. *Geochemistry, Geophysics, Geosystems, 20*, pp. 5556–5564. https://doi.org/10.1029/2019GC008515

Widmer-Schnidrig, R. (2022). Observation of acoustic normal modes of the atmosphere after the 2022 Hunga-Tonga eruption. *EGU 2022, Vienna, Austria*. https://doi.org/10.5194/egusphere-egu22-13581

Wilson, R. I., Admire, A. R., Borrero, J. C., Dengler, L. A., Legg, M. R., Lynett, P., McCrink, T. P., Miller, K. M., Ritchie, A., Sterling, K. and Whitmore, P. M. (2013). Observations and Impacts from the 2010 Chilean and 2011 Japanese Tsunamis in California (USA). *Pure and Applied Geophysics, 170*(6–8), pp.

1127–1147. https://doi.org/10.1007/s00024-012-0527-z

World Shipping Council (WSC) (2023). *The Top 50 Container Ports. WSC webpage*. https://www.worldshipping.org/top-50-ports (accessed 20 October 2023).

Xerandy, X., Znati, T., and Comfort, L.K. (2015). Cost-effective, cognitive undersea network for timely and reliable near-field tsunami warning. *International Journal of Advanced Computer Science and Applications, 6*(7), pp. 224–233.

Yin, J. and Shi, J. (2018). Seasonality patterns in the container shipping freight rate market. *Maritime Policy & Management, 45*(2), pp. 159–173. https://doi.org/10.1080/03088839.2017.1420260

Zimmerman, M. (2012). *Pacific tsunami warning center miscalculated wave impact on Hawaii shores. Hawaii air report online*. http://www.hawaiireporter.com/pacific-tsunami-warning-center-miscalculated-wave-impact-on-hawaii-shores/123 (accessed 20 October 2023).

Authors' biographies

Bruce E. O. Thomas received a M.Sc. degree in geomatics applied to risk and resilience studies at the ENSG-Geomatics and ENTPE engineer schools in France in 2019. He worked on volcanic ground deformation using GNSS data at the University of Hawai'i, Honolulu, USA, as well as tsunami hazard mapping at the Research Institute for Development, Nouméa, New Caledonia. He is now a research assistant and Ph.D. student at the University of Stuttgart, Germany. His current research explores the application of cost-effective geodetic techniques for natural hazard assessment and warning studies in the Pacific region.

Bruce E. O. Thomas

James H. Foster received a B.Sc. degree in geophysics from the University of Edinburgh, Edinburgh, U.K., in 1991 and a Ph.D. degree in geology and geophysics from the University of Hawai'i, Manoa Honolulu, HI, in 2002. He is Professor of Space Geodetic Techniques at the University of Stuttgart. His current research interests include the applications of geodetic techniques to the detection and mitigation of natural hazards.

James H. Foster

Tasnîme Louartani received a M.Sc. degree in geomatics specialized in data science at the ENSG-Geomatics in France in 2023. She worked at the University of Stuttgart on mapping cargo ships in the Pacific Ocean. She is currently a research engineer focusing on data management and exchange in the context of urban research and sustainable development at the University Gustave Eiffel, Champs-sur-Marne, France.

Tasnîme Louartani

PEER–REVIEWED ARTICLE

From volunteer ping to community map – The CHS' Community Hydrography Program

Authors

Mathieu Rondeau[1], Michel Breton[1], Gabriel Montpetit-Allard[1], Michel Leger[1], Yan Bilodeau[1] and Johnny Kasudluak[2]

Abstract

To support coastal communities in collecting and using bathymetric data in the nearshore areas they depend on for travel, hunting, and fishing, the Canadian Hydrographic Service (CHS) launched its Community Hydrography Program in 2022. The Program was developed by examining the successes and shortcomings in the documentation of past community hydrography initiatives. Its method focuses on the timely generation of results, namely to maintain project participants' motivation and engagement. A use case demonstrates how community-collected bathymetry data paired with satellite data led to the creation of a community map in just 18 days.

Keywords

community hydrography · crowdsourced bathymetry · capacity building · satellite-derived bathymetry · non-navigational bathymetric maps

Résumé

Afin d'aider les communautés côtières à recueillir et à utiliser des données bathymétriques dans les zones littorales dont elles dépendent pour leurs déplacements, la chasse et la pêche, le Service hydrographique du Canada (SHC) a lancé son Programme d'hydrographie communautaire en 2022. Le Programme a été élaboré en examinant les réussites et les lacunes dans la documentation des initiatives antérieures d'hydrographie communautaire. Sa méthode est axée sur la production de résultats dans les délais impartis, notamment pour maintenir la motivation et l'engagement des participants au projet. Un cas d'utilisation montre comment des données de bathymétrie collectées par la communauté, associées à des données satellitaires, ont permis de créer une cartographie de la communauté en seulement 18 jours.

Resumen

Para ayudar a las comunidades costeras a recopilar y usar datos batimétricos en las zonas cercanas a la costa de las que dependen para viajes, caza y pesca, el Servicio Hidrográfico de Canadá (CHS) lanzó su Programa de Hidrografía Comunitaria en el 2022. El Programa se desarrolló examinando los éxitos y carencias en la documentación de anteriores iniciativas de hidrografía comunitaria. Su método se centra en la generación puntual de resultados, es decir, para mantener la motivación y compromiso de los participantes en el proyecto. Un caso práctico demuestra cómo los datos batimétricos recopilados por la comunidad combinados con datos de satélite llevaron a la creación de un mapa comunitario en solo 18 días.

✉ Mathieu Rondeau · mathieu.rondeau@dfo-mpo.gc.ca

[1] Department of Fisheries and Oceans Canada (DFO), Canadian Hydrographic Service (CHS), Canada

[2] Northern Village of Inukjuak, Québec, Canada

https://doi.org/10.58440/ihr-30-1-a07

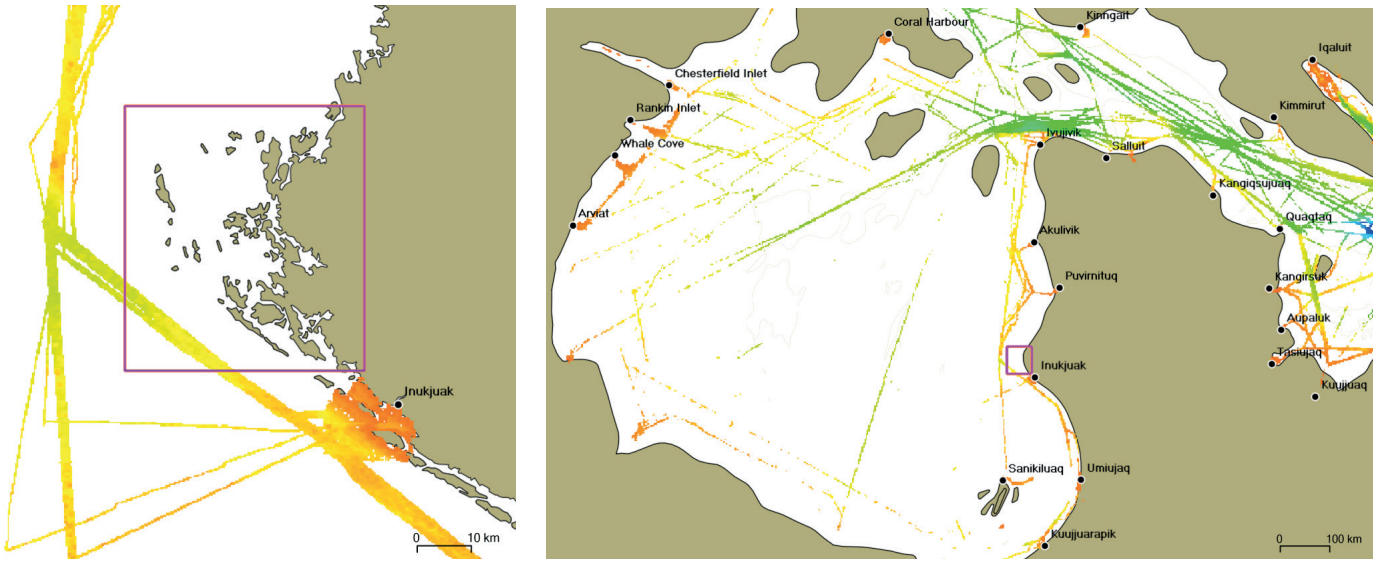

Fig. 1 Non-Navigational (NONNA) bathymetric coverage for Hudson Bay: Only the shipping corridors and community approaches have been surveyed (right). Area of interest in the Inukjuak Marine Region, to the northwest of the community remains unsurveyed (left).

1 Introduction

The International Hydrographic Organization's (IHO) report *Status of Hydrographic Surveying and Charting Worldwide* (IHO, 2023) reveals that within the depth range of 0–200 metres, 23 % of Canada's territorial waters are completely unsurveyed, and 66 % require further resurveying. This is especially true in the Arctic, where an internal report (HDACoE, 2023) states that the estimated gaps in Canada's 100-m resolution bathymetric data elevation model are 87 % in the eastern part of the Arctic and 93 % in the western part.

This situation can be explained twofold: first, Canada has the longest coastline in the world and huge amounts of navigable waters within its boundaries, and second, the Canadian Hydrographic Service (CHS) does not have the resources to survey and chart all these waters. Consequently, CHS decides "which waters to survey and chart in priority, depending on relevant considerations, such as safety of navigation, efficiency and density of maritime traffic, natural features of the area (tides, currents, winds, geography, and hazards), access to ports and waters for ocean-going vessels" (DFO-CHS, 2022).

An example of this approach that is specific to the Arctic is the clearly successful strategy implemented under the Phase 1 of the Ocean Protection Plan (OPP). It involved focusing the CHS' efforts on the corridors used by merchant vessels (Fig. 1, right). As a result, from 2016 to 2022, the CHS succeeded in increasing its bathymetric coverage in the primary and secondary shipping corridors (of the NORDREG Zone specifically) by 12 % (Marshall, 2022), bringing coverage of the latter to 42 % of completion.

Though they obviously depend on shipping corridors for supplies, communities mainly use the near-shore areas for travel, hunting, and fishing. Coastal routes offer shorter transit time and are less exposed to winds and swells and are therefore more convenient for smaller boats. However, these community-used areas, which are often shallower and dotted with shoals and underwater rocks, remain largely unsurveyed (Fig. 1, left).

Though focusing on securing the main shipping corridors, the CHS is attentive to the needs of coastal communities. This is why, the CHS enhanced its contribution to the "Improving Maritime Safety" pillar under Phase 2 of the Ocean Protection Plan (OPP), by creating the Community Hydrography Program. The Program aims to "support Indigenous and coastal communities in the collection and use of bathymetric data to improve the collective understanding of the ocean floor in poorly studied areas" (DFO-CHS, 2023).

Section 2 of this paper begins with an overview of past and current community hydrography initiatives in Canada. The method we propose and detail here is aligned with the Community-Led Engagement for Adaptability and Resilience (CLEAR) approach (Stewart, 2023), which proposes to start adaptability and resilience to climate change efforts by fully understanding coastal communities' needs and cultural practices.

This approach lays the groundwork for the Community Hydrography Program, which the CHS launched in 2022 and that will be presented in Section 3. This latter briefly introduces the concepts for implementing the Program that stem from the takeaways of past and current initiatives. A special focus will be put on the importance of communities seeing rapid results. In Section 4, we will delve into how such a quick turnaround for communities has been efficiently attained, using three main strategies: rapid data routing, automated processing and quality data analysis, and assisted data valorization in the form of bathymetric community maps. Section 5 will examine the case study of Inukjuak Marine Region (IMR) to illustrate how these strategies have come together for community benefit.

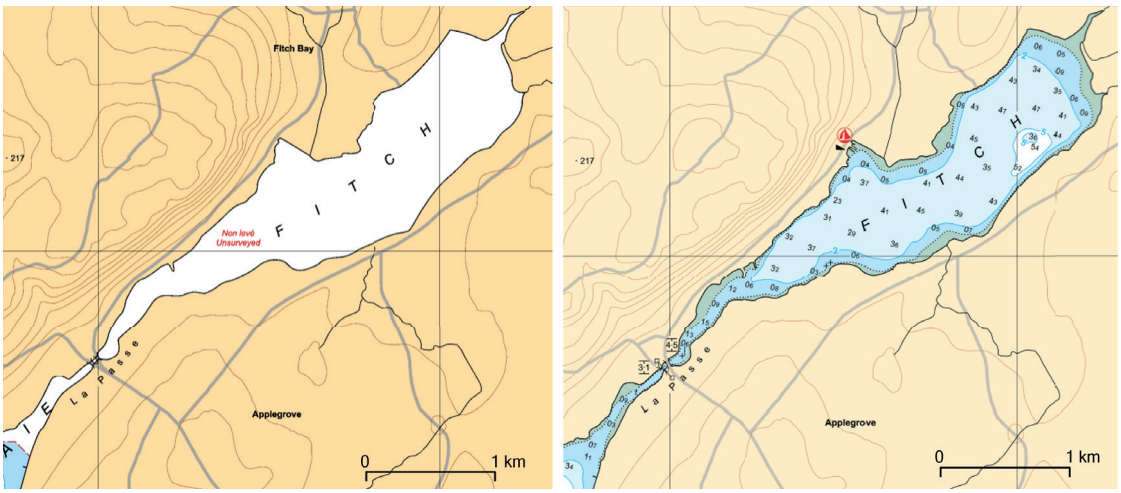

Fig. 2 Chart 1360 – Lake Memphrémagog, with a close-up of Fitch Bay before the project (left) and after the project (right). Credit: Canadian Hydrographic Service.

2 Community hydrography in Canada: an overview

The first known reference to supporting Canadian coastal communities in bathymetric data collection – the BAThyWeb 2.0 proposal (Roche et al., 2011) – dates back to 2011. Although not implemented, BAThyWeb 2.0 had already theorized, more than ten years ago, the type of solution we see today. It consisted of three segments: bathymetric data acquisition, processing, and dissemination. The data acquisition segment was based on a modified low-cost multibeam fish echosounder for depth measurements, linked to a smartphone for position, time and attitude measurements, as well as for data transmission via a cellular network. The data processing segment was based on a web service approach using open-source software to correct data with predicted tides and synthetic sound speed profiles. The data dissemination segment was based on a web portal offering quality management and visualization tools.

Since 2011, coastal communities' interest in bathymetric data collection has grown exponentially. We will start by tracing the evolution of notable community hydrography initiatives in Canada, presenting these initiatives in chronological order.

2.1 Fitch Bay, QC – Memphremagog Conservation (2017)

In 2017, the non-profit Memphremagog Conservation requested the CHS to conduct a bathymetric data collection campaign in Fitch Bay of Lake Memphrémagog. Its objective was to gain bathymetric knowledge of this unsurveyed bay, to improve oversight and regulation of navigation, and thus to reduce the impact of waves generated by power-driven pleasure craft along the shore. The CHS loaned two HydroBalls and trained two Memphremagog Conservation employees on bathymetric data collection. The data was then processed by the CHS and the official chart of the lake was updated (Fig. 2). Seeking to strengthen community capacities in hydrographic data collection, this initiative was the first of its kind documented at the CHS (Côté et al., 2018).

2.2 Crowd-Sourced Bathymetry in Northern Canada, COMREN (2017–2019)

From 2017 to 2019, efforts were made in three communities under the Crowd-Sourced Bathymetry in Northern Canada project funded by the Fund for Innovation and Transformation. The three communities were: 1) Quaqtaq, QC; 2) Gjoa Haven, NU; 3) Iqaluit, NU. Bilingual workshops (English/Inuktitut) were offered to introduce interested participants to crowdsourced bathymetry concepts and benefits, as well as to explain how to deploy the HydroBall and HydroBox bathymetric data collection systems (Desrochers, 2018; Desrochers et al., 2020). In each community, surveys were carried out by trained participants (Figs. 3 and 4).

Here are the four main takeaways from the project report (COMREN, 2019):

1. The report validated the concept of pre-qualified bathymetric data collection systems (HydroBall, HydroBox). These systems allowed individuals without expert knowledge and minimal training to collect high-quality data (IHO orders 1b and 2) (Rondeau & Malouin, 2019). However, several areas of improvement were suggested, such as increasing the HydroBall's survey speed to over four knots, simplifying HydroBox installation with a "universal" pole mount, enhancing compatibility with the NMEA 2000 protocol, automating data transfer when Wi-Fi is available, and reducing acquisition costs to improve accessibility.
2. The report delivered a prototype of an automated processing workflow for crowdsourced

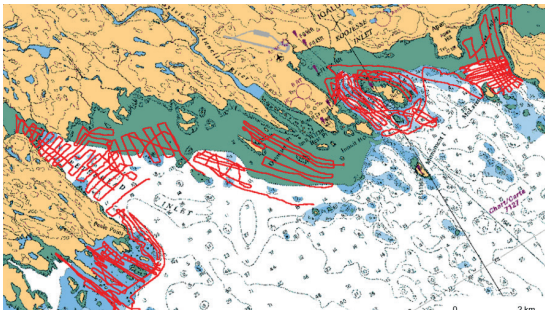

Fig. 3 Survey carried out in Iqaluit, NU.

https://doi.org/10.58440/ihr-30-1-a07

Fig. 4 Residents from the community of Gjoa Haven, NU, who took part in the workshop and training session. Credit: Parks Canada/Barbara Okpik. Survey carried out in Iqaluit, NU.

bathymetric data collected from GNSS-capable loggers (Arfeen, 2019). Additionally, it pointed out the need for developing a water-level reduction algorithm to accommodate data handling from loggers with low-grade positioning capabilities.

3. The report referred to an attempt made to create and disseminate maps to the communities via a web portal.
4. The report suggested a review of the capacity-building approach used during the project. The usual academic-style support materials (lectures and course notes) for training has shown mixed results and may not be adequate. More interactive media, such as video and animation, should be considered. The report also emphasized the importance of having a local coordinator and that monetary compensation may not be enough to ensure participant engagement. Instead, focus should be placed on tangible results and ongoing evaluation of participants' efforts and work.

2.3 Arviat, NU – Aqqiumavvik Society (2020–2021)

The community of Arviat, Nunavut, is located on the west coast of Hudson Bay. It is subject to post-glacial rebound. As the seafloor rises, new shoals emerge, increasing safety risks during navigation. Largely used by community members, the nearshore is unsurveyed for the most part.

In spring 2020, under the leadership of the Aqqiumavvik Society, the community of Arviat acquired the means to chart the seafloor in areas of interest to its members (Tagalik, 2022). The community approached the CIDCO R&D centre and the company M2Ocean to buy a HydroBlock bathymetric data collection system, and to receive training and support for collecting, processing, and validating bathymetric data. The community carried out two survey campaigns in 2020 and 2021, and subsequently, two maps were created (Figs. 5 and 6).

The data was transferred to the CHS and to the Data Centre for Digital Bathymetry (DCDB) via M2Ocean, which acted as a trusted node, a necessary intermediary for the DCDB transfer. The data transferred to the CHS were loaded into the National Bathymetric Database (BDB) and appear in the latest Non-Navigational (NONNA) bathymetric data compilation.

With support from M2Ocean, the Aqqiumavvik Society partnered with SIKU, a social network devoted to Indigenous knowledge sharing, to make the two maps available on the SIKU mobile app.

Arviat is a flagship project and an eloquent example of community capacity building for collecting and validating bathymetric data. The strength of this initiative, which has been widely discussed and shared

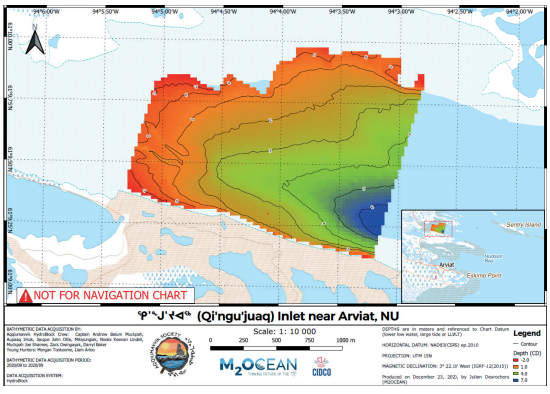

Fig. 5 Map produced following the 2020 survey. Credit: M2Ocean/Julien Desrochers.

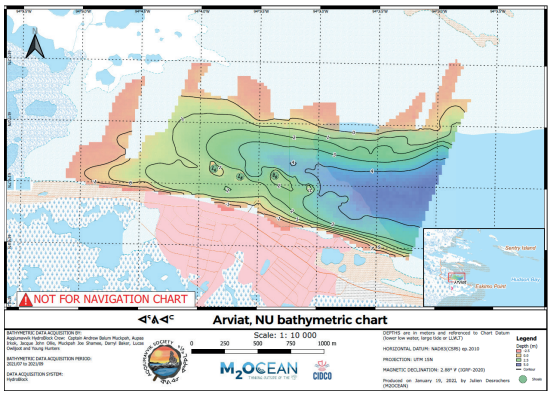

Fig. 6 Map produced following the 2021 survey. Credit: M2Ocean/Julien Desrochers.

Fig. 7 Example of bathymetric data collected in the Rankin Inlet, NU, area in 2022.

(Baker et al., 2021; Desrochers, 2021; Katz, 2022; Trethewey, 2023), lies in the community's willingness to move the project forward.

2.4 Rankin Inlet, NU – Canadian Coast Guard (2021-ongoing)

In 2019, the Canadian Coast Guard (CCG) made a request regarding the need to position uncharted shoals (on CHS navigational charts) along the coast between Chesterfield Inlet and Whale Cove in Nunavut. The goal was to ensure safe navigation for search and rescue vessels that must operate in nearshore areas during the navigation season. Offshore, a secondary shipping corridor is charted to link these communities, but a 10–20-nautical-mile strip along the coast is still unsurveyed.

In response, the CHS designed a low-cost bathymetric data logger, called the BlackBox, to equip both CCG Arctic and CCG Auxiliary search and rescue vessels to collect their own bathymetric data.

The BlackBox can be connected directly to navigation instruments and record positional measurements (latitude and longitude), depth, and time. The first logger was installed onboard a CCG search and rescue vessel *(Rosborough Roughwater 9.11)* at the Arctic Marine Response Station in Rankin Inlet, Nunavut. The data logger was still collecting bathymetric data as of 2023 (Figs. 7 and 8).

An internal report highlights challenges with data routing. On at least one occasion, the data logger's Secure Digital (SD) card was lost in the mail, causing data to be lost. The report suggests data should be transferred by internet to eliminate the need to mail SD cards and thus mitigate such issues in the future. In addition, this approach would streamline the data routing process to processing facilities and expedite data validation.

2.5 Aklavik, NT (2021–ongoing) – Tuktoyaktuk, NT (2022–ongoing)

Several companies manufacture navigational instruments for the recreational boating and fishing markets, including plotter/sounders. These consist of a multi-function display connected to at least an echo sounder and a GPS receiver. Increasingly, the recreational boaters and anglers are using this equipment to collect their own data and produce and share their own navigation charts in areas with little or no official chart coverage. Companies of note in Canada include:

- Garmin, with the ActiveCaptain crowdsourced bathymetry platform and Navionics SonarChart;
- Lowrance, with the C-MAP Genesis crowsourced bathymetry platform; and
- Humminbird, with the LiveShare Map crowsourced bathymetry platform.

We should mention that these companies operate on a service-based business model by which crowdsourced bathymetry data is re-shared with all service subscribers.

The communities of Aklavik and Tuktoyaktuk, both located in the Inuvialuit Settlement Region (ISR) in the Northwest Territories, have chosen to rely on this approach for their respective projects.

In 2021, Aklavik launched a community-based mapping project (Gruben et al., 2022) that was initially funded by Crown Indigenous Relations and Northern Affairs Canada (CIRNAC) to better understand the

Fig. 8 Installation of a CHS BlackBox onboard a CCG search and rescue vessel (*Rosborough Roughwater 9.11)* at the Arctic Marine Response Station in Rankin Inlet, NU. Credit: Canadian Hydrographic Service/Bridgette Bastedo.

https://doi.org/10.58440/ihr-30-1-a07

rapidly changing waters of the Mackenzie Estuary. The community purchased off-the-shelf recreational sports-fishing-grade sonars (Lowrance HDS; Fig. 9) to equip a fleet of 14 local boats. The local boaters collected 10,400 km of linear opportunistic data. This data was then uploaded into the cloud-based C-Map Genesis platform to create bathymetric maps. These maps are available to view through the publicly accessible C-Map Genesis Social Dashboard.

With support from the CHS, Tuktoyaktuk was able to secure funding to conduct their own community-based bathymetry project in 2022. The project took an approach similar to that used in Aklavik: five off-the-shelf sonars (Lowrance HDS) were used to collect bathymetry data using a systematic approach. A coordinated effort was implemented by local boaters to acquire data along prescribed survey lines and areas (Fig. 10). In its first year, the program was able to hire local coordinators to help process and visualize the data in real-time. Real-time feedback of the data and resultant mosaics created a community of practice for sonar operators in the community.

2.6 Paulatuk, NT – Anguniaqvia niqiqyuam Marine Protected Area (2021–ongoing)

The Anguniaqvia niqiqyuam Marine Protected Area (MPA) is the second MPA in the Canadian Arctic to be designated under the Oceans Act, and the first with a conservation objective based solely on Indigenous knowledge.

Bathymetry is recognized as a foundational layer to physical and biological oceanography, which is central to the understanding of MPAs. However, in 2021, the Western Arctic Marine Protected Area Steering Committee, the Anguniaqvia niqiqyuam Marine Protected Area Working Group, and DFO Science identified significant gaps in bathymetry and baseline habitat surveys used to inform the Anguniaqvia niqiqyuam MPA conservation and monitoring strategies. In response to this, a three-year Competitive Science Research Fund (CSRF) project was established by DFO Science, the CHS, and the Paulatuk Hunters and Trappers Committee (PHTC).

Fig. 9 Off-the-shelf sports-fishing sonars purchased by the Hunters and Trappers Committee in Aklavik, NT. Credit: Natural Resources Canada/Dustin Whalen.

Fig. 10 Fleet of four community boats heading out of harbour in Tuktoyaktuk, NT, to conduct a bathymetric survey. Credit: Natalya Saprunova.

To support this project, the CHS: 1) loaned out two portable Norbit multibeam hydrographic survey systems and two bathymetric data loggers; 2) provided training; and 3) supported the community in collecting and processing data to create community maps.

The data collected is bound by a data-sharing agreement articulated around the Ownership, Control, Access, and Possession principles (OCAP®).

2.7 Summary of past initiatives and lessons learned

Hydrography is a complex field of science that requires a specific set of skills for collecting (IHO, 2017a and 2018a) and processing (IHO, 2017b and 2018b) hydrographic data. For this reason, in Canada, the earliest community hydrography initiatives primarily relied on the use of pre-qualified survey systems like the HydroBall (Leighton, 2019). During this initial stage, external projects proponents (universities, research centres, and departments) usually hire community members as subcontractors to assist in data collection. This approach results in a low community engagement.

Over time, a shift to community capacity building was observed. Workshops and training sessions, sometimes given in Inuktitut, were organized. Communities were consulted and their feedback influenced the evolution of data collection methods and tools. However, the main focus stayed on data collection training, with data validation tasks handled externally. While projects were still initiated by external proponents, an increase in community engagement was noted as community members' participation was encouraged and facilitated.

Since 2020, a noticeable change in leadership has been observed. Communities such as Arviat, Aklavik and Tuktoyaktuk have equipped teams for autonomous bathymetric data collection. Despite strides in data collection, these communities still rely on external support for data validation.

In 2022, the community of Paulatuk, NT, addressed a concern about data sovereignty common in Indigenous communities by protecting their data with a data-sharing agreement. This solution adheres to the principles of Ownership, Control, Access, and Possession (OCAP®), as defined by the First Nations Information Governance Centre (FNIGC, 2010), and

https://doi.org/10.58440/ihr-30-1-a07

as such was a milestone in the evolution of community hydrography initiatives.

3 Deployment of the CHS' Community Hydrography Program

Community hydrography is an evolving process with technological improvements and lessons learned from past projects informing future work. Reviewing the past initiatives and meetings with various players has helped develop the current Community Hydrography Program around the following four takeaways.

3.1 Data sovereignty

OCAP® principles are of high importance. It is absolutely essential to ensure both the databases and the platforms hosting the communities' data are secured and aligned with the OCAP® principles. While this can be perceived as counter-intuitive to the open-data concepts promoted by government organizations, applying these principles is a non-negotiable element when building trust with Program participants.

3.2 Synergy with existing initiatives

Communities are heavily solicited. A multitude of projects are presented to them by various federal and provincial agencies, groups, and universities. Consequently, some communities express fatigue and confusion about the number of projects they are asked to participate in. Therefore, it is recommended to align with or fit into programs and initiatives that are already well established in these communities. For example, the Canadian Coast Guard (CCG) and CCG Auxiliary fleets can provide vessels and participants that could be put to use for bathymetric data collection efforts. Similarly, the Enhanced Maritime Situational Awareness (EMSA) portal at Transport Canada, already well implanted and widely used in many communities, could be leveraged for presenting the collected bathymetric data.

3.3 Adequate support

Initiatives focused on academic training have not been particularly successful. The design of training activities and materials should be in line with a given community's prevailing culture. For instance, a "Western" approach, which is often based on theoretical lessons and paper-based training materials, has not worked well. Knowledge-transfer through demonstration, oral transmission, and experience-sharing, however, has shown better results. A more hands-on approach requires building a relationship and meetings in person.

Furthermore, support should not come only in the form of training. To fully engage in collecting bathymetric data, communities need resources. The cost of operating a survey vessel is significant and should not be overlooked. And, as motivated as they may be, community members must be compensated for the time they devote to planning, data collection, and administering the project. The Community Hydrography Program provides resources to some degree (DFO-CHS, 2023).

3.4 Rapid results

To retain and even increase community engagement, it is important for results to be seen quickly. Bathymetric data collection requires a lot of effort and the subsequent steps leading to data utilization should be expected to take time. However, when results from collection efforts are slow in coming or do not come at all, communities disengage from the initial partnership, look for more reactive partners, or try to re organize on their own.

4 Method

Rapid results seek to reduce the time between data collection and its use without skipping the necessary steps of data processing and validation. Rapid results involve optimizing the time it takes to turn raw data collected by a community into qualified data – that is, data with associated uncertainty – all without losing community engagement (Rondeau et al., 2023). To achieve this, action can be taken at three points in the data value chain (Fig. 11): 1) rapidly routing data from the collection area to a secure data warehouse (Section 4.1); 2) transforming raw data into qualified data using a dedicated processing and quality analysis infrastructure (Section 4.2); 3) converting the qualified data into a value-added product, such as a bathymetric community map (Section 4.3).

4.1 Data routing

As observed in several past initiatives, the manual routing of data hinders rapid results. Therefore, automated data transfer from the vessel to the data warehouse should be preferred. However, considerations of limited connectivity and control over the data lead many communities to prefer offline data loggers.

The Community Hydrography Program relies on three types of loggers: the CHS BlackBox, the OFM

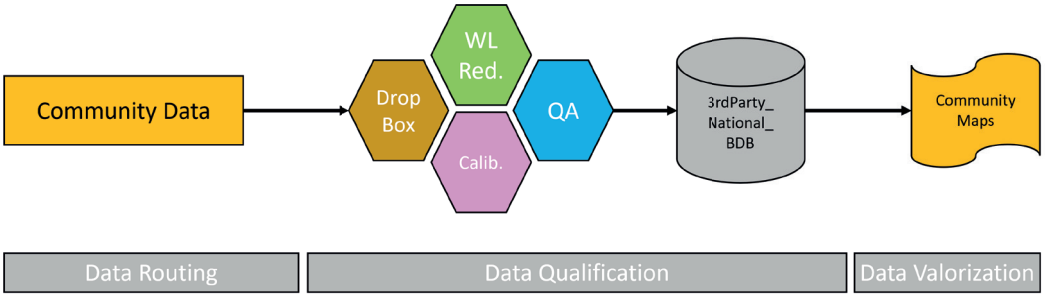

Fig. 11 Conceptual schema showing the efficient value-added chain to transform raw community data into community maps.

https://doi.org/10.58440/ihr-30-1-a07

Mussel Kit and the UNH WIBL. The CHS BlackBox is a basic data logger manufactured in-house. Its current version has no connectivity capabilities. The OFM Mussel Kit is a data logger manufactured by the Canadian company Orange Force Marine (OFM), which works with a subscription-based CSB data collection service. The OFM Mussel Kit is leased to the client and the data collected is transferred to the cloud when in cellular range, where it is processed and made accessible to the client via the Terradepth platform. The OFM solution has been successfully deployed as part of the Lakebed 2030 initiative, supported by the Great Lakes Observing System (GLOS). The Wireless Inexpensive Bathymetric Logger (WIBL) is an open-source project led by the University of New Hampshire (UNH) (Calder et al., 2018; Calder, 2023a). The WIBL data logger has open source hardware and software, and its designs and code are shared on a BitBucket directory (Calder, 2023b).

4.2 Data qualification

Community hydrography data is managed in a dedicated infrastructure where data from the loggers can be safely received, stored, processed, qualified, assessed, and returned to the communities. The infrastructure consists of: 1) a Dropbox™ repository; 2) a processing module for the reduction of water levels; 3) a calibration module that calculates and applies correction for vessel's draft; 4) a validation/quality assurance module; and, 5) a storage module referred to as the 3rdPartyBDB. The processing workflow has been prototyped in Python language, coupled with Caris HIPS and Caris BE command line libraries, PostGIS and spatial Python libraries. Currently the workflow is functional in the Caris environment with plans to modify some modules within the workflow in the future, so that they are functional outside the Caris ecosystem and can be made available to any community wishing to use this workflow independently.

The workflow for the above-described infrastructure is detailed step by step as follows:

In Step 1, data is deposited on the Community Hydrography team's Dropbox™ repository. The files must contain, at a very minimum, the time, date, latitude, longitude, and depth for each measured sounding.

The files can be deposited manually (in the case of a data logger without telecommunication capability) or automatically (if the data logger has telecommunication capability). Currently, CHS BlackBox, OFM Mussel Kit and UNH WIBL are the supported data loggers. As soon as a file is deposited in the repository, it is detected and downloaded onto the CHS network, and an email is sent to the Program team to inform members that data is ready for processing.

In Step 2, data is reduced for water levels. The approach used is similar to that proposed by NOAA (Klemm & Krabiel, 2023). The Integrated Water Level System (IWLS) web service is queried to receive the position of all available tide gauge stations in Canada at the time of the request. A global influence map using the Voronoi polygon principle is then built for all of Canada (Fig. 12). Each Voronoi polygon represents the area of influence of its associated tide gauge station.

Fig. 12 Map of tide gauge stations and their respective areas of influence (Voronoi polygons) for all of Canada. Green = stations for which predictions are available. Pink = stations for which observations are available.

The bounding polygon of the dataset to be reduced is then superimposed on the global influence map (Fig. 13). The Voronoi polygons that touch the survey envelope are retained, and the associated tide gauge stations are queried to see if observation and/or prediction data are available for the time period covered by the dataset. The observation data will be prioritized for a tide gauge station responding with both observation and prediction data.

If a tide gauge station does not respond for observed or predicted tides for the requested time period, its Voronoi polygon is removed and a new influence map is generated (Fig. 14).

The current approach has certain limitations, particularly in complex coastal areas. A more sophisticated method is currently being considered. This method would no longer rely on the area of influence to select tide gauge stations, but rather on the search for the shortest routes (from soundings to closest tide gauge), all while taking into account constraints related to the coastline's morphology, such as the prohibition of crossing a land area.

This processing section ends with the generation of a bathymetric surface at 10-, 15-, or 20-m resolution, according to the user's choice, vertically referenced to Chart Datum.

In Step 3, data is calibrated for the vessel's draft. Even though it is possible for the user to configure a ship geometry file, the calibration module is relevant for correcting residual errors in the draft measurement or even estimating it completely if the boat's geometry is unknown. The idea is to systematically compare the dataset to be calibrated with the best bathymetric surfaces available in the CHS databases, as referred to as peer-consistency assessment in Section 4 of B-12 (IHO, 2022). Here again, the implementation principle is similar to that proposed by NOAA (Klemm & Krabiel, 2023). The bounding polygon of the dataset to be calibrated is used to query all the qualified CatZOC A1 bathymetric surfaces available in the CHS regional databases. A surface

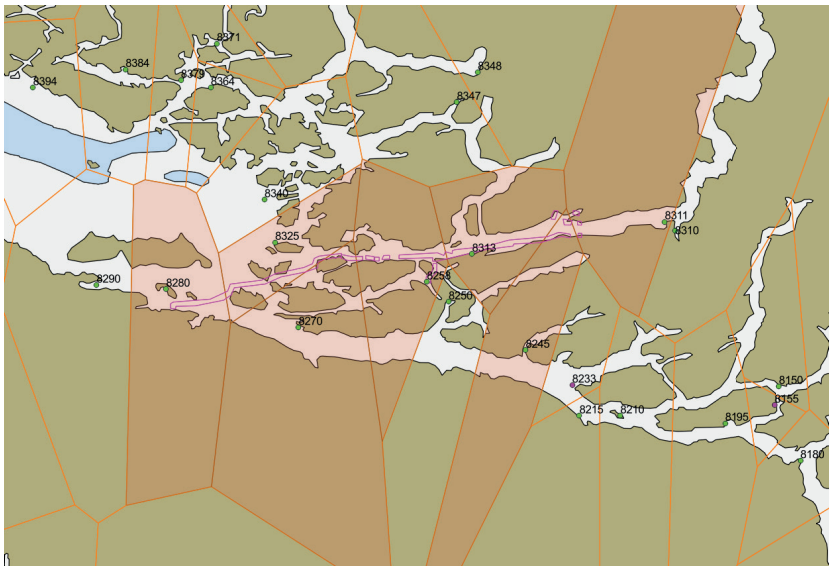

Fig. 13 Bounding polygon of the dataset to be reduced, superimposed on the global influence map. Highlighted are the Voronoi polygons solicited by the dataset to be reduced.

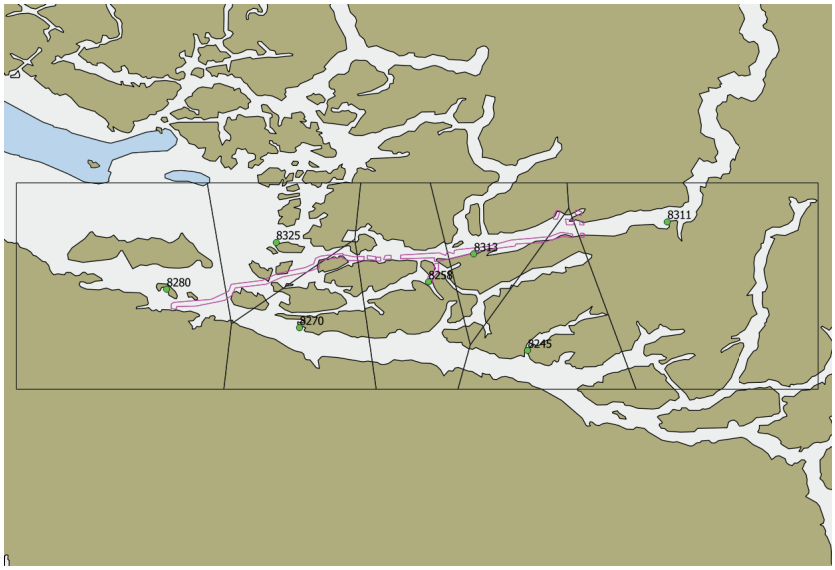

Fig. 14 Final influence map generated to guide the water-level reduction.

difference is calculated for each overlapping CatZOC A1 dataset. A graph and statistics are generated for each overlap. The average of the overlap differences is calculated and a shift value is proposed for application. The user running the script must either accept or deny application of the shift.

In Step 4, the bathymetric surface and its metadata are loaded into the dedicated 3rdPartyBDB.

4.3 Data valorization

For community hydrography data to be fully utilized, it must be transformed and represented in the form of a value-added product, such as a map. In the past, the creation of bathymetric maps was a complex, labour-intensive process, necessitating specialized knowledge and tools. However, recent research and developments in cartography have made this task more accessible. A significant example of this progress was observed during the Speed Mapping Challenge (COMREN, 2022), which took place at the Canadian Hydrographic Conference in 2022. This competition demonstrated the feasibility of rapidly producing bathymetric maps using open data and free software. The innovative solution of the winning team was subsequently presented in (Kastrisios et al., 2023).

Building on this demonstration during the Speed Mapping Challenge, the Program team offered its support in developing a plugin to the QGIS software. This plugin helps communities to draft bathymetric community maps, using both their own bathymetric data and open data of interest (Fig. 15).

The plugin, named UMap, requires three inputs: 1) the extents of the area of interest to be mapped; 2) the coastline of the area of interest; and, 3) one or more bathymetric digital terrain models.

Users are suggested a compilation scale, depending on the area of interest extents, from the scales 1:8,000; 1:12,000; 1:22,000; 1:45,000; 1:90,000; 1:180,000; 1:350,000. The coastline can be provided as a URL link to a Web Feature Service (WFS) or as a vector file. The bathymetric digital terrain models can be provided as a URL link to a Web Coverage Service (WCS), like NONNA in Canadian territorial waters, or as raster files.

Based on the input data, the plugin can produce a community bathymetric map composed of a shoreline, land areas, bathymetric contours, depth areas, and a sounding selection. Four main behaviours have been coded:

The maps created with the UMap plugin are referred to as "community maps" (Fig. 17), which we define as follows:

1. Vertical adjustment: The vertical reference to the map will be that of the reference bathymetric digital terrain model (DEM). If multiple bathymetric DEMs are provided, users must choose the DEM to act as reference. The other DEMs are then shifted toward the reference DEM to ensure overall consistency.
2. Deconfliction: In cases where multiple bathymetric DEMs overlap in the same area, the DEM showing the shallowest bathymetry is preferred.

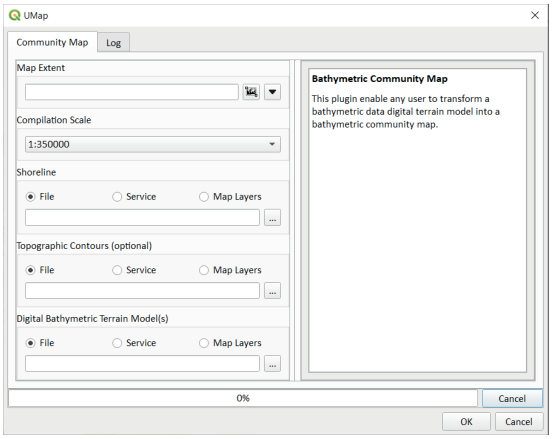

Fig. 15 UMap QGIS plugin. Credit: IIC Technologies.

https://doi.org/10.58440/ihr-30-1-a07

3. Management of partially covered areas: In the case of partially covered areas (commonly known as "spaghetti surveys"), the bathymetric contours are interpolated and adjusted with dotted lines. However, sounding selection is forced on measured data only (Fig. 16).
4. Contours and sounding selection creation: A good bathymetric map is a simplified but accurate representation of the underwater landscape. With a judicious choice of contours and soundings, a good map will facilitate its users' comprehension of the general configuration of the seabed topography. In the context of a bathymetric community map production, for purposes other than navigation, the plugin focuses on the following two main principles during the contour generation and sounding selection stages:
   a. the bathymetric contours and sounding selection must complement each other for map legibility, and
   b. the sounding selection must be limited to show least depths (delineated by a depth contour), shoals, deep and supportive soundings.

"A community map is a map that is created by and for a specific community to support its better understanding of the seafloor topography in a given area. It is most often constructed from open data (for example, non-navigational bathymetric NONNA data in Canadian waters), and can also incorporate data collected by the community. The map uses distinctive symbology to differentiate itself from official navigational products. As it does not adhere to the standards and norms established by hydrographic organizations, a community map is not an official navigational product and should not be used as such."

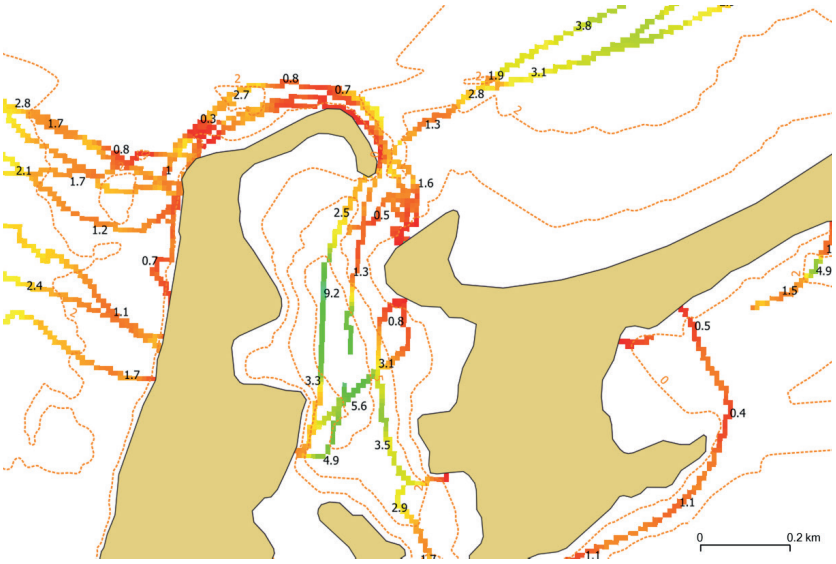

Fig. 16 Management of a partially covered area in Tuktoyaktuk, NT. Rainbow colours = partial "spaghetti" type coverage. Orange dotted line = interpolated contours. Black numbers = forced sounding selection on measured data.

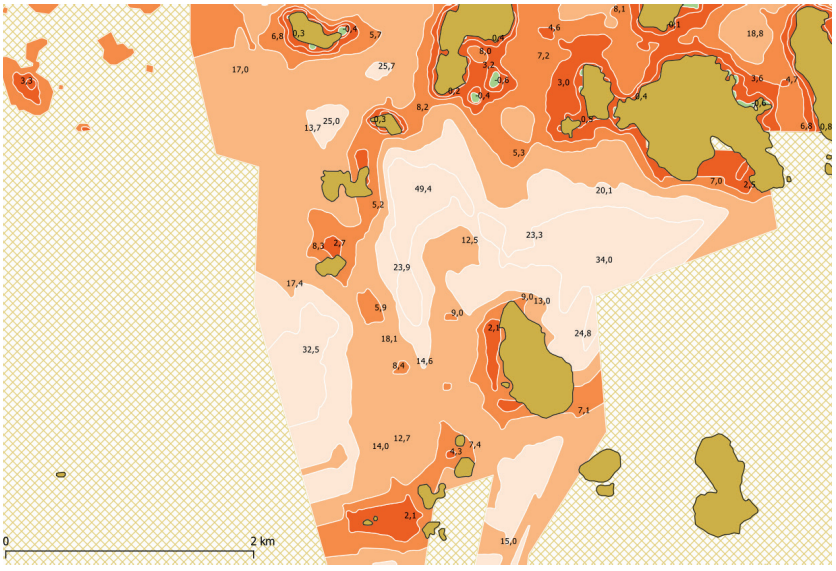

Fig. 17 Community map of part of the Inukjuak Marine Region. The community map is based on bathymetric data collected by the Inukjuak community located on the eastern shore of Hudson Bay.

5 Results

The Inukjuak North Marine Corridor is an eloquent illustration of the method detailed in this paper. The Northern Village of Inukjuak is a municipality on Inuit lands in Quebec, on the eastern shore of the Hudson Bay. Inukjuak faces the same challenges as the above-mentioned community of Arviat, its neighbour across the bay. As post-glacial rebound occurs all around Hudson Bay, coastal areas are becoming progressively more dangerous for harvesters and other land users. The ever-present reality of shallows transform into shoals, and shoals into islands is the norm.

The project took place in the so-called Inukjuak Marine Region (IMR), a vast, secluded area between Innaliit qikitailu Inutjuap taqrangani, a long north-south island chain [also known as the Hopewell and other islands north of Inukjuak] and the Nunavik mainland on the eastern shore of Hudson Bay. This area is almost completely unsurveyed. The available bathymetric data is very old, if not completely non-existent, which, hinders daily activities in the community. In fall 2023, Inukjuak's community members who showed interest in increasing their knowledge of their area's seafloor topography received support from CHS' Community Hydrography Program.

5.1 From volunteer ping to community map in 18 days

A community map was created in just 18 days. The project unfolded day by day, as follows. On Day 1, Johnny Kasudluak, the project coordinator in the Northern Village of Inukjuak, identified the area of interest. On Day 2, an order was placed by the Program team on the EOMAP SDB-Online service; this was presented in a previous issue of IHR (Hartmann et al., 2022). The Satellite-derived Bathymetry (SDB) for the area of interest was requested and received the following day, Day 3. The

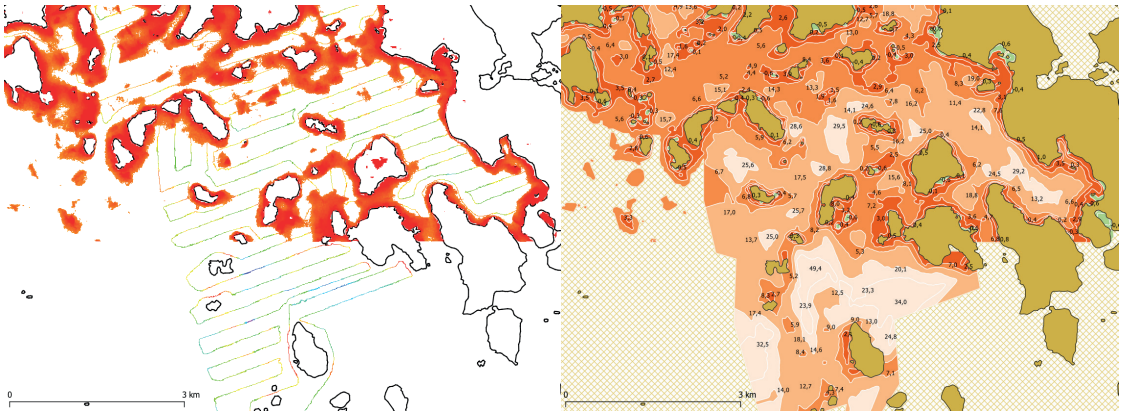

Fig. 18 Left: Bathymetric surface derived from SDB data and bathymetric survey lines collected by the community color coded by depth. The line pattern shape followed by the vessel *Arvik* can be seen. Right: Community map as produced in QGIS with the UMap plugin.

SDB was initially used as a reconnaissance survey to securely plan the deployment and route of the vessel *Arvik*, which had been previously fitted with a CHS BlackBox data logger. A survey-line pattern was drawn jointly by the Program team and Mr. Kasudluak, based on the SDB layer. The line pattern was then sent the same day to the *Arvik* crew in a GPX format so that it could be displayed by the on-board chart plotter. On Day 8, the *Arvik* left Inukjuak harbour with a heading to the area of interest. Surveying was started the very same day. After roughly 20 hours of surveying over four days, the *Arvik* had collected 300 linear kilometres of bathymetric data. At the end of Day 11, just before nightfall, the *Arvik* docked at Inukjuak harbour. On Day 15, the collected bathymetric data was dropped into the Program's Dropbox™ account. On Day 16, the data were automatically processed, qualified, and loaded into the 3rdPartyBDB. On Day 18, the community bathymetric surface and the SDB surface were put into the UMap plugin to create a community map (Fig. 18). The map was then published in Inukjuak's secure space on the Transport Canada's EMSA platform and made available to community members on their smartphones via the EMSA mobile app.

Such rapid results generate engagement and interest for hydrography in coastal communities in Canada. The efficient data-transfer solutions, the automation of data processing, and the UMap QGIS plugin facilitate tangible results for communities, which in turn increases their motivation. The method described in this paper can be implemented entirely or partially by any interested community. It is not finite, but rather a work in progress. The Program team is working on alternative solutions to provide as many options as possible to meet communities' various needs.

5.2 SDB and community-based survey are complementary

This use case demonstrates that "alternative" bathymetric data sources, such as Satellite-derived Bathymetry (SDB) and community-collected data, complement each other exceptionally well. SDB is the ideal reconnaissance survey to secure the deployment of a community vessel in an unsurveyed area. In return, the community survey serves as *in situ* reference data to validate the SDB. The Inukjuak pilot project collected 5,600 community survey soundings overlapping the SDB dataset in the IMR. The collected samples are distributed around an average difference of -0.2m (SDB shows on average shallower depth than the community survey) and a standard deviation of 1.8 m at 95 % confidence.

6 Conclusion

Coastal communities in Canada are struggling with climate change. In some areas the coastline is eroding while elsewhere post-glacial rebound is causing the seafloor to lift and biodiversity is changing. Forced to adapt, northern communities are looking to bathymetric data, which is recognized as a foundational layer for understanding the marine environment and making informed decisions to protect it. The Community Hydrography Program is dedicated to engaging with communities and helping them achieve their hydrographic aspirations in ways that are in line with their values and needs. The Program is articulated around capacity building and the generation of rapid results – and both seem to be successful ways to sustain the motivation of all project participants. Such rapid results rely on quick data routing from field to data warehouse, on automation to transform raw bathymetric data into processed, ready-to-use data, and on community maps as a way for communities to conveniently present and leverage the data collected.

References

Arfeen, K. (2019). *Automated Processing of Arctic Crowd-Sourced Hydrographic Data While Improving Bathymetric Accuracy and Uncertainty Assessment*. Master's thesis, The University of New Brunswick, Canada.

Baker, K., Tagalik, S. and Desrochers, J. (2021). Don't hit rocks – Economic Equity in Ocean Mapping. *Map the Gaps Symposium*, Redux. https://www.youtube.com/watch?v=_tgWFG5Ua6A (accessed 31 January 2023).

Calder, B. R., Dijkstra, S. J., Hoy, S., Himschoot, K. and Schofield,

https://doi.org/10.58440/ihr-30-1-a07

A. (2018). A Design for a Trusted Community Bathymetry System. *2018 Canadian Hydrographic Conference*, March 27–29, Victoria, BC, Canada. Canadian Hydrographic Association.

Calder, B. R. (2023a). Design of a Wireless, Inexpensive Ocean of Things System for Volunteer Bathymetry. *IEEE Internet of Things Journal*, 10(11), pp. 9534–9543. https://doi.org/10.1109/JIOT.2023.3234500

Calder, B. R. (2023b). *Wireless Inexpensive Bathymetric Logger (WIBL) – BitBucket*. https://bitbucket.org/ccomjhc/wibl/src/master/ (accessed 17 March 2023).

COMREN (2019). *Crowd-Sourced Bathymetry in the Northern Canada Area*.

COMREN (2022). *Speed Mapping Challenge*. https://oceanmapping.ca/2022/06/speed-mapping-challenge/ (accessed 16 January 2024).

Côté, R., Biron, A., Bouillon, G. and Lebel, É. (2018). Autonomous vehicules: The Canadian Hydrographic Service Journey, *Canadian Hydrographic Conference*. Vancouver.

Desrochers, J. (2018). A crowdsourced approach for capacity building in North Canada. *Canadian Hydrographic Conference*, Vancouver.

Desrochers, J. (2021). Collaborative Bathymetry in Arviat. *US Hydro Conference 2021*.

Desrochers, J., Ndeh, D. and Regular, K. (2020). Crowd Sourced Bathymetry in Northern Canada. *Proc. Canadian Hydro. Conf.*, 24–27 Feb., Québec City, QC, Canada.

DFO-CHS (2022). *About the Canadian Hydrographic Service – What we do*, *Official CHS web site*. https://www.charts.gc.ca/help-aide/about-apropos/index-eng.html#legal (accessed 24 January 2024).

DFO-CHS (2023). *Community Hydrography*, *Community Hydrography web page*. https://www.dfo-mpo.gc.ca/science/hydrography-hydrographie/opp-ppo/index-eng.html (accessed 14 February 2024).

FNIGC (2010), *The First Nations Principles of OCAP*. https://fnigc.ca/ocap-training/ (accessed 29 January 2024).

Gruben, M., Pascal, J., Whalen, D., Loseto, L., Hunters, A. and Trappers Committee (2022). The Aklavik Mapping Project. *ArcticNet Annual Scientific Meeting*, Toronto. https://doi.org/10.1139/as-2023-000

Hartmann, K., Reithmeier, M., Knauer, K., Wenzel, J., Kleih, C. and Heege, T. (2022). Satellite-derived bathymetry online. *The International Hydrographic Review, 28*, pp. 53–75. https://doi.org/10.58440/ihr-28-a14

HDACoE (2023). *CHS Bathymetric Gap Analysis 2023*. Hydrographic Data Access Centre of Expertise, Canadian Hydrographic Service, Canada.

IHO (2017a). *Standards of Competence for Category 'B' Hydrographic Surveyors*. IHO Publication S-5B, Edition 1.0.1. International Hydrographic Organization, Monaco.

IHO (2017b). *Standards of Competence for Category 'B' Nautical Cartographers*. IHO Publication S-8B, Edition 1.0.0. International Hydrographic Organization, Monaco.

IHO (2018a). *Standards of Competence for Category 'A' Hydrographic Surveyors*. IHO Publication S-5A, Edition 1.0.2. International Hydrographic Organization, Monaco.

IHO (2018b). *Standards of Competence for Category 'A' Nautical Cartographers*. IHO Publication S-8A, Edition 1.0.1. International Hydrographic Organization, Monaco.

IHO (2022). *Guidance on Crowdsourced Bathymetry*. IHO Publication B-12, Edition 3.0.0. International Hydrographic Organization, Monaco.

IHO (2023). *Status of Hydrographic Surveying and Charting Worldwide*. IHO Publication C-55, International Hydrographic Organization, Monaco.

Kastrisios C, Dyer N, Nada T, Contarinis S and Cordero J. (2023). Increasing Efficiency of Nautical Chart Production and Accessibility to Marine Environment Data through an Open-Science Compilation Workflow. *ISPRS International Journal of Geo-Information, 12*(3), p. 116. https://doi.org/10.3390/ijgi12030116

Katz, C. (2022). *With Old Traditions and New Tech, Young Inuit Chart Their Changing Landscape*. https://hakaimagazine.com/features/with-old-traditions-and-new-tech-young-inuit-chart-their-changing-landscape/ (accessed 14 November 2022).

Klemm, A. and Krabiel, T. (2023). From Crowd to Chart: Methods and Applications of Crowdsourced Bathymetry in Support of Safe Navigation. *US Hydro Conference 2023*, Mobile, Alabama. https://github.com/anthonyklemm/Crowdsourced_Bathy_Processing/blob/main/Klemm_CSB_USHYDRO23.pdf (accessed 18 February 2024).

Leighton, S. (2019). The HydroBall Project – Crowd Source Bathymetry in Northern Canada. *The Journal of Ocean Technology, 14*(1).

Marshall, C. (2022). National Report for Canada. *12th ARHC Meeting and Symposium on the Hydrography in Arctic*, St John's, Newfoundland and Labrador, Canada.

Roche, S., Devillers , R., Santerre, R., Nistad, J.-G. and Rondeau, M. (2011). *BAThyWeb 2.0: Bathymetry Affordable Technology on the Web 2.0*. https://doi.org/10.13140/RG.2.2.32856.37129

Rondeau, M. and Malouin, M.-A. (2019). Bad Information Is Better Than No Information At All – Assessing the uncertainty of bathymetric collaborative data collected with a HydroBox system. *Vecteur – CIDCO Symposium*, Rimouski. https://doi.org/10.13140/RG.2.2.34784.10243

Rondeau, M., Gautier, S., Montpetit-Allard, G., Bilodeau, Y. and Breton, M. (2023). «From Volunteer Ping to Community Chart» – Implementation of a «trusted-node» at CHS. *CIDCO Symposium*, Rimouski. https://doi.org/10.13140/RG.2.2.18965.19683

Stewart, H. (2023). The future is CLEAR: Community-Led Engagement for Adaptability and Resilience, *The International Hydrographic Review, 29*(1), pp. 56–64. https://doi.org/10.58440/ihr-29-a06

Tagalik, S. (2022). *Youth Marine Mapping in Arviat, Pinnguaq*. https://pinnguaq.com/stories/youth-marine-mapping-arviat/ (accessed 21 February 2023).

Trethewey, L. (2023). *The Deepest Map: The High-Stakes Race to Chart the World's Oceans* (1st ed.). Harper, ISBN 0063099977, 9780063099975.

Authors' biographies

Mathieu Rondeau

Mathieu Rondeau holds a bachelor's degree in surveying engineering from l'École Supérieure des Géomètres et Topographes (Le Mans, France) and a master's degree in geomatics sciences from Laval University (Quebec, Canada). From 2009 to 2018, he worked for the Interdisciplinary Centre for the Development of Ocean Mapping (Canada), where he gained most of his expertise in hydrographic surveying. Since 2018, he has been employed by the Canadian Hydrographic Service. For the past two years, he has been a part of the Community Hydrography Program team, dedicated to supporting coastal communities in the collection and use of bathymetric data.

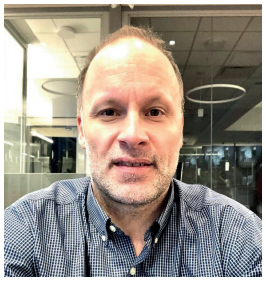

Michel Breton

Michel Breton has 15 years of experience with the Canadian Hydrographic Service (CHS). Michel initially worked as multidisciplinary hydrographer surveying and charting the west coast of Canada. Over time, a knack for innovation and data management led him onto projects meant at improving data integration in the organization. Since 2019, Michel has been involved in the digital transformation initiative at the CHS, with S-100 implementation, and more recently with crowdsourced bathymetry data. Michel is currently managing the Community Hydrography Program, a program designed to enable coastal communities in Canada to collect and utilize bathymetric data. Michel is representative for Canada on the International Hydrographic Organization (IHO) Crowdsourced Bathymetry Working Group (CSBWG).

Gabriel Montpetit-Allard

Gabriel Montpetit-Allard began his career as environment and wildlife technician in the private sector. He later obtained a bachelor's degree in physical geography from the Université du Québec à Rimouski. From 2006 to 2018, he gained professional experience in operational sciences in the private and academic sectors. He then joined the Canadian Hydrographic Service team in 2019. Since 2023, he supervises the bathymetric data acquisition and community outreach unit of the Community Hydrography Program. Through this program, the Community Hydrography team seeks to support coastal communities in their goals to collect, process and use bathymetric data.

Michel Leger

Michel Leger is currently a multidisciplinary hydrographer with the Canadian Hydrographic Service since 2019 at the Bedford Institute of Oceanography. Michel obtained a B.Sc. Eng. in Geomatics from UNB in May 2019. Michel was part of the Community Hydrography team for a four-month position in 2023 as a geomatics technician role tasked with the development and testing of the first iteration of the processing workflow. Michel still provides support and is still interested in the project and looks forward to more opportunities to assist the team in the future.

Yan Bilodeau

Yan Bilodeau, holding a Bachelor's degree in Geography from the Université du Québec à Montréal, joined the Canadian Hydrographic Service in 2017 as a multidisciplinary hydrographer. In 2019, he transitioned into the role of a geomatics specialist within the Geomatics and Technical Support team, focusing on automation projects and contributing to the development of bathymetric data processing and integration pipelines. Since 2023, Yan has been an integral member of the Community Hydrography Program team, dedicated to assisting coastal communities across Canada in collecting and utilizing bathymetric data.

https://doi.org/10.58440/ihr-30-1-a07

As the Lead Project Coordinator for the Arviliit IPCA Establishment Project, based in Inukjuak, Quebec, Johnny Kasudluak spearheads an initiative in Inuit-led conservation and protection of Arviliit (Ottawa Islands). Over the past 3 years and 3 months, they've expertly balanced on-the-ground work with remote coordination and planning. Johnny is driven by a deep-seated belief in safe marine navigation for the local Inuit population, recognizing that existing nautical charts often fail to provide accurate information due to the dynamic nature of the area's bathymetry. This motivates their dedication to driving community hydrography efforts in Inukjuak's marine region, collaborating closely with the Canadian Hydrographic Survey. Their commitment to fostering collaboration and innovation is evident in their role as they develop a pioneering model for community-led hydrographic-bathymetric research. Beyond their professional pursuits, Johnny finds inspiration in nature and the rich cultural heritage of their surroundings

Johnny Kasudluak

https://doi.org/10.58440/ihr-30-1-a07

PEER–REVIEWED ARTICLE

AI-based boulder detection in sonar data – Bridging the gap from experimentation to application

Authors

Matthias Hinz[1,2], Patrick Westfeld[1], Peter Feldens[2], Agata Feldens[3], Sören Themann[3] and Svenja Papenmeier[2]

Abstract

The detection of boulders in hydroacoustic data is essential for a range of environmental, economic and marine planning applications. The manual interpretation of hydroacoustic data for object detection is a non-trivial, tedious and subjective task. Using the conventional means accessible to hydrographic professionals, it is nearly impossible to locate all boulders or rule out their presence for extended areas of interest. Although it has been shown that AI can do the job quickly and reproducibly, earlier work has not progressed beyond scientific experiments. As a result, AI software have not been routinely integrated into the workflows of institutions involved in hydrographic data acquisition and processing, or oceanographic analysis. This paper presents a workflow for fully automated boulder detection in hydroacoustic data. A graphical user interface enables training and evaluation of detection models, boulder detection model execution, and post-processing of detection results without programming. The workflow is demonstrated on data from the southern Baltic Sea. Validation results of the detection for various data inputs include a mAP-50 of 77.83 % for raster images of backscatter intensities based on side-scan sonar, a mAP-50 of 70.46 % for raster images of slope angles based on multibeam echosounder and a mAP-50 of 44.02 % for backscatter and bathymetric data given as 3D point clouds.

Keywords

boulders · neural network · side-scan sonar · multibeam echosounder · backscatter · 3D point cloud · seabed mapping · habitat mapping · big data

✉ Matthias Hinz · matthias.hinz@bsh.de

[1] German Federal Maritime and Hydrographic Agency, Nautical Hydrography, 18057 Rostock, Germany

[2] Leibniz Institute for Baltic Sea Research Warnemünde, Marine Geology, 18119 Rostock, Germany

[3] Subsea Europe Services GmbH, 25469 Halstenbek, Germany

https://doi.org/10.58440/ihr-30-1-a08

Résumé

La détection des blocs rocheux dans les données hydroacoustiques est essentielle pour toute une série d'applications environnementales, économiques et de planification marine. L'interprétation manuelle des données hydroacoustiques pour la détection d'objets est une tâche non négligeable, fastidieuse et subjective. En utilisant les moyens conventionnels accessibles aux professionnels de l'hydrographie, il est pratiquement impossible de localiser tous les blocs rocheux ou d'exclure leur présence dans des zones d'intérêt étendues. Bien qu'il ait été démontré que l'IA peut exécuter le travail rapidement et de manière reproductible, les travaux antérieurs n'ont pas dépassé le stade de l'expérimentation scientifique. Par conséquent, les logiciels d'IA n'ont pas été intégrés de manière routinière dans les flux de travail des institutions engagées dans l'acquisition et le traitement des données hydrographiques ou dans l'analyse océanographique. Cet article présente un flux de travail pour la détection entièrement automatisée des blocs rocheux dans les données hydroacoustiques. Une interface utilisateur graphique permet la formation et l'évaluation de modèles de détection, l'exécution de modèles de détection de blocs rocheux et le post-traitement des résultats de détection sans programmation. Le flux de travail est démontré sur des données provenant du sud de la mer Baltique. Les résultats de la validation de la détection pour diverses entrées de données comprennent un mAP-50 de 77,83 % pour les images matricielles des intensités de rétrodiffusion basées sur le sonar à balayage latéral, un mAP-50 de 70,46 % pour les images matricielles des angles de pente basées sur le sondeur multifaisceaux et un mAP-50 de 44,02 % pour les données de rétrodiffusion et bathymétriques fournies sous forme de nuages de points en 3D.

Resumen

La detección de rocas en los datos hidroacústicos es esencial para una serie de aplicaciones medioambientales, económicas y de planificación marina. La interpretación manual de los datos hidroacústicos para la detección de objetos es una tarea no trivial, tediosa y subjetiva. Usando los medios convencionales al alcance de los profesionales de la hidrografía, es casi imposible localizar todas las rocas o descartar su presencia en áreas extensas de interés. Aunque se ha demostrado que la IA puede hacer el trabajo de forma rápida y reproducible, los trabajos anteriores no han llegado más allá de experimentos científicos. Como resultado, el software de IA no se han integrado de forma habitual en los flujos de trabajo de las instituciones implicadas en la adquisición y procesamiento de datos hidrográficos, o en el análisis oceanográfico. Este artículo presenta un flujo de trabajo para la detección totalmente automatizada de rocas en datos hidroacústicos. Una interfaz gráfica de usuario permite el adiestramiento y evaluación de modelos de detección, la ejecución del modelo de detección de rocas, y el post-procesado de los resultados de la detección sin programación. Se hace una demostración del flujo de trabajo con datos del sur del Mar Báltico. Los resultados de la validación de la detección para varias entradas de datos incluyen un mAP-50 de 77,83 % para imágenes ráster de intensidades de retrodispersión basadas en sonar de barrido lateral, un mAP-50 de 70,46 % para imágenes ráster de ángulos de pendiente basadas en ecosonda multihaz, y un mAP-50 de 44,02 % para datos de retrodispersión y batimétricos proporcionados como nubes de puntos 3D.

https://doi.org/10.58440/ihr-30-1-a08

1 Introduction

The automation of geospatial data acquisition, processing and analysis is a widely researched field that is constantly advancing in terrestrial (Kraus, 1997; Longley et al., 2005; Van Genderen, 2011) and marine environments (Lurton, X, 2002; Jong, 2002; Wu et al., 2021). Optical measurement techniques such as LiDAR (Light Detection and Ranging) and underwater technology such as sonar (Sound Navigation and Ranging) allow large areas of land and water bottom topography and backscatter to be surveyed, producing highly accurate data that can be displayed as either 3D point clouds (Liu et al., 2021) or raster data (Schimel et al., 2018).

Seabed topography, morphology and subsurface characteristics are typically surveyed using hydroacoustic sensors such as side-scan sonar (SSS) and multibeam echosounders (MBES). SSS and MBES are suitable for comprehensive surveys of larger areas in deeper waters. Both sensor technologies provide backscatter information while MBES can also measure depth. The amount of data collected can be classified as Big Data, as a single survey can reach hundreds of millions of data points. Therefore, it is not feasible to perform analysis manually and data handling requires powerful computing and extensive storage solutions (Wlodarczyk-Sielicka & Blaszczak-Bak, 2020).

The need for widespread, accurate and up-to-date information on the shape of the seabed is critical for many marine economic and environmental purposes (Jonas, 2023). In particular, the identification of natural (e.g. boulders) and man-made subsurface objects is becoming increasingly important (Papenmeier et al., 2020). Boulders in particular pose a potential hazard to shipping. Their exact positions must be taken into account in nautical charts, especially in areas where minimum underkeel clearance is required (Mills, 1998). Boulders also provide habitats for many marine species and need to be considered when building or extending offshore infrastructure (Irving, 2009; Grzelak & Kuklinski, 2010; Wenau et al., 2020). Identifying objects such as boulders is also important for creating accurate Digital Terrain Models (DTM) by optimising established Computer Vision (CV) methods that separate ground points from the Digital Surface Model (DSM) generated by sonar and LiDAR (Förstner & Wrobel, 2016; Silva al., 2018).

Identifying small objects such as boulders in large datasets can be challenging. Current best practice, as outlined in official guidelines (Heinicke et al., 2021), recommends the manual identification of boulders when analysing large areas. This is achieved by processing the sonar data into a mosaic with a resolution of 25 cm per pixel and then manually interpreting the data. A grid with a resolution of 25 m × 25 m (coastal waters), 50 m × 50 m (Baltic Sea) or 100 m × 100 m (North Sea) is created for this purpose and categorised according to the number of boulders into three categories: no boulders, 1–5 boulders, more than 5 boulders. This workflow is inefficient, often taking several weeks to complete for larger survey areas, and is less suitable for producing DTMs.

Within the past decade, deep learning based computer vision has emerged for sonar data (Steiniger et al., 2022) and automated boulder detection from hydroacoustic data has been an area of interest for a number of researchers. Michaelis et al. (2019) trained a Haar-like feature detector on 300 kHz SSS data for a 12 km^2 study area within the Sylt Outer Reef, North Sea and could detect up to 62 % of the overall occurrence of boulders. Feldens et al. (2019, 2021) used the YOLOv4 model for object detection on both MBES and SSS data from the west of Fehmarn, Baltic Sea. The highest mean average precision (mAP-50) was 64 % for MBES (slope rasters), and 37 % to 43 % for two different detection models for SSS data. Feldens (2020) used deep learning super-resolution to address the limited resolution of many available side-scan sonar datasets.

Van Unen & Lekkerkerk (2021) demonstrated a classification model on a point cloud derived from MBES measurements, where each point is labelled as either boulder or seabed. The evaluation showed an accuracy of 35.5 %, with almost twice as many false positives as true positives for the boulder labels. The authors concluded that the algorithm is far from trustworthy, but can help surveyors with preliminary detections. Problems included a lack of data quality and quantity, boulders being only partially classified as such, and many small pebbles being detected that would not be classified as boulders. Similar issues arise in other areas of remote sensing, such as optical sensors: Bickel et al. (2019) detected lunar rockfall based on NASA's Lunar Reconnaissance Orbiter narrow angle camera (NAC) images with an AP of 69 % for an Intersection of Union (IoU) of 50 %. Similar to the analysis of SSS data based on backscatter intensities, the analysis of the NAC images based on albedo is limited by a coarse spatial resolution of 0.5 m / pixel, and boulders are identified by an elevated albedo on their surfaces and a long shadow on the sides of the boulders.

Previously published approaches to boulder detection are based on academic case studies. In order to improve boulder detection for practical hydrography and habitat mapping requirements, existing approaches need to be refined and extended. Different hydroacoustic sensors and sensor settings need to be considered for a wide range of applications. It is also important to make these capabilities accessible to a wide range of hydrographic professionals. For this reason, it is necessary to make workflows easy to use. This can be achieved with a graphical user interface (GUI) and automated data processing routines that eliminate the need for coding or manual data transformation.

This study proposes a workflow that automatically detects boulders on both SSS and MBES data. It integrates with the existing data acquisition, processing

https://doi.org/10.58440/ihr-30-1-a08

and interpretation workflows of hydrographic and marine environmental professionals. Object detection algorithms based on Convolutional Neural Networks (CNN) are at the core of the application, but workflows including data management, pre- and post-processing are equally important, as most available AI tools and libraries are not specifically designed to work with hydrographic or geospatial data. A desktop-based user interface is presented to assist users with all key tasks, and a modular design allows for flexible expansion (e.g. support for new models and data types) in the future.

This paper is structured as follows: Section 2 outlines the methodology for AI-based boulder detection, detailing the tasks to be automated for different data inputs and different automated data workflows, as well as the configuration, training and evaluation of different deep learning models. Section 3 describes the software architecture and GUI. Section 4 presents the application of four different models to two different datasets collected using MBES and SSS sensors. The results are discussed in Section 5.

2 Workflows for automated boulder detection

2.1 Object detection of marine boulders

CNN-based object detection models were used to identify boulders in hydroacoustic datasets. A hydroacoustic dataset can be represented as a raster or a point cloud. In a raster representation, geographic space is divided into an array of rectangular or square cells to which attributes are assigned. These cells are sometimes referred to as pixels and form the elements of pictures, images or mosaics (Longley et al., 2005). The term grid, as used in the following, does not refer to the data representation or raster data, but to a network of equally spaced horizontal or vertical lines (Merriam-Webster, 2024), which may also delineate grid cells. 3D point clouds consist of a large number of 3D points. Each point consists of three coordinates that uniquely identify its location and optional attributes (Liu et al., 2021). This format is preferred for many applications related to scene understanding, as it preserves the original geometric information without any discretisation (Guo et al., 2019). Apart from the acoustic waveform, which is not analysed in this paper (Kubicek et al., 2020), backscatter intensities and bathymetry are the most common types of information included in hydroacoustic datasets. Fig. 1 shows how boulders can be visualised using this information and how they are annotated by experts as a basis for object detection. While MBES data include backscatter and bathymetry and can be represented as both point clouds and raster data, SSS data are mostly represented as raster data as they do not include bathymetry. The following Sections 2.3 and 2.4 describe workflows for each of these types of data representation separately, as they require different sets of tools and data preparation. However, several generic concepts form the common basis of both workflows and are explained in the following paragraphs and in Section 2.2.

CNN models for object detection tasks are typically trained on 2D or 3D data supplemented by annotations consisting of bounding boxes. Bounding boxes describe an approximate area in which an object is located by a surrounding rectangle in 2D space or a cuboid in 3D space. Trained detectors can predict similar bounding boxes with confidence scores between 0 and 1 for input data containing similar objects (Szeliski, 2022). Based on these conditions, we have identified the following set of basic tasks (T1–T6) that need to be performed: Boulders need to be annotated on hydroacoustic data (T1). Based on the hydrocoustic data and the annotations, a so-called ground truth (GT) dataset has to be created in

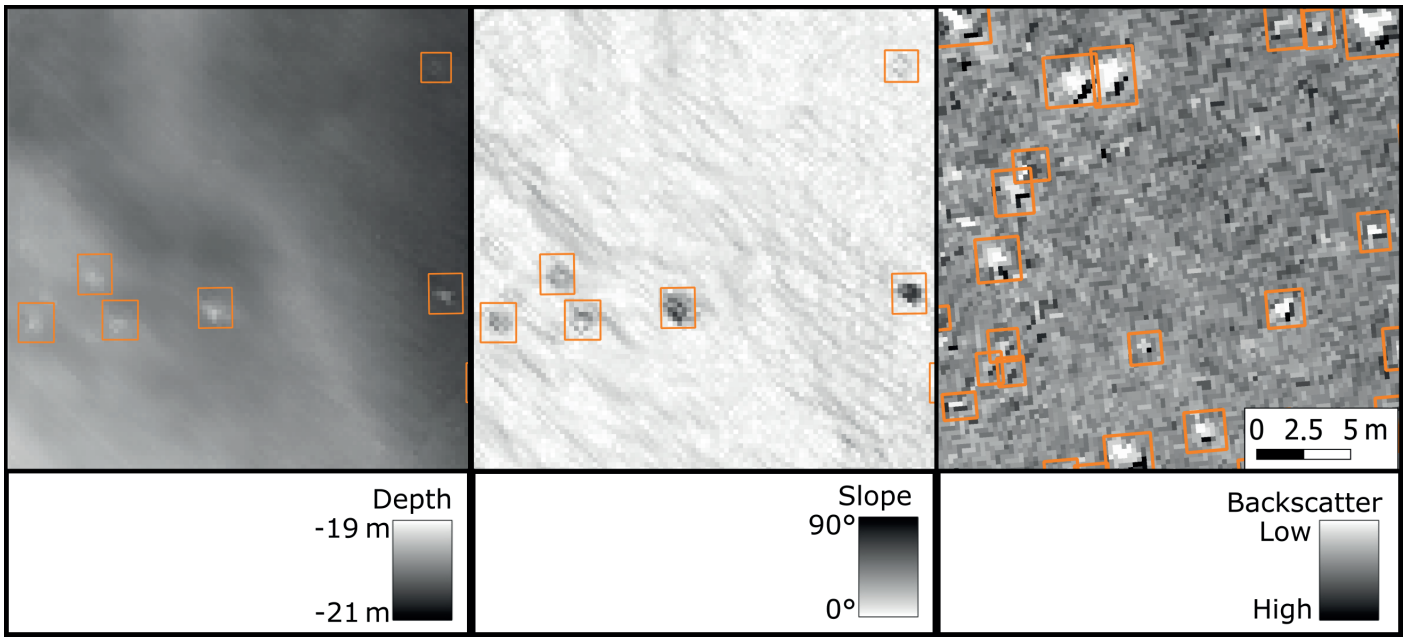

Fig. 1 Raster input data: Bathymetry (left), slope (center), side scan sonar backscatter (right) with boulder annotations shown as orange rectangles.

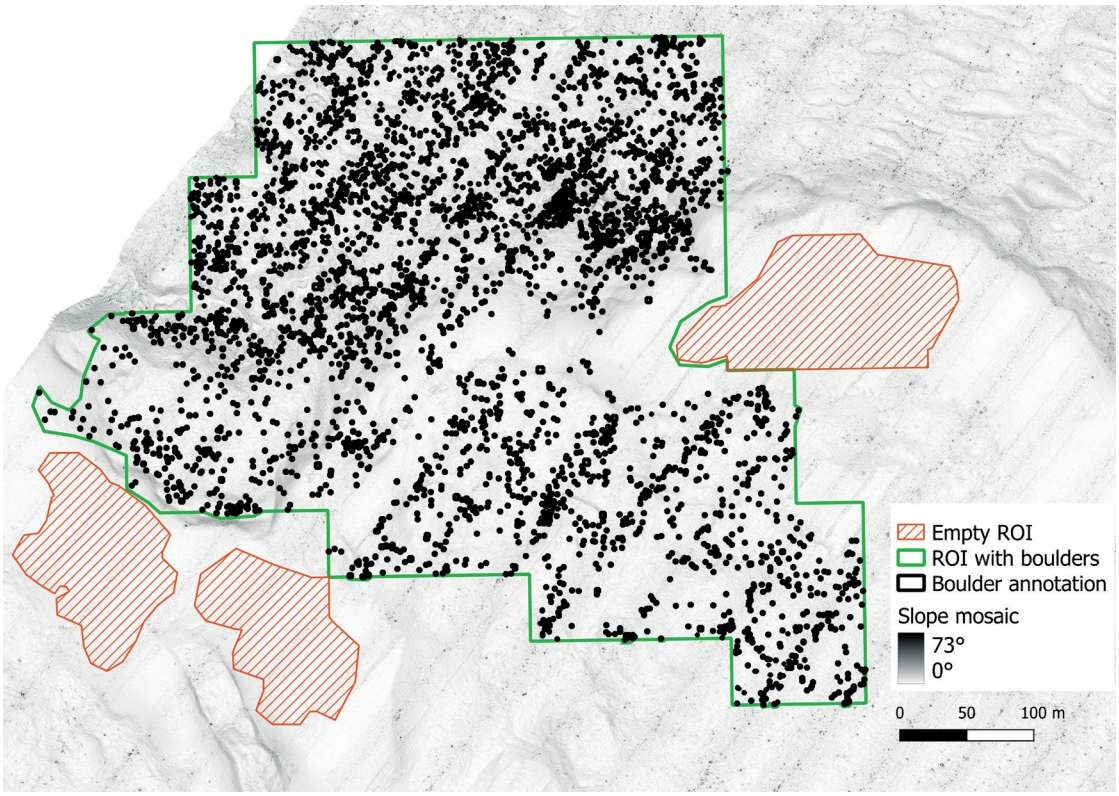

Fig. 2 Slope mosaic from MBES data of the Kadetrinne, German Baltic Sea. The black dots represent the individual annotated boulders.

the specific data format (T2) that is required for the training and validation of a specific CNN model (T3). A trained and validated model needs to be tested (T4) before it can be used to detect boulders on hydroacoustic data in a production environment (T5). The output of the detection can be post-processed to mitigate possible shortcomings of the output or to address specific user needs (T6).

Since experts have to create initial GT annotations manually, the annotation process has to be designed to meet their specific needs and habits of working with data (Fig. 2). Sonar datasets are usually visualised as large raster mosaics within a domain-specific application or a general-purpose GIS such as QGIS and ArcGIS. Within the large mosaics, Regions of Interest (ROI) are defined by polygons where annotations are to be created and later extracted from the original data. As boulders need to be distinguished from seabed and other objects, ROIs without boulders (here called empty ROI) are defined to collect examples of the latter features (similar to Feldens et al., 2021). Allowing experts to define ROIs within a larger dataset is also a means of creating a balanced dataset with sufficient variability.

CNN used for image analysis cannot process large continuous datasets as a whole. Instances of input data are limited to a few thousand pixels or data points, depending on available memory. Therefore, for both raster and point cloud analysis, the data must be retiled or sliced in order to be processed iteratively. This approach is similar to that reported by Feldens et al. (2021) and Bickle et al. (2019). Thus, all input data are overlaid with a regular grid, where the cell size and the overlap between the cells are defined depending on data resolution, object sizes and model characteristics (Fig. 3). It is necessary to define the overlaps because some objects are only partially included at the grid cell boundaries and are therefore difficult to detect. An overlap larger than the size of the expected objects ensures that all available data from each object are included in one grid cell. Cases where objects occur in more than one grid cell due to the overlap, or where objects are truncated at the cell boundaries, must be dealt with by deduplication at a later stage in the workflow. The size of the data slices is limited by the hardware used, such as the performance and memory of the graphics card, and the way in which the chosen algorithm uses it. Working with larger slices results in fewer overlapping areas to deal with, but may result in larger areas of no data at the boundaries of an ROI.

A common pattern for training and evaluating models in machine learning and deep learning is to split the GT data into three parts: A large training dataset for iteratively optimising the model weights and hyperparameters during training, a smaller validation dataset for monitoring error (or performance) metrics during training and selecting the best weights (early stopping), and a test dataset for evaluating the model based on data not involved in training (Lakshmanan et al., 2022). The division between training and validation data in this paper is done by randomly assigning data slices to either the former or the latter in a ratio of 9:1. This ratio is maintained for each ROI as well as for the input dataset as a whole. Since the number of data slices within an ROI is not always

https://doi.org/10.58440/ihr-30-1-a08

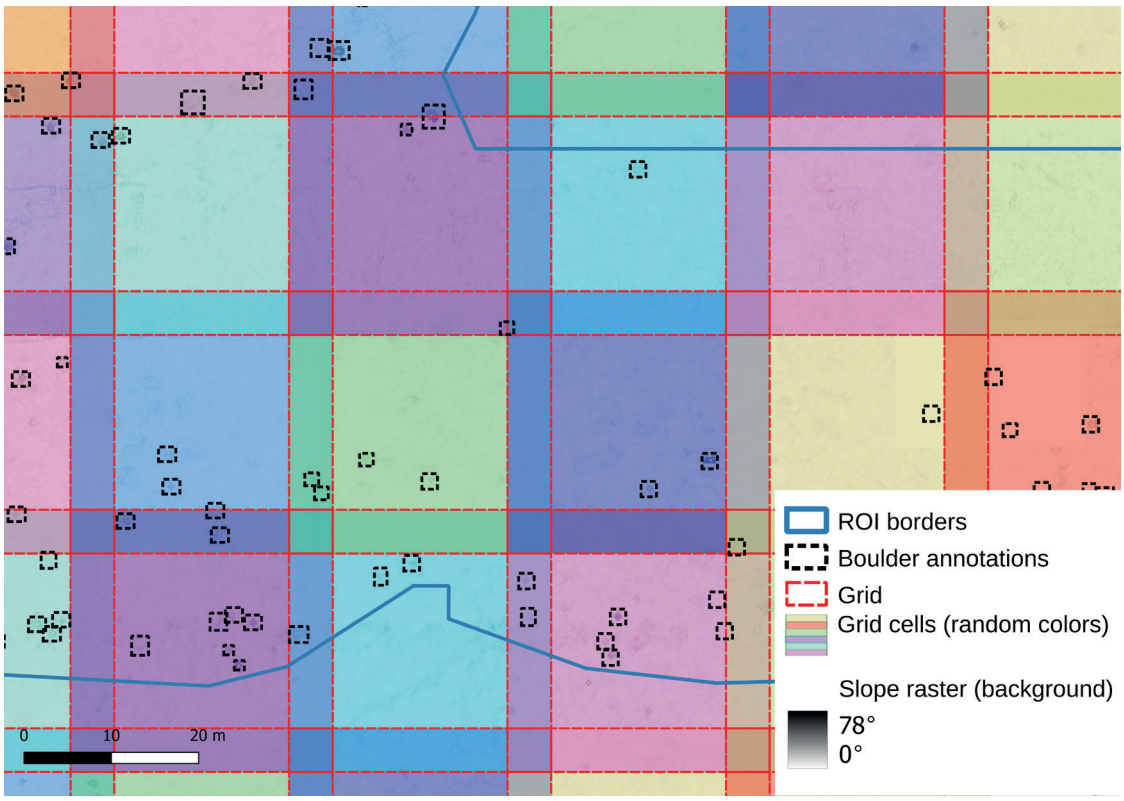

Fig. 3 A 30 m × 30 m grid with 5 m overlap over GT bounding boxes, and an ROI.

divisible by 10, the absolute counts of the assigned slices are rounded to the nearest integers. The test dataset in this work is completely separated from the training and validation data.

For many CV and machine learning tasks, extensive reference datasets exist for benchmarking and comparing algorithms, such as ImageNet (Deng et al., 2009), MS COCO (Lin et al., 2014) and Pascal VOC (Everingham et al., 2014) for image-based tasks and the KITTI (Geiger et al., 2013) and Waymo (Sun et al., 2019) datasets for tasks on 3D objects, point clouds and autonomous driving data. The most common metrics for evaluating such object detection tasks in both 2D and 3D spaces are the mean Average Precision (mAP), an average of all Average Precision (AP) values across different classes or categories, and the Intersection over Union (IoU; Hosang et al., 2016). As the datasets in this paper contain only one class and category, namely *boulder*, the distinction between AP and mAP is not made. However, the mAP is a primary measure for evaluating object detection as it combines multiple important metrics and model outputs into one value. The IoU is based on pairwise comparisons of GT bounding boxes with predicted model bounding boxes, where the common intersection area is divided by the combined area of both shapes, i.e. two identical boxes have an IoU of 1 % or 100 %.

An IoU threshold determines the AP and the measured number of true positives *TP* (predictions that match a GT box), false positives *FP* (predictions that do not match) and false negatives *FN* (GT boxes with no matching prediction), which the metrics precision *TP*/(*TP*+*FP*) and recall *TP*/(*TP*+*FN*) are calculated. In practice, different IoU thresholds are used for AP calculation depending on the task, but it is common to use either a threshold of 50 % or to perform multiple calculations with different thresholds between 50 % and 95 % and calculate the average (Hosang et al., 2016). A high precision model will have few *FP*s relative to its *TP*, without any indication of how many GT instances were actually predicted. High recall indicates that many GT boxes are matched by predictions with no indication of *FP*. Ideally, a model should have both high recall and high precision. However, by filtering predictions with confidence threshold, the model's output could be optimized for either precision or recall. The AP combines precision and recall by calculating an average over different confidence thresholds (e.g. over the precision/recall curve). All of these metrics are also used, with some variation, by the AI libraries and tools described in this paper. They can be given either as values between 0 and 1 or as percentages. As a convention in this work, all mAP, IoU and recall values are expressed as percentages. IoU thresholds are indicated by a number appended to the metric, e.g. mAP-50 for a threshold of 50 %.

2.2 Technical challenges

Most of the available AI tools and libraries, in particular those used in this work (Darknet, MMDetection3D and the Ultralytics framework), are not designed for processing hydrographic or geospatial data. This poses several challenges: If the work is based on such tools, the input data have to be converted into other data formats with a possible loss of information,

i.e. the coordinate reference system, among others. For the output, in turn, spatial references have to be derived from the context of the input. Information on how to transform hydrographic information into non-hydrographic formats and how to contextualise non-hydrographic output with domain knowledge needs to be maintained separately.

It is not only the object detection algorithms that are not ideal for large geospatial and hydrographic datasets, but also the established annotation tools, such as Label Studio[1] for image data and CVAT[2] for image, video and point cloud annotations. In the context of this work, many of the available and framework-compatible tools for 2D image annotation are designed to annotate images of normal image size rather than larger mosaics. The tools available for point cloud annotation are also designed to annotate smaller 3D scenes and do not perform well on multi-gigabyte (GB) datasets. Although it would be possible to first slice the sonar data and then annotate each tile using one of these tools, there are several drawbacks to this approach: Annotations are created in image coordinates or local 3D coordinates and stored in a specific format compatible with a family of algorithms (e.g. YOLO or KITTI format). Geospatial references are not retained, making it difficult to contextualise or integrate these annotations with other hydrographic or geographic information. It would be more difficult for experts to select ROI or get an overview when working from scene to scene than when working with the whole dataset, and they would have to learn to work with new software. It was therefore decided instead, to use established GIS software to draw geographically referenced polygons around boulders, and to write data converters to transform this data into specific annotation formats (Feldens et al., 2021). This approach is also more versatile, as it allows the same data to be reused for different algorithms and grid schemes, depending on changing hardware and software requirements.

The hardware and software requirements also specify the selected AI tools and settings. The experiments and software development were mainly carried out on a Windows 10 workstation computer with an NVIDIA 3080 Ti graphics card. The aim of this work is to enable boulder detection on similarly equipped desktop or server computers. Key considerations for the software and algorithms used in this work include the availability as an actively maintained open source implementation, sufficient stability, and applicability to common object detection use cases.

2.3 Raster-based boulder detection

A previous study by Feldens et al. (2021) used YOLOv4 (Bochkovskiy et al., 2014), implemented on the open source framework Darknet[3] as a backbone for raster-based boulder detection. The current work reuses parts of the publicly available source code[4] and workflows and partially incorporates the newer model architecture YOLOv8[5] , based on PyTorch.

The hydroacoustic data input to this workflow is expected as pre-processed raster files in GeoTIFF format, i.e. gridded sonar data with a resolution of 25 cm × 25 cm per pixel. Data pre-processing is specific to the input types, and is described, for example, in Wilken et al. (2016) for SSS imagery, in Lurton et al. (2015) for MBES backscatter imagery and in Gao (2009) and Ferreira et al. (2022) for bathymetric datasets. Feldens et al. (2021) explored different types of raster derivatives and how well they perform for boulder detection. Based on these publications, it was decided to train SSS-based models with backscatter rasters and to train MBES-based models on rasters of slope values calculated from bathymetry rasters (QGIS.org, 2024). Experiments with YOLO4 and bathymetry rasters, and composite images combining bathymetry resp. slope with backscatter data into multi-channel images, confirmed previous findings that they give worse results than slope data alone (Feldens et al., 2021). These examinations are therefore not included in this paper. Slope data is preferred to hillshading because the latter conversion is more deterministic, results in a fixed range of values between 0 and 90 degrees, and eliminates the absolute depth as a variable from which boulder detections should be independent. The YOLOv4 implementation used is only compatible with 8-bit greyscale images and 32-bit RGB images, which means that each raster cell in a band can only have an integer value in the range [0,255]. Whilst absolute depth values would be constrained by this limitation, slope values could still be represented with reasonable accuracy above the sensor accuracy. The GeoPackage (GPKG) was chosen as the file format for both vector input (boulder annotations and ROI) and detection output.

The first automated step in the raster-based workflow, after data pre-processing and GIS-based annotation (T1), is the creation of a training dataset (T2), as shown in Figs. 4 and 5, divided for visual purposes only. Larger segments of the input raster files are extracted by overlaying them with the polygons defining ROIs (Fig. 4). Rotated copies of these slices are created at different angles, so the CNN is trained with the data of different orientations and learns to recognize boulders independent from their alignment. Rotating larger mosaics instead of small tiles also has the advantage that rotations that are not multiples of 90° will later result in tiles without edges that have no data. Therefore, it is not necessary to crop

[1] Label Studio: https://labelstud.io (accessed 14 March 2024).

[2] Computer Vision Annotation Tool (CVAT): https://www.cvat.ai/ (accessed 14 March 2024).

[3] Darknet implementation of Yolov4: https://github.com/AlexeyAB/darknet (accessed 19 February 2024).

[4] Source code of previous studies: https://gitlab.com/pfeldens/BoulderDetection (accessed 19 February 2024).

[5] YOLOv8: https://github.com/ultralytics/ultralytics (accessed 19 February 2024).

https://doi.org/10.58440/ihr-30-1-a08

and scale these tiles to remove the edges. Next, the slices are divided into small, slightly overlapping tiles of the same size and scale, small enough to be more effectively processed by the CNN.

Once these tiles have been created, it is then determined for each tile whether and where there are boulders in the image (Fig. 5). Since GeoTIFF images can be processed like TIFF images without losing their spatial reference, the overlap between annotations and tiles can be determined using conventional spatial joins. For each tile, a text file is created with the image coordinates of all boulders. Bounding boxes that are partially visible within a tile are included if their dimensions equal or exceed a defined threshold of 75 cm in width and height of the height intersection area, which is equal to 3 pixels in width and height for the given resolution of the input data. In order to not exclude very small boulders by this threshold, bounding boxes are also included if they are at least 25 % visible in width and height. Partially visible bounding boxes are cropped to the visible area of the respective tile. These thresholds are based on empirical reviews of the data where artefacts of 2 pixels or less in either width or height could not be identified as boulders.

Finally, the tiles are randomly divided into training and validation datasets (Section 2.1). As it was found that a disproportionately large number of empty tiles leads to inefficient training with a very slow increasing mAP, it is also possible to limit the percentage of these tiles compared to the tiles with boulders. A limit of 40 % was used in this work.

Training and validation (T3) are entirely performed by the backend software (either Darknet or PyTorch, depending on the model used). The software is configured by the user, facilitated by a GUI. Tested default values are suggested by the software. Various data enhancement techniques such as mosaicking, rescaling, adding noise and varying saturation are also performed internally.

The test (T4) is carried out separately by comparing the GeoPackage of boulder annotations from the test dataset with the GeoPackage of detections, taking

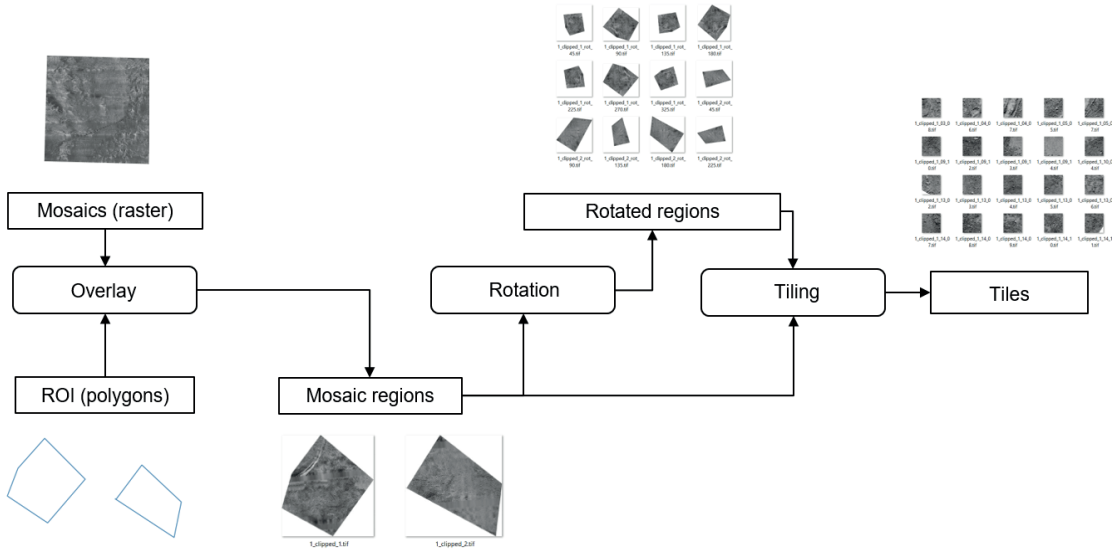

Fig. 4 Extracting ROI and tiles from large mosaics with data augmentation through rotation.

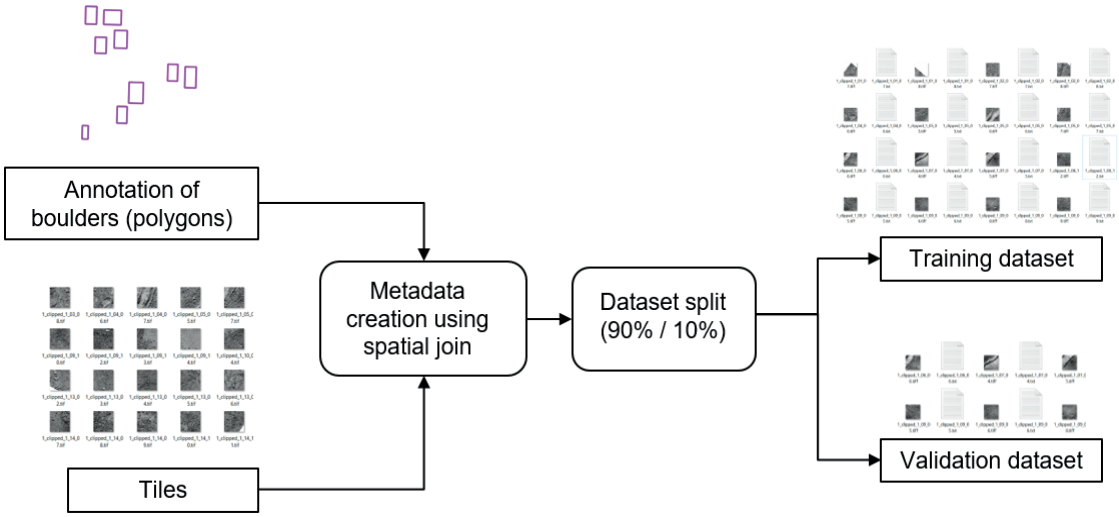

Fig. 5 Inferring annotations and metadata for each tile and performing an optional data split.

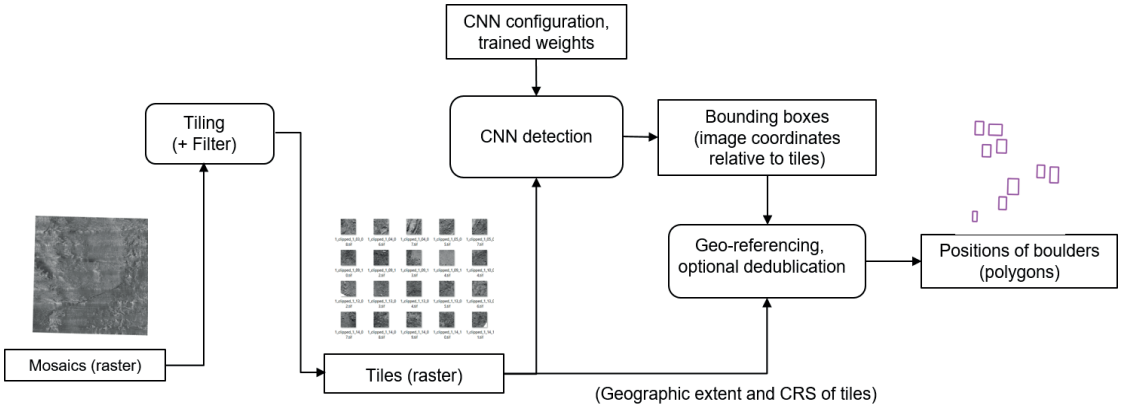

Fig. 6 Workflow for detecting and optional post-processing boulders on raster files.

into account the defined ROIs. Python converters are written to extract the boundaries of each polygon and convert them to the bounding box format expected by the TorchMetrics Python package. The GT and detected data are then filtered and grouped by ROI. If the ROIs are irregular in size and shape, or if they contain much more than 100 GT annotations, it may be necessary to impose a regular grid on the ROI in order to efficiently calculate accurate performance metrics, as shown in Section 4.3.

Fig. 6 shows how the boulder detection (T5) and optional post-processing (T6) are implemented and automated. Similar to the GT data, the input data has to be retiled. The premise of this work is that optimal results are obtained when the tile size is the same as for the GT data, although empirical tests have shown that reasonably good results can be obtained with slight variations in tile size and with adjusted user-defined settings. The detection model predicts bounding boxes in image coordinates relative to the dimensions of each tile. Since GeoTIFF tiles contain geospatial metadata, these local coordinates could be transformed into the coordinate reference system of the input data. All georeferenced bounding boxes are then merged as polygons into a single GeoPackage file.

The model results in their current implementation often have the drawback of detecting the same boulders multiple times, due to the edge case of overlapping tiles (Section 2.1), but also due to properties of the predicted annotations and the algorithm itself. To eliminate these duplicates in a heuristic way, the clustering algorithm DBSCAN (Density-Based Spatial Clustering of Applications with Noise; Ester et al., 1996), as implemented by the Python package Scikit-learn[6], can be applied, using user-defined weights as criteria. In summary, DBSCAN considers objects to be part of a cluster if they are reachable from each other according to a distance function that produces a numerical value that should be below a defined threshold.

This distance function has been replaced by a custom function that only considers overlapping bounding boxes and distinguishes between pairs of bounding boxes that originate from different tiles (edge cases) and those that have a high degree of overlap for other reasons, such as the shadow of a boulder, which is sometimes detected as a second object nearby. The likelihood that two bounding boxes are unique (not duplicates) is computed as a value between 0 and 1. In the first case, where bounding boxes originate from different tiles, the likelihood is computed from the minimum relative separation of two shapes, i.e. 0 indicates that one bounding box is completely contained by the other and 1 indicates that there is no overlap. In the second case, the likelihood is aggregated from three factors: the minimum relative separation, the relative similarity of the areas, and the similarity ratio of width to height. The threshold below which two bounding boxes are considered duplicates and the weighting of each factor in the likelihood calculation are determined empirically.

If a cluster is found, all polygons are merged into one entity using a convex hull. The maximum of all included confidence values is used as the merged cluster detection confidence. Since the worst case complexity of DBSCAN is $O(n^2)$, execution is accelerated by pre-clustering based on a safe threshold of Euclidean distance (larger than the largest observed object), taking advantage of the better performance of the built-in distance metric as opposed to the custom metric.

2.4 Point cloud-based boulder detection

The MMDetection3D[7] platform for general 3D object detection (Zhang 2023) is used for the training, validation and boulder detection of MBES-based point clouds. The platform supports a variety of algorithms for point cloud-based object detection, although they have so far been developed, tested and applied to LiDAR data and not to sonar data. It is assumed that MBES-based and LiDAR-based point clouds are similar enough to apply these algorithms to the given use case. The specific algorithms used here are SECOND (Sparsely Embedded

[6] DBSCAN on Scikit: https://scikit-learn.org/stable/modules/generated/sklearn.cluster.DBSCAN.html (accessed 19 February 2024).

https://doi.org/10.58440/ihr-30-1-a08

Convolutional Detection; Yan et al., 2018) and SA-ASSD (He et al., 2020). On KITTI test data with LiDAR point clouds, SECOND reached an AP-70 between 65.82 % (category *hard*) and 83.34 % (category *easy*) and SA-SSD reached 74.16 % (*hard*) and 88.75 % (*easy*) (He et al., 2020).

Due to the early stage of development, the point cloud-based workflow is not as sophisticated as the grid-based workflow described above. The partitioning of the data, the creation of the GT data and the recognition are inherited from the raster-based approach. The only difference is that instead of retiling raster files, files of 3D points are grouped and optionally split into training and validation data. Groups or sections of points are not explicitly rotated because MMDetection3D can be configured to perform rotations and other geometry manipulations internally. In the current version, GT data is initially annotated in the same way as the raster-based approach, i.e. by drawing 2D polygons in QGIS based on a mosaic file. A converter has been written that converts these polygons to 3D bounding boxes and estimates height / depth based on the shallowest and deepest points that fall within the area of the box. The results are checked and adjusted on a random basis.

The 3D geometries (Fig. 7) used to train the point cloud models are based on UTM projected geographic coordinates and depth. MBES backscatter is introduced as additional information. The MBES data are provided as comma-separated values (CSV) files, where each row represents a data point, including geographic coordinates, depth, signal intensity and beam angles. As part of the data pre-processing, experts have already flagged erroneous data in these files so that they can be excluded from the point cloud. The data points are not presented in any spatial order, but in the chronological order in which they were recorded by the MBES, with each file representing a track line followed by the survey vessel. As with the raster-based approach, the point cloud is usually much too large to be used directly as input data for model training. Instead, the point cloud needs to be broken down into smaller data slices that the AI backend can sequentially process with the available hardware (i.e. graphics cards). Intermediate processing steps using Python also require data slicing, as loading a dataset with millions of data points into the main memory exceeds the capabilities of many desktop and server computers.

The chronological sorting of the points in the raw data does not allow direct partitioning into smaller spatially organised subsets. Due to the large number of points, it is necessary to reorganise and subdivide the data in an efficient and hardware-friendly way: First, all CSV files are read and appended to the same GeoPackage file. Since GeoPackage uses a SpatiaLite database internally, the data can then be queried according to a given spatial extent (bounding box of a grid cell). For the full extent of the dataset, which can also be queried, a spatial grid is constructed where each grid cell is defined by width, height and an overlap with neighbouring cells. Ground truth datasets are then constructed based on all grid cells that overlap with any region of interest. For each grid cell, all data points within the cell and an ROI are written to a separate file. All boulder annotations that overlap (at least partially) both the cell and the ROI are written to an associated annotation file. In this way, the boulders that are only partially visible within the cell are also annotated. The resulting dataset conforms to the standard layout of KITTI datasets (Geiger et al., 2013) and the requirements of the MMDetection3D software documentation for this type of data.

An optional pre-processing step is the de-trending of depth values, which is similar to ground filtering procedures (Silva et al. 2018; Gomes et al. 2023): For each 3D point, the mean depth of the k nearest neighbours is determined using the k-nearest-neighbours search algorithm of the library Open3D, based on FLANN (Muja et al., 2014; the experimental setups mentioned in Section 4.2 used k=200). The actual depth of the points is reduced by this mean depth. The resulting residuals are then used for training and validation data.

For the detection output, 3D bounding boxes are

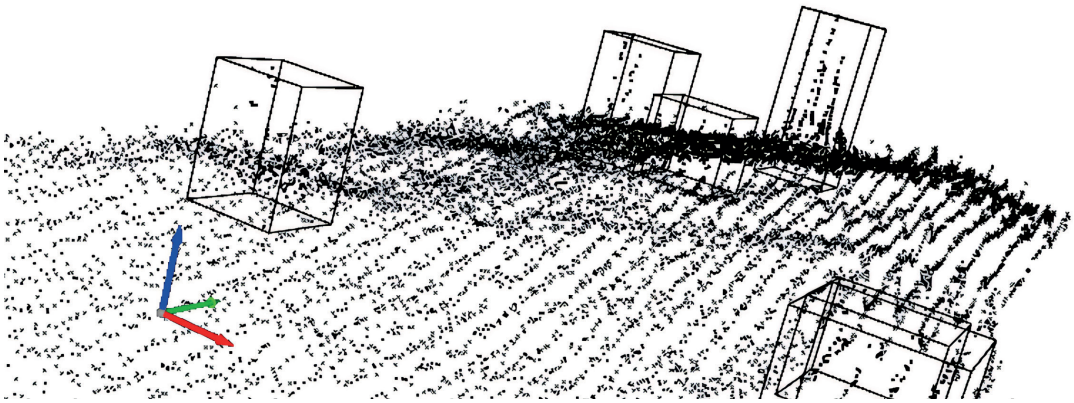

Fig. 7 MBES ground truth data with boulders annotated with 3D bounding boxes.

[7] MMDetection3D: https://github.com/open-mmlab/mmdetection3d (accessed 19 February 2024).

converted and merged into similar GeoPackage files as for the 2D raster-based approach (Section 2.3), but with the bottom depth and the height of each box included in their attributes. As a result, the same optional deduplication methods can be applied and detection performance can be evaluated in 2D space on the same test data that are used for the raster-based models.

3 Software design and realization

A software architecture and a prototype graphical user interface are presented below. They allow seamless integration into the operational workflows of potential users such as hydrographic offices and scientific institutions.

3.1 Software architecture

The software is written in Python 3.10 and was initially based on the public source code published by Feldens et al. (2021). It has been developed from a set of command-line processing tools to a modular software where data representation, workflow functionality and GUI are structured in packages. These types of modules form a functional division of the software into three layers, where the user interface (presentation layer) executes methods from the workflow modules (logical layer). Both the GUI modules and the workflows use object-oriented representations of the data layer for input and output. The data layer has no dependencies on workflows or the GUI, and the workflow has no dependencies on the GUI and can be used by itself as a Python interface. Darknet and MMDetection3D each serve as the AI backends of the software. Due to the modular design, other backends can be added as they become viable for boulder detection and similar tasks. The generic *workflow* package is the common (non-graphical) interface for all backends and provides Python methods for the tasks T2–T6 described in Section 2.1. GIS-based annotation (T1) is not implemented in this software.

The application uses the NumPy and pandas libraries for data processing and numerical operations. Several open source libraries are used for processing geographic vector and raster data, such as GeoPandas, PROJ, GDAL and OGR. The GUI is based on Tkinter (Python interface to Tcl/Tk) and is therefore designed for desktop use. As the software is modularised, different interfaces such as browser-based UIs can be added in the future. In order to organise the data in an efficient way, users can define local workspaces with respect to the workflow, so that input data, derived GT datasets, model configurations, trained models and detected data are organised in separate folders. This is useful because each of these data types can have a one-to-many or many-to-many relationship with the others, i.e. the same input data can be used to create a GT dataset, and a GT dataset can be composed of different input data. Similarly, a model configuration and a GT dataset can be reused to train different models. Models and data can also be shared separately for re-use by other users.

3.2 User interface

In order to make automated boulder detection accessible to non-programmers, a GUI has been developed (Fig. 8). The current version of this interface consists of four horizontal tabs, each corresponding to an automated workflow task (T2: training data preparation, T3: model training and validation, T5: detection, T6: post-processing). A testing interface (T4) will be added in the near future. Each tab contains an input form with mandatory file inputs and outputs and optional settings. All settings can be saved as JSON files, shared as such and reloaded on different

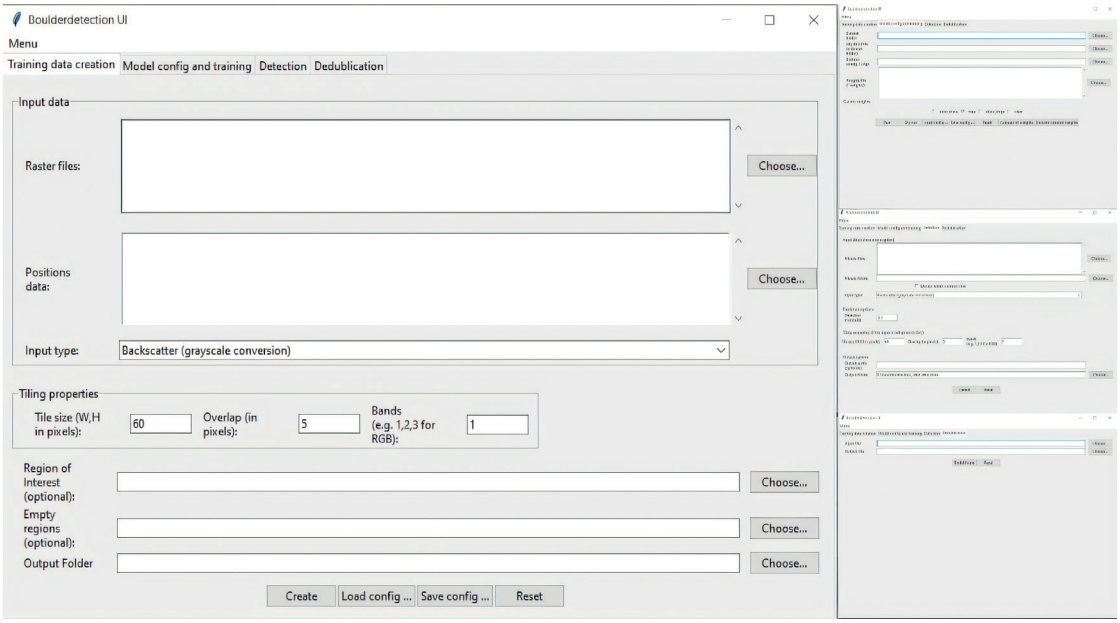

Fig. 8 Prototypical GUI of the boulder detection software.

https://doi.org/10.58440/ihr-30-1-a08

machines. It is planned to develop this interface further in response to user feedback. Different interfaces will be possible in the future, such as a cloud-based server application programming interface (API) and a browser-based GUI.

4 Showcase Baltic Sea

4.1 Ground truth data

Fig. 9 shows where the GT data were collected in the German Baltic Sea. An MBES dataset M-TR from the Kadetrinne and an SSS dataset S-TR from the Western Rönnebank are used for training and validation of the boulder detection models. An MBES dataset M-TE and an SSS dataset S-TE were also acquired within the Western Rönnebank for testing purposes. For the S-TE test dataset there are two different subsets. S-TE1 was collected in 2022 and is based on a different survey than S-TR, which was collected in 2020. S-TE2 is based on the same survey as S-TR. The boulder annotations of M-TE, S-TE1, S-TE2 are based on approximately the same ROIs. None of these ROIs overlap with the ROIs of S-TR.

From the key statistics in Table 1, it can be seen that approximately 6,000–7,000 boulders were annotated for each training dataset and a few thousand boulders were marked for testing. All four datasets were annotated by the same expert by the method described in Section 2.1.

However, the sizes of the bounding boxes are not equally distributed between the training and test data. This is particularly obvious for the dataset S-TR and S-TE1 in comparison (Fig. 10). As all the raster mosaics were rasterized to a resolution of 25 cm × 25 cm per pixel, it can be estimated that the mean bounding box in the S-TR (the largest mean) covers about 71 pixels, while the mean for the S-TE1 is only 25 pixels. One reason is that for S-TE1, the sonar device was towed in a higher altitude by the vessel, with a difference in altitude of 2-4 m. That causes boulder shadows and boulders in general to appear smaller to humans. For S-TR and S-TE2, on the other hand, the distribution of bounding box sizes is similar because the tow altitude and detailed device settings are consistent across both datasets. Similar biases in the distribution of bounding box sizes could be observed for M-TR in comparison to M-TE, although the differences are smaller.

The datasets contain various gaps where data are missing due to measurement errors. Manual inspection showed that some boulders with data gaps could only be detected after filling these gaps by interpolation based on the neighbouring values. However, no significant changes in mAP and IoU could be observed for training with and without filling the gaps in the GT data, possibly because not enough instances of boulders with gaps were part of the validation data.

For M-TR and M-TE, the same annotations for boulders and ROIs were used for both point cloud-based and raster-based boulder detections.

4.2 Model training and validation

The models presented in this paper are the empirical results of 68 documented model training runs, where the training dataset as well as the hyperparameters were iteratively adjusted for optimal results, guided by the validation data. 16 experiments were performed on rasterised SSS data using YOLOv4, 13 on rasterised MBES data using YOLOv4 and 34 on point cloud-based detection using MMDetection3D. Five experiments were performed on YOLOv7 and YOLOv8 with promising results for YOLOv8 (Table 2). Many of these experiments failed due to poor neural network configuration, hardware and software limitations, or very low performance measurements for the validation data. A common reason for poor performance was an inappropriate ratio of network resolution to tile size, which was resolved by increasing the former or decreasing the latter. For MMDetection3D, mAP-50 values did not converge and did not exceed 15 % during trainings with object noise turned on, a setting that rotates and translates points only within 3D bounding

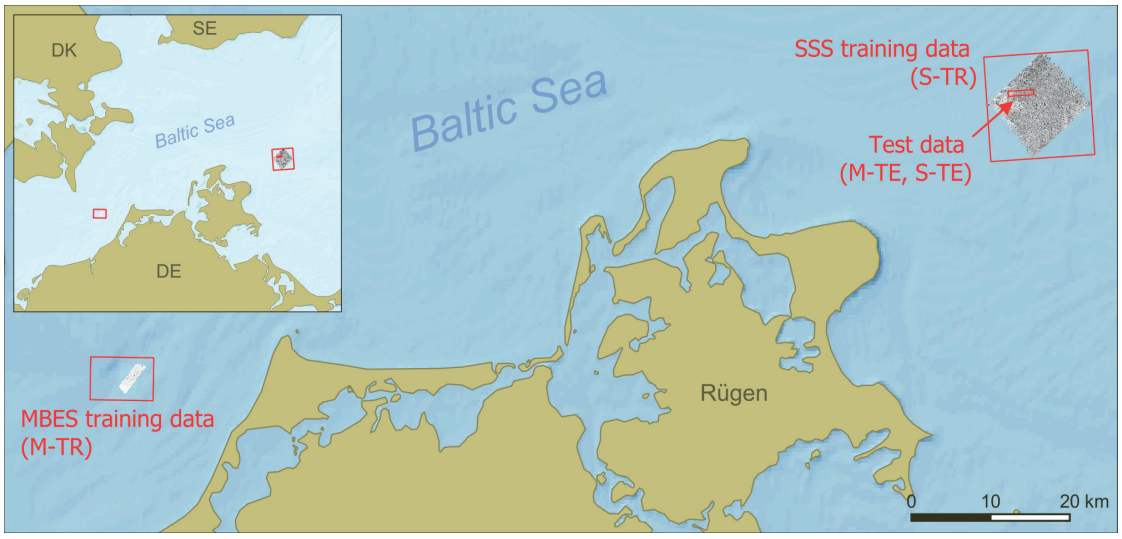

Fig. 9 Study sites from which training, validation and test data are taken.

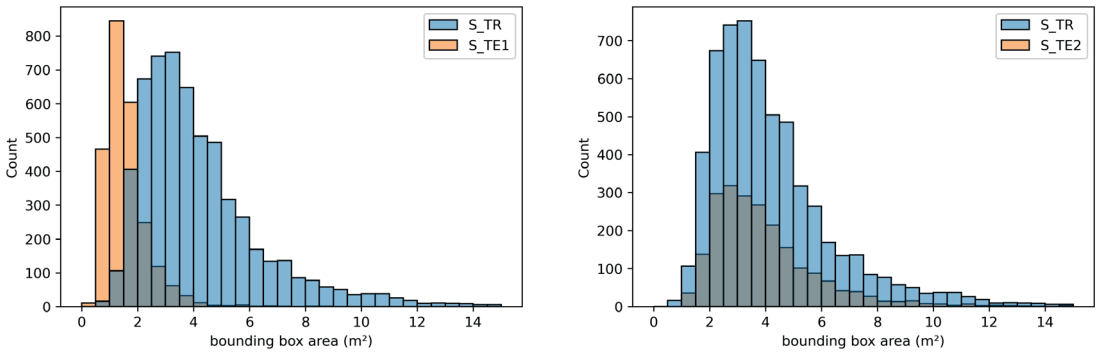

Fig. 10 Bounding box sizes of training (blue bars) and test (orange bars) datasets for SSS in comparison.

boxes. After manual inspection of the boulder detection results, the training data was revised several times in order to ensure that many different views of boulders and the seabed are represented and accurately annotated. In cases where promising results were achieved, the hyperparameters of the neural network (i.e. resolution, learning rate) and the setup of the training dataset were iteratively optimised. For the rasterised MBES data, the best results were obtained with slope-converted data. Experiments with combined bathymetry and backscatter values (e.g. slope values in the R-channel and intensity values in the G-channel of an RGB image) performed worse than slope data alone, which is similar to the findings of Feldens et al. (2021).

Table 2 shows the main results of the study. For each model, the performance metrics (mAP and IoU) were reported by the libraries used (Darknet, MMdetection3D and Ultralytics). Using the above methodology, YOLOv4 achieved a mAP-50 of 65.66 % on SSS backscatter data. However, the result required a workaround for the often-reported weakness of YOLOv4 to not detect small objects well: The tile size was set to 60 px × 60 px, and although the network could be trained with a resolution of 608 px × 608 px on the given hardware, using larger tiles would lead to much worse results. However, model WRB-HF-8c was trained and validated using the exact same GT dataset as WRB-HF-8b, but with all tiles scaled up to 608 px × 608 px using cubic resampling. Although the average IoU is lower for the selected best weights, the mAP-50 increased by almost five percentage points. The same GT dataset was also used to train the YOLOv8 model, with a further improvement of over 8 percentage points. The advantages of YOLOv8 over YOLOv4 could not be further investigated at this stage. With a mAP-50 of around 70.46 %, MBES / slope-based boulder detection performs in the same range or slightly better than backscatter intensities on their respective validation data.

The trials of the point cloud-based models SECOND and SA-SSD achieved mAP-50 and recall-50 values of 24.15 % / 41.85 % and 44.02 % / 48.89 % respectively, based on 3D instead of 2D bounding boxes. An increased recall was measured for KDR-V34, i.e. many bounding boxes from the GT were recognised, albeit with a low accuracy of the IoU. However, the low mAP and visual inspection indicate that the model produces a high number of false positives with the given configuration. The SA-SSD-based model was trained on depth residuals rather than absolute depths. Although the mAP-25 and recall-25 are both lower than for KDR-V34, the results for mAP-50 and recall-50 are better, with fewer indications of false positives. However, the SA-SSD model could not be investigated further due to technical difficulties. Not shown in Table 2 is a model based on SECOND trained

Table 1 Key statistics of the training and test datasets.

	M-TR	M-TE	S-TR	S-TE1	S-TE2
Sensor	MBES: Teledyne-Reson Seabat 7125-SV2	MBES: R2Sonic 2024	SSS: Klein Marine Systems - Klein 4000	SSS: Klein Marine Systems - Klein 4000	SSS: Klein Marine Systems - Klein 4000
Frequency (kHz)	400	400	400	400	400
Marked boulders	6,836	1,291	5,909	2,417	2,180
Area of ROI (in m²)	489,028	155,167	827,500	155,167	155,167
Area of empty ROI (in m²)	719,141	34,096.8	2,202,500	34,096.8	34,096.8
Bounding box area in m²					
Min	0.71	0.94	0.62	0.33	1.01
1st quartile	3.14	1.88	2.72	1.09	2.61
Mean / Median	3.83 / 4.0	2.47 / 2.31	4.42 / 3.7	1.59 / 1.43	4.03 / 3.51
3rd quartile	4.0	3.14	5.13	1.88	4.71
Max	25.50	8.44	57.78	8.98	19.85

https://doi.org/10.58440/ihr-30-1-a08

on depth residuals. This is because the results were very similar to KDR-V34 and were therefore considered redundant.

4.3 Model testing and comparison

This section describes how the trained models that performed best on their respective validation data (10 % of the tiles from M-TR and S-TR) were applied to the M-TE and S-TE test datasets and finally evaluated. Overall, all models perform worse than on the validation data. This is to be expected, as the datasets are not involved in the training, but also due to other differences such as the discrepancy in the bounding box size distribution.

Fig. 11 shows GT data and boulder detections for a small area of approximately 420 m². The small numbers in the boxes indicate the confidence of the prediction, ranging from 0 to 1. Predictions less than 0.1 have been suppressed for all models except KDR-V34. For KDR-V34, the number of predictions with low confidence was so high that the filter had to be set to 0.15 in order to obtain a useful output based on visual assessment. From visual observation, the model with the best fit to the GT data is KDR-Slope-1d and the WRB-HFc model in respect to S-TE2 only. KDR-V34 makes plausible predictions for boulders that are easy to detect, but the false positives degrade the result. Both SSS-based models fail to predict small bounding boxes, particularly in S-TE1.

Table 3 and 4 show the performance metrics of four models and basic statistics of the GT data of the test regions. Each performance measure includes two values per model: the first value is derived from the output of the detection workflow, and the second from the deduplicated predictions. For each ROI, the predictions and GT annotations were used as input to the Python package TorchMetrics, using the package pycocotools as a backend to calculate metrics such as mAP and IoU. Pycocotools is based on the official API used to benchmark object detection and segmentation models (Hosang et al., 2016) on the MS COCO dataset (Lin et al., 2014), and is integrated into several applications, including YOLO8 / Ultralytics and MMdetection3D. Typically, object detection images are computed individually per image and then aggregated across all images and object categories. However, for evaluating boulder detection tasks, the area over which GT and predictions are compared is critical. Calculating metrics per ROI without considering the irregular areas of the ROIs, especially for M-TE and S-TE, would lead to biased aggregation results. The scoring algorithm also becomes inefficient if too many predictions are included per image. By default, the number of predictions evaluated is limited to 100. Therefore, it was decided to overlay a grid and thus compute and aggregate detection metrics for equally sized grid cells (Fig. 12). A bounding box is included in an input slice if at least 50 % of its area is within the corresponding grid cell. The cell size of 15 m × 15 m was empirically chosen to closely match the shapes of the grid and the ROIs and to keep the number of predictions per grid cell sufficiently low. At the same time, the number of grid cells should be small in order to avoid edge cases. Tables 3 and 4 show the detailed results of the test evaluation. The differences in the GT area and the number of GT instances compared to Table 2 are a result of the gridding process.

5 Discussion

Data acquisition in the marine domain is time consuming and therefore expensive, and the collected data must serve multiple purposes ("map once, use many times"). It is therefore necessary to have efficient data processing and analysis techniques at hand. As we show in this study, boulder detection is possible with high accuracy and reliability from different input data (data and data derivatives from MBES and SSS) supported by the developed workflow.

Some disadvantages of SSS-based boulder surveys are evident from the drastic decrease in mAP (Table 4), down to 0 for mAP-50, for SSS models,

Table 2 Boulder detection models and validation results.

Code name	Training dataset	Model architecture / library	Best performance (Validation data)
WRB-HF-8b	S-TR / backscatter mosaic	YOLOv4 / Darknet	avg. IoU = 66.70 % mAP-50 = 65.66 % mAP-25 = 71.36 %
WRB-HF-8c	S-TR / backscatter mosaic upscaled tiles	YOLOv4 / Darknet	avg. IoU = 62.32 % mAP-50 = 69.39 % mAP-25 = 73.75 %
WRB-HF-8-y8-a	WRB SSS-mosaic backscatter upscaled tiles	YOLOv8 / Ultralytics	mAP-50: 77.83 % mAP-50:95: 44.71 % Recall: 69 % Precision: 75.67 %
KDR-Slope-1d	M-TR / slope mosaic	YOLOv4 / Darknet	mAP-50 = 70.46 % avg. IoU = 64.63 %
KDR-V34	M-TR / point cloud bathymetry	SECOND / MMdetection3D	mAP-25: 59.15 % Recall-25: 81,56 % mAP-50: 24.15 % Recall-50: 41.85%
KDR-SA-SSD-V24	M-TRPoint cloud detrended bathymetry	SA-SSD / MMdetection3D	mAP-25: 52.6 % Recall-25: 55.24 % mAP-50: 44.02 % Recall-50:48.89 %

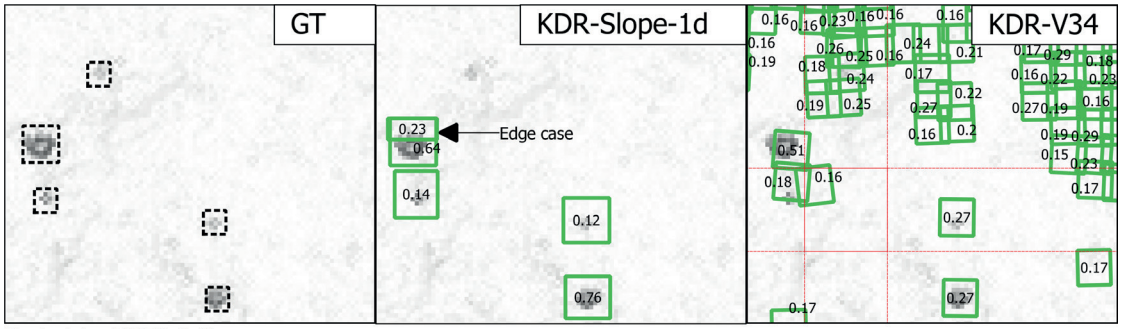

Fig. 11 GT and detection data for a selected area within M-TE and S-TE1.

depending on the test area. The appearance of boulders in SSS data does not reflect their true geometry, but is a result of the insonification angle (similar to work on lunar rockfalls, Bickel et al. 2019). This depends on the distance of a boulder from the side-scan sonar and the tow geometry, and may contribute to a different appearance of boulders at a survey site compared to the training dataset. For site S–TE1 (Fig. 10) this resulted in apparently smaller boulders that the trained model was unable to detect. Where the boulder characteristics were similar between test and training sites (site S–TE2, Fig. 10 and Table 4), the results of the model trained on SSS data were in line with the expected performance based on the validation datasets. The MBES data more closely represent the actual boulder geometry and are therefore less affected by changing survey geometries (the resolution still changes with increasing cross-track distances), and the MBES data are suitable for segmentation of boulder geometries in the next step of the modular software. On the other hand, in shallow waters of less than 10 m, MBES surveys are time consuming (Schneider von Deimling & Feldens 2021) and SSS data can be collected more quickly. Therefore, there is no inherently superior data collection method, and hydrographic professionals must decide on the appropriate collection method based on the actual application.

The largest source of uncertainty in model evaluation is the collection and annotation of GT data. Feldens et al. (2021) highlighted that the annotation of boulders by different experts can vary by as much as 30 %, demonstrating the subjective nature of this manual process of generating label data to evaluate model performance. The majority of boulders in the databases have only been identified by a single expert, but in images that contain artefacts and sometimes high noise (a prominent example in the Baltic Sea are artefacts due to acoustic scattering in a stratified water body). As a result, there are a significant

Table 3 Performance of models on MBES test dataset before and after deduplication.

	M-TE	
GT instances	1,193	
GT area (m²)	201,600	
Model	KDR-Slope-1d	KDR-V34
mAP-10	57.10 / 61.03	13.08 / -
mAP-25	43.81 / 44.76	8.23 / -
mAP-50	1.11 / 0.63	0.70 / -
recall -10	64.63 / 62.78	96.65 / -
recall -25	53.98 / 51.05	85.33 / -
recall-50	8.21 / 5.87	17.18 / -
Predictions	1,024 / 813	48,557 / -

https://doi.org/10.58440/ihr-30-1-a08

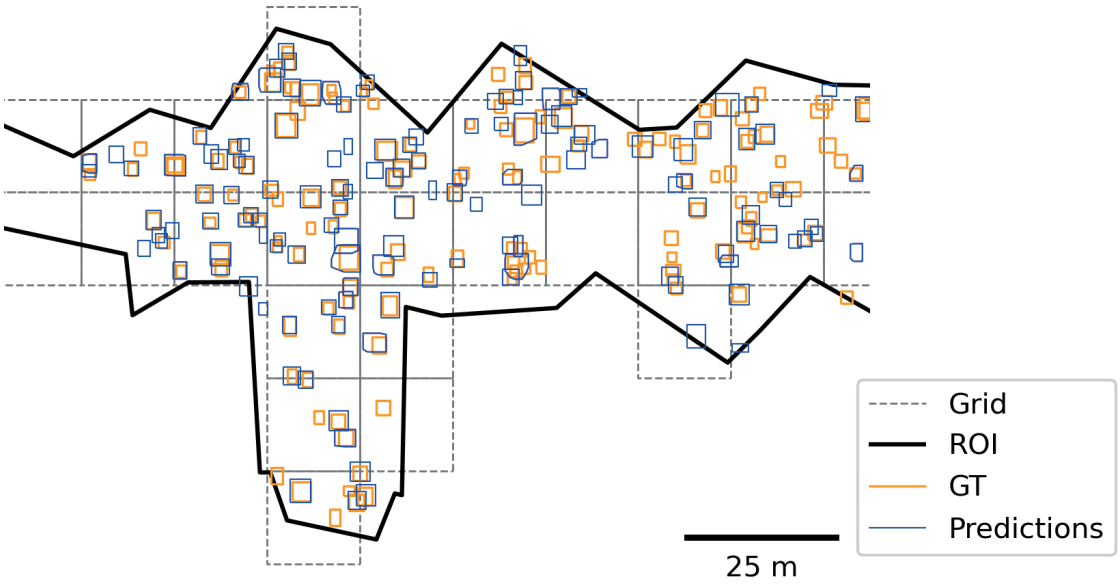

Fig. 12 Grid overlay of ROI and bounding boxes from GT and model predictions.

number of boulders that may not be detected by the expert, as well as a number of anomalies that are misidentified as boulders. Apart from geometric artefacts, certain types of boulders (e.g. small boulders), artefacts or seabed conditions may in principle be under-represented in the training and validation data and their inclusion could improve the results on the test datasets. It is uncertain to what extent these false positives, false negatives and sub-optimal training data adjustments present in the GT database affect model performance. Another factor is the accuracy with which the bounding boxes can be repeatedly drawn by the human expert. A shift of a few pixels can change the size of the bounding boxes significantly (e.g. when annotating different scales of view, on rotated images or by different experts) and thus change the IoU comparison with the model results, especially for smaller boulders. This is indicated by reduced mAP-50 values for the test datasets, where the mAP-25 values more accurately represent model performance. This problem of variable size bounding boxes is more inherent to side scan sonar mosaics, i.e. due to the geometric effects of bounding box size for non E-W or N-S oriented lines causing oblique shadows. A more nuanced but practical way of evaluating boulder detection models could be to categorise boulders by difficulty of identification, e.g. into classes of hard, moderate and easy. This approach is used with the classes of the KITTI dataset (Geiger et al., 2013). Difficulty of identification is also relevant to the interpretation and use of model outputs. Users of the software could benefit from making various uncertainties in the detection results explicit in the detection results ("uncertainty awareness"), as far as they can be derived from the data and metadata. This could include, for example, identifying nadir artefacts or noisy data (i.e. areas affected by water column stratification) and marking them as zones of high uncertainty.

Therefore, both the collection of reliable ground truth data representative of geological conditions and common artefacts encountered during acoustic surveys and the accurate fusion with hydroacoustic data remain challenging tasks. The workflow developed allows for incorporation of new GTs as they become available. For the present approach, however, the criterion for a well-performing model is how closely the automated boulder detection resembles the expert

Table 4 Performance of models on SSS test datasets before and after deduplication.

	S-TE1		S-TE2	
GT instances	2,242		2,033	
GT area (m²)	201,600		201,600	
Model	WRB-HF8b	WRB-HF8c	WRB-HF8b	WRB-HF8c
mAP-10	11.64 / 11.35	17.24 / 17.47	58.48 / 61.31	67.31 / 70.84
mAP-25	4.12 / 3.64	5.35 / 4.69	55.82 /57.68	64.85 / 67.02
mAP-50	0.01 / 0.01	0 / 0	24.43 / 23.13	33.99 / 31.88
recall-10	12.27 / 11.73	19.85 / 18.60	68.67 / 66.31	79.78 / 77.08
recall-25	6.6 / 5.84	9.77 / 8.21	66.26 / 63.99	77.72 / 74.77
recall-50	0.09 / 0.04	0.09 / 0	40.33 / 37.24	51.99 / 47.71
Predictions	348 / 301	589 / 496	2122 / 1732	2728 / 2213

judgement, despite the inherent problems discussed above. A correct deduplication of the detected boulders is therefore essential for the evaluation of the model results. Previous approaches (Feldens et al. 2019, 2020, 2021) used a simple method of a minimum distance threshold between individual boulders. Such an approach does not match field observations, where boulders can be densely packed and stacked, especially in formerly glaciated areas such as the Baltic Sea. The heuristic approach based on DBSCAN presented in this study (Section 2.3) represents a step forward in solving this problem. In the past, Bickel et al. (2019) also mentioned the problem of double detections in their work on lunar rockfalls. Bickel et al. (2019) suggest deduplication through post-processing algorithms such as Non-Maximum-Suppression (NMS). While this established algorithm mainly uses the IoU and confidence to remove duplicates, our proposed solution has a higher degree of customisation to account for the highly variable geological conditions on the seabed. Further work could be devoted to numerically optimising the deduplication parameters against GT data and the efficiency of the algorithm.

Annotating data for models operating on 3D datasets has arguably the greatest potential for improvement, both in terms of ground truthing and model development: A large number of specialised neural networks have been developed that operate on 2D images (ranging from face detection to media applications, Dhillon & Verma, 2019). The current approach of annotating boulders based on 2D raster mosaics is also practical for hydrographic professionals (with the caveats described above), even considering that thousands of boulders need to be marked in training datasets. However, there are few tools available for annotating 3D data, and annotating such datasets takes considerably more time. Integrating an efficient 3D view into the annotation process (e.g. including automatic setting of minimum and maximum depths in an area) could therefore produce more reliable data and improve 3D model results. In addition to the improvement of GT databases discussed above, the further optimisation of point cloud algorithms holds potential for the interpretation of acoustic remote sensing data. Point cloud analysis would allow the detection of smaller boulders due to the increased resolution, which is less affected by the gridding process. The detection of smaller boulders has been problematic in the majority of previous studies dealing with automatic boulder detection, but is crucial to meet EU regulations that authorities must comply with when reporting (e.g. Article 17 of the Habitats Directive, German Federal Nature Conservation Act – BNatSchG).

The input data to algorithms that are capable of detecting objects in point clouds is not gridded. Instead, the SECOND and SA-SSD algorithms rely on grouping points into voxels. Voxels can be described as 3D pixels and therefore have more flexibility than 2D raster datasets. One of their advantages is that they can be irregularly shaped and each dimension (i.e. height, width and depth) can be defined separately. Thus, voxel sizes could be adapted to the variable along, across and vertical resolution of an MBES when the 3D points are transformed into a local coordinate system aligned with the direction of the vessel. Another relevant functionality is the combination and integration of different data types. 3D object detection algorithms are already able to combine co-registered LiDAR point clouds, stereo camera street view imagery and bird's eye view. With further research, a similar setup could be realised with MBES, interferometric SSS and other sensor types such as optical sensors, cameras or radar. This is particularly relevant for the economically and ecologically important shallow waters down to about 10 m depth, where hydroacoustic coverage, especially for MBES, is limited.

Ground filtering of 3D point data is a widely used procedure in machine learning applications for automotive LiDAR data (Gomes et al., 2023), 3D object detection (Wang et al., 2022), and digital terrain modelling (Silva et al., 2018), which could not be fully explored in this study. As a disadvantage, the technique adds an additional processing step before model training and detection, which could be time consuming. It also adds another transformation step with possible uncertainties if absolute depths (e.g. from the bounding boxes) are to be estimated from the residuals. On the other hand, de-trended point clouds have a smaller vertical range of values (about -5 to 6.3 compared to -21 to 20 for normalised values in 30 m × 30 m scenes of M-TR), which allows for more efficient model training and prediction, since the same hardware could process either 3D scenes with higher vertical resolution or larger scenes with the same resolution in the same time. From an initial visual inspection, point clouds based on depth residuals appear to have a flatter terrain and boulders are easier for humans to distinguish. The scenes also appear to be more similar to the street scenes from KITTI and Waymo, where the ground (i.e. roads) is rather flat and the algorithms used are reported to perform well (Yan et al., 2018; He et al. 2020).

6 Conclusion and outlook

This study demonstrates the automation of boulder detection, evolving from basic object detection approaches to a comprehensive framework tailored to hydrographic and marine environmental applications. It outlines a set of tasks which are then refined to meet the specific needs of hydrographic professionals. This process has resulted in the development of a versatile hydrographic object detection software. This software accommodates a variety of input types (such as SSS and MBES derived grids, point clouds) and algorithms (including YOLOv4, YOLOv8, SECOND, SA-SSD), providing users with a range of options to achieve optimal results. Future developments of this software may include the integration of a web-based front-end for cloud-based computing.

The experimental setup, which included a training

https://doi.org/10.58440/ihr-30-1-a08

area and a test area for MBES and SSS data, highlighted the difficulties in achieving operationally useful results due to environmental conditions, such as the variability of seabed and water column conditions, bounding box size distribution, and methodological challenges, such as the potential homogeneity of data from a single survey mission. These conditions introduce uncertainties in the boulder detection results that could be mitigated in the future by employing ensemble methods or incorporating domain knowledge into the model training.

Despite these limitations, the experimental setup allows the comparison of different algorithms and datasets operating on 2D and 3D input data. In particular, it has been demonstrated that 3D object detection algorithms originally developed for LiDAR data can be effectively applied to hydroacoustic point clouds. The exploration of different data pre- and post-processing methods also provides a valuable avenue for future research and implementation in similar applications.

Acknowledgments

We gratefully acknowledge financial support of the project "OTC Rostock: Automatische Lokalisierung von Steinen in akustischen Datensätzen mit neuronalen Netzwerken (OTC-Stone)" by Forschungszentrum Jülich GmbH with funds from the German Federal Ministry of Education and Research (BMBF) under grant no. 03ZU1107HA, 03ZU1107HB and 03ZU1107HC.

We would like to thank the three reviewers for their thorough reviews and valuable recommendations.

References

Bickel, V. T., Lanaras, C., Manconi, A., Loew, S. and Mall, U. (2019). Automated Detection of Lunar Rockfalls Using a Convolutional Neural Network. *IEEE Transactions on Geoscience and Remote Sensing, 57*(6), pp. 3501–3511. https://doi.org/10.1109/tgrs.2018.2885280

Bochkovskiy, Alexey, Wang, Chien-Yao and Liao, Hong-Yuan Mark (2020). Yolov4: Optimal speed and accuracy of object detection. *arXiv preprint arXiv:2004.10934*. 2020

Wang, B., Lan, J. and Gao, J. (2022). LiDAR Filtering in 3D Object Detection Based on Improved RANSAC. *Remote Sensing*, 14(9), 2110. https://doi.org/10.3390/rs14092110

Deng, J., Dong, W., Socher, R., Li, L.-J., Li, K. and Fei-Fei, L. (2009). ImageNet: A large-scale hierarchical image database. *2009 IEEE Conference on Computer Vision and Pattern Recognition*. https://doi.org/10.1109/cvpr.2009.5206848

Dhillon, A. and Verma, G. K. (2019). Convolutional neural network: a review of models, methodologies and applications to object detection. *Progress in Artificial Intelligence, 9*(2), pp. 85–112. https://doi.org/10.1007/s13748-019-00203-0

Ester, M., Kriegel, H.-P., Sander, J., Xu, X. and others. (1996). A density-based algorithm for discovering clusters in large spatial databases with noise. *Kdd, 96*, pp. 226–231.

Everingham, M., Eslami, S. M. A., Van Gool, L., Williams, C. K. I., Winn, J. and Zisserman, A. (2014). The Pascal Visual Object Classes Challenge: A Retrospective. *International Journal of Computer Vision, 111*(1), pp. 98–136. doi: 10.1007/s11263-014-0733-5

Ferreira, I. O., Andrade, L. C. d., Teixeira, V. G. and Santos, F. C. M. (2022). State of art of bathymetric surveys. *Boletim de Ciências Geodésicas, 28*(1). https://doi.org/10.1590/s1982-21702022000100002

Feldens, P., Darr, A., Feldens, A. and Tauber, F. (2019). Detection of Boulders in Side Scan Sonar Mosaics by a Neural Network. *Geosciences (Switzerland), 9*(4), p. 159. https://doi.org/10.3390/geosciences9040159

Feldens, P. (2020). Super Resolution by Deep Learning Improves Boulder Detection in Side Scan Sonar Backscatter Mosaics. *Remote Sensing, 12*(14), p. 2284. https://doi.org/10.3390/rs12142284

Feldens, P., Westfeld, P., Valerius, J., Feldens, A. and Papenmeier, S. (2021). Automatic detection of boulders by neural networks: A comparison of multibeam echo sounder and side-scan sonar performance. *Hydrographische Nachrichten*, pp. 6–17. https://doi.org/10.23784/HN119-01

Förstner, W. and Wrobel, B. P. (2016). Surface Reconstruction. In *Photogrammetric Computer Vision: Statistics, Geometry, Orientation and Reconstruction* (pp. 727–766). Cham: Springer International Publishing. https://doi.org/10.1007/978-3-319-11550-4_16

Gao, J. (2009). Bathymetric mapping by means of remote sensing: methods, accuracy and limitations. *Progress in Physical Geography: Earth and Environment, 33*(1), pp. 103–116. https://doi.org/10.3390/s23020601

Geiger, A., Lenz, P., Stiller, C. and Urtasun, R. (2013). Vision meets robotics: The KITTI dataset. *The International Journal of Robotics Research, 32*(11), pp. 1231–1237. https://doi.org/10.1177/0278364913491297

Gomes, T., Matias, D., Campos, A., Cunha, L. and Roriz, R. (2023). A Survey on Ground Segmentation Methods for Automotive LiDAR Sensors. *Sensors, 23*(2), p. 601. https://doi.org/10.3390/s23020601

Grzelak, K. and Kuklinski, P. (2010). Benthic assemblages associated with rocks in a brackish environment of the southern Baltic Sea. *Journal of the Marine Biological Association of the United Kingdom, 90*(1), pp. 115–124. https://doi.org/10.1017/s0025315409991378

Van Genderen, J. L. (2011). Airborne and terrestrial laser scanning. *International Journal of Digital Earth, 4*(2), pp. 183–184. https://doi.org/10.1080/17538947.2011.553487

Guo, Y., Wang, H., Hu, Q., Liu, H., Liu, L. and Bennamoun, M. (2019). Deep Learning for 3D Point Clouds: A Survey. *CoRR, abs/1912.12033*. https://doi.org/10.48550/arXiv.1912.12033

He, C., Zeng, H., Huang, J., Hua, X.-S. and Zhang, L. (2020). Structure aware single-stage 3d object detection from point cloud. *In Proceedings of the IEEE/CVF conference on computer vision and pattern recognition* (pp. 11873–11882).

Heinicke, K., Bildstein, T., Reimers, H.-C. and Boedeker, D. (2021). *Leitfaden zur großflächigen Abgrenzung und Kartierung des Lebensraumtyps „Riffe" in der deutschen Ostsee (EU-Code 1170; Untertyp: geogene Riffe)*. Bundesamt für Naturschutz. https://doi.org/10.19217/skr612

Held, P. and Schneider von Deimling, J. (2019). New Feature Classes for Acoustic Habitat Mapping—A Multibeam Echosounder Point Cloud Analysis for Mapping Submerged Aquatic Vegetation (SAV). *Geosciences, 9*(5), 235. https://doi.org/10.3390/geosciences9050235

Hosang, J., Benenson, R., Dollar, P. and Schiele, B. (2016). What Makes for Effective Detection Proposals? *IEEE Transactions on Pattern Analysis and Machine Intelligence, 38*(4), 814–830. https://doi.org/10.1109/tpami.2015.2465908

Irving, R. (2009). The identification of the main characteristics of stony reef habitats under the Habitats Directive. Summary report of an inter-agency workshop 26-27 March 2008. *JNCC Report*, 432.

Jong, C. D. (2002). *Hydrography*. Delft: DUP Blue Print.

Kraus, K. (1997). *Photogrammetry, Advanced Methods and Applications. With Contributions by Josef Jansa and Helmut Kager. Transl. by Peter Stewardson* (4th ed., Vol. 2). Bonn: Dümmler.

Kubicek, B., Sen Gupta, A. and Kirsteins, I. (2020). Sonar target representation using two-dimensional Gabor wavelet features. *The Journal of the Acoustical Society of America, 148*(4), pp. 2061–2072. https://doi.org/10.1121/10.0002168

Lakshmanan, V., Robinson, S., Munn, M. and Langenau, F. (2022). *Design Patterns für Machine Learning* (1st ed.). Heidelberg: O'Reilley.

Lin, T.-Y., Maire, M., Belongie, S., Bourdev, L., Girshick, R., Hays, J., Perona, P., Ramanan, D., Zitnick, C. L. and Dollár, P. (2014). *Microsoft COCO: Common Objects in Context*. arXiv. https://doi.org/10.48550/ARXIV.1405.0312

Liu, S., Zhang, M., Kadam, P. and Kuo, C.-C. J. (2021). Introduction. *In 3D Point Cloud Analysis: Traditional, Deep Learning, and Explainable Machine Learning Methods* (pp. 1–13). Cham: Springer International Publishing. https://doi.org/10.1007/978-3-030-89180-0_1

Lurton, X., Lamarche, G., Brown, C., Lucieer, V., Rice, G., Schimel, A. and Weber, T. (2015). *Backscatter measurements by seafloor–mapping sonars. Guidelines and Recommendations*. GeoHab. https://doi.org/10.5281/ZENODO.10089261

Longley, P. A., Goodchild, M., Maguire, D. J. and Rhind, D. W. (2005). Representing Geography. In Geographical information systems and science (2nd ed.). Chichester: Wiley.

Lurton, X. (2002). *An introduction to underwater acoustics*. Berlin: Springer, Chichester: Praxis Publ.

Merriam-Webster. (2024). *Grid*. Merriam-Webster.com Dictionary. https://www.merriam-webster.com/dictionary/grid (accessed 14 March 2024).

Michaelis, R., Hass, H. C., Papenmeier, S. and Wiltshire, K. H. (2019). Automated Stone Detection on Side-Scan Sonar Mosaics Using Haar-Like Features. *Geosciences, 9*(5), p. 216.

Mills, G. B. (1998). International hydrographic survey standards. *The International Hydrographic Review, LXXV*(2), pp. 79–85.

Muja, M. and Lowe, D. G. (2014). Scalable Nearest Neighbor Algorithms for High Dimensional Data. *Pattern Analysis and Machine Intelligence, IEEE Transactions On, 36*(11), 2227–2240. https://doi.org/10.1109/tpami.2014.2321376

Papenmeier, S., Darr, A., Feldens, P. and Michaelis, R. (2020). Hydroacoustic mapping of geogenic hard substrates: Challenges and review of German approaches. *Geosciences (Switzerland), 10*(3), p. 100. https://doi.org/10.3390/geosciences10030100

QGIS.org. (2024). *Raster terrain analysis*. QGIS 3.34. Geographic Information System User Guide. QGIS Association. https://docs.qgis.org/3.34/en/docs/user_manual/processing_algs/qgis/rasterterrainanalysis.html (accessed 13 March 2024).

Schimel, A. C. G., Beaudoin, J., Parnum, I. M., Le Bas, T., Schmidt, V., Keith, G. and Ierodiaconou, D. (2018). Multibeam sonar backscatter data processing. *Marine Geophysical Research, 39*(1–2), 121–137. https://doi.org/10.1007/s11001-018-9341-z

Silva, C. A., Klauberg, C., Hentz, Â. M. K., Corte, A. P. D., Ribeiro, U. and Liesenberg, V. (2018). Comparing the Performance of Ground Filtering Algorithms for Terrain Modeling in a Forest Environment Using Airborne LiDAR Data. *Floresta E Ambiente, 25*(2). https://doi.org/10.1590/2179-8087.015016

Schneider von Deimling, J. and Feldens, P. (2021). ECOMAP Habitatkartierung mittels innovativer optischer und akustischer Fernerkundungs- und Auswerteverfahren. *Hydrographische Nachrichten*, pp. 13–22. https://doi.org/10.23784/HN120-02

Szeliski, R. (2022). Recognition. In *Computer Vision: Algorithms and Applications* (pp. 273–331). Cham: Springer International Publishing. https://doi.org/10.1007/978-3-030-34372-9_6

Steiniger, Y., Kraus, D. and Meisen, T. (2022). Survey on deep learning based computer vision for sonar imagery. *Engineering Applications of Artificial Intelligence, 114*, 105157. https://doi.org/10.1016/j.engappai.2022.105157

Sun, P., Kretzschmar, H., Dotiwalla, X., Chouard, A., Patnaik, V., Tsui, P., Guo, J., Zhou, Y., Chai, Y., Caine, B., Vasudevan, V., Han, W., Ngiam, J., Zhao, H., Timofeev, A., Ettinger, S., Krivokon, M., Gao, A., Joshi, A., et al. (2019). *Scalability in Perception for Autonomous Driving: Waymo Open Dataset*. arXiv. https://doi.org/0.48550/ARXIV.1912.04838

Van Unen, P. and Lekkerkerk, H.-J. (2021). Machine Learning as a Tool: Detecting Boulders in a Multibeam Point Cloud. *Hydro International*. https://www.hydro-international.com/content/article/machine-learning-as-a-tool (accessed 26 April 2023).

Wenau, S., Römer-Stange, N., Keil, H., Spiess, V. and Preu, B. (2020). Sub-Seafloor Object Detection through Dedicated Diffraction Imaging. *NSG2020 4th Applied Shallow Marine Geophysics Conference*. https://doi.org/10.3997/2214-4609.202020157

Wlodarczyk-Sielicka, M. and Blaszczak-Bak, W. (2020). Processing of Bathymetric Data: The Fusion of New Reduction Methods for Spatial Big Data. *Sensors, 20*(21), p. 6207. https://doi.org/10.3390/s20216207

Wu, Z., Yang, F. and Tang, Y. (2021). *High-resolution Seafloor Survey and Applications. Springer Singapore*. https://doi.org/10.1007/978-981-15-9750-3

Yan, Y., Mao, Y. and Li, B. (2018). SECOND: Sparsely Embedded Convolutional Detection. *Sensors, 18*(10). https://doi.org/10.3390/s18103337

Zhang, W. (2023). *Exploring versatile neural architectures across modalities and perception tasks*, School of Computer Science and Engineering, Nanyang Technological University.

https://doi.org/10.58440/ihr-30-1-a08

Authors' biographies

Matthias Hinz studied Geoinformatics at the University of Münster in Germany, where he graduated in 2016. From 2017 to 2021, he worked as a research associate at the University of Rostock for two R&D projects focussing on e-learning with open geodata and the development of an urban spatial decision support system. Before and after graduation, he worked on several other projects in the fields of web GIS, spatial statistics, remote sensing, and reproducible research. Since 2022, he works for the German Federal Maritime and Hydrographic Agency (BSH) and the Leibniz Institute for Baltic Sea Research Warnemünde (IOW) in the project OTC-Stone.

Matthias Hinz

Dr.-Ing. Patrick Westfeld graduated as a geodesist from TU Dresden (Germany) in 2005. He conducted research in the fields of photogrammetry and laser scanning and completed his PhD in 2012 on geometric-stochastic modelling and motion analysis. Since 2017, Dr Westfeld has been Head of R&D in Hydrography and Geodesy at BSH, the German Federal Maritime and Hydrographic Agency. The activities of his division range from conceptual issues pertaining to hydroacoustic and imaging sensor technologies, sensor integration and modelling, algorithm development up to application-specific implementation and practical transfer into the production environment.

Patrick Westfeld

Dr. Peter Feldens is a geologist who graduated from the University of Kiel in 2008. After completing his PhD in the TUNWAT project ("Tsunami deposits in near-shore and coastal waters of Thailand") at Kiel University in 2011, he worked on the Late Pleistocene and Holocene development of the Baltic and North Sea. At GEOMAR he participated in fieldwork in the Caspian Sea and researched the behaviour of salt glaciers in the Red Sea, be-fore returning to the Department of Marine Geophysics and Hydroacoustics at Kiel University. Since 2015, he has been a scientist at the Leibniz Institute for Baltic Sea Research Warnemünde, focusing on applied habitat mapping using remote sensing and the geological evolution of marginal seas.

Peter Feldens

Agata Feldens is part of the Subsea Europe Services GmbH, where she is responsible for hydroacoustic data interpretation. Her focus is on the object interpretation in the OTC-Stone project. Before joining the company in 2022, she worked in the "Marine Geophysics" group at the Leibniz institute for Baltic Sea Research Warnemünde and the "Sedimentology, Coastal- and Continental Shelf Research" group of the Christian-Albrechts-University in Kiel. Her expertise lies in the interpretation of hydroacoustic data, with a special emphasis on geology and sedimentology.

Agata Feldens

Sören Themann offers two decades of multifaceted experience in marine geology and subsea technology, under-pinned by a solid foundation in marine geology and geophysics from Kiel University. His professional journey has touched upon science, R&D, sales, and thoughtful executive management, with a particular focus on nurturing startups and leading innovative projects at companies such as Kongsberg Maritime. His collaborative efforts in R&D teams have supported progress in underwater monitoring and hydroacoustic mapping. Themann's dedication to blending scientific expertise with strategic development has quietly contributed to the advancement of marine geophysical research.

Sören Themann

https://doi.org/10.58440/ihr-30-1-a08

Svenja Papenmeier

Dr. Svenja Papenmeier studied geosciences and marine geosciences at the University of Bremen, graduating in 2007. In 2012, she completed her PhD at Kiel University, where she investigated the properties and dynamics of suspended load and near-bed fine cohesive sediments in highly impacted estuaries such as the Weser, Ems and Elbe. During her PostDoc, Dr. Svenja Papenmeier worked at the Alfred Wegener Institute, Helmholtz Centre for Polar and Marine Research, focusing on hydroacoustic sediment and habitat mapping in the German North Sea in close cooperation with the German Federal Maritime and Hydrographic Agency and the Federal Agency for Nature Conservation. Since 2019, she has been a senior scientist at the Leibniz Institute for Baltic Sea Research Warnemünde, where she continues to work on seafloor mapping in the Baltic Sea. Her work has a strong focus on the delineation of geogenic reefs and the automation of boulder detection. The author has provided support for several field and ship campaigns, including those in the Siberian Laptev Sea, around the Antarctic Peninsula, Chilean and Norwegian Fjords, and Hudson Bay, through hydroacoustic mapping of the seafloor surface and subsurface.

https://doi.org/10.58440/ihr-30-1-a08

PEER–REVIEWED ARTICLE

Improving a ship's energy efficiency in Korean coastal waters using tidal current information

Authors

Jinyoung Yang[1] and Do-Seong Byun[2]

Abstract

This study investigates the impact of tidal currents on a ship's speed, fuel consumption, and energy efficiency for Greenhouse Gas (GHG) reduction. The research was conducted in Korean coastal waters from Busan Port to Incheon Port during spring and neap tides. The results show that if a tanker sails with the most favorable tidal current, it can improve fuel efficiency by up to 2.46 % and reduce sailing hours by up to 2.17 hr. This change can also improve the Carbon Intensity Indicator (CII) Rating from "B" to "A". The study concludes that utilizing tidal currents can enhance energy efficiency and contribute to GHG reduction without any financial investment.

Keywords

tidal current · spring and neap tides · energy efficiency · fuel consumption · GHG reduction · global climate change

Résumé

Cette étude examine l'impact des courants de marée sur la vitesse des navires, la consommation de carburant et l'efficacité énergétique en vue de la réduction des gaz à effet de serre (GES). La recherche a été menée dans les eaux côtières coréennes, du port de Busan au port d'Incheon, pendant les marées de vives-eaux et de mortes-eaux. Les résultats montrent que si un pétrolier navigue avec le courant de marée le plus favorable, il peut améliorer son rendement énergétique jusqu'à 2,46 % et réduire ses heures de navigation jusqu'à 2,17 heures. Ce changement peut également améliorer le classement de l'indicateur d'intensité carbonique (CII) de « B » à « A ». L'étude conclut que l'utilisation des courants de marée peut améliorer l'efficacité énergétique et contribuer à la réduction des GES sans aucun investissement financier.

Resumen

Este estudio investiga el impacto de las corrientes de marea en la velocidad de los buques, el consumo de combustible y la eficiencia energética para la reducción de Gases de Efecto Invernadero (GEI). La investigación se realizó en aguas costeras de Corea desde el Puerto de Busan al Puerto de Incheon durante mareas vivas y muertas. Los resultados muestran que si un petrolero navega con la corriente de marea más favorable, puede mejorar la eficiencia del combustible hasta un 2,46 % y reducir las horas de navegación hasta en 2,17 hrs. Este cambio también puede mejorar la Clasificación del Indicador de Intensidad de Carbono (CII) de "B" a "A". El estudio concluye que la utilización de corrientes de marea puede mejorar la eficiencia energética y contribuir a la reducción de GEI sin ninguna inversión financiera.

✉ Do-Seong Byun · dsbyun@korea.kr

[1] Korea Maritime Safety Tribunal, Sejeong 30121, Republic of Korea

[2] Oceanographic Forecast Division, Korea Hydrographic and Oceanographic Agency, Busan 49111, Republic of Korea

https://doi.org/10.58440/ihr-30-1-a06

1 Introduction

The international shipping industry, which contributed about 2.89 % of global Greenhouse Gas (GHG) emissions in 2018, has been urged to energy efficient operations of ships to address global climate change (Dewan & Godina, 2023). Ships with a gross tonnage (G/T) of 400 and above, built on or after January 1, 2013, are required to comply with the Energy Efficiency Design Index (EEDI) as per Regulation 24 of Annex 6 of the International Convention for the Prevention of Pollution from Ships (MARPOL). Ship built before January 1, 2013, have been subject to the Energy Efficiency Existing Ship Index (EEXI), a legal control similar to the EEDI, since November 1, 2022, in accordance with Regulation 25 of Annex 6 of MARPOL. Further, Regulation 28 of the Convention requires an operational Carbon Intensity Indicator (CII), a new measure for reducing GHG emissions, to be applied to ships of 5,000 G/T and above, regardless of their build date, starting from 2023 (IMO, 2021a).

The annual CII of individual ships is calculated as the ratio of the total mass of CO_2 emitted to the total transport work undertaken in a given calendar year. The total mass of CO_2 is equivalent to the sum of CO_2 emissions from all the fuel oil consumed during the specific year. The annual CII of individual ships is categorized into five ratings, i.e. rating A, B, C, D or E which indicates a major superior, minor superior, moderate, minor inferior or inferior performance levels, respectively. It was analyzed that around 37.3 % of 684 ships registered in the Republic of Korea fell under ratings A and B, while about 34.2 % fell into the ratings D and E (Kim & Won, 2022). Another sample study on 140 ships, over 800 voyages calling at the South Asian ports between January 2021 and January 2022 showed that 34 % of the ships would have a non-compliant rating of CII in 2023 and it would rise to around 52 % of the ships in 2026 (Directorate General of Shipping, 2022). If a ship is rated as D of CII for three consecutive years or rated as E, it must submit its revised Ship Energy Efficiency Management Plan (SEEMP) to its Administration and take corrective actions to improve its CII level. Therefore, each vessel should consider how to maintain and improve a fair CII level. This implies that the ship is eager to save fuel oil to transport a cargo per mile. In other words, sailing longer distances with the same amount of fuel oil results in a better CII rating.

While new technologies such as hull air lubrication, automated fuel ejection timing systems, and energy recovery devices have been adopted to achieve a better EEDI (Rehmatulla & Tristan, 2020), several approaches of the operational measure like slow steaming, trim adjustment, route optimization, hull fouling removal and just-in-time operation in ports are being considered to improve the CII rating and EEXI by consuming less fuel oil (ICCT, 2021). The shipping industry should consider how to meet the CII rating requirements by implementing practical and efficient options to increase the energy efficiency of its fleet.

The energy efficiency of a ship can be simply defined by the distance a vessel travels with a given amount of fuel. Given that a ship propels itself using energy primarily generated by an internal combustion engine and sails at sea, both internal and external factors can affect the ship's energy efficiency. The internal factors are related to the ship's characteristics, including hull design, engine and propulsion efficiency. On the other hand, external factors that influence energy efficiency, particularly in coastal regions, include natural forces such as winds, waves, and tidal currents. If the external forces become significantly stronger in an adverse manner, the energy efficiency of a ship might gradually deteriorate under such conditions, as the amount of energy loss is likely to increase.

Natural forces, such as wind and tidal currents, have been harnessed for over a millennium to propel ships (Whitewright, 2018). Distinct from wind, tidal currents are characterized by their long-term predictability and relative insusceptibility to seasonal and global climatic variations (Byun et al., 2013). Tidal current velocity is significantly changed by the topography of the seabed and spring-neap tidal cycles. Consequently, the speed of a ship operating in coastal waters can be temporally and spatially influenced by tidal currents, thereby affecting the ship's fuel consumption and energy efficiency. Navigation under favorable conditions yields superior economic and energy efficiency compared to navigation under adverse conditions (Casson, 1951).

Numerous studies have focused on speed optimization for the purpose of fuel conservation and reduction of energy consumption (Degiuli et al., 2021; Yang et al., 2020; Yu et al., 2019; Fagerholt et al., 2010; Corbett et al., 2009). Several approaches have investigated the impact of voyage optimization at the operational level on the reduction of greenhouse gas (GHG) emissions (Du et al., 2021; Wang et al., 2021; Safaei et al., 2019; Zaccone et al., 2018; Lu et al., 2015; Prpić-Oršić et al., 2014). However, it is evident that these studies primarily concentrate on the speed control of ocean-navigating vessels, which have additional operational options such as weather routing, trim/draft optimization, and arrival time adjustment to mitigate GHG emissions (Klakeel et al., 2023). These operational options, however, are unlikely to be selected for coastal shipping due to the constraints of limited alternative sailing routes and short distances that do not permit significant differentials from the options. Therefore, coastal shipping may need to explore other operational measures.

Considering that coastal regions are more consistently and predictably affected by tidal currents compared to external variables, this study aims to investigate the effect of tidal currents on the sailing speed of ships and their energy efficiency. In particular, we scrutinize these effects under different departure times within the tidal regime of the Korean coast (Fig. 1). For this analysis, we employ the

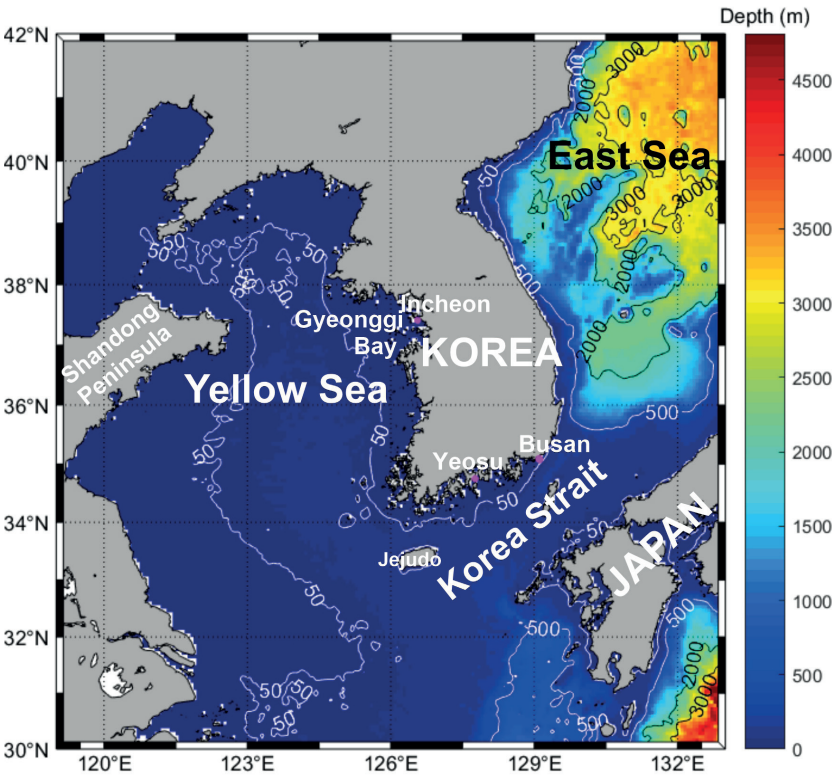

Fig. 1 Map showing the Korean coastal waters including the Korea Strait. The white and black lines represent depth contours (in meters), derived from the ETOPO1, a 1arc-minute global digital elevation model of the Earth's surface, dataset.

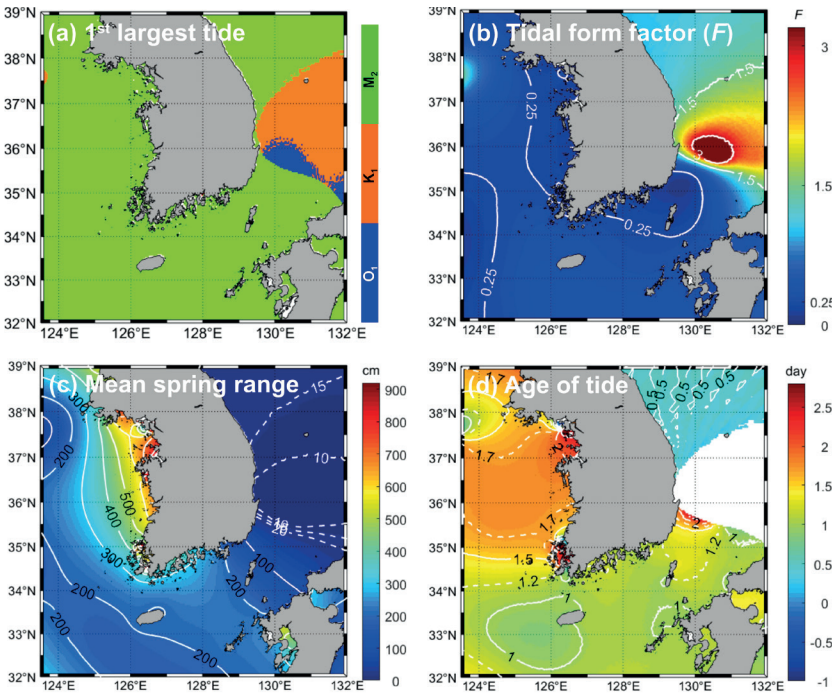

Fig. 2 Distributions of the (a) 1st largest tidal constituent, (b) tidal form factors *F*, (c) mean spring range and (d) the age of the tide around the Korean coast waters including Korea Strait, calculated from the TPXO9 model database. F is the ratio of the tidal amplitudes $(M_2 + S_2)/(K_1 + O_1)$ classified by semidiurnal ($F<0.25$), mixed ($0.25<F<3$) and diurnal tidal regimes ($F>3$). The mean spring range and the age of the tide with $0.25<F<3$ are calculated from the sum of amplitudes and difference of the tidal phase lags of M_2 and S_2 tides, respectively. Note that the age of tide that corresponds to diurnal tidal regimes has been excluded, as shown in the white area in (d).

Numerical Tidal Current Software (NTICS), developed by the Korea Hydrographic and Oceanographic Agency (KHOA), in tandem with actual performance data from a ship navigating between Yeosu Port and Incheon Port. Throughout this study, this software will be referred to as KHOA-NTICS.

2 Characteristics of tides and tidal currents

The west and south coasts of Korea are characterized by the M_2-predominated semidiurnal tidal regime (Figs. 2a and 2b), showing different tide and tidal current characteristics. The mean spring tidal ranges (yielded as twice the sum of the M_2 and S_2 amplitudes) vary between 300 cm and 800 cm on the west coast but between 100 cm and 400 cm on the south coast of Korea (Fig. 2c). It is noteworthy that, in addition to these distinct tidal ranges, the west and south coasts also exhibit different degrees of spring retardation, also referred to as the age of the tide (calculated from the difference in phase lag, divided by the difference in angular speed between the S_2 and M_2 tides; Fig. 2d): the west coastal water shows higher delay values (>2 days), while the south coastal water exhibits lower delay values (ranging between >1 day and <1.5 days).

Compared to tides, tidal currents are more significantly influenced by bathymetry, including narrow waterways (Byun et al., 2013). Greater tidal ranges are observed in Gyeonggi Bay (>900 cm) on the west coast, while stronger (>4 m/s) tidal currents are present off the western tip of southwest Korea. The maximum flood currents in coastal areas are generally observed to flow towards the Korean Peninsula with a clockwise rotation during flood tides (Fig. 3a). In contrast, the maximum ebb currents tend to flow away from the Korean Peninsula with an anticlockwise rotation during ebb tides (Fig. 3b). More specifically, within the regional area, the flood (ebb) currents in the Korea Strait are inclined to flow from east (west) to west (east). Conversely, on the west coast of Korea, they flow towards (away from) the west of the Korean Peninsula (Fig. 3).

3 Methodology

3.1 Tidal current prediction using harmonic constants

Numerical models are commonly used worldwide to understand the characteristics of tidal regimes (Byun et al., 2004; Song et al., 2013) and to predict tides and tidal currents (Blain et al., 2002; Byun & Cho, 2009; Byun & Hart, 2022). Further, harmonic analyses of simulated tidal elevation and tidal-current results are used to produce information on the tidal constants (amplitudes and phase-lags) and tidal ellipse parameters (semi-major and semi-minor axes, inclination and phase) for the harmonic constituents. This information can be employed, in turn, in tide and tidal-current predicting and hindcasting through their prediction algorithms (Byun et al., 2023). Examples include the

https://doi.org/10.58440/ihr-30-1-a06

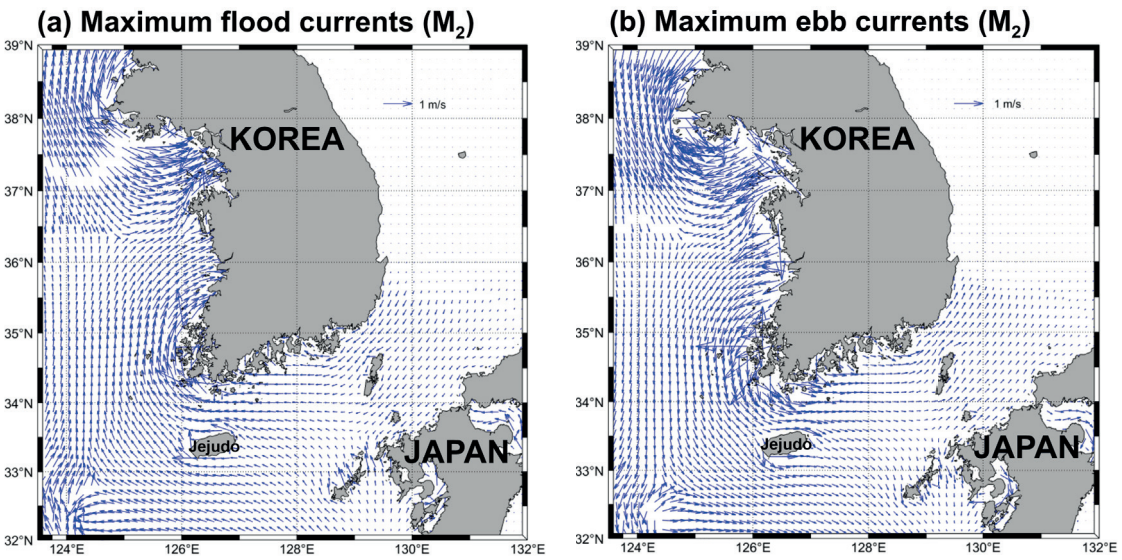

Fig. 3 Distributions of M_2 maximum (a) flood currents and (b) ebb currents around Korean coastal waters including Korea Strait, calculated from TPXO9 model harmonic constants.

Polpred Offshore Tidal Software and Poltips Coastal Tidal Software programs developed by NOC (National Oceanography Centre Laboratory), and NTICS of KHOA, which are tide and tidal current prediction and visualization software. KHOA-NTICS has 16 tidal harmonic constant (M_2, S_2, K_2, N_2, L_2, $2N_2$, T_2, Mu_2 and Nu2 for semidiurnal tides and K_1, O_1, P_1, Q_1, OO_1, J_1 and M_1 for diurnal tides) database of three different horizontal resolutions of 250 m for Korean coastal water, and 500 m and 1 km for the Yellow Sea and Korea Strait in surface, middle and bottom layers. This study used the surface layer database of 500 m. Since 2006 (Kwon & Kang, 2007), this software has been gradually renovated.

Tidal current velocity C ($=U+iV$) can be predicted using harmonic constants for the easterly U and northerly V velocity components or their tidal ellipse parameters. Each component of tidal current velocity can be expressed by Byun & Hart (2017):

$$U(\tau) = \sum_{k=1}^{n} f_k(\tau)(u_u)_k \cos[w_k t + V_k(t_0) + u_k(\tau) - (g_u)_k] = \sum_{k=1}^{n} f_k(\tau)\,[a_k \cos\Phi_k \cos(\omega_k t + V_k(\tau_0) + u_k(\tau) - \phi_k) - b_k \sin\Phi_k \sin(\omega_k t + V_k(\tau_0) + u_k(\tau) - \phi_k)] \quad (1)$$

$$V(\tau) = \sum_{k=1}^{n} f_k(\tau)(v_v)_k \cos[w_k t + V_k(t_0) + u_k(\tau) - (g_v)_k] = \sum_{k=1}^{n} f_k(\tau)\,[a_k \sin\Phi_k \cos(\omega_k t + V_k(\tau_0) + u_k(\tau) - \phi_k) + b_k \cos\Phi_k \sin(\omega_k t + V_k(\tau_0) + u_k(\tau) - \phi_k)] \quad (2)$$

where the subscript k denotes each tidal current constituent; n is the total number of tidal current constituents; V_k is the astronomical arguments; $(u_u)_k$ and $(v_v)_k$ are the tidal harmonic constituent amplitudes and $(g_u)_k$ and $(g_v)_k$ are local time phase lags for u- and v-velocities components, respectively; ω_k is the angular frequency; τ ($=t_0+t$) is the reference time t_0 plus the t elapsed since t_0; ϕ_k is the phase of the maximum current; Φ_k is the inclination of the semi-major axis, measured anticlockwise from the x-axis; and f_k and u_k are the nodal amplitude factors and the nodal angles for the 18.61-year nodal modulation correction, respectively.

3.2 Calculating actual sailing distance

KHOA-NTICS, a tidal current prediction software based on a numerical model-derived harmonic constants, incorporates a feature that computes the anticipated arrival time along a chosen sailing route. This calculation takes into account the ship's departure time and varying tidal current velocity fields. Under the conditions that tidal current velocity $\vec{c}$ field and a ship speed $|\vec{s}|$ or r_s are given and actual ship's sailing direction θ_l is known (Fig. 4a), actual ship sailing speed r_l on the given route in a certain time Δt from point A can be calcuated as shown in Fig. 4b. The displacement of point D from point A is determined by the product of $\vec{c}$ and Δt. Unknown $|\vec{l}|$ or r_l is yielded by finding intersection point C between straight line $\overline{AB}$ and a circle with radius r_l at point D (Fig. 4b). Distance vectors for each velocity in a certain time are expressed as $\vec{R}_c(=\vec{c}\Delta t)$ for tidal current velocity, $\vec{R}_s(=\vec{s}\Delta t)$ for ship velocity $\vec{s}$, and $\vec{R}_l(=\vec{l}\Delta t)$ for actual ship velocity $\vec{l}$.

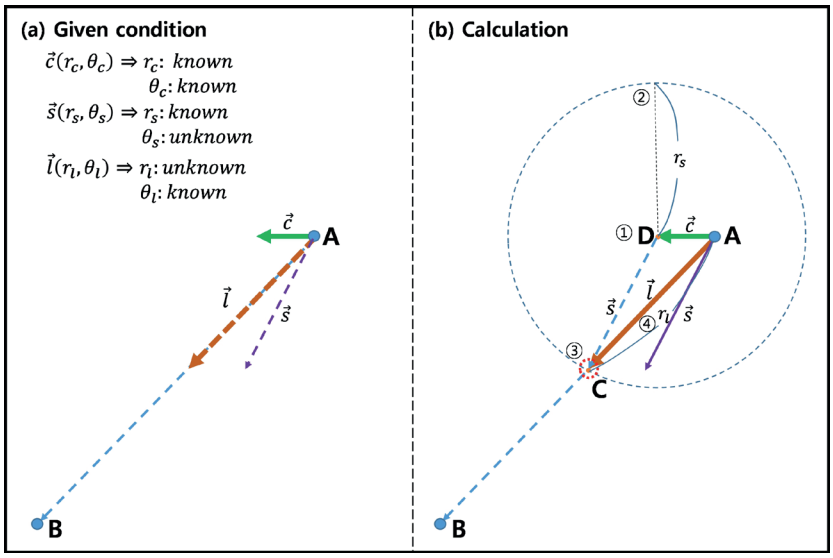

Fig. 4 Schematic diagram for procedures of calculating actual ship sailing speed r_l between A and C denote the direction of each vector. The circled numbers in (b) denote the sequence in which r_l is calculated.

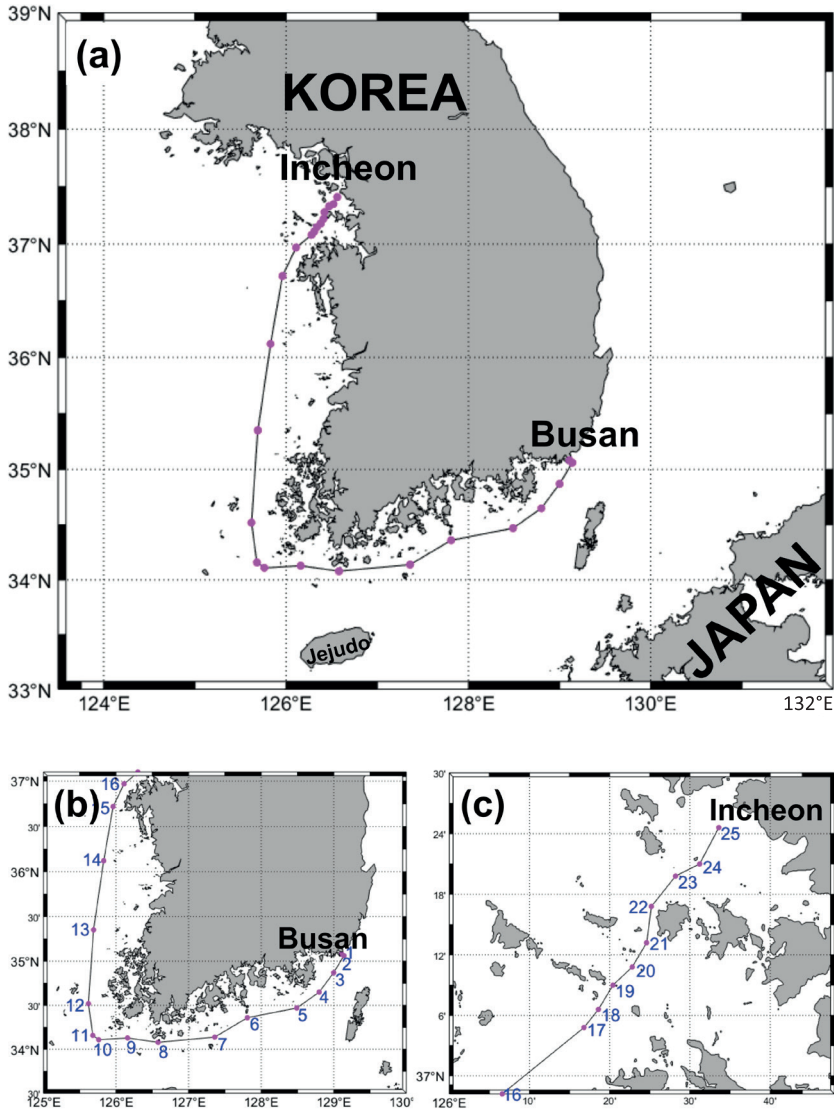

Fig. 5 Map showing an experimental ship route with 25 points from Busan to Incheon Ports, Korea.

3.3 Experiment setting

In tidally dominated coastal environments, the ship's speed is significantly influenced by the velocity of tidal current and the relative direction between the tidal current and the ship's heading. The effect of tidal currents on a ship's speed along Korea's west and south coasts was analysed for spring (13–14 August 2022) and neap (20–21 August 2022) tidal periods using KHOA-NTICS. For this experiment, the sailing route is determined with selected 25 waypoints from Busan Port to Incheon Port, two major ports located on the southeast coast and west coast in Korea, respectively (Fig. 5). This sailing course, spanning a distance of 744 km (402 NM), was selected to draw waypoints to observe traffic separation schemes. The schemes were designed to reduce the likelihood of encountering reciprocal courses or crossing ahead of other vessel in area of heavy traffic, and to ensure safe passage by avoiding dangerous waters such as islands and rocks. In this study, we assumed a ship's sailing speed in still water (absent the influence of tidal currents) to be 12.0 knots. By using KHOA-NTICS with the still water option, the travel time for the designated route is estimated to be 35 hr and 40 min.

Considering the variation in the tidal current velocity field at 10-minute intervals as provide by KHOA-NTICS, the experiments were primarily designed so that a vessel departs from the Busan Port at hourly intervals, starting from the high tide of the day. A fundamental procedure of calculating actual sailing distance in a changing tidal current velocity field is illustrated in Fig. 4. The actual tidal effect on a ship's headway can be calculated from the composition of two vectors, i.e. the speed and direction of a ship in still water, and the corresponding direction and speed of the tidal current.

A vessel that sails with a tidal current experiences an increase in speed, while a ship that sails against the current experiences a reduction in headway. This suggests that when a ship sailing encounters the direction of the tidal current from the ship's heading, the actual speed of the ship decreases due to the current acting as resistance to the ship's headway, compared to the speed of sailing in still water. Conversely, when the tidal current comes from the ship's stern, the ship sails at a faster speed than a ship that does not benefit from the tidal current.

4 Results and discussion

4.1 The effect of tidal current depending on different departing times

The effect of tidal currents on arrival times, with departures at 1 hr intervals departing times, was quantitatively examined for two different periods of spring and neap tides using a function of the ship's arrival and departure in KHOA-NTICS. The travel time between two consecutive points varied from the individual departure times, as the effect of the tidal current on the ship's headway at each point changes depending on the time a vessel passes that location.

https://doi.org/10.58440/ihr-30-1-a06

If the tidal current effects on the ship's headway at each point are accumulated, it results in the total sailing hours from the departure point to the destination. For convenience, 10 out of 25 points (Fig. 5) from Busan to Incheon Ports were selected to examine the travel time between them.

As shown in Fig. 6, the sailing hours calculated between each pair of points (P1–P5, P5–P6, P6–P8, P8–P10, P10–P12, P12–P13, P13–P14, P14–P16, and P16–P25) demonstrate that tidal currents affect the sailing hours, significantly more in spring tides than in neap tides. The arrival time at the specific point varied depending on departure time due to different tidal currents with the different tidal periods, indicating a ship faced with diverse fair or disadvantage tidal currents at every place during the voyage.

During the spring tide period (Fig. 6a), the travel duration between the two ports fluctuated depending on the various departure times, spanning from 34 hr and 50 min to 36 hr and 50 min. Importantly, this range indicates an extension of over an hour when compared to the case where the effect of tidal currents is not considered (35 hr and 40 min).

The shortest journey during the spring tide occurred with departure times of S+6 and S+9, which was one hour shorter than sailing in still water. However, the departure windows from S+6 to S+9 and from S+18 to S+20 were more than half an hour shorter. Among 24 cases, these cases demonstrate that the vessel predominantly sailed with a favorable tidal current during the voyage. Conversely, the longest journey occurred with a departure time of S, which was 1 hr and 10 min longer than sailing in still water. If a vessel navigates against the current, its travel time will exceed that of moving in still water or with the current.

In contrast, during the 24 neap tide cases, the shortest sailing time occurred at the departure time of N+1, which was 30 minutes shorter than sailing in still water, as shown in Fig. 6b. Conversely, the longest travel time was associated with the departure times of N+15 and N+16, which were 30 minutes longer compared to sailing in still water.

The effect of tidal currents on sailing ships, compared to still water conditions, exhibited a range from -1.167 hr to 1.00 hr during spring tides, and from -0.50 hr to 0.50 hr during neap tides across the 24 cases of varying departure times. Specifically, sailing with the most favorable tidal current among these 24 cases resulted in time savings of 2.167 hr during spring tides and 1.00 hr during neap tides, in contrast to sailing against the most adverse current. Notably, the standard deviation was 0.601 hr for spring tides and 0.282 hr for neap tides, indicating that tidal current variations are more pronounced during spring tides than neap tides.

During spring tides, it is noteworthy that the most significant variation in navigation hours, compared to sailing in still water, occurs between two adjacent departure times. Specifically, this difference is adversely 0.833 hr, corresponding to 0.50 hr at S+11 and -0.333 hr at S+12. In contrast, the navigation time that experiences the most positive reduction between adjacent departure times is 0.50 hr, occurring between -1.167 hr at S and -0.667 hr at S+1. Similar differences are observed between adjacent departure times at S+3 and S+4, S+4 and S+5, and S+5 and S+6. Additionally, the time span between S+14 and S+15 exhibits the same value of 0.167 hr, representing the smallest difference during spring tides.

For the neap tide cases, the largest difference in sailing hours between two adjacent departure times was 0.50 hr. Specifically, this difference occurred between -0.167 hr at N+6 and 0.333 hr at N+7, as well as between 0.00 hr at N+14 and -0.50 hr at N+16. Notably, there were several instances of identical sailing hours between adjacent departure times during this period. For instance, sailing times were 0.167 hr at N+2 and N+3, from N+8 to N+13, and

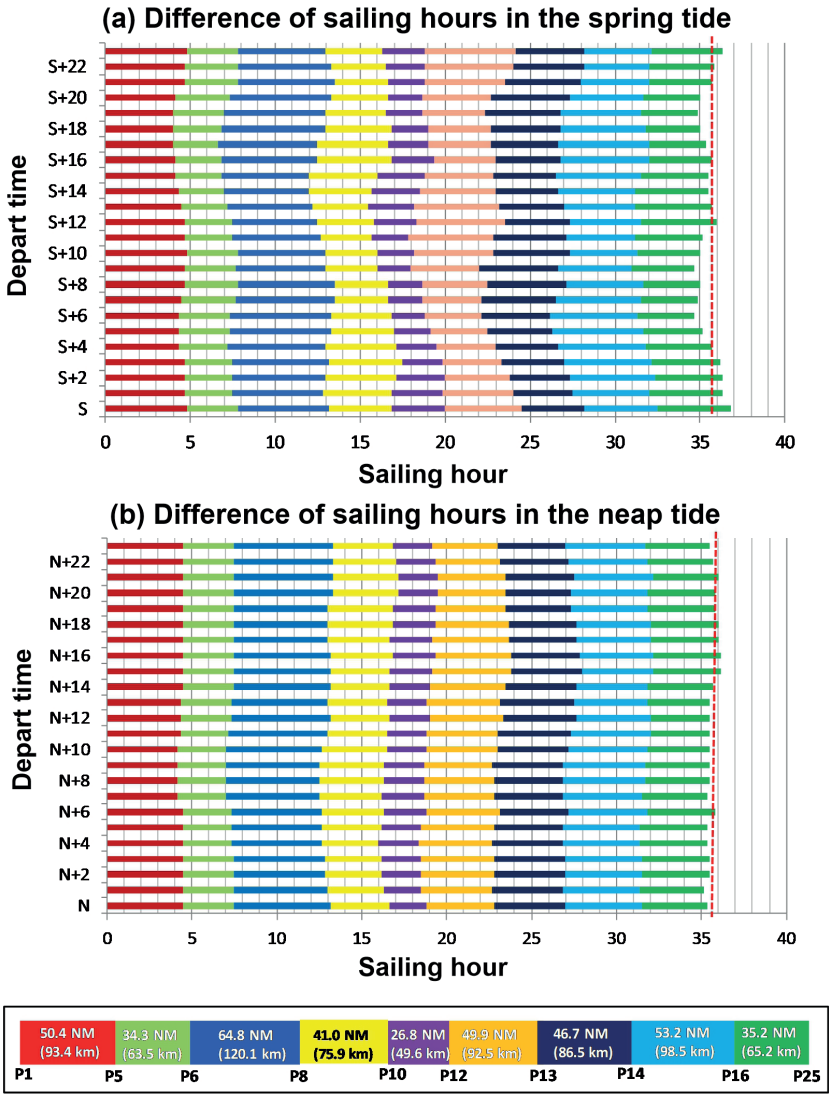

Fig. 6 The difference in sailing hours due to tidal currents at 10 waypoints (1, 5, 6, 8, 10, 12, 13, 14, 16, and 25 as shown in Fig. 5) from Busan to Incheon Ports during spring (13–14 August 2022) and neap (20–21 August 2022) tides. For instance, S+2 or N+2 on the left axis indicates departure two hours after high tide in spring (S) or neap (N) tide at the departure point, Busan Port. The numbers in the legend represent the distance in nautical miles and kilometers (in parentheses) between the waypoints. The red-dashed line on the right side of each panel indicates the sailing time (35.67 hr) as calculated in still water.

Table 1 The simulated fuel efficiency and CII ratings for a ship at various departure times. Note that sailing time and fuel consumption are calculated for the critical cases in Fig. 6 based on the actual ship's performance between Yeosu Port and Incheon Port and the correlation between the ship's speed and fuel consumption.

	Tidal condition	Sailing speed (knot)	Distance (miles)	Sailing time (hr)	Fuel consumption (ton)	Fuel efficiency (kg/mile)	Attained CII	CII Ratio (Rating) in 2023
	Actual performance	12.51	358.58	28.67	19.09	53.227	5.809	0.862 (B)
	Speed in still water	12.00	402	33.51	19.69	48.964	5.412	0.803 (A)
Spring tide	Maximum counter-current	11.60	402	34.67	20.37	50.669	5.601	0.831 (B)
	Maximum fair current	12.37	402	32.51	19.10	47.503	5.251	0.780 (A)
	Maximum gap between two adjacent departure	12.18	402	33.01	19.39	48.233	5.332	0.792 (A)
		11.88	402	33.84	19.88	49.451	5.466	0.811 (A)
Neap tide	Maximum counter-current	11.82	402	34.01	19.98	49.695	5.493	0.815 (A)
	Maximum fair current	12.18	402	33.01	19.39	48.233	5.332	0.792 (A)
	Maximum gap between two adjacent departure	12.12	402	33.17	19.49	48.477	5.359	0.796 (A)
		11.94	402	33.67	19.78	49.208	5.439	0.807 (A)

0.333 hr at N+4 and N+5. Additionally, there were negative differences of -0.333 hr at N+17 and N+18, and -0.167 hr at N+19 and N+20, respectively.

These results indicate that tidal currents exert a more pronounced influence on ship speed during spring tides compared to neap tides. For instance, the maximum time difference between voyages with favorable currents (S+9 case) and opposing currents (S case) on a spring tide day was up to two hours and 10 minutes. Conversely, during neap tides, the maximum time difference between sailing times (N+1 and N+15 cases) was only one hour – half of that demonstrated during spring tides. Furthermore, the results indicate that the variation in sailing times between adjacent departure times is greater in spring tides due to differing tidal current velocities, as summarized in Table 1.

4.2 Effect of tidal currents on ship's energy efficiency

Reducing the sailing time for the same distance by leveraging the tidal current leads to a decrease in fuel consumption and an improvement in energy efficiency. The actual operating data between Yeosu Port and Incheon Port, which follow a similar route (accounting for 89.2 % of our total distance) as depicted in Fig. 1, were analyzed to assess the influence of tidal currents on a ship's operational energy efficiency. Specifically, a tanker with a gross tonnage of 29,404 serviced 72 domestic voyages from May 17, 2018, to August 30, 2019. During this period, the tanker, carrying an average of 38,554.30 kiloliters of cargo for each laden leg, consumed 1,374.18 metric tons (M/T) of fuel oil for her west-north bound journey of 358.58 miles. This journey, at an average speed of 12.51 knots, lasted 28.67 hours, resulting in an average fuel consumption of about 0.6657 M/T per hour, or 53.2266 kg per mile.

The actual performance of the oil tanker, as previously mentioned, along with the following four guidelines (G1, G2, G3, and G4) developed by the International Maritime Organization (IMO), were utilized to assess the energy efficiency of the ship. According to Resolution MEPC.353(78), the 2022 Guidelines on the Reference Lines for use with operational Carbon Intensity Indicators (CII Reference Lines Guidelines, G2) (IMO, 2021c), which was adopted on 10 June 2022, the CII Reference line of the tanker is formulated as follows:

$$CII_{ref} = a \times Capacity^{-c} \quad (3)$$

The parameters of *a* and *c* in the above formula for the tanker from the G2 Guidelines are 5,247 and 0.610, respectively. Therefore, considering that the capacity (deadweight) of the tanker is 50,542, the CII Reference Line for the tanker could be obtained 7.0906 gCO_2/(dwt.nmile) from Eq. 3.

The required annual operational CII for the tanker for 2023 is calculated by Resolution MEPC.338(76), which is the CII Reduction Factors Guidelines, G3 (IMO, 2021d), as follows:

$$\text{Required Annual operational CII} = (1–Z/100) \times CII_{ref} \quad (4)$$

In Eq. 4, Z generally refers to the reduction factors for the required annual operational CII from 2020 to 2030 relative to the 2019 reference line. Considering

https://doi.org/10.58440/ihr-30-1-a06

that reduction factor Z for 2023 is allocated to 5 % according to the G3 Guidelines, the tanker's required annual operational CII for 2023 is 6.7361. The required annual operational CII for the ship for 2024, 2025 and 2026 is allocated to 6.5943, 6.4524 and 6.3106, respectively.

The CII of an individual ship is obtained as the ratio of the total mass of CO_2 (M) emitted to the total transport work (W) in a given calendar year. The Attained CII value for individual ships is formulated by Resolution MEPC.352(78), which is the CII Guidelines, G1 (IMO, 2021b), as follows:

$$\text{Attained CII} = M/W = (FCj \times CFj) / (C \times Dt) \quad (5)$$

In Eq. 5, FCj represents the total mass of fuel oil consumed in a year, measured in grams, while CFj is the CO_2 conversion factor for the specific type of fuel oil used. C represents the ship's Deadweight tonnage (DWT) for tankers, and Dt represents the total distance travelled. According to the Third GHG study of the IMO, the CFj values for Heavy Fuel Oil (HFO) and Marine Gas Oil (MGO) are 3,114 and 3,206 kg CO_2 /tonne fuel, respectively.

Shifting focus to the assessment of the tidal current effect on a ship's energy efficiency, it is estimated that a tanker sailing 402 miles of the simulated route at a speed of 12.00 knots would consume 19.69 M/T of fuel oil over a duration of 33.51 hr. This projection is based on the ship's performance and the general cubic relationship (Fuel consumption α (ship speed)^3) between the ship's speed and fuel consumption (IMO, 2016). By employing slow steaming, fuel efficiency improves from 53.227 to 48.964 kg of fuel oil per mile, compared to the performance at 12.51 knots. Consequently, the Attained CII for 2023, calculated using Eq. 5, will be 5.412. In this way, it can assume sailing time, fuel consumption, fuel efficiency and Attained CII for the cases of different departing times, as shown in Table 1. When the ship sails with the fairest tidal current of 0.37 knots among 24 cases of hourly different departure times at Busan Port during the spring tide, its travel time will be 32.51 hr. Fuel efficiency improves to 47.503 kg of fuel oil per mile, which results in the Attained CII in 2023 of 5.251. This shortens the journey by 1.00 hr and 2.17 hr compared to sailing in still water and against the strongest countercurrent, respectively, expected to achieve fuel savings of 2.98 % and 6.25 %. In the case of sailing under the most favourable conditions during the spring tide, the Attained CII will be 5.251, which is 0.780 of the CII ratio and rated as "A", the superior boundary, by the ratio of Attained CII to the required annual operational CII. The ratio of Attained CII is an operational energy efficiency performance rating, assigned by Resolution MEPC.354(78), the CII Rating Guidelines, G4 (IMO, 2021e). The CII Rating of this tanker sailing under the strongest countercurrent during the spring tide is 0.831 for 2023, allocated a rating of "B", the lower boundary. If the ship changes its departure time by an hour, the sailing speed increases from 11.88 knots to 12.18 knots, with a 2.46 % improvement in fuel efficiency, improving the CII ratio from 0.811 to 0.792.

During the neap tide, choosing to sail with the most favourable current of 0.18 knots from among 24 cases results in a journey duration of 33.01 hours. This represents a reduction of half an hour and one hour, respectively, compared to sailing without considering the tidal current and sailing under the most adverse current. When travelling with the most favourable tidal current, the Attained CII will be 0.792, which corresponds to an "A" rating. However, the value increases to 0.815 when sailing under the most adverse current.

The results above indicate that both sailing hours and fuel consumption are influenced by the vessel's departure time and the effect of tidal currents on the ship's progress, even within a single day. Therefore, it is seen as a viable strategy to alleviate the pressure of reducing GHG emissions in the coastal shipping industry by choosing a departure time that minimizes both sailing time and fuel consumption, thus leveraging the most favorable tidal current during the voyage. For example, if a ship adjusts its departure time from Busan Port by merely an hour, the sailing hours on the same route can either increase by up to 0.33 hours or decrease by 0.50 hours, leading to substantial variations in fuel consumption and energy efficiency.

5 Conclusions

The international shipping industry should take an appropriate measure to address new regulation on the reduction of GHG emissions from vessels by the IMO. Starting from 2022, the industry should be satisfied with the CII Rating of the MARPOL Convention as well as EEDI for a new ship. Therefore, shipping companies are exploring ways to reduce fuel consumption during various ship operations, including sailing and while in port.

In regions where tides are dominant, leveraging predictable tidal currents presents an attractive and straightforward option. Given the limited operational measures available for improving energy efficiency in coastal shipping, optimizing fuel consumption becomes critical. This study investigates the effect of tidal currents on ship speeds (arrival times) between Busan Port and Incheon Port in the Republic of Korea. More specifically, we examine the potential for saving sailing hours and reducing fuel consumption during spring and neap tides using the tidal current prediction software, KHOA-NTICS.

The results indicate a decrease of 0.40 knots under the strongest countercurrent, but an increase of 0.37 knots under the most favorable conditions, assuming the ship's speed is 12.0 knots in still water. The findings also suggest that the ship can reduce

its travel time by more than half an hour compared to sailing in still water, if it departs during the time

windows from S+6 to S+9 and from S+18 to S+20.

These outcomes lead to different CII ratings: a "B" rating for the first case and an "A" rating for the latter, reflecting a 6.25 % improvement in energy efficiency. Notably, this improvement aligns with an analysis of 14,452 voyages involving tankers and dry bulk carriers based on the Blue Visby Solution. The latter was expected to achieve an average of 7.5 % fuel savings (Sung et al., 2022).

Furthermore, it is noted that adjusting the hourly departure time can lead to an enhancement of up to 0.30 knots in speed, corresponding to a 2.46 % improvement in fuel efficiency. This underscores the potential benefits of leveraging accurate tidal current prediction information for coastal shipping companies. Such utilization allows them to achieve GHG reduction without significant investments in technical measures. With limited options for decarbonization, optimizing fuel consumption becomes crucial for maintaining their CII rating. Consequently, the development of a dedicated system that computes the optimal departure time and sailing speeds, considering ship size and performance, using operational forecasting systems-derived ocean currents and tidal current predictions, is recommended.

Acknowledgment

Thank you to the Korea Hydrographic and Oceanographic Agency (KHOA) for making the Numerical TIdal Current Software (NTICS) available.

Additionally, we express our gratitude to an anonymous reviewer for the helpful and constructive comments that helped us to clarify the manuscript.

References

Blain, C. A., Preller, R. H. and Rivera, A. P. (2002). Tidal prediction using the advanced circulation model (ADCIRC) and a relocatable PC-based system. *Oceanography, 15*(1), 77–87. https://doi:10.5670/oceanog.2002.38

Byun, D.-S., Hart, D. E. and Jeong, W.-J. (2013). Tidal Current Energy Resources off the South and West Coasts of Korea: Preliminary Observation-Derived Estimates. *Energies*, 6, pp. 566–578. https://doi:10.3390/en6020566

Byun, D.-S., Wang, X. H. and Holloway, P. E. (2004). Tidal characteristic adjustment due to dyke and seawall construction in the Mokpo Coastal Zone, Korea. *Estuarine Coastal Shelf Science, 59*, pp. 185–196. https://doi:10.1016/j.ecss.2003.08.007

Byun, D.-S. and Cho, C.-W. (2009). Exploring conventional tidal prediction schemes for improved coastal numerical forecast modeling. *Ocean Modelling, 28*(4), pp. 193–202. https://doi:10.1016/j.ocemod.2009.02.001

Byun, D.-S. and Hart, D. E. (2022). Tidal current classification insights for search, rescue and recovery operations in the Yellow and East China Seas and Korea Strait. *Continental Shelf Research, 232*, p. 104632. https://doi.org/10.1016/j.csr.2021.104632

Byun, D.-S., Choi, B.-J. and Hart, D. E. (2023). Overcoming tide-related challenges to successful regional and coastal ocean modeling. *Frontiers in Marine Science, 10*, p. 1150305. https://doi:10.3389/fmars.2023.1150305

Byun, D.-S. and Hart, D. E. (2017). A robust interpolation procedure for producing tidal current ellipse inputs for regional and coastal ocean numerical models. *Ocean Dynamics, 67*, pp. 451–463. https://doi:10.1007/s10236-017-1037-4

Casson, L. (1951). Speed under Sail of Ancient Ships. *Transactions of the American Philological Association, 82*, pp. 136–148.

Corbett, J., Wang, H. and Winebrake, J. (2009). The effectiveness and costs of speed reductions on emissions from international shipping. *Transportation Research Part D: Transport and Environment, 14*, pp. 593–598. https://doi:10.1016/j.trd.2009.08.005

Degiuli, N., Martic, I. and Farkas, A. and Gospic, I. (2021). The impact of slow steaming on reducing CO_2 emissions in the Mediterranean Sea. *Energy Reports, 7*, pp. 8131–8141. https://doi:10.1016/j.egyr.2021.02.046

Dewan, M. H. and Godina, R. (2023). Effective Training of Seafarers on Energy Efficient Operations of Ships in the Maritime Industry. *Procedia Computer Science, 217*, pp. 1688-1698. https://doi.org/10.1016/j.procs.2022.12.369

Directorate General of Shipping (2022). *Comments on the Report of the Correspondence Group on Carbon Intensity Reduction (TOR 3)*. https:/dgshipping.gov.in/WriteReadData/userfiles/file/MEPC %2078-7-22 %20- %20Comments %20on %20the %20report %20of %20the %20Correspondence %20Group %20on %20Carbon %20Intensity %20Reduction %20(TOR %203) %20(India) %20(3).pdf (accessed 2 November 2022).

Du, W., Li, Y., Zhang, G., Wang, C., Chen, P. and Qiao, J. (2021). Estimation of ship routes considering weather and constraints. *Ocean Engineering, 228*, p. 108695. https://doi:10.1016/j.oceaneng.2021.108695

Fagerholt, K., Laporte, G. and Norstad, I. (2010). Reducing fuel emissions by optimizing speed on shipping routes. *Journal of the Operational Research Society, 61*, pp. 523–529. https://doi:10.1057/jors.2009.77

ICCT (International Council on Clean Transportation) (2021). Reducing Greenhouse Gas Emissions from Ships - Cost Effectiveness of Available Options. https://theicct.org/wp-content/uploads/2021/06/ICCT_GHGfromships_jun2011.pdf (accessed 28 October 2023).

IMO (International Maritime Organization) (2016). *IMO Train the trainer (TTT) course on Energy Efficient Ship Operation, Module 3 – From Management to Operation.* https://wwwcdn.imo.org/localresources/en/OurWork/Environment/Documents/Air %20pollution/M3 %20from %20management %20to %20operation %20final.pdf (accessed 28 October 2023).

IMO (International Maritime Organization) (2021a). *Further Shipping GHG Emission Reduction Measures Adopted*. https://www.imo.org/en/MediaCentre/PressBriefings/pages/MEPC76.aspx (accessed 28 October 2023).

IMO (International Maritime Organization) (2021b). *Guidelines on the operational Carbon Intensity Indicators and the Calculation Methods (CII Guidelines, G1)*. https://wwwcdn.imo.org/localresources/en/KnowledgeCentre/IndexofIMOResolutions/MEPCDocuments/MEPC.336(76).pdf (accessed 28 October

https://doi.org/10.58440/ihr-30-1-a06

2023).

IMO (International Maritime Organization) (2021c). *Guidelines on the Reference Lines for use with operational Carbon Intensity Indicators (CII Reference Lines Guidelines, G2)*. https://wwwcdn.imo.org/localresources/en/KnowledgeCentre/IndexofIMOResolutions/MEPCDocuments/MEPC.337(76).pdf (accessed 28 October 2023).

IMO (International Maritime Organization) (2021d). *Guidelines on the operational Carbon Intensity Reduction Factors relative to Reference Lines (CII Reduction Factors Guidelines, G3)*. https://wwwcdn.imo.org/localresources/en/KnowledgeCentre/IndexofIMOResolutions/MEPCDocuments/MEPC.338(76).pdf (accessed 28 October 2023).

IMO (International Maritime Organization) (2021e). *Guidelines on the operational Carbon Intensity Rating of Ships (CII Rating Guidelines, G4)*. https://wwwcdn.imo.org/localresources/en/KnowledgeCentre/IndexofIMOResolutions/MEPCDocuments/MEPC.339(76).pdf (viewed 28 October 2023).

Kim, J. and Won, J. (2022). *The Risk and Impacts by Upcoming Regulation for the Decarbonization of Existing Ships. Korea Investors Service, Inc.* https://m.kisrating.com/fileDown.do?menuCd=R1&gubun=1&-fileName=SR20220323-4.pdf&writedate=20220323 (accessed 2 November 2022).

Klakeel, T., Anantharaman, M., Rabiul Islan, T. M. and Garaniya, V. (2023). Effectiveness of current technology in GHG Reduction – A Literature Survey. *The International Journal on Marine Navigation and Safety of Sea Transportation, 17*(1), pp. 171–176. https://doi.org/10.12716/1001.17.01.18

Kwon, S. J. and Kang, T.-S. (2007). Numerical simulation for behavior of tidal elevation and tidal currents in the South Sea. *Journal of Korean Society of Coastal and Ocean Engineers* (in Korean), *19*(3), pp. 253–265.

Lu, R., Turan, O., Boulougouris, E., Banks, C. and Incecik, A. (2015). A semi-empirical ship operational performance prediction model for voyage optimization towards energy efficient shipping. *Ocean Engineering, 110*, pp. 18–28. https://doi:10.1016/j.oceaneng.2015.07.042

Rehmatulla, N. and Tristan, S. (2020). The Impact of Split Incentives on Energy Efficiency Technology Investments in Maritime Transport. *Energy Policy, 147*, p. 111721. https://doi.org/10.1016/j.enpol.2020.111721

Prpić-Oršić, J., Vettor, R., Guedes Soares, C. and Faltinsen, O. (2014). Influence of ship routes on fuel consumption and CO_2 emission. In C. Guedes Soares, & T.A. Santos (Eds.). *Maritime Technology and Engineering*, pp. 857–864. Taylor & Francis Group.

Safaei, A. A., Ghassemi, H. and Ghiasi, M. (2019). VLCC's fuel consumption prediction modeling based on noon report and automatic identification system. *Cogent Engineering, 6*, p. 1595292. https://doi:10.1080/23311916.2019.1595292

Song, D., Wang, X. H., Zhu, X. and Bao, X. (2013). Modeling studies of the far-field effects of tidal flat reclamation on tidal dynamics in the East China Seas. *Estuarine, Coastal Shelf Science, 133*, pp. 147–160. https://doi.org/10.1016/j.ecss.2013.08.023

Sung, I., Zografakis, H. and Nielsen, P. (2022). Multi-Lateral Ocean Voyage Optimization for Cargo Vessels as a Decarbonization Method. *Transportation Research Part D: Transport and Environment, 110*, p. 103407. https://doi.org/10.1016/j.trd.2022.103407

Wang, H., Lang, X. and Mao, W. (2021). Voyage Optimization Combining Genetic Algorithm and Dynamic Programming for Fuel/Emissions Reduction. *Transportation Research Part D: Transport and Environment, 90*, 102670. https://doi:10.1016/j.trd.2020.102670

Whitewright, J. (2018). Sailing and Sailing Rigs in the Ancient Mediterranean: Implications of Continuity, Variation and Change in Propulsion Technology. *International Journal of Nautical Archaeology, 47*, pp. 28–44. https://doi:10.1111/1095-9270.12278

Yang, L., Chen, G., Zhao, J. and Rytter, N. G. M. (2020). Ship Speed Optimization Considering Ocean Currents to Enhance Environmental Sustainability in Maritime Shipping. *Sustainability, 12*(9), 3649. https://doi:10.3390/su12093649

Yu, B., Peng, Z., Tian, Z. and Baozhen, Y. (2019). Sailing speed optimization for tramp ships with fuzzy time window. *Flexible Services and Manufacturing Journal, 31*(2), pp. 308–330. https://doi:10.1007/s10696-017-9296-4

Zaccone, R., Ottaviani, E., Figari, M. and Altosole, M. (2018). Ship voyage optimization for safe and energy-efficient navigation: A dynamic programming approach. *Ocean Engineering, 153*, pp. 215–224. https://doi:10.1016/j.oceaneng.2018.01.100

Authors' biographies

Jinyoung Yang

Jinyoung Yang worked in commercial vessels as a deck officer and holds the First Class Deck Officer Certificate. He has served in the Korean Maritime Administration over 25 years, which makes the policies and efforts to promote the safety and environment protection at sea. He studied the science of maritime affairs in the World Maritime University and Mokpo Maritime University, from the point of view of the safety and environment protection at sea. His recent main studying areas are the prevention of air pollution and mitigation of climate change by ships.

Do-Seong Byun

Do-Seong Byun, a senior researcher at the Korea Hydrographic and Oceanographic Agency (KHOA), holds a BS and MS in Oceanography from Chonnam National University in Korea, and a PhD in Oceanography from the University of New South Wales, Australia. Currently, he is in charge of Ocean Forecast Team at Oceanographic Forecast Division in KHOA. His main research interests are the analysis and prediction of tides and tidal currents in coastal regimes, and ocean forecasting modelling.

https://doi.org/10.58440/ihr-30-1-a06

PEER–REVIEWED ARTICLE

Exploring the possibility of adding DGGS support to the S-100 Universal Hydrographic Data Model

Authors
Kimberly Mason[1] and Jens Schröder-Fürstenberg[1]

Abstract

Discrete Global Grid Systems (DGGS) have many advantages over traditional coordinate reference systems. A DGGS is a spatial reference system consisting of multiple layers of grids with increasing resolution which partition the globe into polygon shaped cells of equal area. Individual cells can be easily identified and basic Geographic Information System (GIS) operations can be performed on data stored within the cells. Advantages of using DGGS for spatial data include the ability to integrate data layers of different data types in a statistically uniform way, the possibility to avoid distortions caused from projection, and the capability to scale analysis across multiple resolution levels. The benefits of using DGGS for hydrographic data, specifically Electronic Navigational Charts (ENC) are examined. The addition of DGGS to S-100 would provide a uniform gridding system for ENC cells, and would eliminate distortions in the Polar Regions caused when projecting rectangular cells based on latitude and longitude. The Open Geospatial Consortium (OGC) led a pilot project for which one of the participants developed a server that offers S-100 marine protected area data organized according to DGGS. Because of this success and the availability of open-source software for the implementation of DGGS, the BSH (German Federal Maritime and Hydrographic Agency) investigated the feasibility and possible benefits of using Discrete Global Grid Systems for S-100 data. The outcome was successful. However, it is recognized that DGGS as a standard is not yet advanced enough and the available software tools are inadequate for wide implementation. More investigation needs to be done, and additionally the best grid shape, orientation and aperture for a uniform grid for hydrographic data need to be determined. Overall, DGGS should be considered for future versions of S-100, the new universal hydrographic data model, because the benefits for ENCs and hydrographic data are clear and in the future, it is expected that DGGS will revolutionize GIS.

Keywords
Discrete Global Grid System · S-100 · coordinate reference system · gridding · hydrographic data · marine protected area · electronic navigational chart

✉ Kimberly Mason · kimberly.mason@bsh.de
[1] German Federal Maritime and Hydrographic Agency, Nautical Hydrography, D-18057 Rostock, Germany

https://doi.org/10.58440/ihr-30-1-a01

Résumé

Les systèmes de grilles globales discrètes (DGGS) présentent de nombreux avantages par rapport aux systèmes de coordonnées de référence traditionnels. Un DGGS est un système de référence spatiale composé de plusieurs couches de grilles à résolution croissante qui divisent le globe en cellules en forme de polygone de superficie égale. Les cellules individuelles peuvent être facilement identifiées et les opérations de base des systèmes d'information géographique (SIG) peuvent être effectuées sur les données stockées dans les cellules. Les avantages de l'utilisation de DGGS pour les données spatiales sont notamment la capacité d'intégrer des couches de données de différents types de manière statistiquement uniforme, la possibilité d'éviter les distorsions causées par la projection et la capacité d'échelonner l'analyse sur plusieurs niveaux de résolution. Les avantages de l'utilisation de DGGS pour les données hydrographiques, en particulier les cartes électroniques de navigation (ENC), sont examinés. L'ajout de DGGS à la S-100 fournirait un système de grille uniforme pour les cellules des ENC, et éliminerait les distorsions dans les régions polaires causées par la projection de cellules rectangulaires basées sur la latitude et la longitude. L'Open Geospatial Consortium (OGC) a mené un projet pilote pour lequel l'un des participants a développé un serveur qui offre des données S-100 sur les aires marines protégées organisées selon un DGGS. En raison de ce succès et de la disponibilité de logiciels libres pour la mise en œuvre de DGGS, le BSH (Agence fédérale maritime et hydrographique allemande) a étudié la faisabilité et les avantages éventuels de l'utilisation de systèmes de grilles globales discrètes pour les données S-100. Cette étude a été couronnée de succès. Cependant, il est reconnu que la norme sur les DGGS n'est pas encore assez avancée et que les outils logiciels disponibles sont inadéquats pour une mise en œuvre à grande échelle. Il convient de poursuivre les recherches et de déterminer la meilleure forme, orientation et ouverture de grille, en vue d'obtenir une grille uniforme pour les données hydrographiques. Dans l'ensemble, les DGGS devront être pris en considération pour les futures versions de la S-100, le nouveau modèle universel de données hydrographiques, car les avantages pour les ENC et les données hydrographiques sont évidents et, à l'avenir, on s'attend à ce que les DGGS révolutionnent les SIG.

Resumen

Los Sistemas de Mallas Globales y Discretas (DGGS) tienen muchas ventajas sobre los sistemas tradicionales de referencia por coordenadas. Un DGGS es un sistema de referencia espacial que comprende múltiples capas de mallas de resolución creciente que dividen el globo en celdas poligonales de igual superficie. Las celdas individuales se pueden identificar fácilmente y pueden realizarse operaciones básicas del Sistema de Información Geográfica (SIG) con los datos almacenados en las celdas. Las ventajas de usar DGGS para datos espaciales incluyen la capacidad de integrar capas de datos de diferentes tipos de manera estadísticamente uniforme, la posibilidad de evitar distorsiones causadas por la proyección, y la capacidad de escalar el análisis a través de múltiples niveles de resolución. Se examinan las ventajas de usar DGGS para datos hidrográficos, concretamente Cartas Náuticas Electrónicas (ENC). Añadir el DGGS a la S-100 proporcionaría un sistema uniforme de mallas para las celdas ENC y eliminaría las distorsiones en las Regiones Polares producidas al proyectar celdas rectangulares basadas en latitud y longitud. El Consorcio Geoespacial Abierto (OGC) dirigió un proyecto piloto para el que uno de los participantes desarrolló un servidor que ofrece datos S-100 de áreas marinas protegidas organizados por el DGGS. Debido a este éxito y a la disponibilidad de software de código abierto para la implementación del DGGS, la BSH (Agencia Federal Marítima e Hidrográfica de Alemania) investigó la viabilidad y posibles beneficios de utilizar Sistemas de Mallas Globales y Discretas para datos S-100. El resultado fue un éxito. El resultado fue un éxito. Sin embargo, se reconoce que el DGGS como norma aún no está suficientemente avanzado, y que las herramientas de software disponibles son inadecuadas para una implementación generalizada. Es necesario seguir investigando y, además hay que determinar la mejor forma, orientación y apertura de cuadrícula para una malla uniforme de datos hidrográficos. En general, se debería tener en cuenta al DGGS para futuras versiones de la S-100, el nuevo modelo universal de datos hidrográficos, ya que los beneficios para las ENC y datos hidrográficos son evidentes y, se espera que en el futuro el DGGS revolucione los SIG.

https://doi.org/10.58440/ihr-30-1-a01

1 Introduction

The International Hydrographic Organization (IHO) has developed the S-100 Universal Hydrographic Data Model to modernize and enhance the exchange and use of hydrographic data. The S-100 standard uses ISO 8211 (file interchange format), HDF5 and Geography Markup Language (GML) encoding formats and is a framework for the development of dependent product specifications. S-101 is the new product specification for Electronic Navigational Charts (ENCs), which will replace S-57, the standard data format currently used for digital hydrographic data. S-101 offers many improvements; for example, it is fully machine-readable, it supports data that are more complex, it makes updating ENC data easier, and provides dynamic under-keel clearance (Mellor, 2023). S-102 is for bathymetric surfaces and S-122 encodes marine protected areas as some further examples of product specifications. Hydrographic offices and industry are currently working towards the transition to S-100, a huge shift for hydrographic data, particularly for Electronic Chart Display and Information Systems (ECDIS). In 2026, S-100 data are available for ECDIS and new ECDIS systems are required to be compatible with S-100 by 2029 (Navtor AS, 2022). The advantages of the S-100 model are that it complies with ISO (International Organization for Standardization) standards, is machine readable, and will provide global consistency (IHO, 2022).

Although the S-100 model makes many advancements, there is still the problem that ECDIS needs to support multiple projections for the display of ENCs. According to the Performance Standards for Electronic Chart Display and Information Systems (ECDIS) published by the International Maritime Organization (IMO), ECDIS requires that positional data be referenced to the WGS 84 or PE-90 geodetic datum (IMO, 2022). However, the Performance Standards do not specify any projections and many ECDIS manufacturers use one projection for lower latitudes and one for Polar Regions where distortions become severe. Another challenge relating to ENCs that is present in S-57 and S-101 is that no uniform gridding system has been implemented. ENCs are divided into cells (files) so that the ECDIS system is able to load and unload cells as necessary while navigating and make updating easier (Palikaris & Mavraeidopoulos, 2020). Many hydrographic offices still base ENC cells on paper chart boundaries, or have their own gridding systems for ENCs, which consist of square cells based on latitude and longitude. In both cases, gridding systems do not match at borders between countries, and Polar Regions present exceptional challenges. IHO working groups, among others, have discussed the idea of implementing a uniform system on multiple occasions in the past.

A global spatial indexing system for S-101 data was proposed in a discussion paper from the 18th IHO Transfer Standard Maintenance and Application Development Working Group (TSMAD) meeting in 2009. The paper proposed a C-squares indexing system using numbered squares measured by latitude and longitude. Advantages of implementing a global spatial indexing system are listed in the paper, including, having a common system and standardized structure not tied to any national scheme. Advantages of the C-squares indexing system are that it can be extended indefinitely to any resolution, and is efficient for data storage and searching (Pharaoh, 2009). A second paper from the 12th Worldwide ENC Database Working Group Meeting (WENDWG12) in February 2022 reports on the progress of the ENC Scheming Guidelines Drafting Group. The drafting group was established at WENDWG11 to do a feasibility and impact study on new grid-based schemes for ENCs. The following important factors to consider when developing a gridding scheme were determined: interoperability, overlap, number of ENC cells, flexibility of the arrangement, and maintenance (JHOD, 2022). At the 12th Arctic Regional Hydrographic Commission Meeting (ARHC12) in September 2022, IIC Technologies presented results from the Arctic Grid Project. The project proposed three candidates for a grid scheme for the Arctic region, one of which was a DGGS (Pritchard, 2022).

Discrete Global Grid Systems (DGGS) are a type of spatial reference system in which the globe is divided into nested layers of polygon shaped cells. DGGS offers the same advantages as C-squares (and a uniform system) and does not depend on latitude and longitude, which introduces distortions, particularly in the Polar Regions. The use of DGGS for S-100 will be investigated and discussed in this article. The concept of DGGS has been around for a long time, but the Open Geospatial Consortium (OGC) recently published it as an international standard in 2017. In 2021, the OGC conducted a pilot project, with the goal of enhancing marine spatial data infrastructure, which focused on the IHO S-122 standard for marine protected areas. As part of this project, a data server that ingests S-122 data and uses DGGS was developed (Japan Hydrographic and Oceanographic Department, 2022). Open source DGGS implementation tools and software exist and the BSH's endeavor to produce a test DGGS dataset is presented.

2 Discrete Global Grid Systems

A Geographic Information System (GIS) is a computer system for storing, analyzing, and displaying spatial data. Multiple data layers can be imported, and overlaying these layers helps understand patterns and relationships in the data (National Geographic, 2024). There are two common formats of GIS data, vector (points, lines and polygons) and raster (grids of rectangular cells). Before analysis can be performed on data layers, they need to be converted to a common format. Maps created from GIS require a projection to transform coordinates on Earth's curved

https://doi.org/10.58440/ihr-30-1-a01

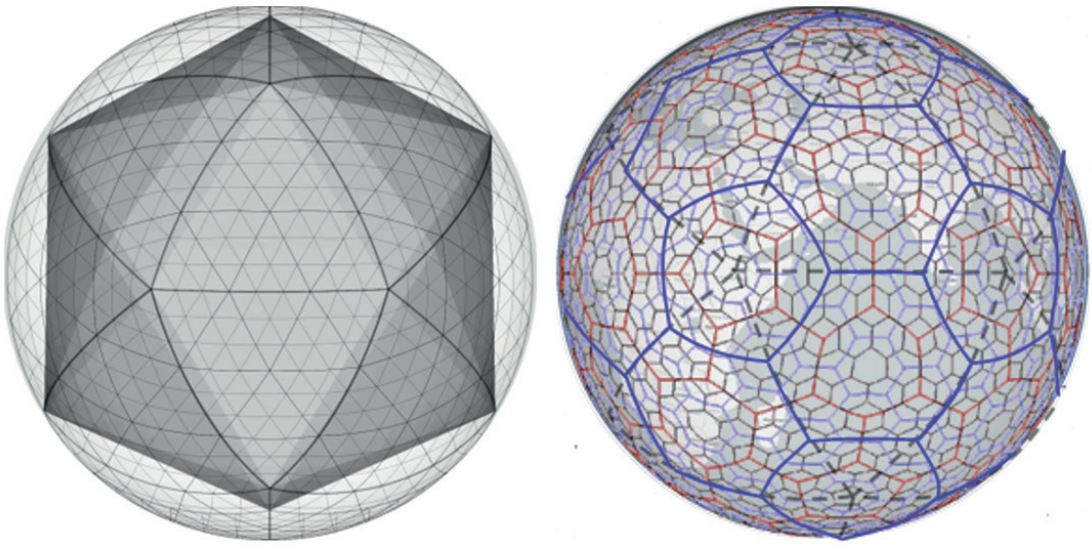

Fig. 1 Examples of DGGS (Gibb, 2021).

surface to a flat area. Map projections always a have a distortion in either shape or size, or both. The authors of the article 'Geospatial Operations of Discrete Global Grid Systems – a Comparison with Traditional GIS' suggest three issues with traditional GIS (Li & Stefanakis, 2020). First, when performing an overlay analysis in GIS, the different spatial data layers are stored in separate files and therefore are not vertically integrated and associated with a location. Second, in GIS software it is necessary to use a projection to visualize the Earth's surface on a flat screen. This causes distortions that the viewer needs to interpret. Third, GIS analysis is typically performed at a single resolution level and it is not efficient to scale the data or store many layers of the data at different scales. The use of Discrete Global Grid Systems can address these three issues.

As defined by the OGC, "a Discrete Global Grid System is a spatial reference system that uses a hierarchical tessellation of cells to partition and address the globe" (OGC, 2023). A DGGS contains a "spatio-temporal referencing by zonal identifiers and functions for quantization, zonal query, and interoperability" (Gibb, 2021). The OGC Abstract Specification Topic on DGGS (Gibb, 2021) describes the terms used to define a DGGS. Tessellation refers to the partitioning of the globe into equal-area polygons, so that the globe is completely covered by the polygons and there is no overlap of the polygons. The polygons are referred to as cells, when discussing the geometry, or zones as the containers for storing data. One tessellation of cells is referred to as a discrete global grid. A Discrete Global Grid System contains many levels of discrete global grids with different cell sizes. The process of subdividing cells to form a tessellation of smaller cells is called cell refinement. The refinement ratio, or aperture, is the ratio of the number of cells in one tessellation to the number of cells in the immediate next tessellation level with the next largest cell size (parent cell to children cells). It is not necessary for children cells to be uniquely covered by a single parent cell (Alderson et al., 2020). Hierarchical refers to the organization or numerical order of the refinement levels of discrete global grids based on their decreasing cell size. Fig. 1 shows two examples of DGGS.

To construct the initial tessellation, a regular polyhedron is scaled so that its vertices touch an ellipsoidal (or spherical) earth model, and the vertices are joined with arcs on the ellipsoid. The tessellations shown in Fig. 1 were constructed from the regular polyhedron icosahedron, and the icosahedron is visible under the tessellation on the left. The tessellation on the left was constructed exactly as described above. The tessellation on the right was constructed from a truncated icosahedron, meaning that hexagons fill the triangular faces and pentagons cover the flattened vertices. Different orientations of the icosahedron are possible. Common approaches are to align vertices with the poles, symmetrical placement about the equator, or orient the icosahedron so that no vertex touches land (SOU, 2024).

The zones are identified with a unique spatio-temporal reference called a zonal identifier. The zonal identifier is an index, a label or code that indicates a position or time period or both. The indexing of DGGS is very efficient and makes for rapid calculations on data in the grid. Quantization is the process of how data get into the grid. Quantization functions assign data to zones. Different strategies exist for quantization, and it is possible to integrate vector and raster data for example. A zonal query function uses zonal identifiers to specify geometry and retrieve data from a zone. Spatial Relation Operations are used for cell navigation. Examples of relation operations are finding a cell's parent cell or finding all cells from a smaller tessellation that are covered by a certain cell (Li & Stefanakis, 2020). Interoperability functions are used to transfer data from a DGGS externally. "Information recorded about phenomena at a location can be easily referenced to the explicit area of the associated cell, integrated with other cell values,

and provides statistically valid summaries based on any chosen selection of cells. With equal area partitioning, spatial analysis can be replicated consistently anywhere on the Earth independent of resolution or scale (Gibb, 2021)."

Conventional global coordinate reference systems (such as latitude/longitude) currently used in GIS software, work well for navigation, which is what they were originally designed for. But, because one degree of longitude, does not represent the same distance everywhere on the globe, uncertainties and distortions are present when producing analyses or visualizations. Many of these uncertainties and distortions can be eliminated with DGGS, which uses equal area cells that represent the earth in a uniform way. DGGS are designed for information, to support data storage, processing, analysis, transmission, and visualization. With DGGS, layers of spatial data can be integrated by location, meaning vector and raster data can both be integrated in the DGGS grid and analyzed together without converting formats. Additionally, scalability is built into the DGGS system, meaning data can be easily viewed and analyzed at multiple resolutions (Li & Stefanakis, 2020).

3 State of the art

The OGC is an international organization of geospatial experts from various fields that work together to innovate and develop open standards for geospatial data. OGC's mission is to make location information FAIR – Findable, Accessible, Interoperable, and Reusable (OGC, 2023). OGC developed an international standard for DGGS consisting of structural and functional requirements, published in 2017 (OGC, 2017). The standard was later published as an ISO standard, ISO 19170, in 2021 (ISO, 2021; Alderson et al., 2020). Additionally, OGC develops Application Programming Interface (API) standards designed to provide and access geospatial data on the web, which have been widely implemented. A draft OGC API for accessing data organised according to Discrete Global Grid Systems is currently under development (OGC, 2023).

Although limited, open-source software solutions exist for DGGS implementation, and researchers and companies have begun using DGGS for GIS analysis. The authors of 'Geospatial Operations of Discrete Global Grid Systems – a Comparison with Traditional GIS' (Li & Stefanakis, 2020) made an in-depth comparison of available DGGS implementation software. They discuss the DGGS operations currently required by the OGC's Discrete Global Grid Systems Abstract Specification and extended operations that are currently supported by traditional GIS and are foreseen to be developed for DGGS in the future. The basic functions are: quantization operations, spatial relation operations, and interoperability operations. The extended operations discussed in the article are: database techniques, data pre-processing and manipulation, spatial analysis and data interpretation, data computation, and data visualization. Only some basic functions have been implemented in the DGGS software available today. Four examples of DGGS implementation software that are available open-source are presented below. They are: HEALPix, geogrid, DGGRID, and H3. Then, two examples of analysis performed with open-source DGGS are described.

HEALPix is a DGGS implementation that was developed to support the analysis of very large multi-frequency satellite derived datasets at a high resolution (HEALPix Team, 2019). Three properties of HEALPix allow the execution of Fourier analysis with spherical harmonics on the sphere, and not be too slow. These properties are: a hierarchical structure, equal area cells, and an iso-latitude distribution of the cells, meaning the cell centres are located on rings of constant latitude. (Górski et al., 2022). The grid is based on an octahedron with its points at the north and south poles. Diamonds cover the four vertices at the equator and the eight faces. To construct each finer resolution grid, each face is split into four diamonds. HEALPix is available in the following program languages: C, C++, Fortran90, IDL, Java and Python; and offers many features, including: generation and query of the DGGS, manipulation of satellite datasets, spherical harmonics transformations, and visualization (HEALPix Team, 2019).

The DGGS implementation geogrid was developed at Heidelberg University and allows the generation and handling of the Icosahedral Snyder Equal Area Aperture 3 Hexagon (ISEA3H) Discrete Global Grid System (Mocnik, 2021). ISEA3H is a projection that maps the icosahedron onto the sphere. Aperture 3 is the refinement ratio, or in other words, the number of children cells per parent cell. Hexagon is the cell shape (Sahr et al., 2013). geogrid is programmed in Java and includes the following functions: translation of coordinates to grid cells, indexing, cell geometry calculations and visualization.

DGGRID is another example of an open-source DGGS implementation. DGGRID allows the generation and manipulation of icosahedral discrete global grids (Sahr, 2024). It is possible to specify the following parameters to create a customized DGGS: the orientation of the base icosahedron, the projection used to transfer the base icosahedron edges onto the sphere, the cell shape (hexagon, triangle, or diamond), the aperture, the resolution, and the earth radius (Sahr, 2023). Kevin Sahr wrote DGGRID in C++, and based on this library; Richard Barnes developed an R package, dggridR, with much of the same functionality (Barnes & Sahr, 2017). Barnes intends dggridR to be used for spatial statistics, as it allows binning in evenly sized cells instead of using a rectangular grid based on latitude and longitude, which introduces distortions.

H3, Uber's hexagonal hierarchical spatial index, is a DGGS implementation developed by the ride-sharing and food delivery company for their specific purposes, and made available open-source (Brodsky,

https://doi.org/10.58440/ihr-30-1-a01

2018). The H3 grid, shown in Fig. 2, was constructed from a truncated icosahedron, where pentagons cover the twelve vertices, and ten (partial) hexagons cover each of the twenty faces. The base level grid (resolution 0) has 110 hexagonal cells and 12 pentagon cells. The area of the hexagon cells within one resolution differ based on their distance to the pentagon cells. The ratio between the minimum and maximum area of cells within one resolution is nearly 2 (Uber, 2024) and the area of the pentagons is close to the area of the smallest hexagons. There are sixteen resolution levels, the largest have an average area of 4 million square kilometers and the smallest 0.9 square meters. The grid is positioned on the globe so that the pentagons are centered over water, to avoid pentagons in Uber's use of analysing drivers and riders across a city and be able to cluster cells to represent neighbourhoods (Brodsky, 2018). H3 was written in C and bindings are available for Java and Python. The basic functions available are indexing, transforming latitude and longitude coordinates to cell addresses, locating neighbouring cells, and representing movement between cells.

The author of 'Discrete Global Grid Systems as scalable geospatial frameworks for characterizing coastal environments' did an analysis of coastal temperature data, aggregating and interpolating the data in a hexagonal DGGS using both the H3 Python library and the dggridR R package (Bousquin, 2021).

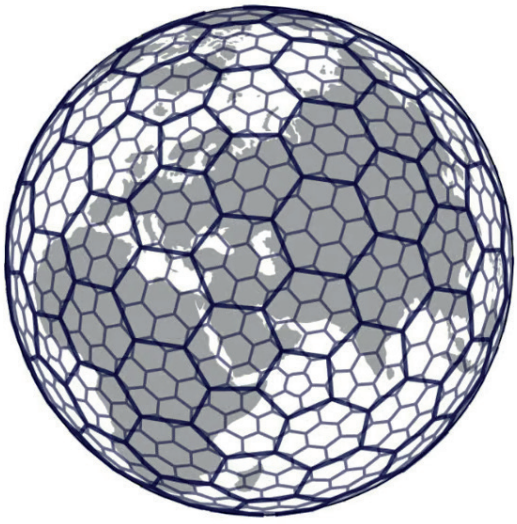

Fig. 2 The H3 DGGS (Brodsky, 2018).

The paper identified advantages of using a hexagonal grid compared to a square grid. First, with a hexagonal grid, the centroids of each cell are equidistant to the centroids of all neighbouring cells, which is an advantage for path analysis. Second, because a hexagon more closely resembles a circle, when point datasets are aggregated there is less bias from edge effects. One disadvantage of hexagonal DGGS is that child cells are not uniquely covered by one parent cell and the amount of overlap depends on the aperture (Bousquin, 2021). Bousquin identified an advantage of H3; neighbours of a cell can be determined directly from the cell index and do not need to be stored in a separate table. The authors of 'Integrating the Who, What, and Where of U.S. Retail Center Geographies' used H3 for an analysis of retail centres in the United States (Ballantyne, Singleton, Dolega and Macdonald, 2022). Three datasets, more than three million retails places points and their building footprints, and retail land-use polygons from OpenStreetMap, were aggregated to an H3 grid at resolution 11. Major retail centres, defined as having more than fifty retail places within neighbouring cells were extracted. An R package, h3jsr, for spatial operations on H3 DGGS was used for the analysis on characteristics of retail centres. This research is an example where DGGS was successfully used in place of traditional GIS methods.

4 Federated Marine Spatial Data Infrastructure Pilot Phase II

The Federated Marine Spatial Data Infrastructure (FMSDI) Pilot Phase II is an OGC Innovation Program initiative with the objective of enhancing Marine Spatial Data Infrastructures (MSDI), to better understand MSDI maturity, and to demonstrate the power of FAIR data in the context of the marine environment (Taleisnik & Idol, 2022). The goal of the initiative was to transform and interoperate with S-100 data, using S-122 as the example. First, Marine Protected Area (MPA) data were transformed into S-122 and served through OGC APIs, then the IHO and OGC standards and how the standards influence the interoperability and usage of MPA data were investigated, and finally, a roadmap for MSDI development was created. The initiative is described in an OGC Engineering Report.

The Marine Protected Area Product Specification IHO Publication S-122 (IHO, 2019) was produced by the IHO Nautical Information Provision Working Group (NIPWG) to encode the extent and relevant information of MPAs for use in ECDIS. The United Nations Convention on the Law of the Sea (UNCLOS) identifies categories of Marine Protected Areas and places a general obligation on states to implement measures to protect the marine environment. A Marine Protected Area is an area of the ocean, including the water, flora, fauna and features, reserved to protect the enclosed environment. MPAs can be located in territorial waters, the exclusive economic zone, or even international waters. The S-122 Product Specification is a feature-based vector product based on the S-100 General Feature Model (Taleisnik & Idol, 2022). Participants of the initiative (IIC Technologies, Pelagis, Helyx Secure Information Systems Ltd., The University of Calgary, and Compusult) demonstrated seven server and client components. The servers ingested MPA data (and in some cases, other data) in the Baltic and North Seas from various sources, and transformed it to S-122. The clients served the data through OGC APIs, and displayed outputs to end users.

IIC Technologies demonstrated one Baltic/North Sea Server. Pelagis and Helyx Secure Information Systems Ltd. each demonstrated clients designed to ingest data from the server (from various sources). IIC Technologies and the University of Calgary demonstrated two Data Fusion Servers that ingest various datasets. Data Fused Clients were demonstrated by Compusult and Pelagis. The server demonstrated by IIC Technologies was designed to ingest MPA data from various sources, transform it to S-122, and offer it through an OGC API. The MPA data were provided in shapefile and Web Feature Service (WFS) format and were first reduced to PostGIS database tables, then the fields were mapped individually to the S-122 fields and a custom tool used for the transformation. Many MPA have borders along the shoreline, and shorelines often have a high point density. Therefore, downloading from the server and viewing so many vertices was challenging. Using a DGGS would improve performance because MPAs could be efficiently partitioned to the grid. The MPA polygons would need to be partitioned according to the grid system, downloaded, and pieced together again. Some grid cells would have partial coverage so a data coverage concept would be necessary. The University of Calgary's Fusion Server published data processed into an Icosahedral Snyder Equal Area Aperture 3 Hexagonal (ISEA3H) DGGS. The server ingests coverage data and vector data from different sources, and these data are mapped together into a hierarchy of hexagonal cells. A GeoJSON encoding was used for the data and they were delivered using an Environmental Data Retrieval (EDR) API accessed via Web Coverage Services (WCS). The use of DGGS is still in the experimental stage and what data structure to use to deliver the data is unknown, but an extension of WCS could be an option. Clients requesting location data from the server need knowledge of the DGGS geometry. Additionally, the data structure needs to support the functionality to search the data, which so far has not been implemented, but could possibly be done with Common Query Language (CQL).

The Engineering Report makes suggestions to add a number of new attributes to the S-122 model and discusses potential solutions to the challenges encountered with DGGS. A major difficulty with DGGS is that clients accessing data stored in DGGS need to know how to decode cell location information, meaning that they need to be able to translate the DGGS geometry to coordinates. Additional developments that would be beneficial include, support for temporal extents, and the possibility to query by tessellation level. The servers and clients developed for the Pilot project used a GeoJSON encoding instead of the GML that is used in the S-122 standard. The reason stated in the report for using GeoJSON is because of the interoperability of the format and wide adoption and support in mapping software (Taleisnik & Idol, 2022). Further, the report discusses challenges between the S-122 standard and the GeoJSON encoding. The report recommends the use of ISO 19152 for more complex restrictions and suggests adding new attributes to the S-122 model.

Phase III of the pilot builds on the work accomplished during phase II. The goal of phase III was to enhance MSDI and advance the implementation of open data standards through use cases on the

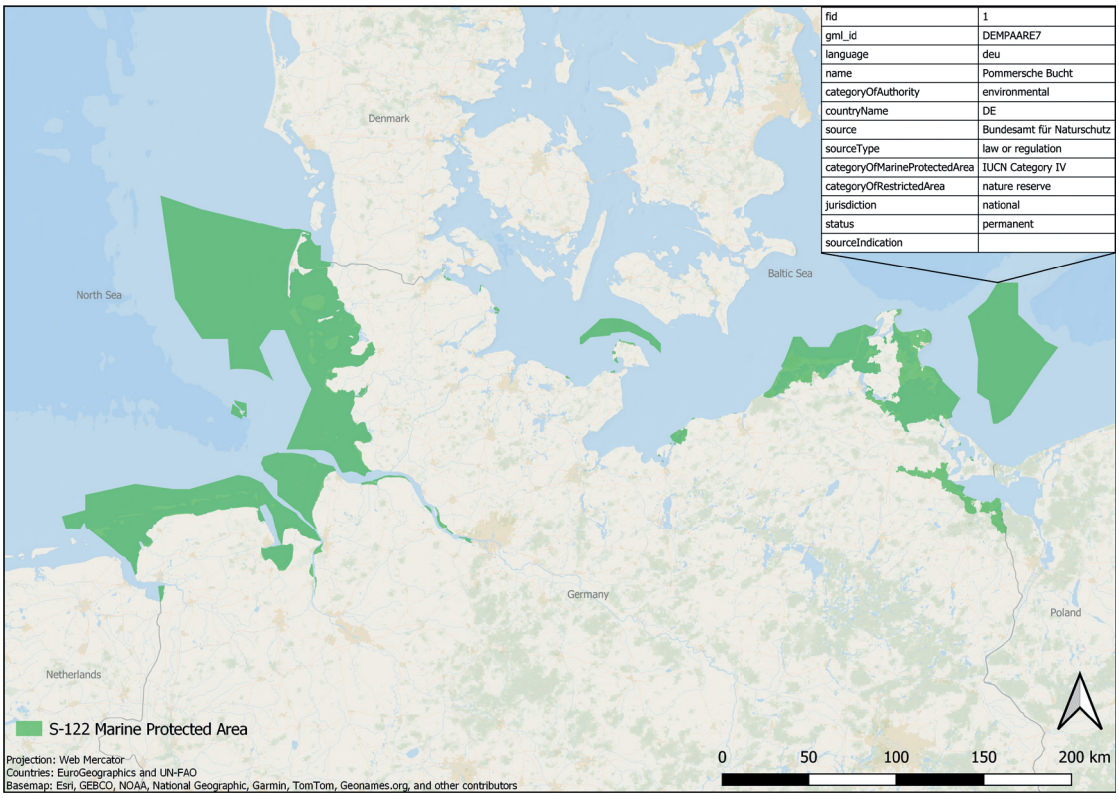

Fig. 3 BSH's S-122 test dataset – Marine Protected Areas.

https://doi.org/10.58440/ihr-30-1-a01

integration of marine and terrestrial data in the Arctic. One of the participants, the University of Calgary, contributed a Discrete Global Grid System server and another participant, Ecere Corporation, implemented a DGGS client interacting with this server. An ISEA3H DGGS was used to integrate elevation, land cover, population, ship lanes, MPA and additional data to model and visualize three sub-scenarios – coastal erosion, flooding, and navigational hazards. Results, challenges encountered during the development and lessons learned are detailed in the OGC Engineering Report on phase III (Thomas & Saeedi, 2023).

5 Investigation

This section presents the investigation into DGGS done by the BSH (German Federal Maritime and Hydrographic Agency). It describes the production of an S-122 dataset and shows the conversion of the S-122 Marine Protected Areas to a DGGS. Additionally, it discusses a comparison of DGGS grid cells and finally it provides a summary of the investigation.

5.1 S-122 dataset production

The BSH has produced a test S-122 dataset of Marine Protected Areas (MPA) within the German Exclusive Economic Zone (EEZ). The S-122 data were produced from the existing S-57 feature RESARE (Restricted Area) data in BSH's primary production tool CARIS Hydrographic Production Database (HPD), and Marine Protected Area data from the International Union for Conservation of Nature (IUCN) downloaded from Protected Planet. The data were imported to QGIS in shapefile format. Errors in the IUCN data were first cleaned up, and then both datasets were imported to an SQLite database and a table was created to represent S-122 attributes. Additional tables were created and filled for RestrictedArea, DataCoverage, Authority, ContactDetails, Applicability, and Regulations. A Python script was used to generate the S-122 GML from the SQLite database. Finally, the output GML was validated against the S-122 schema in XMLSpy. Fig. 3 shows the Marine Protected Areas encoded in the S-122 test dataset. The data encoded for the area Pommersche Bucht is displayed in the table in the top right corner of the map.

5.2 Converting S-122 data to DGGS

To test the feasibility of using DGGS for S-100 data, the Marine Protected Area data were organized according to a DGGS. Uber's DGGS implementation H3 Python binding was used for the investigation because Python is accessible and interoperable with BSH processes and therefore using H3 was quick and efficient for producing some test data. H3 uses hexagonal cells with aperture 7 and all basic DGGS operations are implemented. However, H3 is optimized for land data; but the purpose here was to test how DGGS data work, not to present a permanent solution of a DGGS grid for hydrographic data.

The MPA polygons were transformed to groups of hexagonal cells using the polygon_to_cells function. Cell resolution 8 was used which has an average cell area of 0.7 km2 (Uber, 2024). Because no visualization operation has so far been built into the DGGS functionality, the hexagonal cells must be converted to traditional GIS polygons and exported to a common GIS file format in order to produce a map of the data. This process is very slow because of the large number of small hexagonal polygons now making up the original areas. Therefore, a smaller DGGS cell size was not feasible for the scale of the whole German EEZ. A smaller cell size is, however, not necessary at this scale. When comparing Fig. 3 above of the MPA GML polygons and Fig. 4 below showing the MPA data arranged to a DGGS, at this scale it is not possible to see the edges. In the zoom window in the top right of the map below it is possible

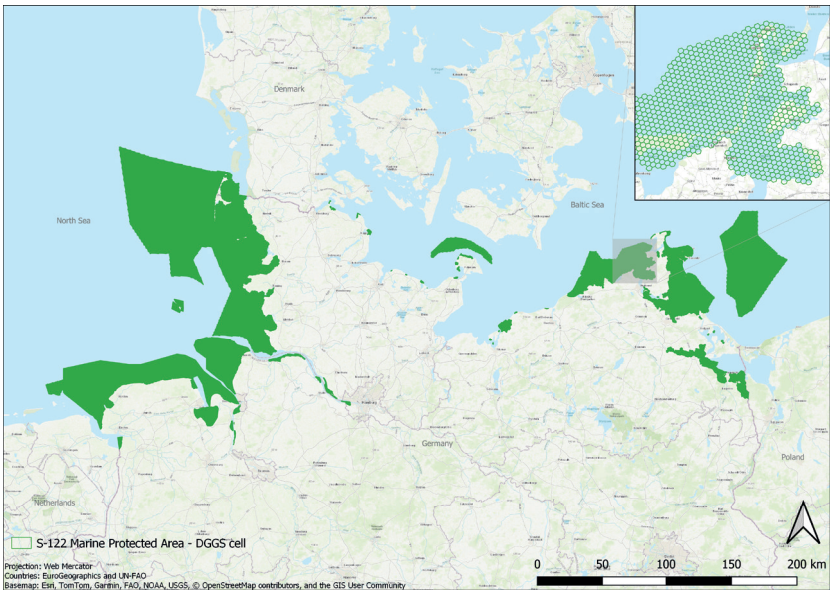

Fig. 4 BSH's S-122 test dataset arranged according to a DGGS.

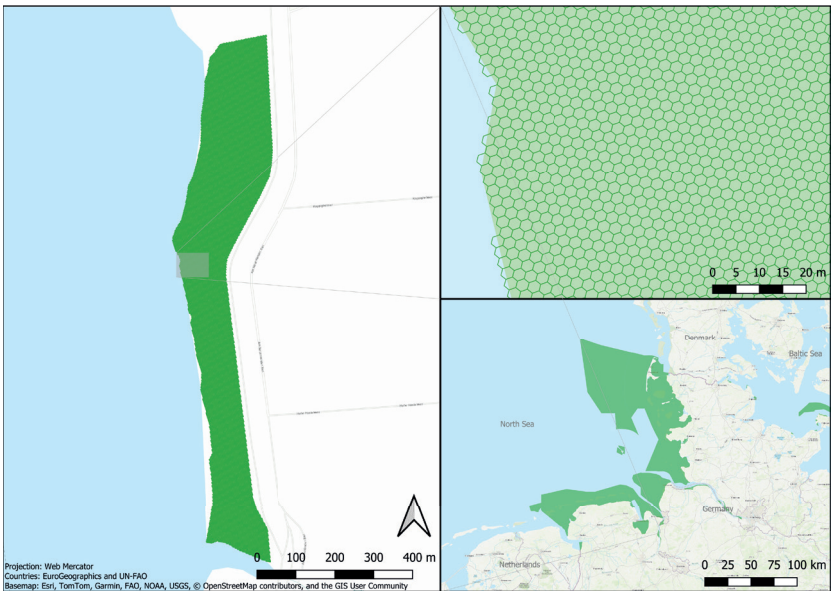

Fig. 5 The Neuenlander Außendeich MPA in a high resolution DGGS.

to see that the MPA areas are made up of many small hexagons and the boundary has changed slightly to match the hexagon pattern.

The highest resolution possible with H3 is resolution 15, which has an average cell size of 0.9 m^2. The second highest resolution possible, resolution 14, has an average cell area of 6.3 m^2 (Uber, 2024). The smallest MPA in the S-122 test dataset, Neuenlander Außendeich, was converted to DGGS at resolution 14. The area is approximately 150 m by 1,000 m. It is shown in Fig. 5 below on the left. In the overview map on the bottom right, the area is nearly not even visible on the River Weser south of Bremerhaven. On the top right is a zoom of a small area where the individual hexagons are visible and the polygon area from the S-122 GML dataset is displayed underneath so that the differing edge border is visible. At resolution 14, the maximum difference of the edge location between the original polygon and the DGGS is approximately 1.5 m. The original polygon covers an area of 173,996 m^2 and the DGGS area covers 174,010 m^2. This is a difference of 14 m^2 or 0.008 % of the original polygon area. It would need to be considered whether this change of the MPA boundary is acceptable at a certain scale, whether the legally defined limits of the MPA should not be modified at all, or whether an extension of the MPA to match the hexagonal grid, while ensuring the entire MPA is contained, would be acceptable.

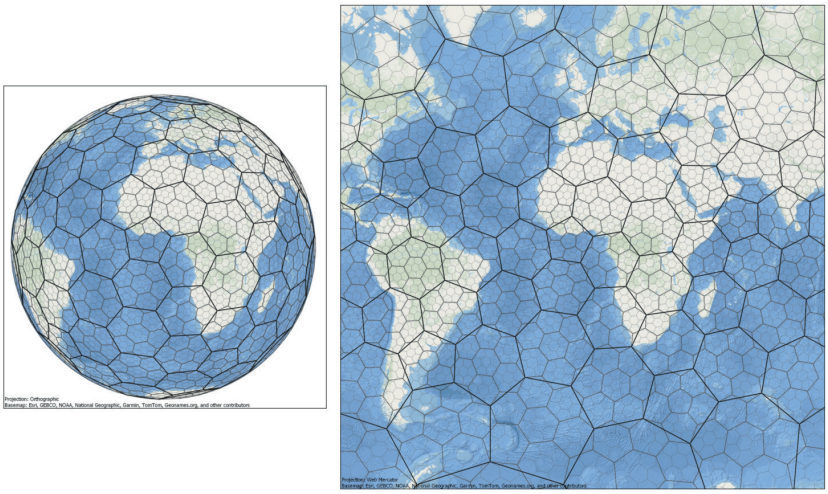

Fig. 6 An orthographic and a Mercator projection of the H3 DGGS.

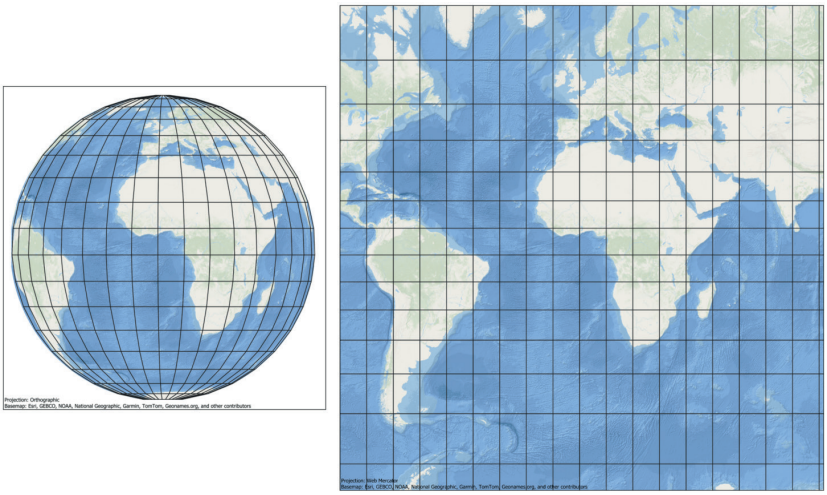

Fig. 7 An orthographic and a Mercator projection of a grid based on latitude and longitude.

5.3 Modelling DGGS grid cells

DGGS can be a system for organizing data layers, but also has the benefit that because DGGS consists of (almost) equal area cells around the globe, including in the Polar Regions, it could be used for an Electronic Navigational Chart (ENC) gridding system and the same system could be used everywhere. Fig. 6 shows the three largest cell sizes of the H3 DGGS (resolution 0, 1 and 2 with corresponding approximate average cell areas 4 million km^2, 610,000 km^2 and 87,000 km^2; Uber, 2024). There are sixteen resolutions in H3 and the smallest has an average cell area of 0.9 km^2. Therefore, the scalability of the cell sizes would be beneficial for different ENC cell sizes for different scales. Again, H3 is just used here as an example, but any DGGS would offer the same scalability option and could be optimized for the specific purpose of ENC cells. On the left is an orthographic projection that shows how the hexagons look on the globe and the (almost) equal area of the cells is visible. On the right, a Mercator projection is used, which is a typical projection used for navigation. Here the distortions are present and become extreme near the poles. As a comparison, a 10° latitude by 10° longitude grid is shown below in Fig. 7. In the orthographic projection on the left, it is clear that as the lines of longitude converge at the poles, the cells become narrower towards the poles, however, in the Mercator projection, these cells appear much larger. When cells sizes are not equal, the distortions from the Mercator projection are much harder to interpret.

5.4 Summary

The BSH successfully transformed an S-122 test dataset to DGGS. Although, because visualization is not implemented in H3, the hexagons need to be exported to traditional GIS format and viewed in GIS software or a web map, but this is very slow for many small hexagons because traditional GIS software has no knowledge of DGGS yet. Exporting polygons as dissolved areas of hexagons would be more efficient. It is difficult to show the advantages of DGGS as a data format because the tools for implementing and working with DGGS are not yet advanced enough, however, it is relatively easy to convert polygons to DGGS. The advantage of using equal area cells for ENCs and hence avoiding distortions can clearly be seen when comparing hexagonal DGGS cells to cells based on latitude and longitude. Equal area cells also have the advantage that especially when the data inside are arranged according to DGGS, the size of ENC files including all data should be similar when the cell sizes are equal. A

https://doi.org/10.58440/ihr-30-1-a01

uniform system for ENC cells is perhaps currently the strongest advantage of using DGGS.

6 Outlook and conclusion

Discrete Global Grid Systems are a spatial reference system in which the globe is partitioned into equal area polygons, and the polygons form cells arranged into hierarchical grids. The cells can be referenced via zonal identifiers, and spatial operations based on the cells are possible. The OGC published an international standard describing DGGS and basic operations in 2017. Open-source software is available for the implementation of DGGS, and analysis is possible with the basic operations implemented so far. Advantages for using DGGS for S-122 data were identified through the Federated Marine Spatial Data Infrastructure (FMSDI) Pilot Project Phase II, for example, that DGGS would eliminate the challenges with high point densities. BSH has successfully produced an S-122 dataset according to the current standard and organized the dataset according to DGGS. Discrete Global Grid Systems offer advantages over traditional GIS methods and coordinate systems because DGGS is designed for information, multiple data types can be integrated, and it is efficient to scale.

There are still many challenges to overcome before DGGS can be widely implemented for hydrographic data. First, a further investigation would be necessary into the operability of DGGS with different file formats such as hdf5, raster, vector, point clouds, and even digital twin data. The interoperability between files in different formats and whether the effects are related to the gridding system or file formats would need to be identified. One example of such a test would be to combine raster bathymetry data and ENC vector data to DGGS cells. A second investigation into the operability of DGGS for ENCs would be necessary. ENCs are used for navigation and therefore require a reference system conversion between the ship's Global Navigation Satellite System (GNSS) signal and the chart horizontal reference system. How this works when the chart is referenced to a DGGS would need to be determined. Thirdly, the scalability of DGGS would need to be investigated. The kRing function implemented in H3 allows for the compacting of hexagons making it possible to represent an area in higher detail with fewer hexagons (Brodsky, 2018). An example is shown in Fig. 8. Additionally, the level of detail necessary would need to be determined and the idea of coverage coming from OGC's pilot project investigated. Finally, the benefits of using DGGS for other S-100 products need to be investigated, possibly including the use of routeing and/or clustering operations already implemented in available DGGS software.

Although there are still challenges to be worked out relating to the operations and data structure to be used, it is possible to implement S-122 data according to a DGGS. Using Discrete Global Grid Systems, instead of traditional coordinate systems, to organize data, offers many advantages. For example, datasets with global coverage can be represented in a uniform way and many distortions that would be present with traditional coordinate systems can be eliminated. Hydrographic offices around the world are currently working towards the transition to S-100 hydrographic data. One major component of S-100 is the new S-101 standard for ENCs. ECDIS systems currently require at least two projections, one for displaying charts in the Polar Regions, and one for navigation in lower latitudes. S-100 does not specify a standard to address this issue. Another thing not addressed with S-100 is a uniform gridding system for ENC cells. Currently, countries have their own systems, largely based on latitude and longitude. Benefits of using DGGS for S-100 have been identified. First, a DGGS grid would provide one global uniform system for displaying charts in ECDIS, with seamless coverage and no distortions in the Polar Regions. Second, DGGS can be a gridding system for ENC cells that is consistent across all nations and matches at borders and the possibility of implementing a common scaling. This has been discussed many times in the past. Third, DGGS can handle large amounts of data and can combine different types of data, for example bathymetry data (raster) for ENCs (vector). Advantages of using DGGS for a server to store, transmit, and visualize Marine Protected Area data and combine datasets were shown from OGC's pilot project.

Software for the implementation of DGGS is not yet advanced enough and at this point cannot compare to traditional GIS software in functionality and operability. However, DGGS will be used in the future for many applications as the tools become available and advantages are realized. DGGS has the possibility to be better than traditional GIS and even replace it in the future. Therefore, it would be beneficial for S-100 to support DGGS in the future. This would be a long-term goal, but the development of the next edition of the S-100 framework to

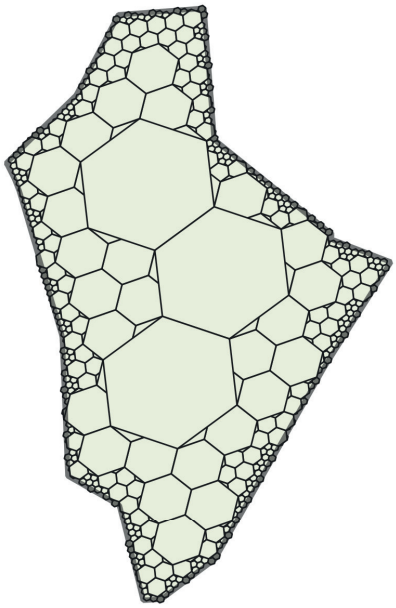

Fig. 8 Example of what would be possible with the kRing function.

enable the possibility of supporting DGGS should be thought about now. Questions to be answered are: is the S-100 GML encoding interoperable enough and how advanced do standards need to be before it is feasible to add DGGS support. A single, customized DGGS for hydrographic data would need to be developed. The cell shape, aperture, and orientation would need to be optimized. Ideally, in the future, systems used for the production of navigational charts will support automatic integration of DGGS. Discrete Global Grid Systems are a solution designed for data storage, analysis, and visualization and have the potential to improve interoperability, FAIRness and advancement of Marine Spatial Data Infrastructure (MSDI) implementation.

Acknowledgements

The authors would like to thank Daniel Zühr, Andreas Sommer, and Elena Gnehm for their involvement in the production of BSH's initial S-122 GML test dataset.

References

Alderson, T., Purss, M., Du, X., Mahdavi-Amiri, A. and Samavati, F. (2020). Digital Earth Platforms. In H. Guo, M. Goodchild and A. Annoni, *Manual of Digital Earth* (pp. 25–54). Singapore: Springer. https://doi.org/10.1007/978-981-32-9915-3_2

Ballantyne, P., Singleton, A., Dolega, L. and Macdonald, J. (2022). Integrating the Who, What, and Where of U.S. Retail Center Geographies. *Annals of the American Association of Geographers, 113*:2, pp. 488–510, https://doi.org/10.1080/24694452.2022.2098087

Barnes, R. and Sahr, K. (2017). *Discrete Global Grids for R: Spatial Analysis Done Right*. https://github.com/r-barnes/dggridR (accessed 1 March 2024).

Bousquin, J. (2021). Discrete Global Grid Systems as scalable geospatial frameworks for characterizing coastal environments. *Environmental Modelling & Software, 146*, https://doi.org/10.1016/j.envsoft.2021.105210

Brodsky, I. (2018). *H3: Uber's Hexagonal Hierarchical Spatial Index*. https://www.uber.com/en-DE/blog/h3/ (accessed 1 March 2024).

Gibb, R. (2021). *Topic 21 - Discrete Global Grid Systems - Part 1 Core Reference System and Operations and Equal Area Earth Reference System*. OGC Document: 20-040R3, Open Geospatial Consortium. https://docs.ogc.org/as/20-040r3/20-040r3.pdf (accessed 1 March 2024).

Górski, K., Wandelt, B., Hivon, E., Hanson, F. and Banday, A. (2022). *The HEALPix Primer*. https://healpix.sourceforge.io/html/intro.htm (accessed 1 March 2024).

HEALPix Team (2019). *HEALPix – Data Analysis, Simulations and Visualization on the Sphere*. https://healpix.sourceforge.io/index.php (accessed 1 March 2024).

IHO (2019). *Marine Protected Area Product Specification*. IHO Publication S-122, International Hydrographic Organization, Monaco. https://iho.int/en/nipwg-product-specifications (accessed 1 March 2024).

IHO (2022). *Universal Hydrographic Data Model*. International Hydrographic Organization, Monaco. https://iho.int/uploads/user/pubs/standards/s-100/S-100_5.0.0_Final_Clean_Web.pdf (accessed 1 March 2024).

IMO (2022). *Performance Standards for Electronic Chart Display and Information Systems (ECDIS)*. International Maritime Organization, Monaco. https://wwwcdn.imo.org/localresources/en/KnowledgeCentre/IndexofIMOResolutions/MSCResolutions/MSC.530(106).pdf (accessed 1 March 2024).

ISO (2021). *ISO 19170-1:2021 - Geographic information - Discrete Global Grid Systems Specifications*. International Organization for Standardization, ISO/TC 211, 35.240.70, 106 pp. https://www.iso.org/standard/32588.html (accessed 1 March 2024).

JHOD (2022). *Interim Report on the development of S-101 ENC Scheming Guidelines*. Japan Hydrographic and Oceanographic Department. https://iho.int/uploads/user/Inter-Regional%20Coordination/WEND-WG/WENDWG12/WENDWG12_2022_04.2A_EN_Scheming_ver4.pdf (accessed 1 March 2024).

Li, M. and Stefanakis, E. (2020). Geospatial Operations of Discrete Global Grid Systems – a Comparison with Traditional GIS. *Journal of Geovisualization and Spatial Analysis, 4*(26). https://doi.org/10.1007/s41651-020-00066-3

Mellor, T. (2023). *S-57 to S-101: Explaining the IHO standards for ECDIS*. UK Hydrographic Office, Admiralty Maritime Data Solutions. https://www.admiralty.co.uk/news/s-57-s-101-explaining-iho-standards-ecdis (accessed 1 March 2024).

Mocnik, F.-B. (2021). *Library for Discrete Global Grid Systems*. https://github.com/giscience/geogrid (accessed 1 March 2024).

National Geographic (2024). *GIS (Geographic Information System)*. National Geographic Society. https://education.nationalgeographic.org/resource/geographic-information-system-gis/ (accessed 1 March 2024).

Navtor AS (2022). *The 101 on S-100: what YOU need to know about maritime's big data transformation*. NAVTOR AS, Egersund, Norway. https://www.navtor.com/post/the-101-on-s-100-what-you-need-to-know-about-maritime-s-big-data-transformation (accessed 1 March 2024).

OGC (2017). *Topic 21: Discrete Global Grid Systems Abstract Specification*. OGC 15-104r5, Open Geospatial Consortium, USA. https://portal.ogc.org/files/15-104r5 (accessed 1 March 2024).

OGC (2023). *About*. Open Geospatial Consortium, USA. https://www.ogc.org/about-ogc/ (accessed 1 March 2024).

OGC (2023). *OGC API - Discrete Global Grid Systems*. Open Geospatial Consortium, USA. https://ogcapi.ogc.org/dggs/overview.html (accessed 1 March 2024).

Palikaris, A. and Mavraeidopoulos, A. (2020). Electronic Navigational Charts: International Standards and Map Projections. *GNSS and Geomatics Application for Navigation and Marine Engineering, 8*:248. https://doi.org/10.3390/jmse8040248

Pharaoh, T. (2009). *S-101 Coverage Referencing System – Discussion Paper*. 18th TSMAD Meeting, 4th to 8th May 2009, Ottawa, Canada. https://legacy.iho.int/mtg_docs/com_wg/TSMAD/TSMAD18/TSMAD18-16.3F_IndexSystem.pdf (accessed 1 March 2024).

Pritchard, J. (2022). *The Arctic Grid Project*. IIC Technologies. https://iho.int/uploads/user/Inter-Regional%20Coordination/

https://doi.org/10.58440/ihr-30-1-a01

RHC/ARHC/ARHC12/ARHC12_2022_C2A_EN_Arctic%20Grid%20Project%20report.pdf (accessed 22 March 2024).

Sahr, K. (2023). *DGGRID version 8.0b User Documentation for Discrete Global Grid Generation Software*. Southern Oregon University Department of Computer Science, Southern Terra Cognita Laboratory. https://discreteglobal.wpengine.com/wp-content/uploads/2024/01/dggridManualV80b.pdf (accessed 1 March 2024).

Sahr, K. (2024, January 10). *DGGRID – A command-line application that generates and manipulates icosahedral discrete global grids*. https://github.com/sahrk/DGGRID (accessed 1 March 2024).

Sahr, K., White, D. and Kimerling, A. (2013, March 14). Geodesic Discrete Global Grid Systems. *Cartography and Geographic Information Science, 30*:2, pp. 121–134. https://doi.org/10.1559/152304003100011090

SOU (2024). *DGG Orientation*. Southern Oregon University Department of Computer Science, Southern Terra Cognita Laboratory. https://discreteglobal.wpengine.com/dgg-orientation/ (accessed 1 March 2024).

Taleisnik, S. and Idol, T. (2022). *Towards a Federated Marine SDI: IHO and OGC Standards Applied to Marine Protected Area Data Engineering Report.* OGC Document: 22-013R3, Open Geospatial Consortium. https://docs.ogc.org/per/22-013r3.pdf (accessed 1 March 2024).

Thomas, R. and Saeedi, S. (2023). *Towards a Federated Marine SDI: Connecting Land and Sea to Protect the Arctic Environment Engineering Report*. OGC Document: 23-010, Open Geospatial Consortium. https://docs.ogc.org/per/23-010.html (accessed 25 March 2024).

Uber (2024). *Tables of Cell Statistics Across Resolutions*. H3 – Hexagonal hierarchical geospatial indexing system, Uber Technologies Inc. https://h3geo.org/docs/core-library/restable (accessed 1 March 2024).

Authors' biographies

Kimberly Mason is a Geoinformatics Specialist in the Nautical Editorial Office at BSH, the German Federal Maritime and Hydrographic Agency. Her responsibilities involve generating S-100 data and automating the production of maps and nautical publications. She has previous work experience as a GIS Analyst and Database Analyst. She graduated from the University of Waterloo in Canada in 2019 with a Bachelor of Mathematics in Statistics, Computer Science and GIS. She completed a Master of Science in Geodesy and Geoinformatics with a specialization in Hydrography in 2022 at HafenCity University in Hamburg, Germany.

Kimberly Mason

Jens Schröder-Fürstenberg is a Master Mariner who studied Navigation at the University of Rostock. He sailed on bulk carrier and container feeder vessels and worked in ship operation and handling for many years. He is working with the German Maritime and Hydrographic Agency (BSH) since 1999 and he is the Head of the Nautical Information Service Division. Jens was Chairman of the IHO Nautical Information Provision Working Group for about 10 years and he is now the Chairman of the IHO Wordwide ENC Database Working Group. From 2003 to 2022, he worked as ECDIS basics instructor at the Maritime Education and Training Centre Warnemünde of University of Applied Sciences Wismar.

Jens Schröder-Fürstenberg

Greetings from HYDRO 2023 Organizing Committee

Aldo Monaca

Greetings to all readers of The International Hydrographic Review! It is with great pleasure and pride that we extend our warmest welcome to the upcoming issue featuring selected contributions from HYDRO 2023 in Genoa. As members of the Organizing Committee, we are delighted to offer this foreword as a testament to the success and significance of HYDRO 2023.

The conference held in Genoa was a resounding success, bringing together experts, professionals, and enthusiasts from around the globe to engage in fruitful discussions, exchange insights, and explore advancements in hydrography and related fields. We are immensely grateful to all participants, presenters, sponsors, and organizers whose contributions made this event possible.

HYDRO 2023 marked a significant milestone as it was the first time that Italy had the honor of hosting the conference. This historic occasion underscored Italy's rich maritime heritage and its commitment to advancing hydrographic science and technology on the global stage.

At HYDRO 2023, seven main topics took center stage, encompassing a diverse array of subjects vital to the advancement of hydrography:

1. Coastal Resilience: Discussions surrounding coastal resilience delved into strategies and technologies aimed at mitigating the impacts of coastal hazards and climate change, ensuring the sustainability of coastal communities and ecosystems.
2. Sustainable Underwater Infrastructures: Exploring the theme of sustainability, sessions focused on the development and maintenance of underwater infrastructures, with an emphasis on environmentally friendly practices and solutions.
3. Blue Transition: Highlighting the shift towards a sustainable blue economy, this topic examined innovative approaches to ocean resource management, renewable energy generation, and economic development while preserving marine ecosystems.
4. Ocean Exploration: From deep-sea exploration to the discovery of marine biodiversity hotspots, discussions under this track showcased the latest advancements in ocean exploration technologies and methodologies.

Impressions from HYDRO 2023, 7–9 November, Genoa, Italy.

https://doi.org/10.58440/ihr-30-1-e02

1. Collaboration and Partnerships: Recognizing the importance of collaboration, sessions in this track explored partnerships between governments, industries, academia, and non-profit organizations to address common challenges and achieve shared goals in hydrography and oceanography.
2. Quality: Ensuring data quality and accuracy is fundamental to hydrographic operations. Topics under this track focused on quality assurance, standards compliance, and best practices in data collection, processing, and dissemination.
3. Enabling Technologies: Rapid advancements in technology continue to drive innovation in hydrography. Sessions in this topic area highlighted emerging technologies such as artificial intelligence, autonomous systems, and remote sensing, and their applications in marine surveying and mapping.

Throughout HYDRO 2023, attendees were treated to a myriad of enlightening presentations and networking opportunities, the conference was a beacon of innovation and collaboration.

We extend our heartfelt thanks to all the speakers whose expertise and insights enriched our discussions and contributed to the success of HYDRO 2023. Your dedication to advancing the field of hydrography is truly commendable. Additionally, we express our sincere appreciation to our sponsors for their generous support, which played a pivotal role in making HYDRO 2023 a memorable and impactful event. Your commitment to advancing hydrographic research and education is invaluable.

As we reflect on the highlights of HYDRO 2023, we are reminded of the collective passion and dedication of the hydrographic community to advancing our understanding of the world's oceans and waterways. We hope that the selected contributions showcased in this issue will inspire further dialogue and propel the field of hydrography to new heights.

Finally, we wish the organizers and participants of HYDRO 2024 in Rostock the very best of luck for a successful and fruitful conference. May it be filled with insightful discussions, groundbreaking discoveries, and enduring collaborations.

Aldo Monaca
President of HYDRO 2023 Organizing Committee

https://doi.org/10.58440/ihr-30-1-e02

CONFERENCE PAPER

Exploration of hydrothermal venting sites using deep-towed multibeam echo sounder data

Authors

Tanja Dufek[1], Ralf Freitag[2], Thomas Kuhn[2] and Harald Sternberg[1]

Preamble

The following work was presented at the Hydrographic Conference HYDRO 2023, 7–9 November 2023, Genoa, Italy in the oral session *Ocean Exploration*.

Abstract

The Federal Institute for Geosciences and Natural Resources (BGR) obtained a contract for the exploration of polymetallic sulphides from the International Seabed Authority (ISA) in an area of 10,000 km^2 located in the southwestern Indian Ocean. Since obtaining this contract of exploration in 2015, BGR has conducted annual research cruises to this area and continuously improves the exploration methods for seafloor sulphides deposits. One of the main instruments is HOMESIDE, a deep-towed multibeam echo sounder (MBES) sled. Its water column data allows to visualize and therefore locate discharge sites of hydrothermal fluid – active hydrothermal venting sites (or commonly also referred to as "black smokers"). Additionally, its bathymetric data is used for geological mapping and therefore greater analysis of the seafloor geomorphology. HOMESIDE is typically towed at an altitude of about 100 m above the seabed in a water depth of approximately 3,000 m, allowing a resolution of the derived digital terrain model (DTM) of 2 m. Due to malfunction of individual positioning sensors or operational errors, the navigation data might need to be further corrected in post-processing. Navigation offsets between adjacent lines are mostly apparent in overlapping swath data. The tool *mbnavadjust* of the open-source software *MB-System* showed to be a valuable tool to improve the data quality subsequently in areas with data overlap and systematic navigation offsets. Data mismatches of more than 10 m are processed with this tool and can, therefore, be reduced significantly. In this paper, firstly, the role of deep-towed MBES as exploration tool for hydrothermal sites is presented. Secondly, the importance of post-processing MBES navigation based on the swath data especially for this project is highlighted. The workflow as well as the results are presented and show significant improvement.

Keywords

deep-towed MBES platform · high-resolution bathymetry · navigation adjustment · exploration of polymetallic sulphides

✉ Tanja Dufek · tanja.dufek@hcu-hamburg.de

[1] HafenCity University Hamburg, D-20457 Hamburg, Germany

[2] Federal Institute for Geosciences and Natural Resources, D-30655 Hannover, Germany

https://doi.org/10.58440/ihr-30-1-c01

1 Introduction

Mineral resources are generally limited and new deposits or sources of new origin are of large interest. It is not even 50 years ago that marine discharge sites of hydrothermal fluid have been discovered. Typically, such sites are located on top of sulphide mounds and large metal-rich sulphide deposits can be found underneath. Even today, the general knowledge of them is still limited, as hydrothermal sites usually occur in remote deep-sea areas and are comparably small in size. Typical sulphide mounds have a diameter of 100 m to 200 m and heights of several tens of metres. This correlates roughly with the resolution of a ship-borne multibeam echo sounder (MBES) in such great water depth, and illustrates the challenge of mapping and identifying them.

Over the last years, the number of known hydrothermal sites has increased. The current version 3.4 of the *InterRidge Global Database of Active Submarine Hydrothermal Vent Fields* (Beaulieu and Szafranski, 2020) lists 721 vent locations. These have been identified by anomaly detection in the water column or direct observations. Different estimations of the number of existing sites as well as their density of occurrence can be found in literature. The proposed distances between them can range from about 3–12 km (Baker et al., 2016) to 54 km at fast-spreading ridges and approximately 174 km at slow-spreading ridges (Hannington et al., 2011). Hydrothermal sites occur typically in a cluster/field. The sulphide deposits form within the seabed beneath the discharge site of the hydrothermal fluid. Therefore, the knowledge about their size and composition is typically very limited. Methods of subsurface geophysics, sampling, and drilling need to be applied to gain such information. The composition of deposits can greatly vary within a small distance. It depends on the temperature and chemistry of fluids, their duration over time, and the environment like tectonic setting or host rocks.

As described above, the exploration of hydrothermal sites and the associated deposits is very challenging due to their relatively small size and because the sulphide deposits are lying subsurface. It is estimated, that most sites and deposits are still unknown. The general knowledge about known sites is still limited as well. Over the last decades, the instrumentation for their detection and identification has been improved in accuracy and resolution, allowing for a constant development and advancement of the exploration methods. Within this paper, the current exploration approach utilized by BGR in its polymetallic contract area will be outlined with emphasis on the role of the hydrographic MBES data. Then, the utilized tool for navigation adjustment based on overlapping swath bathymetry of the MBES data in post-processing is described and some data examples are shown to illustrate the improvement in data quality.

2 Formation of hydrothermal sites and current exploration methods

Hydrothermal sites are commonly also referred to as black smokers. But the name is misleading, as they do not discharge air, but hot fluid. They usually occur in tectonic active areas like mid-ocean ridges or back-arc spreading centres (Hannington et al., 2005). Such tectonic activity results in fracture and faults in the seafloor, which allow the seawater to penetrate into the oceanic crust down to a few kilometres. As this water descends, it gets closer to the underlying heat source – magma – and starts heating up. This way seawater is changing into a hot (> 400°C), reducing, and acid fluid and as such it will dissolve metals from ambient rocks, which will be enriched in the hydrothermal fluid. At a certain point, the fluid density has decreased and it starts ascending again, until it is emitted at the seafloor. When the hot reducing fluid gets into contact with cold, oxic seawater, it will suddenly cool down and precipitate the dissolved metals as sulphides. A certain share of the sulphides will form small particles (1–3 μm) which will be discharged into the water column as black smoke plumes (SPC, 2013).

The hydrothermal fluid that is discharged has a lower density than the surrounding seawater and therefore ascends through the water column. As it mixes quickly with the surrounding deep-sea water, it will only rise to between 100 m and 300 m above the seafloor. The plume will then start to move horizontally for up to several kilometres away from the discharge site. Most of the dissolved metal in the fluid is carried away by the currents, but some part precipitates in the vicinity of the site or forms the typical chimney structure (Fig. 1 top left). Such chimneys can reach heights of several tens of metres. By the precipitation and collapsing of the chimney structures, sulphide mounds form as part of the sulphide deposits at the sites. Like mentioned above, such mounds have a typical diameter of 100 m to 200 m. But the majority of the sulphide deposits are found under the seafloor. If allowed by the environmental circumstances, seafloor massive sulphide deposits of several hundred metres of diameter and high concentration of economically interesting ore minerals can develop (Hannington et al., 2011). Typically, they are enriched in base (iron, zinc, copper, lead), special (cobalt, nickel, indium, germanium), or precious metals (gold and silver; Boschen et al., 2013). Over time, an active hydrothermal site becomes inactive and gets extinct as it moves away from the heat source due to tectonic plate motion. Due to the small size and their typical deep-sea environment, hydrothermal sites are challenging to detect and identify. Exploration concepts and methods are constantly improved and high-resolution MBES data plays an important role as exploration tool.

BGR conducts annual cruises into the contract area located along the Central and South-Eastern Indian Ridge. It has a size of 10,000 km^2, which is

https://doi.org/10.58440/ihr-30-1-c01

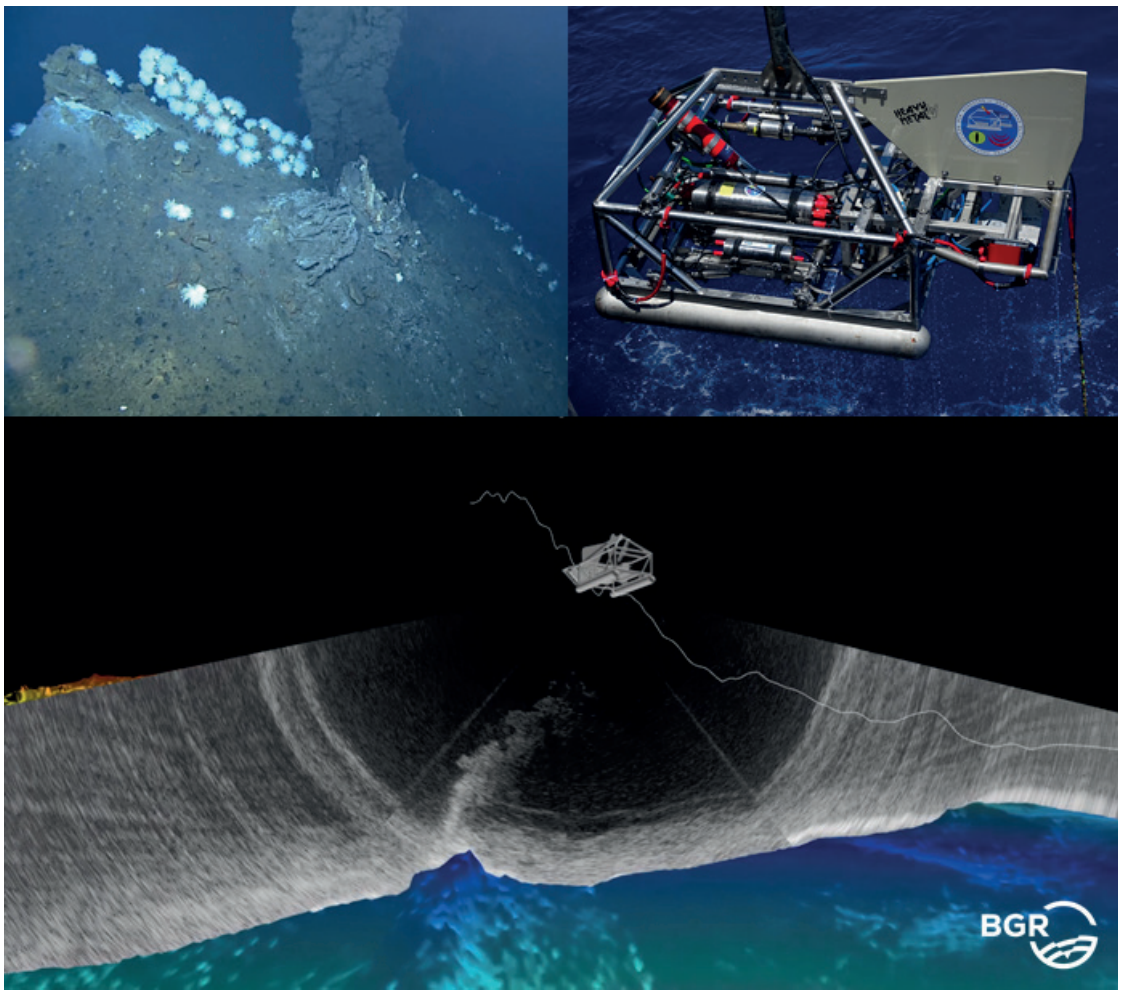

Fig. 1 Top right: A photo of an active hydrothermal venting site showing the associated mound structure as well as the black hydrothermal fluid discharged in a plume; Top right: a picture of the deep-towed HOMESIDE sled; Bottom: A 3D visualization of HOMESIDE and the high-resolution bathymetry combined with a depiction of the water column data showing the plume of an active venting site.

about the size of the island of Cyprus or Hawaii and is organized in 12 clusters consisting of 5 to 17 blocks of 10 × 10 km^2 each. To detect new hydrothermal vent sites, at first, likely areas for hydrothermal activity are identified using ship-borne bathymetry. Then, a "plume-hunting" sled equipped with chemical sensors for temperature, oxidation-reduction potential, and turbidity, is deployed to detect water column anomalies. If such water column anomalies have been detected, the BGR-developed deep-towed MBES sled HOMESIDE (Fig. 1 top right) is deployed in the area of potential origin of the anomaly. It is towed about 100 m to 120 m above the seafloor in 3,000 m water depth, allowing to obtain terrain models of a resolution of 2 m. This is sufficient to map the sulphide mounds in adequate detail. But more importantly, in regard of localization of the discharge site, the hydrothermal plume can directly be visualized within the MBES water column data. In Fig. 1 bottom, a 3D visualization of the bathymetry, HOMESIDE and real swath water column data collected over a venting site are shown. The HOMESIDE data is streamed in real-time during acquisition to the lab via the towing cable. Therefore, the acquisition parameters can directly be adjusted accordingly. Unlike active venting, inactive sites do not discharge hydrothermal fluid and therefore no water column anomaly can be used for their detection. Therefore, since 2019, a string for the detection of self-potential anomalies has been added to HOMESIDE. A self-potential anomaly is an electric field that forms in the seawater over a metal-bearing area in or on top of the seabed. To detect it, the voltage between different electrodes is measured in an array attached at the lower end of the string. Such anomalies can indicate sulphide deposits whether a site is active or not. To allow the probe to be as close as possible to the seafloor, the length of the string is about 90 m. After a new hydrothermal site has been located, camera carrying devices like ROVs or video sleds are deployed to gather visual information. It is also sampled to proof the occurrence of sulphides at the new site.

A high position accuracy of HOMESIDE data is crucial to correctly locate the hydrothermal sites, but also to reduce mismatches between overlapping bathymetric data. Due to sensor malfunction or operational errors, the navigation solution might not fulfil the high accuracy requirements. As a result, position mismatches of ROV deployments and bathymetric maps might occur. Furthermore, the mismatches in

https://doi.org/10.58440/ihr-30-1-c01

the overlap might reduce the visibility of small bathymetric features. This then decreases the ability to correctly identify potential interesting structures in DTMs, like inactive sites. Therefore, the bathymetric data needs to be further post-processed in case the navigation data exceeds an accuracy of about 10 m. In the following chapter the instrumentation and the data-based navigation correction are described.

3 HOMESIDE: Instrumentation and navigation correction in post-processing

The deep-towed sled HOMESIDE is equipped with a Kongsberg EM 2040 multibeam echo sounder. It is generally operated with 300 kHz (frequency modulated signal) and 400 soundings per ping when towed at an altitude of 100 m to 120 m. It is a dual-receiver MBES achieving typically a swath width of about 500 m. For navigation, the INS (*Exail Phins 6000*) is aided by an USBL (ultra-short baseline) underwater positioning system, a DVL (Doppler velocity log) *Teledyne RDI Workhorse Navigator 600*, and a CTD *Valeport Midas SVX*. Additional chemical sensors, like for turbidity and oxidation-reduction potential are also integrated on HOMESIDE for plume detection of active vent sites.

The utilized USBL system varies with the research vessel employed, therefore, over the years, multiple USBL systems have been used. BGR also deploys a mobile *Sonardyne Ranger 2* USBL system and has used it additionally to - or instead - of the ship-owned system. The accuracy of the final HOMESIDE navigation depends largely on the accuracy of the USBL, which again depends mainly on the geometry (distance of transceiver and transponder) and utilized sound speed profile (SSP), assuming the calibration is valid. The accuracy of the HOMESIDE's INS is given by the manufacturers as three times better than the USBL accuracy (Exail, 2018), which is about 0.2 % of the slant range for the *Sonardyne Ranger 2* (Sonardyne, 2014). The distance between the vessel and HOMESIDE varies during one tow. It is typically shorter - and about the water depth - in the beginning of a deployment, and increases during the deployment as the ship speed is usually higher than the one of HOMESIDE. To maintain the altitude, the cable length has to be increased. If the distance gets too large, the communication of the USBL transceiver and the transponder can start failing occasionally. In such cases, the ship speed is reduced to improve the reception. With a typical slant range of 5,000 m, the expected positioning accuracy of the USBL is about 10 m and of the INS hence about 3 m (assuming no large systematic offsets due to drop outs of important aiding sensors for example). The real-time INS data is firstly post-processed by using the software *Exail Delph INS*. It allows a re-computation of the navigation by excluding certain aiding sensors (also just temporarily) or including additional ones, if they have been recorded separately. Further, smoothing filters can be applied. This way, the navigation can be much improved. But it does not include any corrections for incorrect SSP (e.g., in case an older one is applied). Due to time constraints, an SSP cannot be taken before each HOMESIDE tow, sometimes not even before the first station when starting the instrument deployment in a new cluster. Therefore, a slight decrease in accuracy can be assumed for stations where the SSP is older. The resulting effects are noticeable in the bathymetric data of HOMESIDE: Typically, mismatches between two adjacent data sets of up to 10 m can be expected. This is considered as no large systematic offset. If there are offsets of up to 50 m or so (e.g., due to completely wrong SSP or false calibration values), typically a dependency of the tow direction can be noticed. Such large offsets need to be adjusted, but minor mismatches reduce the quality of the final DTM and the ability to identify small bathymetric features as well.

To reduce mismatches between overlapping HOMESIDE data sets in post-processing, the open source software *MB-System* is used. It is a software

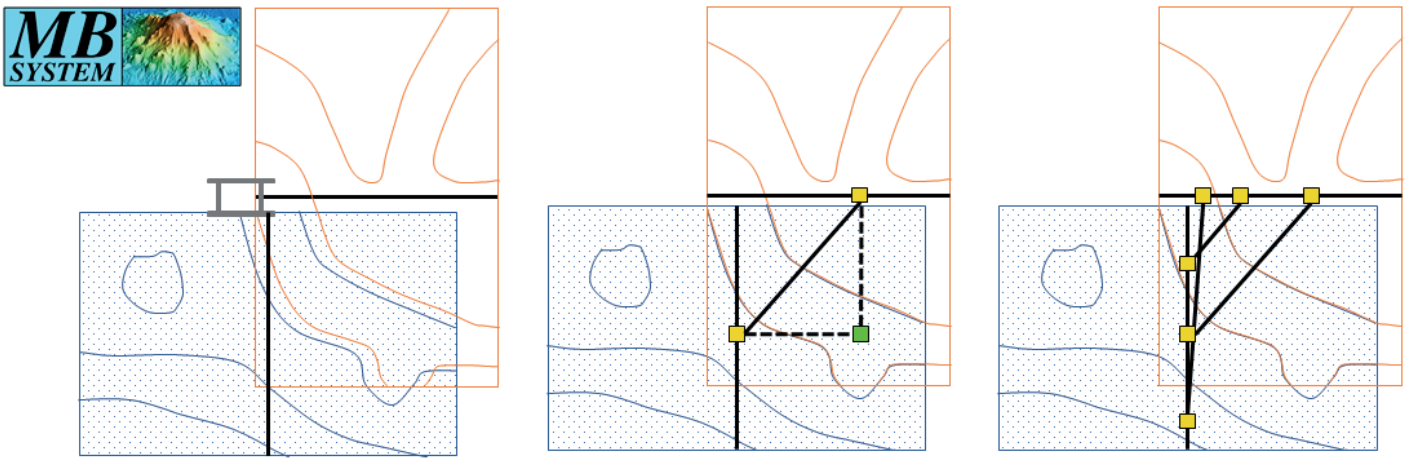

Fig. 2 Schematic depiction of the working principle for the navigation adjustment in *MB-System*'s tool *mbnavadjust*. Left: Two data files overlap but the bathymetry represented as contour lines does not coincide. Middle: The offset is determined in one location (green square) and stored as tie point in correspondence to the navigation control points (yellow squares). Right: Typically, multiple ties points for one overlap at different locations are set.

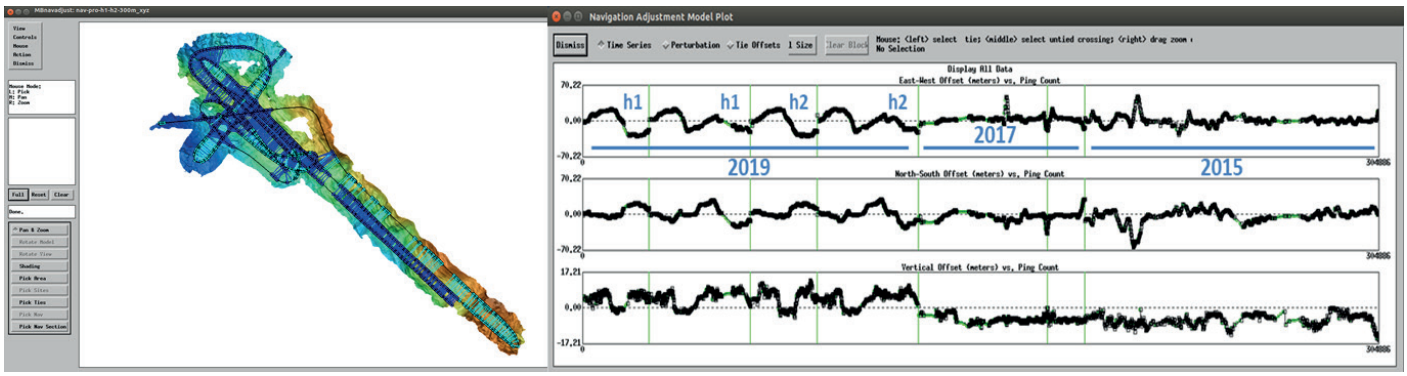

Fig. 3 Overview of MBES data with navigation control points (circles) and tie points (lines connecting corresponding navigation control points). Cyan coloured circles and lines represent ties within a survey (one block of data without time gap) and dark circles and lines indicate ties between two different surveys. Right: *MB-System mbnavadjust* model plot after inversion showing the offsets in longitude (top), latitude (middle), and depth (bottom) in a time series.

to process and visualize MBES and side scan data and was developed by the Lamount-Doherty Earth Observatory of Columbia University and is now maintained by the Monterey Bay Aquarium Research Institute (MBARI), University of New Hampshire, and MARUM. *MB-System* is LINUX-based and consists of numerous tools that can be executed within a terminal window. The main component used for the navigation adjustment is *mbnavadjust*. This tool allows relative navigation adjustment of data files based on features present in overlapping areas. In Fig. 2, the principle of the navigation adjustment in *mbnavadjust* is schematically depicted: Two overlapping files (represented in red and blue) show mismatches when comparing their bathymetry – represented via contour lines (left). For a certain location in the overlap (bright green square), the relative offset between the data sets is determined. The offset is stored as tie point in conjunction with the two corresponding navigation control points (yellow squares, centre). For each overlap, multiple tie points are set for different locations of an overlap, if possible (right). The tool offers an automatic determination of the offsets (in *xyz* or *xy* only), but also the operator can manually shift the data sets until they match visually and choose the shifting values as offsets to be stored. The tie points are set manually. When processing HOMESIDE data, typically, all data overlaps larger than 10 % are inspected and tie points are set.

After all tie points are set, a least square adjustment is performed, which tries to find the optimum fit of all data sets to each other by minimizing the offsets. The user has the possibility, to assign different weights to individual surveys: fixed (no adjustment), good (takes part in the adjustment), or poor (will be fitted after adjustment). The set tie points and the applied shifts can be inspected and changed if necessary. In Fig. 3, an example of a smaller data set is depicted. This data set has the advantage that, in the northern part, multiple data sets of different years were run over another, resulting in large data overlaps. On the left-hand side in Fig. 3, the DTM and the tie points are shown as connections between the navigation control points are shown (in cyan for ties within a survey and in blue for ties between different surveys). The right-hand side shows a model plot with the offsets after adjustment and which will be applied for longitude, latitude, and depth (top to bottom).

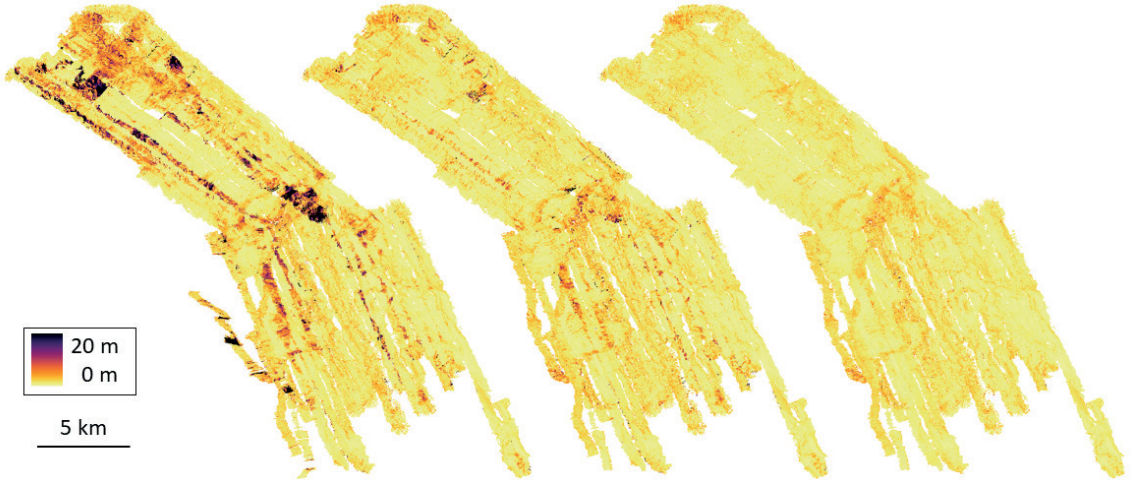

Fig. 4 Uncertainty of HOMESIDE MBES data compilation (2 m resolution, at 95 % confidence level) to visualise the mismatches in the data before (left) and after (middle) navigation adjustment in *MB-System*. The depiction on the right shows the final result after additional data editing.

https://doi.org/10.58440/ihr-30-1-c01

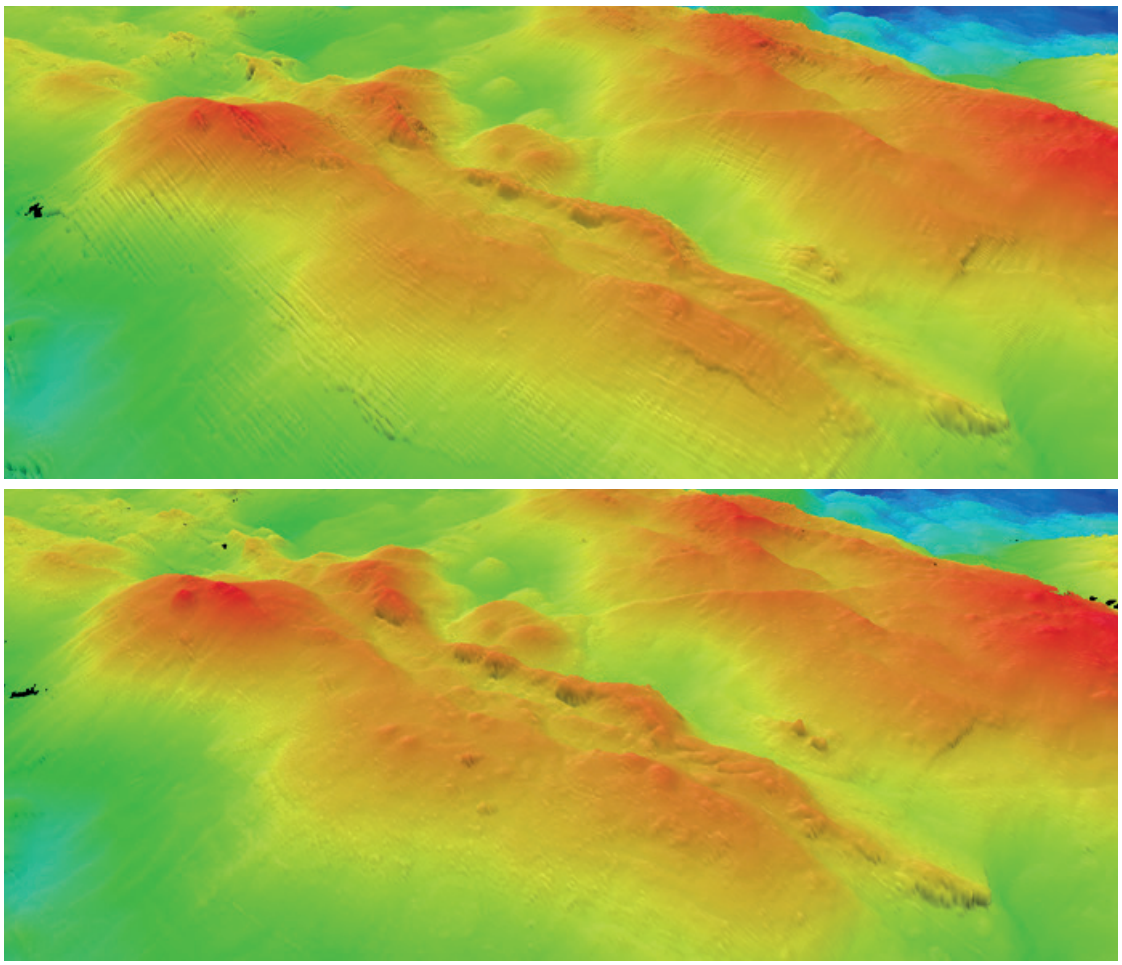

Fig. 5 3D view of HOMESIDE data (2m DTM) before (top) and after (bottom) navigation adjustment in *MB-System.*

In the model plot, the different years of data acquisition are highlighted: 2015, 2017, and 2019. In 2019, the dual-receiver configuration of the MBES on HOMESIDE was used the first time. Both sensor heads were imported separately into *MB-System*, indicated by "h1" and "h2" in the model plot. Examining the offsets closer, large systematic offsets in the 2019 data of up to 50 m can be noticed (especially in longitudinal direction). Each of the four data sets of 2019, consists of two profiles run in opposite direction and the dependency on towing direction as well as cable length can be recognized: firstly, the offsets are small in the beginning, turns, and end of the station where the cable length is short. And secondly, the offsets have different signs (+/-) depending on the towing direction. These large offsets in this example occurred because an SSP of another area was applied in the USBL.

After navigation adjustment in *MB-System*, the new navigation is then applied to the original bathymetric data in the MBES bathymetry processing software *QPS Qimera* and finally edited. Within the editing process, wrong depth measurements are removed and small remaining mismatches in overlapping data reduced by excluding certain soundings from the DTM computation.

4 Results and discussion

The best way to visualize the improvement of data quality, is the depiction of DTMs created from various data stages coloured by uncertainty (95 % confidence interval). The colours indicate therefore how good the soundings within one DTM cell (2 m) fit together. In Fig. 4, a large compilation of different HOMESIDE data sets collected between 2015 and 2022 is shown in different processing stages. The depictions are coloured by uncertainty: darker areas represent DTM cells where the sounding depths deviate stronger from each other than in the brighter cells. The data compilation consists of over 3,200 data files and 24,200 tie points were set manually. The improvement of how the measurements fit together is clearly visible from the left side (before *MB-System*) to the centre (after *MB-System*) and to the right (after final data editing).

A section of the same data is shown in Fig. 5 in a 3D representation. The depiction on the top shows the data before and at the bottom after the navigation adjustment in *MB-System*. The artefacts caused by the navigation offsets can be clearly be noticed in the top picture. Small mounds and other details in the bathymetry can be more clearly recognized in the bottom picture.

Currently, the majority of the high-resolution data collected in the contract area has been

post-processed in *MB-System* to improve the navigation. This approach is especially suited when there is a large amount of data sets with big overlaps. The additional navigation correction is particularly important when it includes data with large systematic positioning errors. The adjustment using *MB-System* showed to improve the overall data quality greatly. Within the current stage of the project, every year data sets are added to already existing larger data compilations. The possibility of weighting the different data sets or even keep certain files fixed, is an important and useful feature of the tool, as complete re-adjustments of the overall data should be avoided, but the newly collected data should be fitted to the existing data.

The disadvantage of using *MB-System* is the amount of manual work. It is very time consuming to set every tie point manually. For an intermediate sized data set, it takes about two weeks to set all tie points. The time can be reduced when decreasing the amount of tie points, but this influences also the quality of the adjustment. Furthermore, *MB-System* has the disadvantage that both MBES heads can only be imported separately. After the least squares adjustment, the two individual navigation solutions for each head are again averaged to one final navigation solution, which impairs the original results from the adjustment. Additionally, possible alternative tools to shift new data sets based on mismatches in the overlap to older data in a more time efficient way are tested.

5 Conclusion

Hydrothermal sites and the associated sulphide deposits are of interest as possible mineral recourses in the future. Research methods to explore and understand them are continuously improving. Hydrography plays an important role herein, as based on the MBES water column data discharge sites of hydrothermal fluid can be located. Furthermore, the bathymetric data allows the visualization of the investigation area, which in turn is the basis for further investigations and analysis. The data collected within this project is unique, as it is rare that such a large amount of data is collected over so many years in such a remote area and with such high requirements for accuracy and resolution. Whereas high accuracy positioning on the water surface is available, high accuracy under water positioning is still challenging and not easily achievable. The availability of MBES post-processing tools that provide possibilities for data-based navigation adjustment, is crucial for fulfilling the high data requirements for an underwater platform like in this project.

References

Baker, E. T., Resing, J. A., Haymon, R. M., Tunnicliffe, V., Lavelle, J. W., Martinez, F., Ferrini, V., Walker, S. L. and Nakamura, K. (2016). How many vent fields? New estimates on vent field populations on ocean ridges from precise mapping of hydrothermal discharge locations. *Earth and Planetary Science Letters, 449*, pp. 186–196. https://doi.org/10.1016/j.epsl.2016.05.031

Beaulieu, S. E. and Szafranski, K. (2020). *InterRidge Global Database of Active Submarine Hydrothermal Vent Fields Version 3.4*. PANGAEA – Data Publisher for Earth & Environmental science. https://doi.org/10.1594/PANGAEA.917894

Boschen, R. E., Rowden, A. A., Clark, M. R. and Gardner, J. (2013). Mining the deep-sea seafloor massive sulphides: A review of the deposits, their benthic communities, impacts from mining, regulatory frameworks and management strategies. *Ocean & Coastal Management*, *84*, pp. 54–67. https://doi.org/10.1016/j.ocecoaman.2013.07.005

Exail (2018): *PHINS 6000 Datasheet*. https://rts.as/wp-content/uploads/2018/09/iXBlue-PHINS-6000-Subsea.pdf (accessed 1 October 2023).

Hannington, M. D., de Ronde, C. E. J. and Petersen, S. (2005). Sea-floor tectonics and submarine hydrothermal systems. In J. W. Hefenquist, J. F. H. Thompson, R. J. Goldfarb and J. P. Richards (Eds.), *Economic Geology*. Society of Economic Geologists, Littleton, Colorado. https://doi.org/10.5371/AV100.06

Hannington, M., Jamieson, J., Monecke, T., Petersen, S. and Beaulieu, S. (2011). The abundance of seafloor massive sulphide deposits. *Geology*, *39*(12), pp. 1155–1158. https://doi.org/10.1130/G32468.1

Sonardyne (2014). *Datasheet Sonardyne Ranger 2 USBL*. https://www.uniquegroup.com/wp-content/uploads/2022/10/Sonardyne-Ranger-2-USBL.pdf (accessed 1 October 2023.

SPC – Secretariat of the Pacific Community (2013). *Deep sea minerals: Sea-floor massive sulphides, a physical, biological, environmental, and technical review* (E. Backer and Y. Beaudoin, Eds.), Vol 1A.

https://doi.org/10.58440/ihr-30-1-c01

CONFERENCE PAPER

Closing the data gap – Automated seafloor health maps to accelerate nature-based solutions

Authors

Hannah Brocke[1], Tadzio Holtrop[1], Raja Kandukuri[1], Guy Rigot[1], Anna-Lea Lesage[1], Nils Oehlmann[1] and Joost den Haan[1]

Preamble

The following work was presented at the Hydrographic Conference HYDRO 2023, 7–9 November 2023, Genoa, Italy in the oral session *Blue Transition*.

Abstract

This article delves into the pivotal role of the oceans, specifically the seafloor, in addressing climate change and food security. Despite its significance, a lack of detailed data on the seafloor hampers informed decision-making by policymakers, impedes sustainable blue economy investments, and hinders the development of blue carbon and biodiversity credit markets. PlanBlue, an innovative technology company, has devised a groundbreaking solution using advanced imaging, underwater navigation, and machine learning to automate seafloor mapping. This article explores the importance of seafloor data, the barriers to access data, and how PlanBlue's technology can improve our understanding of the ocean's potential. The discussion encompasses the significant role of the seafloor as a carbon sink, the necessity for credible data in ocean conservation, and the crucial link between seafloor mapping and effective marine spatial planning. PlanBlue's innovative approach not only adds speed and scale to data collection but also provides multi-layered insights into species health, biomass, and more, contributing to the credibility of marine conservation efforts. The article concludes with a scientific review highlighting the accuracy and meaningfulness of PlanBlue's methodology, validating its transformative impact on the blue carbon industry and seafloor habitat monitoring.

Keywords

ocean data · blue carbon · biodiversity · ocean health · habitat mapping · marine ecosystems

✉ Hannah Brocke · h.brocke@planblue.com

[1] PlanBlue GmbH D-28359 Bremen, Germany

https://doi.org/10.58440/ihr-30-1-c03

1 Introduction

Climate change and food security are among the most pressing challenges for life on earth today. The oceans, specifically the seafloor, play a key role in tackling exactly those two challenges. Yet, we are facing a major problem: there is a severe lack of detailed data on the seafloor to maximize its potential. Policymakers require data to make informed decisions on ocean policies (e.g. pollution regulation), attract new investments in the sustainable blue economy (e.g. offshore wind), and scale nature-based solutions through the upcoming blue carbon and biodiversity credit markets (e.g. seagrass meadows and kelp forests).

There are technologies that can map the seafloor at scale, including satellite imagery and airborne mapping. To add credibility to what is observed from a distance, these methods are dependent on so-called 'ground-truth' data. Observations close to the seafloor verify the done remote measurements and add information about the health state of habitats. Not having credible, objective, high-detail ground-truth data reduces the opportunity our seafloor provides in tackling climate change and food security. As this has been a manual and time intensive process, the availability of ground-truthing data is limited.

PlanBlue has developed a solution to bridge this knowledge gap (Fig. 1). They combine advanced imaging, underwater navigation, and machine learning into a full automated data processing methodology. The result is geo-referenced seafloor maps, which provide, for the first time, highly detailed insights on health, biomass, carbon sequestration potential, biodiversity, pollution, and human-made materials. The technology is fast and scalable, significantly improving time-to-data from weeks or months to just hours.

This article goes further into the role of the ocean for climate change and food security, the pivotal role of data, the barriers to access this data, and how PlanBlue's solution can help close the (data) gap. We discuss the challenges they overcame to ensure the results are accurate. Lastly, we will look ahead where the future of these advanced data products can bring us, from adding credibility to the blue carbon market, to delivering data to support aquacultural regulations, and enabling more ecosystem friendly development of offshore infrastructure.

2 The seafloor, an undervalued and underfinanced carbon sink

Seventy percent of Earth's surface is covered by the oceans. They regulate climate, are major sinks for carbon dioxide, provide food, and support biodiversity. The seafloor, as far as we know, is the best carbon sequester, as it can fix CO_2 up to 30x faster than for example trees on land. Notably, seagrass exhibits remarkable carbon dioxide capture efficiency. Despite their pivotal role in mitigating climate change, seagrass meadows face inadequate recognition and protection due to limited data on their health state. For most people seagrass meadows are out of sight, out of mind. They are underrepresented in policy making and finance decisions around climate mitigation. Of all United Nations Sustainable Development Goals, Goal 14 "Life Below Water" has received the least amount of public money (UN, 2022). To tap into the large carbon sequestration potential of the ocean, we need funds for seafloor restoration and preservation projects. Access to credible data is essential to accelerate the blue carbon market, including blue carbon credits and National Determined Contributions (NDCs) to meet the Paris Agreement. Monetizing the seafloor can foster the flow of funding into ocean conservation.

3 Feeding the world, safeguarding access to protein and livelihoods

The oceans feed more than 3 billion people and provide a livelihood for 10–12 % of the world's population. The global population is still growing and access to protein is high on the agenda of world leaders. Protection of wild fish stocks and their habitats is one piece of the puzzle, aquaculture is by many seen as another. However, aquaculture can have huge destructive consequences for ocean life, for example through nutrient pollution (eutrophication) coming from the farms, affecting the seafloor. There is an urgent need for better legal regulations. Poorer coastal communities remain dependent on nature-based food sources, and poorly regulated aquaculture production jeopardizes their food security.

4 In the dark, knowledge that lies on the bottom of the ocean

To stress how little we know about the ocean, often the comparison is made that we know more about the surface of Mars or the Moon than we know about the ocean floor. For this article, we like to give this statement a little more context and depth.

Seabed 2030, an initiative launched with the sole purpose to map 100 % of the seabed by 2030 was founded in 2017 with the awareness that, at the time, only 6 % had been mapped to an adequate resolution. They defined this as the absence of detailed underwater topography, or bathymetric data. In their most recent roadmap, they state that mapping coverage has increased to nearly 20 %, which they now define more specifically as 'at a resolution of 1km using the echo sounding method' as a minimum. So more than 80 % of the world ocean floor is still not mapped to this coarse level.

Jon Copley, Associate Professor of Marine Ecology, University of Southampton, digs a bit deeper into the different levels of detail of seafloor mapping in his 2014 article in The Conversation (Copley, 2014). He wrote this article following the release of the new global map of the seafloor (Witze, 2014) published by David Sandwell of Scripps Institute of Oceanography in San Diego and colleagues. With this map, the entire ocean floor has now been mapped to a maximum resolution of around 5 km, which means we can see most features larger than 5km across in those maps.

https://doi.org/10.58440/ihr-30-1-c03

However, as Copley states, that global map of the ocean floor is admittedly less detailed than maps of Mars, the Moon, or Venus. This is caused by our planet's watery veil, as he states it. Or in other words, the water is in the way. NASA, for example, mapped 98 % of the surface of Venus to a resolution of around 100 meters. To map the ocean floor in that level of detail, we can't use satellites. Modern sonar systems aboard ships, however, can map the ocean floor to a resolution of around 100 meters across a narrow strip below the ship. At the time of the writing of that article, in 2014, about 10–15 % of the oceans were covered to that level of detail.

He goes on that if we want to detect things just a few meters in size on the ocean floor, such as the wreckage of missing aircraft, the mineral spires of undersea volcanic vents, or the state of the marine habitat, we need to take our sonar systems much closer

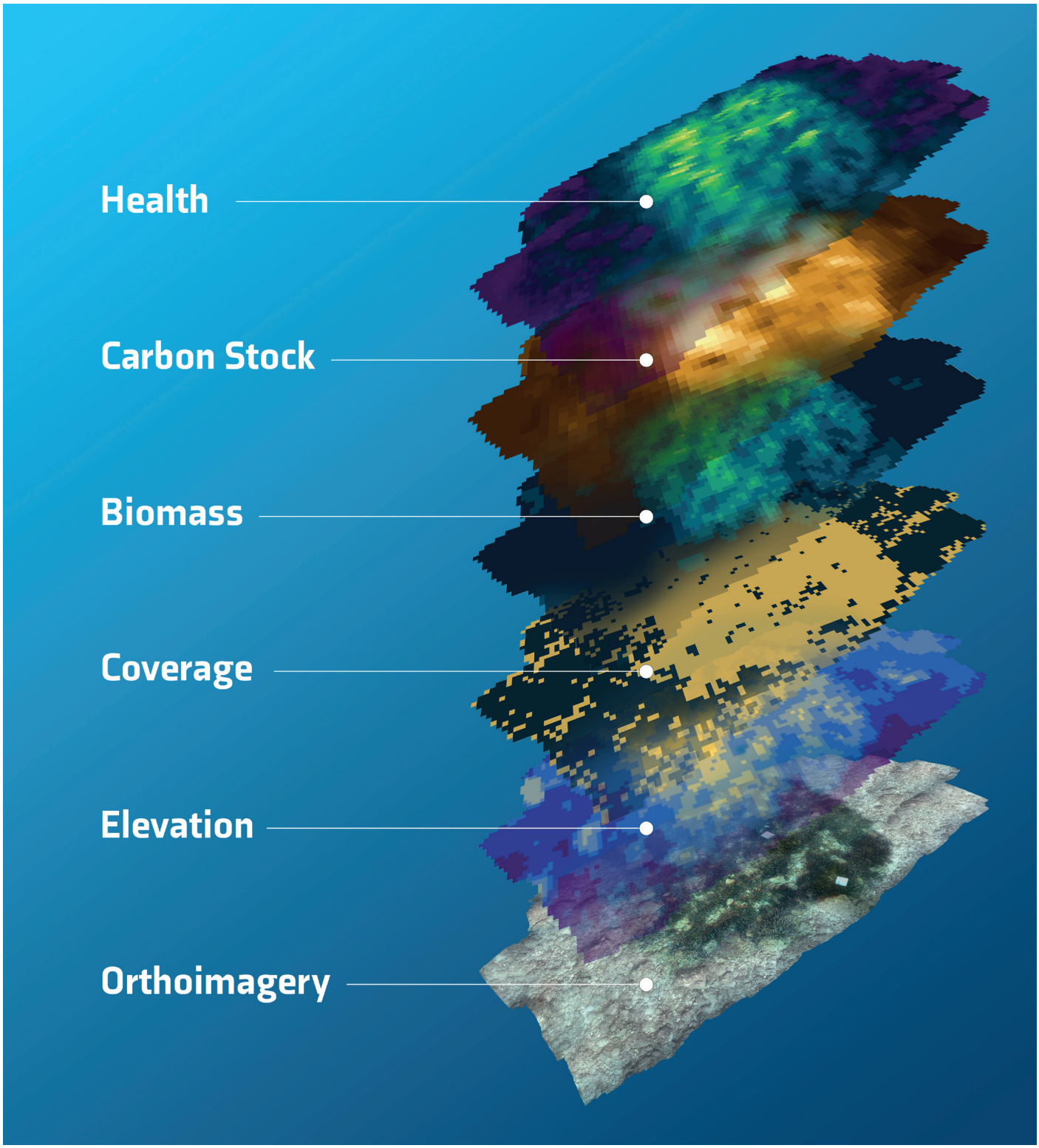

Fig. 1 Overview of PlanBlue's data products.

https://doi.org/10.58440/ihr-30-1-c03

to the seabed. Working with data from closer to the seabed, is exactly what the PlanBlue team sets out to do. To understand the carbon sequestration capacity or the state of biodiversity in the marine ecosystems, we require information at marine habitat level, not just the rough topography of the seafloor. At the time of writing of Copley's article in 2014, less than 0.05 % of the ocean floor had been mapped to that highest level of detail, which is an area roughly equivalent in size to Tasmania.

5 Mapping the seafloor, measuring habitat features, such as health and carbon

With the explicit goal to emphasize the ecologic and economic value of the seafloor, PlanBlue is processing seafloor data from around the globe, using a novel seafloor mapping solution. Founded in 2017 by two former marine scientists and two engineers to enable high-quality seafloor mapping, PlanBlue replaced traditional seafloor mapping methods with highly automated and scalable processing pipelines. Their goal is to add in-depth information to bathymetric maps, including health state of the seafloor, carbon sequestration potential, biomass, pollution, and biodiversity. The technology is capable surveying anything on the seabed and map a diversity of carbon sequestering ecosystems including corals and seaweeds. PlanBlue doesn't just aspire to add detail to seafloor mapping, but also to do so at scale.

6 Time is running out, adding speed and scale

As the International Panel on Climate Change (IPCC) and the Biodiversity Treaty of Kunming Montreal make clear, we are running out of time to turn the tide on climate change and protect biodiversity. For this reason, an important part of PlanBlue's mission is to add speed and scale. Their solution replaces manual processes with automated pipelines, based on state-of-the-art computing and AI.

PlanBlue's core business is to sell data products. Traditional methods of ground-truthing aerial and satellite data require a time intensive process of in-situ collection of data. This means divers going down with a clipboard, doing line transects, underwater counting, and photo and video assessments. PlanBlue's technology largely replaces this with near in-situ remote sensing, using hyperspectral cameras and a selection of sensors to correct distortions of the images in the water column. By controlling the entire data chain, they can ensure a seamless and speedy process, even in areas with limited internet access during field campaigns. With the streamlined processes PlanBlue can reduce time-to-data from weeks or sometimes months, to a timeline of days or even hours.

7 A new dimension, adding layers of insights to seafloor mapping

With the ambition to create a comprehensive representation of underwater areas and their changes over time, the first step for PlanBlue is the creation of orthoimagery of the seafloor. Through their automated pipelines PlanBlue's technology can stitch thousands of images together in less than 24 hours after the collected seafloor data has been uploaded to the cloud. For accurate mapping and meaningful data processing, underwater navigation and geo-location are essential. PlanBlue developed their in-house navigation system that ensures precise positioning of the imagery on the seabed, which is essential for the data processing models, to develop geo-referenced maps, and provide year-on-year comparisons.

As PlanBlue is working with hyperspectral data, another challenge comes in. The hyperspectral camera is a push-broom scanner. Because of this, movement of the camera through the water introduces distortions in the captured images. Using data from the navigation and other sensors, PlanBlue adjusts for that motion as part of the data processing. By doing this, PlanBlue can create an overlay of hyperspectral data on top of an RGB image, generating unique maps of the seafloor.

8 Clearing things up, adjusting for turbid water

This is not the only correction of distortion of the observations that PlanBlue's technology accounts for. PlanBlue's near in-situ data collection vehicles are typically operated about two meters above the seafloor. To accurately assess the property of the vegetation or sediment, the observations need to be compensated for the water column between the vehicle and the seabed.

While the space community has worked for decades on compensation for the light traveling through the atmosphere, this kind of work is still in early stages underwater. PlanBlue integrated sensors that gather data required to adjust for different conditions like depth, weather, turbidity, and other environmental circumstances.

For data to be meaningful, it should be comparable over time and across locations. The comparability of the insights was demonstrated by two surveys in the Mediterranean Sea with similar ecosystems, observing the same species of seagrass, *Posidonia oceanica* (Fig. 2). With environmental circumstances ranging from bright and sunny, to cloudy and rainy and observations at a depth of 5–6 meters in one location to 25–30 meters of depth in another, they were perfect circumstances to confirm the coherence of the findings. With these objective measurements that are agnostic to the conditions encountered in the field or caused by the device, PlanBlue can provide invaluable insights that are essential for effective marine spatial planning, and monetization of the seafloor.

https://doi.org/10.58440/ihr-30-1-c03

9 A multi-layered picture, turning raw data into calibrated and validated insights

To make the outcomes of the analysis visual, the data processing pipelines generate maps and overlays. Based on photogrammetry, PlanBlue provides an accurate elevation model of the scanned area, with a resolution of 1 cm × 1 cm and a vertical accuracy in the sub-cm range. These maps can be used to validate existing bathymetry data of lower resolution and serve as the foundation for example for calculating the canopy height of a seagrass meadow. This can then be used to estimate seagrass biomass. The next overlay distinguishes living and attached seagrass meadows in the orthoimagery, generating a data set that provides the coverage of seagrass as a percent value. PlanBlue is also working on incorporating additional benthic organisms and (human-made) structures into this overlay. Consequent layers can provide a reliable estimation of above-ground seagrass biomass, in kg/m^2 and the quantification of carbon content (estimated in kg/m^2) within seagrass meadows, operating at a spatial resolution of 10 cm × 10 cm.

Ultimately, they add a seafloor health overlay. The hyperspectral camera can look beyond the mere structure of the seafloor. Through a range of (pre-determined) indices, the data can provide a unique insight into the health and productivity of seafloor habitats, like seagrass meadows. This includes for example chlorophyll data, which helps to determine species' health. The comparability of the data over time, makes it possible to visualize seasonal changes in marine ecosystems, which are instrumental to better understand the behavior of these valuable habitats, and measure the impact of policy interventions.

10 Adding credibility to marine conservation efforts

The insights about the health, biomass, and density of seagrass, and other key vegetation of the seafloor, can revolutionize marine conservation, preservation, and restoration. Knowing not just whether seagrass, kelp, or coral is present or not, but also the state it is in, can ensure policy makers' focus on the areas where most impact can be made.

For example, unhealthy seagrass meadows can become net emitters of CO_2 and other climate gases, while healthy seagrass sequesters carbon up to 30 times faster than a rainforest. Thorough assessment of seagrass meadows (Fig. 3) can take Blue Carbon projects to the next level and provide the credibility that is needed to attract investors and accelerate the market.

Projects aiming to increase biodiversity require robust baseline information and methods to assess impact for them to be of interest to investors and to be prioritized by governments. New initiatives that intend to enhance biodiversity in offshore energy projects can attract interest of investors with sustainability mandates, and for example issue blue bonds.

Monetizing the seafloor is a viable approach to ensure enough financial means come in to protect and restore these vital ecosystems. However, reliable monitoring and evaluation methodologies are required to get access to these financial advantages.

Another example of use can be found in advancing the developments of aquaculture in a responsible

Fig. 2 PlanBlue collecting seagrass data during a campaign in Nice, France.

https://doi.org/10.58440/ihr-30-1-c03

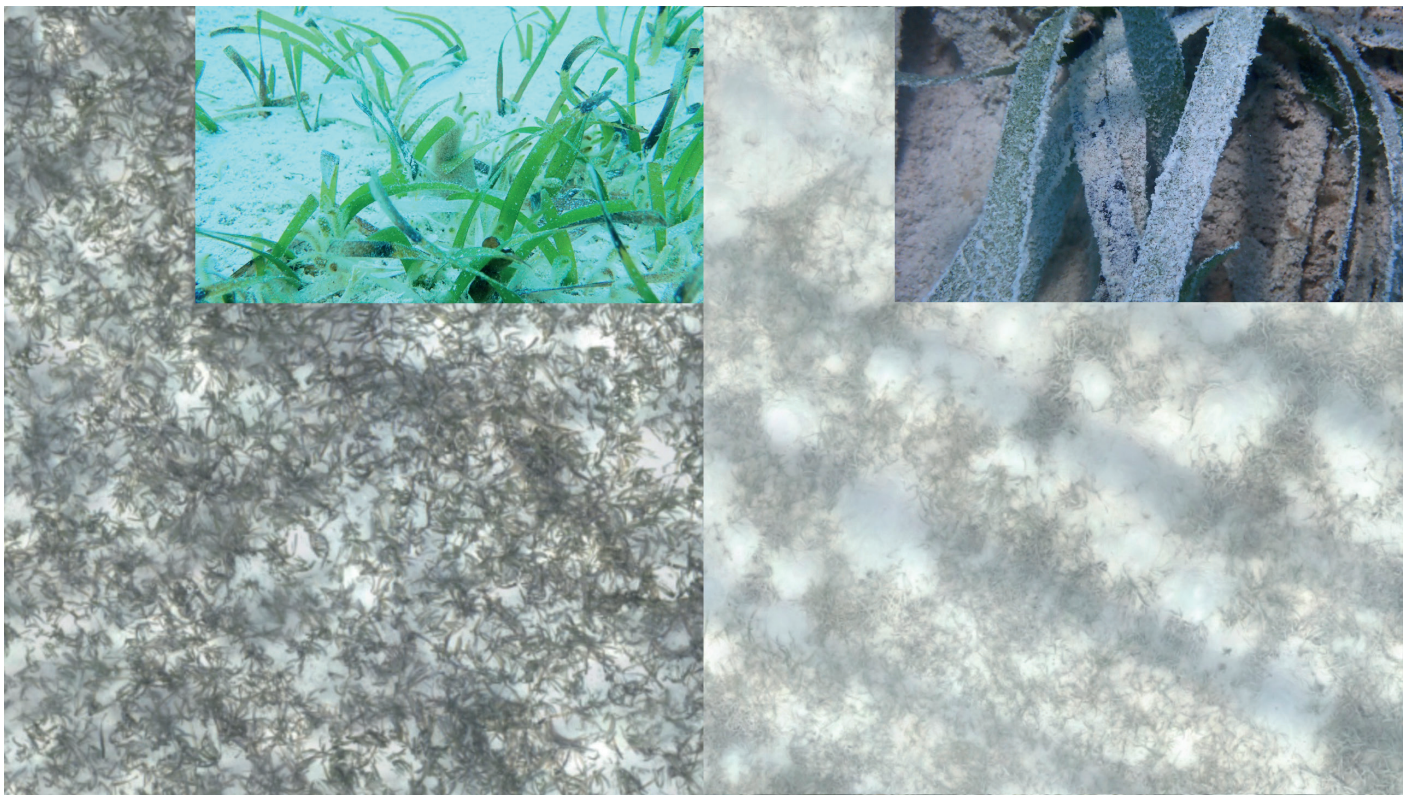

Fig. 3 Assessment of seagrass health.

manner. Although by many seen as a key solution, expanding large scale aquaculture has severe risks. To manage this, policy makers are working to improve regulations. Without accurate data this is an impossible task. PlanBlue's habitat maps can provide standardized data to base new regulations on.

11 Scientific review of the results

While one of PlanBlue's unique selling points is to significantly scale up the detailed data on the seafloor in a short period of time, added speed and scale are of little value when the outcomes are not accurate, comparable, and meaningful. Scientific validation of the methodology is at the center of the development of PlanBlue's work. The rigor of the data analysis methodology has been developed and tested in collaboration with internationally renowned research institutes and local experts. Two of these studies have recently been published in peer-reviewed articles.

An article in the journal Restoration Ecology discussed a study of the Université Côte d'Azur in 2020 (Riera et al., 2023), to assess the effectiveness of artificial reefs to simulate natural habitats. The study compared old artificial reefs, with 3D-printed artificial reefs, and natural reefs. PlanBlue's seafloor habitat mapping technology was used and assessed as part of the study.

The study concluded that PlanBlue's technology was able to identify the relative differences in the signals of the ecosystem in different habitats, and reduce human effort and time required for these underwater observations. In the study, one diver could sample 24 transects on five different sites at 30-m depth over 3 days, much faster than traditional methods. There were recommendations on how to further enhance visual cross-identification in low light conditions that have since been implemented in the current version of PlanBlue's technology. Another opportunity that was identified for further development was using spectral fingerprinting to distinguish between photosynthetic and non-photosynthetic organisms. This was an area of focus in the field study with University of Guam, USA, in 2019.

The results of that study were published in Scientific Reports (Mills et al., 2023). The focus of this collaboration with the University of Guam was to assess whether PlanBlue's technology can be used for effective surveying and monitoring of coral reef ecosystems. The team surveyed eight reefs in Guam, USA, and used two approaches for benthic classification. PlanBlue's method was compared with manually conducted surveys to determine the accuracy and utility as a proxy for reef surveys.

The findings show that if a well-annotated library is available, underwater hyperspectral imaging can be used to quickly, repeatedly, and accurately monitor and map dynamic benthic communities on tropical reefs using broad benthic categories.

12 Conclusion

PlanBlue's underwater geo-spatial technology is driving a transformation in the blue carbon industry and seafloor habitat monitoring, speeding up the protection of vital marine ecosystems with almost instant, credible, and accurate data. The seafloor plays a critical role in regulating climate, absorbing

carbon dioxide, and supporting biodiversity. However, it remains an undervalued and underfinanced carbon sink, lacking detailed information to drive meaningful conservation efforts.

PlanBlue has tested and improved their innovative seafloor mapping solution, with local partners and international research institutes. Equipped with hyperspectral and RGB imaging capabilities, the company has successfully created objective ground truth data, that provides insights into seafloor health, biomass, carbon sequestration potential, biodiversity, pollution, and human-made materials. The potential of the methodology has been validated in peer-reviewed academic studies, and ongoing collaborations continue to advance the underlying analysis and technology. With reliable data, investors and policy makers can focus their efforts where they can make the most significant impact, both economically and ecologically.

References

Copley, J. (2014). *Just how little do we know about the ocean floor?* The Conversation. http://theconversation.com/just-how-little-do-we-know-about-the-ocean-floor-32751 (accessed 20 February 2024).

Mills, M. S., Ungermann, M., Rigot, G., den Haan, J., Leon, J. X. and Schils, T. (2023). Assessment of the utility of underwater hyperspectral imaging for surveying and monitoring coral reef ecosystems. *Sci. Rep., 13*, 21103. https://doi.org/10.1038/s41598-023-48263-6

Riera, E., Hubas, C., Ungermann, M., Rigot, G., Pey, A., Francour, P. and Rossi, F. (2023). Artificial reef effectiveness changes among types as revealed by underwater hyperspectral imagery. *Restor. Ecol., 31*, e13978. https://doi.org/10.1111/rec.13978

Witze, A. (2014). Gravity map uncovers sea-floor surprises. *Nature*. https://doi.org/10.1038/nature.2014.16048

UN (2022). *Accelerating Investments in SDG 14 and the Sustainable Blue Economy*. UN Department of Economic and Social Affairs. https://sdgs.un.org/events/accelerating-investments-sdg-14-and-sustainable-blue-economy-48934 (accessed 15 March 2024).

https://doi.org/10.58440/ihr-30-1-c03

CONFERENCE PAPER

Unlock insights from hydrographic data with GeoAI

Author
Matthew Woodlief[1]

Preamble

The following work was presented at the Hydrographic Conference HYDRO 2023, 7–9 November 2023, Genoa, Italy in the oral session *Collaboration and Partnership, Quality, Enabling Technologies and Ocean Literacy.*

Abstract

Hydrographic offices are collecting hundreds of terabytes of data every day. This information not only comes from bathymetry data sensors, but also from weather stations, radar, ships, satellites, aerial and drone imagery, and other sensors. With all this data pouring in, hydrographic offices need to be able to automate time consuming processes and adopt modern technologies. One such technology is GeoAI, the intersection of spatial data and artificial intelligence. GeoAI can be considered an enabling technology, in that it allows you collect the data once and apply different algorithms to the data for it to be for multiple purposes. Data collected from multibeam echo sounders can be analyzed to update ENCs by finding new obstructions such as rocks and shipwrecks. Using that same point cloud, GeoAI can then be used to understand marine animal habitat by identifying underwater structures and seafloor patterns that lead to increased biodiversity. GeoAI can be used to aid in coastal resilience projects by analyzing aerial imagery from drones captured in multiple seasons and years for change detection, highlight the areas that need the most attention. Machine Learning, a part of the GeoAI portfolio, can additionally use that same imagery data set to run predictive analytics, highlighting areas that are susceptible to erosion, flooding, and landslides. Many of the same GeoAI algorithms can be used to help maximize investments in the blue economy by bringing location intelligence to the decision-making process. Models can predict the best locations to establish aquaculture, Marine Protected Areas, and offshore energy production. In addition to its applications in coastal resilience projects and maximizing investments in the blue economy, GeoAI offers a wide array of benefits in the domain of hydrospatial data management. The integration of GeoAI in hydrographic offices revolutionizes the way hydrographic data is processed and utilized. Traditionally, processing and interpreting vast amounts of hydrospatial data, including bathymetry, weather, radar, and imagery, required extensive human resources and time-consuming manual efforts. However, with GeoAI, these offices can automate complex tasks and streamline data analysis, significantly improving efficiency and accuracy.

Keywords
GeoAI · automation · hydrospatial · GIS

✉ Matthew Woodlief · mwoodlief@esri.com

[1] Environmental System Research Institute (ESRI Inc.), St. Charles, Missouri, United States of America

https://doi.org/10.58440/ihr-30-1-c02

1 Introduction

Hydrographic offices are collecting hundreds of terabytes of data every day. This hydrospatial information not only comes from bathymetry data sensors, but also from weather stations, radar, ships, satellites, aerial and drone imagery, and other sensors. With all this data pouring in, hydrographic offices need to be able to automate time consuming processes and adopt new technologies. One such technology is called GeoAI, the intersection of spatial data and artificial intelligence. GeoAI is an enabling technology, in that it allows you collect the data once and apply different algorithms to the data for it to be used for multiple purposes. Data collected from multibeam echo sounders can be analyzed to update Electronic Navigation Charts (ENCs) by finding hazards to navigation, new obstructions such as rocks and shipwrecks. Using that same point cloud, GeoAI can then be used to understand marine animal habitat by identifying underwater structures and seafloor patterns that lead to increased biodiversity. GeoAI can be used to aid in coastal resilience projects by analyzing Satellite-Derived Bathymetry (SDB) data and/or aerial imagery from drones captured in multiple seasons and years for change detection, highlighting the areas that need the most attention. Machine Learning, a part of the GeoAI portfolio, can additionally use that same imagery data set to run predictive analytics, highlighting areas that are susceptible to sedimentation, erosion, flooding, and landslides. Many of the same GeoAI algorithms can be used to help maximize investments in the blue economy by bringing location intelligence to the decision-making process. Models can predict the best locations to establish aquaculture, Marine Protected Areas, and offshore energy production in the hydrospatial domain.

In addition to its applications in coastal resilience projects and maximizing investments in the blue economy, GeoAI offers a wide array of benefits in the domain of hydrospatial data management (Hains et al., 2022). The integration of GeoAI in hydrographic offices revolutionizes the way hydrographic data is processed and utilized. Traditionally, processing and interpreting vast amounts of hydrospatial data, including bathymetry, weather, radar, and imagery, required extensive human resources and time-consuming manual efforts. However, with GeoAI, these offices can automate complex tasks and streamline data analysis, significantly improving efficiency and accuracy.

This paper also aims to answer the question, how? by outlining the systems that need to be in place, the architecture of those systems, and the methodologies required for this analysis. The presentation at HYDRO 2023 used a few of the use cases above as examples to clarify the workflows. It also showed how a modern GIS, a platform that includes desktop, server, and web components, is essential to taking advantage of GeoAI capabilities.

2 What is GeoAI?

GeoAI is the application of Artificial Intelligence (AI) fused with geospatial data, science, and technology to solve geographic based problem sets (ESRI, 2024). AI can be considered an umbrella term for any task performed by a machine that would traditionally require human intelligence, such as perception, reasoning, and learning. To solve spatial problems, we typically turn to two types of AI, Machine Learning (ML) and Deep Learning (DL). Machine learning is a subset of AI that refers to techniques that allow computers to learn patterns withing data and acquire knowledge without being explicitly programmed to do so. As a subset of Machine Learning, Deep learning uses a specific machine learning process called an artificial neural network which is inspired by the layered approach to learning taken by the human brain. The relationship between AI, ML, and DL is best illustrated by the diagram Fig 1a. Spatial analysis tools are integrated with AI Models to help them find patterns, find anomalies, and make predictions. Geographic problems are solved through spatial analysis by using vector data, image and raster data, spatiotemporal statistics, and modeling. A non-exhaustive list of Spatial Analysis techniques is shown in Fig 1b. Put simply, the combining of AI techniques and spatial analysis is GeoAI. GeoAI, therefore, is not a product to be bought and sold, but an integrated method for conducting spatial analysis using the power of computers. As Machine Learning is the method that is best fit for the hydrospatial data collected by hydrographic offices, the focus will be on that process.

3 Machine learning

Machine learning has been tagged as “Revolutionizing”, or “Game Changing”. Removing that hyperbole, Machine learning can be used for five main tasks: Extracting features from imagery and LiDAR, finding patterns and clusters, detecting anomalies, extracting insights from unstructured text, and making predictions. As hydrographic organization are being asked to go beyond chart production and provide additional hydrospatial services such as supplying scientific data, reporting on vessel traffic patterns, and using data to protect and promote the blue economy, leveraging some or all these capabilities becomes essential. For organizations that are beginning their journey of fulfilling these new mandates, the swirling of terms, processes, and technologies can be overwhelming. To get the most return for their efforts and investment, leveraging machine learning and deep learning algorithms integrated with image analysis tools.

4 Image classification

Image analysis is an excellent gateway into the realm of GeoAI for many organizations. Looking at the types and formats of data collected by the hydrographic survey teams and the types and formats of data available to them from other government entities, it is

https://doi.org/10.58440/ihr-30-1-c02

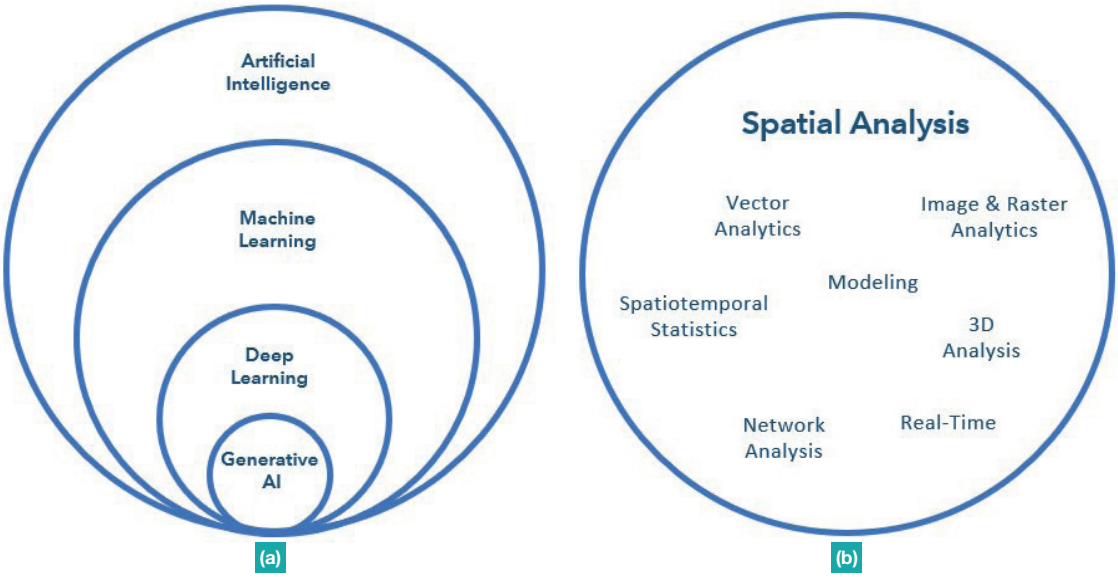

Fig. 1 (a) The relationship between AI, ML, and DL. (b) Spatial Analysis techniques.

easy to see why. From imagery collected by drones, planes and satellites to data collected by various flavors of echosounders and LiDAR scanners, these offices are sitting on virtual mountains of data in raster or point cloud format. These data formats are rich in information just waiting to be extracted. Furthermore, with GeoAI, the notion of imagery can be expanded to include the visual output from echosounders and the raster output of multidimensional raster datasets.

Image analysis takes many forms, but the end goal is to extract information out of an image. The classic image analysis technique is image classification in which analysts quantify the identification of features or objects in Imagery Classification is lumped into two categories, Supervised or Unsupervised, depending on the interaction with the analyst. Supervised classification involves creating training samples to "teach" the ML algorithm what it needs to find in the imagery or how to classify groups of pixels with the same value. This method can be a more time consuming as you need to create the training samples yourself until you have a representative amount for each class you want to detect. The reward is usually a more accurate result as it is comparing known quantities. There are three main supervised classification algorithms to know and they are simplified here. Maximum Likelihood (ML), Artificial Neural Network (ANN), and Support Vector Machines (SVM). Maximum Likelihood works by calculating a probability score based on the value of the pixel. The pixel gets assigned to the class with the highest probability score (NV5, 2024). Neural Networks are built to function similarly to the human brain. Like your brain, it contains numerous nodes (neurons) that are connected in layers of experience. By leveraging the "experience" of each layer the algorithm makes a guess on the value of the node, checks if the guess was correct. This "path" to the answer is given a higher value. For each data point this feedback loop is repeated until all the pixels have been classified (AWS, 2024). Support Vector Machines work similarly to Neural Networks in that they have input and output layers, but it also considers the number of features in the input data set to find the optimal sets of classification (IBM, 2023). SVM has been found to be more accurate in smaller datasets (Pal & Mather, 2005).

In supervised classification methods the analyst needs to have some subject matter expertise to create viable training samples. In a real-world example, this could be a workflow for identifying the characteristics of the sea floor as it can be used to distinguish between rock, sand, and vegetation which can aid in undersea cable routing or sea life habitat studies. The analyst would provide the samples of what each region "looks" like and feed those into the algorithm. Another example would be shoreline delineation. At the mesh point of land and sea, the littoral zone provides a great opportunity for the usage of GeoAI. The analyst can create training samples of what the water pixels look like and what the land pixels look like. We could even go as far as assigning soil type attributes to the shoreline by comparing the spectral signatures of different materials.

Unsupervised classification, as its name implies, does not rely on input from the analyst or training samples. Instead, it uses clustering algorithms based on the spectral characteristics of the image to assign the classes. The most common of these algorithms is *K*-Means Clustering (Madhugiri, 2022). *K* is the only value needed for input and reflects the number of classes in which to sort the pixels. In the Land Classification example, it is necessary to separate water, impervious surfaces, and pervious surfaces, so *K* would equal three. A centroid is selected for each

https://doi.org/10.58440/ihr-30-1-c02

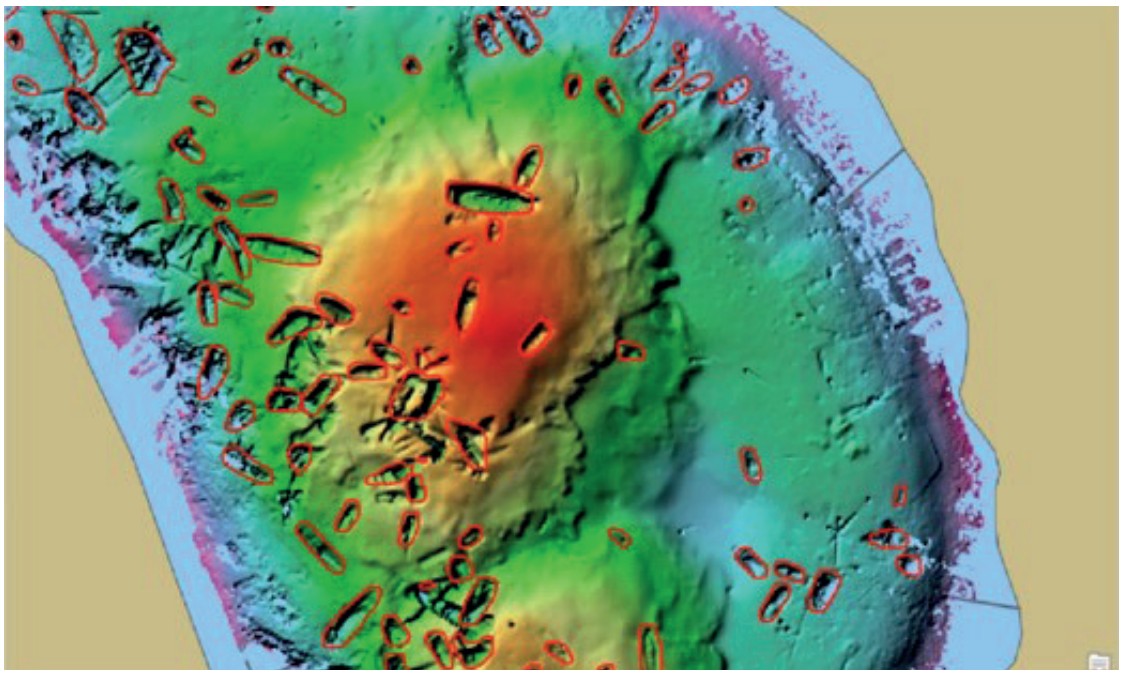

Fig. 2 Shipwrecks have a pattern in bathymetric surfaces that can identified by GeoAI models.

cluster and distances are calculated. The centroid and clustering process is repeated until convergence has been met or all data points have been classified. Again, this is an oversimplification of the methodology, but it is good background information. Unsupervised classification has a couple advantages, one is analysts do not need to create training data as input. Second, it can quickly detect patterns that may be difficult to detect otherwise. These advantages make unsupervised classification perfect for exploratory analysis or anomaly detection (Madhugiri, 2022). In a real-world example, this could be leveraged to find shipwreck or plane crash debris from rasters generated from echo sounder point clouds. Simply point the algorithm at a folder full of images and tell it to look for anything abnormal. This method, however, is less accurate as the algorithm treats all anomalies as equals.

Another method that needs to be discussed is the Object Based Imagery Analysis (OBIA). The key to OBIA is segmentation. Segmentation can mimic the way the human eye can pick out certain objects by grouping similar pixels into objects, rather than assigning individual pixels to classes (GISGeography, 2023). Due to the initial segmentation, objects are classified not only by their spectral signature, but also their shape, size, and spatial properties. Buildings, cars, swimming pools, etc. are all objects that are easily detected by OBIA. For hydrographic purposes, shipwrecks are an example, as are coral reef or sea grass patches. The method for detecting shipwrecks has been well documented by Rohit Singh and Vinay Viswambharan of Esri (Singh & Viswambharan, 2020). The goal of their research was to update the S-57 Chart with new shipwrecks after a disaster such as a hurricane. Manually searching for and digitizing all of the shipwrecks would have been a herculean effort as their study area represented over 100 km^2. in Jamaica Bay, NY. By combining segmentation methods with supervised classification, they were able to identify 100s of uncharted wrecks (Fig. 2).

GeoAI does not need to constrained to search for stationary objects on the sea floor. Vessel traffic monitoring is now a common task that has been laid at the feet of hydrographic offices. GeoAI models can be used to detect moving vessels and reconstruct their paths to understand patterns in a given port. Likewise, fragile ecosystems can be monitored with space-borne sensors. Vessels that turn their AIS off hoping to avoid detection can still be found. As seen in Fig. 3, the spectral signature of a vessel (bright white) is easily distinguishable from the black of the sea surface. This imagery is from Synthetic Aperture Radar (SAR) which can penetrate cloud cover and

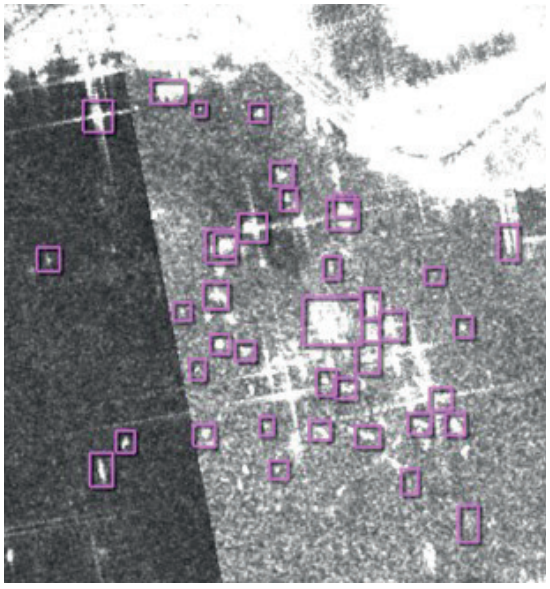

Fig. 3 Vessels detected using GeoAI models with Synthetic Aperture Radar.

does not rely on light from the sun. Meaning, that critical areas can be monitored in all types of weather and all times of day. By employing GeoAI to sort through the noise, humans only need to be notified if there is a new detection.

5 The case for GIS

The advantages of using GeoAI are numerous. Hydrographic offices can save time and money when updating charts and providing datasets to the public. They can also spare manpower to aid in the conversion to S-100 standards. For all the clarity on the advantages brought by GeoAI, machine learning, deep learning, etc., how to leverage these tools is much less apparent. Integrating GeoAI into your workflows is not without challenge. New skills need to be developed, potentially new hardware needs to be purchased, and legal hurdles need to be cleared. However, the barrier of entry can be lowered by turning to a modern Geographic Information System (GIS). The modern GIS, such as ArcGIS produced by ESRI contains a multitude of tools, wizards, and pre-trained models that enable the analyst to leverage GeoAI methodologies in a comprehensive package. From Image management, to training and running the models, to deriving insights, you only need one system. Many users get what they need from a single desktop application called ArcGIS Pro. Analysts do not have to run the analytics in one application, interpret the results in another, and share them in yet another application.

The models, algorithms, and methods described above involve complex mathematics and statistical modeling techniques that have been limited to use by data scientists and statisticians. Using a modern GIS, such as ArcGIS, allows the everyday GIS analyst to leverage the power of GeoAI by using tools that have the algorithms already built-in. For example, the Image Classification Wizard in ArcGIS Pro can take the analyst from training sample creation, to training the model, all the way to final classifications. GIS also can reduce the time it takes to create the training samples for supervised classification. The ArcGIS Living Atlas has over sixty pre-trained models, including shipwreck detection and models for detecting moving vessels. Vessel detection models can be used over streaming datasets for real-time monitoring in traffic management situations or even run on a schedule, only alerting humans if there is a detection as seen in Fig. 4 of an ArcGIS Dashboard. Pre-trained models can also be retrained to cope with the challenges presented by new geographies. With GIS and an integration with Python it is possible to organizations to create their own domain specific models, with the only limitation being the imagination of the analyst.

6 Closing

Hydrographic offices need to be able to meet their main mission of providing for safe navigation for the waters in their country while also meeting the changing of political wills along with the demand for data and analysis. They are constantly being asked to do more with less or unchanging budgets. They must also prepare for the migration to S-100 standards. With all of these pressing needs occurring simultaneously, these offices need to leverage new technology. GeoAI and the associated methods and algorithms provide the tools needed for these organizations to be more efficient in their daily work. GeoAI

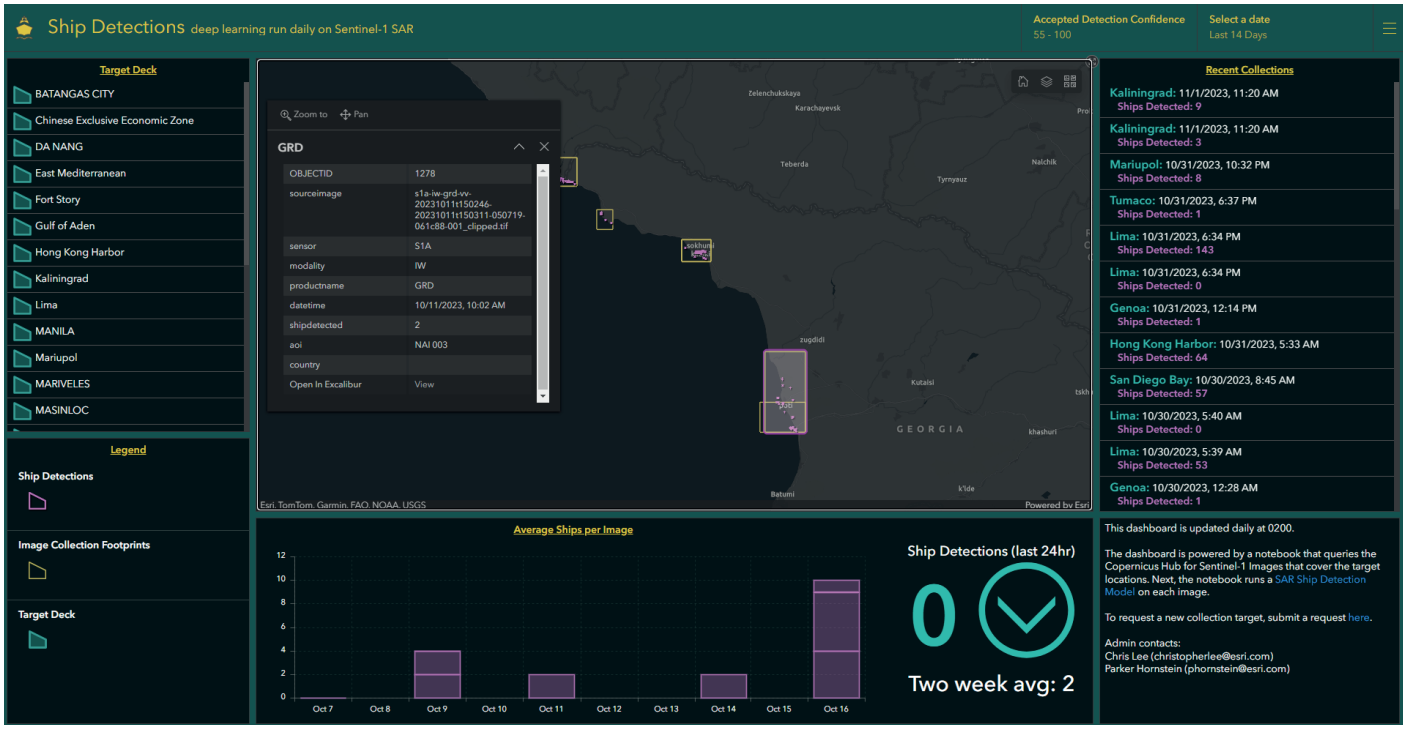

Fig. 4 GeoAI models can be ran on a schedule so analysts received new updates every morning.

https://doi.org/10.58440/ihr-30-1-c02

also provides many options and opportunities for automation. Examples include creating a data pipeline to update S-57 and S-100 charts from the same source data, creating seafloor classification from side scan sonar point clouds, and monitoring coastline changes. GIS provides the starting point and the system for taking advantage of the efficiencies to be gained by using GeoAI. Using GIS, offices can leverage supervised, unsupervised, and object-based classification to find uncharted hazards, detect new patterns from older datasets, and create authoritative mapping of the sea floor for use by other scientific organizations.

References

AWS (2024). *What is a neural network?.* Amazon Web Services, Inc. https://aws.amazon.com/what-is/neural-network/ (accessed 1 February 2024).

ESRI (2024). *What Is GeoAI? | Accelerated Data Generation & Spatial Problem-Solving.* https://www.esri.com/en-us/capabilities/geoai/overview (accessed 1 February 2024).

GISGeography. (2023, September 6). Obia - object-based image analysis (GEOBIA). GIS Geography. https://gisgeography.com/obia-object-based-image-analysis-geobia/

Hains, D., Schiller, L., Ponce, R., Bergmann, M., Cawthra, H. C., Cove, K., Echeverry, P., Gaunavou, L., Kim, S.-P., Lavagnino, A. C., Maschke, J., Mihailov, M. E., Obura, V., Oei, P., Pang, P. Y., Njanaseelan, G. P., Sharma, S. L. (2022). Hydrospatial – Update and progress in the definition of this term. *The International Hydrographic Review, 28,* pp. 221–225. https://doi.org/10.58440/ihr-28-n14

IBM (2023). *What are support vector machines (SVMs)?.* The International Business Machines Corporation. https://www.ibm.com/topics/support-vector-machine (accessed 1 February 2024).

Madhugiri, D. (2022). *Unsupervised learning in Image Classification – Everything to Know.* https://www.amygb.ai/blog/unsupervised-learning-in-image-classification (accessed 1 February 2024).

NV5 (2024). *Maximum Likelihood. Maximum likelihood.* NV5 Geospatial Solutions, Inc. https://www.nv5geospatialsoftware.com/docs/MaximumLikelihood.html (accessed 1 February 2024).

Singh, R. and Viswambharan, V. (2020). *Detecting Shipwrecks Using Deep Learning.* https://www.esri.com/arcgis-blog/products/arcgis-pro/analytics/detecting-shipwrecks-using-deep-learning/ (accessed 1 February 2024).

Pal M. and Mather, P. M. (2005). Support vector machines for classification in remote sensing. I*nternational Journal of Remote Sensing, 26*(5), 1007–1011, https://doi.org/10.1080/01431160512331314083

NOTE / TECHNICAL REPORT

CSB as part of the modern hydrographic toolbox

Authors

Jennifer Jencks[1] and Belen Jimenez Baron[2]

Preamble

This paper is intended as a response to a Note by Philip Payne, published in The International Hydrographic Review (IHR, https://ihr.iho.int/) in November 2023: Payne, P. (2023). Crowdsourced bathymetry and its use to support resurvey activity in the North Sea region. *The International Hydrographic Review, 29*(2), pp. 248–253. https://doi.org/10.58440/ihr-29-2-n16

1 Introduction

It is well established that hydrographic surveys with multibeam echosounders (MBES) are the most ideal and preferred way to collect data for the purpose of producing nautical charts. It is also acknowledged that this standard method is constrained in many ways, from survey platforms to personnel to equipment requirements (Masetti, 2020a). Around the world it is uncommon to see a hydrographic authority that has adequately and completely surveyed and mapped their entire area of responsibility (IHO, 2024). Therefore, while the intention here is not to debate whether crowdsourced bathymetry (CSB) can or should be considered "as good as" a hydrographic survey using MBES, this is an invitation for the reader to consider CSB as a supplementary data source which can aid decision making, prioritization and potentially fill data gaps when the well adopted methods do not or cannot.

In the November 2023 edition of The International Hydrographic Review (IHR), the article *Crowdsourced bathymetry and its use to support resurvey activity in the North Sea region* was published (Payne, 2023). While the article highlighted potential uses and benefits of CSB, it primarily focused on considerations to be taken into account when considering the use of CSB in planning a resurvey scheme in the North Sea.

From the perspective of the chair and vice-chair of the International Hydrographic Organization (IHO) Crowdsourced Bathymetry Working Group (CSBWG), we would like to provide information in response to some of the stated concerns and remind readers that many of the issues raised should either not be taken as general statements or should be recognized as not being unique to CSB data. We would also like to provide the reader with updates about the progress of CSB within the context of CSBWG and a summary on the potential of not just considering, but embracing, CSB as an additional data source by hydrographic offices and other relevant stakeholders. Our intent is to encourage hydrographic offices to continue to pursue their own investigations into whether CSB data may be of benefit to them.

2 Background

As has been described previously in the IHR (Jencks et al., 2021), it was at the 2014 Fifth Extraordinary International Hydrographic Conference, that the IHO recognized that traditional survey vessels alone could not be relied upon to solve data deficiency issues and

✉ Jennifer Jencks · jennifer.jencks@noaa.gov

[1] National Centers for Environmental Information (NCEI), National Oceanic and Atmospheric Administration (NOAA), Boulder, CO, United States of America

[2] National Institute of Water & Atmospheric Research Ltd (NIWA), Wellington 6021, New Zealand

https://doi.org/10.58440/ihr-30-1-n03

agreed there was a need to encourage and support all mariners in an effort to "map the gaps". One outcome of the conference was an initiative to support and enable mariners to collect CSB. A Crowdsourced Bathymetry Working Group[1] was established and tasked to draft a new IHO publication, initially published in 2019, to provide best practices for collecting and contributing crowdsourced depth data. Edition 3.0 of the IHO publication B-12 *Guidance on Crowdsourced Bathymetry* (IHO, 2022a) was approved in October 2022 and included updates such as incorporating feedback from operational use and experience, making the document more "equipment agnostic", simplifying the document and making it more accessible to all readers (e.g. data collectors, providers and users). The latest edition also takes into account a wider representation of hydrographic authorities, addressing specific issues such as quality assessment of the data and legal considerations in waters of national jurisdiction.

(IHO, 2022a) defines crowdsourced bathymetry as *the collection and sharing of depth measurements from vessels, using standard navigation instruments, while engaged in routine maritime operations*.

Today, the CSBWG focuses on investigating and highlighting use cases of CSB data, providing guidance on data quality and standards in liaison with the IHO Data Quality Working Group (DQWG) and considering incentives to increase data contributions by mariners. The CSBWG is particularly tasked to work in cooperation and coordination with other IHO bodies, including the 15 Regional Hydrographic Commissions (RHCs) and relevant industry stakeholders, to understand regional perspectives, technical capabilities and to encourage a harmonized approach to data gathering and the resultant datasets. Thanks to the active participation of the CSBWG members, a comprehensive work plan has been established (CSBWG, 2023) and efforts are being put towards building a bridge between stakeholders needs, identified challenges and the operationalisation of CSB supported by the development of open source tools.

3 CSB as part of the modern hydrographic toolbox

It is understood within the hydrographic community that the fast evolution of technology is creating the need to redefine the role of the hydrographers, cartographers and managers of hydrographic authorities around the world. This is not just limited to upgrading personnel skills, but also to changing the ways in which data is treated and processes and organizations are managed (Foroutan et al., 2022). Part of this transformation requires thinking out of the box, considering alternative methodologies, diversifying data sources and engaging in new partnerships. We would like to invite the reader to embrace this reality whenever considering testing or using non-traditional data sources such as CSB.

Furthermore, hydrographic offices around the world are today expanding their scope to more than just safety of navigation. This is reflected in the vision and mission statements of many offices and authorities, which include supporting scientific research and contributing to a more sustainable use of the oceans (e.g. Directorate of Hydrography and Navigation of Peru, Canadian Hydrographic Service). There are also hydrographic offices which contribute nationally and internationally to the prediction and damage mitigation of tsunamis and sea level rise. Therefore, when considering new data sources, it is important to evaluate how this data can contribute to the overall mission of a hydrographic authority, rather than determine only whether a specific sounding will qualify to be displayed in a nautical chart.

It is the ultimate responsibility of each organization to decide whether CSB should be considered as a source of data. In addition to the well explained use case for seabed or feature monitoring (Payne, 2023), we would like to provide a few additional examples of the potential benefits of CSB for the consideration of such organizations.

3.1 Recognizing the value of CSB in uncharted areas

CSB data collected in areas routinely visited by vessels where hydrographic surveys do not reach is typically the first use case that is considered. Fig. 1 shows an example of a considerable amount of CSB data collected beyond the extents of a hydrographic survey. Given that this data was collected by one or more vessels conducting their routine maritime operations, the value of increasing the information provided in the existing charts is clear, especially when there is evidence that the uncharted areas are frequently transited.

3.2 Considering CSB in chart adequacy assessments

In heavily used maritime areas of the world, where chart information is vast, CSB also has the potential to make a significant contribution. These data can be used to identify previously uncharted features (Fig. 2), assist in verifying charted information and confirm whether charts are still appropriate for the latest traffic patterns. As described by Calder (2021), increased number of observations can significantly contribute to increasing the quality and value of CSB data (Fig. 3).

3.3 Improving the general knowledge of the seabed

In parts of the coastal world where the nature of the seabed may be ever changing, the advantage of CSB data would most certainly be in the identification of potential change which could assist in the prioritization of surveys (Fig. 4). If pockets of these regions have to be lower prioritized due to resource constraints, CSB can help in the identification of potential change. Making this data and derived products available to the public

[1] https://iho.int/en/csbwg/ (accessed 1 April 2024).

can also support a wide range of environmental, marine and oceanographic research, specially where a continuous digital model of the seabed is more important than reaching high accuracies.

4 An asset does not (necessarily) equate to a replacement

One can easily compare the adoption of CSB to that of LiDAR (light detection and ranging) and satellite derived bathymetry (SDB). These methodologies also provide an alternative for, or addition to, bathymetric surveys in areas where traditional methods such as acoustic-based hydrographic surveys are missing, historically lower prioritized by hydrographic authorities or simply too expensive to conduct due to the inefficiency of MBES in extremely shallow areas. Despite the facing of some barriers at the beginning, these data acquisition methods have now gained extensive popularity. In many cases LiDAR is now accepted as a way to deliver high accuracy S-44 compliant surveys (Cooper, 2021), with the added benefit of also providing a continuous model for land and water. The ability for SDB to detect shoals at a very low cost is also evident and SDB datasets have been commissioned by hydrographic authorities around the world, achieving results which can meet the standards Category Zone of Confidence (CATZOC) B and C (EOMAP, 2019).

As demonstrated in Fig. 5, it is relevant to note, that neither SDB or LiDAR have become a replacement to multibeam, rather it is the combination of methods which can optimize resources and capabilities of a hydrographic authority in fulfilling their primary task to enable safe navigation (Cooper, 2021).

5 But is the data any good?

Hydrographic offices and authorities have always accepted observations from mariners to update their charting area of responsibility. Typically, these are marked "position doubtful", "existence doubtful", or the local equivalent, to indicate some level of assessment. There is also an established process for mariner reporting: "Hydrographic Note" in some jurisdictions. The use of modern CSB is not, fundamentally, different from this in quality, in fact, one could argue it is better. Instead of one mariner saying "depth here is 10 m", theoretically one might have dozens of mariners supplying data consistently reporting the same value. This section provides an overview on accuracy, suitability and quality of CSB data, inviting the reader to consider how to use CSB based on the assessment of those three points.

5.1 Accuracy

The concern around the accuracy of CSB soundings is often raised, and for good reason. Uncontrolled CSB is unlikely to account for offsets and other corrections that would be expected for hydrographic data. However, this situation is not uncorrectable. Vertical offsets and approximate sound speed can often be estimated and corrected for, and has been shown to then match calibrated authoritative data quite well (Klemm & Krabiel, 2023).

Today, the majority of CSB data within the IHO framework is collected with single beam sounders. As explained in Fig. 6, this reduces the problem of resolving for the position and depth of the ensonified seabed to a simple georeferencing equation. As done with any other depth data, having a good understanding of the different error sources can enable the quantification of the uncertainties associated with the determination of position and depth.

If CSB data can be assessed and its accuracy can be calculated, there should be no judgment to

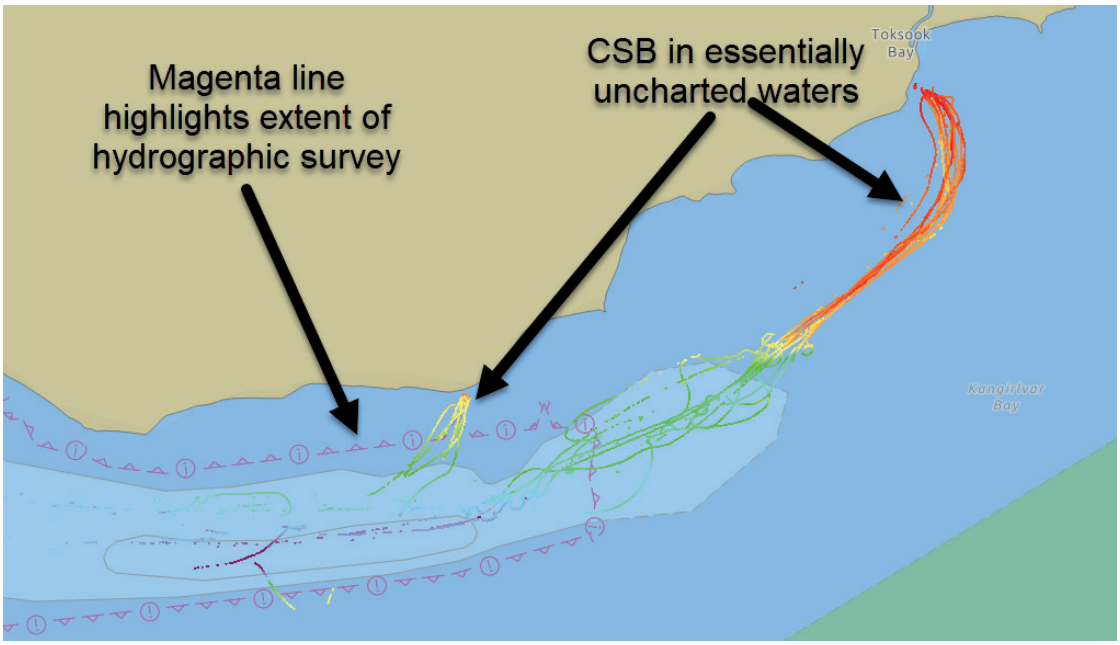

Fig. 1 CSB tracks collected through and past the extent of a NOAA hydrographic survey in Toksook Bay, Alaska. Image courtesy of NOAA.

https://doi.org/10.58440/ihr-30-1-n03

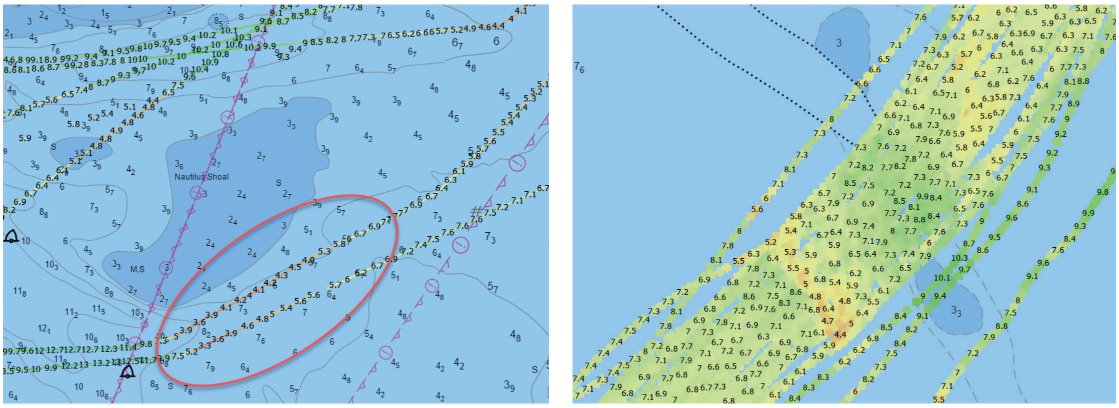

Fig. 2 Mischarted shoals detected in heavily trafficked Chesapeake Bay (left) and Delaware Bay (right). Image courtesy of NOAA.

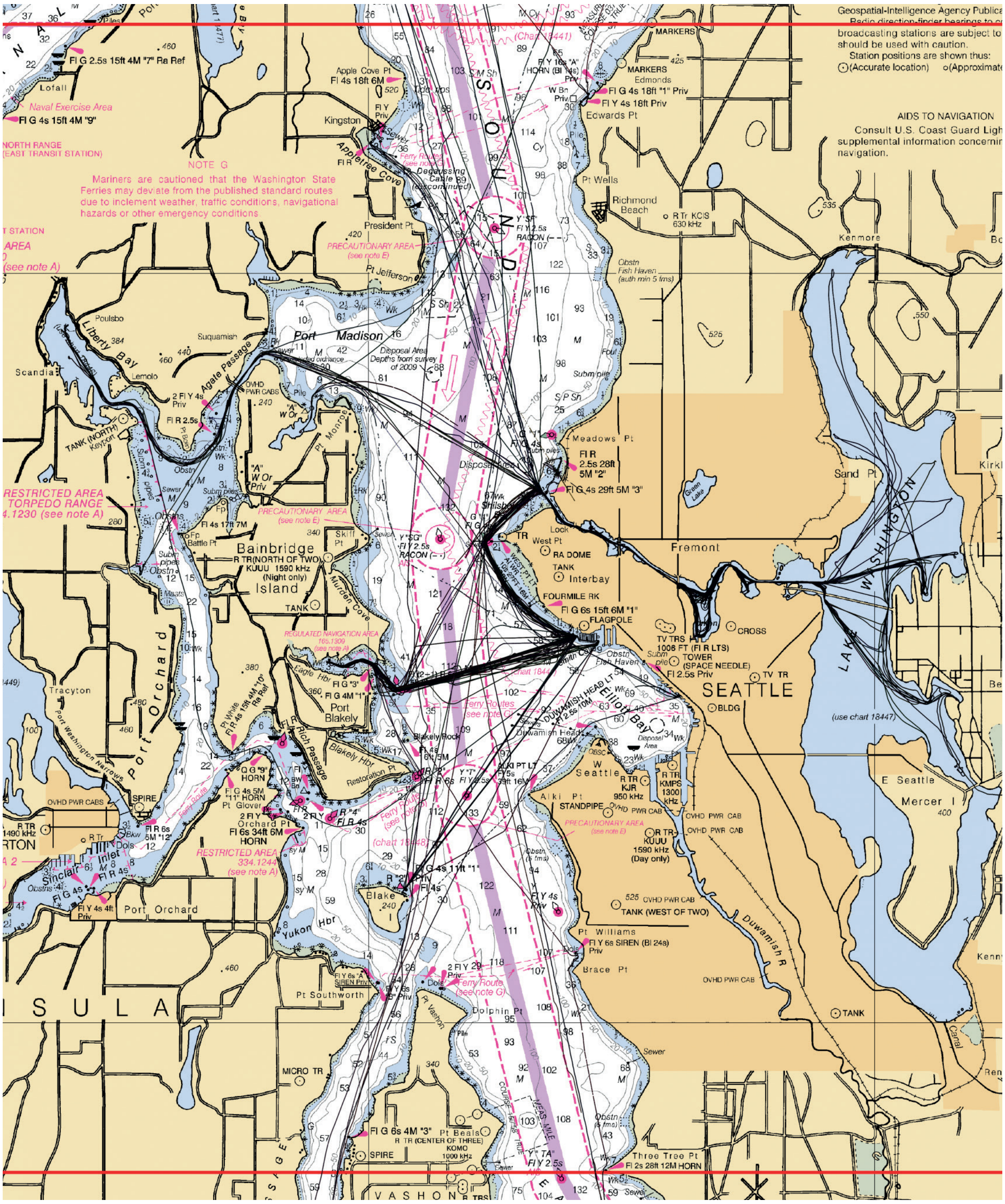

Fig. 3 Data selected for experiments conducted in (Calder, 2021), because of the data density and supporting authoritative data for the area around Seattle, WA in southern Puget Sound.

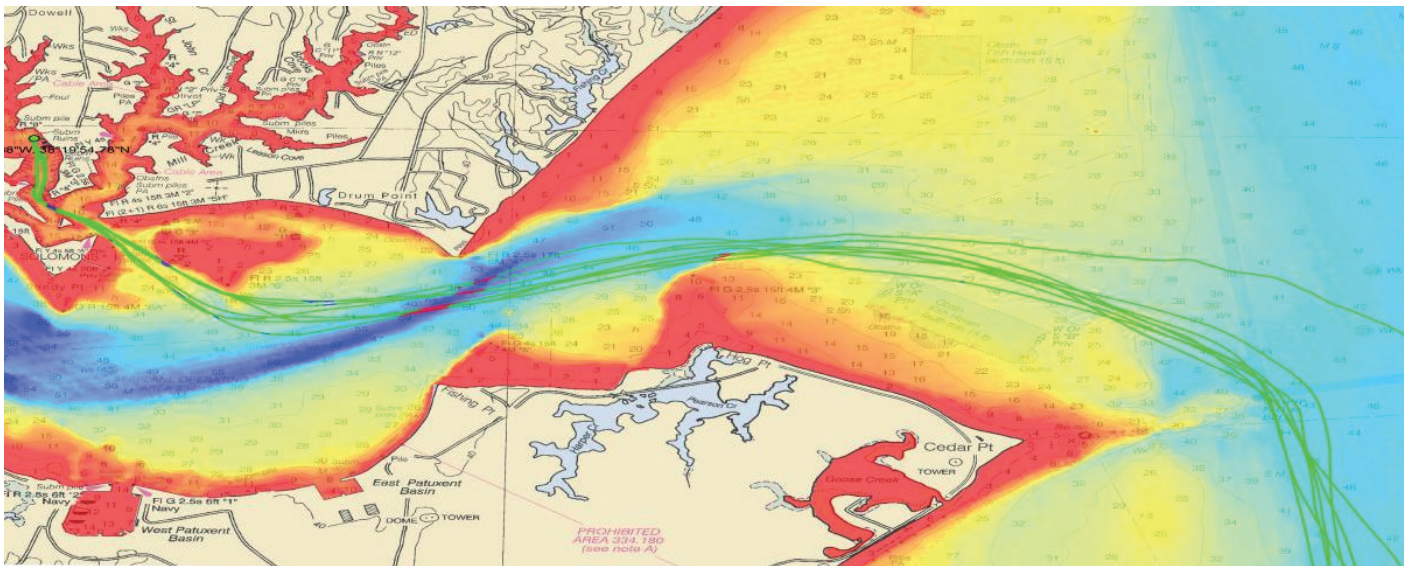

Fig. 4 CSB test tracks collected on NOAA's Research Vessel Bay Hydro II in green overlaid on multibeam survey data demonstrates how changes can be detected. Image courtesy of NOAA.

which data collection method was used. Whenever the highest orders of S-44 have to be met, the right equipment should be chosen and the finest attention paid to the procedures by the experienced hydrographer. However, deploying such a setup for mapping an area which does not require the highest standards would be excessive and inefficient, and this is why some areas are down-prioritized with respect to others by hydrographic authorities.

As explained by Calder et al. (2020) and Masetti et al. (2020a), implementation of trusted CSB networks under the supervision of the competent authorities can significantly improve the chances of CSB data to qualify for appearing in nautical charts. Fig. 7 shows how data credibility and "chartability" is not just a function of the method used, but also depends on the level of involvement of competent agencies such as hydrographic authorities.

5.2 Suitability

Another concern is around the suitability of CSB data in nautical charting. For example, the North Sea Hydrographic Commission (NSHC) Resurvey Working Group (RSWG) examined and concluded that CSB was not suitable for charting in many areas of the NSHC area (Payne, 2023). While the article made it clear they were referring only to the North Sea, we would like to stress that what might be ruled as unsuitable for one region, may very well be suitable for another. In fact, other hydrographic authorities, such as the Canadian Hydrographic Service (CHS) and the National Oceanic and Atmospheric Administration (NOAA) have been exploring the use of CSB data for years and have provided several positive examples (Jencks, et al., 2021; Klemm & Krabiel, 2023).

Industry is also recognizing the power of CSB. DockTech Ltd. (Tel Aviv-Jaffa, Israel) offers a real-time status of waterway conditions and is demonstrating that in harbors, one of the most critical navigation areas, port operators, pilots and mariners find CSB data a useful addition to their official navigation products (Grinker et al., 2022).

5.3 Data Quality

Data quality is not an inherent quality of a specific methodology or equipment used to collect the data. Hydrographers know that each dataset is unique and needs to be assessed independently. Equipment, experienced operators, and good procedures make the three elements which will ultimately constrain the quality of a specific dataset (IHO, 2022b).

All types of externally sourced surveys present a challenge, and it is still today a work in progress to have charting authorities fully embrace alternative data sources even, for example, multibeam surveys from scientific cruises. While it is true that this type of data may lack some of the essential elements of quality assurance as defined by S-44 (people, procedures, equipment), the gap between the quality of such surveys and the ones planned for safety of navigation has significantly been narrowed. Today some hydrographic authorities have begun to embrace externally sourced data and include it in their products, while others are working on the right procedures to make this happen.

CSB is unlikely to ever reach the uncertainty and quality achieved by professionally collected data. However, in the phrase "best available data" the key word is "available". When a specific area is covered by volunteer soundings only, a charting authority may consider using this data, with appropriate warnings, rather than leave an area marked as unsurveyed or inaccurate (Fig. 8).

Metadata is critical to the understanding of any dataset. To allow for an assessment of the quality of the data, it is important to document certain additional information together with the data. This is why we strongly encourage active and potential

https://doi.org/10.58440/ihr-30-1-n03

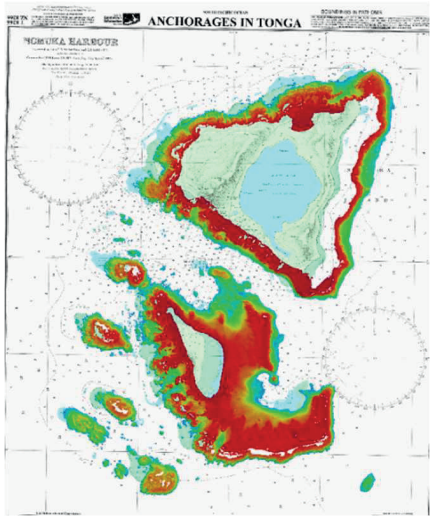

SDB Coverage and previously georeferenced fathoms chart

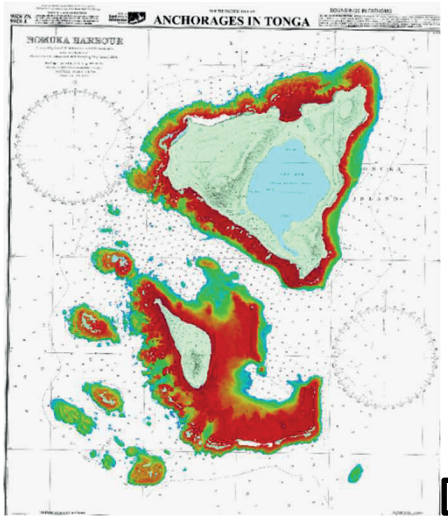

SDB Coverage used to correct fathoms chart georeferencing

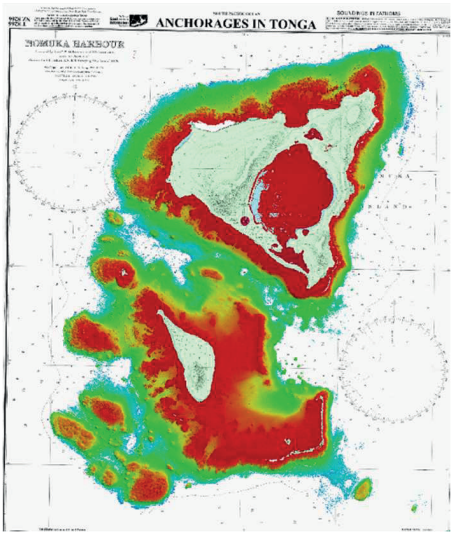

ALB Coverage against correctly georeferenced fathoms chart

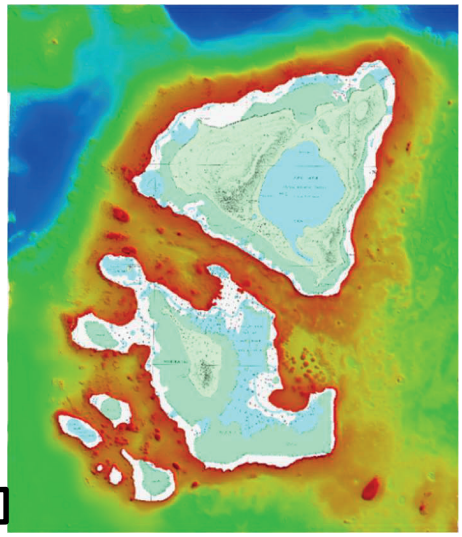

MBES Coverage against correctly georeferenced fathoms chart

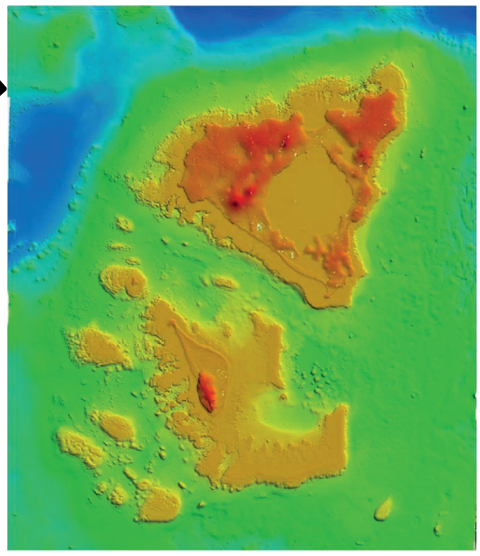

All coverage (including topographic lidar coverage acquired with ALB)

Fig. 5 Progression of the multi sensor survey on the Nomuka datasets (Cooper, 2021).

data collectors to provide as much extra information as they can (e.g., offsets between global navigation satellite system (GNSS) and echo sounder, type of corrections applied, if any, etc.). The metadata associated with a data set provides valuable supporting information relating to how the data collection was performed and enables appropriate processing, corrections and an informed assessment of the data quality to be made. The CSBWG recommends the review of B-12, specifically *Chapter 3: Data & Metadata* (IHO, 2022a, pp. 22–29) and *Chapter 4: Data Quality Assessment* (IHO, 2022a, pp. 30–33), which describe metadata requirements, suggested metadata, and delve into data quality concepts like uncertainty and data consistency. The guidance document also discusses how to provide

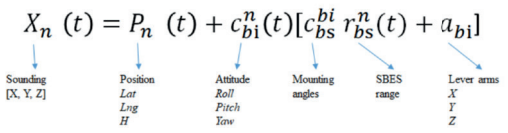

Fig. 6 Georeferencing equation for single beam acoustic measurements (Masetti et al., 2020b).

feedback and suggestions to the CSB data contributor for improving future contributions.

The latest edition of S-44 also includes a matrix, which allows for the classification of any data at a more granular level (IHO, 2022b). This is meant as a tool for the hydrographers to assess the quality of the data beyond the S-44 Order, and to allow for alternative data sources, which might not fully comply with a specific S-44 order, to be assessed in a standardized way. It is encouraged to use such a table to communicate the quality of CSB data, which ultimately will provide the input to decide what the specific data can be used for.

Once the data has been assessed and its quality can be defined in terms of the IHO S-44 matrix, it can be considered whether this data is appropriate for use in a nautical chart. Using the CATZOC table (Fig. 9) the competent authority can estimate if the data is compatible with a specific Zone of Confidence (ZOC), and then decide whether it should be used in the nautical chart (IHO, 2020). As stated by DQWG (2019), *"Good data quality does not mean that the quality of the data has to be good. It means that the end user is well informed how good the data is."*

6 Resource considerations

It is a fact that the ever increasing size of a global fleet contributing CSB data can translate to an unpredictable amount of new data, and therefore there is much outspoken concern from hydrographic authorities about becoming quickly overwhelmed. Although this concern is valid, it should not be used as the main argument to systematically dismiss CSB data, but rather as an incentive to optimize and customize workflows that are more appropriate for this purpose. Instead of insisting to fit this data into an existing system, designed to manage different types of data, the way forward is designing specific workflows, based on the same principles and good practice that we apply for any other data source, but customized to fit CSB. Following this trend, many are already developing new tools and processes to assist hydrographic offices, industry and the greater community (for e.g. Debroisse, 2023; Masetti et al., 2020a; Klemm & Kraibel, 2023; Grinker et al., 2022; Salaudeen, 2023). The evolution of these tools, and the needs that are trying to be met, are topics of every CSBWG meeting.

One example is a CSB Processing Tool, developed by NOAA's Office of Coast Survey. Though it is currently a simple and preliminary solution, it is an important step in unlocking the full potential of CSB data. The script and source-code can be accessed from GitHub[2], and the tool is also distributed through NOAA's Office of Coast Survey's Pydro Tool Suite, which is a collection of tools meant to streamline and automate the hydrographic workflow. Both are free and open to the public (Klemm, 2023).

The CSBWG is actively encouraging community-led projects to develop best-in-class "community vetted"

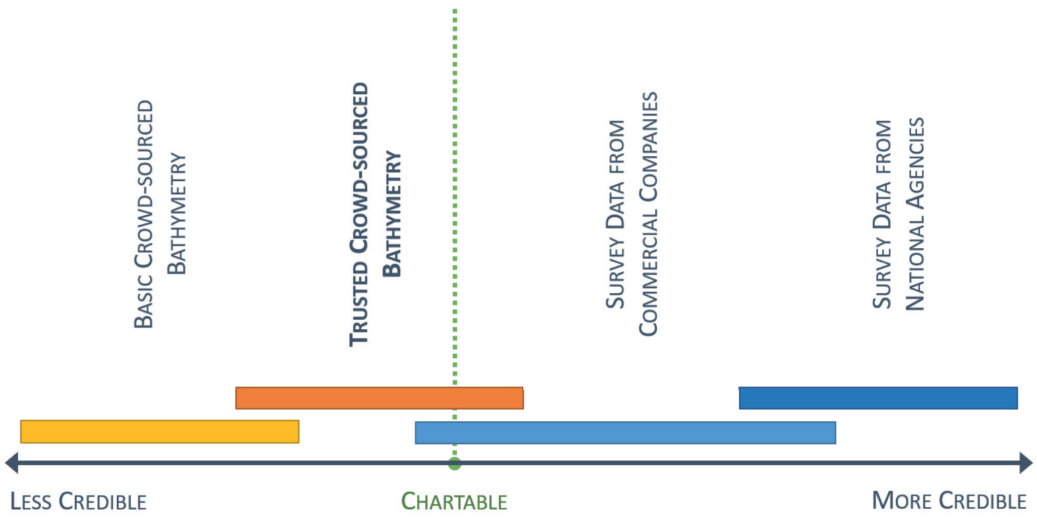

Fig. 7 Example of credibility plot comparing different hydrographic data sources (Masetti et al., 2020a). A possible minimum level of credibility required for making the geospatial information 'chartable' is marked in dashed green.

https://doi.org/10.58440/ihr-30-1-n03

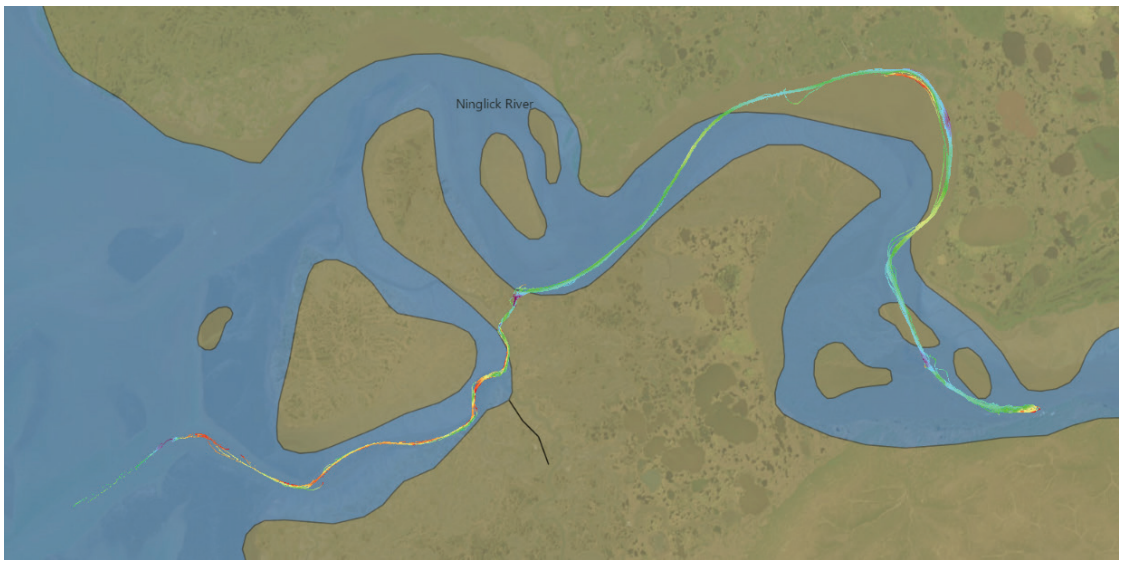

Fig. 8 Along the Ninglick River, where mariners routinely navigate. Image courtesy of NOAA.

algorithms in open-source projects that will support these processes in the future. Much of this work has been published (Calder, 2021; Grinker et al., 2022; Salaudeen, 2023) and we encourage the community to read more about it.

In addition to technology, the skills of the (future) hydrographer and cartographer are constantly being re-defined. The emphasis on data management within hydrographic authorities is evidence of this and having alternative data sources as part of their workflow is something that takes time and effort. We must all be cautious of becoming short-sighted and resist discounting a specific data source simply based on its definition or the volume of the task as to ensure we do not limit the potential for the benefits associated with wider observation of the seabed depths.

Finally, we acknowledge that activities related to CSB data collection and use will likely require resources and funding. However, professional surveyors, vessel time, echo sounders, positioning systems and data management infrastructures all require significant investment. The cost to collect CSB data ranges between free to minimal. Currently The Nippon Foundation GEBCO – Seabed 2030 provides free data loggers and support to those willing to contribute data to the project. The resources and expertise needed to process CSB data are already available within hydrographic authorities. A cost-benefit analysis would be the most appropriate way to decide whether a specific authority should include CSB data in their workflows.

7 Currently available CSB datasets

Over the last several years, contributions of CSB data to the IHO Data Centre for Digital Bathymetry (DCDB) has grown significantly (Fig. 10). The IHO DCDB Viewer (ncei.noaa.gov/maps/iho_dcdb/)[3] allows the public to discover and download these data. At the same time, most data are concentrated around just a few areas. It should be noted that this is not necessarily because of a lack of data being collected (though that might certainly be one reason), but that it also reflects coastal States responses (or lack of responses) to Annex B IHO Circular Letter (CL) 11/2019[4] and to the questionnaire in Enclosure to IHO CL 21/2020[5].

If we were to focus on just one region, for example the North Sea (Fig. 11), we would observe a significant amount of CSB data off the coast of Norway,

Table 4-1 –ZOC Categories

ZOC	Position accuracy	Depth accuracy	Seafloor coverage
A1	± 5 m + 5% depth	0.50 m + 1% depth	Full area search undertaken. Significant seafloor features detected and depths measured.
A2	± 20 m	1.00 m + 2% depth	Full area search undertaken. Significant seafloor features detected and depths measured.
B	± 50 m	1.00 m + 2% depth	Full area search not achieved; uncharted features hazardous surface navigation are not expected but may exist.
C	± 500 m	2.00 m + 5% depth	Full area search not achieved, depth anomalies may be expected.
D	Worse than ZOC C	Worse than ZOC C	Full area search not achieved, large depth anomalies may be expected.
U	Unassessed – The quality of the depth data has yet to be assessed.		

Fig. 9 Simplified version of CATZOC Categories. See original publication for the full table (IHO, 2020, Annex A).

some off of Germany, Belgium and the Netherlands, and data within the exclusive economic zone (EEZ) of Sweden. This is the result of both data contributions within the region, but also of the positive response to the circular letters that the States provided. The lack of discoverable data along the coastlines of Denmark and France is because these offices have requested the ability to pre-approve data within their waters of national jurisdiction before it is made publicly discoverable. The IHO DCDB has developed the necessary tools and interface to allow for countries with such a requirement to undertake the review. Denmark and France have been involved in beta testing and have provided valuable feedback to DCDB. Neither the United Kingdom nor Ireland have provided replies to the circular letters, therefore data collected within their areas of national jurisdiction are not allowed to be made discoverable.

The list of all coastal States that have replied positively to the questionnaire in Annex B to IHO CL 11/2019 and to the questionnaire in Enclosure to IHO CL 21/2020 can be found online[6].

It should also be acknowledged that the responses to IHO CL 11/2019 and 21/2020 currently total 34 coastal States. We are optimistic that this number will grow, especially when coastal States who have responded positively to the circular letters encourage others to do the same and strive to work together to share, not only data, but also lessons learned and approaches to data collection, processing and application of CSB.

8 Conclusion

We would like to thank the editor of the IHR for the opportunity to respond to *"Crowdsourced bathymetry and its use to support resurvey activity in the North Sea region"* published in November 2023 (Payne, 2023). We would also like to thank those authors for acknowledging the potential uses and many benefits of CSB and also for taking part in a much-needed dialogue about the concerns of hydrographic authorities regarding CSB data, as it allows for the CSBWG to address such concerns.

As the IHO effort to encourage the acceptance of CSB and to provide guidance and structure on how to collect and use CSB data is still quite new, we understand and would expect that it will take time until this data source is fully adopted by hydrographic authorities.

It is well known that despite the great work that hydrographic authorities around the world are doing to provide a service, there are a number of unofficial products, essentially populated by CSB, that are distributed and widely used by mariners. The use of unofficial charts over official ones will continue to increase unless hydrographic authorities get involved in considering the application of CSB. As long as these services remain unofficial and unsupervised by qualified hydrographers and cartographers, the full potential of CSB will not be unlocked, while a large percentage of mariners worldwide will continue to demand products in areas outside of the priorities of the local hydrographic authorities.

As data volumes and public interest grow, we are hopeful that hydrographic authorities and academic institutions will take on these issues, perform analyses, create products, etc. In the meantime, the IHO DCDB is always looking for feedback to enhance the way CSB is served to the public.

While the collection of bathymetric data by mariners is not new, we acknowledge that the hydrographic community is still in the early stages of understanding

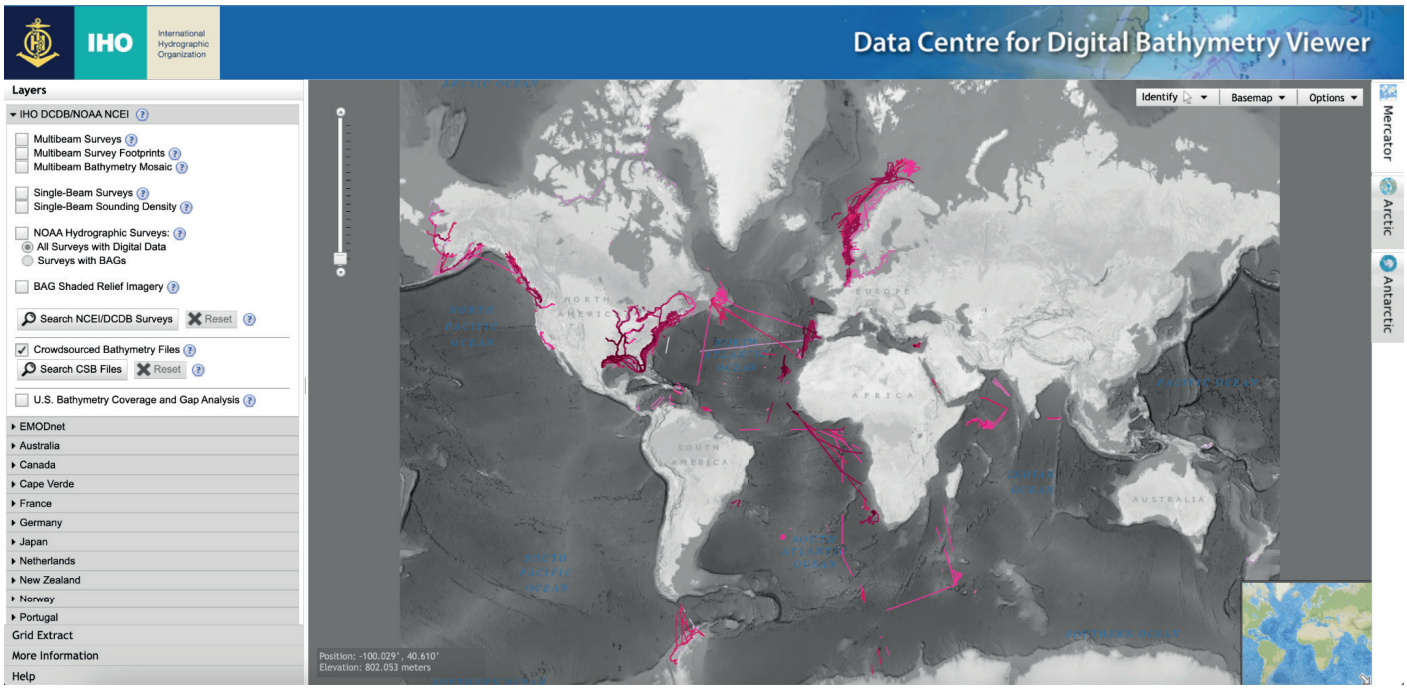

Fig. 10 DCDB screenshot of the global collection of CSB data (5 March 2024).

https://doi.org/10.58440/ihr-30-1-n03

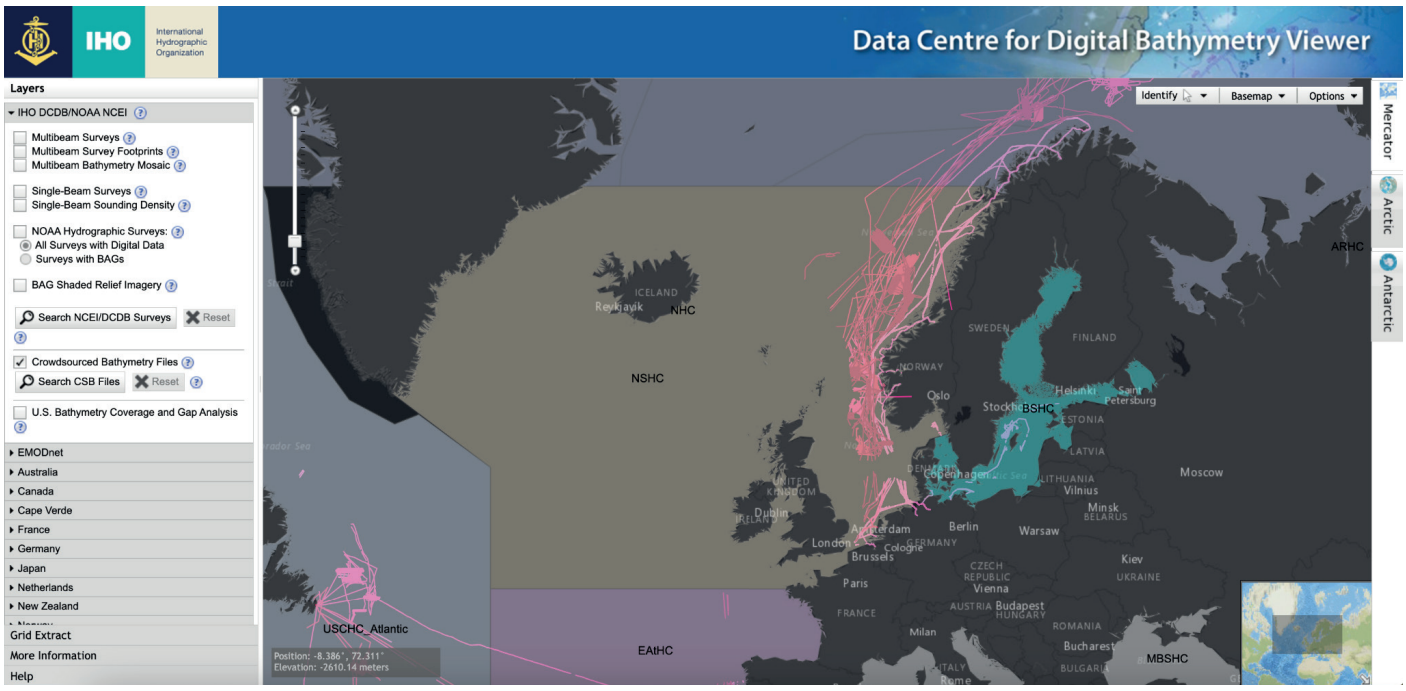

Fig. 11 DCDB screenshot of the CSB data within the NSHC (5 March 2024).

and implementing CSB within the IHO framework and that much of what has been written is about potential. However, in a world where our global seafloor is still only 25 % mapped with publicly available data (GEBCO Bathymetric Compilation Group, 2023) and our coastal waters only 50 % charted (IHO, 2024), we believe it is a great disservice to discourage the consideration of any bathymetric data type, especially one that is readily available to everyone.

The IHO strongly encourages all coastal States to permit the CSB data collected within their waters of national jurisdiction to be made publicly available and to work with others in the field who are currently developing ways and ideas to best use these data, whether for nautical charting or other purposes. Healthy skepticism is good and needed, especially when safety of navigation is involved. However, we encourage all hydrographic authorities to consider the use and application of these data on their own.

We also encourage all hydrographic authorities to attend future CSBWG meetings where their concerns, suggestions, and work would be most welcome to discuss. The next IHO CSBWG, hosted by the IHO, will be 23–25 April 2024, followed by an IRCC Workshop on Crowdsourced Bathymetry (CSB) on 26 April. Please also consult our website[1] for information on future meeting dates.

References

Calder, B. R. (2021). Estimating Observer and Data Reputation in Mariner Volunteered Bathymetry. *The International Hydrographic Review, 25*, pp. 77–96. https://ihr.iho.int/articles/estimating-observer-and-data-reputation-in-mariner-volunteered-bathymetry/

Calder, B. R., Dijkstra, S. J., Hoy, S., Himschoot, K. and Schofield, A. (2020). A Design for a Trusted Community Bathymetry System. *Marine Geodesy, 43*(4), pp. 327–358. https://doi.org/10.1080/01490419.2020.1718255

CSBWG (2023). *Crowdsourced Bathymetry Working Group Work Plan 2023*. Crowdsourced Bathymetry Working Group, Inter-Regional Coordination Committee, International Hydrographic Organization. https://iho.int/uploads/user/Inter-Regional%20Coordination/CSBWG/MISC/CSBWG_WorkPlan_13December2023.pdf (accessed 1 April 2024).

Cooper, B. (2021). Effectively Mapping and Charting of Remote Locations with Satellites, Lasers and Acoustics. *The International Hydrographic Review, 26*, pp. 61–83. https://ihr.iho.int/articles/effectively-mapping-and-charting-of-remote-locations-with-satellites-lasers-and-acoustics/ (accessed 1 April 2024).

Debroisse, P. J., (2023). *Towards Automation of Volunteered and Authoritative Bathymetric Data Comparisons* [Master's thesis, University of New Hampshire]. https://ccom.unh.edu/sites/default/files/publications/Debroisse_Thesis_Final.pdf (accessed 1 April 2024).

DQWG (2019). *Combining S-101 and S-102 and definitions of depth* [presentation]. Data Quality Working Group, S-100 Test Strategy

[2] https://github.com/anthonyklemm/Crowdsourced_Bathy_Processing (accessed 1 April 2024).

[3] http://ncei.noaa.gov/maps/iho_dcdb/ (accessed 5 March 2024).

[4] https://legacy.iho.int/mtg_docs/circular_letters/english/2019/CL11_2019_EN_v1.pdf (accessed 1 April 2024).

[5] https://iho.int/uploads/user/circular_letters/eng_2020/CL21_2020_EN_v1.pdf (accessed 1 April 2024).

[6] https://iho.int/uploads/user/Inter-Regional%20Coordination/CSBWG/MISC/B-12_2023_EN_Acceptance_of_CSB_Data_in_NWJ_v7.0.pdf (accessed 1 April 2024).

Meeting 7, Monaco, 23–26 September 2019. Hydrographic Services and Standards Committee, International Hydrographic Organization. https://legacy.iho.int/mtg_docs/com_wg/S-100WG/TSM7/TSM7_2019_5.5_DataQualityV1.pdf (accessed 1 April 2024).

EOMAP (2019). *Satellite-Derived Bathymetry in Hydrographic Surveys* [presentation]. South West Pacific Hydrographic Commission, 16th Meeting 13–15 February 2019, Niue. https://iho.int/uploads/user/Inter-Regional%20Coordination/RHC/SWPHC/SWPHC16/SWPHC16-16.2-EOMAP.pdf (accessed 1 April 2024).

Foroutan, M., Bhatia S. and Béchard, G. (2022). The Hydrographer of the Future – Reflections on an International Virtual Workshop. *The International Hydrographic Review, 28*, pp. 172–180. https://doi.org/10.58440/ihr-28-n12

GEBCO Bathymetric Compilation Group (2023). The GEBCO_2023 Grid a continuous terrain model of the global oceans and land. NERC EDS British Oceanographic Data Centre NOC. https://doi.org/10.5285/f98b053b-0cbc-6c23-e053-6c86abc0af7b

Grinker, B., Solomon, S. and Hassin, A. (2022). Evaluation of a Crowd Sourced Bathymetric Approach. *The International Hydrographic Review, 28*, pp. 158–171. https://doi.org/10.58440/ihr-28-a08

IHO (2020). *Mariners' Guide to Accuracy of Depth Information in Electronic Navigational Charts (ENC)* (1st ed.). IHO Special Publication S-67, International Hydrographic Organization, Monaco. https://iho.int/uploads/user/pubs/standards/S-67/S-67%20Ed%201.0.0%20Mariners%20Guide%20to%20Accuracy%20of%20Depth%20Information%20in%20an%20ENC_EN.pdf (accessed 1 April 2024).

IHO (2022a). *Guidance to crowdsourced bathymetry* (3rd ed.). IHO Publication B-12, International Hydrographic Organization, Monaco. https://iho.int/uploads/user/pubs/bathy/B_12_CSB-Guidance_Document-Edition_3.0.0_Final.pdf (accessed 1 April 2024).

IHO (2022b). *Standards for Hydrographic Surveys* (6th ed.). IHO Special Publication S-44, International Hydrographic Organization, Monaco. https://iho.int/uploads/user/pubs/standards/s-44/S-44_Edition_6.1.0.pdf (accessed 1 April 2024).

IHO (2024). *Status of Hydrographic Surveying and Charting Worldwide*. IHO Publication C-55, International Hydrographic Organization, Monaco. https://iho.int/uploads/user/pubs/cb/c-55/c55.pdf (accessed 1 April 2024).

Jencks, J., Wyatt, D., Pratellesi, M. and Wills, P. (2021). A Commitment to Crowdsourced Bathymetry Citizen Sourced Data. *The International Hydrographic Review, 26*, pp. 119–126. https://ihr.iho.int/articles/a-commitment-to-crowdsourced-bathymetry-citizen-sourced-data-help-reveal-the-deep-and-share-your-data/ (accessed 1 April 2024).

Klemm, A. R. (2023). Introduction to Crowdsourced Bathymetry: The Power of Community. *Medium*. https://medium.com/@anthony.klemm/introduction-to-crowd-sourced-bathymetry-the-power-of-community-ad941ac20469 (accessed 1 April 2024).

Klemm A. R. and Krabiel T. (2023). *Crowd to Chart: Methods and Applications of Crowdsourced Bathymetry in Support of Safe Navigation*. US Hydro 2023, March 2023, Mobile, Alabama. https://github.com/anthonyklemm/Crowdsourced_Bathy_Processing/blob/main/Klemm_CSB_USHYDRO23.pdf (accessed 1 April 2024).

Masetti, G., Rondeau, M., Jimenez Baron, B., Wills, P., Petersen, Y. M. and Salmia, J. (2020a). *Trusted Crowd-Sourced Bathymetry – From the Trusted Crowd to the Chart*. A whitepaper jointly prepared by Danish Geodata Agency and Canadian Hydrographic Service. https://eng.gst.dk/media/9079/trusted-crowd-sourced-bathymetry-from-the-trusted-crowd-to-the-chart20200621.pdf (accessed 1 April 2024).

Masetti, G., Rondeau, M., Jimenez Baron, B., Wills, P., Petersen, Y. M. and Salmia, J. (2020b). *"Trusted Crowd-Sourced Bathymetry" Project: From the Trusted Crowd to the Chart* [presentation]. 9th Meeting of the IHO Crowdsourced Bathymetry Working Group, Stavanger, Norway, 29 June – 2 July 2020. https://www.researchgate.net/publication/342638911_Trusted_Crowd-Sourced_Bathymetry_Project_From_the_Trusted_Crowd_to_the_Chart (accessed 1 April 2024).

Payne, P. (2023). Crowdsourced bathymetry and its use to support resurvey activity in the North Sea region. *The International Hydrographic Review, 29*(2), pp. 248–253. https://doi.org/10.58440/ihr-29-2-n16

Salaudeen, I. (2023). Assessing CSB data reliability – Estimating vertical uncertainty of sample CSB data by comparing with reference multibeam data. *Journal of Applied Hydrography, 124*, pp. 14–19. https://doi.org/10.23784/HN124-03

https://doi.org/10.58440/ihr-30-1-n03

NOTE / TECHNICAL REPORT

Citizen Hydrospatial Sciences – To csB or not to csB, that is the question!

Authors

Denis Hains[1], Steven Geoffrey Keating[2], Chandana Rathnayake[3], Victoria Obura[4], Shereen Sharma[5] and Stephen Hall[6]

Abstract

Citizen science, where individuals and interested groups of people contribute to scientific research, has been growing significantly. In the hydrospatial realm, covering everything from the water's surface and column, to its depths, to its bottom and its sub-bottom composition and its coastal areas; citizen scientists collect valuable data. This note is using Citizen Hydrospatial Sciences as an overall introduction and context. The note really focuses and dives into the Crowdsourced Bathymetry (CSB) topic challenges and opportunities facing the global hydrographic community. Surprisingly, only about a third of the International Hydrographic Organization's (IHO) Member States (MS) and/or Hydrographic Offices (HOs) have responded to the IHO Secretariat's call for supporting the CSB initiative. Although this constitutes a great achievement and commitment, this raises questions: Why are not more HOs getting involved? Denis Hains discussed this in its Keynote address at the Hydro 2023 Conference in Genoa, Italy, sparking further discussion. This note follows up on Hains' talk, looking more particularly into the CSB data quality and legal concerns worries some HOs seem to have. It is important to indicate, though, that while this note explores these issues, it does not offer legal advice.

Keywords

citizen hydrospatial sciences · crowdsourced bathymetry · hydrographic offices · data quality · legal · risk management · navigation safety

✉ Denis Hains · dhains@h2i.ca

[1] CIDCO (Interdisciplinary Development Centre for Ocean Mapping), Rinouski, QC, Canada

[2] United States Observer to the Advisory Board on the Law of the Sea, United States of America

[3] EGS International Ltd, Bordon, United Kingdom

[4] Hydrospatial Movement Club – African Node, Nairobi, Kenya

[5] Survey & Spatial Consultants, Perth, Australia

[6] SaltwaterSteve Ocean Consultancy, Swansea, United Kingdom

https://doi.org/10.58440/ihr-30-1-n02

1 Introduction

The foundational part of the hydrospatial sciences (Hains et al., 2022) is the science of hydrography, which is defined as the branch of applied sciences which deals with the measurement and description of the physical features of oceans, seas, coastal areas, lakes and rivers, as well as with the prediction of their change over time, for the primary purpose of safety of navigation and in support of all other marine activities, including economic development, security and defence, scientific research, and environmental protection[1]. More than 70 % of our planet is covered by water; we call it – "all the Blue of our Blue Planet and its contiguous zones" (Hains et al., 2022). According to The Nippon Foundation – GEBCO (GEneral Bathymetric Charts of the Oceans[2]), Seabed 2030 Project[3], as of June 2023 only 24.9 % of the oceans have been mapped to adequate modern measurement techniques and standards. "Detailed knowledge of the shape of the seafloor is crucial to humankind. Bathymetry data is critical for safety of navigation and is used for many other applications" (Wölfl et al., 2019). The increase from 6 % in 2016 to 24.9 % in 2023 in data and knowledge since the inception of The Nippon Foundation- GEBCO Seabed 2030 Project is great progress.

However, at this rate, if the future progress is not better than linear, with the traditional means of measuring the bathymetry of our waters by specialized ship-based platforms, the best we could anticipate achieving would be about 50 % of coverage by 2030. While this would still be a positive achievement, it would fall short by about a half of the target for 2030.

So how can we possibly meet this exciting challenge and great opportunity of measuring and mapping our waters by 2030? Citizen Hydrospatial Sciences, Crowdsourced Bathymetry (CSB) and the increased use of new technologies, such as remotely operated underwater, surface and airborne hydrospatial survey vehicles, often called the rise of robotic systems, stand to be an essential part of the solution to fill this gap. Citizen Sciences have proven to be critical in the fields of Ecology and Biodiversity monitoring (e.g., bird-watching and behaviours); as well as in Environmental Monitoring, such as pollution tracking of water and air; Public Health and epidemiology; and Conservation and Habitat restoration.

2 Citizen hydrospatial sciences

With the impacts of climate change becoming more apparent, private citizens are increasingly interested in contributing to solutions by observing, questioning, studying, designing, collecting, analyzing data and communicating their perspectives to applicable stakeholders. (Fig. 1).

Now that the Citizen Science is clarified, we can define the hydrospatial terms associated with Citizen Science in the title of this note, a definition which comes from the Hydrospatial Movement Club and Community's adopted definitions:

- **hydrospatial** – *adjective*
  Relating to hydrospatial sciences or denoting data, information and knowledge that is associated with a particular location and time of the earth's waters and their contiguous zones.

Fig. 1 Citizen Science circular process (Esteban, 2022).

[1] IHO Hydrographic Dictionary (English). http://iho-ohi.net/S32/engView.php?quick_filter=hydrography&quick_filter_operator=Contains (accessed 10 January 2024).

[2] https://www.gebco.net/ (accessed 19 April 2024).

[3] https://seabed2030.org/ (accessed 19 April 2024).

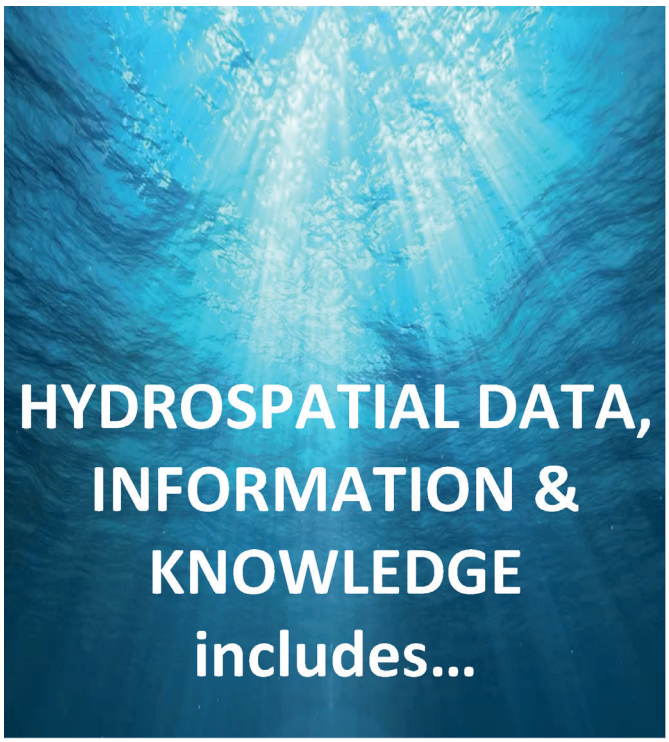

- Hydrography
- Oceanography
- Oceans & Cables
- Water Resources Management
- Fisheries & Marine Habitat
- Marine Protected Areas
- Marine Spatial Areas
- Coastal Zones & Erosion
- Flooding Areas
- Marine Mineral Resources
- Ocean Mapping
- Marine Biology
- Marine Geology
- Marine Geophysics
- Marine Environment
- Marine Ecosystems
- Marine Geography
- Marine Shipping
- Marine Ports
- Marine Pilotage
- Marine Weather & Meteorology

...and much more...

Fig. 2 List of examples of hydrospatial sciences (Hains, 2023).

- **hydrospatial sciences** – *plural-only noun (plurale tantum)*
  All sciences dealing with the study of the earth's waters and their contiguous zones.

The hydrospatial sciences are numerous (Fig. 2). Given the size and the scope of all the hydrospatial sciences, it is unrealistic to consider that traditional measurements with current technologies and limited ship-based approaches will suffice to cover the requirement for data, information and associated knowledge. Like previously perceived unsurmountable challenges, a step-by-step and collaborative approach is needed to achieve the objectives of the United Nations (UN) Decade for Ocean Science & Sustainability as well as Seabed 2030. With limited resources, all Governmental and Non-Governmental Organizations may benefit from willing non-expert unpartisan science groups. This voluntary, citizen help should not be rejected; rather, it should be encouraged and be framed within logical constraints and standards. Citizen Science must be embraced and categorized accordingly to understand the relative value of different data sets and the reliability of the information integrated into common databases.

3 Is crowdsourced bathymetry the same as citizen hydrospatial sciences?

The set of Citizen Hydrospatial Sciences is much broader than CSB. CSB is however a subset of bathymetry, an important contributor to it, and an essential layer for most of the hydrospatial sciences. CSB is defined by the IHO in its publication B-12 as (IHO, 2022):

"[…] the collection and sharing of depth measurements from vessels, using standard navigation instruments, while engaged in routine maritime operations."

From that definition, we can see that the emphasis is on "[…] depth measurements […]", and therefore the logical nexus to bathymetry. The definition also specifies that CSB is "[…] from vessels, […]", so meaning boats and ships using their "[…] standard navigation instruments, […]", a set which includes echosounders and positioning systems. The quality of today's positioning systems and echosounders is continually improving; accordingly, these can offer valuable data for a better knowledge and understanding of bathymetry, particularly in areas with very old, sparse or no existing bathymetric data. The last part of the CSB definition demonstrates that CSB results from vessels "[…] while engaged in routine maritime operations (RMO)" reflecting that the main purpose of the RMO are not systematic surveying (neither hydrographic surveying nor Marine Scientific Research (MSR)) but rather operations such as a passage from one place to another, conducting fishing operations, or eco-tourism. The beauty of CSB is that RMO can produce the collateral benefit of contributing to a bigger cause, i.e., the exponential increase in reported soundings over geolocations that lack sounding data, as well as providing repeat soundings over heavily trafficked channels. The latter may provide change detection, revealing the following: undefined features, newly detected wrecks; and hazardous maritime debris (Sedaghat et al., 2013; Payne, 2013). The benefits contribute to mobile seabed monitoring, increased data availability, cost-effectiveness, timeliness, community engagement, risk mitigation, support for scientific research, complimentary methods, and encouragement to innovation.

https://doi.org/10.58440/ihr-30-1-n02

4 "To csB or not to csB – that is the question…"

Just as William Shakespeare's Hamlet is famous for stating the philosophical question "To be, or not to be, […]" (Act 3, Scene. 1), the global maritime community faces an equally important philosophical question of To csB or Not to csB...to Map the Sea and waters. The idea of leveraging a crowd of stakeholders to collect bathymetric data is not a new phenomenon (IHO, 2020a) – in fact, a GEBCO established Working Group in 1995 made a recommendation that "[…] attempts should be made to get funds from agencies such as the [United States] Defense Mapping Agency to fund echo-sounding on commercial transits" (Carpine-Lancre et al., 2003, p. 127). The former Defense Mapping Agency (now called The National Geospatial-Intelligence Agency) has the legislated mission to "improve the means of safe navigation […] which includes the production and dissemination of nautical charts" (United States Code, 2024). The pressing question today, however, is how this data may be used by the global community of stakeholders, including HOs; how to use CSB was the rationale for the creation of the IHO's Crowdsourced Bathymetry Initiative, which resulted in the creation of the IHO's Crowdsourced Bathymetry Working Group (CSBWG; IHO 2020a).

According to its Terms of Reference, the CSBWG is composed of "…representatives of IHO Member States (MS), invited expert contributors, including members of IHO-IOC (Intergovernmental Oceanographic Commission) Technical Sub Committee on Ocean mapping (TSCOM), and observers from accredited NGIOs (National Geospatial Information Organizations) and the secretarial role of this WG is played by a representative of the IHO Secretariat" (IHO, 2021).

As of the end of 2023, approximately only a third of the MS of the IHO had responded to the International Hydrographic Organization (IHO) Circular Letters (CLs), namely Annex B to IHO CL 11/2019 (IHO, 2019) and to the questionnaire in Enclosure to IHO CL 21/2020 (IHO, 2020b). These IHO-CLs stipulate the support to CSB activities in waters of national jurisdiction as a means to contribute to the IHO Data Centre for Digital Bathymetry (DCDB) for archive and public distribution. From the unofficial communication with MS who have responded unsupportive or with restrictions and also with MS who have not yet responded to the CL, the IHO CSBWG has interpreted and extrapolated some reasons for the hesitance of these HOs to support the free and open sharing of CSB. The list of ten points in Fig. 3 is a starting point, only an assessment that requires further work. While the authors of this note respect all MS and HO perspectives for not yet endorsing the CSB activities at this time, we do offer counterarguments to some or most of the ten items listed below. In this note, the authors will focus only on the item 4 – Data Quality and Accuracy Concerns; and, item 5 – Legal and Liability Issues.

5 Whatever the data source is… "A shoal is a shoal!"

It might be useful to first define the terms precision, accuracy, quality, uncertainty and ambiguity (Heiskanen & Moritz, 1967):

- Precision refers to the degree of exactness or reproducibility of measurements. High precision implies that repeated measurements yield very similar while not necessarily aligned with the true value.
- Accuracy refers to how close a measured value is to the true or accepted value. High accuracy implies that measured values are close to the true values.
- Quality refers to the reliability, accuracy, and consistency of measurements.
- Uncertainty refers to the lack of exact knowledge about the true value due to various sources of errors.

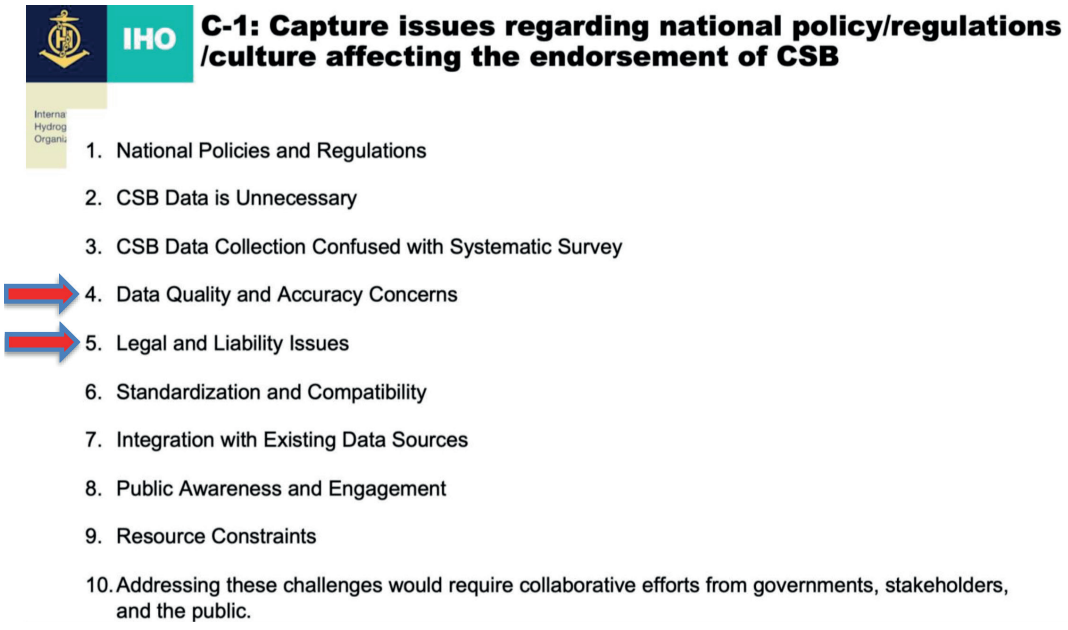

Fig. 3 Issues affecting endorsement of CSB (Hains, 2023).

- Ambiguity arises when there are multiple possible interpretations or solutions to a problem leading to the uncertainty about the correct solution.

Data quality and accuracy are often associated with precision and uncertainty (Fig. 4). The authors argue that regardless of the ambiguity or uncertainty in the data, shallower depths detected in potentially less precise CSB datasets are likely to also be identified in higher precision datasets. This means that all shallower depths and other information provided via CSB should not be disregarded; they could serve as indicators of potential hazards to navigation. The authors suggest that the primary focus, or fundamental purpose of a Hydrographic Office (HO) should be ensuring the safety of navigation by using the best available data. Given the constraints of limited resources and the varying priorities of different HOs, the best data may not always come from the most accurate or precise sources and may sometimes originate from outside the HO itself. Therefore, the use of data from various sources (including CSB) could improve the safety of navigation.

As shown in Figure 4, the aim shall always be to have the highest accuracy and most precise data possible. However, when nothing else is available, and if the data is very old, the lower accuracy and lower precision data might well be the best data available. It is not recommended to discard any data. But it is essential to educate users of the variable uncertainty or ambiguity of data provided. The authors of this note do not agree the premise that an HO is potentially encouraging a mariner to unsafely navigate poorly surveyed waters by using CSB soundings when no other soundings exist. Datasets can and should be categorized and illustrated accordingly, ideally quantified or if necessary rated for its quality. With level of confidence of the datasets published, mariners/navigators can and should assess risk management themselves, the reliability with respect to their own needs, and then mitigate the relative risks. Using CSB soundings on nautical products may further lower the risks for users who would decide to navigate the areas anyway, according to their local knowledge. Ensuring data quality is and will remain a big challenge, but the authors argue that not sharing CSB data is sub-optimal, as it removes potentially relevant information from the set of data inputs a navigator needs to make shipboard decisions for safe navigation. Fundamentally, ultimate responsibility for safe navigation rests with the ship and its navigator. For example, in the Norwegian appellate case following the 2004 grounding of the M/V Rocknes in the Vatlestraumen passage near Bergen, Norway, the Court of Appeal is reported to have stated "responsibility for safe navigation always lies with the ship's captain and navigator, and not with the mapping agency that provides quality-assured nautical charts" (Hydro International, 2011; IMORules, 2024). In the alternative, even if CSB data is not used by the navigator, the IHO recognizes that "While CSB data may not meet the accuracy requirement for charting (Nautical charts) areas of critical under-keel clearance, it holds limitless potential for myriad other uses." (IHO, 2022).

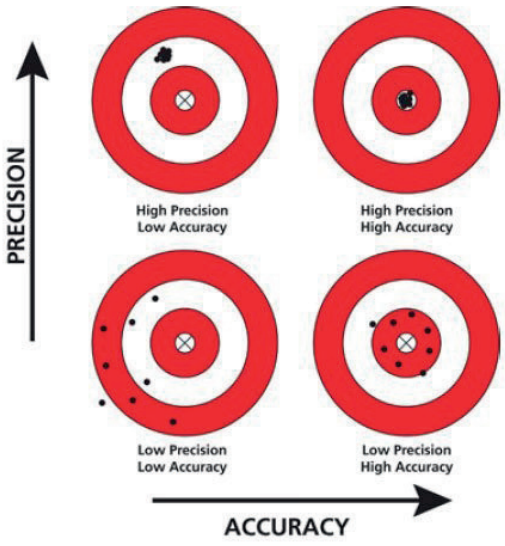

Fig. 4 Accuracy versus precision (Drayer & Ernest, 2017).

Even in cases where highly accurate and precise data exist, depending on the age of this data, the siltation rate of the site or other local regime, it is always possible that debris or hazards could have appeared on the seabed since the last highly accurate survey took place. In that circumstance, a more recent CSB data set might detect a hazard to navigation that might have appeared since, and then bring up the requirement for a temporary navigational warning, or a Notice to Mariner requirement until a new highly accurate survey may take place.

6 Legal and liability issues

While this part of the note will touch upon particular legal issues that HOs may find relevant to the adoption of CSB in official products, this note does not represent legal advice. While the intent of this segment is to offer insights into potential legal determinations, each HO is represented by its respective legal counsel and each HO is responsible for its decisions.

Legal analysis of CSB can fit two categories: (1) at the front end, the legal propriety of CSB data as incidental to safe navigation and being distinct from hydrographic surveying and Marine Scientific Research, and (2), at the back end, the legal ramifications of HO use of CSB in updating official charts or the veto against public availability of CSB via the DCDB. The front end is discussed in detail in recent literature (Keating, 2023, pp. 81–103). this note examines the back end, that is the arguments arising from the perceived or pre-supposed risk of making CSB data publicly available.

6.1 Legal risk

The potential and actual liability of HOs for their official products has been the subject of international litigation. (Obloy & Peruzi, 1995, p. 217). Specific examples include cases where an HO was held not liable for obstructions it had not surveyed and were not part of a chart used as source materials for the

https://doi.org/10.58440/ihr-30-1-n02

U.S. chart and the fault of the collision rested with the vessel. (Empire Transport v. United States, 1974). In another case, the Cunard Corporation brought suit against the United States for not correctly charting a shoal upon which the S.S. Queen Elizabeth II ran aground in the waters near Martha's Vineyard, Massachusetts. In that case, the U.S. appellate court affirmed the lower court's decision that the alleged error to chart the actual depth of the hazard was not the proximate cause of the grounding but rather the unsafe navigation of the vessel was. (Cunard v. United States, 1998). These prior cases reflect the discretion that HOs have in charting hazards, and also indicate that groundings can occur when a hazard has not been charted. (United Cook Inlet Drift Assoc. v. Trinidad Corporation, 1995). More recently, the Norwegian cases involving the M/V Rocknes tragedy demonstrate ongoing, relevance of alleged HO liability and ultimate responsibility of the vessel and navigators. (Hydro International, 2014).

Academics have also commented on the potential and actual liability of HOs in charting. The academic discussions have been vigorous and normally related to how changes in technology (e.g., electronic charts and displays) impact the responsibilities of State HOs and the science of hydrography discussion (Obloy & Peruzzi, 1995; Buhl, 2008; Pogson, 2008; Clark, 2010).

Usually, legal risk indicates potential legal actions against an entity for negligence, i.e., failing to sustain a duty of care under tort law or products liability under contract law (Obloy & Peruzzi, 1995, p. 219; Pogson, 2008; Clark, 2010). A review of fairly recent judicial decisions shows that suits have been brought because an actual hazard had not been plotted on a chart due to an omission or a discretionary choice to not print a feature on a chart (In re Glacier Bay, 1995, p. 1450; Hydro International, 2011). It may be that HOs are concerned that by plotting CSB soundings, that the HO will take ownership of the representation of the reported depth, and that the HO does not want to assume risk on the potential error of a CSB sounding. However, a review of the case law does not indicate that courts hold HOs liable for including additional information that might be informative to the navigator. As is discussed below in Additional Risk Management Options, there may be a way to report a CSB sounding on an official chart in a manner that distinguishes it from an HO certified sounding on its own or as part of an HO-developed methodology and standards. While it is generally accepted that an HO has an intellectual property interest in a chart, as the creative products of the application hydrographic sciences, a reported CSB sounding is a fact that a particular vessel reported a unique depth at a reported geocoordinate, at a specific date-time instance, with reported metadata. All of this information is factual – this does not mean that a reported sounding is exact or without error, but it does provide a baseline of knowledge where any knowledge has heretofore been non-existent. The authors argue that one or an aggregation of CSB soundings is factual data, and as the European Commission has noted, ideas and facts are not covered by copyright, but the expression of them is (European Commission Public Domain News Blog, 2020). See also the European Commission's Open Science and Intellectual Property Rights document which states "When it comes to data and IPR, it could be summarised that data and facts do not have protection under copyright, but databases do." (European Commission, 2022, p. 5). For the sake of argument, even if an HO may have a copyright on the expression of reported CSB soundings, as in a chart, the HO could caveat the presentation with language that CSB soundings have not been verified but are being provided to give the navigator some reported depth, where no depths may have been reported before, and that navigators should operate with caution over such areas. The maritime domain is a dynamic and often unpredictable environment, so risk is inherent in all aspects of maritime operations. Accordingly, it is practically impossible for an HO to operate without legal risk, so HOs must manage risk (Pogson, 2008).

6.2 Risk aversion is not risk management

At present, it appears that various HOs are averse to CSB data being made available by the IHO's DCDB in waters subject to their respective national jurisdictions, because the CSB data has not been rigorously evaluated, in accordance with hydrographic survey standards. In the case of CSB, it would appear that HOs assume that by precluding CSB reported soundings on charts, these HOs would avoid accidents or grounding, making it safer for the mariner, and also reducing liability for the HO from legal action for charting erroneous information. The authors offer a different perspective. In the case of a grounding, where hazard information had been obtained from CSB, and an HO did not use it, the HO may believe that it reduced navigational risk of potentially imprecise data, but in reality, the HO may have increased actual risk for navigators, if the CSB data happens to be the only or most recent data available for a particular area.

Some might claim that using data from a third party, or unknown source might create legal and liability risks. Requirements for validation, and the assessment of the ambiguity, the uncertainty and the quality of data must always be done, to demonstrate duty of care. But still, if a possible hazard to navigation is detected from a CSB data set, and the HO does not assess and take appropriate actions, this may actually increase grounding risk to a ship . For example, in the National Geospatial-Intelligence Agency (NGA) Index to Special Notice to Mariners, para. 23, states: "Mariners will occasionally discover uncharted shoals […] or other dangerous situations that should be made known to other navigators […] those items that can be classified as urgent should be reported by any rapid means to the closest responsible charting authority." (NGA, 2024). As an

example, if a shipowner learned that the HO had access to additional CSB sounding data over an area with no prior recorded soundings in the location of a grounding, but did not integrate it, or make it available with a caution note, that shipowner might bring legal action against the HO, for not making new sounding information (however imprecise) available to the knowledge of mariners. How would a National Hydrographer be viewed in Court, acknowledging that a potential "shoal discovered" in a lower quality CSB data set was not published, because it did not meet the HO survey data quality? While a court might determine that the failure to provide notice was not the proximate cause of the grounding, the decision of the HO may nonetheless be subject to criticism. This is purely speculative, but possible, and the authors consider that not publishing or broadcasting a potential hazard to navigation, constitutes a risk aversion rather than risk management. What must be remembered, is that every case will be reviewed, in accordance with specific facts applied to the law of the applicable jurisdiction. Some jurisdictions recognize sovereign or statutory immunity, or recognize that certain HOs have significant discretion, as to how to chart hazards to navigation.

This notion of risk aversion is even more important in the context of using new technologies, not yet integrated within the hydrographic standards, where clearly the accuracy and precision is not yet as good as bathymetric LiDAR (Light Detection And Ranging), nor Multi Beam Echo Sounder surveys. Detecting a hazard to navigation with CSB or newer satellite-based technology, Satellite-Derived Bathymetry (SDB), and not representing it on official chart, might be considered a risk worth taking for the safety and efficiency of navigation, until higher quality data is available; however, the question remains, as to whether the ship's master or navigators should have access to the broadest range of relevant information to make fully informed decisions, as to the charted course for a vessel? The authors acknowledge the challenges faced by HOs, organizations that have limited resources and may not allow them to fully validate and integrate all the available CSB and new technologies data. Hopefully, with increased automation and Artificial Intelligence (AI) and machine learning (ML), it might be possible to develop algorithms facilitating quality assessment and hazards detection. AI and ML might be useful to run models to analyze the potentially vast amount of CSB data, to determine whether CSB soundings might detect seamounts, or other unreported features. AI and ML could then triage what variances detected by CSB would be worthy of more extensive examination by the HO with responsibility over the zone.

6.3 Other considerations for CSB

CSB also offers the opportunity for change detection, i.e., repeatable sounding reports in highly trafficked areas. For example, if repeated CSB soundings for a specific geographic location remain within a reasonable range, might the sample size of repeated CSB soundings offer the HO some indication of relative accuracy of the CSB data gathered over time? This might be very useful in an area of highly trafficked water, that has either no official sounding at a single position, or where the CSB soundings represent a change from the original charted depth. For example, heavy weather causes containers and other deck cargo to fall off vessels, and would not this change detection be valuable to enhance safety of navigation, if a series of CSB soundings demonstrate a shallowing in the metric range equivalent to the dimensions of a missing container?

The authors recognize the proposition that CSB may not be as precise nor subjected to the rigorous collection standards of a hydrographic survey (Radic et al., 2023), but the abundance of CSB data should not be ignored nor should it be kept from public availability. Proponents for Seabed 2030 and GEBCO seek the broadest public availability for CSB data, because the broader range of CSB stakeholders may be able to develop additional technology and tools, to process the growing set of CSB data. In addition, the quality and affordability of data logging equipment, with GNSS receiver capability is expected to continually improve. (Calder et al., 2020) A prudent mariner is expected to use all available means to navigate the vessel (Mielstrup & Thomas, 2017). CSB can fill voids in a charted area, so why not provide that information to the navigator, who is the ultimate holder of the risk in operating a vessel, with clear metadata documenting the limitation of this data? The sheer volume of CSB data will grow significantly, and this offers a baseline for knowledge, especially in formerly icebound areas, which are now opening up to navigation. The hydrospatial domain is vast, and the CSB data might be critical for outcomes related to the Hydrospatial (Marine Spatial) Data Infrastructure (HDI or MSDI), in addition to improving the means for safe navigation.

6.4 Additional risk management options

The authors suggest that IHO via its existing hierarchical structure of Working Groups, Committees, the Council, and/or the Assembly if needed, continues suporting CSB. The supplemental use of CSB in hydrographic products could be done in the future using distinctive coloration, or providing caveats that the CSB data is pending verification, or clear warning of CSB data, or has not yet been verified by the HO, but that the data was reported by a transiting vessel using standard navigational instrumentation. In this way, CSB may be distinguishable from verified sounding data, and the provision of some data to the navigator is preferable to no data. (Rondeau, 2019)

In the alternative, if national law or a coastal State's HO policy prevents CSB data from being published on the HO's official charts unless it has been verified by the HO in question, then why not allow the IHO-DCDB to make the CSB data available for discovery

https://doi.org/10.58440/ihr-30-1-n02

by the public? First of all, there is inherent value in public availability of CSB, to support the laudable objectives of Seabed 2030 and the U.N. Decade of Ocean Science and Sustainability. Second, and arguably even more important, is the need to make these data available to local and regional communities. Nautical charts are only one form of product, the hydrospatial domain is much broader, and includes also coastal zone modelling, habitat mapping, etc., all of which are also improved upon with CSB data.

The fundamental fact is, one cannot adequately protect what has not been mapped! CSB has demonstrated value to expand our baseline measurements of the ocean bottom (no matter how unrefined). The availability of the increasing body of CSB data can propel technological improvements, to enhance safety of navigation by private enterprise, making additional data sets and presentational software available to navigators, especially in areas where official hydrographic products provide sparse soundings.

7 Conclusion and next steps

The primary purpose of this note is to underscore the significance of incorporating properly validated Citizen Hydrospatial Sciences and particularly the Crowdsourced Bathymetry, into both national and international databases, as well as official products. Such integration contributes substantially to enhancing our understanding, of all the blue of our blue planet and its contiguous zones.

It is crucial to recognize, and document the variable quality, uncertainty, of data, including metadata, originating from Citizen Hydrospatial Sciences and Crowdsourced Bathymetry. To maximize their utility, it is imperative to assess, consider, and transparently represent their value to end-users.

While acknowledging, that challenges may arise concerning the quality and uncertainty of data, and legal and liability issues associated with Crowdsourced Bathymetry, the overall value and importance of these initiatives to the hydrospatial domain are overwhelmingly positive. The suggestion is to consider embracing these contributions for the sake of safer, more efficient and more sustainable navigation and hydrospatial activities.

It is vital to stress once more that the present note does not provide legal guidance, nor conduct a comprehensive quality analysis. Instead, this note offers a high level, professional and policy perspective, on the merits of utilizing Crowdsourced Bathymetry and Citizen Hydrospatial Sciences, leaving and respecting the decision to embrace these methodologies, to the discretion of relevant entities and authorities. The note represents the individual and collective opinions of the authors and does not necessarily represent the opinions or positions of their respective organizations or countries.

References

Calder, B. R., Dijkstra, S. J., Hoy, S., Himschoot, K. and Schofield, A. (2020). A Design for a Trusted Community Bathymetry System. *Marine Geodesy, 43*(4), 327–358. https://doi.org/10.1080/01490419.2020.1718255

Carpine-Lancre, J., Fisher, R., Harper, B., Hunter, P., Jones, M., Kerr, A., Laughton, A., Ritchie, S., Scott, D. and Whitmarsh, M. (2003), *The History of GEBCO, 1903–2003 (1st ed.)*. GITC bv, Lemmer, The Netherlands. https://www.gebco.net/data_and_products/history_of_gebco/ (accessed 9 April 2024).

Clark, P. (2010). *Liability Exposure for Hydrographic Surveyors*. The Wire, Jan. 3, 2010. https://www.itic-insure.com/our-publications/the-wire/liability-exposure-for-hydrographic-surveyors-2607/ (accessed 19 January 2024).

Cunard Line v. United States, 1998 U.S. App. LEXIS 22085 (1988).

Drayer D. and Ernest Z. (2017). *How would you create a sketch illustrating the difference between the terms accuracy and precision in scientific measurement?* https://socratic.org/questions/how-would-you-create-a-sketch-illustrating-the-difference-between-the-terms-accu (accessed 22 April 2024).

Empire Transport v. United States, 524 F.2d 1, 1975 U.S. App. LEXIS 13868 (2nd Cir.1974).

Esteban, R. G. (2022). *Science for all: a visit to the citizen science projects of PRBB centres*. https://ellipse.prbb.org/science-for-all-a-visit-to-the-citizen-science-projects-of-prbb-centres/ (accessed 22 April 2024).

European Commission (2020), *Public domain*. News & Events, European Commission. https://intellectual-property-helpdesk.ec.europa.eu/news-events/news/public-domain-2020-11-19_en. (accessed 21 April 2024).

European Commission (2022). *Open science and intellectual property rights: How can they better interact? State of the art and reflections: Executive summary*. European Commission, Directorate-General for Research and Innovation, Publications Office of the European Union. https://data.europa.eu/doi/10.2777/347305 (accessed 1 September 2022).

Hains, D. (2023). *Citizen Hydrospatial Sciences!* [Conference presentation]. HYDRO 2023 Conference, Genoa, Italy. https://www.italianhydrographicsociety.it/wp-content/uploads/2024/04/Hains_Keynote_Hydro2023-2.pdf (accessed 22 April 2024).

Hains, D., Schiller, L., Ponce, R., Bergmann, M., Cawthra, H. C., Cove, K., Echeverry, P., Gaunavou, L., Kim, S.-P., Lavagnino, A. C., Maschke, J., Mihailov, M. E., Obura, V., Oei, P., Pang, P. Y., Njanaseelan, G. P., Sharma, S. L. (2022). Hydrospatial – update and progress in the definition of this term. *The International Hydrographic Review, 28*, pp. 221–225. https://doi.org/10.58440/ihr-28-n14

Hains D., Mihailov M. E., Obura V., Oei, P. and Maschke J. (2022). *Hydrospatial: it's all about the blue of our blue planet and its contiguous zones*. ECO Magazine, February 17, 2022. https://www.ecomagazine.com/in-depth/hydrospatial-it-s-all-about-the-blue-of-our-blue-planet-and-it-s-contiguous-zones (accessed 22 April 2024).

Hains, D. and Ponce, R. (2023). *Hydrospatial – The Extension of Hydrography*. https://storymaps.arcgis.com/stories/418dde64aff54c41b2d94efffc6ba6c0 (accessed 22 April 2024).

Heiskanen, W. A. and Moritz, H. (1967). Physical geodesy. *Bull. Geodesique, 86*, pp. 491–492. https://doi.org/10.1007/BF02525647

Hydro International (2011). *Rocknes Claims Appeal Dismissed*. https://www.hydro-international.com/content/news/rocknes-claims-appeal-dismissed (accessed 22 April 2024).

IHO (2019). *Call for Approval of Edition 2.0.0 of IHO Publication B-12*. IHO Circular Letter 11/2019. https://legacy.iho.int/mtg_docs/circular_letters/english/2019/CL11_2019_EN_v1.pdf (accessed 22 April 2024).

IHO (2020a). *IHO Crowdsourced Bathymetry Initiative*. https://iho.int/en/iho-crowdsourced-bathymetry-initiative (accessed 22 April 2024).

IHO (2020b). *IHO Crowdsourced Bathymetry (CSB) Data for Public Domain*. IHO Circular Letter 21/2020. https://iho.int/uploads/user/circular_letters/eng_2020/CL21_2020_EN_v1.pdf (accessed 22 April 2024).

IHO (2021). *Crowdsourced Bathymetry Working Group (CSBWG) – Terms of Reference*. https://iho.int/uploads/user/Services%20and%20Standards/TOR/CSBWG_TOR.pdf (accessed 22 April 2024).

IHO (2022). *Guidance to crowdsourced bathymetry (3rd ed.)*. IHO Publication B-12, International Hydrographic Organization, Monaco. https://iho.int/uploads/user/pubs/bathy/B_12_CSB-Guidance_Document-Edition_3.0.0_Final.pdf (accessed 22 April 2024).

IMORules (2024). *Principles to be observed in keeping a navigational watch*. Part 4-1, para. 13. https://www.imorules.com/Chunk531586986.html (accessed 22 April 2024).

Keating, S. G. (2023). Crowdsourced bathymetry and automation: An evolutionary process to improve the means of navigation. In T. M. Johansson, D. Dalaklis, J. E. Fernandez, A. Pastra and M. Lennan (Eds.), *Smart ports and robotic systems: Navigating the waves of techno-regulation and governance*. Palgrave Macmillan.

Meilstrup, M. and Thomas, C. (2017). Instill the Fundamentals of Seamanship and Navigation. *Proceedings Magazine, Vol. 143/8/1,374*, https://www.usni.org/magazines/proceedings/2017/august/instill-fundamentals-seamanship-and-navigation (accessed 9 February 2024).

NGA (2024). *Reporting of Dangers to Navigation* (para. 23, p. 16). Notices to Mariners Special Paragraphs 2024 Edition. National Geospatial-Intelligence Agency, United Stated of America. https://msi.nga.mil/api/publications/download?key=16920954/SFH00000/UNTM/Special_Notice.pdf&type=view (accessed 9 April 2024)

Obloy, E. J. and Perruzzi, J. E. (1995). The Electronic Chart Display and Information System (ECDIS): Is it the "Legal Equivalent of a Paper Chart" and What Potential Liabilities Does its Use Introduce? *J. Mar. L. & Com., 26*, p. 215.

Payne, P. (2023). Crowdsourced bathymetry and its use to support resurvey activity in the North Sea region. *The International Hydrographic Review, 29*(2), 248–253. https://doi.org/10.58440/ihr-29-2-n16

Pogson, K. (2008). Legal Considerations for Hydrographic Authorities: The need for effective risk management strategies, *Hydro International*. https://www.hydro-international.com/content/article/legal-considerations-for-hydrographic-authorities (accessed 22 April 2024).

Radič, T., Pavič, I., Mišković, J. (2023) Comparison of Hydrographic Survey Data with Crowdsourced Bathymetry Data. *International Journal of Maritime Science & Technology, 70*(2), pp. 115–125. https://doi.org/10.17818/NM/2023/2.3

Rondeau, M. (2019). *Bad information is better than no information at all – Assessing the uncertainty of bathymetric collaborative data collected with a HydroBox system* [Conference presentation]. Vecteuer 2019, Rimouski. https://doi.org/10.13140/RG.2.2.34784.10243

Sedaghat, L., Hersey, J. and McGuire, M. P. (2013). Detecting Spatio-Temporal Outliers in Crowdsourced Bathymetry Data. *GEOCROWD '13: Proceedings of the Second ACM SIGSPATIAL International Workshop on Crowdsourced and Volunteered Geographic Information*, pp. 55–62. https://doi.org/10.1145/2534732.2534739

United Cook Inlet Drift Assoc. v. Trinidad Corp. *(In re Glacier Bay), 1995, 71 F.3d 1447, 1995 U.S. App. LEXIS 33288* (9th Cir. 1995).

United States Code, Title 10 Section 442 (2024).

Wölfl, A.-C., Snaith, H., Amirebrahime, S. et al. (2019). Seafloor Mapping – The Challenge of a Truly Global Ocean Bathymetry. *Front. Mar. Sci., 6*. https://doi.org/10.3389/fmars.2019.00283

NOTE / TECHNICAL REPORT

Science Monitoring And Reliable Technology (SMART) to monitor the ocean using submarine cables

Author
Matías Sifón[1]

Abstract
The Ocean is a fundamental part of life on Earth and therefore its observation is essential; however, there are currently no seabed monitoring networks that cover large areas. The Science Monitoring and Reliable Telecommunications (SMART) Cables initiative aims to combine the growing telecommunications industry with ocean sciences, leveraging the infrastructure of the former to deploy sensors to obtain essential ocean data on the seafloor in real time.

Keywords
SMART · cables · telecommunications · ocean · monitoring

The ocean covers almost 70 % of our planet. It is responsible for approximately 50 % of the oxygen we breathe, makes all life on our planet possible, and is also responsible for making the Earth look blue when viewed from space. The ocean plays a fundamental role in regulating the climate. It produces most of the water vapour, which condenses and creates clouds, which is then released as precipitation.

Better knowledge of the ocean is essential to understanding the various threats facing society, including: climate change, sea level rise, global warming, tsunamis, and earthquakes. Deep ocean seafloor observation could improve tsunami monitoring and climate change causes and effects, like sea level rise. For example, a better understanding of deep ocean circulation and sea level rise could improve the complexity and accuracy of models of ocean-atmosphere interaction which contribute to our understanding of global climate.

Despite the potential benefits, the deep ocean floor remains poorly observed and monitored. Given the size of the ocean, its exploration is difficult and expensive. For example, to detect and monitor tsunamis, the most commonly deployed method is the use of Deep-ocean Assessment and Reporting of Tsunami (DART) buoys to measure pressure; however, the buoys are mostly placed near the coasts of the countries that control them due to high operating costs.

The Global Ocean Observing System (GOOS) has defined temperature and pressure as two of the Essential Ocean Variables (EOV's) to effectively provide oceanographic forecasts and early warning, climate projections and assessments. These variables are currently being monitored mainly *in situ*, by boats, buoys, anchoring systems or floats, and by remote sensing, such as the various existing satellite techniques for both information acquisition and processing.

Submarine cables are critical to the provision of commercial internet, and are the main means of data transmission globally (Fig. 1). There are more than 1 million km of operational submarine telecommunications cables (Howe et al., 2022), though the number of existing cables and their distribution is not even. There exists a clear difference between the northern and southern hemispheres, leaving an important area without cable coverage in the South Pacific.

The Science Monitoring and Reliable Telecommunications (SMART) Cables initiative (SMART Cables, 2024) could improve the rate of acquisition of seabed data (i.e. pressure, temperature

✉ Matías Sifón · msifon@shoa.cl
[1] Hydrographic and Oceanographic Service of the Chilean Navy (SHOA), Chile

https://doi.org/10.58440/ihr-30-1-n01

and acceleration mainly) by integrating sensors that measure various ocean variables using the infrastructure of submarine telecommunications cables. These cables could potentially be the most extensive and cost-effective system for achieving such measurements (Howe et al., 2022). The Humboldt transoceanic cable project that would connect Sydney, Australia with Valparaiso, Chile seeks to improve coverage of telecommunications cables in this region and presents an opportunity to deploy SMART cables as well.

The idea of taking advantage of the efforts of the submarine telecommunications cable industry to measure essential ocean variables is a promising solution to obtain information from large areas in real time, while having a minimal impact on both the environment and the telecommunications industry. Since the telecommunications cable will be deployed, the infrastructure needed to install the sensors and transmit the data is already in place, leaving as the principal challenges the achievement of minimal environmental impact and the engineering of the sensors to ensure maintenance-free operation for the lifespan of the cable. This configuration would lead to economic savings due to the high cost of deploying both systems independently.

By using the infrastructure of submarine cables, it is possible to monitor hard-to-reach places very efficiently, especially considering that there are already dedicated submarine cables for scientific research, so their integration with telecommunications cables should not be complex. The ideal result would be for the cables represented by lines in Fig. 1 to have SMART repeaters every 70 km, which would allow for a virtually global monitoring network of the ocean floor. Obviously, the separation between each SMART repeater can vary depending on the reality of each project, also considering the challenge of processing the information acquired through these systems.

Sensors would be installed on SMART repeaters, defined by Howe et al. (2019), that can theoretically measure as many variables as desired; however, for this exercise, temperature and pressure sensors have been chosen, in conjunction with accelerometers (a possible configuration of SMART repeaters and their sensors is shown in Fig. 2). It should be noted that, due to the nature of the parameters to be measured, both the pressure and temperature sensors must be in direct contact with the environment, while the accelerometer can be inside the housing.

In this design, the data generated by the sensors is transmitted through the same telecommunications network and uses the network's infrastructure for power supply. Installation and maintenance efforts being matched with those of cables and the potential for rich data collection already represent significant advantages, but there are also other benefits to consider. Since the sensors are on the seabed, the possibility of vandalism of the instruments is drastically reduced, mitigating one of the problems that maintainers of other observing systems such as buoys or ground stations must deal with, as well as intermittency in transmissions, whether these are due to power supply problems or the transmission method itself (satellite, cellular network, etc.).

Inaccessibility also poses a challenge in terms of engineering since sensors must be able to function maintenance-free for the lifespan of the cables, which is around 25 years. Currently, most oceanographic sensors operate with regular maintenance, so the design of both the SMART sensors (pressure, temperature and accelerometers) and the repeaters must be durable. Among other issues, the best way to deal with biofouling and also to prevent interference with

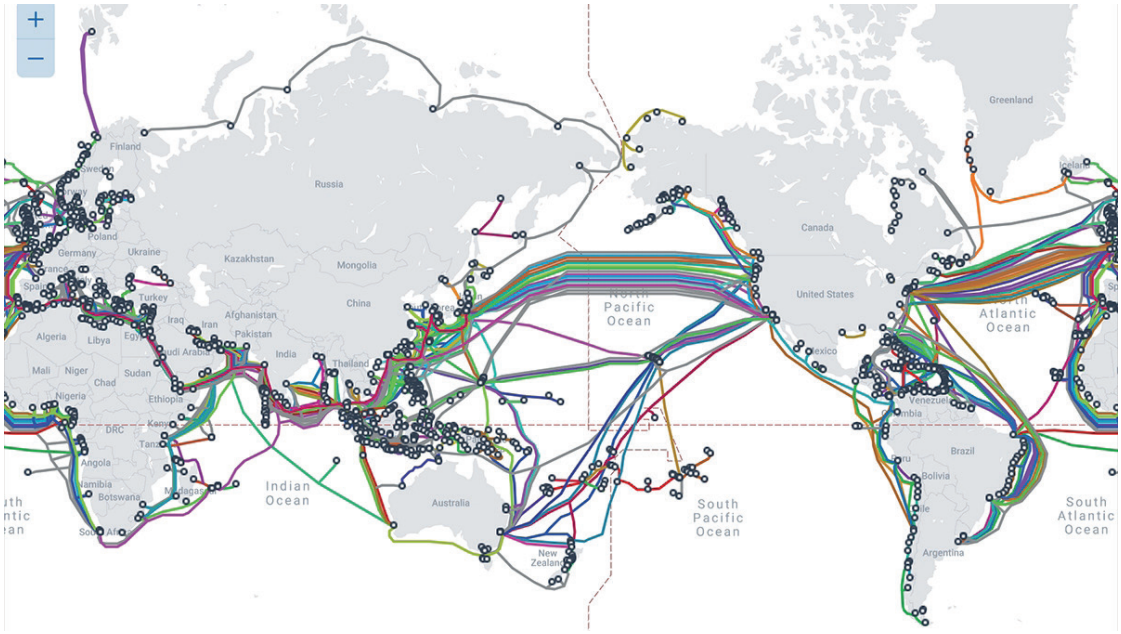

Fig. 1 Global distribution of submarine cables (Bischof et al., 2018): The coloured lines represent the wires and circles, the points where a wire has a connection to some point on a continent.

the adjoining telecommunications systems is still a matter of study.

Overcoming the challenges to develop a robust seafloor monitoring network is important because these networks of sensors can greatly improve our understanding of climate. For example, deep Antarctic waters are known to be warming due to the constant absorption of heat, contributing to sea level rise. In addition, the South Atlantic circulation is changing, which is associated with variations in ocean temperature, heat flux at the ocean-atmosphere interface, and sea level, suggesting that deep circulation is a relevant element in the global climate. Thus, the temperature sensors of the SMART cables would provide data with a greater spatial and temporal density in the deep ocean and in real time than current techniques allow, with which we could better understand these phenomena, helping to understand their implications for the planet and the society.

Variations in sea level can impact coastal communities and various marine species. Even in terms of international policy, sea level rise could affect the boundaries established between countries and some islands countries could see the surface of their territory reduced considerably. Global warming has caused sea level rise to occur on average at rates of 3.0 ± 0.4 mm/year since 1992, with an estimated acceleration of 0.084 ± 0.025 mm/year^2, implying that, if these values were maintained, sea level would have risen by 65 cm by the year 2100 (Howe et al., 2022), However, this change is not homogeneous mainly due to the effects of changes in mass resulting from the melting of ice, expansion of water due to warming, changes in ocean volume, changes in land heights, etc., so measurement techniques with broad spatial coverage and sensors that measure pressure and temperature are required to contribute to the study of the particular contributions in each place.

Wind waves, with periods of less than 30 s, play a crucial role in the exchange of heat and gases between the ocean and the atmosphere and can be a threat to coastal areas. Due to their wavelength, which in deep waters are always much smaller than depth, they cannot be measured from the seabed at more than 1000 m, so satellites and floating buoys are used. However, the need for the observation of these waves in the vicinity of the coast and in real time is increasing, so the SMART sensors on the continental shelf and areas near the coast constitute a valuable alternative that could provide information on wave amplitude, period and even direction (Howe et al., 2019).

Another relevant point is the monitoring of tsunamis, oceanographic waves with periods considerably longer than the wind waves described in the previous paragraph, which is done by measuring pressure variations from the seabed mainly using DART technology developed by NOAA. The DART technology allows for discrete measurement in real time, with high support and maintenance costs, requiring installations to be close to the coast. The information is transmitted by means of satellite systems through a buoy, while the sensor installed on the seabed has electrical power systems through batteries, which require frequent renewal. To avoid unnecessary use of the batteries, consumption is reduced through few transmissions per day, which increase their frequency if activated as a result of the occurrence of an earthquake or tsunami. Despite its limitations, the DART system is currently considered one of the best alternatives for real-time tsunami monitoring in the deep ocean, which allows the generation of tsunami propagation models for both early warning and scientific research. To maintain its concept of operability for tsunami hazard risk management, however, monitoring frequency must be sacrificed.

Tsunami observation in open waters through direct data is important because their geophysical characteristics give these waves the ability to cross the ocean and affect coasts that are thousands of kilometres from their place of origin, causing great damage. Timely alerting of coastal communities is therefore essential. However, it is important to be able to determine whether a tsunami will truly affect

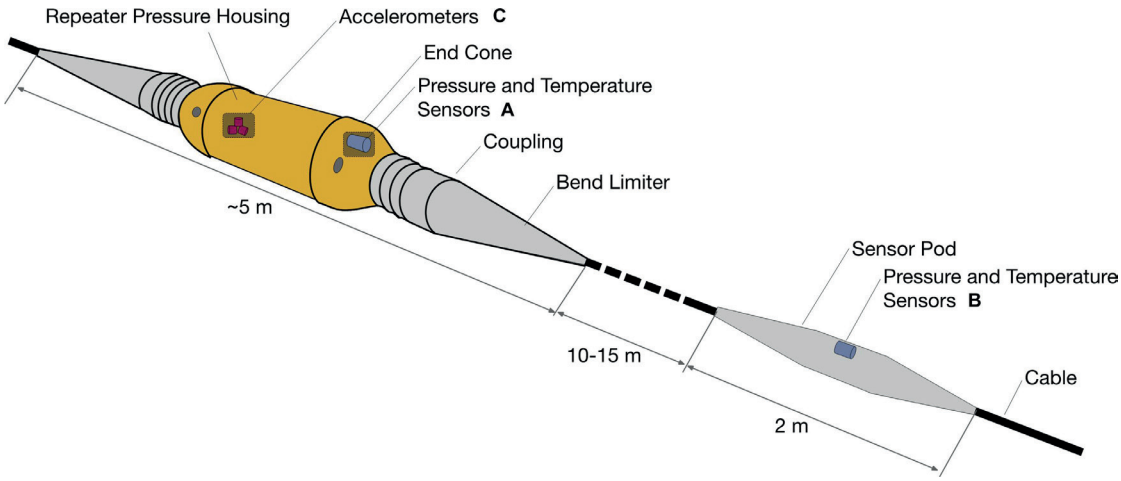

Fig. 2 Illustration of a SMART repeater housing showing possible configurations (Howe et al., 2019): (A) at the end of the repeater housing under the bell, (B) in an outer sheath. (C) The accelerometers are mounted inside the pressure housing.

https://doi.org/10.58440/ihr-30-1-n01

a particular community, preventing an unnecessary evacuation, which comes at a high cost (economic, credibility, community effort, possible accidents during the evacuation process, etc.).

Computational modelling is used by early warning systems to estimate the generation and propagation of tsunamis generated by subduction mega earthquakes (Maule, 2010; Tohoku-Oki, 2011; Valdivia, 1960). These models allow us to estimate effectively the possible impact of this type of tsunami, which can take several hours to reach distant coasts. Robust monitoring of the propagation of a tsunami in deep waters allows for the corroboration of computational models.

For tsunamis generated by sources other than subduction mega earthquakes, like the tsunami resulting from the eruption of the Hunga-Tonga Hunga-Ha'apai volcano in January 2022, there are no computer models that are able to estimate the tsunami threat to carry out a timely evacuation. This is mainly due to the complexity of the source of tsunami generation (Fig. 3), which for this case and many others, cannot be determined in useful times for early warning, so monitoring the spread of the tsunami is essential to alert coastal communities. Although DART buoys are an excellent tool, as they are installed close to the coast, they are not enough, and there are blind areas, such as in the South Pacific Ocean (Fig. 4).

In the case of seismicity, as with the other variables, there are also blind spots to cover. The cost of installing underwater seismological instrumentation is very high, so most of the instruments are on land, which complicates analyses. Currently in Chile, for example, seismic monitoring is practical only in a north-south direction, due to the geomorphology and orientation of the territory, complicating the determination of some earthquake parameters. In the South Pacific, there are few sensors toward the centre of the ocean. If accelerometers were to be installed on submarine cables, the study of seismicity would be enhanced both in science and in early warning systems, as well as for engineering studies, directly benefiting mainly coastal communities.

One way to improve the seismological network would be via the implementation of SMART Cables with accelerometer sensors, although, at present, there is no submarine cable that crosses the South Pacific Ocean. However, the Humboldt telecommunications project mentioned above, which aims to link Australia, New Zealand and Chile by means of fibre optic cables (Fig. 5), not only covers that blind space, but also crosses four major tectonic plates, which would allow for a very powerful study of seismicity and provide a direct contribution to the early warning of earthquakes and tsunamis.

While there are many benefits to be gained from SMART technology, the Joint Task Force (JTF) has decided to use it primarily to address two issues: (1) the permanent acquisition of data to evaluate phenomena associated with climate change and (2) to contribute to the sea level monitoring network to enhance tsunami early warning systems, through temperature and pressure sensors, in conjunction with accelerometers. JTF SMART Cables is an initiative led primarily by three United Nations agencies: the International Telecommunication Union (ITU), the World Meteorological Organization (WMO) and the Intergovernmental Oceanographic Commission (IOC/UNESCO).

Currently, there are different projects that are in the process of analysis with SMART cables, the most notable being the one that will link New Caledonia with Vanuatu and the one in Portugal, which will link Lisbon, Madeira and Azores. These two projects have funding for the implementation of this technology and are expected to be the first to come into operation. The first of these will have an extension of about 300 km, with between two and four SMART repeaters, while the second will be 3,700 km, with 50 repeaters. Other projects that are expected in the future to include SMART repeaters are the aforementioned Humboldt project, as well as the one that will link New Zealand with Antarctica and Australia with Antarctica.

The implementation of SMART technology would substantially improve our understanding of the ocean and some geophysical processes such as ocean temperature, ocean circulation, sea level rises, tides, currents, tsunami and seismic, enhancing engineering, early warning systems, climate change mitigation measures and more.

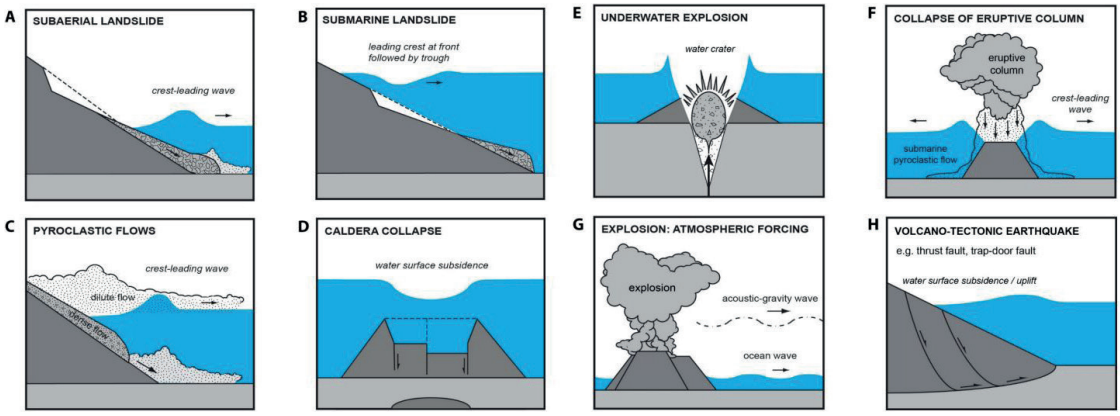

Fig. 3 Different possible mechanisms of tsunami generation from a volcanic eruption (Schidell, 2023).

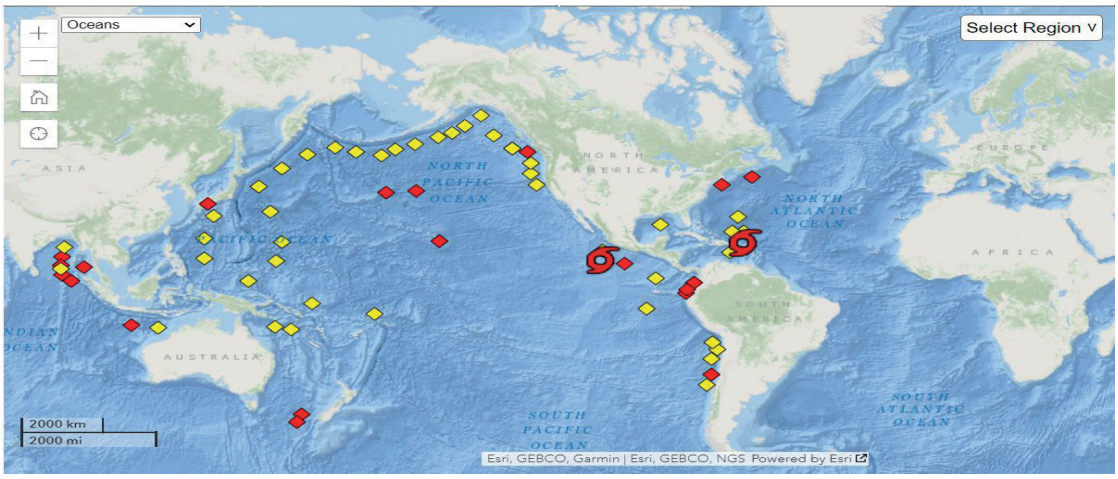

Fig. 4 Tsunami monitoring network using DART buoys[1] : Yellow markers indicate DART buoys that are operational, while red buoys indicate non-operational buoys. The circular red symbols indicate storms under monitoring (at the time of capture). This online monitoring system is maintained by the U.S. National Buoy Data Center (NDBC).

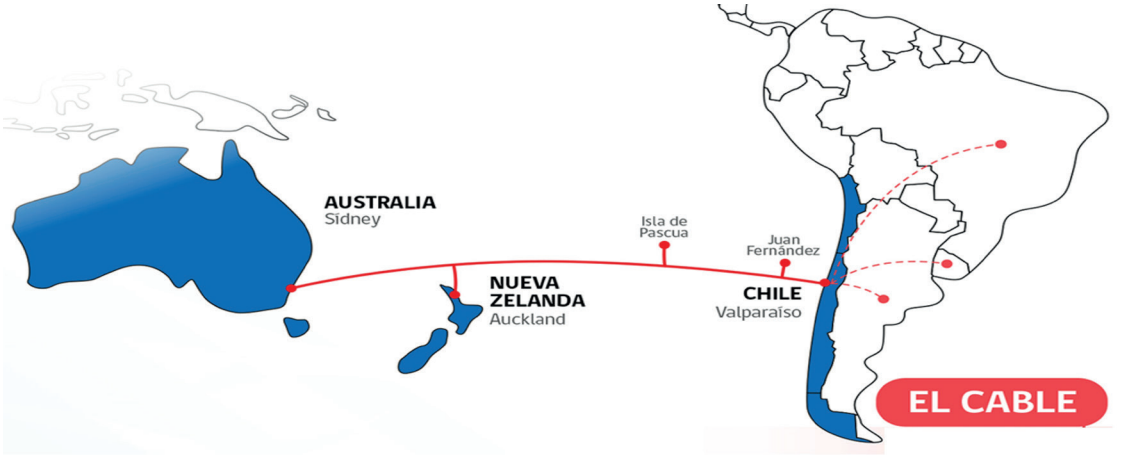

Fig. 5 Illustration of the route of the submarine telecommunications cable belonging to the Humboldt project (final route yet to be defined). The image corresponds to an excerpt from the infographic that can be found on the project's website[2].

In this way, SMART Cables combines two key concepts in today's society: the increase in pressure to achieve greater global connectivity and the urgent need to coherently address climate change and ocean management, achieving a synergy widely discussed today under the concepts of Blue Economy and Ocean Discovery, as well as by the United Nations Sustainable Development Goals. The telecommunications industry will continue to install submarine cables, so the question is, what if we take advantage of that infrastructure to do science for the direct benefit of the planet and society? How would it improve our understanding of the planet?

References

Bischof, Z. S., Fontugne, R. and Bustamante, F. E. (2018). Untangling the world-wide mesh of undersea cables. *Proceedings of the 17th ACM Workshop on Hot Topics in Networks (HotNets '18)*, Association for Computing Machinery, New York, NY, USA, pp. 78–84. https://doi.org/10.1145/3286062.3286074

Howe, B. M., Arbic, B. K., Aucan, J., Barnes, C.R., Bayliff, N., Becker, N., Butler, R., Doyle, L., Elipot, S., Johnson, G. C., Landerer, F., Lentz, S., Luther, D. S., Müller, M., Mariano, J., Panayotou, K., Rowe, C., Ota, H., Song, Y. T., Thomas, M., Thomas, P. N., Thompson, P., Tilmann, F., Weber, T. and Weinstein, S. (2019). SMART Cables for Observing the Global Ocean: Science and Implementation. *Front. Mar. Sci., 6*:424. https://doi.org/10.3389/fmars.2019.00424

Howe, B. M., Angove, M., Aucan, J., Barnes, C. R., Barros, J. S., Bayliff, N., Becker, N. C., Carrilho, F., Fouch, M. J., Fry, B., Jamelot, A., Janiszewski, H., Kong, L. S. L., Lentz, S., Luther, D. S., Marinaro, G., Matias, L. M., Rowe, C. A., Sakya, A. E., Salaree, A., Thiele, T., Tilmann, F. J., von Hillebrandt-Andrade, C., Wallace, L., Weinstein, S. and Wilcock, W. (2022). SMART Subsea Cables for Observing the Earth and Ocean,

[1] https://www.ndbc.noaa.gov/ (accessed 3 October 2023).

[2] https://www.subtel.gob.cl/cable-humboldt/ (accessed 1 October 2023).

https://doi.org/10.58440/ihr-30-1-n01

Mitigating Environmental Hazards, and Supporting the Blue Economy. *Front. Earth Sci., 9*:775544. https://doi.org/10.3389/feart.2021.775544

Schindelé, F. (2023). *Tsunami Generated by Volcanoes (TGV), IOC Report (Feb 2023)*. 8th Joint ICG/PTWS – IUGG JTC Technical Workshop, 11th September 2023, Nuku'alofa, Tonga. https://oceanexpert.org/downloadFile/54669 (accessed 18 February 2024).

SMART Cables (2024). SMART Systems – Launched, SMART Cables. https://www.smartcables.org/ (accessed 31 March 2024).

NOTE / TECHNICAL REPORT

Shared waters, same standards – The Baltic Sea e-Nav project: A partnership for the future of marine navigation

Authors

Benjamin Hell[1], Magnus Wallhagen[1], Patrick Westfeld[2], Sophie Hohwü-Christensen[3], Rainer Mustaniemi[4], Antti Värre[5] and James Harper[6]

Abstract

In order to deploy the first layers of S-100 based navigation products in the Baltic Sea, and do so in a regionally harmonized manner, the Hydrographic Offices involved are partnering with academia and industry in the Baltic Sea e-Nav project. To unlock the full potential of the S-100 paradigm shift towards e-navigation, there is a need for transnational collaboration to build capacity and ensure seamless, harmonized products. In addition, the project will test S-100 products from an end-user perspective to ensure the most relevant and useable navigation data possible. The recently started project will continue until 2026 and is co-financed by the EU Interreg Baltic Sea Region programme.

Keywords

S-100 · Baltic Sea · ECDIS · international collaboration · EU project

1 Introduction

During the past decades, the countries around the Baltic Sea have cooperated in the process of conducting modern hydrographic surveys of the main shipping areas of this highly navigated region, to obtain detailed, quality assured hydrographic data. By using the Baltic Sea as a testbed, surrounding countries will now take the next step towards the development of navigation in the Baltic Sea and implement the next generation of navigational products based on the new S-100 standard, developed by the International Hydrographic Organisation (IHO). The International Maritime Organization (IMO) has agreed to require S-100 compliance in the IMO ECDIS Performance Standards (IMO, 2022) for the next generation of vessel navigation systems and has defined S-100 as the underlying data model for e-navigation (IMO, 2018).

Introducing these machine-readable products and services is a major step towards digitalized and more automated sea traffic. Electronic Navigational Charts (ENC) compliant with the new S-101 product specification will be the new base layer in the next generation of S-100 compatible navigation systems. Combining these ENCs with other S-100 products will make it possible to calculate more precise under keel margins, and give the navigators a better situational awareness of the navigable waters around them. Depth contours, currently portrayed at static depth intervals, will be able to be generated from more detailed and dynamic information, and consequently provide the navigators with

✉ Benjamin Hell · benjamin.hell@sjofartsverket.se

[1] Swedish Maritime Administration, 60178 Norrköping, Sweden

[2] German Federal Maritime and Hydrographic Agency, Nautical Hydrography, 18057 Rostock, Germany

[3] Danish Geodata Agency, 9400 Nørresundby, Denmark

[4] Finnish Transport and Communications Agency Traficom, 00520 Helsinki, Finland

[5] Satakunta University of Applied Sciences, 28130 Pori, Finland

[6] IC-ENC, TA1 2DN Taunton, United Kingdom

https://doi.org/10.58440/ihr-30-1-n04

more relevant and precise "go and no-go areas".

Expected benefits are increased safety for both people and environment, new opportunities for vessels to optimize their routes and cargo loading, and thereby more eco-efficient solutions for shipping. The new S-100 products also address the increasing cyber security threats by raising data protection in navigation systems to current standards and best practice. Additionally, S-100 will be a major step towards automated navigation and autonomous shipping as the data becomes more machine readable.

For the Baltic Sea e-Nav project, the goal is – by the end of the project in 2026 – to achieve significant and regionally harmonised S-100 compliant product coverage of the Baltic Sea with commercial ENC (S-101), detailed bathymetry data along important shipping routes (S-102), and prototype water level and current services (S-104 and S-111).

2 The challenges to implement S-100 products in the Baltic Sea

While there have been various testbed projects for S-100 products, on-going or finished (e.g. CHS, 2018; UKHO, 2022; Jang et al., 2023), that investigate different aspects of the S-100 potential, the Baltic Sea e-Nav project is probably the foremost project looking at S-100 from a truly multinational perspective: How do S-100 data producers need to collaborate across borders, to ensure that the end users can navigate with the help of seamlessly harmonized data products? How should one manage the S-100 product rollout in an area where most vessel voyages stretch across the areas of responsibility of several coastal states? And how can the data producers' varied, shared expertise be leveraged for an efficient, collaborative transition to the S-100 world?

To trigger market adoption of S-100 products and S-100 compatible end user systems, especially for the highly regulated market segment of Electronic Chart Display and Information Systems (ECDIS), sufficient and relevant S-100 product availability is a key factor. The challenge to upgrade ECDIS on-board existing vessels to S-100 compatible systems requires that S-100 products provide a significant added benefit for the navigators. Probably ENC alone, even in S-101 format, will not be enough to justify the investment in new bridge systems. Still, coverage with S-101 products being the ENC base layer are needed to enable the use of other products, such as more detailed S-102 gridded bathymetry. Consequently, the hydrographic offices need to produce and update S-101 ENCs with at least the same informational content and up-to-datedness as the corresponding legacy S-57 ENCs, which also need to be maintained in the product portfolios.

This increased product portfolio complexity, together with the challenge to implement entirely new products for navigation, such as S-102 gridded detailed bathymetry products or S-104 and S-111 oceanographic services, is a major challenge for the data producers in making the transition to S-100. The technical capacity and production readiness for S-100 varies between the different Baltic Sea countries. Therefore, the common Baltic Sea e-Nav project for S-100 implementation is also a platform for sharing experience and capacity building, which will streamline the rather rapid rollout of S-100 products until the agreed upon transition period for ECDIS between 2026 and 2029.

The degree of maturity for the development of data according to the new standards is different in different Baltic Sea countries. Testing of the new standards against relevant use cases is essential at this phase of S-100 implementation. The project will utilize the Baltic Sea as a testbed for this, to test, analyse and refine the new navigational products. The results will be spread to all relevant actors in the Baltic Sea Region, and also beyond through the regular international collaboration within the IHO.

Finally, in an area such as the geographically confined Baltic Sea which is highly used for ship traffic, it is vital for the navigators' decision making that the navigation products they use are harmonised across borders and well-adopted to the particular regional conditions. A patchwork of differing national interpretations of S-100 based product specifications could otherwise lead to a worsened user experience and thereby potentially decreased navigational safety.

Therefore, the Baltic Sea Hydrographic Commission (BSHC) has decided that S-100 products in the region should be as harmonised as possible regarding criteria such as information content, coverage, spatial resolution and availability. For this purpose, the Baltic Sea e-Nav project will coordinate the development of common guidelines for S-100 data producers, to be adopted by the BSHC for application in the Baltic Sea region.

3 The project partnership

The project consortium consists of several building blocks, which together comprise the full value chain from product development through distribution of navigation data to the potential end consumers (Fig. 1).

Firstly, the core of the partnership are data producers in the form of all Baltic Sea coastal EU member states' respective hydrographic offices, with full partners from Denmark, Estonia, Finland, Germany, Latvia and Sweden, as well as associated partners from Lithuania and Poland. Together they form the majority of the BSHC. Furthermore, the partnership includes the Finnish Meteorological Institute as one of the relevant national meteorological and oceanographic agencies, which are important partners for the oceanographic S-100 products for navigation (water level and surface currents).

Secondly, two applied research institutes in the field of shipping technology, RISE Research Institutes of Sweden and the Finnish Satakunta University of Applied Sciences, will lead the testing activities and help the data producers with structured development and refinement of their products.

Thirdly, the navigation system manufacturing company FURUNO Finland will supply the project with the

https://doi.org/10.58440/ihr-30-1-n04

needed S-100 navigation system technology and further insight from their close relation to the end users of navigation data products.

Finally, the two ENC distribution hubs PRIMAR and IC-ENC will, as associated partners, support the project in aspects related to the S-100 product distribution chain.

Most of the project partners have a long record of productive collaboration, both in various projects but also as members of the BSHC.

4 The scope and expected outputs of the project

4.1 A harmonized Baltic Sea e-Nav base package

The Baltic Sea e-Nav project will achieve two specific outputs: Firstly, the rollout of a number of commercial S-100 based products with significant coverage in the Baltic Sea, the "Baltic Sea e-Nav base package". Secondly, the project will develop detailed product harmonisation guidelines for the data producers in the Baltic Sea region.

The primary goal of the project is to introduce significant coverage of relevant S-100 products in a regionally coordinated manner, both with regard to the timing, the geographic coverage and also the informational content of the products.

In order to ensure a seamless user experience when navigating with products from different producers, but also to make capacity building and international collaboration easier, the project will develop concrete product harmonisation guidelines for data producers. This will be done in liaison with the BSHC and its relevant working groups, so that the BSHC eventually will formally adopt the guidelines. Similar cross-border harmonisation guidelines already exist for (legacy) S-57 ENC in the Baltic Sea, which even have been re-used as examples in other regions in the World.

4.2 Focus on four important S-100 products

The project will develop a set of four different S-100 based product lines: ENC and bathymetry products, as well as water level and surface currents services.

For ENCs, by the end of the project there will be full coverage of the major shipping routes in the Baltic Sea with S-101 ENC, with usage bands and

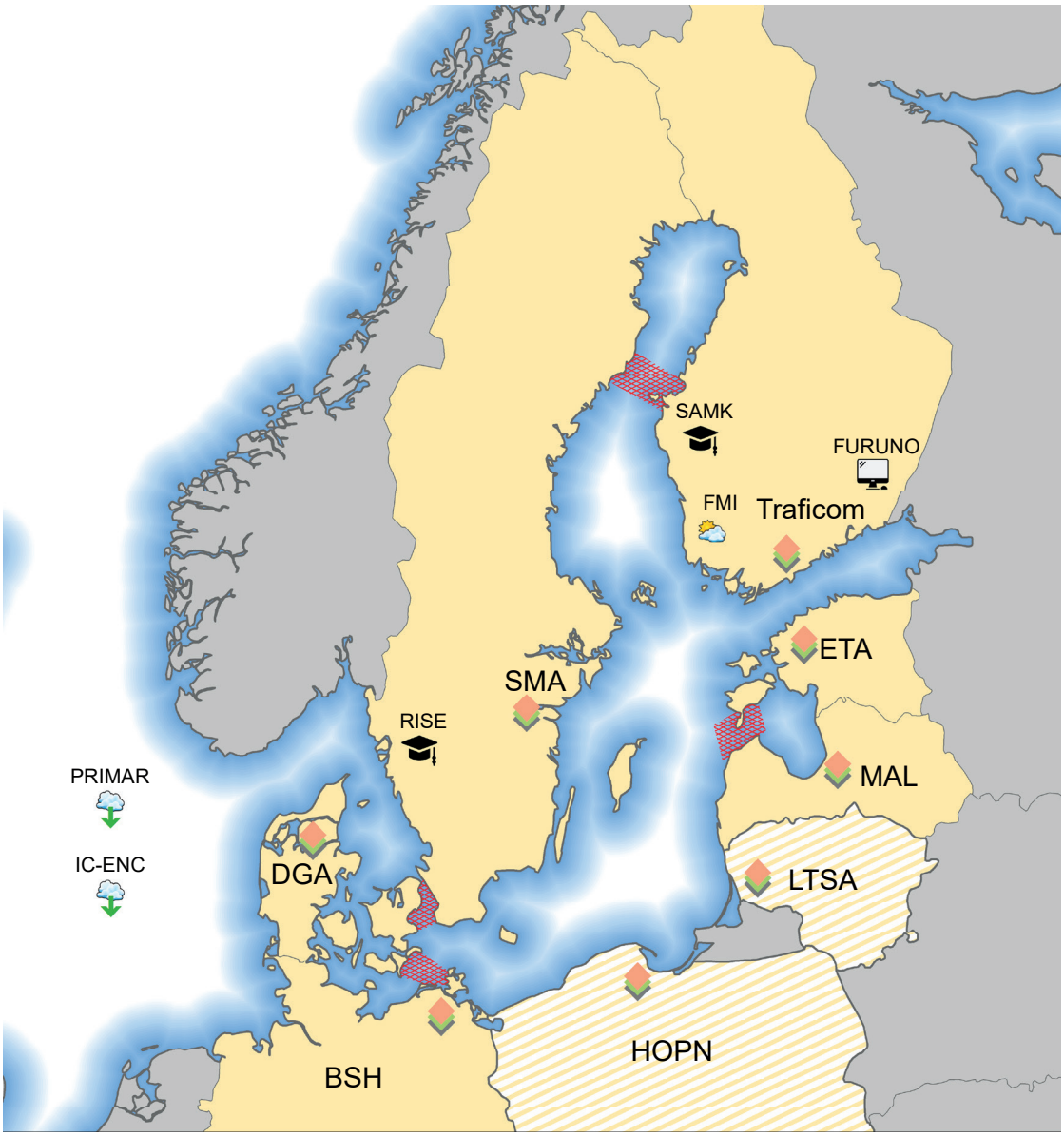

Fig. 1 The partnership of the Baltic Sea e-Nav project covers (almost) the entire area of the Baltic Sea, with partners being the Hydrographic Offices of Denmark, Estonia, Finland, Germany, Latvia, Lithuania (associated), Poland (associated) and Sweden, as well as the Finnish Meteorological Institute (FMI), Satakunta University of Applied Sciences (SAMK), RISE Research Institutes of Sweden, Furuno Finland and the associated partners PRIMAR and IC-ENC. The initial testing of S-100 products will be carried out in cross-border areas with some level of navigational challenges (red).

https://doi.org/10.58440/ihr-30-1-n04

geographic coverage equivalent to present S-57 ENCs.

Additionally, in relevant shipping areas, which are surveyed to modern standards, S-102 bathymetry products will become available for navigation. The S-102 coverage will likely vary depending on individual countries' specific conditions, and the informational content of these entirely new products is still being worked on.

Overview services for the oceanographic products S-104 water level and S-111 sea surface currents will probably cover mainly the Finnish areas of the Baltic Sea, and may still be prototypes at the end of the project. But the project will contribute to a solid understanding of what would be required to fully operationalize S-104 and S-111 services for navigation, covering the entire Baltic Sea.

4.3 Prototyping, testing and upscaling

The work in the project will be carried out in three phases, beginning with product prototyping, which is followed by testing and refinement before the final upscaling of the production for rollout.

In the beginning, product prototypes are being developed at the same time as testbeds are prepared. This includes the development of a navigation system prototype to be used in the existing bridge simulators that several partners own. Furthermore, based on a number of criteria, suitable geographic areas for product testing are being defined and particular navigation scenarios are being translated into testbed protocols.

In the second phase, product testing and refinement are being carried out iteratively. The bridge simulator tests will be conducted in virtual versions of real-world locations (Fig. 1) and relevant navigation scenarios, in order to bring a realistic end user perspective into the tests. Based on test findings, the S-100 products and harmonisation guidelines will be refined and tested again.

In parallel, the third phase of the project will be initialized by the data producers who need to upgrade their production workflows for the new products. As soon as the products are tested and defined, the data producers will start with the production of the Baltic Sea e-Nav base package.

According to plan, there will be a significant amount of relevant S-100 products available in the Baltic Sea when the first commercial end user systems in the form of S-100 ECDIS hit the market in 2026.

Acknowledgement

The Baltic Sea e-Nav project is co-funded by the European Union Interreg Baltic Sea Region programme, priority 2 (water-smart societies) objective 2.2 (blue economy).

Information about the project's progress will be published on the project web site available at https://interreg-baltic.eu/project/baltic-sea-e-nav/.

References

CHS (2018). *Notice of interest for the development of S-102 product display applications and software*. Canadian Hydrographic Service, Canada. https://www.charts.gc.ca/documents/data-gestion/s-102/S-102_Notice_of_interest_CHS.pdf (accessed 26 April 2024).

IMO (2018). *E-Navigation Strategy Implementation Plan – Update 1, MSC.1/Circ.1595, 2018*. International Maritime Organization, London, United Kingdom. https://www.imo.org/en/OurWork/Safety/Pages/eNavigation.aspx (accessed 7 April 2024).

IMO (2022). *IMO Resolution MSC.530(106): Performance Standards for Electronic Chart Display and Information Systems (ECDIS), adopted 2022-11-07*. International Maritime Organization, London, United Kingdom. https://wwwcdn.imo.org/localresources/en/KnowledgeCentre/IndexofIMOResolutions/MSCResolutions/MSC.530(106).pdf (accessed 20 April 2024).

Jang, J., Park, S., Oh, S. and Kim, I. (2023). The effectiveness of S-100 ECDIS capable of ENDS in the view of ship officers' visual characteristics. *The International Hydrographic Review, 29*(2), pp. 164–171. https://doi.org/10.58440/ihr-29-2-a27

UKHO (2022). *UKHO provides S-100 navigation data for Mayflower Autonomous Ship during at-sea testing before departure for US coast*. https://www.gov.uk/government/news/ukho-provides-s-100-navigation-data-for-mayflower-autonomous-ship-during-at-sea-testing-before-departure-for-us-coast (accessed 22 April 2024).

GENERAL INFORMATION

Empowering hydrographic professionals: Highlights from IFHS Student Awards and insights into the Hydrographic Professional Accreditation Scheme

Authors

Huibert-Jan Lekkerkerk[1], David Vincentelli[1], Tanja Dufek[1] and Yvonne Liversidge[1]

1 IFHS Student Award 2023

We are delighted to announce that Manuela Ammann (University of Applied Sciences Northwestern Switzerland), holding a Masters in Geomatics, has been named the recipient of the Student Award 2023 of the International Federation of Hydrographic Societies (IFHS).

The Award was presented by IFHS Chairman, David Vincentelli, at the flagship HYDRO 2023 event in Genoa, Italy, receiving a £1,500 prize and also a historic map of Genoa port provided by the Italian Navy Institute.

Nominated by the German Hydrographic Society (DHyG), Manuela is the first Swiss recipient of the IFHS Award, which she secured for her paper titled Robotic Photogrammetric Underwater Inspection of Hydropower Plants (see pp. 38-44 of this issue)[2] which highlighted her excellent, innovative and practice-relevant work.

The IFHS also offers a Best Student Presentation Prize, and is committed to ensuring that all HYDRO conferences continue to include sessions on education and training and an opportunity to present their work to a global hydrographic audience.

We eagerly await submissions for the next Student Awards! See all IFHS Student Award information at https://hydrography.earth/awards/.

2 IFHS empowers the younger generation – a pathway for students and trainees through the Hydrographic Professional Accreditation Scheme

Manuela's achievement stands as a beacon of inspiration for those considering a career in Hydrography. It is highly celebrated by the IFHS and its member societies, whose fundamental mission is to support all students and trainees on their career journey. In addition to awards, prizes and opportunities at events, the IFHS offers students and trainees support through an entry-level Affiliate status of the Hydrographic Professional Accreditation Scheme (HPAS).

Raising awareness among young professionals about the importance of individual accreditation is crucial, and this Scheme enables students and trainees to demonstrate their commitment to the profession during their education and training.

This Affiliate level requires no experience. While it is not an accreditation in itself, it provides students, apprentices, survey assistants, data processing assistants and those starting out in their careers, with a crucial pathway and structured route to activate their professional development journey and work towards future individual accreditation.

In 2024, the IFHS has seen a rise in Affiliate applications to the Scheme and some previous Affiliates have begun advancing through the levels of Accreditation. This is encouraging, and we

✉ Yvonne Liversidge · coordinator@ths-uki.org

[1] The International Federation of Hydrographic Societies

[2] Ammann, M. (2024). Robotic photogrammetric underwater inspection of hydropower plants. *The International Hydrographic Review*, *30*(1), pp. 38-44. https://doi.org/10.58440/ihr-30-1-a04

https://doi.org/10.58440/ihr-30-1-i02

Student Award 2023 of the International Federation of Hydrographic Societies (IFHS): Award winner Manuela Ammann (right) and IFHS Chair David Vincentelli (left) at HYDRO 2023 in Genoa, Italy.

https://doi.org/10.58440/ihr-30-1-i02

look forward to the ongoing expansion of Affiliates within the HPAS scheme.

For further information on the pathways and application process for the Hydrographic Professional Accreditation Scheme, insights into how it can empower the younger generation to progress in their early careers, and the advantages of individual accreditation, please continue reading below.

Here's to continued excellence in the field of hydrography!

3 HPAS – The Hydrographic Professional Accreditation Scheme by the International Federation of Hydrographic Societies

In such an international branch as hydrography, the need for standards – especially in the accreditation of individual personnel – is of great importance. The recently introduced multinational Hydrographic Professional Accreditation Scheme by the IFHS, allows individuals to gain a professional accreditation based on educational qualifications, practical experience and continuing professional development (CPD). The HPAS has received recognition by the IBSC (FIG/IHO/ICA International Board on Standards of Competence) offering those without a certificate from a recognised Cat-A or Cat-B programme an alternative which increases the likelihood that individual accreditation will become more established in the professional field of hydrography.

3.1 Towards a standardised, follow-up for, and international recognition of hydrographic skills

HPAS, the Hydrographic Professional Accreditation Scheme, is the IFHS individual certification scheme, recognised by the IBSC created to follow and accredit professional hydrographers.

Multiple questions may arise regards the Scheme, such as: Why the need for a new scheme? What are the differences between HPAS and a certificate from a recognised Cat-A and Cat-B programme?

We shall first outline the differences between diploma and certification. Certificates from a recognised Cat-A and Cat-B programme are well known and accepted within the industry and beyond. This recognition is however given by the IBSC to educational programmes rather than to individuals. The individual is thus not certified but the programme. Depending on the programme the certificate, diploma or a side-letter will be issued stating that the student has completed a programme meeting the requirements for a Cat-A or Cat-B according to the relevant S5 standard of competence from the IBSC. This indicates that the holder of such a certificate has completed all the relevant theoretical competencies as listed in the S5-A or S5-B standard as well as completed a Field Training Project. It does not qualify the holder of such a degree or certificate as a competent hydrographic surveyor just yet. In effect, one might go to a completely different industry for years still holding the same degree without ever practising hydrography at all.

Certification schemes, such as the HPAS, certify the capacity of an individual to be a recognised and qualified hydrographic surveyor, not only due to their educational qualifications but also based on the technical and/or management experience gained during their hydrographic career as well as their contribution to hydrographic surveying in general. This means that accredited HPAS members (or indeed those from other IBSC recognised schemes) have demonstrated not only how to apply the theoretical knowledge in a practical environment but also that they have accumulated enough practical experience to be proficient in their work as hydrographic surveyors. This should aid employers and clients in their selection of the right person for the (hydrographic) job.

The main objectives of a certification scheme compared to a diploma or certificate from a recognised course are:

- To demonstrate the practical proficiency of a hydrographic surveyor through a documented and peer-reviewed record of experience.
- To ensure the continuous development of an individual.
- To allow individuals with a non-hydrographic educational background in a related science to be certified as a hydrographic surveyor at a certain level.

The multinational HPAS scheme is developed and maintained by the IFHS which, as a federation consists of six hydrographic societies: THS:UKI for the UK and Ireland, DHyG for Germany, HSB for Benelux, IHS for Italy, AFHy for francophone countries and HSSA for South Africa. The development of the scheme was driven by the general need for such an accreditation scheme in industry, governmental and educational/research institutions.

HPAS is not the first scheme to become certified by the IBSC. It follows the path of Canada, Australasia, and the USA in that way, with the early goal to bridge the interest of the six associated

https://doi.org/10.58440/ihr-30-1-i02

societies, becoming a multi-national standard, and with the ambition to be recognised by all other IBSC approved schemes, helping the employment of professional hydrographers worldwide and increasing the confidence of the employers and clients of hydrographic professionals.

To that effect a Memorandum of Understanding mutually recognising each other's accreditation is in place with the Canadian ACLS International Hydrographer Certification Scheme.

3.2 How to apply for HPAS?

HPAS offers three levels of accreditation and an affiliate level for Students or those who have just started their career in hydrographic surveying. For each level multiple pathways are possible as shown in the illustration below. Level 2 (AH-L2) is a practical hydrographic surveyor or survey technician who can execute various survey tasks and instructions. A level 1 (AH-L1) surveyor has progressed to a supervisory/senior level and is able to plan and lead complex multidisciplinary field projects. Level 0 (AH-L0) is the highest level given to professionals who have not only advanced their knowledge but also developed management and leadership skills and become people of repute in the profession.

The exact pathway depends on the educational background and experience of the applicant. For those holding a certificate or diploma from an IBSC recognised Cat-A programme there are no further academic qualifications required for any of the pathways, they do however need to meet the experience criteria.

The minimum duration of work experience given in the illustration below must be understood as an absolute minimum. The variety of tasks and types of executed projects as well as the assigned responsibilities and roles are of greater importance.

Those holding a certificate from an IBSC recognised Cat-B programme and have the appropriate amount of experience can apply for a Level 2 accreditation. When they wish to apply for a Level 1 accreditation, they will need to demonstrate that they have obtained additional formal qualifications equivalent to those of a recognised Cat-A programme. Similarly, those entering with a degree from a programme that is not recognised will need to demonstrate their formal theoretical knowledge on a level equivalent to that of a Cat-A or Cat-B recognised programme in addition to the required amount of practical experience.

For Affiliate status, no experience is required, as this is an entry level designed for Student, apprentice, or survey assistant, data processing assistant. The affiliate status does not provide an accredited professional status but enables students and trainees to show commitment to the profession during their education and training.

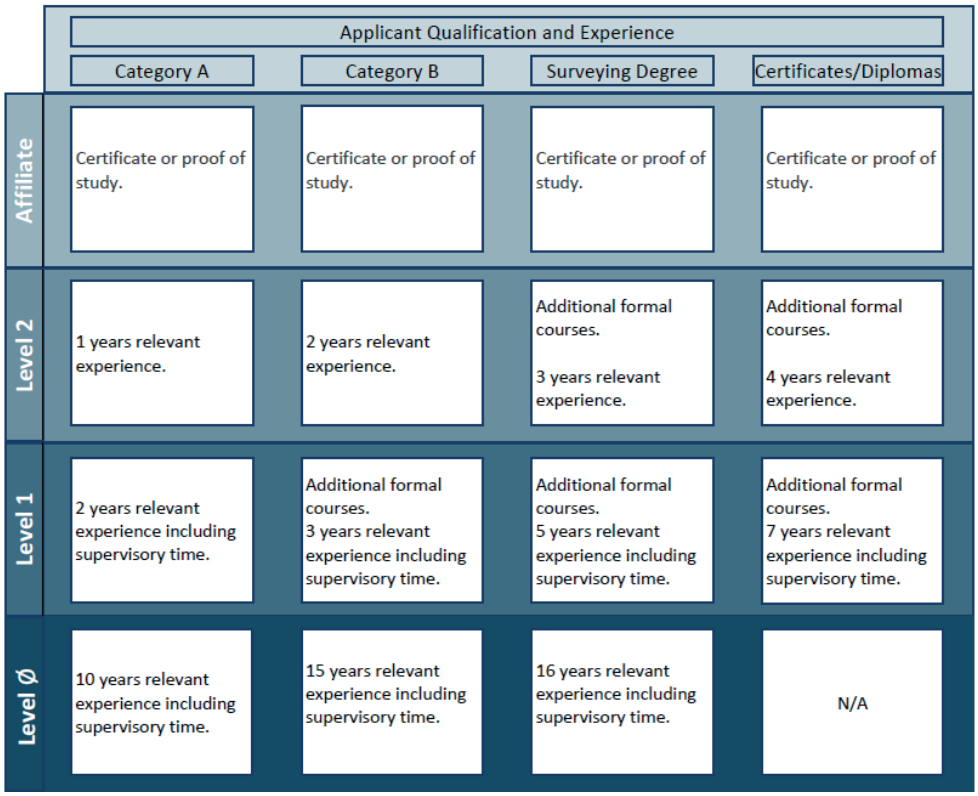

HPAS levels and pathways.

To apply to HPAS, proof of educational qualifications and work experience must be provided. The required documentation varies according to the level sought and the preconditions of the applicant and may include:

- A CV with references and/or referees.
- A logbook of hydrographic survey activities covering the required amount of experience,
- Recent survey reports or products with a critique providing detailed information about the applicant's role in the provided projects as well as an evaluation.
- An experience matrix, which lists different survey types and tasks. The applicant must indicate which kind of projects and in which responsibilities they have been involved.Depending on the level applied for, a certain number of tasks and types as well as roles are expected to be accomplished.
- A qualification mapping for those without the required certificate or degree from an IBSC recognised programme including a mapping for those applying to L1 or L0 and holding a certificate from a recognised Cat-B programme indicating how they have obtained the additional formal competencies at a Cat-A level.
- Records of Continuous Professional Development for those transitioning between levels.

Once applications are submitted, these are reviewed by the HPAS panel. The panel consists of at least eight members from IFHS societies coming from industry, academia or government and are in office for three years. IFHS will advertise the vacant panel seats annually and nominations are then received by the HPAS steering committee, which selects the panel member. The steering committee consists of representatives of the IFHS societies and gives strategic direction and guidance to the HPAS.

The HPAS panel will scrutinise the provided information and base their decision to award or deny a certain level sought on the supplied information. In case certain aspects regards the accreditation level cannot be clarified from the provided documentation the panel may ask for additional information, contact referees or invite the applicant to an interview.

3.3 What support and guidance are available?

Support tools and events are available to guide potential candidates with their applications. A level-specific overview of necessary documents, examples of filled forms and a detailed explanation of them for each level are given in the HPAS Applicant Guide. The Panel has recently developed an Interactive Application Guide to help candidates assess their qualifications and experience to apply for the correct level. The IFHS has also just launched regular free Webinars titled 'HPAS-Building a successful Application', which are held in advance of each intake deadline, where attendees benefit from an overview of key information, tips, and advice along with a live Q&A and informal mentoring with the HPAS Panel. All of this information, links to the Guide, Interactive tool, webinar dates/recordings and contact details for the HPAS coordinator are all available at 'HPAS Corner' following https://hydrography.earth/hpas/.

3.4 When are application deadlines and what are the fees?

There are two HPAS application deadlines per year: 31 March and 31 October. The time between the application deadline and being informed about the decision might take about 15 weeks. The regular accreditation fee of 140–200 € (depending on the level sought) is reduced to 70–100 € for members of the IFHS societies. The annual renewal is 30–50 € for members.

Affiliates who are members of IFHS societies can attain Affiliate status free of charge.

3.5 How to maintain an HPAS level?

To maintain their accreditation, members must show that they have been employed in the hydrographic field for at least 6 months of the last 12 and submit a record of at least 40 hours of CPD from that year. The CPD log ensures that accredited HPAS members stay current with hydrographic developments and keep enhancing their skills. For the CPD record different professional, educational or voluntary activities related to hydrography are supported. They include non-technical skills to improve personal competencies and soft skills, as well as formal and informal time. The minimum required time of formal CPD is 20 hours per year and includes activities of structured learning that have a clear learning objective like a professional course, technical authorship, or a learning activity with assessment measures. Informal CPDs are self-managed learning like private study, on-the-job practical training, attendance at informal seminars or events focusing on knowledge sharing.

Accredited HPAS members can also transition from one level to the next after gaining more experience and educational or other qualifications. Depending on the transition level,

https://doi.org/10.58440/ihr-30-1-i02

the applicant must hand in some, or all the documents listed above for the regular application. They will also need to demonstrate that they have fulfilled all CPD requirements.

3.6 Conclusion

The first two years of HPAS operations have demonstrated the interest of public and private sector professionals to apply for HPAS accreditation. A majority of the applicants did not have a degree or certificate from an IBSC recognised Cat-A or Cat-B programme.

Within the IFHS community, accreditation of individuals is new and the Scheme needs to be advertised and Introduced further. Its successful establishment in such an internationally operating field as hydrography has a lot of benefits, especially if schemes which accredit individuals can be mutually recognised. It facilitates, for example, the staff recruitment, tenders, company-internal CPD or general administration.

The CPD requirements may well stimulate those offering training and other formal courses to consider registering the participants and issuing them with certificates stating which competencies have been covered. In addition, the international training industry offering e-learning and online trainings may develop further. They may constitute the foundation for a new international standard in the hydrographic profession which not only recognises theoretical education but also practical achievements.

https://doi.org/10.58440/ihr-30-1-i02

GENERAL INFORMATION

FIG Commission 4 Work Plan 2023–2026: Targeting the next challenges in the hydrospatial domain

Authors

Gunathilaka, M. D. Eranda K.[1], Gordon Johnston[2], Geoff Lawes[3], Samuel Ironside[4], Wee, K. T. K.[5], Mick Filmer[6], Tanja Dufek[7], Jakovljevic Gordana[8], Denis Hains[9] and Ashraf Dewan[6]

Abstract

The evolution of hydrographic science and technology is continually shaped by emerging trends and challenges, influencing our comprehension and governance of marine environments. Commission 4 (Hydrography) of the International Federation of Surveyors (FIG) is charged with anticipating the impact of these developments on hydrospatial professionals and addressing emerging issues in its forthcoming four-year work plan. This necessitates staying informed about the latest advancements and navigating the interplay of factors within the hydrospatial domain. Commission 4 also aims to engage with the hydrospatial community to gain insights into the effects of current trends on global hydrospatial work at various levels. Establishing collaborations with key organisations, including the International Hydrographic Organization, professional bodies, standards bodies, global taskforces, and other FIG commissions and networks, is integral to ensuring the hydrospatial community can deliver the highest level of professional output for global hydrospatial information users. This article seeks to enhance community awareness and understanding of the roles played by FIG Commission 4 and its associated working groups. It provides an update on the changes and goals outlined in the FIG Commission 4 work plan for the term 2023–2026, introduces the term "hydrospatial" in lieu of "geospatial" for ocean and related domains, and introduces a new working group (WG 4.5) focused on addressing the impacts of climate change.

✉ M. D. Eranda K. Gunathilaka · erandakan@geo.sab.ac.lk

[1] Faculty of Geomatics, Sabaragamuwa University of Sri Lanka, Sri Lanka

[2] Venture Geomatics Limited, Sutton, United Kingdom

[3] Revelare Systems Pty Ltd, Queensland, Australia

[4] Land Information New Zealand (LINZ), Wellington, New Zealand

[5] Faculty of Built Environment & Surveying, Universiti Teknologi Malaysia (UTM), Johor Bahru, Malaysia

[6] School of Earth and Planetary Sciences, Curtin University, Perth, Australia

[7] HafenCity Universität, Hamburg, Germany

[8] Faculty of Architecture, Civil Engineering and Geodesy, University of Banja Luka, Bosnia and Herzegovina

[9] H2i Hains Hydrospatial International Inc., Ottawa, Ontario, Canada

https://doi.org/10.58440/ihr-30-1-i01

1 Introduction

The International Federation of Surveyors (FIG), founded in 1878, is a United Nations (UN) and World Bank recognised non-governmental international professional organisation. FIG member organisations include professional bodies and academic institutions in over 120 countries, representing those who measure, locate, map, value, plan, construct, develop and manage the land, the seas, and any human-built structures with a vision to extend the usefulness of surveying for the benefit of society, the environment, and the economy.

FIG's technical work is led by ten Commissions. FIG Commission 4 is focused on the field of hydrographic surveying and includes the entire hydrospatial domain (Hains et al., 2022). There are also several Task Forces (TFs) that have been established within FIG to research and advise on matters of an administrative or general policy nature to FIG; and several Networks comprising industry professionals, organisations, and affiliated institutions, serving as a platform for collaboration, knowledge exchange, and advocacy in the surveying, geospatial and hydrospatial community.

According to its constitution, in each four-year term, the FIG council must develop a new work plan. Subsequently, each commission generates subordinate plans to align with the FIG council's plans, considering the latest trends in their scope. Led by the newly elected commission chair, and several new team members, FIG commission 4 has developed a new work plan that reflects a forward-looking approach to address evolving challenges in the hydrospatial domain (FIG, 2023).

2 Future challenges

The hydrospatial domain is undergoing a transformative impact of automation that reaches all areas of the blue planet, including the blue zone and contiguous zones. Consequently, the routine of the hydrographic surveyor is likely to change radically over the next four years with more remote operations and autonomous systems, including Autonomous Underwater Vehicles (AUVs), Uncrewed Surface Vehicles (USVs) and Uncrewed Airborne Vehicles (UAVs) as well as a variety of remote-sensing systems such as Satellite Derived Bathymetry (SDB) undertaking hydrospatial data acquisition.

It is also likely that Artificial Intelligence (AI) will be used in some aspects of data processing and more types of spatiotemporal data from novel sources will permeate the hydrospatial domain, leading to an increase in data volumes and changes in data management, storage, and use.

Climate change poses significant challenges and opportunities in the hydrospatial domain, especially where ocean circulation and the coastal zone are affected by rising sea levels and increased frequency of extreme weather events.

By recognising the interplay between global issues and the hydrospatial domain, we can better leverage interdisciplinary collaborations to work toward holistic solutions to address the complex socio-environmental challenges facing the marine environment.

3 New plan

During the previous term (2019–2022), FIG Commission 4 operated four working groups (WGs), namely *WG 4.1 – Standards and Guidelines for Hydrography*, *WG 4.2 – Blue Growth & UN Sustainable Development Goal 14*, *WG 4.3 – Mapping the Plastic* and *WG 4.4 – Marine Development and Administration*. The terms of reference for the existing working groups have been updated for the new term (2023–2026), and a new *WG 4.5 – Climate Change induced Sea Level Rise and Adaptation* has been established.

We report and discuss progress at our annual event the *Working Week*. The next two of these events being FIG Working Week 2024 in Accra, Ghana[1] and FIG Working Week 2025 in Brisbane, Australia[2].

Also invite you to join our commission LinkedIn page and keep in touch with us[3].

3.1 WG 4.1 – Hydrographic Standards and Guidelines

Hydrographic standards and guidelines are developed and maintained through international collaboration among national hydrographic offices, maritime organisations, standards bodies, and industry stakeholders. By adhering to standardised practices and procedures, stakeholders can ensure the integrity and utility of hydrographic data for supporting safe navigation, sustainable resource management, environmental protection, and disaster preparedness and response efforts. WG 4.1 aims to engage with standards organisations and stakeholders to ensure that the

[1] https://www.fig.net/fig2024/ (accessed 18 February 2024).

[2] https://www.fig.net/fig2025/ (accessed 18 February 2024).

[3] https://www.linkedin.com/showcase/fig-commission-4-hydrography (accessed 18 February 2024).

Commission Chair Eranda Gunathilaka (left) and Vice Chair Gordon Johnston (right).

concerns and experience of hydrospatial professionals are heard when standards are being developed or considered for adoption within the hydrospatial domain.

During the 2023–2026 term, WG 4.1 seeks to encourage and advocate for open standards that help to ensure transparency, traceability, posterity, and integrity of hydrospatial data. One such example is the Bathymetry Attributed Grid (BAG) format, which is under consideration as an Open Geospatial Consortium (OGC) community standard. WG 4.1 is represented in the Open Navigation Surface Working Group (ONSWG) and continues to advocate for the needs of hydrospatial professionals in relation to data transfer standards such as BAG.

In keeping with this theme of encouraging open standards and transparency, WG 4.1 aims to develop a new guideline during this term, focussed on processing of bathymetric data with significant data redundancy. This is an area where repeatable spatial processing methodologies and human-based manual processes are being challenged by large data volumes and AI-based processing approaches. WG 4.1 seeks to establish useful and practical guidance for surveyors to create awareness and build the trust necessary to effectively deploy emerging technology in this area.

3.2 WG 4.2 – Sustainable Oceans and Hydrography

WG 4.2 aims to foster collaboration with international governmental and non-governmental entities to enhance understanding and awareness of the significance of marine and oceanic environments. Emphasis is placed on the integration of emerging technologies to improve operational efficiency and anticipate future workforce needs. Additionally, WG 4.2 will explore the utilisation of established project planning methodologies and intends to develop a standardised tool to evaluate the socio-economic and regional impacts of hydrographic projects comprehensively. The surveyor, and in particular, the hydrographic surveyor has a key role in developing an understanding of our seas and oceans for the wider social benefits and Commission 4 aims to promote this role, the benefits and offer case studies of participation and support. WG 4.2's work is related to the United Nations Sustainable Development Goal 14: *Life Below Water*.

3.3 WG 4.3 – Mapping the Plastic

WG 4.3 was formed in 2018 as an initiative of the FIG Young Surveyors Network (YSN) and Commission 4 (Hydrography) as FIG's response to the issue of plastic pollution. The question that is posed to WG 4.3 is: how can spatial science professionals best contribute to the global plastic battle? Almost every piece of plastic ever made is still on our planet in some form and UN estimates suggest that more than 75 % of all the plastic produced since 1950 is now waste, with most discarded into landfills or dumped into marine environments. The UN Environment Programme (UNEP) has conventionally calculated that each year more than eight million tonnes of plastic ends up in our oceans. Therefore, given our specific spatial information, remote sensing, hydrographic surveying, project management and overall measurement

https://doi.org/10.58440/ihr-30-1-i01

science skillsets, WG 4.3 is decided to focus on better understanding the quantity and type of plastic waste being transported in waterways before they reach our oceans.

Plastic waste floats on the surface and upper limits of rivers or settles on banks, estuaries, and coastlines during the transportation process. Here, sensing data from satellites and airborne platforms available in different spatial, spectral, and temporal resolutions has long been recognised as a potentially reliable source of long-term qualitative and quantitative information over large geographic areas. WG 4.3 has focussed on harnessing the potential of remote sensing and developed survey and processing methodologies to accurately map floating plastic in rivers and the surrounding environment at localised 'hot spot' areas using data from UAV orthophotos combined with artificial intelligence algorithms and software tools in near real time. The fundamental objective of WG 4.3 is to generate methodologies to control and eradicate plastic pollution in our oceans (Jakovljevic et. al, 2020). With the support of the international surveying community, our networks within the plastics movement, our academic and industry partners and the donor community FIG can contribute meaningfully to this goal. Raising awareness of the issue is a key component of this and we undertake more plastics surveys, refine our methods and techniques, WG 4.3 will be able to offer support to more countries and regions inundated with plastic pollution.

3.4 WG 4.4 – Hydrospatial Domain and Marine Administration

WG 4.4 was renamed to incorporate the term hydrospatial in recognition of a broader context. It shall seek to promote and engage with international government and non-governmental organisations to increase the understanding and awareness of the importance of the hydrospatial domain and marine administration. This includes assisting in the development of indigenous hydrospatial data infrastructure management, assisting in the development of institutional policy and frameworks, assisting in the development of conceptual and technical standards, guidelines and practice, reviewing of national and international hydrospatial domain and marine administration policies, standards and guidelines and finally to instigate sustainable collaboration by promoting best practices, including citizen science activities, such as Crowd-Sourced Bathymetry (CSB) for development of information and knowledge in the hydrospatial domain. The beneficiaries include global governments and associated national mapping and charting agencies; and relevant international non-governmental organisations, hydrospatial industry and academia.

3.5 WG 4.5 – Climate Change induced Sea Level Rise and Adaptation

Climate change induced sea level rise refers to the gradual increase in the average global sea level because of climate change, primarily driven by the thermal expansion of seawater and the melting of glaciers and polar ice caps. The consequences of sea level rise are significant, impacting coastal communities, ecosystems, and infrastructure. Coastal areas are particularly vulnerable to the effects of sea level rise, facing increased risks of flooding, erosion, saltwater intrusion, and coastal inundation during storm events. Low-lying islands and coastal cities are at elevated risk of displacement, loss of habitat, and damage to critical infrastructure.

However, in most of the developing countries, there is no accurate estimation of sea level rise rates and prediction of its trend according to the IPCC's projections, and evaluation of the impact through potential inundation of low-lying coastal regions. At several places, problems limit successful outcomes, often due to the lack of long-term tidal data and/or accurate digital elevation models (DEMs) over coastal areas.

Since this is a global challenge, Commission 4 established a new WG 4.5 to undertake planning and development of guidelines aligned with global standards to support hydrospatial professionals working in this domain.

WG 4.5 seeks to:

- Review existing practices, tools, and techniques to monitor and analyse sea level rise and associated issues;
- identify existing, and further develop best practices, tools and capacity related to the quantification and analysis of climate change consequences such as mean sea level (MSL),local/regional rela tive sea level rise estimation and coastal inundation;
- support multidisciplinary collaboration between surveying, geospatial sciences, hydrog raphy, and oceanography;
- use satellite data for improved sea level rise estimation and use high resolution remote sensing images, UAV sensors and GIS (Geospatial Information System) tools for coastal inundation modelling; andestablish links and collaboration with existing sea level research groups, building on previous work.

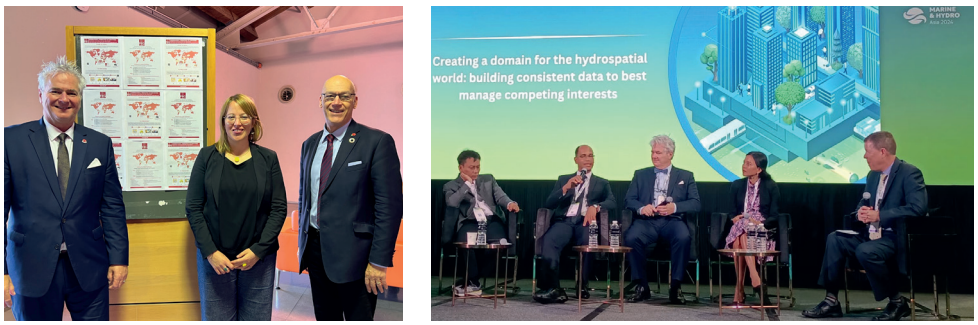

Some events represented by the FIG Commission 4 (left: Hydro 2023, right: Geo Connect Aisa 2024).

4 Summary

FIG Commission 4 has developed a forward-looking work plan for 2023–2026 to tackle emerging challenges in the hydrospatial domain. These challenges encompass the transformative impact of automation, the integration of Artificial Intelligence (AI), and the effects of climate change. The new plan includes five working groups (WGs) focusing on standards and guidelines, sustainable oceans, plastic pollution mapping, hydrospatial domain and marine administration, and climate change-induced sea level rise and adaptation. Emphasising open standards, sustainability, and effective response to sea level rise, FIG seeks to foster interdisciplinary collaboration and contribute significantly to societal, environmental, and economic betterment in the hydrospatial field. Hydrospatial professionals are encouraged to contact the commission representatives and actively get involved in these crucial initiatives.

References

FIG (2023). *Commission 4 Work Pan 2023–2026*. International Federation of Surveyors. https://www.fig.net/organisation/comm/4/workplan_23-26.asp (accessed 27 January 2024).

Hains, D., Schiller, L., Ponce, R., Bergmann, M., Cawthra, H. C., Cove, K., Echeverry, P., Gaunavou, L., Kim, S.-P., Lavagnino, A. C., Maschke, J., Mihailov, M. E., Obura, V., Oei, P., Pang, P. Y., Njanaseelan, G. P. and Sharma, S. L. (2022). Hydrospatial – Update and progress in the definition of this term. *The International Hydrographic Review*, *28*, pp. 221–225. https://doi.org/10.58440/ihr-28-n14

Jakovljevic, G., Govedarica, M. and Alvarez-Taboada, F. (2020). A Deep Learning Model for Automatic Plastic Mapping Using Unmanned Aerial Vehicle (UAV) Data. *Remote Sensing*, *12*(9):1515. https://doi.org/10.3390/rs12091515

https://doi.org/10.58440/ihr-30-1-i01

BOOK REVIEW

The deepest map – The high-stakes race to chart the world's oceans

By Laura Tretheway, published by HarperCollins Publishers LLC, New York City, New York, U.S.A. in 2023. Goose Lane Editions, 304 p., ISBN 978-0063099951.

Author
Douglas Paul Brunt[1]

Award-winning environmental and ocean journalist Laura Tretheway takes readers on an interesting and informative voyage into the seascape of ocean mapping in their 2023 book, *The Deepest Map – The High-Stakes Race to Chart the World's Oceans.*

Using the author's own firsthand experiences with the ship and crew of the *E/V Nautilus* plus the recollections of a new hydrographer who worked with the high-profile Five Deeps expeditions as the main story arc, the book explores many of the key issues surrounding the quest to map the world's oceans.

Not surprisingly, the Nippon Foundation – GEBCO Seabed 2030 Project quickly surfaces and becomes a main theme in the book. The book is not overly technical, instead, it provides just enough detail for the average reader to appreciate the technological challenges and advancements associated with hydrographic surveying and how that plays into the to the perils and the politics of ocean mapping. At the same time, it tries to answer the fundamental question: Why is it important to fill the gaps in our collective knowledge of the oceans?

Any time that "the ocean" is the subject of investigation, trying to find the appropriate scope of the work can be daunting. However, through a series of interrelated chapters, the author deftly and concisely ties together the personal, hands-on experiences of those doing the surveying and driving innovation with what transpires in meeting rooms and board rooms at the national, regional, and global levels.

For cartographers, the chapter on the Marie Tharp maps dives deeply into why these are regarded as revolutionary: These maps, the first being published by *National Geographic* in 1967, were the first to give the public a glimpse of what the seafloor truly looked like. However, the author also points out that these maps gave the impression that the world's oceans were well mapped when, in fact, the maps were more akin to illustrations as they were based on very sparse data. This early impression persists today in many minds and presents a challenge to those seeking more support for continued ocean mapping. Importantly, the chapter is a reflection on the power of maps to change society's perception of the world's oceans and seas.

To make significant and rapid progress towards better and more complete maps of the oceans, innovations in ocean mapping technology and how the problem is approached will be required. Examples of each are discussed in chapters on crowdsourcing and the application of automation (e.g., robotics) to hydrography.

In the chapter, "Buried History," the author reminds us that even with the vast body of knowledge humans have acquired about the oceans over millennia, the rate of new discoveries has not abated. These discoveries, whether of natural features, biology, or archeological, help us to better understand not only the ocean itself but also the human-ocean relationship. With each discovery, questions of ownership and who has the right to exploit (or not) these finds, come to the fore.

Politics is inescapable when talking about ocean mapping and Tretheway gives the reader a window into this world with chapters on the workings of the GEBCO Sub-Committee on

✉ Douglas Paul Brunt · douglas.paul@brunt.name
[1] Retired; formerly Government of Canada, Department of Fisheries and Ocean Canada, Canadian Hydrographic Service, Ottawa, Canada

https://doi.org/10.58440/ihr-30-1-b01

Undersea Feature Names (SCUFN) and the International Seabed Authority (ISA). The former struggles to maintain an apolitical stance; a position made more difficult by the increase in bathymetric data, which, in turn, permits better definition of existing and new undersea features. Increasingly nationalistic positions, particularly when meetings move out from behind closed doors, further complicate matters. Matters also get complicated when commercial, national, and international interests overlap as it is the case with the ISA, which was formed in 1994 as an autonomous international organization under the Agreement relating to the Implementation of Part XI of the United Nations Convention on the Law of the Sea (1994 Agreement). By shining more light on this organization, the author provides the reader with valuable insights at a time when everyone should be considering the good and adverse consequences of seabed mining.

Throughout the book, the issue of diversity and inclusion (and corresponding respect), particularly as it relates to gender, is touched upon. The gender imbalance within the hydrographic community is well documented (including within the IHR) and it is important that the author draws attention to the situation. For those readers outside the hydrographic community, some information on the steps being taken today to address diversity would have been useful. Obviously, there is more work to be done to bring a gender-balance to all levels of the discipline.

Within the scope of the investigation, the author has sought out the input of many subject matter experts and the author's diligence in researching is evident from the extensive references cited. These sources, references, and the list of acknowledgements contain some of the most well-known and respected names in the hydrographic and ocean mapping communities, including many who are active within the International Hydrographic Organization (IHO) and would be familiar to IHR readers.

The author answers the "why map the ocean" question thoroughly and convincingly and addresses the fear that this information could also be used by bad actors. In the end, however, it is concluded that while maps have always been used as tools for exploitation, they are also critical for conservation, protection, and management of the ocean environment.

The Deepest Map engages and enlightens the reader, and we are grateful for it. This is a recommended read.

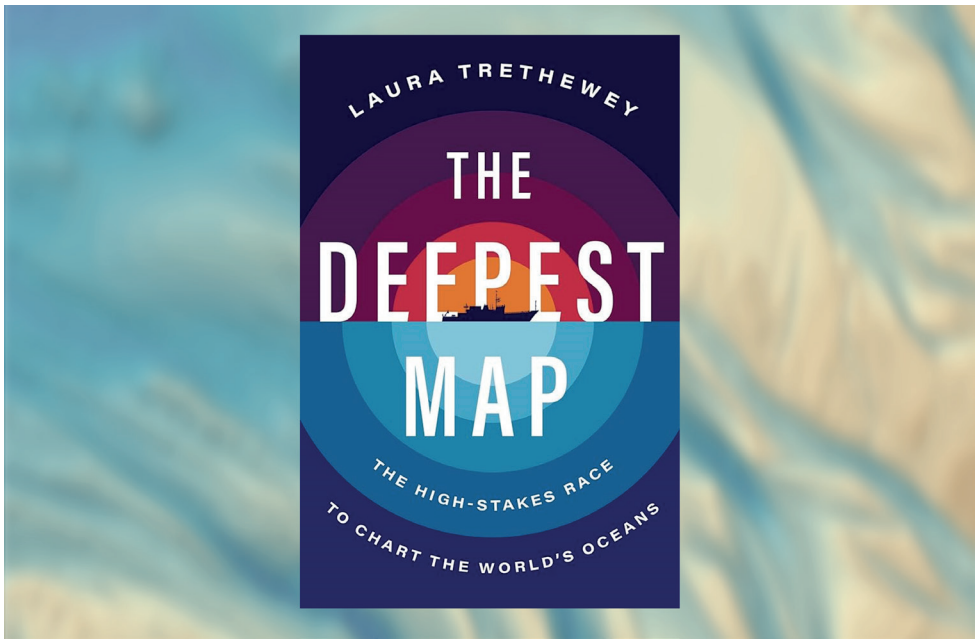

Cover of the book "The deepest map – The high-stakes race to chart the world's oceans" by Laura Tretheway.

https://doi.org/10.58440/ihr-30-1-b01


IHO
International
Hydrographic
Organization